UNIVERSITAT ROVIRA I VIRGIL

SECOND-ROW TRANSITION-METAL COMPLEXES RELEVANT TO CO2 REDUCTION AND WATER OXIDATION

Takashi Ono

Dipòsit Legal: T 1108-2014

ADVERTIMENT. L'accés als continguts d'aquesta tesi doctoral i la seva utilització ha de respectar els drets de la persona autora. Pot ser utilitzada per a consulta o estudi personal, així com en activitats o materials d'investigació i docència en els termes establerts a l'art. 32 del Text Refós de la Llei de Propietat Intel·lectual (RDL 1/1996). Per altres utilitzacions es requereix l'autorització prèvia i expressa de la persona autora. En qualsevol cas, en la utilització dels seus continguts caldrà indicar de forma clara el nom i cognoms de la persona autora i el títol de la tesi doctoral. No s'autoritza la seva reproducció o altres formes d'explotació efectuades amb finalitats de lucre ni la seva comunicació pública des d'un lloc aliè al servei TDX. Tampoc s'autoritza la presentació del seu contingut en una finestra o marc aliè a TDX (framing). Aquesta reserva de drets afecta tant als continguts de la tesi com als seus resums i índexs.

ADVERTENCIA. El acceso a los contenidos de esta tesis doctoral y su utilización debe respetar los derechos de la persona autora. Puede ser utilizada para consulta o estudio personal, así como en actividades o materiales de investigación y docencia en los términos establecidos en el art. 32 del Texto Refundido de la Ley de Propiedad Intelectual (RDL 1/1996). Para otros usos se requiere la autorización previa y expresa de la persona autora. En cualquier caso, en la utilización de sus contenidos se deberá indicar de forma clara el nombre y apellidos de la persona autora y el título de la tesis doctoral. No se autoriza su reproducción u otras formas de explotación efectuadas con fines lucrativos ni su comunicación pública desde un sitio ajeno al servicio TDR. Tampoco se autoriza la presentación de su contenido en una ventana o marco ajeno a TDR (framing). Esta reserva de derechos afecta tanto al contenido de la tesis como a sus resúmenes e índices.

WARNING. Access to the contents of this doctoral thesis and its use must respect the rights of the author. It can be used for reference or private study, as well as research and learning activities or materials in the terms established by the 32nd article of the Spanish Consolidated Copyright Act (RDL 1/1996). Express and previous authorization of the author is required for any other uses. In any case, when using its content, full name of the author and title of the thesis must be clearly indicated. Reproduction or other forms of for profit use or public communication from outside TDX service is not allowed. Presentation of its content in a window or frame external to TDX (framing) is not authorized either. These rights affect both the content of the thesis and its abstracts and indexes.

UNIVERSITAT ROVIRA I VIRGILI
SECOND-ROW TRANSITION-METAL COMPLEXES RELEVANT TO CO2 REDUCTION AND WATER OXIDATION
Takashi Ono
DL:T 1108-2014

UNIVERSITAT ROVIRA I VIRGILI
SECOND-ROW TRANSITION-METAL COMPLEXES RELEVANT TO CO2 REDUCTION AND WATER OXIDATION
Takashi Ono
DL:T 1108-2014

UNIVERSITAT ROVIRA I VIRGILI
SECOND-ROW TRANSITION-METAL COMPLEXES RELEVANT TO CO2 REDUCTION AND WATER OXIDATION
Takashi Ono
DL:T 1108-2014

Takashi Ono

Second-Row Transition-Metal Complexes Relevant to CO_2 Reduction and Water Oxidation

DOCTORAL THESIS

Supervised by Prof. Antoni Llobet Dalmases

Institute of Chemical Research of Catalonia (ICIQ)

2014

Tarragona

UNIVERSITAT ROVIRA I VIRGILI

UNIVERSITAT ROVIRA I VIRGILI
SECOND-ROW TRANSITION-METAL COMPLEXES RELEVANT TO CO2 REDUCTION AND WATER OXIDATION
Takashi Ono
DL:T 1108-2014

UNIVERSITAT ROVIRA I VIRGILI
SECOND-ROW TRANSITION-METAL COMPLEXES RELEVANT TO CO2 REDUCTION AND WATER OXIDATION
Takashi Ono
DL:T 1108-2014

Antoni Llobet Dalmases, Group Leader at the Institute of Chemical Research of Catalonia (ICIQ) in Tarragona and Full Professor of Chemistry at the Universitat Autònoma de Barcelona (UAB),

STATES that the present research work, entitled "**Second-Row Transition-Metal Complexes Relevant to CO_2 Reduction and Water Oxidation**", presented by Takashi Ono for the award of the degree of Doctor, has been carried out under my supervision at the Institute of Chemical Research of Catalonia (ICIQ) and that it fulfils all the requirements to be eligible for the International Doctorate Award.

Tarragona, April 2014

Doctoral Thesis Supervisor

Prof. Dr. Antoni Llobet Dalmases

ICIQ
Institut Català d'Investigació Química

UNIVERSITAT ROVIRA I VIRGILI

UNIVERSITAT ROVIRA I VIRGILI
SECOND-ROW TRANSITION-METAL COMPLEXES RELEVANT TO CO2 REDUCTION AND WATER OXIDATION
Takashi Ono
DL:T 1108-2014

UNIVERSITAT ROVIRA I VIRGILI
SECOND-ROW TRANSITION-METAL COMPLEXES RELEVANT TO CO2 REDUCTION AND WATER OXIDATION
Takashi Ono
DL:T 1108-2014

To my family

UNIVERSITAT ROVIRA I VIRGILI
SECOND-ROW TRANSITION-METAL COMPLEXES RELEVANT TO CO2 REDUCTION AND WATER OXIDATION
Takashi Ono
DL:T 1108-2014

Acknowledgments.

First of all, I would like to give thanks to my supervisor Professor Antoni Llobet for all his support and guidance during all these years. And for allowing me to take part of this motivating project; and the opportunity to meet all my labmates even the ones that have already left and the newcomers.

The development of this thesis was possible thanks to the financial support of FPU Ministery of Spain, help making this experience possible abroad. Including four years in Spain, and also half a year in the USA as a visiting student.

My gratitude also goes to ICIQ, who provided me with the cutting-edge technology and wonderful scientific technicians; In which is the base of all the work presented in this Memory.

To Professor Christopher C. Cummins at MIT, USA for accepting me, and being my host during my visit student program. Thank you, in addition for allowing me to take part of his research team, and for his kind support. To all my lab associates there for their support during my stay Cesar, Daniel, Runyu, Alexandra and Nazario, especially to Ioana for her successful work that she carried out in the same project, which released a brilliant paper.

To Professor Christopher J. Cramer and Laura Gagliardi at Minnesota University, USA. for their kind collaboration on DFT calculations and fruitful discussions. Also, a big thanks to the team at Minnesota, Pere, Mehmed and Michelle; And absolutely all of my lab associates at ICIQ who have helped, and supported me during these years.

A special thanks to ICIQ secretaries, and group secretaries who always helpful and took good care of my issues.

To my family, my wife Rocio Arteaga-Muller and my two little daughters Sarah Emmari and Leah Lynette, thank you for all your support and the time that you sacrificed being so far, in order to complete this project.

To my parents Koji and Kimiyo Ono and sister Yukiko, for your encouragement and your never ending support. Thank you.

UNIVERSITAT ROVIRA I VIRGILI
SECOND-ROW TRANSITION-METAL COMPLEXES RELEVANT TO CO2 REDUCTION AND WATER OXIDATION
Takashi Ono
DL:T 1108-2014

The work performed in the present doctoral thesis has been possible thanks to the funding of:

- Institut Català d'Investigació Quimica (ICIQ)
- Ministerio de Educación. Beca FPU: AP-2009-0789
- Ministerio de Ciencia e Innovación: CTQ2010-21497
- AGAUR: 2009 SGR 69
- Ministerio de Ciencia e Innovación dentro del Programa Nacional de Internacionalización de la I+D (Proyectos y Acciones Internacionales): EUI2009-04139

UNIVERSITAT ROVIRA I VIRGILI
SECOND-ROW TRANSITION-METAL COMPLEXES RELEVANT TO CO2 REDUCTION AND WATER OXIDATION
Takashi Ono
DL:T 1108-2014

UNIVERSITAT ROVIRA I VIRGILI
SECOND-ROW TRANSITION-METAL COMPLEXES RELEVANT TO CO2 REDUCTION AND WATER OXIDATION
Takashi Ono
DL:T 1108-2014

UNIVERSITAT ROVIRA I VIRGILI
SECOND-ROW TRANSITION-METAL COMPLEXES RELEVANT TO CO2 REDUCTION AND WATER OXIDATION
Takashi Ono
DL:T 1108-2014

Graphical abstracts

Chapter I. General Introduction

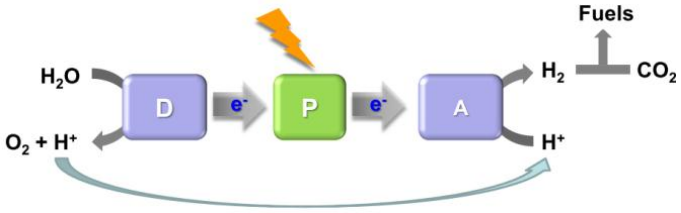

Artificial photosynthesis is a promising solution to the problem that our society faces. In order to achieve, efficient water oxidation catalysts have to be developed. As well, the reduction of CO_2 as useful chemicals is desired. An overview of the most representative catalysts for water oxidation and hydrogenative CO_2 reduction is provided.

Chapter II. Objectives

Chapter III

III-1. Carbon Dioxide Reduction Catalyzed by Mononuclear Ruthenium Polypyridyl Complexes

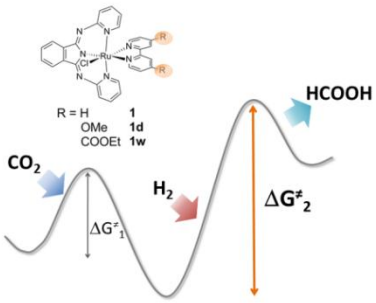

Mononuclear Ru polypyridyl complexes are shown to efficiently catalyze the hydrogenative reduction of CO_2 to formic acid. Electronic perturbation to the metal centre exerted by the pyridyl ligands produce dramatic effects in the catalytic performance. DFT calculations provides detailed mechanistic information and allow to rationalize the relationship between electronic perturbation and catalytic performance.

III-2. Carbon Dioxide Reduction Catalyzed by Mononuclear Ruthenium Polypyridyl Complexes: Electronic and Steric Effects

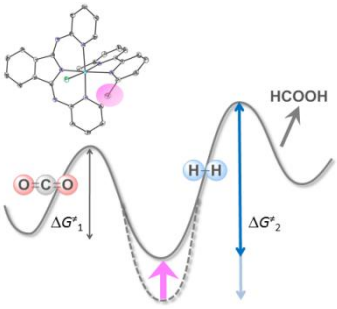

This section contains extended studies for hydrogenative CO_2 reduction. Systematic modification on electronic properties of the Ru complexes revealed the relationship between catalytic activity and their redox potentials. Furthermore, the effect of steric group on catalytic performance was studied experimentally and computationally.

Chapter IV

IV-1. Carbon Dioxide Reduction Catalyzed by Dinuclear Ruthenium Polypyridyl Complexes

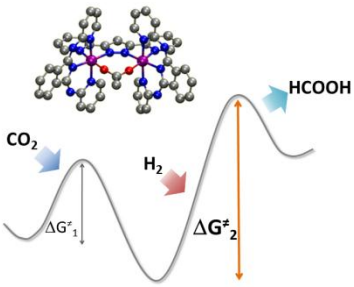

Dinuclear ruthenium polypyridyl complexes have been applied to the hydrogenative reduction of CO_2. The kinetics associated with the catalytic cycle were studied experimentally and a full catalytic cycle was determined on the basis of DFT calculations, which complements the experimental results.

IV-2. Dinuclear Ruthenium Hydride Complexes Containing Hbpp and Terpyridine Ligands: Synthesis and Reactivity

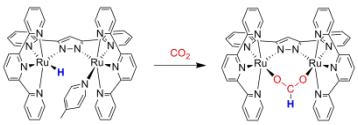

In this section, we report the synthesis and characterization of dinuclear ruthenium mono- and dihydrido complexes formed in-situ by hydride source apart from dihydrogen as well as the reactivity toward CO_2.

UNIVERSITAT ROVIRA I VIRGILI
SECOND-ROW TRANSITION-METAL COMPLEXES RELEVANT TO CO2 REDUCTION AND WATER OXIDATION
Takashi Ono
DL:T 1108-2014

UNIVERSITAT ROVIRA I VIRGILI
SECOND-ROW TRANSITION-METAL COMPLEXES RELEVANT TO CO2 REDUCTION AND WATER OXIDATION
Takashi Ono
DL:T 1108-2014

UNIVERSITAT ROVIRA I VIRGILI
SECOND-ROW TRANSITION-METAL COMPLEXES RELEVANT TO CO2 REDUCTION AND WATER OXIDATION
Takashi Ono
DL:T 1108-2014

Table of Contents

UNIVERSITAT ROVIRA I VIRGILI
SECOND-ROW TRANSITION-METAL COMPLEXES RELEVANT TO CO2 REDUCTION AND WATER OXIDATION
Takashi Ono
DL:T 1108-2014

UNIVERSITAT ROVIRA I VIRGILI
SECOND-ROW TRANSITION-METAL COMPLEXES RELEVANT TO CO2 REDUCTION AND WATER OXIDATION
Takashi Ono
DL:T 1108-2014

UNIVERSITAT ROVIRA I VIRGILI
SECOND-ROW TRANSITION-METAL COMPLEXES RELEVANT TO CO2 REDUCTION AND WATER OXIDATION
Takashi Ono
DL:T 1108-2014

Glossary of terms and abbreviations

1D	Monodimensional
2D	Bidimensional
AcO^-	Acetate
bid^-	(1*Z*,3*Z*)-1,3-bis(pyridin-2-ylimino)isoindolin-2-ide
bpp^-	3,5-bis(2-pyridyl)pyrazolate
Bpy	2,2'-bipyridine
br	Broad
BzOH	Benzyl alcohol
COSY	Correlation spectroscopy
CV	Cyclic voltammetry
D	Doublet
δ	Chemical shift
DCM	Dichloromethane
DFT	Density functional theory
DMF	N,N-Dimethylformamide
dmso	Dimethyl sulfoxide
dpb^-	2,6-di(pyridin-2-yl)benzen-1-ide
DPV	Differential pulse voltammetry
E	Potential
E^0	Standard potential
$E_{1/2}$	Half wave potential
$E_{p,a}$	Anodic peak potential
$E_{p,c}$	Cathodic peak potential
ESI-MS	Electrospray ionization mass spectrometry
ET	Electron transfer
g	gram
GC	Glassy carbon
HOTf	Trifluoromethanesulfonic acid or triflic acid

Hz	Heltz
ITO	Indium tin oxide
J	Coupling constant
J	Current density
L	Ligand, litre
λ	Wavelength
M	Molar, Metal
m	Multiplet
μ	Ionic force
μA	Microampere
m/z	Mass-to-charge ratio
mg	miligram
mL	Mililitre
μL	Microlitre
MLCT	Metal to ligand charge transfer
mm	Milimeter
mmol	Milimol
MS	Mass spectrometry
NADPH	Nicotinamide adenine dinucleotide phosphate
n-Bu_4NPF_6	Tetra(*N*-butyl)ammonium hexafluorophosphate
NHE	Normal hydrogen electrode
NMR	Nuclear magnetic resonance
NOESY	Nuclear Overhauser spectroscopy
OEC	Oxygen evolving center
Ortep	Oak Ridge thermal ellipsoid plot
OTf^-	OSO_2CF_3
PCET	Proton coupled electron transfer
Ph	Phenyl
POM	Polyoxometalate
ppm	Parts per millon

PSI	Photosystem I
PSII	Photosystem II
PT	Proton transfer
Py	Pyridine
Q	Quartet
Rds	Rate determining step
RT	Room temperature
S	Singlet, second
$scCO_2$	Super critical carbon dioxide
sh	Shoulder
SSCE	Sodium saturated Calomel electrode
SPS	Solvent purification system
SQWV	Square wave voltammetry
T	Triplet
$TBAPF_6$	Tetra(*N*-butyl)ammonium hexafluorophosphate
TFE	2,2,2-Trifluoroethanol
TOF	Turnover frequency
TOF_i	Initial turnover frequency
TON	Turnover number
Trpy	2,2':6',2''-terpyridine
UV-vis	Ultraviolet-visible spectroscopy
V	Volt
WOC	Water oxidation catalyst

UNIVERSITAT ROVIRA I VIRGILI
SECOND-ROW TRANSITION-METAL COMPLEXES RELEVANT TO CO2 REDUCTION AND WATER OXIDATION
Takashi Ono
DL:T 1108-2014

UNIVERSITAT ROVIRA I VIRGILI
SECOND-ROW TRANSITION-METAL COMPLEXES RELEVANT TO CO2 REDUCTION AND WATER OXIDATION
Takashi Ono
DL:T 1108-2014

Electronic Supplementary Material

- cif files for the crystal structure data presented in this thesis.
- pdf files of additional Supporting Information for Chapter III-1, III-2, IV-1, and VI.

UNIVERSITAT ROVIRA I VIRGILI
SECOND-ROW TRANSITION-METAL COMPLEXES RELEVANT TO CO2 REDUCTION AND WATER OXIDATION
Takashi Ono
DL:T 1108-2014

UNIVERSITAT ROVIRA I VIRGILI
SECOND-ROW TRANSITION-METAL COMPLEXES RELEVANT TO CO2 REDUCTION AND WATER OXIDATION
Takashi Ono
DL:T 1108-2014

General Introduction

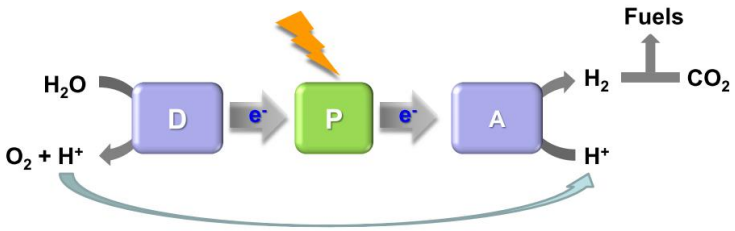

Table of Contents

UNIVERSITAT ROVIRA I VIRGILI
SECOND-ROW TRANSITION-METAL COMPLEXES RELEVANT TO CO2 REDUCTION AND WATER OXIDATION
Takashi Ono
DL:T 1108-2014

I.1. Energy demand and climate change

Energy demand and its consumption have been rising with population and economic growths. It has been reported that world energy consumption increased from 354 British thermal units (Btu) in 1990 to 524 quadrillion Btu in 2010 and is estimated to be 820 quadrillion Btu in 2040[1]. As can be seen in Figure 1, about 80% of energy use is covered by fossil fuels, such as coal, oils and natural gas, in 2011.[2] And this trend is predicted to continue through 2040 (Figure 2). However, the fossil fuels are limited resources and these carbon-based fuels emit CO_2, which has been considered as one of the greenhouse gases (GHGs), causing serious global climate change, such as an increase of global surface temperature, glacier retreat, rise in sea level, and ocean acidification. According to 4th report of Intergovernmental Panel on Climate Change (IPCC),[3] before industry revolution, atmospheric concentration of CO_2 remained at less than 300 ppm, but it reached 379 ppm in 2005 (Figure3) and it is predicted to rise to higher level.

In order to avoid the serious scenario, the increased attention has been paid for alternative energy resources, such as renewable and nuclear energies, that contribute to low-carbon emission. Considering the radiation hazard potentially caused by nuclear accident, the utilization of renewable energy sources such as solar, hydro, wind,

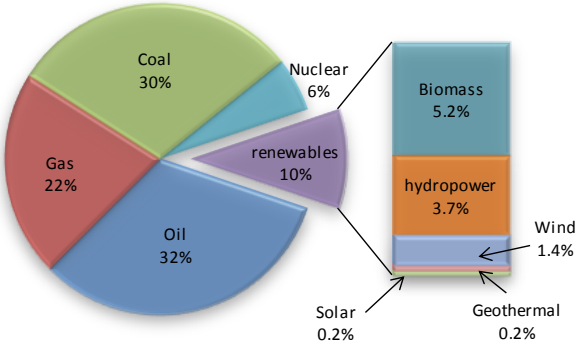

Figure 1. Primary energy consumption by fuel types in 2011.

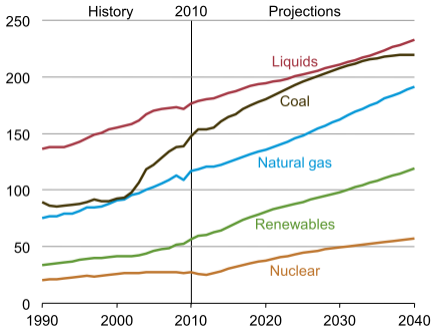

Figure 2. World energy consumption by fuel type, 1990-2040 (unit:quadrillion Btu).

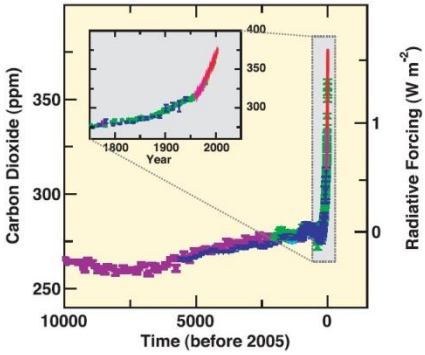

Figure 3. Atmospheric concentrations of carbon dioxide over the last 10000 years and since 1750 (inset). Figure from IPCC 4th report.

biomass and geothermal, has been desired for the alternatives to the human energy demand, even though it still accounts for only 10% in 2011 (Figure 1). Since solar energy that reached to earth in only one day could fulfil the yearly human energy consumption,[4] its efficient utilization is a desired approach for the future energy demand.

Converting solar energy into chemical energy, so-called solar fuels, is highly desirable process since this possesses advantages in that they can be stored and transported, unlike the photovoltaic system which directly converts solar energy into electricity. A potential solution to this challenging task is to mimic the system of nature known as photosynthesis, responsible for the conversion of solar energy into the chemical energy as the form of carbohydrates.

UNIVERSITAT ROVIRA I VIRGILI
SECOND-ROW TRANSITION-METAL COMPLEXES RELEVANT TO CO2 REDUCTION AND WATER OXIDATION
Takashi Ono
DL:T 1108-2014

1.2. Photosynthesis

1.2.1. Natural Photosynthesis

In nature, organisms such as higher plants, green algae and cyanobacteria convert, using solar energy efficiently, CO_2 into carbohydrates as an energy-rich compound along with oxidation of water to molecular oxygen (eqn. 1).[5]

$$6CO_2 + 6H_2O + h\nu \longrightarrow 6/n(CH_2O)_n + 6O_2 \qquad (1)$$

This process, carried out in chloroplast in those orgasms, is divided into two parts. 1) One is called as the *light-dependent reactions*, where oxidation of water to molecular oxygen takes place by solar energy, which creates energy-rich ATP and NADPH necessary for driving the reduction of thermodynamically stable CO_2 molecule (eqn.2). 2) The other is called as *light-independent reactions* or *Calvin cycle*, where carbohydrates are produced from reduction of CO_2 using ATP and NADPH (eqn. 3).

Light dependent reaction

$$2H_2O + 2NADP^+ + 3ADP + 3Pi + h\nu \longrightarrow 2NADPH + 2H^+ + 3ATP + O_2 \qquad (2)$$

Light independent reaction (Calvin cycle)

$$CO_2 + 2NADPH + 3ATP + 2H^+ \longrightarrow 1/n(CH_2O)_n + 2NADP^+ + 3ADP + 3Pi + H_2O \qquad (3)$$

I.2.1.1. Light-dependent reaction

Light dependent reactions take place on the thylacoid membranes, where four multisubunit protein complexes work together; 1) Photosystem II (PSII), 2) Cytochrome b_6f (Cyt b_6f), 3) Photosystem I (PSI), and 4) ATP synthase (Figure 4). The key features in the process of light-dependent reaction are as follows;

1) Light harvesting and energy transfer
2) Successive charge separation and stabilization *via* electron transport chains
3) Accumulation of oxidizing and reducing equivalents

In PSII, solar energy is efficiently used to excite chlorophyll P680 to P680* after absorption by antenna pigments (chlorophyll, carotenoid, and phycobillin) located on

UNIVERSITAT ROVIRA I VIRGILI
SECOND-ROW TRANSITION-METAL COMPLEXES RELEVANT TO CO2 REDUCTION AND WATER OXIDATION
Takashi Ono
DL:T 1108-2014

thylakoid membranes. P680* induces an electron transfer to primary electron acceptor, pheophytin (pheo), generating charge separated radical ions $P680^{\cdot+}pheo^{\cdot-}$. $P680^{\cdot+}$ oxidizes tyrosine (Yz) to tyrosine radical ($Yz^{\cdot}$), which then used for the accumulation of four oxidative equivalents in Mn_4CaO_5 cluster, so called oxygen-evolving complex (OEC), triggering the oxidation of water to oxygen and proton. On the other hand, an electron is stabilized, by coupled with a proton from stroma, in the form of Q_BH_2 (plastquinol) through the electron transport chain ($pheo^{\cdot-}$, primary protein-bound plastquinone (Q_A), and secondary plastquinone (Q_B)). The formed Q_BH_2 further transfer its electron to cytochrome b_6f complex (Cyt b_6f) with a concomitant release of proton in lumen, which, combined with protons released from water oxidation, results in proton gradient across the thylacoid membranes. This proton gradient drives the synthesis of ATP by ATP synthase. At a moment, the electron is transferred from reduced Cyt b_6f to plastocyanine (PC) and enters to PSI for reducing photooxidized $P700^+$. The electron from photoexcited P700* goes to iron-sulfur cluster ferredoxin (Fd) through a series of membrane-bound, iron-sulfur centres, FeS-X, FeS-B and FeS-A. And finally $NADP^+$ is reduced to NADPH by Fd· $NADP^+$ reductase (FNR).

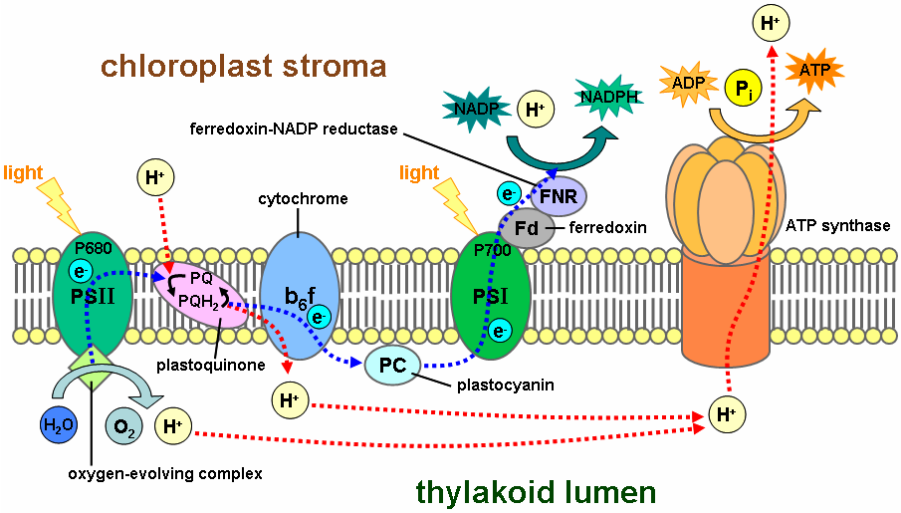

Figure 4. Simplified illustration of the oxygenic photosynthesis systems of green plants, algeas and cyanobacterias.

Oxygen evolving complex (OEC)

Recently, Umena and Kamiya *et al*. obtained an X-ray structure of PSII at an atomic resolution of 1.9 Å, which revealed the reaction centre as distorted chair-like Mn_4CaO_5 cluster with four water molecules (W1-4, in Figure 5); two to Mn4 and two to Ca.[6] In addition, protein environment around Mn_4CaO_5 cluster is believed to control reaction coordinates during water oxidation reaction as well as the paths for generated proton, oxygen and incoming water.[6-7]

As hypothesized by Kok, it is believed that the water oxidation reaction proceed by the catalytic cycle shown in Figure. 5. There are five oxidation states of the OEC, referred to as an 'S-state' (S_i: i = 0 to 4, the lowest oxidation to the highest). Mn_4O_5Ca cluster can efficiently accumulates four oxidative equivalents by transferring electron to $P680^+$ and releasing proton (proton-coupled electron transfer), and finally S_4 state triggers the formation of oxygen. Although the key step of the O-O bond formation in the OEC is not fully understood, proposed mechanisms[8-10] can be broadly classified into: (A) nucleophilic water (or hydroxy) attack to the Mn(V)-oxo moiety in the cluster core and (B) oxo/oxyl radical coupling reaction, at S_4 state of the OEC. Recent computational and spectroscopic studies suggested that O5 (in Figure 5) might be involved in O-O bond formation through oxo/oxyl radical coupling.[9,11]

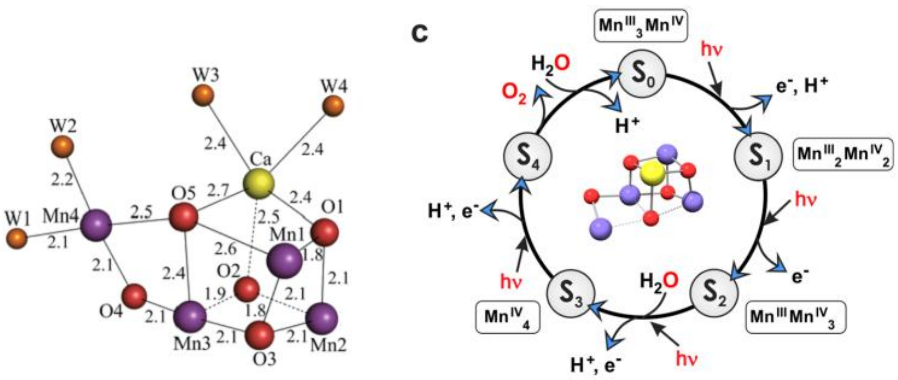

Figure 5. Left: Structure of the Mn_4O_5Ca cluster (W refers to water molecules). Right: Kok cycle

UNIVERSITAT ROVIRA I VIRGILI
SECOND-ROW TRANSITION-METAL COMPLEXES RELEVANT TO CO2 REDUCTION AND WATER OXIDATION
Takashi Ono
DL:T 1108-2014

I.2.1.2.Light independent reactions, Calvin cycle

The other half process of photosynthesis is the conversion of CO_2 into carbohydrates where chemical energy is stored in the form of chemical bond of carbohydrates, produced by energy-rich compounds, ATP and NADPH, with CO_2 (eqn. 3). Although there are six pathways for CO_2 fixation,[12] predominant pathway in higher plants is known as Calvin cycle (Figure 6). Calvin cycle is the initial pathway of photosynthetic CO_2 fixation, consisting of 13 reactions catalyzed by 11 different enzymes in stroma phase of chloroplast. The cycle is simply classified into 3 parts (Figiure 6): 1) fixation of CO_2 *via* carboxylation, 2) reduction of 3-phosphoglycerate (PGA) to glyceraldehyde 3-phosphate (G3P) and 3) regeneration of Ribulose 1,5-bisphosphate (RuBP) from G3P

1) The first part is carboxylation process, where three molecules of CO_2 are fixed into three molecules of ribulose 1,5-bisphosphate (RuBP) catalyzed by **R**ib**u**lose 1,5-**bis**phosphate **c**arboxylase/**o**xygenase (Rubisco), producing six molecules of 3-phosphoglycerate (PGA).
2) The second part is reduction process of PGA, where six molecules of PGA convert into 6 molecules of glyceraldehyde 3-phosphate (G3P) *via* phosphorylation and reduction by ATP and NADPH derived from light-dependent reaction.
3) The last part is regeneration process of RuBP. Five molecules of G3P undergo a series of reactions, regenerating three molecules of RuBP. One molecule of G3P is utilized for the production of either starch in the chloroplast or sugars in cytosol.

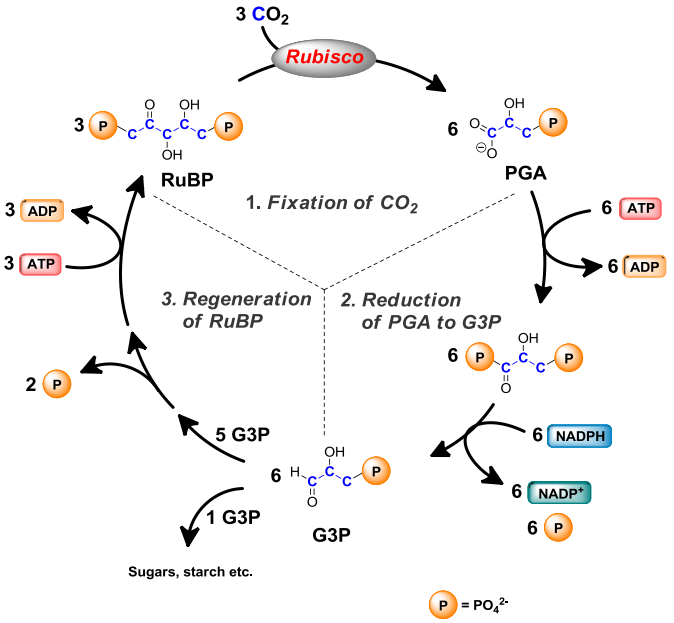

Figure 6. Schematic diagram of the Calvin cycle.

Rubisco enzyme

Key reaction of Calvin cycle is carboxylation of RuBP, which is catalyzed by Rubisco (Scheme 1). Structural mechanism of Rubisco has been mostly elucidated.[13-15] Firstly, Rubisco is activated upon carbamylation of ε-amino group on Lys201 by 'activator' CO_2, generating KCX201 which then stabilizes Mg^{II} ion together with the coordination of Asp203 and Glu204. Subsequently, substrate RuBP or its enolate form binds to Mg^{II} forming octahedral coordination with one water molecule. At this point, 'substrate' CO_2 coordinates to metal centre along with large conformation change, resulting in the isolation of active site from the solvent. After carboxylation on C_2 to form six-carbon intermediate (Scheme 1b), a series of subsequent reactions shown in Scheme 1a undergo to produce two molecules of PGA with the returning to the initial conformation.

UNIVERSITAT ROVIRA I VIRGILI
SECOND-ROW TRANSITION-METAL COMPLEXES RELEVANT TO CO2 REDUCTION AND WATER OXIDATION
Takashi Ono
DL:T 1108-2014

Scheme 1. a) Sequence of reactions catalyzed by Rubisco; enolization assisted by proton abstraction from C_3, carboxylation, hydration, C_2-C_3 bond cleavage and stereospecific protonation on C_2. b) proposed mechanism of carboxylation by Rubisco leading to six-carbon intermediate

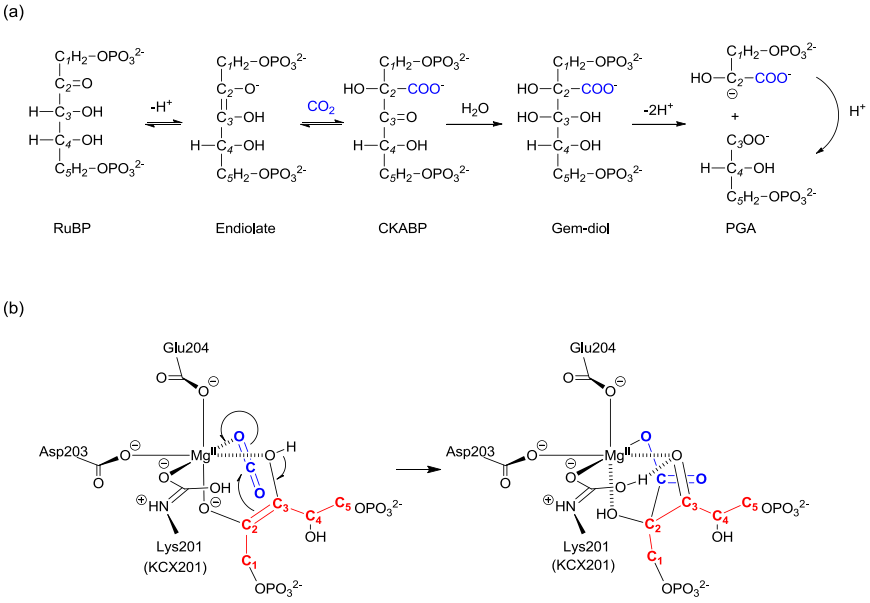

I.2.2. Artificial Photosynthesis

As described above, photosynthetic process consists of the highly complicated multiple processes. However, we can see that the essentials of this process are electron transfer induced by light, concomitant formation of the oxidative and reductive equivalents, and both oxidation and reduction reactions. Thus, in order to mimic photosynthesis artificially, it needs to construct a photoelectrochemical system comprised of a photosensitizer P which absorbs light, and an electron donor D which is capable of oxidizing water and provides electron to P, and an electron acceptor A which produces solar fuels by reducing proton and/or CO_2 (Figure 7). Unlike in natural system, solar fuels are not necessarily to be carbohydrates, but simpler and useful reduction products, such as hydrogen from proton or CO, HCOOH, CH_3OH and CH_4 from CO_2 (Figure 7).

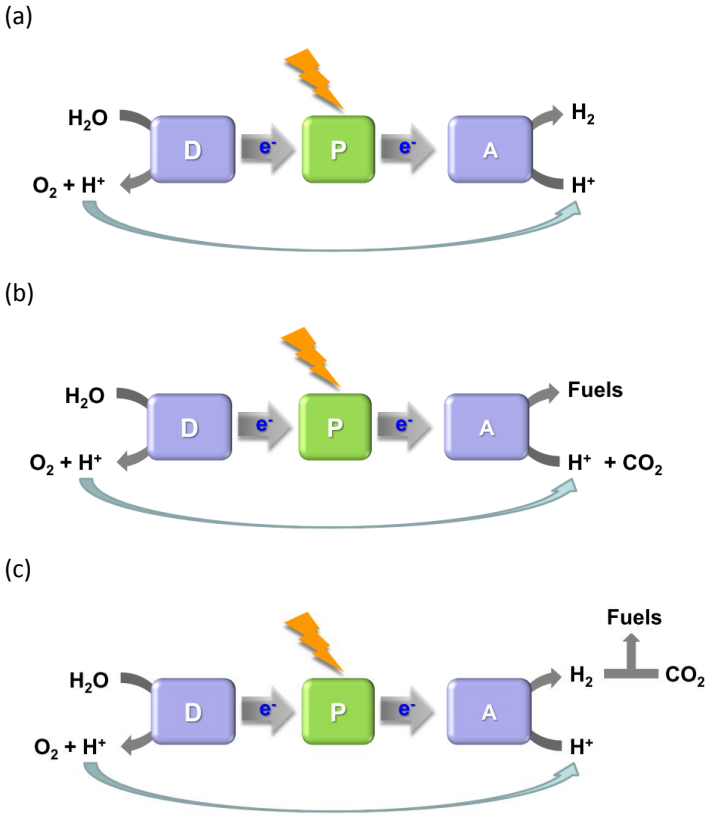

Figure 7. Schematic representation of artificial photosynthesis.

Photosensitizer

The $[Ru(bpy)^3]^{2+}$-type of complexes are most commonly used photosensitizer because they have been studied for several decades as a result of their strong ^{3}MLCT absorption, long-lived excited state lifetimes, high chemical and thermal stability, and easy functionalization. As well, the redox properties of $[Ru(bpy)_3]^{2+}$ are fulfilled to drive oxidation of water to O_2 thermodynamically at pH 7. ($E_{1/2}$ = 1.26 vs. NHE at pH 7.2)

UNIVERSITAT ROVIRA I VIRGILI
SECOND-ROW TRANSITION-METAL COMPLEXES RELEVANT TO CO2 REDUCTION AND WATER OXIDATION
Takashi Ono
DL:T 1108-2014

1.3 Water Oxidation

Four electron oxidation of water to O_2 is a thermodynamically demanding reaction (0.94 V vs. SSCE at pH 1; 0.58 V at pH 7, Table 1), which means that it requires strong oxidant to make this reaction thermodynamically favourable. However, since this process includes high molecular complexity such that four O-H bonds from two water molecules have to be broken together with the formation of O-O double bond, a catalyst which possesses multiple electron transfer property is required. As we have seen above, in order to achieve multiple electron transfer reactions, Mn_4CaO_5 cluster applies proton-coupled electron transfer (PCET) processes since this process offers a facile way to accumulate the oxidative equivalents without having high-energy intermediates and electrostatic charge build-up during the reactions.

Table 1. Standard potentials for water oxidation at pH 1 and pH 7.

Redox Process	$E°$/V (vs. NHE)	
	pH 1	pH 7
$\cdot OH + 1H^+ + 1e^- \rightarrow H_2O$	2.74	2.39
$HO\text{-}OH + 2H^+ + 2e^- \rightarrow 2H_2O$	1.72	1.37
$HO\text{-}O\cdot + 3H^+ + 3e^- \rightarrow 2H_2O$	1.61	1.26
$O{=}O + 4H^+ + 4e^- \rightarrow 2H_2O$	1.18	0.81

1.3.1. Proton-Coupled Electron Transfer (PCET)

Polypyridyl ruthenium-aqua/oxo (Ru-OH_2/Ru=O) system is considered as one of the important system for PCET reactions.[16-17] The example complex for PCET, $[Ru^{II}(trpy)(bpy)(OH_2)]^{2+}$ studied by Meyer *et al.*[18] is shown in Scheme 2 by comparing with non-aqua complex *cis*-$[Ru^{II}(bpy)_2Cl_2]$.[19] The difference ($\Delta E_{1/2}$) between two redox potentials of Ru(IV/III) and Ru(III/II) couples in *cis*-$[Ru^{II}(bpy)_2Cl_2]$ is 1.7 V due to increase in charge and oxidation state, while $\Delta E_{1/2}$ for Ru(IV/III) and Ru(III/II) in $[Ru^{II}(trpy)(bpy)(OH_2)]^{2+}$ is only 0.11 V, caused by sequential proton losses and electronic stabilization of the higher oxidation state by σ-π donation of the oxo moiety (Figure 8).

UNIVERSITAT ROVIRA I VIRGILI
SECOND-ROW TRANSITION-METAL COMPLEXES RELEVANT TO CO2 REDUCTION AND WATER OXIDATION
Takashi Ono
DL:T 1108-2014

Scheme 2. Latimer diagram of ruthenium polypyridyl complexes (a) without and (b) with a coordinated water molecule.

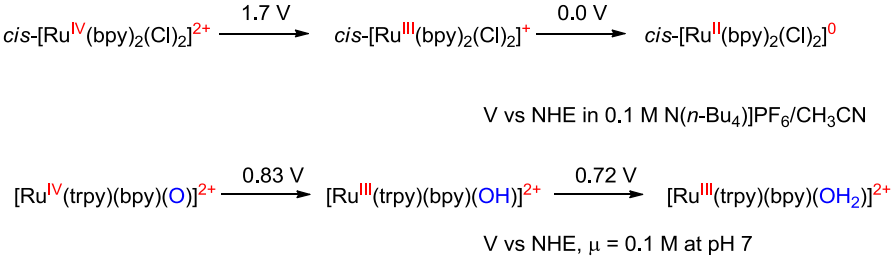

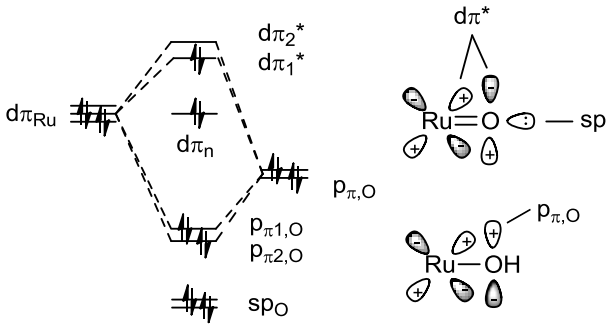

Figure 8. Ru ^{IV}=O schematic energy orbital diagram.

1.3.2. Mechanism of *O-O bond formation*

Two mechanisms have been established for the key O-O bond formation step with molecular catalysts; (a) water nucleophilic attack (WNA),[20-21] and (b) interaction of two M-O units (I2M).[22-24] For the former, the HOMO of water molecule interacts with the dπ* character of the LUMO of the metal-oxo moiety, resulting in the formation of O-O single bond with the concomitant cleavage of an M-O π bond leading to the formal two-electron reduction of the metal. (Figure 9a). Additionally, the WNA pathway requires a metal-oxo fragment that has enough electrophilicity to undergo a nucleophilic attack by water molecule to form the O-O bond. For the latter, two metal oxo units couple to each other, forming a peroxo intermediate (Figure 9b). This pathway involves the coupling of two metal–oxo units bearing radical character.

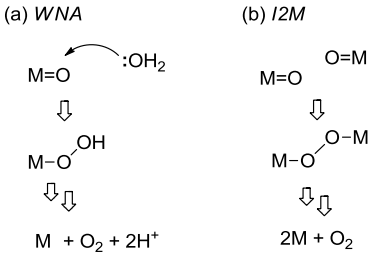

Figure 9. Two mechanism for the O-O bond formation.

1.3.3. Water Oxidation Catalysts (WOCs)

Water oxidation catalysis has been recognized as a bottleneck for the development of the artificial photosynthesis. Thus, many efforts have focused on discovering water oxidation catalysts (WOCs). Compared to heterogeneous metal oxides, molecular catalysts have the advantage of facile modification of the structure and can be incorporated into molecular assemblies by means of adsorption or anchoring on heterogeneous surfaces. Recently, a number of WOCs have been reported based on homogeneous Ru, Mn, Ir, Co,[25-27] Fe,[28-31] and Cu[32-33] transition-metal complexes, polyoxometalate, and metal oxides. Since a number of reviews summarizes the recent advances,[23,34-36] the Ru-based WOCs with neutral and negatively charged ligands will be described.

Most of the reported Ru-based WOCs consist of neutral N-donor ligand, which generally suffers from their high oxidation potential for the formation of the catalytic active Ru(V)=O species. For instance, the onset potentials for the oxidation of water with $Ru(NNN)(NN)(OH_2)^{2+}$ (NNN = tridentate ligand, NN = bidentate ligand) type of complexes are beyond ~1.5 V vs NHE[20,37-40] which is close to the redox potentials of $(NH_4)_2Ce^{IV}(NO_3)_6$ (CAN). However, in order to establish a light driven water oxidation process for the development of artificial photosynthesis, CAN has to be replaced to commonly used photosensitizer, $[Ru(bpy)_3]^{3+}$ type of complexes. In this respect, lowering the oxidation potentials of the catalysts could be advantageous and it has been recently reported that the complexes containing negatively charged ligand such

UNIVERSITAT ROVIRA I VIRGILI
SECOND-ROW TRANSITION-METAL COMPLEXES RELEVANT TO CO2 REDUCTION AND WATER OXIDATION
Takashi Ono
DL:T 1108-2014

as carboxylate group showed significant effect on lowering the oxidation potentials of high-valent Ru species.

Ruthenium WOCs based on neutral N-donor ligand

In 1982, Meyer *et al*. reported first homogeneous dinuclear ruthenium WOC, *cis*,*cis*-$[(bpy)_2(H_2O)Ru^{III}ORu^{III}(H_2O)(bpy)_2]^{4+}$, **1** (Figure 9), known as 'the blue dimer', capable of catalyzing the oxidation of water to oxygen.[41-42] It undergoes sequential losses of proton and electron ($4e^-/4H^+$) to reach its highest oxidation states *cis*,*cis*-$[(bpy)_2(O)Ru^{V}ORu^{V}(O)(bpy)_2]^{4+}$ by chemical oxidants. Using CAN as the oxidant, this dinuclear complex showed TON 13.2[43] and TOF 4.2 x 10^{-3}.[44] Light-driven water oxidation using COOEt-substituted $[Ru(bpy')_3]^{2+}$ and $S_2O_8^{2-}$ was also achieved.

In 2004, Llobet *et al*. presented[45] a dinuclear WOC, $\{[Ru(trpy)(H_2O)]_2(\mu\text{-bpp})\}^{3+}$, **2** (Figure 9), in which both metal centres are linked by polypyridyl chelating *bpp*$^-$ (bis(2-pyridyl)-3,5-pyrazolate) ligand instead of the μ-oxo bridge in the blue dimer, providing a robust bridge that prevents a reductive cleavage (TON 18.6 using 100 equiv. of CAN). Furthermore, it has been proven that two oxo ligands oriented in a close proximity induced by rigidity of the chelating *bpp*$^-$ ligand favours intermolecular coupling (I2M).[22,46] Later on, Thummel *et al.* reported a series of dinuclear Ru complexes **3** (Figure 9) based on polypyridyl bridging ligands, showing the high TON (up to 689) toward water oxidation using 5000 equiv. of CAN as the oxidant,[47-48] although mechanistic studies have not been carried out in detail.

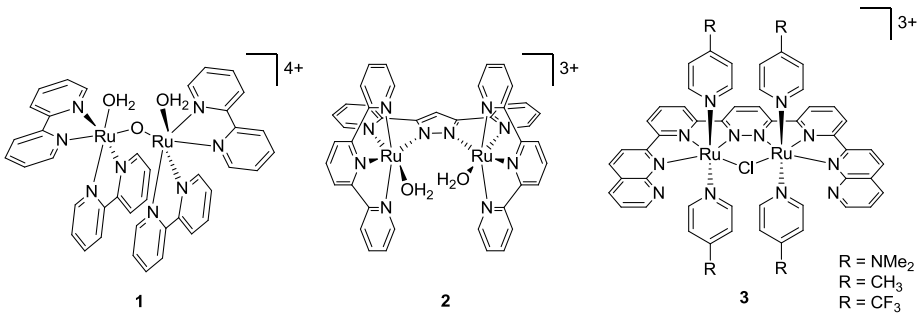

1 2 3

Figure 9. Representatives of the dinuclear Ru-based WOCs.

UNIVERSITAT ROVIRA I VIRGILI
SECOND-ROW TRANSITION-METAL COMPLEXES RELEVANT TO CO2 REDUCTION AND WATER OXIDATION
Takashi Ono
DL:T 1108-2014

Although it has been long believed that multi-metal centres are required for WOCs as that for natural system, recently it has been proven that single-site is enough for catalysing water oxidation reaction. In contrast to the dinuclear WOCs, mononuclear ones potentially have advantages in terms of easier synthesis. Therefore, a large number of mononuclear WOCs have been developed after the first discovery by Thummel *et al*. (Figure 10, **4**) Later on, Meyer *et al*. have also shown that $[Ru(trpy)(NN)(OH_2)]^{2+}$, **5** (Figure 10), where NN = *bpm* (2,2'-bipyrimidine) or *bpz* (2,2'-bipyrazine), is capable of catalytically oxidizing water and the mechanistic details have been provided,[20] presenting that the presence of two metal centres is not necessary for the design of an efficient water oxidation catalyst. These breakthroughs led a development of mononuclear ruthenium-based WOCs.

It is noteworthy to mention here that Llobet *et al*. has very recently reported that mononuclear complexes $[Ru(trpy)(5,5'\text{-}X_2\text{-}bpy)(OH_2)]^{2+}$ (X = H: **7a**$^{2+}$, or F: **7b**$^{2+}$) are slowly and irreversibly converted into dinuclear complexes $[(trpy)(5,5'\text{-}X_2\text{-}bpy)Ru^{IV}(m\text{-}O)Ru^{IV}(trpy)(O)(OH_2)]^{4+}$, **8a-b**$^{4+}$, in the presence of CAN at pH 1 (Figure 11).[49] These dinuclear complexes showed comparable TOFs with respect to mononuclear ones but dinuclear ones are much more robust than the mononuclear precursors, leading to a higher TON of 14930 (for **7a**$^{2+}$ vs 6683 for **8a**$^{4+}$) with electrochemical WOC at an applied potential of 1.6 V vs. SSCE.

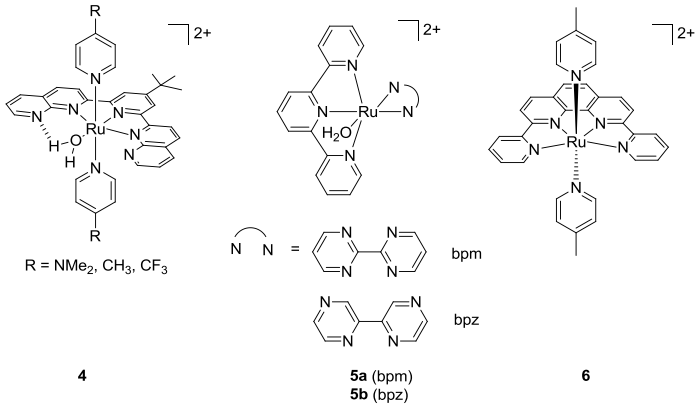

Figure 10. Mononuclear Ru-WOCs with/without aqua group.

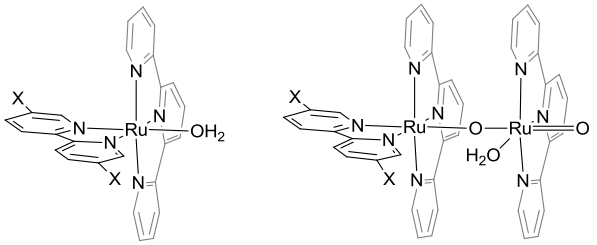

Figure 11. Dinuclear WOCs **8** from their mononuclear counterparts **7**.

By taking advantages of synthetic ease for mononuclear complexes, Thummel *et al.* have published a series of non-aqua $Ru^{II}N6$ complexes whose metal centre is coordinatively saturated with N-donor ligand.[50-51] Although there is no detailed experimental result, they have proposed a mechanism involving seven-coordinated Ru(IV)=O species which is generated as shown in Scheme 3; Two electron oxidation of $Ru^{II}N6$ leads to a 16-electron $Ru^{IV}N6$ species that is possibly coordinated by water molecule, followed by PCET processes of the Ru^{IV}-OH_2 complex to generate a high-valent Ru^{VI}=O. The nucleophilic attack of a second molecule of water leads to the formation of hydroperoxide intermediate, Ru^{IV}-OOH. An intramolecular electron transfer from peroxide to Ru^{IV} results in the generation of oxygen and regeneration of $Ru^{II}N6$. An example of a mononuclear Ru(II)N6 catalyst (consisting of one tetradentate

Scheme 3. Proposed mechanism for water oxidation catalyzed by mononuclear RuN6 complexes.

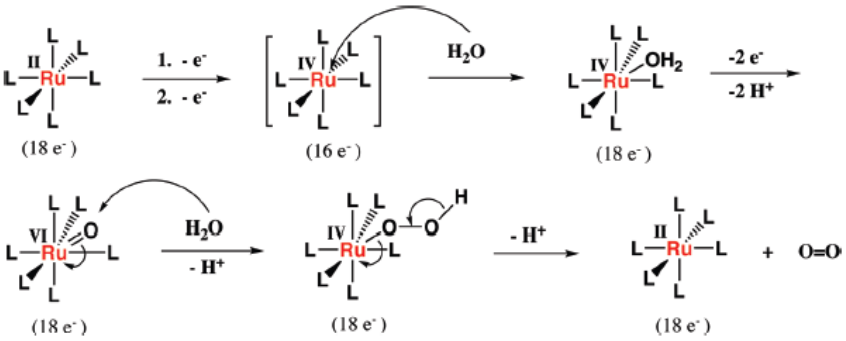

and two monodentate ligands) $[Ru(dpp)(pic)_2]^{2+}$ (*dpp* = 2,9-di(pyrid-2'-yl)-1,10-phenanthroline, *pic* = 4-picoline) **6** (Figure 10) is able to generate O_2 with TON of 416 using CAN as the oxidant.[51]

Ruthenium WOCs based on negatively charged ligand

Sun *et al*. synthesized new dinuclear complexes **9-10** containing negatively charged carboxylate groups[52-53] (Figure 12), which resemble Thummel's dinuclear complex **3**. These complexes gave TON of *ca*. 4700 and 10400, respectively, in the presence of CAN (10^5 equiv.) as the oxidant at pH 1. Interestingly, both complexes shows dramatically lowered onset potential for water oxidation at pH 7.2; for **9**, at *ca*. 1.3 V vs NHE, and for **9**, at *ca*. 1.2 V. As expected, both catalysts were able to catalyze photochemical water oxidation.[53-54] A system based on the former WOC, COOEt-modified $[Ru(bpy')_3]$ as photosensitizer and $S_2O_8^{2-}$ as sacrificial electron acceptor achieved TON of 370 and TOF of 0.26 s^{-1}. The latter showed TON of *ca*. 60 and TOF 0.1 s^{-1} even with non-substituted $[Ru(bpy)_3]^{2+}$.

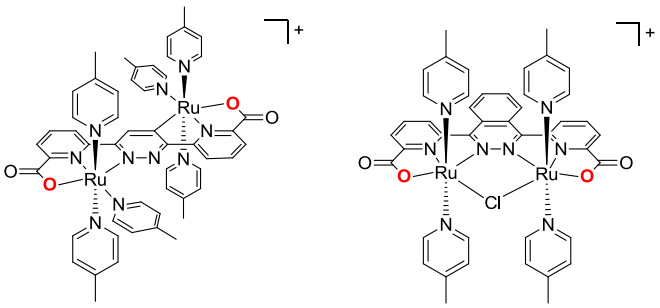

Figure 12. Sun's dinuclear catalysts based on anionic donor ligands.

With the success of the lowering potential with dinuclear complexes, Sun *et al*. and Åkermark *et al*. also developed mononuclear Ru catalysts based on the negatively charged ligands shown in Figure 13.[55-61]

UNIVERSITAT ROVIRA I VIRGILI
SECOND-ROW TRANSITION-METAL COMPLEXES RELEVANT TO CO2 REDUCTION AND WATER OXIDATION
Takashi Ono
DL:T 1108-2014

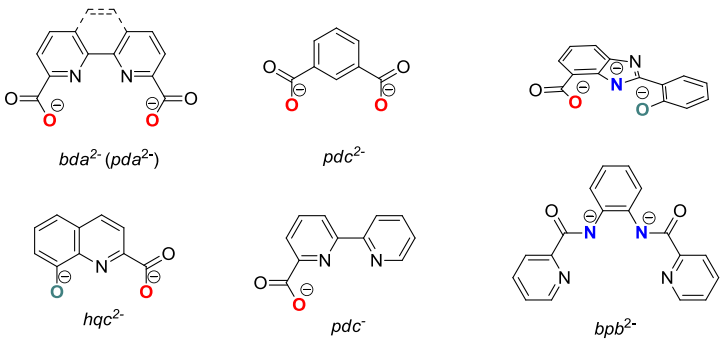

Figure 13. Negatively charged ligands used for mononuclear Ru-WOCs.

Complex Ru(bda)(pic)$_2$ (*bda*$^{2-}$ = 2,2'-bipyridine-6,6'-dicarboxylate, *pic* = 4-picoline) **11** reported by Sun *et al*. represented a breakthrough of mononuclear water oxidation catalysts.[55] Stabilization of higher oxidation state by two anionic carboxylate groups allowed them to isolate a seven coordinated species (Figure 14) which is in relation with the previously proposed seven-coordinated species by Thummel for their RuN6 complexes.[50] Since this complex shows electrocatalytic activity toward water oxidation at very low onset potential of *ca*. 1.0 V vs. NHE at pH 7.0, light-driven water oxidation was examined using $[Ru(bpy)_3]^{2+}$ as photosensitizer and $Na_2S_2O_8$ as sacrificial electron acceptor, resulting in TOF of >0.35 s^{-1}.[62]

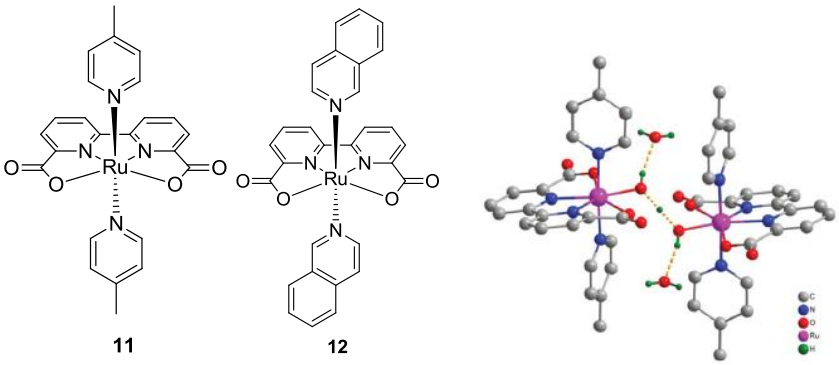

Figure 14. Left: Ru(bda)(pic)$_2$, **11**. Centre: Ru(bda)(isoq)$_2$, **12**. Right: X-ray structure of dinuclear seven-coordinate species $[Ru(bda)(pic)_2]_2(\mu\text{-}O_2H_3)\cdot 2H_2O$

Recently, it has been demonstrated that the catalytic activity of this complex is highly sensitive to the modification on both equatorial *bda*$^{2-}$ and axial monodentate ligand.[57,63-67] For instance, when axial 4-picoline ligands were replaced by isoquinoline, the highest TOF of 300 s^{-1} was obtained using CAN as the oxidant (Figure 14, **12**).[63] The proposed mechanism for the O-O bond formation is bimolecular I2M pathway in which two Ru^{V}=O (Ru^{IV}-O·) units couple to generate Ru^{IV}-O-O-Ru^{IV}. This species liberates O_2 or in the presence of excess CAN, is further oxidized to Ru^{IV}-O⁻O-Ru^{IV} that liberates O_2 (Scheme 4).[63] Accelerated catalytic performance of isoquinoline derivative was rationalized by that the stacking of isoquinoline facilitates the dimer formation.

Scheme 4. O_2 generation pathways of complex [Ru(bda)(isoq)$_2$] **12** with stoichiometric and excess amounts of Ce^{IV} at pH 1.

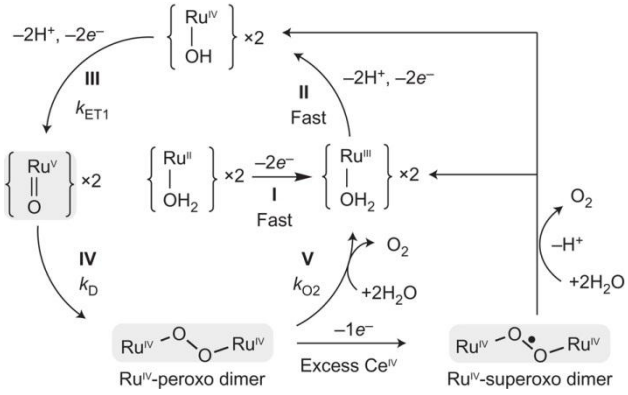

It is of interest to see the different electronic effect of carboxylate and phenolate group. For instance, the calculated redox potentials for the aqua complexes generated from complexes Ru(pdc)(pic)$_3$ (*pdc*$^{2-}$ = pyridine-2,6-dicarboxylate), **13**, and Ru(hqc)(pic)$_3$ (*hqc*$^{2-}$ = 8-oxidoquinoline-2-carboxylate), **14**, are shown in Scheme 5.[56,58] The *hqc*-based complex shows 0.15 V low potential (1.23 V for *hqc*-based complex and 1.38 V for *pdc*-based complex) in the 1e^{-} transfer process, that is the Ru^{V}=O/Ru^{IV}=O couple, at pH 7 with respect to the *pdc*-based complex owing to stronger π-donating phenolate than carboxylate. By contrast, the difference of their redox potentials (both

UNIVERSITAT ROVIRA I VIRGILI
SECOND-ROW TRANSITION-METAL COMPLEXES RELEVANT TO CO2 REDUCTION AND WATER OXIDATION
Takashi Ono
DL:T 1108-2014

0.78 V) for Ru^{IV}=O/Ru^{III}-OH couple at pH 7 diminish, because the higher electron density of *hqc*-based Ru centre restrains the release of proton which makes PCET process difficult. At pH 0, this PCET effect becomes more pronounced; for the *hqc*-based complex, Ru^{V}=O species is generated at 0.11 V higher potential than that for the *pdc*-based complex.

Scheme 5. Calculated redox potentials for the complexes based on hqc^{2-} and pdc^{2-}

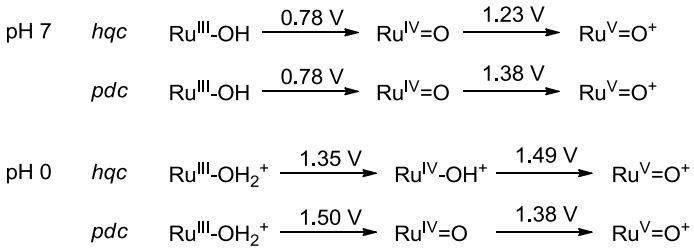

Lastly the groups of Hill and Bonchio independently reported the polyoxometalate complex $[\{Ru^{IV}_4(\mu\text{-}O)_4(\mu\text{-}OH)_2(H_2O)_4\}(\gamma\text{-}SiW_{10}O_{36})_2]^{10-}$ **15** (Figure 15).[68-69] These polyanionic nature of POM ligands and bridged oxo and hydroxo ligands are strong σ-donors responsible for the facile access to the high oxidation states required for water oxidation. This Ru-POM catalyzes the oxidation of water with up to 500 TON and a TOF of 0.125 s^{-1} in the presence of CAN.[68] When $[Ru(bpy)_3]^{2+}$ and $S_2O_8^{2-}$ were used as oxidant and sacrificial electron acceptor, TON of ~350 and TOF of ~0.08 s^{-1} were obtained.[70]

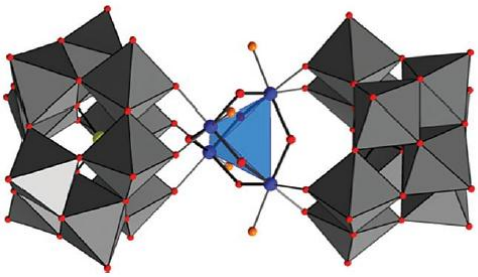

Figure 15. Structure of Ru-polyoxometalate **15**.

UNIVERSITAT ROVIRA I VIRGILI
SECOND-ROW TRANSITION-METAL COMPLEXES RELEVANT TO CO2 REDUCTION AND WATER OXIDATION
Takashi Ono
DL:T 1108-2014

I.4. CO_2 utilization

There is a growing need to mitigate CO_2 emissions because of steadily increasing anthropogenic CO_2 emissions of *ca*. 25 Gt/year.[71] Some of the strategies for the mitigation are carbon capture and storage (CCS), and carbon capture and recycling (CCR) to useful chemicals and fuels. There are several advantages for producing chemicals from CO_2 because it is non-toxic, non-flammable, cheap, and renewable feedstock. Although the industrial uses of CO_2 are still limited to some chemical processes (110 CO_2 Mt/year),[71] including the synthesis of urea salicylic acid, organic/inorganic carbonates, and polycarbonates, there are a number of investigations on the chemical transformation of CO_2 to organic chemicals, polymers, and fuels.[72-73]

Among them, the reduction of CO_2 to fuels has attracted increasing attention. Because the amount of fuels we use is much greater than that of some chemicals, an approach for recycling CO_2 as fuels could be more effective for mitigating CO_2 emissions. However, since CO_2 is a highly oxidized and thermodynamically stable molecule, a large energy input is required for the reduction of CO_2. Thus, CO_2 reduction into fuels would be feasible economically only when renewable energy is sufficiently supplied from solar energy, which can be utilized by: (1) artificial photosynthesis, (2) electrochemical reduction using photovoltaic systems, and (3) hydrogenative reduction of CO_2 using solar-produced hydrogen.

Possible products of reduction of CO_2 with its reduction potentials are summarized in Table 2. From the thermodynamic point of view, more favourable pathway is to reduce CO_2 through multiple PCET processes. As can been seen in Table 2, the more reduced the products become, the more favourable the processes become. To overcome the kinetic barriers for the CO_2 reduction, molecular catalysts are required. There are a number of developments in the area of CO_2 reduction by homogeneous transition-metal catalysts, which can be categorized into (1) hydrogenative CO_2 reduction (CO_2 hydrogenation), (2) electrocatalytic CO_2 reduction, and (3) photocatalytic CO_2 reduction.

UNIVERSITAT ROVIRA I VIRGILI
SECOND-ROW TRANSITION-METAL COMPLEXES RELEVANT TO CO2 REDUCTION AND WATER OXIDATION
Takashi Ono
DL:T 1108-2014

Table 2. CO_2 reduction potentials.

reaction			$E°$ (V vs NHE) at pH 7
$CO_2 + e^-$	→	$CO_2^{\cdot -}$	-1.90
$CO_2 + 2H^+ + 2e^-$	→	HCO_2H	-0.61
$CO_2 + 2H^+ + 2e^-$	→	$CO + H_2O$	-0.53
$CO_2 + 4H^+ + 4e^-$	→	$HCHO + H_2O$	-0.48
$CO_2 + 6H^+ + 6e^-$	→	$CH_3OH + H_2O$	-0.38
$CO_2 + 8H^+ + 8e^-$	→	$CH_4 + 2H_2O$	-0.24

I.4.1. Hydrogenative CO_2 Reduction

Transition metal catalyzed hydrogenative reduction of carbon dioxide is one of the methodologies to reduce CO_2 to other useful C1 chemicals. One of the well-documented systems for the reduction of CO_2 utilizes H_2 as a reducing agent, and most of the reported systems produce formic acid and its derivatives such as *N*,*N*-dimethylformamide and formate ester as main products. There have been a number of systems which generates higher reduced products, such as formaldehyde,[74] methanol,[75-77] and methane.[78-79] However, these systems require expensive hydride source such as hydrosilane and pinacolborane (4,4,5,5-Tetramethyl-1,3,2-dioxaborolan) and their catalytic activities are low and most of the systems require harsh reaction conditions, that is, it requires high energy cost and is economically unfavourable.

Beside the direct use of formic acid as fuels or the C1 chemical for further transformation into higher hydrocarbons, recently, particular attention has been paid for the use of formic acid as a hydrogen storage material[80-82] from the viewpoint of safety handling. Formic acid is liquid (density: 1.220 g/mL) and contains 4.4 wt% and 53 g/L of hydrogen at ambient conditions in contrast to 22.9 g/L at 350 bar for compressed H_2 at room temperature.[80,83] Furthermore, a number of the reports on the decomposition of formic acid into gaseous products H_2/CO_2 catalyzed by homogeneous transition metal catalysts has appeared.[84-88] Combined with the catalytic

UNIVERSITAT ROVIRA I VIRGILI
SECOND-ROW TRANSITION-METAL COMPLEXES RELEVANT TO CO2 REDUCTION AND WATER OXIDATION
Takashi Ono
DL:T 1108-2014

decomposition reaction of formic acid, hydrogenative CO_2 reduction can be considered as a promising method for the storage-transportation of H_2 (Figure 16).

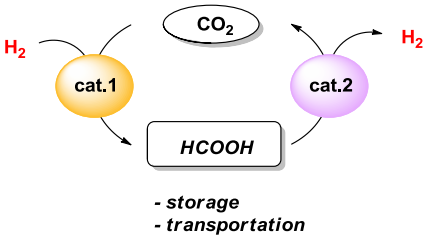

Figure 16. Schematic representation for the hydrogen storage methodology.

The hydrogenative CO_2 reduction into formic acid based on molecular catalysts has been carried out in organic solvents, water, supercritical CO_2 ($scCO_2$),[89-92] and even in ionic liquid.[93-94] The formation of formic acid from CO_2 and H_2 in gas phase is thermodynamically unfavourable ($\Delta G_{298}°$ = +32.9 kJ/mol) (eqn.4). This is in contrast to that for the reaction in water, which has standard Gibbs free energy of -4 kJ/mol (eqn.5). Furthermore, addition of a base (inorganic, organic bases) favours this reaction by stabilizing it as ionic form (eqn.6) as in many reported systems different kind of bases had been used for achieving the catalytic reaction. In organic media, amines are preferred, whereas in water, KOH or carbonates are used. In addition, it has been reported that base plays a role in the H_2 activation step as described below.

		$\Delta G_{298}°$ [kJ/mol]	$\Delta H°$ [kJ/mol]	$\Delta S°$ [J/mol·K]
$CO_2(g) + H_2(g) \rightarrow HCOOH(l)$	(4)	32.9	-31.2	-215
$CO_2(aq) + H_2(aq) \rightarrow HCO_2H(aq)$	(5)	-4	—	—
$CO_2(aq) + H_2(aq) + NH_3(aq) \rightarrow HCO_2^-(aq) + NH_4^+(aq)$	(6)	-9.5	-84.3	-250

I.4.1.1. Catalytic Mechanism

To understand the mechanism for the hydrogenative CO_2 reduction and to design efficient catalyst, the mechanisms have been investigated experimentally and

theoretically. Catalytic mechanism for hydrogenative CO_2 reduction generally consists of following three different steps (Figure 17): (a) insertion of CO_2 into metal-hydrido (M-H) bond to form metal-formato (M-OCHO) species, (b) coordination of H_2 together with release of the product, and (c) regeneration of metal-hydrido species. The key step in the catalytic cycle is step (c), the formation of metal-hydrido species through heterolytic cleavage of H-H bond. The heterolytic cleavage of H_2 is assisted by an external base or internal ancillary ligand (:B).

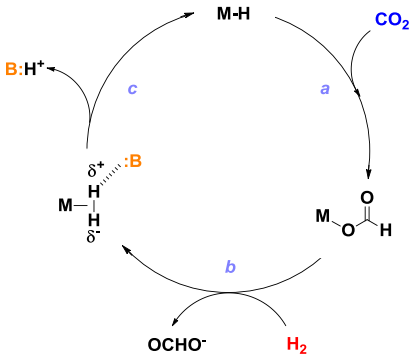

Figure 17. General catalytic mechanism for the hydrogenative CO_2 reduction. :B = base. Step a: CO_2 insertion into M-H bond, step b: H_2 coordination with release of the formate, step c: regeneration of M-H species through heterolytic cleavage of H_2 assisted by a base.

H_2 activation

Metal hydrides are an important class of complexes involved in a number of catalytic hydrogenation processes.[95] There are mainly two ways that transition metal catalysts activate H_2 molecule to generate metal-hydrido species (Scheme 6).[96-97] One is oxidative addition of H_2 along with an increase of oxidation state (+2) of metal centre, and the other is heterolytic cleavage in which oxidation state of metal centre unchanged. The pathway depends on the degree of back donation on metal centre.[96] Nucleophilic metal centre favours oxidative addition due to back donation from metal $d\pi$ orbital into σ^* orbital of H_2 molecule, whereas electrophilic metal centre favours heterolytic cleavage because of increased acidity of H_2 molecule upon coordination to

metal centre which facilitates deprotonation by an external base. Many reported Ru(II)-catalyzed hydrogenation proceeds through heterolytic activation pathway .In addition, it has been developed that H_2 activation could be assisted by an internal base on an ancillary ligand as can be found in biological system. For example, based on the structure of Fe-Fe hydrogenases,[98] H_2 activation has been proposed to occur via addition of H_2 to a metal centre followed by heterolytic cleavage of the coordinated H_2 by pendant amine.

Scheme 6. Two mechanisms for H_2 activation by metal centre

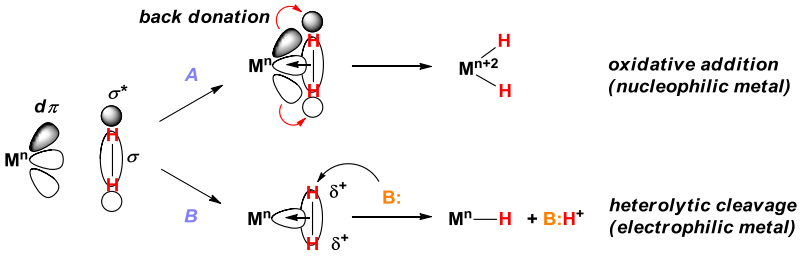

CO_2 insertion

From a mechanistic point of view, the insertion of CO_2 into the M-H bond can proceed in two routes (Scheme 7): (A) the pre-coordination of CO_2 to the metal centre followed by hydride migration to CO_2 or (B) the direct addition of hydride to CO_2 and the subsequent rotation of the formato ligand. Although route (A) is commonly accepted, it has been proposed theoretically that route (B) is also possible, depending on the catalyst and its coordination environment.

Scheme 7. Two pathways for CO_2 insertion into the metal-hydrido bond

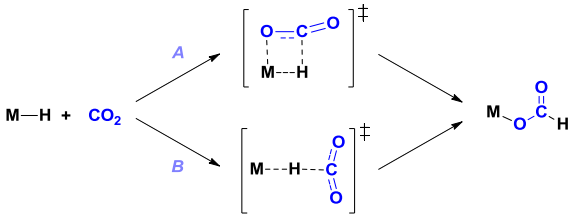

UNIVERSITAT ROVIRA I VIRGILI
SECOND-ROW TRANSITION-METAL COMPLEXES RELEVANT TO CO2 REDUCTION AND WATER OXIDATION
Takashi Ono
DL:T 1108-2014

I.4.1.2. Homogenous Catalysts for Hydrogenative CO_2 Reduction to Formic Acid

Some of the reported catalysts are listed in Table 3.

First reported homogeneous catalysts for hydrogenative CO_2 reduction were pioneered by Inoue *et al.* in 1976, in which the groups 8-10 transition-metal with phosphine ligands were used as catalyst precursors.[99] Since then, a number of catalysts based on the combination of groups 8-10 metal such as Ru, [89-92,100-107] Rh,[101-102,108-111] Ir,[101,112] and Pd,[101] and various phosphines have been reported to be effective for the reaction. At the same time, the catalytic systems in water as the solvent have been also investigated especially by groups of Joó and Laurenczy[101-105,112] using water soluble metal-phosphine complexes. In the last decade, complexes containing σ-donating pincer ligands[113-114] or nitrogen donor ligands[115-122] have attracted an attention due to their high catalytic activities. $Ir(PN^{Py}P)H_3$ ($PN^{Py}P$ = 2,6-C_5H_3N ($CH_2P^iPr_2$)$_2$), **16**, is the best homogeneous catalyst in terms of TON to date. In addition, there are also increased attentions for the use of catalysts based on non-precious metal, such as Co,[123-124] Fe.[125-127]

Table 3. A comparison of catalytic systems for the hydrogenative reduction of CO_2 or carbonate to formic acid.

Complex	solvent	additives	P_{H2}/P_{CO2} (bar)	T (°C)	t (h)	TON	TOF (h^{-1})	*ref*
Rh(dcpb)(hfacac)	DMSO	NEt_3	20/20	25	-	-	1335	111
$RhCl(tppts)_3$	H_2O	$NHMe_2$	20/20	RT	12	3439	287	109
$RhCl(tppts)_3$	H_2O	$NHMe_2$	20/20	81	0.5	-	7260	109
$RuH_2(PMe_3)_4$	$scCO_2$	NEt_3, H_2O	85/120	50	1	1400	1400	89
$RuCl_2(PMe_3)_4$	$scCO_2$	NEt_3, H_2O	80/140	50	47	7200	153	90
$RuCl(OAc)(PMe_3)_4$	$scCO_2$	NEt_3, C_6F_5OH	70/120	50	0.3	32000	95000	91
$TpRuH(PPh_3)(CH_3CN)$	THF/H_2O	NEt_3	25/25	100	16	720	45	128
$TpRuH(PPh_3)(CH_3CN)$	TFE	NEt_3	25/25	100	16	1815	113	129
$[C_6Me_6Ru(bpy)Cl](Cl)$	H_2O	KOH	20/20	80	20	68	3.4	118
$[C_6Me_6Ru(4DHBP)Cl](Cl)$	H_2O	KOH	20/20	80	20	4400	220	118

UNIVERSITAT ROVIRA I VIRGILI
SECOND-ROW TRANSITION-METAL COMPLEXES RELEVANT TO CO2 REDUCTION AND WATER OXIDATION
Takashi Ono
DL:T 1108-2014

Table 3. (continued)

Complex	solvent	additives	P_{H2}/P_{CO2} (bar)	T (°C)	t (h)	TON	TOF (h^{-1})	*ref*
[Cp*Ir(bpy)Cl](Cl)	H_2O	KOH	20/20	80	20	105	(6)	118
[Cp*Ir(4DHBP)Cl](Cl)	H_2O	KOH	20/20	80	20	6770	(7960)	118
[Cp*Ir(4DHBP)(OH_2)](SO_4)	H_2O	KOH	0.5/0.5	25	24	92	(7)	122
[Cp*Ir(6DHBP)(OH_2)](SO_4)	H_2O	KOH	0.5/0.5	25	33	330	(27)	122
$Ir(PN^{py}P)H_3$	H_2O/THF	KOH	40/40	120	48	$3.5x10^6$	73000	113
$Ir(PN^{H}P)H_3$	H_2O	KOH	28/28	185	24	$3.5x10^5$	14500	114
$Fe(BF_4)_2{\cdot}6H_2O/PP_3$'	MeOH	$NaHCO_3$	60/-	100	20	7546	377	126
$Co(BF_4)_2{\cdot}6H_2O/PP_3$	MeOH	$NaHCO_3$	60/-	120	20	3877	194	123
$CoH(dmpe)_2$	THF-d_8	Vkd	0.5/0.5	21	-	2000	3400	124

Parenceces shows initial TOFs. dcpb: 1,4-bis(dicyclohexylphosphino)butane, tppts: tris(3-sulfonatophenyl)phosphine, Tp: hydrotris(pyrazolyl)borate, XDHBP: X,X'-dihydroxy-2,2'-bipyridine, $PN^{py}P$: 2,6-bis((diisopropylphosphino)methyl)pyridine, $PN^{H}P$: bis(2-(diisopropylphosphino)ethyl)amine, PP3: tris(2-(diphenylphosphino)ethyl)phosphine, PP3': tris(2-(diarylphosphino)aryl)phosphine, dmpe: TFE: 2,2,2-trifluoroethanol, Vkd: Verkade's base, 2,8,9-triisopropyl-2,5,8,9-tetraaza-1-phosphabicyclo[3,3,3]undecane.

Phosphine ligand-based catalysts

Among the phosphine based catalysts, a series of rhodium(I)-diphosphine precatalysts, Rh(diphosphine)(hfacac) (diphosphine: $PR_2(CH_2)_nPR_2$, n = 2-6, R = Me, iPr, Cy, and Ph, hfacac = hexafluoroacetylacetonate), **17**, reported by Leitner *et al*. were intensively investigated for the catalytic hydrogenative CO_2 reduction in organic solvent (DMSO).[110-111] For example, Rh(dcpb)(hfacac) (dcpb: R =Cy, n = 4), **17a**, precatalyst showed turnover frequencies (TOF) of 1335 h^{-1} under relatively mild reaction conditions (at 25 °C under 40 bar of 1/1 mixture of H_2 and CO_2). From both experimental and theoretical results (Figure 18),[110] they have suggested that the rate-determining step is formic acid elimination step, and heterolytic H_2 activation is associated with the oxygen atom of bound formate (Path A) rather than oxidative addition of H_2 followed by reductive coupling between formato and hydrido ligands

(Path B). It was suggested that amine could be involved as a base in the step of H-H bond cleavage.

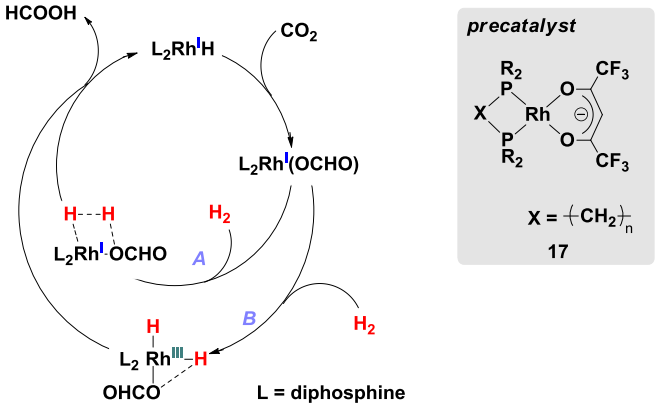

Figure 18. Proposed catalytic mechanism for the hydrogenative CO_2 reduction based on Rh(I)-diphosphine catalysts. Path A: H_2 coordination followed by heterolytic cleavage of H_2 between Rh-formato and H-H bonds. Path B: oxidative addition of H_2 followed by reductive coupling to HCOOH.

Ruthenium(II)-phosphine complexes, *cis*-$Ru(X)_2(PMe_3)_4$ (X = H, or Cl), **18**, developed by Noyori, Ikariya, Jessop *et al*. is of particular importance because of high TON 7200 for the hydrogenative CO_2 reduction at that time.[89-90] The reaction was carried out in $scCO_2$. They also demonstrated that the addition of small amount of water significantly enhanced the reaction rate. Later, the mechanism was investigated theoretically by Sakaki and Musashi using *cis*-$RuH_2(PH_3)_4$ as a model system.[130] It was found that the rate-determining step was insertion of CO_2 into Ru-H bond. However, this was inconsistent with the experimental observation where the reaction rate depended on the H_2 pressure, suggesting incorporation of H_2 in the rate-determining step. In 2006, Sakaki *et al.* eliminated this discrepancy by considering the water molecule effect which decreased the activation barrier in the step of CO_2 insertion through the intermediate shown in Figure 19.[131] In addition, the rate-determining step now became the regeneration of Ru-H species through σ-bond metathesis between Ru-OCHO and H-H moieties (Figure 18). It is also noteworthy that in the presence of

UNIVERSITAT ROVIRA I VIRGILI
SECOND-ROW TRANSITION-METAL COMPLEXES RELEVANT TO CO2 REDUCTION AND WATER OXIDATION
Takashi Ono
DL:T 1108-2014

water, the activation barrier of the metathesis step becomes slightly large with respect to that for the system in the absence of water due to decreased nucleophilicity of formato oxygen atom by making hydrogen bonding. Additionally, they demonstrated theoretically that both alcohol (MeOH) and amine (NMe_2H) could work in the same manner as water molecule.

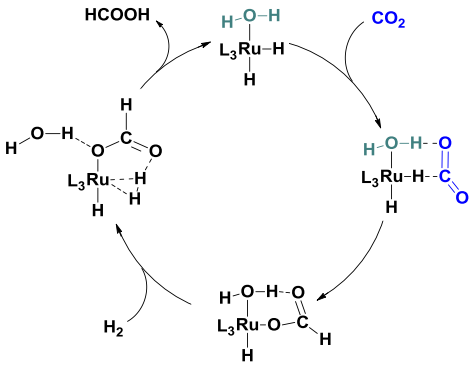

Figure 19. Proposed mechanism of *cis*-$RuH_2(PMe_3)_3$-catalyzed hydrogenative CO_2 reduction in the presence of water molecules. L = PMe_3

Similar promoting effects of water and alcohol have been reported by different groups. Lau *et. al*. have found that the catalytic reaction by $TpRuH(PPh_3)(CH_3CN)$ (Tp = hydrotris(pyrazolyl)borate), **19**, enhanced by adding 5% of water in THF. (TON 30 vs 720).[128] In the same catalyst system, they also demonstrated that using an acidic alcohol, 2,2,2-trifluoroethanol (TFE) as the solvent the TON has further increased to 1815 presumably due to stronger interaction between alcohol hydrogen atom and oxygen atom of CO_2.[129] Jessop *et al*. also demonstrated that through their extensive work on additive effects, the system of $RuCl(OAc)(PMe_3)_4$, **20**, combined with perfluoro phenol (C_6F_5OH) as additive showed one of the highest TOF (95000 h^{-1}) to date.[91]

N donor type ligand based catalysts

In 2009, Nozaki *et al*. designed Ir(III) trihydride complexes **16** containing strong s-dononating alkylphosphine- and pyridine-based $PN^{py}P$ pincer ligand ($PN^{py}P$ = 2,6-C_5H_3N

UNIVERSITAT ROVIRA I VIRGILI
SECOND-ROW TRANSITION-METAL COMPLEXES RELEVANT TO CO2 REDUCTION AND WATER OXIDATION
Takashi Ono
DL:T 1108-2014

($CH_2P^iPr_2)_2$) that was employed as strong electron donor (Figure 20a). This complex was used for the hydrogenative CO_2 reduction in a mixture of H_2O/THF solvent and showed highest TON (3500000) and TOF (150000 h^{-1}) to date.[113]

In 2011, Hazari *et al.* evaluated the thermodynamics of the CO_2 insertion step for analogues of Nozaki's Ir(III)-trihydride complex using computational method.[114] They found that Ir(III)-PN^HP complex (PN^HP = $HN(^iPr_2PC_2H_4)_2$), **21**, (Figure 20b), which has H-bond donor in the secondary coordination sphere, is favourable for the CO_2 insertion with $\Delta G°$ of -20.4 kJ/mol with respect to +3.4 kJ/mol for an analogue (Me groups on the phosphorous atoms instead of ^{i}Pr groups) of the Nozaki's complex. Furthermore, they experimentally isolated air- and moisture-stable formate complex. However, no clear advantages of an H-bond donor in the secondary coordination sphere were observed in the catalytic rate, as can be found from its maximum TON of 348000 and TOF of 18780 h^{-1}, which is one order of magnitude lower than the best system reported by Nozaki.

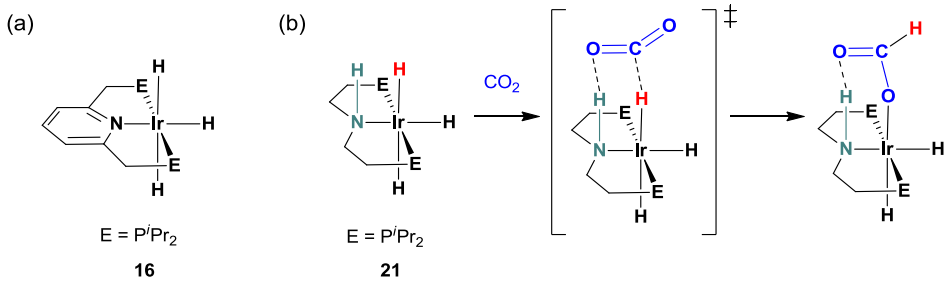

Figure 20. Ir-PNP pincer complexes reported by (a) Nozaki *et al*, and (b) Hazari *et al*.

Bipyridine-based ligand systems have been intensively investigated by Himeda *et al.* in the last decade. They evaluated the catalytic activity for the hydrogenative CO_2 reduction in aqueous basic solution using Ru, Rh, and Ir-based half-sandwich complexes containing substituted bipyridine (*bpy*) or phenanthrorine (*phen*) ligands.[118-119] By taking advantage of facile alteration of electronic properties of *bpy*-based complex, a relationship between initial rates and the substituents (H, OMe, Me, COOH,

UNIVERSITAT ROVIRA I VIRGILI
SECOND-ROW TRANSITION-METAL COMPLEXES RELEVANT TO CO2 REDUCTION AND WATER OXIDATION
Takashi Ono
DL:T 1108-2014

and OH) on *bpy* was systematically investigated (Figure 21). They observed the clear correlation in Hammet plot; for example, Ir-catalyst containing OH groups on *bpy*, which are deprotonated to form oxyanion, O^- *in situ* leading to strong electron donating substituent, showed initial TOF (TOF_i) of 7960 h^{-1}, whereas non-substituted complex showed only TOF_i of 6 h^{-1}.[118] Furthermore, they have shown that locating the OH group close to the reactive site (6,6'-positions of *bpy*) enhanced the catalytic rates 4 times higher with respect to that for the complex based on 4,4'-$(OH)_2$-bpy.[120,122] Theoretical studies revealed that this additional enhancement derived from the facile cleavage of H-H bond by the O^- group close to the reactive site. This was found experimentally, where 95% of $Cp^*Ir(OH_2)(6,6'\text{-}(OH)_2\text{-bpy})^{2+}$, **25**, converted to Ir-H species in 30 minutes at room temperature under 0.2 MPa of H_2 whereas only 90% of $Cp^*Ir(OH_2)(4,4'\text{-}(OH)_2\text{-bpy})^{2+}$ converted to Ir-H species after 40 hours under 0.5 MPa of H_2.[120,122] Interestingly, the catalytic activity was observed even under atmospheric pressures of H_2 and CO_2 at 25 °C with TON 330 and TOF 27 h^{-1} for $Cp^*Ir(OH_2)(4,4'\text{-}(OH)_2\text{-bpy})^{2+}$.

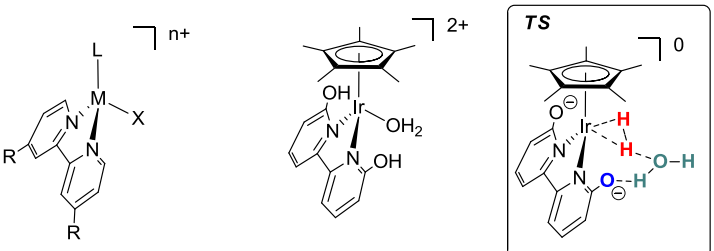

22: M = Ru^{II}, L = C_6Me_6
23: M = Rh^{III}, L Cp*
24: M = Ir^{III}, L = Cp*

25

X = Cl (n = 1) or OH_2 (n = 2)
R = H (**a**), Me (**b**), OMe (**c**), COOH (**d**), OH (**e**)

Figure 21. Left and middle: A series of half sandwich complexes for the hydrogenative CO_2 reduction reported by Himeda *et al*.. Right: transition state in the H_2 activation step for $[Cp^*Ir(OH_2)(6,6'\text{-}(OH)_2\text{-bpy})]^{2+}$ complex.

Fukuzumi *et al*. reported that water-soluble Ru and Ir aqua complexes containing *bpy* ligand, [LM(4,4'-R_2-bpy)(OH_2)](SO_4) (**26**: R = H or OMe; M = Ru^{II}, **27**: L = η^6-C_6Me_6;

UNIVERSITAT ROVIRA I VIRGILI
SECOND-ROW TRANSITION-METAL COMPLEXES RELEVANT TO CO2 REDUCTION AND WATER OXIDATION
Takashi Ono
DL:T 1108-2014

M = Ir^{III}, L = Cp*), can catalyze the hydrogenative reduction of CO_2 into formic acid under acidic conditions (pH of 2.5–5.0) without any base in water.[116] Among them, the highest TOF (27 h^{-1}) was obtained using [Cp*Ir(4,4'-OMe_2-bpy)(OH_2)](SO_4) and they found that electron-donating groups enhanced catalytic rates as similar trend were found with Himeda's catalysts. It was demonstrated that the catalytic cycle for both Ru and Ir complexes proceeded through the similar mechanism, but differ in the rate-determining step. The rate-determining step for the Ru catalysts is the reaction of the Ru-OH_2 with H_2, whereas for the Ir catalysts the rate-determining step is the reaction of Ir-H with CO_2.

On the other hand, polypyridyl metal hydrides have been of interest for many years because they play important roles as intermediates for the electro- and photocatalytic CO_2 reduction. For example, Ru(II)-hydrido complex, *cis*-$Ru^{II}(bpy)_2(CO)H^+$, can catalyze electrochemical CO_2 reduction to formate and CO.[132] The catalytic intermediate species for the formation of formate is Ru-H species which is electrogenerated in the presence of H_2O as a hydride source and further ligand-based reduction of Ru-H species triggers the insertion of CO_2. Due to the stabilization by π-acidic ligands such as CO, or PPh_3, polypyridyl Ru(II)-hydrido complexes themselves have low reactivity toward CO_2. Only a few polypyridyl Ru(II)-hydrido complexes without π-acidic ligands have been isolated and characterized including [Ru^{II}(trpy)(4,4'-R_2-bpy)(H)]$^+$ (R = H or OMe) reported by Ishitani *et al*.. They demonstrated that these Ru(II)-H complexes readily react with CO_2 in organic solvents at room temperature to quantitatively form the Ru-formato complexes. However, there have been very few precedents for the hydrogenative CO_2 reduction using Ru(II)-polypyridyl complexes.[133]

Non-noble metal catalysts

Recently, it has been reported by Beller *et al*. that the system based on abundant non-precious metals, such as Fe and Co, and tetraphos (PP3) ligands (Figure 22a, **28-30**) showed catalytic activity for the hydrogenative reduction of bicarbonate (HCO_3^-) and CO_2 (TON up to 7546 for Fe, 3877 for Co)[123,125-126]. Milstein also reported that Fe-PNP pincer ligand system (**31** in Figure 22b) was capable for the hydrogenative

UNIVERSITAT ROVIRA I VIRGILI
SECOND-ROW TRANSITION-METAL COMPLEXES RELEVANT TO CO2 REDUCTION AND WATER OXIDATION
Takashi Ono
DL:T 1108-2014

reduction of CO_2 and HCO_3^- with mild conditions (80 °C, total gas pressure ≤ 10 bar, TON up to 788).[127] Very recently, Linehan and co-workers described a cobalt hydride catalyst **32** (Figure 22c) that showed TON 2000 and TOF 3400 h^{-1} under 1 atm of CO_2/H_2 = 1/1 at room temperature comparable to some of the best noble metal catalysts.[124] This system, however, requires stoichiometric quantities of the strong basic (pK_a 33.6 for its conjugate acid) and expensive base, called as Vercade's base (Vkd, 2,8,9-triisopropyl-2,5,8,9-tetraaza-1-phosphabicyclo[3.3.3]-undecane).

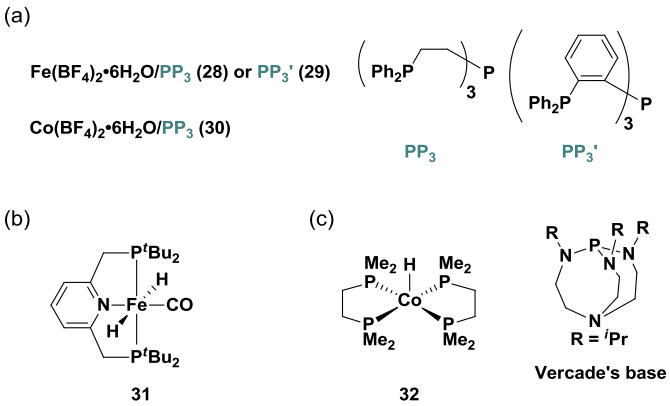

Figure 22. Catalytic systems based on non-noble metal for the hydrogenative reduction of CO_2.

Converstion of CO_2 to MeOH using H_2

Apart from the production of formic acid, recently, various research groups have investigated homogeneous catalysts for indirect/direct conversion from CO_2 to methanol using H_2 as reducing agent.

In 2011, Sanford *et al* proposed the cascade reaction in which three different catalysts were combined together for achieving the sequential transformations from CO_2 to MeOH in one reactor.[134] In detail, this reaction consists of following three consecutive catalytic reactions using reported catalysts: a) hydrogenative CO_2 reduction to formic acid (cat. A), b) esterification of formic acid to formate ester (cat. B), c) hydrogenation of the ester to release MeOH (cat. C) (Scheme 8). Although this straightforward methodology is interesting, catalytic performance (TON 21) is quite low and it needs to be improved.

UNIVERSITAT ROVIRA I VIRGILI
SECOND-ROW TRANSITION-METAL COMPLEXES RELEVANT TO CO2 REDUCTION AND WATER OXIDATION
Takashi Ono
DL:T 1108-2014

Scheme 8. Proposed sequential transformations from CO_2 to MeOH

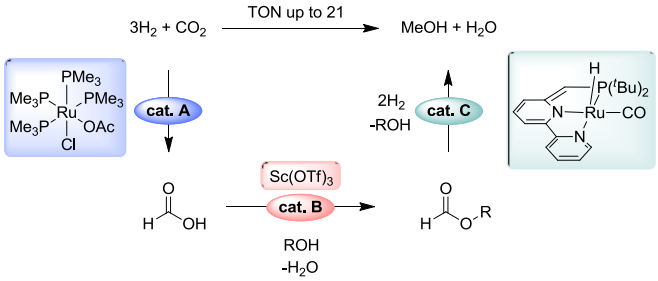

Klankermayer and Leitner *et al*. presented a Ru-phosphine complex, [Ru(triphos)(tmm)] (triphos = 1,1,1-tris(diphenylphosphinomethyl)ethane, and tmm = trimethlenemethane), **33**, (Figure 23) for the direct hydrogenation of CO_2 to methanol.[135] Although this system showed better results (TON up to 221), catalytic activity still remains insufficient. The system requires one equivalent of acid for the formation of active species $[(Triphos)RuH(H_2)]^+$ which was suggested for the reduction of C=O functionalities.[136] Although the final products are not MeOH, Leitner *et al*.[137] and Beller *et al*.[138] independently achieved the *N*-methylation of amine and aniline using H_2 and CO_2 as a methylating reagent with Ru/triphos system. N-methylation of amine is of importance in the area of fine chemical. Therefore, this system could offer valuable way for the utilization of CO_2.

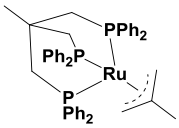

33

Figure 23. Ru(triphos)(tmm) **33** for the catalytic conversion of CO_2 to MeOH

I.4.2. Electrocatalytic CO_2 reduction

The products obtained from most of the systems reported so far are either CO or formic acid or a mixture of those, in case, with H_2 as a side product.[139] Although in general, the mechanism[139-140] for the formation of CO is thought to occur *via* M-COO^-

UNIVERSITAT ROVIRA I VIRGILI
SECOND-ROW TRANSITION-METAL COMPLEXES RELEVANT TO CO2 REDUCTION AND WATER OXIDATION
Takashi Ono
DL:T 1108-2014

intermediate, followed by C-O bond cleavage assisted by proton, the mechanism for the production of formic acid still remains controversial. One proposed pathway[141] is the formation of metal hydrido intermediate (M-H) from reduced metal centre with H^+, followed by CO_2 insertion into M-H bond to form metal formato species (M-OCHO). In addition, H_2 can be formed from the reaction with M-H with H^+.

The catalysts for electrocatalytic reduction of CO_2 can be divided into three types based on ligand type[140]: 1) metal (Ni, Co and Fe) catalysts with macrocyclic ligands, 2) metal (Re, Ru and Rh) catalysts with bipyridine ligands, and 3) metal (Rh, Pd, Cu and Ir) catalysts with phosphine ligands. Among them, one of the systematically studied complexes is Fe-tetraphenylporphyrin (FeTPP) complexes by the Savéant group,[142-145] which showed efficient and selective CO formation and high stability in the presence of Lewis acid[144] or weak Bronsted acid,[142-143] but this system requires large overpotential (≈ 1 V). Observation on the important role of proton donors prompt them to modify the TPP ligand by introducing the phenolic group (Figure.24, **34**), leading to the dramatic increase of catalytic activity with TON of 50 million at low overpotential (η = 0.465 V).[145]

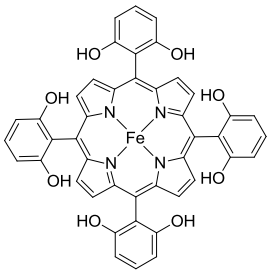

34

Figure 24. Electrocatalysts for the reduction of CO_2 to CO.

I.4.3. Photocatalytic CO_2 reduction

In general, upon light irradiation, photosensitizer P is excited to P*, which is reductively quenched by a sacrificial electron donor, typically triethanolamine (TEOA)

UNIVERSITAT ROVIRA I VIRGILI
SECOND-ROW TRANSITION-METAL COMPLEXES RELEVANT TO CO2 REDUCTION AND WATER OXIDATION
Takashi Ono
DL:T 1108-2014

to yield a reduced sensitizer, P^-. P^- is responsible for electron transfer to transition metal catalyst and then, its reduced form triggers reduction of CO_2.

The reported catalytic systems can be classified into two types[146-147]: 1) a combination of photosensitizer and catalyst (Ni and Co), 2) catalyst (Fe, Co, and Re) which itself functions as both a photosensitizer Although Fe and Co conjugated macrocycles (porphyrin, corrin, phthalocyanine and corrole) complexes of type 2 strongly absorbs visible light, these system displayed low quantum yield Φ and low TON partly due to the short lifetime of the excited states. The other type 2 complexes, *fac*-Re(bpy)$(CO)_3$X (X = Cl, Br), reported by Lehn and co-workers,[148-149] showed high $\Phi_{CO} = 0.14$ with selective CO formation. However, this catalyst only absorbs light at wavelength shorter than 400 nm, which is the drawback of this catalyst for the use of solar light. Ishitani *et al*. have developed supramolecular photocatysts **35** (Figure 25) using $[Ru(bpy)_3]^{2+}$ type photosensitizer covalently connected to the Re complex (Figure 24). The catalyst **33** showed the best result with $\Phi_{CO} = 0.21$ and TON_{CO} 232 under visible light irradiation.[150]

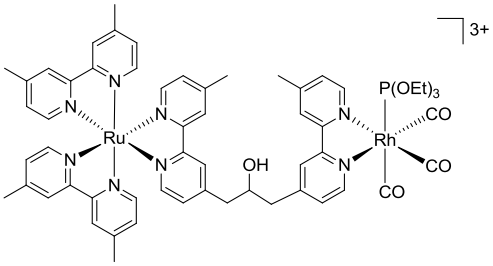

35

Figure 25. Ru-Rh supramolecular complex **35** for photocatalytic CO_2 reduction under visible light.

I.5. References

(1) *U.S. Energy Information Administration, International Energy Outlook 2013* http://www.eia.gov/forecasts/ieo/

(2) *U.S. Energy Information Administration 2012* http://www.eia.gov/totalenergy/data/annual/index.cfm

(3) *Intergovernmental Panel on Climate Change (IPCC) 2007 Fourth Assesment Report: Climate Change 2007 (AR4)* http://www.ipcc.ch/publications_and_data/ar4/wg1/en/contents.html

UNIVERSITAT ROVIRA I VIRGILI
SECOND-ROW TRANSITION-METAL COMPLEXES RELEVANT TO CO2 REDUCTION AND WATER OXIDATION
Takashi Ono
DL:T 1108-2014

(4) Lewis, N. S.; Nocera, D. G. *Proc. Natl. Acad. Sci. U.S.A.* **2006**, *103*, 15729-15735.
(5) Ke, B. *Photosynthesis Photobiochemistry and Photobiophysics*; Kluwer Academic, Dodrecht, 2001; Vol. 10.
(6) Umena, Y.; Kawakami, K.; Shen, J.-R.; Kamiya, N. *Nature* **2011**, *473*, 55-60.
(7) Guskov, A.; Kern, J.; Gabdulkhakov, A.; Broser, M.; Zouni, A.; Saenger, W. *Nat Struct Mol Biol* **2009**, *16*, 334-342.
(8) Siegbahn, P. E. M. *Acc. Chem. Res.* **2009**, *42*, 1871-1880.
(9) Cox, N.; Pantazis, D. A.; Neese, F.; Lubitz, W. *Acc. Chem. Res.* **2013**, *46*, 1588-1596.
(10) Najafpour, M. M.; Moghaddam, A. N.; Allakhverdiev, S. I.; Govindjee *Biochimica et Biophysica Acta (BBA) - Bioenergetics* **2012**, *1817*, 1110-1121.
(11) Pantazis, D. A.; Ames, W.; Cox, N.; Lubitz, W.; Neese, F. *Angew. Chem., Int. Ed.* **2012**, *51*, 9935-9940.
(12) Fuchs, G. *Annual Review of Microbiology* **2011**, *65*, 631-658.
(13) Andersson, I. *J. Mol. Biol.* **1996**, *259*, 160-174.
(14) Cleland, W. W.; Andrews, T. J.; Gutteridge, S.; Hartman, F. C.; Lorimer, G. H. *Chem. Rev.* **1998**, *98*, 549-562.
(15) Stec, B. *Proc. Natl. Acad. Sci. U.S.A.* **2012**, *109*, 18785-18790.
(16) Huynh, M. H. V.; Meyer, T. J. *Chem. Rev.* **2007**, *107*, 5004-5064.
(17) Weinberg, D. R.; Gagliardi, C. J.; Hull, J. F.; Murphy, C. F.; Kent, C. A.; Westlake, B. C.; Paul, A.; Ess, D. H.; McCafferty, D. G.; Meyer, T. J. *Chem. Rev.* **2012**, *112*, 4016-4093.
(18) Takeuchi, K. J.; Thompson, M. S.; Pipes, D. W.; Meyer, T. J. *Inorg. Chem.* **1984**, *23*, 1845-1851.
(19) Meyer, T. J.; Huynh, M. H. V. *Inorg. Chem.* **2003**, *42*, 8140-8160.
(20) Concepcion, J. J.; Jurss, J. W.; Templeton, J. L.; Meyer, T. J. *J. Am. Chem. Soc.* **2008**, *130*, 16462-16463.
(21) Concepcion, J. J.; Tsai, M.-K.; Muckerman, J. T.; Meyer, T. J. *J. Am. Chem. Soc.* **2010**, *132*, 1545-1557.
(22) Romain, S.; Bozoglian, F.; Sala, X.; Llobet, A. *J. Am. Chem. Soc.* **2009**, *131*, 2768-2769.
(23) Romain, S.; Vigara, L.; Llobet, A. *Acc. Chem. Res.* **2009**, *42*, 1944-1953.
(24) Nyhlén, J.; Duan, L.; Åkermark, B.; Sun, L.; Privalov, T. *Angew. Chem., Int. Ed.* **2010**, *49*, 1773-1777.
(25) Wasylenko, D. J.; Ganesamoorthy, C.; Borau-Garcia, J.; Berlinguette, C. P. *Chem. Commun.* **2011**, *47*, 4249-4251.
(26) Rigsby, M. L.; Mandal, S.; Nam, W.; Spencer, L. C.; Llobet, A.; Stahl, S. S. *Chemical Science* **2012**, *3*, 3058-3062.
(27) Pizzolato, E.; Natali, M.; Posocco, B.; Montellano Lopez, A.; Bazzan, I.; Di Valentin, M.; Galloni, P.; Conte, V.; Bonchio, M.; Scandola, F.; Sartorel, A. *Chem. Commun.* **2013**, *49*, 9941-9943.
(28) Ellis, W. C.; McDaniel, N. D.; Bernhard, S.; Collins, T. J. *J. Am. Chem. Soc.* **2010**, *132*, 10990-10991.
(29) Chen, G.; Chen, L.; Ng, S.-M.; Man, W.-L.; Lau, T.-C. *Angew. Chem., Int. Ed.* **2013**, *52*, 1789-1791.
(30) Hong, D.; Mandal, S.; Yamada, Y.; Lee, Y.-M.; Nam, W.; Llobet, A.; Fukuzumi, S. *Inorg. Chem.* **2013**, *52*, 9522-9531.
(31) Coggins, M. K.; Zhang, M.-T.; Vannucci, A. K.; Dares, C. J.; Meyer, T. J. *J. Am. Chem. Soc.* **2014**, *136*, 5531-5534.
(32) Barnett, S. M.; Goldberg, K. I.; Mayer, J. M. *Nat Chem* **2012**, *4*, 498-502.
(33) Zhang, M.-T.; Chen, Z.; Kang, P.; Meyer, T. J. *J. Am. Chem. Soc.* **2013**, *135*, 2048-2051.

UNIVERSITAT ROVIRA I VIRGILI
SECOND-ROW TRANSITION-METAL COMPLEXES RELEVANT TO CO2 REDUCTION AND WATER OXIDATION
Takashi Ono
DL:T 1108-2014

(34) Sala, X.; Romero, I.; Rodríguez, M.; Escriche, L.; Llobet, A. *Angew. Chem., Int. Ed.* **2009**, *48*, 2842-2852.
(35) Cao, R.; Lai, W.; Du, P. *Energy Environ. Sci.* **2012**, *5*, 8134-8157.
(36) Limburg, B.; Bouwman, E.; Bonnet, S. *Coord. Chem. Rev.* **2012**, *256*, 1451-1467.
(37) Wasylenko, D. J.; Ganesamoorthy, C.; Henderson, M. A.; Koivisto, B. D.; Osthoff, H. D.; Berlinguette, C. P. *J. Am. Chem. Soc.* **2010**, *132*, 16094-16106.
(38) Maji, S.; López, I.; Bozoglian, F.; Benet-Buchholz, J.; Llobet, A. *Inorg. Chem.* **2013**, *52*, 3591-3593.
(39) Yoshida, M.; Masaoka, S.; Abe, J.; Sakai, K. *Chemistry – An Asian Journal* **2010**, *5*, 2369-2378.
(40) Concepcion, J. J.; Jurss, J. W.; Norris, M. R.; Chen, Z.; Templeton, J. L.; Meyer, T. J. *Inorg. Chem.* **2010**, *49*, 1277-1279.
(41) Gersten, S. W.; Samuels, G. J.; Meyer, T. J. *J. Am. Chem. Soc.* **1982**, *104*, 4029-4030.
(42) Gilbert, J. A.; Eggleston, D. S.; Murphy, W. R.; Geselowitz, D. A.; Gersten, S. W.; Hodgson, D. J.; Meyer, T. J. *J. Am. Chem. Soc.* **1985**, *107*, 3855-3864.
(43) Collin, J. P.; Sauvage, J. P. *Inorg. Chem.* **1986**, *25*, 135-141.
(44) Nagoshi, K.; Yamashita, S.; Yagi, M.; Kaneko, M. *J. Mol. Catal. A: Chem.* **1999**, *144*, 71-76.
(45) Sens, C.; Romero, I.; Rodríguez, M.; Llobet, A.; Parella, T.; Benet-Buchholz, J. *J. Am. Chem. Soc.* **2004**, *126*, 7798-7799.
(46) Bozoglian, F.; Romain, S.; Ertem, M. Z.; Todorova, T. K.; Sens, C.; Mola, J.; Rodríguez, M.; Romero, I.; Benet-Buchholz, J.; Fontrodona, X.; Cramer, C. J.; Gagliardi, L.; Llobet, A. *J. Am. Chem. Soc.* **2009**, *131*, 15176-15187.
(47) Zong, R.; Thummel, R. P. *J. Am. Chem. Soc.* **2005**, *127*, 12802-12803.
(48) Deng, Z.; Tseng, H.-W.; Zong, R.; Wang, D.; Thummel, R. *Inorg. Chem.* **2008**, *47*, 1835-1848.
(49) López, I.; Ertem, M. Z.; Maji, S.; Benet-Buchholz, J.; Keidel, A.; Kuhlmann, U.; Hildebrandt, P.; Cramer, C. J.; Batista, V. S.; Llobet, A. *Angew. Chem., Int. Ed.* **2014**, *53*, 205-209.
(50) Tseng, H.-W.; Zong, R.; Muckerman, J. T.; Thummel, R. *Inorg. Chem. (Washington, DC, U. S.)* **2008**, *47*, 11763-11773.
(51) Zhang, G.; Zong, R.; Tseng, H.-W.; Thummel, R. P. *Inorg. Chem.* **2008**, *47*, 990-998.
(52) Xu, Y.; Åkermark, T.; Gyollai, V.; Zou, D.; Eriksson, L.; Duan, L.; Zhang, R.; Åkermark, B.; Sun, L. *Inorg. Chem.* **2009**, *48*, 2717-2719.
(53) Xu, Y.; Fischer, A.; Duan, L.; Tong, L.; Gabrielsson, E.; Åkermark, B.; Sun, L. *Angew. Chem., Int. Ed.* **2010**, *49*, 8934-8937.
(54) Xu, Y.; Duan, L.; Tong, L.; Akermark, B.; Sun, L. *Chem. Commun.* **2010**, *46*, 6506-6508.
(55) Duan, L.; Fischer, A.; Xu, Y.; Sun, L. *J. Am. Chem. Soc.* **2009**, *131*, 10397-10399.
(56) Duan, L.; Xu, Y.; Gorlov, M.; Tong, L.; Andersson, S.; Sun, L. *Chem. —Eur. J.* **2010**, *16*, 4659-4668.
(57) Tong, L.; Duan, L.; Xu, Y.; Privalov, T.; Sun , L. *Angew. Chem., Int. Ed.* **2011**, *50*, 445-449.
(58) Tong, L.; Wang, Y.; Duan, L.; Xu, Y.; Cheng, X.; Fischer, A.; Ahlquist, M. S. G.; Sun, L. *Inorg. Chem.* **2012**, *51*, 3388-3398.
(59) Tong, L.; Inge, A. K.; Duan, L.; Wang, L.; Zou, X.; Sun, L. *Inorg. Chem.* **2013**, *52*, 2505-2518.
(60) Kärkäs, M. D.; Åkermark, T.; Johnston, E. V.; Karim, S. R.; Laine, T. M.; Lee, B.-L.; Åkermark, T.; Privalov, T.; Åkermark, B. *Angew. Chem., Int. Ed.* **2012**, *51*, 11589-11593.
(61) Kärkäs, M. D.; Åkermark, T.; Chen, H.; Sun, J.; Åkermark, B. *Angew. Chem., Int. Ed.* **2013**, *52*, 4189-4193.

UNIVERSITAT ROVIRA I VIRGILI
SECOND-ROW TRANSITION-METAL COMPLEXES RELEVANT TO CO2 REDUCTION AND WATER OXIDATION
Takashi Ono
DL:T 1108-2014

(62) Duan, L.; Xu, Y.; Zhang, P.; Wang, M.; Sun, L. *Inorg. Chem.* **2010**, *49*, 209-215.
(63) Duan, L.; Bozoglian, F.; Mandal, S.; Stewart, B.; Privalov, T.; Llobet, A.; Sun, L. *Nat Chem* **2012**, *4*, 418-423.
(64) Wang, L.; Duan, L.; Stewart, B.; Pu, M.; Liu, J.; Privalov, T.; Sun, L. *J. Am. Chem. Soc.* **2012**, *134*, 18868-18880.
(65) Duan, L.; Araujo, C. M.; Ahlquist, M. S. G.; Sun, L. *Proc. Natl. Acad. Sci. U.S.A.* **2012**, *109*, 15584-15588.
(66) Duan, L.; Wang, L.; Inge, A. K.; Fischer, A.; Zou, X.; Sun, L. *Inorg. Chem.* **2013**, *52*, 7844-7852.
(67) Jiang, Y.; Li, F.; Zhang, B.; Li, X.; Wang, X.; Huang, F.; Sun, L. *Angew. Chem., Int. Ed.* **2013**, *52*, 3398-3401.
(68) Sartorel, A.; Carraro, M.; Scorrano, G.; Zorzi, R. D.; Geremia, S.; McDaniel, N. D.; Bernhard, S.; Bonchio, M. *J. Am. Chem. Soc.* **2008**, *130*, 5006-5007.
(69) Geletii, Y. V.; Botar, B.; Kögerler, P.; Hillesheim, D. A.; Musaev, D. G.; Hill, C. L. *Angew. Chem., Int. Ed.* **2008**, *47*, 3896-3899.
(70) Geletii, Y. V.; Huang, Z.; Hou, Y.; Musaev, D. G.; Lian, T.; Hill, C. L. *J. Am. Chem. Soc.* **2009**, *131*, 7522-7523.
(71) Aresta, M.; Dibenedetto, A. *Dalton Trans.* **2007**, 2975-2992.
(72) Sakakura, T.; Choi, J.-C.; Yasuda, H. *Chem. Rev.* **2007**, *107*, 2365-2387.
(73) Cokoja, M.; Bruckmeier, C.; Rieger, B.; Herrmann, W. A.; Kühn, F. E. *Angew. Chem., Int. Ed.* **2011**, *50*, 8510-8537.
(74) Bontemps, S.; Vendier, L.; Sabo-Etienne, S. *J. Am. Chem. Soc.* **2014**, *136*, 4419-4425.
(75) Sgro, M. J.; Stephan, D. W. *Angew. Chem., Int. Ed.* **2012**, *51*, 11343-11345.
(76) Chakraborty, S.; Patel, Y. J.; Krause, J. A.; Guan, H. *Polyhedron* **2012**, *32*, 30-34.
(77) Chakraborty, S.; Zhang, J.; Krause, J. A.; Guan, H. *J. Am. Chem. Soc.* **2010**, *132*, 8872-8873.
(78) Matsuo, T.; Kawaguchi, H. *J. Am. Chem. Soc.* **2006**, *128*, 12362-12363.
(79) Park, S.; Bézier, D.; Brookhart, M. *J. Am. Chem. Soc.* **2012**, *134*, 11404-11407.
(80) Boddien, A.; Gärtner, F.; Federsel, C.; Sponholz, P.; Mellmann, D.; Jackstell, R.; Junge, H.; Beller, M. *Angew. Chem., Int. Ed.* **2011**, *50*, 6411-6414.
(81) Johnson, T. C.; Morris, D. J.; Wills, M. *Chem. Soc. Rev.* **2010**, *39*, 81-88.
(82) Enthaler, S.; von Langermann, J.; Schmidt, T. *Energy Environ. Sci.* **2010**, *3*, 1207-1217.
(83) Zhang, J.; Ramachandran, P. V.; Gore, J. P.; Mudawar, I.; Fisher, T. S. *J. Heat Transfer* **2005**, *127*, 1391-1399.
(84) Morris, D. J.; Clarkson, G. J.; Wills, M. *Organometallics* **2009**, *28*, 4133-4140.
(85) Fellay, C.; Dyson, P. J.; Laurenczy, G. *Angew. Chem., Int. Ed.* **2008**, *47*, 3966-3968.
(86) Gao, Y.; Kuncheria, J.; J. Puddephatt, R.; P. A. Yap, G. *Chem. Commun.* **1998**, 2365-2366.
(87) Boddien, A.; Mellmann, D.; Gärtner, F.; Jackstell, R.; Junge, H.; Dyson, P. J.; Laurenczy, G.; Ludwig, R.; Beller, M. *Science* **2011**, *333*, 1733-1736.
(88) Fujita, E.; Muckerman, J. T.; Himeda, Y. *Biochimica et Biophysica Acta (BBA) - Bioenergetics* **2013**, *1827*, 1031-1038.
(89) Jessop, P. G.; Ikariya, T.; Noyori, R. *Nature* **1994**, *368*, 231-233.
(90) Jessop, P. G.; Hsiao, Y.; Ikariya, T.; Noyori, R. *J. Am. Chem. Soc.* **1996**, *118*, 344-355.
(91) Munshi, P.; Main, A. D.; Linehan, J. C.; Tai, C.-C.; Jessop, P. G. *J. Am. Chem. Soc.* **2002**, *124*, 7963-7971.
(92) Getty, A. D.; Tai, C.-C.; Linehan, J. C.; Jessop, P. G.; Olmstead, M. M.; Rheingold, A. L. *Organometallics* **2009**, *28*, 5466-5477.
(93) Zhang, Z.; Hu, S.; Song, J.; Li, W.; Yang, G.; Han, B. *ChemSusChem* **2009**, *2*, 234-238.

UNIVERSITAT ROVIRA I VIRGILI
SECOND-ROW TRANSITION-METAL COMPLEXES RELEVANT TO CO2 REDUCTION AND WATER OXIDATION
Takashi Ono
DL:T 1108-2014

(94) Zhang, Z.; Xie, Y.; Li, W.; Hu, S.; Song, J.; Jiang, T.; Han, B. *Angew. Chem., Int. Ed.* **2008**, *47*, 1127-1129.
(95) Lau, C. P.; Ng, S. M.; Jia, G.; Lin, Z. *Coord. Chem. Rev.* **2007**, *251*, 2223-2237.
(96) Kubas, G. J. *J. Organomet. Chem.* **2014**, *751*, 33-49.
(97) Kubas, G. J. *Chem. Rev.* **2007**, *107*, 4152-4205.
(98) Nicolet, Y.; de Lacey, A. L.; Vernède, X.; Fernandez, V. M.; Hatchikian, E. C.; Fontecilla-Camps, J. C. *J. Am. Chem. Soc.* **2001**, *123*, 1596-1601.
(99) Inoue, Y.; Izumida, H.; Sasaki, Y.; Hashimoto, H. *Chem. Lett.* **1976**, *5*, 863-864.
(100) Jessop, P. G. In *The Handbook of Homogeneous Hydrogenation*; Wiley-VCH Verlag GmbH: 2008, p 489-511.
(101) Joo, F.; Nadasdi, L.; Elek, J.; Laurenczy, G. *Chem. Commun.* **1999**, 971-972.
(102) Joó, F.; Laurenczy, G.; Karády, P.; Elek, J.; Nádasdi, L.; Roulet, R. *Appl. Organomet. Chem.* **2000**, *14*, 857-859.
(103) Laurenczy, G.; Joó, F.; Nádasdi, L. *Inorg. Chem.* **2000**, *39*, 5083-5088.
(104) Elek, J.; Nádasdi, L.; Papp, G.; Laurenczy, G.; Joó, F. *Applied Catalysis A: General* **2003**, *255*, 59-67.
(105) Papp, G.; Horvath, H.; Laurenczy, G.; Szatmari, I.; Katho, A.; Joo, F. *Dalton Trans.* **2013**, *42*, 521-529.
(106) Urakawa, A.; Iannuzzi, M.; Hutter, J.; Baiker, A. *Chem. —Eur. J.* **2007**, *13*, 6828-6840.
(107) Urakawa, A.; Jutz, F.; Laurenczy, G.; Baiker, A. *Chem. —Eur. J.* **2007**, *13*, 3886-3899.
(108) Graf, E.; Leitner, W. *J. Chem. Soc., Chem. Commun.* **1992**, 623-624.
(109) Gassner, F.; Leitner, W. *J. Chem. Soc., Chem. Commun.* **1993**, 1465-1466.
(110) Hutschka, F.; Dedieu, A.; Eichberger, M.; Fornika, R.; Leitner, W. *J. Am. Chem. Soc.* **1997**, *119*, 4432-4443.
(111) Angermund, K.; Baumann, W.; Dinjus, E.; Fornika, R.; Görls, H.; Kessler, M.; Krüger, C.; Leitner, W.; Lutz, F. *Chem. —Eur. J.* **1997**, *3*, 755-764.
(112) Erlandsson, M.; Landaeta, V. R.; Gonsalvi, L.; Peruzzini, M.; Phillips, A. D.; Dyson, P. J.; Laurenczy, G. *Eur. J. Inorg. Chem.* **2008**, *2008*, 620-627.
(113) Tanaka, R.; Yamashita, M.; Nozaki, K. *J. Am. Chem. Soc.* **2009**, *131*, 14168-14169.
(114) Schmeier, T. J.; Dobereiner, G. E.; Crabtree, R. H.; Hazari, N. *J. Am. Chem. Soc.* **2011**, *133*, 9274-9277.
(115) Maenaka, Y.; Suenobu, T.; Fukuzumi, S. *Energy Environ. Sci.* **2012**, *5*, 7360-7367.
(116) Ogo, S.; Kabe, R.; Hayashi, H.; Harada, R.; Fukuzumi, S. *Dalton Trans.* **2006**, 4657-4663.
(117) Hayashi, H.; Ogo, S.; Fukuzumi, S. *Chem. Commun.* **2004**, 2714-2715.
(118) Himeda, Y.; Onozawa-Komatsuzaki, N.; Sugihara, H.; Kasuga, K. *Organometallics* **2007**, *26*, 702-712.
(119) Himeda, Y.; Miyazawa, S.; Hirose, T. *ChemSusChem* **2011**, *4*, 487-493.
(120) Hull, J. F.; Himeda, Y.; Wang, W.-H.; Hashiguchi, B.; Periana, R.; Szalda, D. J.; Muckerman, J. T.; Fujita, E. *Nat. Chem.* **2012**, *4*, 383-388.
(121) Wang, W.-H.; Hull, J. F.; Muckerman, J. T.; Fujita, E.; Himeda, Y. *Energy Environ. Sci.* **2012**, *5*, 7923-7926.
(122) Wang, W.-H.; Muckerman, J. T.; Fujita, E.; Himeda, Y. *ACS Catal.* **2013**, *3*, 856-860.
(123) Federsel, C.; Ziebart, C.; Jackstell, R.; Baumann, W.; Beller, M. *Chem. —Eur. J.* **2012**, *18*, 72-75.
(124) Jeletic, M. S.; Mock, M. T.; Appel, A. M.; Linehan, J. C. *J. Am. Chem. Soc.* **2013**, *135*, 11533-11536.
(125) Federsel, C.; Boddien, A.; Jackstell, R.; Jennerjahn, R.; Dyson, P. J.; Scopelliti, R.; Laurenczy, G.; Beller, M. *Angew. Chem., Int. Ed.* **2010**, *49*, 9777-9780.

UNIVERSITAT ROVIRA I VIRGILI
SECOND-ROW TRANSITION-METAL COMPLEXES RELEVANT TO CO2 REDUCTION AND WATER OXIDATION
Takashi Ono
DL:T 1108-2014

(126) Ziebart, C.; Federsel, C.; Anbarasan, P.; Jackstell, R.; Baumann, W.; Spannenberg, A.; Beller, M. *J. Am. Chem. Soc.* **2012**, *134*, 20701-20704.
(127) Langer, R.; Diskin-Posner, Y.; Leitus, G.; Shimon, L. J. W.; Ben-David, Y.; Milstein, D. *Angew. Chem., Int. Ed.* **2011**, *50*, 9948-9952.
(128) Yin, C.; Xu, Z.; Yang, S.-Y.; Ng, S. M.; Wong, K. Y.; Lin, Z.; Lau, C. P. *Organometallics* **2001**, *20*, 1216-1222.
(129) Ng, S. M.; Yin, C.; Yeung, C. H.; Chan, T. C.; Lau, C. P. *Eur. J. Inorg. Chem.* **2004**, *2004*, 1788-1793.
(130) Musashi, Y.; Sakaki, S. *J. Am. Chem. Soc.* **2000**, *122*, 3867-3877.
(131) Ohnishi, Y.-y.; Nakao, Y.; Sato, H.; Sakaki, S. *Organometallics* **2006**, *25*, 3352-3363.
(132) Pugh, J. R.; Bruce, M. R. M.; Sullivan, B. P.; Meyer, T. J. *Inorg. Chem.* **1991**, *30*, 86-91.
(133) Lau, C. P.; Chen, Y. Z. *J. Mol. Catal. A: Chem.* **1995**, *101*, 33-36.
(134) Huff, C. A.; Sanford, M. S. *J. Am. Chem. Soc.* **2011**, *133*, 18122-18125.
(135) Wesselbaum, S.; vom Stein, T.; Klankermayer, J.; Leitner, W. *Angew. Chem., Int. Ed.* **2012**, *51*, 7499-7502.
(136) Geilen, F. M. A.; Engendahl, B.; Hölscher, M.; Klankermayer, J.; Leitner, W. *J. Am. Chem. Soc.* **2011**, *133*, 14349-14358.
(137) Beydoun, K.; vom Stein, T.; Klankermayer, J.; Leitner, W. *Angew. Chem., Int. Ed.* **2013**, *52*, 9554-9557.
(138) Li, Y.; Sorribes, I.; Yan, T.; Junge, K.; Beller, M. *Angew. Chem., Int. Ed.* **2013**, *52*, 12156-12160.
(139) Savéant, J.-M. *Chem. Rev.* **2008**, *108*, 2348-2378.
(140) Benson, E. E.; Kubiak, C. P.; Sathrum, A. J.; Smieja, J. M. *Chem. Soc. Rev.* **2009**, *38*, 89-99.
(141) Costentin, C.; Robert, M.; Saveant, J.-M. *Chem. Soc. Rev.* **2013**, *42*, 2423-2436.
(142) Bhugun, I.; Lexa, D.; Saveant, J.-M. *J. Am. Chem. Soc.* **1994**, *116*, 5015-5016.
(143) Bhugun, I.; Lexa, D.; Savéant, J.-M. *J. Am. Chem. Soc.* **1996**, *118*, 1769-1776.
(144) Bhugun, I.; Lexa, D.; Savéant, J.-M. *J. Am. Chem. Soc.* **1996**, *118*, 3982-3983.
(145) Costentin, C.; Drouet, S.; Robert, M.; Savéant, J.-M. *Science* **2012**, *338*, 90-94.
(146) Kumar, B.; Llorente, M.; Froehlich, J.; Dang, T.; Sathrum, A.; Kubiak, C. P. *Annu. Rev. Phys. Chem.* **2012**, *63*, 541-569.
(147) Morris, A. J.; Meyer, G. J.; Fujita, E. *Acc. Chem. Res.* **2009**, *42*, 1983-1994.
(148) Hawecker, J.; Lehn, J.-M.; Ziessel, R. *J. Chem. Soc., Chem. Commun.* **1983**, 536-538.
(149) Hawecker, J.; Lehn, J.-M.; Ziessel, R. *Helv. Chim. Acta* **1986**, *69*, 1990-2012.
(150) Sato, S.; Koike, K.; Inoue, H.; Ishitani, O. *Photochemical & Photobiological Sciences* **2007**, *6*, 454-461.

UNIVERSITAT ROVIRA I VIRGILI
SECOND-ROW TRANSITION-METAL COMPLEXES RELEVANT TO CO2 REDUCTION AND WATER OXIDATION
Takashi Ono
DL:T 1108-2014

Chapter II

Objectives

UNIVERSITAT ROVIRA I VIRGILI
SECOND-ROW TRANSITION-METAL COMPLEXES RELEVANT TO CO2 REDUCTION AND WATER OXIDATION
Takashi Ono
DL:T 1108-2014

The aim of this thesis is to investigate the new transition-metal complexes to be applied to CO_2 reduction and water oxidation which are primary importance in today's society.

The objective of **Chapter III** and **IV** includes;

- The synthesis and characterization of a new family of mono- and dinuclear Ru polypyridyl complexes for catalytic hydrogenative CO_2 reduction.
- The study on the influences of the electronic, steric properties, and nuclearity of the complexes on their catalytic performance, in terms of the reaction kinetics, in order to elucidate the catalytic mechanism.

The objective of **Chapter V** includes;

- The investigation on the salts of molybdate dianion in order to determine the reactivity with CO_2 as either the potential basis for a new homogeneous catalytic system or as a soluble model for known heterogeneous oxide catalysts.

The objective of **Chapter VI** and **VII** includes;

- The synthesis and characterization of new mono- and dinuclear complexes containing negatively charged cyclometalating ligand, in order to study the influence of negatively charged ligand on their electrochemical properties and the reactivity toward water oxidation.

UNIVERSITAT ROVIRA I VIRGILI
SECOND-ROW TRANSITION-METAL COMPLEXES RELEVANT TO CO2 REDUCTION AND WATER OXIDATION
Takashi Ono
DL:T 1108-2014

UNIVERSITAT ROVIRA I VIRGILI
SECOND-ROW TRANSITION-METAL COMPLEXES RELEVANT TO CO2 REDUCTION AND WATER OXIDATION
Takashi Ono
DL:T 1108-2014

Chapter III-1

Carbon Dioxide Reduction Catalyzed by Mononuclear Ruthenium Polypyridyl Complexes

Phys. Chem. Chem. Phys. **2011**, *13*, 19480–19484. DOI: 10.1039/c1cp22814e

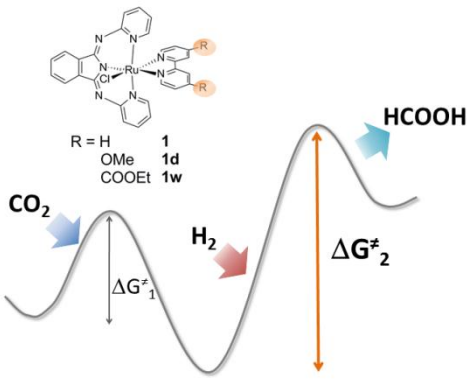

Table of Contents

UNIVERSITAT ROVIRA I VIRGILI
SECOND-ROW TRANSITION-METAL COMPLEXES RELEVANT TO CO2 REDUCTION AND WATER OXIDATION
Takashi Ono
DL:T 1108-2014

III-1.1. Abstract

New mononuclear ruthenium complexes with general formula [Ru(bid)(B)(Cl)] (*bid*$^-$ is (1*Z*,3*Z*)-1,3-bis(pyridin-2-ylimino)isoindolin-2-ide; B = bidentate ligand, *bpy* = 2,2'-bipyridine or 4,4'-R_2-*bpy*, where R = COOEt or OMe) were synthesized and tested as precatalysts for the hydrogenative CO_2 reduction in 2,2,2-trifluoroethanol (TFE) as solvent with added NEt_3 . Significant amounts of formic acid were produced by these catalysts and a kinetic analysis based on initial rate constants was carried out. The potential mechanisms including intermediate species for these catalytic systems were investigated by means of quantum chemical calculations to gain deeper insight into the processes. The effect of electron-donating and electron-withdrawing groups on catalyst performance was studied both experimentally and theoretically.

III-1.2. Introduction

The use of carbon dioxide (CO_2) as a raw material for chemical synthesis is the subject of growing attention, driven by environmental, legal, and social concerns. Atmospheric carbon dioxide is the most abundant greenhouse gas and the scientific community now agrees that the increase of its concentration in the atmosphere is mainly anthropogenic in origin[1-3]. Although to date the use of CO_2 in chemical synthesis has contributed very little to any decrease of CO_2 concentration in the atmosphere, several other factors render CO_2 an interesting chemical feedstock, including its high abundance, low toxicity, low cost, and low critical temperature.

Hydrogenative CO_2 reduction promoted by transition-metal catalysts represents one viable way to obtain reduced C1 products (which include formic acid, formaldehyde, methanol, and, ultimately, methane). Rhodium and, to a lesser extent, ruthenium and iridium complexes bearing phosphine ligands have been reported to reduce CO_2 catalytically to formaldehyde and formic acid and its derivatives.[4-14] In all cases the production of formic acid is thought to be the first required step for any further synthesis. It is thus of particular importance to understand the mechanistic details governing catalytic hydrogenative CO_2 reduction.

UNIVERSITAT ROVIRA I VIRGILI
SECOND-ROW TRANSITION-METAL COMPLEXES RELEVANT TO CO2 REDUCTION AND WATER OXIDATION
Takashi Ono
DL:T 1108-2014

In this paper we report the results of a combined experimental and computational study on a new family of catalysts for hydrogenative reduction of CO_2 to formic acid. Mononuclear ruthenium complexes with general formula $[Ru(T)(B)(Cl)]^{n+}$ (T = tridentate meridional ligand, *trpy* = 2,2':6',6''-terpyridine or anionic *bid*$^-$ = (1*Z*,3*Z*)-1,3-bis(pyridin-2-ylimino)isoindolin-2-ide; B = bidentate ligand, *bpy* = 2,2'-bipyridine or 4,4'-R_2-*bpy*, where R = COOEt or OMe *n* = charge ranging from 0 to 1+; See Figure 1 and 2 for ligand drawing and for general nomenclature and structure) were synthesized and their catalytic activities assayed. The effects of ligand modification and associated electronic tuning on the activities of the ruthenium catalysts were investigated. Quantum chemical modeling was employed to characterize in detail the energetics associated with elementary steps in the overall catalytic cycle.

III-1.3. Results and Discussion

III-1.3.1. Synthesis, Structure and Redox Properties.

Synthesis

All *bid*$^-$-containing compounds **1**, **1d** and **1w** (see Figure 1) were synthesized following the same "one pot" procedure: An ethanol solution with a mixture of $[RuCl_3(Hbid)]$ and the bidentate ligand 4,4'-R_2-*bpy* (R = H, OMe or COOEt) was heated at reflux for one hour. Subsequent addition of an excess of NEt_3 and LiCl was followed by four more hours of reflux. Cooling the solution yielded the desired product as a crystalline powder.

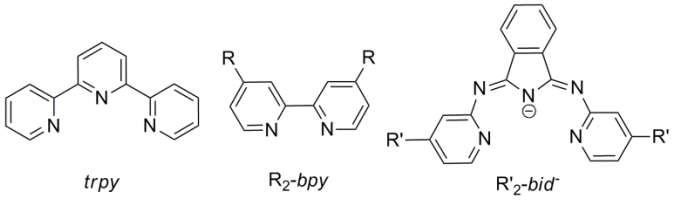

$[Ru(R'_2\text{-bid})(R_2\text{-bpy})Cl]$

1: R = H, R' = H
1d: R = -OMe, R' = H
1w: R = -COOEt, R' = H
1d': R = H, R' = -OMe
1w': R = H, R' = -COOMe

Figure 1. Top, polydentate ligands employed. Bottom, nomenclature used for Ru-Cl complexes.

Structure

Complex **1** was characterized by single crystal X-Ray diffraction analysis and the structure is shown in Figure 2. The metal center adopts an octahedral geometry distorted by the constrained bite angles of the chelating ligands and, possibly, crystal packing in the solid state. Bond distances and angles are in agreement with related complexes[15-17] and are displayed in Table 1 together with DFT calculated structures for **1** and $\mathbf{2}^{+}$.

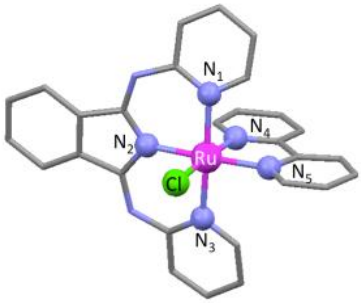

Figure 2. Mixed capped stick and ball and stick (first coordination sphere) representation for the X-Ray structure of compound **1**. Color codes: Ru, violet; Cl, green; N, blue; C, grey. Hydrogen atoms are not shown for clarity.

Table 1. Selected bond lengths (Å) and angles (°) for complexes **1** and $\mathbf{2}^{+}$ (Atom labelling is depicted in Figure 2).

	1		$\mathbf{2}^{+}$
	DFT	**X-Ray**	**DFT**
Ru-Cl	2.488	2.420	2.456
Ru-N1	2.098	2.121	2.071
Ru-N2	2.014	2.013	1.955
Ru-N3	2.108	2.115	2.071
Ru-N4	2.029	2.007	2.041
Ru-N5	2.064	2.056	2.081
N1-Ru-N3	177.3	175.00	159.0
N1-Ru-Cl	88.6	91.22	89.6
N4-Ru-Cl	174.7	176.21	172.9
N1-Ru-N5	92.5	92.74	100.5

Redox properties

Electrochemical measurements were carried out by means of Cyclic Voltammetry and allowed to calculate $E_{1/2}$ values for the Ru(III/II) couple that are presented in Table 2 together with additional catalytic data.

It is interesting to see that the replacement of *trpy* by the anionic *bid*$^-$ ligand produces a large cathodic shift larger than 500 mV, and that the *bpy* substitutents allow for fine tuning of 127 mV cathodic shift for **1d** and of 112 mV anodic shift for **1w**, with regard to the redox potential of the unsubstituted *bpy* complex **1**.

Table 2. Redox and Catalytic Data for complexes **1-2**$^+$.

Catalyst	$E_{1/2}$ [a]	TOF_i [b]	TON [c]
2$^+$	0.865	0.5 (1)	44
1	0.295 (0.570)	155.3 (310.6)	1090
1d	0.168 (0.697)	120.3 (240.6)	880
1w	0.407 (0.458)	193.4 (386.8)	1354

[a] $E_{1/2}$ (V) vs. SSCE obtained from $(E_{p,a} + E_{p,c})/2$ vs. SSCE. Scan rate 100 mV/s in glassy carbon working electrode and a Pt disk counter electrode. In parenthesis the difference between $E_{1/2}$(**2**$^+$) – $E_{1/2}$(**complex**) in V. [b] TOF_i in h^{-1}. Initial turnover frequencies, considering the first 130 minutes. In parenthesis values normalized with regard to **2**. [c] TON of HCOOH detected after 7 days for all catalysts except for **2** (92 h).

III-1.3.2. Catalytic Experiments

Each Ru-Cl complex was tested as a catalyst precursor for the hydrogenative reduction of CO_2, and in all cases formic acid was the sole product detected. Details of catalytic activity are reported in Table 2 for all catalysts. Figure 3 illustrates the formic acid produced quantified by turnover number (TON) measured over the first 140 minutes and over the full range of catalyst activity.

The catalysts derived from **1**, **1d** and **1w**, were studied over 7 days (10000 minutes), after which time all three catalysts were deactivated. A maximum TON of 1354 was reached by **1w**, which represents a 24% improvement compared to unsubstituted **1**. By contrast, substitution with electron-donating groups led to a 19% decrease in the activity of **1d** compared to **1**. Furthermore it was corroborated that **2**$^+$ is a poor catalyst consistent with previously reported data in the literature.[18-20] This

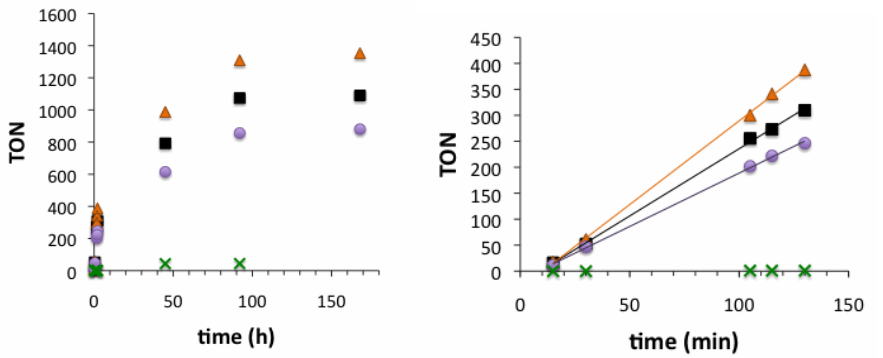

Figure 3. Catalytic performance of a 0.3 mM solution of complexes **1**, **1w**, **1d** and **2**$^{+}$ dissolved in a 8:1 mixture of TFE and NEt_3 at 45 bars of 1:1 CO_2/H_2 at 100 ^{o}C. Left, complete reaction. Right, initial reaction.

poor performance likely derives from the demonstrated high stability of the corresponding hydride species, $[Ru(trpy)(bpy)(H)]^+$ (**2-H**$^{+}$) which had been previously crystallized from aqueous solution.[21] By contrast, the hydride species derived from **1**, [Ru(bid)(bpy)(H)] (**1-H**) is highly reactive. This hydride was generated in rigorously dry DMF-d_7 with the addition of excess $NaBH_4$ and monitored by NMR spectroscopy (δ_{Ru-H} = –8.5 ppm vs. TMS; See Figures S4-7). Once generated, the hydride reacts very rapidly with CO_2 forming [Ru(bid)(bpy)(OCHO)].

It is striking to see that for **1** the initial TOF_i is 311 times that of **2**$^{+}$ and thus manifest the strong sensitivity of the reaction rate with regard to the electronic perturbation. However further electron donation exerted through the *bpy* ligand in **1d** decreases the rate with regard to the unsubstituted *bpy* complex **1.** Surprisingly the complex containing the electron withdrawing *bpy* ligand **1w** produces the opposite effect and achieves a rate that is 387 times faster than **2**$^{+}$. These results show that there isn't a straightforward relationship between electronic perturbation and catalyst performance and thus put forward the need of a detailed and thorough DFT analysis that is presented in the next section.

The rate dependence of initial HCOOH formation was studied for the cases of **1**, **1w**, and **1d**, and a first-order behavior with respect to both precatalyst and H_2

UNIVERSITAT ROVIRA I VIRGILI
SECOND-ROW TRANSITION-METAL COMPLEXES RELEVANT TO CO2 REDUCTION AND WATER OXIDATION
Takashi Ono
DL:T 1108-2014

concentrations was found. In addition, the initial rates were found to be independent of CO_2 concentration (Figures S8-11).

III-1.3.3. DFT Calculations

Density functional theory (DFT, M06-L functional) calculations were undertaken to study the reaction pathway for the overall catalytic process and illuminate the influence of different ligands and substituents. The ability of computational modeling to illuminate a catalytic cycle in full detail for hydrogenative reduction of CO_2 has recently been demonstrated by Yang for Pincer supported transition metal systems.[22] Following Jessop *et al.*[13-14] and Urakawa *et al.*[23-24] the proposed catalytic mechanism consists of four general steps (Figure 4).

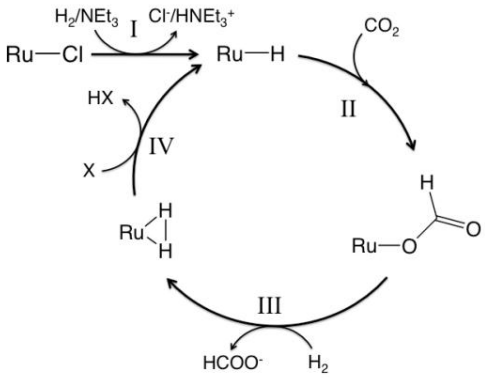

Figure 4. Catalytic cycle for hydrogenative CO_2 reduction. First the Ru-Cl complex is converted to a ruthenium hydride (I), which is the active catalytic species. Then three consecutive steps complete the catalytic cycle: CO_2 insertion into the metal hydrido (II), substitution of the formato ligand by dihydrogen (III), and regeneration of the hydride by heterolytic cleavage (IV).

In addition to the catalysts studied experimentally (**1**, **1d**, **1w** and **2**$^+$), two additional derivatives of **1** substituted on the *bid*$^-$ ligand with -OMe (complex **1d'**) and -COOMe (complex **1w'**) groups were considered (Figure 1). Selected structural parameters for **1** and **2**$^+$ are presented in Table 1 (see supporting information for other structures). The DFT structures for **1** are in good agreement with those obtained from X-Ray single crystal diffraction analysis.

The catalytic steps labeled I to IV in Figure 4 were further associated with elementary (microscopic) steps as follows (T and *bpy* ligands are not indicated):

Entrance to the cycle

$[Ru\text{-}Cl] + H_2 \rightarrow [Ru\text{-}H] + HCl$ (I)

CO_2 insertion

$[Ru\text{-}H] + CO_2 \rightarrow [Ru\text{-}H\cdots CO_2]^{\neq}$ (II-a)

$[Ru\text{-}H\cdots CO_2]^{\neq} \rightarrow [Ru\cdots H\text{-}CO_2]$ (II-b)

$[Ru\cdots H\text{-}CO_2] \rightarrow [Ru\text{-}O\text{-}CHO]$ (II-c)

Substitution

$[Ru\text{-}O\text{-}CHO] \rightarrow [Ru\cdots O\text{-}CHO]^{\neq}$ (III-a)

$[Ru\cdots O\text{-}CHO]^{\neq} \rightarrow [Ru] + HCOO^-$ (III-b)

$[Ru] + H_2 \rightarrow [Ru\text{-}H_2]$ (III-c)

Heterolytic cleavage

$[Ru\text{-}H_2] + X \rightarrow [Ru\text{-}H\cdots H\cdots X]^{\neq}$ (IV-a-Y)

$[Ru\text{-}H\cdots H\cdots X]^{\neq} \rightarrow [Ru\text{-}H] + HX$ (IV-b-Y)

(Y=O for X=$HCOO^-$ or Y=N for X=NMe_3)

Optimized intermediate and transition-state (TS) structures and energy profiles for the catalytic cycles for systems **1**, **1w**, and **1d** are shown in Figure 5. Initial hydride addition to CO_2 generates, through a TS structure with associated $\Delta G^{\neq}_1$, a hydrogen-coordinated formato intermediate (II-b) that is unstable relative to an oxygen-coordinated isomer (II-c). Substitution of the "formato" ligand by dihydrogen proceeds by formate dissociation and dihydrogen association (an equilibrium process that is endergonic) followed by hydrido regeneration through a heterolytic cleavage assisted by the formato anion (Steps III and IV-a-O with associated $\Delta G^{\neq}_2$). For the last step (IV), we also considered the amine acting as the active base, but in all cases the activation free energies for IV-a-N where higher than the corresponding ones for IV-a-O. The importance of the amine is instead associated with driving the catalytic process by deprotonating the product formic acid. This is computed to contribute 4.8 kcal/mol of additional driving force according to (IV-ON):

UNIVERSITAT ROVIRA I VIRGILI
SECOND-ROW TRANSITION-METAL COMPLEXES RELEVANT TO CO2 REDUCTION AND WATER OXIDATION
Takashi Ono
DL:T 1108-2014

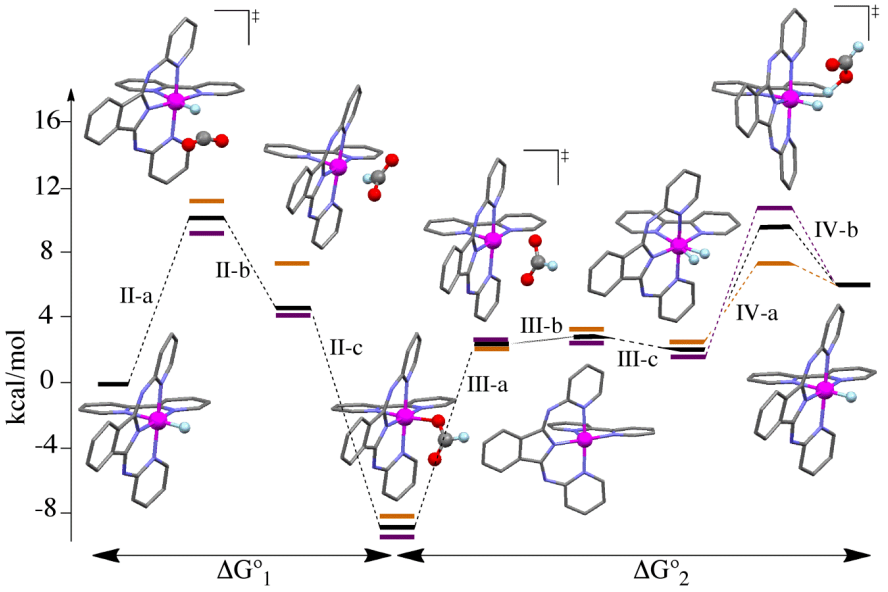

Figure 5. Computed free energy profiles (kcal/mol) for the catalytic cycles of compounds derived from **1** (black), **1d** (purple), and **1w** (orange). The initial Ru-H species define the relative zero of energy. Transition state structures for formate dissociation are stationary on the potential energy surface, but are lower in free energy than infinitely separated products. All free energies relative to [Ru-H] + CO_2 + H_2.

$$[\text{Ru-H}\cdots\text{H}\cdots\text{OCHO}]^{\neq} + \text{NMe}_3 \rightarrow [\text{Ru-H}] + [\text{HCOO}][\text{HNMe}_3]$$

With an overpressure of H_2 and/or CO_2, this is sufficient to render the catalytic process net exergonic. The free energies for each microscopic step involved in processes I to IV for each catalytic system are provided in the supporting information. Some key trends are apparent as indicated in Figure 5. Catalysts bearing ligands substituted with electron-donating groups (**1d** and **1d'**) have more nucleophilic hydrido and correspondingly lower free energies of activation for step II-a and stabilize formato ligand substitution by dihydrogen corresponding to process III. Conversely, those catalysts bearing ligands substituted with electron-withdrawing groups (**1w** and **1w'**) increase the acidity of the dihydrogen ligand and reduce the free energy of activation associated with the heterolytic cleavage step IV-a-O.

In all cases, the free energy of activation associated with reaching the TS

structure for heterolytic cleavage of the dihydrogen intermediate, from the formato intermediate ($\Delta G^{\neq}_2$), is found to be rate-determining. This free energy of activation is predicted to be greater than that for CO_2 insertion ($\Delta G^{\neq}_1$) by 5-7 kcal/mol for **1w** and **1w'**, by 8.8 kcal/mol for **1**, and by 12-13 kcal/mol for **1d** and **1d'**. The absolute free energy of activation for $\Delta G^{\neq}_2$ is computed to be 16.6, 19.0, 22.0, and 25.2 kcal/mol for compounds **1w**, **1**, **1d**, and $\mathbf{2}^+$ ($\mathbf{2}^+$ is not shown in Figure 5), respectively. This trend exactly tracks the relative rates summarized in Table 2 and Figure 3. Substituents on the *bid*$^-$ ligand are predicted to have a much smaller influence on $\Delta G^{\neq}_2$; the activation free energies for this step for **1w'** and **1d'** differ from that for **1** by less than 0.5 kcal/mol.

The key influence of the *bid*$^-$ ligand in **1** and its derivatives, compared to the *trpy* ligand in $\mathbf{2}^+$, which leads to substantially improved catalytic activity for the former compounds, is the destabilization of the formato intermediate relative to the dihydrogen-substituted intermediate. This effect is associated with the anionic charge of the *bid*$^-$ ligand compared to the neutral *trpy* ligand. While this leads to free energies of activation for the heterolytic cleavage step relative to the dihydrogen intermediate that are 3-7 kcal/mol higher for compounds **1** than for $\mathbf{2}^+$, this is more than offset by the equilibrium between the dihydrogen and formato intermediates that is 10-12 kcal/mol less favorable for $\mathbf{2}^+$ than for **1**. Interestingly, the free energy of activation for the hydride addition to CO_2 ($\Delta G^{\neq}_1$) is much less sensitive to *bid*$^-$ vs. *trpy* ligation. While it is smaller, as expected, for *bid*$^-$ compared to *trpy*, the effect is only 1-5 kcal/mol, reflecting the greater intrinsic reactivity of the metal-hydrido compared to the formate/dihydrogen substitution reaction.

III-1.4. Conclusions

We have prepared and characterized a family of new mononuclear complexes of general formula [Ru(bid)(B)(Cl)] (B = 4,4'-R_2-*bpy*, R = H, COOEt or OMe) and test their activity with regard to hydrogenative CO_2 reduction to form formic acid. Their activity has been compared to that of the known complex $[Ru(trpy)(bpy)(Cl)]^+$. The ligands of

UNIVERSITAT ROVIRA I VIRGILI
SECOND-ROW TRANSITION-METAL COMPLEXES RELEVANT TO CO2 REDUCTION AND WATER OXIDATION
Takashi Ono
DL:T 1108-2014

these non-phosphine-containing ruthenium polypyridyl compounds have been systematically modified and substituted so as to alter the electronic properties of derived catalysts in a controlled manner while maintaining the structure. The substitution of *trpy* by the anionic *bid*$^-$ ligand produces a remarkable enhancement of both TON and TOF_i and puts forward to viability of a single Ru-H bond to catalyze the CO_2 reduction reaction efficiently. In particular **1w** reacts nearly 400 times faster than **2**$^+$ and ends up generating 30 times more HCOOH. This dramatic effect manifests the importance of electronic perturbations on catalyst performance. DFT calculations provides detailed mechanistic information in agreement with experiments that allow rationalizing the effect of electronic perturbations exerted by the ligands into the kinetics of the catalytic CO_2 reduction process.

III-1.5. Experimental Section

Materials

All reagents used in present work were obtained from Aldrich Chemical Co., Alfa Aesar or Carbosynth Ltd. and were used without further purification. Synthesis grade organic solvents were obtained from SDS and were routinely degassed with Argon. Ethanol was dried with 3.5 Å molecular sieves and DCM, hexane and diethyl ether were used from the SPS. 2,2,2-Trifluoroethanol (TFE) was obtained from Alfa Aesar and was used without further purification. 4,4'-Dimethoxy-2,2'-bipyridine and $NaBH_4$ were purchased from Aldrich Chemical Co. and 4,4'-Bis(ethoxycarbonyl)-2,2'-bipyridine were purchased from Carbosynth Ltd. and used without further purification. CO_2 (Premier with a purity code of 4.5) and H_2 (BIP with a purity code of 5.7) gases were obtained from Carburos Metalicos, S.A. $[Ru^{III}(Hbid)Cl_3]$[25-26], $[Ru^{II}(bpy)(trpy)(Cl)]PF_6$,[27] were prepared as described in the literature. All synthetic manipulations were routinely performed under argon or nitrogen atmosphere using Schlenk and vacuum line techniques.

Synthesis

Scheme 1. NMR Labeling scheme for complexes **1**, **1d**, and **1w**.

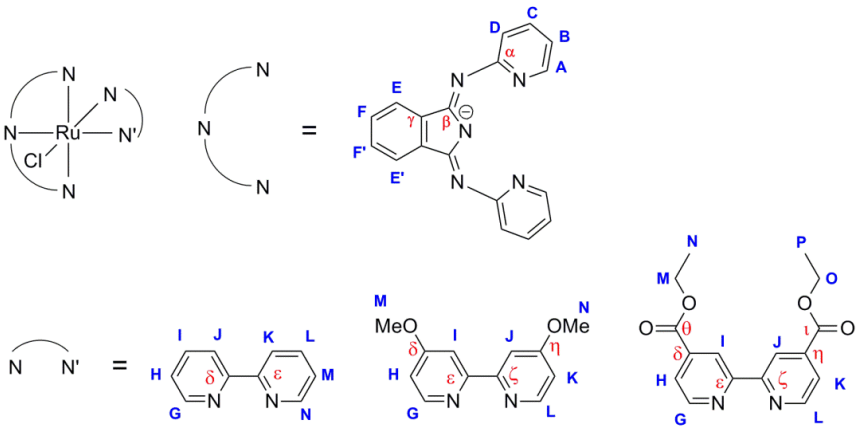

Synthesis of Ru^{II}(bid)(bpy)Cl·0.5LiCl·0.5Et_2O, (1 0.5LiCl·0.5Et_2O)

100 mg (0.197 mmol) of Ru(Hbid)Cl_3 were solved in 50 mL of ethanol. 37.0 mg (0.237 mmol) of 2,2'-bipyridine were added. The mixture was heated to reflux for 1 h. 42 mg (0.986 mmol) of LiCl and 0.10 mL (0.790 mmol) of triethylamine were added. The mixture was heated to reflux for 4 hs. Complex **1** was separated by filtration and cleaned with Et_2O. Yield 50.0 mg (0.0846 mmol), 42.9%. Anal. Calcd. for $C_{30}H_{25}Cl_{1.5}Li_{0.}5N_7O_{0.5}Ru$: C, 55.49; H, 3.88; N, 15.10. Found: C, 55.23; H, 3.91; N, 14.73. ^{1}H NMR (500 MHz, DMF-d_7, 298 K): δ 10.31 (d, 1H, J_{NM} = 5.4 Hz, H_N), 8.84 (d, 1H, J_{KL} = 7.6 Hz, H_K), 8.55 (d, 1H, J_{JI} = 8.0 Hz, H_J), 8.31 (td, 1H, J_{LK} = J_{LM} = 7.6 Hz, J_{LN} = 1.5 Hz, H_L), 8.18 (dd, 2H, J_{EF} = 5.4 Hz, $J_{EF'}$ = 3.0 Hz, H_E), 8.06 (ddd, 1H, J_{MN} = 7.6 Hz, J_{ML} = 5.4 Hz, J_{MK} = 1.2 Hz, H_M), 7.72 (dd, 2H, J_{FE} = 5.4 Hz, $J_{FE'}$ = 3.0 Hz, H_F), 7.65 (ddd, 1H, J_{IJ} = 7.2 Hz, J_{IH} = 8.0 Hz, J_{IG} = 1.4 Hz, H_I), 7.61-7.56 (m, 4H, H_A and H_C), 7.55-7.49 (m, 3H, H_G and H_D), 7.06 (ddd, 1H, J_{HG} = 7.2 Hz, J_{HI} = 5.9 Hz, J_{HJ} = 1.3 Hz, H_H), 6.55 (td, 2H, J_{BA} = J_{BC} = 6.6 Hz, J_{BD} = 1.7 Hz, H_B). ^{13}C NMR (125 MHz, DMF-d_7, 298 K): δ 160.5 ($C_δ$), 160.2 ($C_ε$), 158.2 ($C_α$), 154.5 (C_N), 153.0 (C_A), 152.4 ($C_β$), 150.9 (C_G), 142.1 ($C_γ$), 136.4 (C_L), 135.0 (C_I), 134.6 (C_C), 130.0 (C_F), 128.4 (C_M), 128.2 (C_D), 126.2 (C_H), 124.5 (C_K), 124.2 (C_J), 121.1 (C_E), 117.1 (C_B). MALDI(+)-MS (DCM): *m/z* 556 $[M\text{-}Cl]^+$.

UNIVERSITAT ROVIRA I VIRGILI
SECOND-ROW TRANSITION-METAL COMPLEXES RELEVANT TO CO2 REDUCTION AND WATER OXIDATION
Takashi Ono
DL:T 1108-2014

Synthesis of Ru^{II}(bid)(4,4'-$(MeO)_2$-bpy)Cl·1.5H_2O (1d·1.5H_2O)

To a mixture of 50.0 mg (0.0987 mmol) of Ru(HBid)Cl_3 and 25.6 mg (0.237 mmol) of 4,4'-methoxy-2,2'-bipyridine were dissolved in 20 mL of ethanol. After the mixture was heated to reflux for 1 h, 21.8 mg (0.495 mmol) of LiCl and 50.0 μL (0.359 mmol) of triethylamine were added. The mixture was heated to reflux for 4 h. Upon cooling to room temperature, the precipitate appeared which was separated by filtration and cleaned with diethyl ether. Yield. 50.3 mg (0.0773 mmol), 77.8%. Anal. Calcd. for $C_{30}H_{27}ClN_7O_{3.5}Ru$: C, 53.14; H, 4.01; N, 14.46. Found: C, 53.22; H, 3.56; N, 14.23. ^{1}H NMR (500 MHz, DMF-d_7, 298 K): δ 9.99 (d, 1H, J_{LK} = 6.4 Hz, H_L), 8.52 (d, 1H, J_{JK} = 2.7 Hz, H_J), 8.23 (d, 1H, J_{IH} = 2.8 Hz, H_I), 8.18 (dd, 2H, J_{EF} = 5.4 Hz, $J_{EF'}$ = 3.0 Hz, H_E), 7.79 (dd, 1H, J_{DC} = 6.5 Hz, J_{DB} = 1.6 Hz, H_D), 7.73 (dd, 2H, J_{KL} = 6.4 Hz, J_{KJ} = 2.7 Hz, H_K), 7.70 (dd, 2H, J_{FE} = 5.4 Hz, $J_{FE'}$ = 3.0 Hz, H_F), 7.58 (ddd, 2H, J_{BA} = 7.8 Hz, J_{BC} = 6.5 Hz, J_{BD} = 1.6 Hz, H_B), 7.54 (dd, 2H, J_{AB} = 7.8 Hz, J_{AC} = 1.6 Hz, H_A), 7.09 (d, 1H, J_{GH} = 6.7 Hz, H_G), 6.71 (dd, 1H, J_{HG} = 6.7 Hz, J_{HI} = 2.8 Hz, H_H), 6.55 (td, 2H, J_{CB} = J_{CD} = 6.5 Hz, J_{CA} = 1.6 Hz, H_C), 4.23 (s, 3H, H_N), 3.84 (s, 3H, H_M). ^{13}C NMR (125 MHz, DMF-d_7, 298 K): δ 166.9 (C_η), 165.9 (C_δ), 161.1 (C_ε), 160.9 (C_ζ), 158.4 (C_α), 154.9 (C_L), 153.4 (C_D), 151.3 (C_G), 151.3 (C_β), 142.4 (C_γ), 133.8 (C_B), 129.6 (C_F), 128.3 (C_A), 120.8 (C_E), 116.5 (C_C), 115.6 (C_K), 112.9 (C_H), 111.0 (C_J), 111.0 (C_I), 57.1 (C_N), 56.7 (C_M). MALDI(+)-MS (DCM): *m/z* 651 $[M]^+$, 616 $[M\text{-}Cl]^+$.

Synthesis of Ru^{II}(bid)(4,4'-$(COOEt)_2$-bpy)Cl·LiCl (1w·LiCl)

To a mixture of 100 mg (0.197 mmol) of Ru(HBid)Cl_3 and 71.2 mg (0.237 mmol) of 4,4'-ethoxycarbonyl-2,2'-bipyridine were dissolved in 20 mL of ethanol. After the mixture was heated to reflux for 1 h, 45.6 mg (1.08 mmol) of LiCl and 100 μL (0.718 mmol) of triethylamine were added. The mixture was heated to reflux for 4 h. After cooling to room temperature the resulting solution was kept in the freezer overnight. The precipitate obtained was separated by filtration and cleaned with diethyl ether. Yield. 65.2 mg (0.0887 mmol), 45.0%. Anal. Calcd. for $C_{34}H_{28}Cl_2LiN_7O_4Ru$: C, 52.52, H, 3.63; N, 12.61. Found: C, 52.34; H, 3.64; N, 12.48. ^{1}H NMR (400 MHz, DMF-d_7, 298 K): δ 10.56 (d, 1H, J_{LK} = 5.9 Hz, H_L), 9.32 (s, 1H, H_J), 9.01 (s, 1H, H_I), 8.50 (d, 1H, J_{KL} = 5.9 Hz, H_K),

8.16 (dd, 2H, J_{EF} = 5.4 Hz, $J_{EF'}$ = 3.0 Hz, H_E), 8.04 (d, 1H, J_{GH} = 6.2 Hz, H_G), 7.74 (dd, 2H, J_{FE} = 5.4 Hz, $J_{FE'}$ = 3.0 Hz, H_F), 7.61 (ddd, 2H, J_{BA} = 7.8 Hz, J_{BC} = 6.3 Hz, J_{BD} = 1.3 Hz, H_B), 7.53 (d, 1H, J_{HG} = 6.2 Hz, H_H), 7.48 (dd, 2H, J_{AB} = 7.8 Hz, J_{AC} = 1.4 Hz, H_A), 7.42 (dd, 2H, J_{DC} = 6.3 Hz, J_{DB} = 1.3 Hz, H_D), 6.58 (td, 2H, J_{CB} = J_{CD} = 6.3 Hz, J_{CA} = 1.4 Hz, H_C), 4.58 (q, 2H, J_{OP} = 7.1 Hz, H_O), 4.31 (q, 2H, J_{MN} = 7.1 Hz, H_M), 1.50 (t, 3H, J_{PO} = 7.1 Hz, H_P), 1.29 (t, 3H, J_{NM} = 7.1 Hz, H_N). ^{13}C NMR (100 MHz, DMF-d_7, 298 K): δ 165.1 (C_ι), 164.5 (C_θ), 161.6 (C_ε), 161.2 (C_ζ), 158.0 (C_α), 155.6 (C_L), 153.7 (C_β), 153.0 (C_D), 152.2 (C_G), 141.9 (C_γ), 136.3 (C_η), 135.7 (C_B), 135.1 (C_δ), 130.3 (C_F), 128.2 (C_A), 127.4 (C_K), 125.1 (C_H), 124.0 (C_J), 123.4 (C_I), 121.3 (C_E), 118.0 (C_C), 62.9 (C_O), 62.5 (C_M), 14.4 (C_P), 14.2 (C_N). MALDI(+)-MS (DCM): *m/z* 735 $[M]^+$, 700 $[M\text{-}Cl]^+$.

Generation of ruthenium hydride (1-H) species and ruthenium formate species (1-OCHO).

To a gas tight NMR tube 0.3 mL of 16.9 mM dry DMF-d_7 solution of complex **1** (5.0 μmol), 0.2 mL of 250 mM dry DMF-d_7 solution of $NaBH_4$ (50 μmol, 10 eq.) and 0.1 mL of 54.6 mM DMF-d_7 solution of Cp_2Fe (5.5 μmol, as internal standard) were added. This reaction was monitored every 10 min for 130 min by ^{1}H NMR spectroscopy at 65 °C. After 130 min, reaction mixture was cooled down to room temperature and 1 bar of CO_2 was introduced. The colour of reaction mixture immediately turned dark green to dark blue green. ^{1}H NMR (500 MHz, DMF-d_7, 338 K) for Ru-H species (**1-H**): δ 10.11 (d, 1H), 8.65 (d, 1H), 8.48 (d, 1H), 8.16 (br, 2H), 8.03 (overlapped with the signal of DMF, 1H), 7.91 (br d, 2H), 7.68- (m, 2H), 7.55 (br, 2H), 7.45 (t, 2H), 7.36 (br, 2H), 7.17 (br d, 1H), 7.11 (br t, 1H), 6.18 (td, 1H), -8.48 (s, 1H, Ru-*H*). ^{1}H NMR (500 MHz, DMF-d_7, 298 K) for Ru-O-CHO species (**1-O-CHO**): δ 9.76 (d, 1H), 8.90 (d, 1H), 8.59 (d, 1H), 8.37 (overlapped with unknown product derived from $NaBH_4$ with CO_2, 1H), 8.21 (dd, 2H), 8.11 (t, 1H), 7.75 (dd, 2H), 7.7-7.6 (m, 5H) , 7.57 (d, 2H), 7.45 (d, 1H), 7.25 (s, 1H, Ru-OC*H*O), 7.06 (t, 1H), 6.63 (td, 2H).

UNIVERSITAT ROVIRA I VIRGILI
SECOND-ROW TRANSITION-METAL COMPLEXES RELEVANT TO CO2 REDUCTION AND WATER OXIDATION
Takashi Ono
DL:T 1108-2014

Alternative method for the direct generation of ruthenium formate species (1-OCHO) from complex 1.

To a gas tight NMR tube 2.0 mg (3.4 μmol) of complex **1**, 1.1 mg (17 μmol) of NaOCHO and 0.6 mL of DMF-d_7 were added. This reaction mixture was heated to 80 °C for 20 hours. 18% of complex **1** converted to formate species (**1-OCHO**).

Standard procedure for catalytic hydrogenative CO_2 reduction

Method A: HEL multi reactor: Catalytic reactions were run with a HEL multireactor autoclave which consists on a cylindrical vessel (7.5 cm of diameter and 15 cm high in 316ss), it has drilled holes to take 24 vials (10 mm diameter x 75 mm high). A cover is placed over the 24 vials, acting as a condenser to prevent solvent loss. This cover has fittings to allow active flow of coolant and also "cold fingers" to ensure refluxing (All wetted parts are made of 316ss). This cover is secured to the base with a screw-on ring. In each vial of the reactor 0.8 mL of complex solution were added and in the cases using 0.1 mL of amine. After having all the solvents and reagents distributed in all the tubes, the multireactor was closed and degassed three times with nitrogen gas. After that, the autoclave's lid was cooled to 5 ºC (and was kept at this temperature during the reaction with an oil circulation bath) and the reactor was introduced to an oil bath previously heated at the desired temperature. At that moment stirring at 500 rpm also started and was considered to be the initial time of the reaction. To stop the reaction the multireactor was cooled with an ice bath and the temperature of the reactor's lid warmed to 25 ºC. The whole reactor was depressurized and this was considered the final time of the reaction. The samples were analyzed by ^{1}H NMR, taking 0.2 mL of the reaction solution and mixing with them with 0.25 mL of D_2O containing DMF as internal standard (120 μL in 10 mL). Three replicates were performed for each measurement. **Method B: SPR16 Slurry Phase Reactor (parallel autoclave system):** Catalytic reactions were run with an SPR16 Slurry Phase Reactor which is a completely automated reactor system consisting 16 autoclaves (15 mL). Once programme started, firstly leak test for each autoclave was done and then each reactor was purged with nitrogen gas. Afterwards, into each autoclave of the reactor 4.0 mL (solvent/amine =

9/1) of complex solution were added from top of the vessel under flow of nitrogen gas. After having all the solvents and reagents distributed in all the vessels, stirring at 1000 rpm started, followed by pressurizing with CO_2 gas and then H_2 gas at the desired pressures. After this, temperature was increased to the desired temperature. When reached at desired temperature, that moment was considered to be the initial time. After the reaction time, each reactor was cooled down to room temperature and depressurized. When started cooling, that moment was considered to be the final time of the reaction. . The samples were analyzed by ^{1}H NMR, taking 0.3 mL of the reaction solution and mixing with them with 0.2 mL of D_2O containing DMF as internal standard (120 μL in 10 mL). Two replicates were performed for each measurement.

Instrumentation and measurements

Cyclic voltammetric (CV) experiments were performed in a IJ-Cambria IH-660 potentiostat, using a three electrode cell. Glassy carbon disk electrodes (3 mm diameter) from BASi were used as working electrode, platinum disk as auxiliary and SSCE as the reference electrode. Cyclic voltammograms were recorded at 100 mV/s scan rate under nitrogen atmosphere. The complexes were dissolved in previously degassed dichloromethane containing the necessary amount of (n-Bu_4N)(PF_6), used as supporting electrolyte, to yield a 0.1 M ionic strength solution. All $E_{1/2}$ values reported in this work were estimated from cyclic voltammetry as the average of the oxidative and reductive peak potentials ($E_{p,a}$+$E_{p,c}$)/2. Unless explicitly mentioned the concentration of the complexes were approximately 1 mM. The NMR spectroscopy was performed on Bruker Avance 400 MHz Bruker Avance II and Bruker Avance 500 MHz. The MALDI mass spectroscopy experiments were performed on a Waters Micromass LCT Premier equipment, respectively. UV-Vis spectroscopy was performed on a Cary bio 50 UV-vis spectrophotometer with 1 cm quartz cells.

X-Ray structure determination

Crystals for complex **1** were grown by slow diffusion of diethyl ether into a solution of complex in dichloromethane. CCDC 833745 contains the supplementary

UNIVERSITAT ROVIRA I VIRGILI
SECOND-ROW TRANSITION-METAL COMPLEXES RELEVANT TO CO2 REDUCTION AND WATER OXIDATION
Takashi Ono
DL:T 1108-2014

crystallographic data for complex **1**. These data can be obtained free of charge from the Cambridge Crystallographic Data Centre via www.ccdc.cam.ac.uk/data_request/cif. The measured crystals were prepared under inert conditions immersed in perfluoropolyether as protecting oil for manipulation. The measured crystals were mounted using a nylon loop directly from the crystallization solution to the diffractometer equipped with an APPEX 2 4K CCD area detector, a FR591 rotating anode with MoK_{α} radiation, Montel mirrors as monochromator and a Kryoflex low temperature device (*T* = -173 °C). Full-sphere data collection was used with ω and φ scans. *Programs used*: Data collection Apex-2[28]; data reduction, Bruker Saint V/.60 A[4] [29]; absorption correction, SADABS[30]; structure solution and refinement, SHELXTL[31].

Computational Details

All geometries were fully optimized at the M06-L level[32] of density functional theory with the Gaussian 09 electronic structure program suite[33] using the Stuttgart [8s7p6d2f | 6s5p3d2f] ECP28MWB contracted pseudopotential basis set on Ru,[34] the MIDI! basis set[35] on nitrogen-based ligands and the 6-31G(d) basis set on all the other atoms.[36] Integral evaluation made use of the grid defined as ultrafine in the Gaussian 09 program. The nature of all stationary points was verified by analytic computation of vibrational frequencies, which were also used for the computation of zero-point vibrational energies and molecular partition functions for use in computing 298 K thermal contributions to free energy.[37] Solvent effects of 2,2,2-trifluoroethanol were included with the SMD continuum solvation model.[38] The energies were subsequently computed with a larger basis set using the same basis set on Ru[34] but the 6-311+G(2df,2p) basis set on all other atoms.[36] Ethyl groups of -COOEt substituents and in NEt_3 were modeled as methyl groups for efficiency.

III-1.6. Acknowledgements

Support form SOLAR-H2 (EU 212508), ACS (PRF 46819-AC3), MEC (CTQ2007-67918 and CTQ2008-06866-CO2-02), US NSF (CHE09-52054), and from the Consolider Ingenio

UNIVERSITAT ROVIRA I VIRGILI
SECOND-ROW TRANSITION-METAL COMPLEXES RELEVANT TO CO2 REDUCTION AND WATER OXIDATION
Takashi Ono
DL:T 1108-2014

2010 (CSD2006-0003) are gratefully acknowledged. TO thanks MINECO for a doctoral grant.

I have carried out a part of synthesis, characterization and kinetic analyses. A part of catalytic experiments was carried out by Nora Planas as her Ph.D. thesis in the group of A. Llobet at the Institute of Chemical Research of Catalonia (ICIQ). DFT calculations were performed by Dr. P. Miro in the group of Prof. C. J. Cramer at the University of Minnesota and Nora Planas during her short stay in the group of Prof. Laura Gagliardi at the University of Minnesota. X-ray structure analyses were carried out by Dr. Jordi Benet-Buchholz at ICIQ.

III-1.7. References

(1) Canadell, J. G.; Le Quéré, C.; Raupach, M. R.; Field, C. B.; Buitenhuis, E. T.; Ciais, P.; Conway, T. J.; Gillett, N. P.; Houghton, R. A.; Marland, G. *Proc. Natl. Acad. Sci. U.S.A.* **2007**, *104*, 18866-18870.
(2) Karl, T. R.; Trenberth, K. E. *Science* **2003**, *302*, 1719-1723.
(3) Raupach, M. R.; Marland, G.; Ciais, P.; Le Quéré, C.; Canadell, J. G.; Klepper, G.; Field, C. B. *Proc. Natl. Acad. Sci. U.S.A.* **2007**, *104*, 10288-10293.
(4) Federsel, C.; Jackstell, R.; Beller, M. *Angew. Chem., Int. Ed.* **2010**, *49*, 6254-6257.
(5) Jessop, P. G. In *The Handbook of Homogeneous Hydrogenation*; Wiley-VCH Verlag GmbH: 2008, p 489-511.
(6) Jessop, P. G.; Joó, F.; Tai, C.-C. *Coord. Chem. Rev.* **2004**, *248*, 2425-2442.
(7) Hutschka, F.; Dedieu, A.; Eichberger, M.; Fornika, R.; Leitner, W. *J. Am. Chem. Soc.* **1997**, *119*, 4432-4443.
(8) Gassner, F.; Leitner, W. *J. Chem. Soc., Chem. Commun.* **1993**, 1465-1466.
(9) Angermund, K.; Baumann, W.; Dinjus, E.; Fornika, R.; Görls, H.; Kessler, M.; Krüger, C.; Leitner, W.; Lutz, F. *Chem. —Eur. J.* **1997**, *3*, 755-764.
(10) Tanaka, R.; Yamashita, M.; Nozaki, K. *J. Am. Chem. Soc.* **2009**, *131*, 14168-14169.
(11) Ng, S. M.; Yin, C.; Yeung, C. H.; Chan, T. C.; Lau, C. P. *Eur. J. Inorg. Chem.* **2004**, *2004*, 1788-1793.
(12) Himeda, Y.; Onozawa-Komatsuzaki, N.; Sugihara, H.; Kasuga, K. *Organometallics* **2007**, *26*, 702-712.
(13) Jessop, P. G.; Hsiao, Y.; Ikariya, T.; Noyori, R. *J. Am. Chem. Soc.* **1996**, *118*, 344-355.
(14) Munshi, P.; Main, A. D.; Linehan, J. C.; Tai, C.-C.; Jessop, P. G. *J. Am. Chem. Soc.* **2002**, *124*, 7963-7971.
(15) Sala, X.; Santana, N.; Serrano, I.; Plantalech, E.; Romero, I.; Rodríguez, M.; Llobet, A.; Jansat, S.; Gómez, M.; Fontrodona, X. *Eur. J. Inorg. Chem.* **2007**, *2007*, 5207-5214.
(16) Serrano, I.; Sala, X.; Plantalech, E.; Rodríguez, M.; Romero, I.; Jansat, S.; Gómez, M.; Parella, T.; Stoeckli-Evans, H.; Solans, X.; Font-Bardia, M.; Vidjayacoumar, B.; Llobet, A. *Inorg. Chem.* **2007**, *46*, 5381-5389.
(17) Masllorens, E.; Rodríguez, M.; Romero, I.; Roglans, A.; Parella, T.; Benet-Buchholz, J.; Poyatos, M.; Llobet, A. *J. Am. Chem. Soc.* **2006**, *128*, 5306-5307.

UNIVERSITAT ROVIRA I VIRGILI
SECOND-ROW TRANSITION-METAL COMPLEXES RELEVANT TO CO2 REDUCTION AND WATER OXIDATION
Takashi Ono
DL:T 1108-2014

(18) Creutz, C.; Chou, M. H. *J. Am. Chem. Soc.* **2007**, *129*, 10108-10109.
(19) Creutz, C.; Chou, M. H. *J. Am. Chem. Soc.* **2009**, *131*, 2794-2795.
(20) Creutz, C.; Chou, M. H.; Hou, H.; Muckerman, J. T. *Inorg. Chem.* **2010**, *49*, 9809-9822.
(21) Konno, H.; Kobayashi, A.; Sakamoto, K.; Fagalde, F.; Katz, N. E.; Saitoh, H.; Ishitani, O. *Inorg. Chim. Acta* **2000**, *299*, 155-163.
(22) Yang, X. *ACS Catal.* **2011**, *1*, 849-854.
(23) Urakawa, A.; Jutz, F.; Laurenczy, G.; Baiker, A. *Chem. —Eur. J.* **2007**, *13*, 3886-3899.
(24) Urakawa, A.; Iannuzzi, M.; Hutter, J.; Baiker, A. *Chem. —Eur. J.* **2007**, *13*, 6828-6840.
(25) Gagne, R. R.; Marritt, W. A.; Marks, D. N.; Siegl, W. O. *Inorg. Chem.* **1981**, *20*, 3260-3267.
(26) Marks, D. N.; Siegl, W. O.; Gagne, R. R. *Inorg. Chem.* **1982**, *21*, 3140-3147.
(27) Rasmussen, S. C.; Ronco, S. E.; Mlsna, D. A.; Billadeau, M. A.; Pennington, W. T.; Kolis, J. W.; Petersen, J. D. *Inorg. Chem.* **1995**, *34*, 821-829.
(28) *Data collection with APEX II* versions v1.0-22, v2009.1-0 and v2009.1-02, Bruker AXS inc., Madison, Wisconsin, USA, **2007**
(29) *Data reduction with Bruker SAINT* versions V.2.10(2003), V/.60A and V7.60A, Bruker AXS inc., Madison, Wisconsin, USA, **2007**
(30) *SADABS:* V.2.10(2003); V2008 and V2008/1, Bruker AXS inc., Madison, Wisconsin, USA, **2001**
(31) Sheldrick, G. M. *Acta Crystallogr. Sect. A* **2008**, *64*, 112-122.
(32) Zhao, Y.; Truhlar, D. G. *J. Chem. Phys.* **2006**, *125*, 194101.
(33) Gaussian 09, Revision A.1, Frisch, M. J.; Trucks, G. W.; Schlegel, H. B.; Scuseria, G. E.; Robb, M. A.; Cheeseman, J. R.; Scalmani, G.; Barone, V.; Mennucci, B.; Petersson, G. A.; Nakatsuji, H.; Caricato, M.; Li, X.; Hratchian, H. P.; Izmaylov, A. F.; Bloino, J.; Zheng, G.; Sonnenberg, J. L.; Hada, M.; Ehara, M.; Toyota, K.; Fukuda, R.; Hasegawa, J.; Ishida, M.; Nakajima, T.; Honda, Y.; Kitao, O.; Nakai, H.; Vreven, T.; Montgomery, J., J. A.; Peralta, J. E.; Ogliaro, F.; Bearpark, M.; Heyd, J. J.; Brothers, E.; Kudin, K. N.; Staroverov, V. N.; Kobayashi, R.; Normand, J.; Raghavachari, K.; Rendell, A.; Burant, J. C.; Iyengar, S. S.; Tomasi, J.; Cossi, M.; Rega, N.; Millam, J. M.; Klene, M.; Knox, J. E.; Cross, J. B.; Bakken, V.; Adamo, C.; Jaramillo, J.; Gomperts, R.; Stratmann, R. E.; Yazyev, O.; Austin, A. J.; Cammi, R.; Pomelli, C.; Ochterski, J. W.; Martin, R. L.; Morokuma, K.; Zakrzewski, V. G.; Voth, G. A.; Salvador, P.; Dannenberg, J. J.; Dapprich, S.; Daniels, A. D.; Farkas, Ö.; Foresman, J. B.; Ortiz, J. V.; Cioslowski, J.; Fox, D. J., Gaussian, Inc., Wallingford CT, 2009.
(34) Andrae, D.; Häußermann, U.; Dolg, M.; Stoll, H.; Preuß, H. *Theoret. Chim. Acta* **1990**, *77*, 123-141.
(35) Easton, R. E.; Giesen, D.; Welch, A.; Cramer, C.; Truhlar, D. *Theoret. Chim. Acta* **1996**, *93*, 281-301.
(36) Hehre, W. J.; Radom, L.; Schleyer, P. v. R.; Pople, J. *Ab Initio Molecular Orbital Theory*; Wiley: New York, 1986.
(37) Cramer, C. J. *Essentials of Computational Chemistry: Theories and Models*; 2nd ed.; Wiley: Chichester, 2004.
(38) Marenich, A. V.; Cramer, C. J.; Truhlar, D. G. *J. Phys. Chem. B* **2009**, *113*, 6378-6396.

UNIVERSITAT ROVIRA I VIRGILI
SECOND-ROW TRANSITION-METAL COMPLEXES RELEVANT TO CO2 REDUCTION AND WATER OXIDATION
Takashi Ono
DL:T 1108-2014

Supporting Information for:

Carbon Dioxide Reduction Catalyzed by Mononuclear Ruthenium Polypyridyl Complexes

Table of contents

UNIVERSITAT ROVIRA I VIRGILI
SECOND-ROW TRANSITION-METAL COMPLEXES RELEVANT TO CO2 REDUCTION AND WATER OXIDATION
Takashi Ono
DL:T 1108-2014

S1. NMR:

Figure S1. 1D and 2D NMR spectra (500 MHz, 298K, DMF-d_7) for complex **1:** (a) ^{1}H NMR, (b) COSY, and (c) NOESY.

(a)

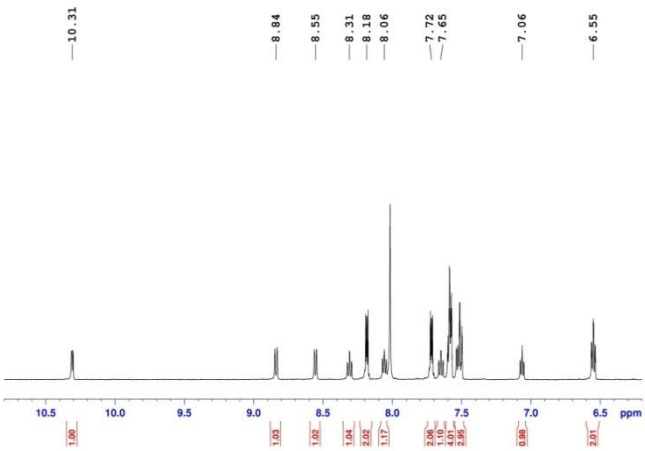

(b)

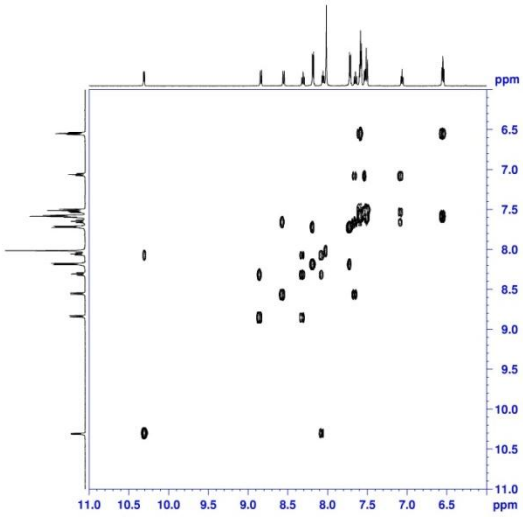

(c)

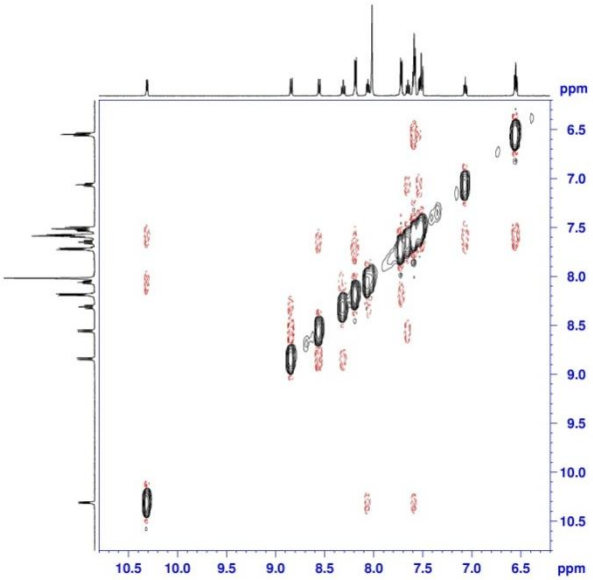

Figure S2. 1D and 2D NMR spectra (500 MHz, 298K, DMF-d_7) for complex **1d:** (a) ^{1}H NMR, (b) COSY, and (c) NOESY.

(a)

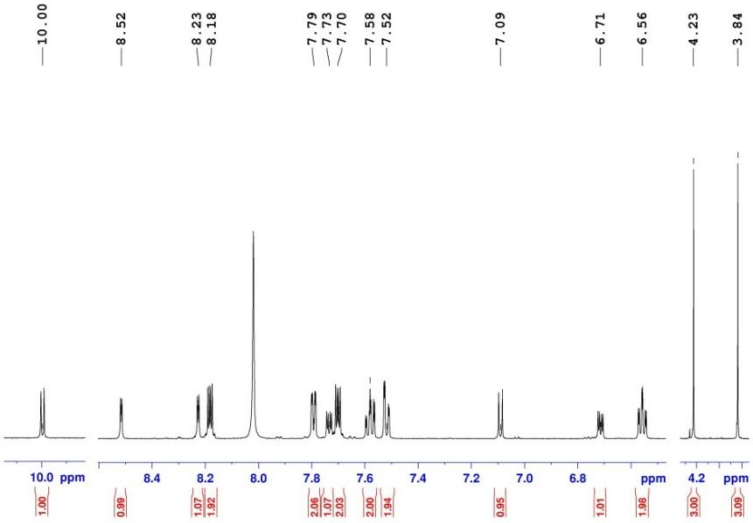

UNIVERSITAT ROVIRA I VIRGILI
SECOND-ROW TRANSITION-METAL COMPLEXES RELEVANT TO CO2 REDUCTION AND WATER OXIDATION
Takashi Ono
DL:T 1108-2014

(b)

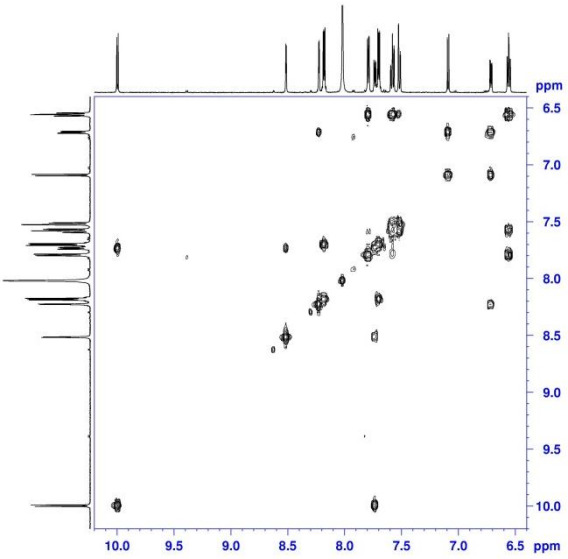

(c)

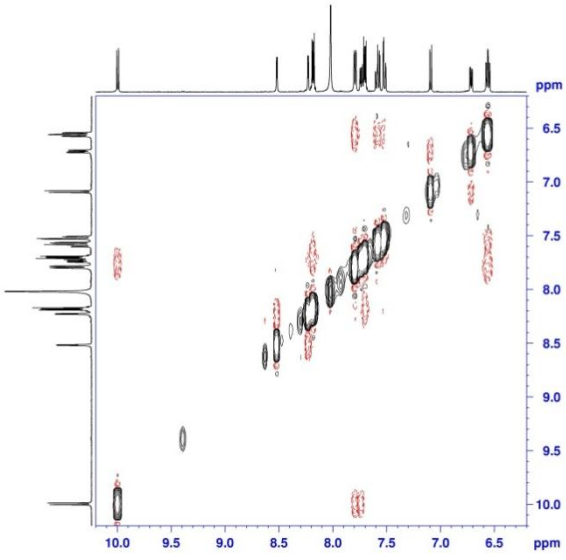

Figure S3. 1D and 2D NMR spectra (400 MHz, 298K, DMF-d_7) for complex **1w:** (a) ^{1}H-NMR, (b) COSY, and (c) NOESY.

(a)

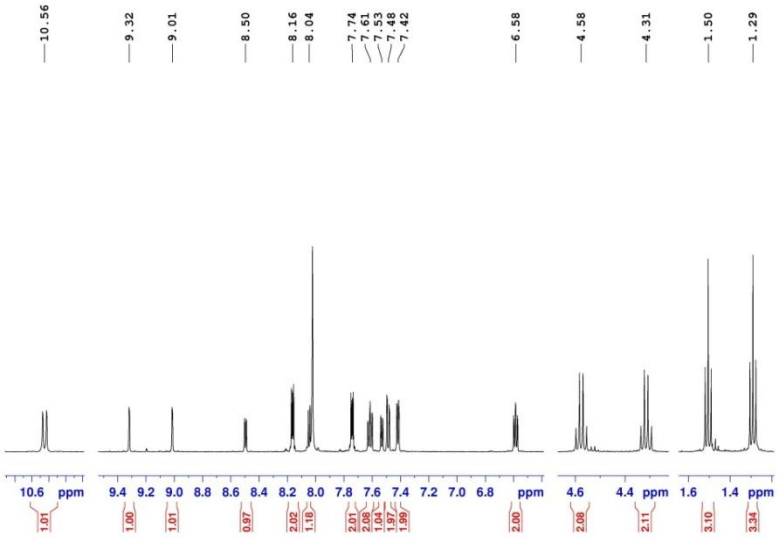

(b)

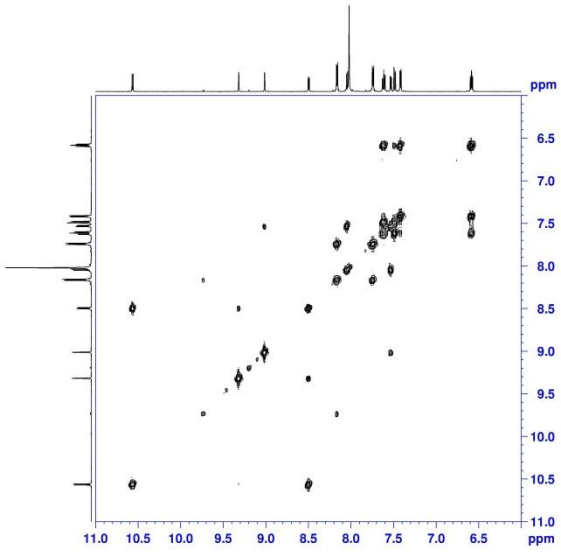

(c)

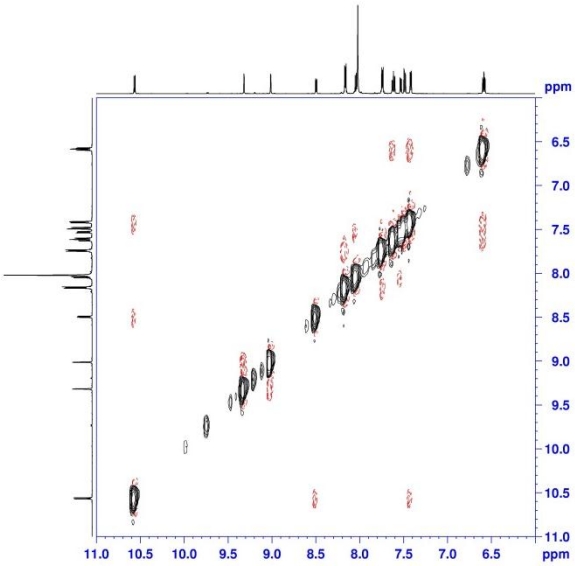
ppm
6.5
7.0
7.5
8.0
8.5
9.0
9.5
10.0
10.5
11.0
11.0 10.5 10.0 9.5 9.0 8.5 8.0 7.5 7.0 6.5
ppm

Figure S4. ^{1}H NMR spectra (500 MHz, 298 K) of reaction mixture of [Ru(bid)(bpy)Cl] (**1**) with 40 equiv. of $NaBH_4$ in DMF-d_7. (a) as mixed, (b) 4 hours at 60 °C, (c) (b)+ 1 hour at 80 °C. (d) (c)+ 1 hour at 80 °C. (e) next day at RT, and (f) free 2,2'-bipyridine.

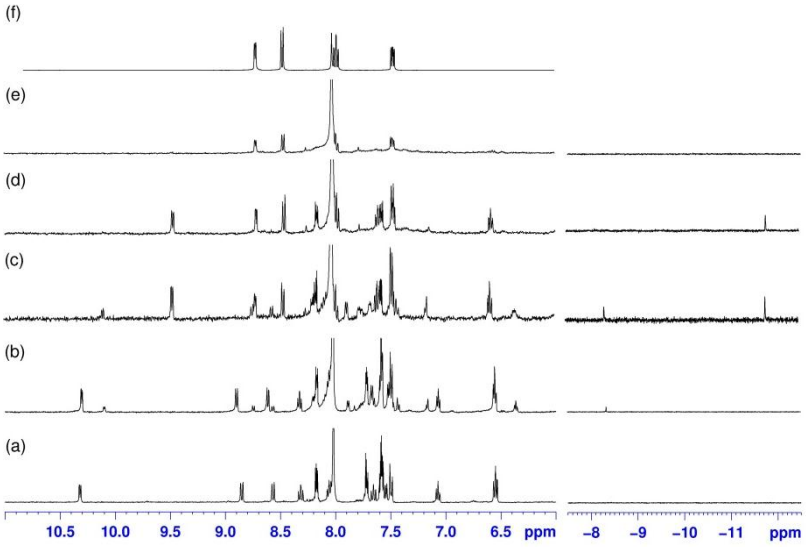

1 partially converted to new species **1-H** which contains one hydride ligand ((a) to (b)). After increased temperature, **1** fully converted to **1-H** and a second hydride species (δ_{Ru-H}: -11.80 ppm) ((b) to (c) and to (d)). After being kept at room temperature overnight, the second hydride species decomposed and free 2,2'-bipyridine was observed. ((d) to (e)). In order to avoid the decomposition process, reaction was further examined at lower temperature (Figure S5).

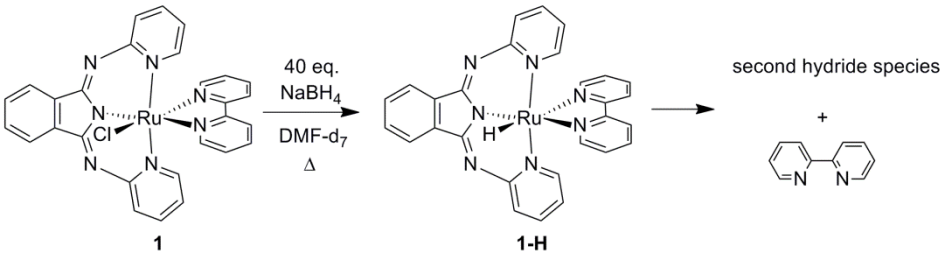

UNIVERSITAT ROVIRA I VIRGILI
SECOND-ROW TRANSITION-METAL COMPLEXES RELEVANT TO CO2 REDUCTION AND WATER OXIDATION
Takashi Ono
DL:T 1108-2014

Figure S5. ^{1}H NMR spectra (500 MHz, 298 K) of reaction mixture of [Ru(bid)(bpy)Cl] (**1)** with 10 equiv. of $NaBH_4$ in DMF-d_7. Top: from 13 ppm to -15 ppm, bottom: aromatic region and hydride region. (A) 0 min at RT. (B) 30 min at 65 °C. (C) 60 min at 65 °C. (D) 90 min at 65 °C. (E) 120 min at 65 °C. *: Ru(bid)(bpy)H (F) after adding CO_2 (1 bar) at RT. ●: Ru(bid)(bpy)(OCHO) (G) Ru(bid)(bpy)Cl with NaOCHO in DMF-d_7. See experimental section for further experimental details.

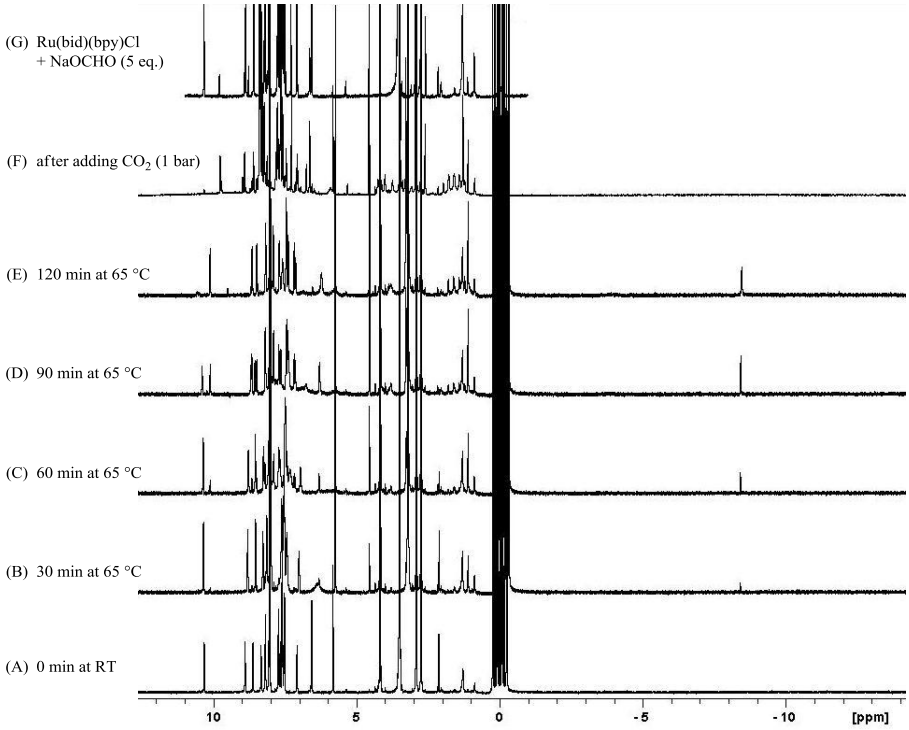

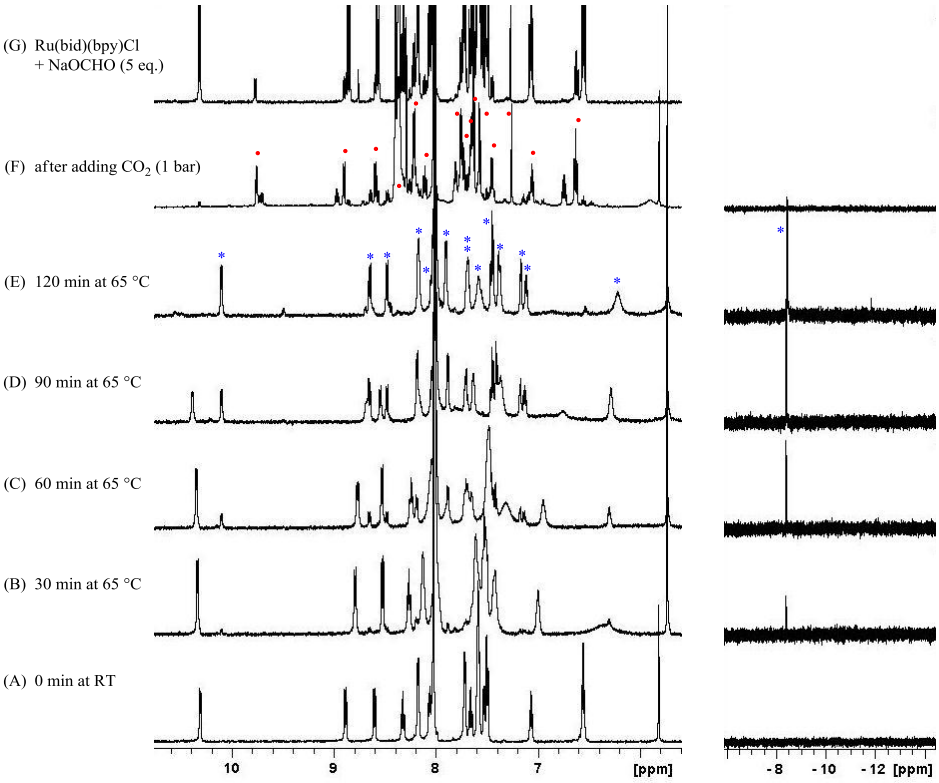
(G) Ru(bid)(bpy)Cl
+ NaOCHO (5 eq.)
(F) after adding CO_2 (1 bar)
(E) 120 min at 65 °C
(D) 90 min at 65 °C
(C) 60 min at 65 °C
(B) 30 min at 65 °C
(A) 0 min at RT
10
9
8
7
[ppm]
-8
-10
-12
[ppm]

Figure S6. COSY spectrum (top) and NOESY spectrum (bottom) of reaction mixture after 130 min reaction time.

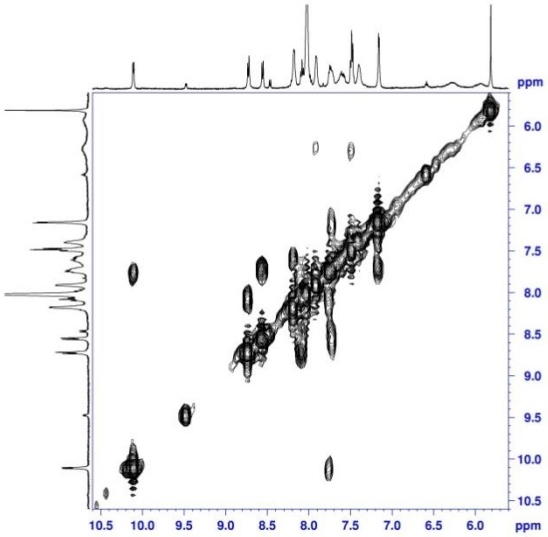

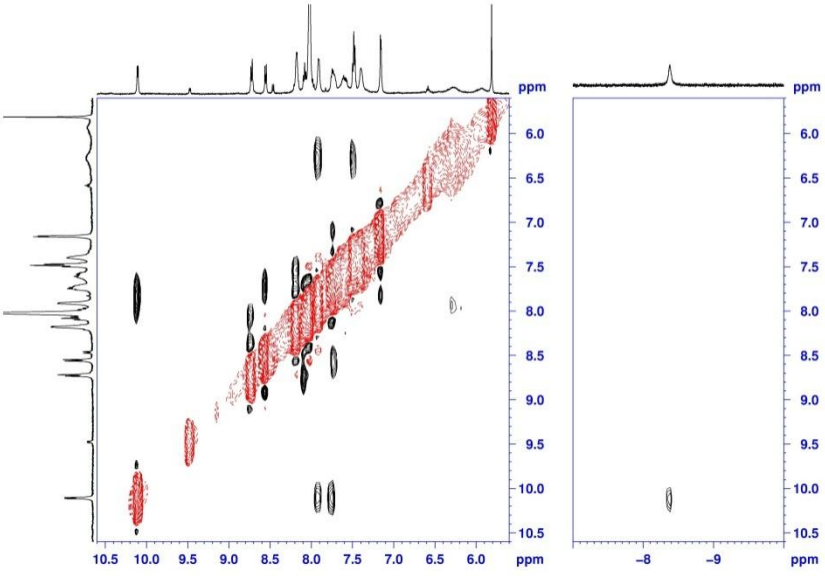

Figure S7. Catalytic example: ^{1}H NMR spectrum of aliquot solution in D_2O after catalytic reaction (using 0.3 mM of complex **1**, CO_2 25 bar and H_2 25 bar at 100 °C for 20 min).

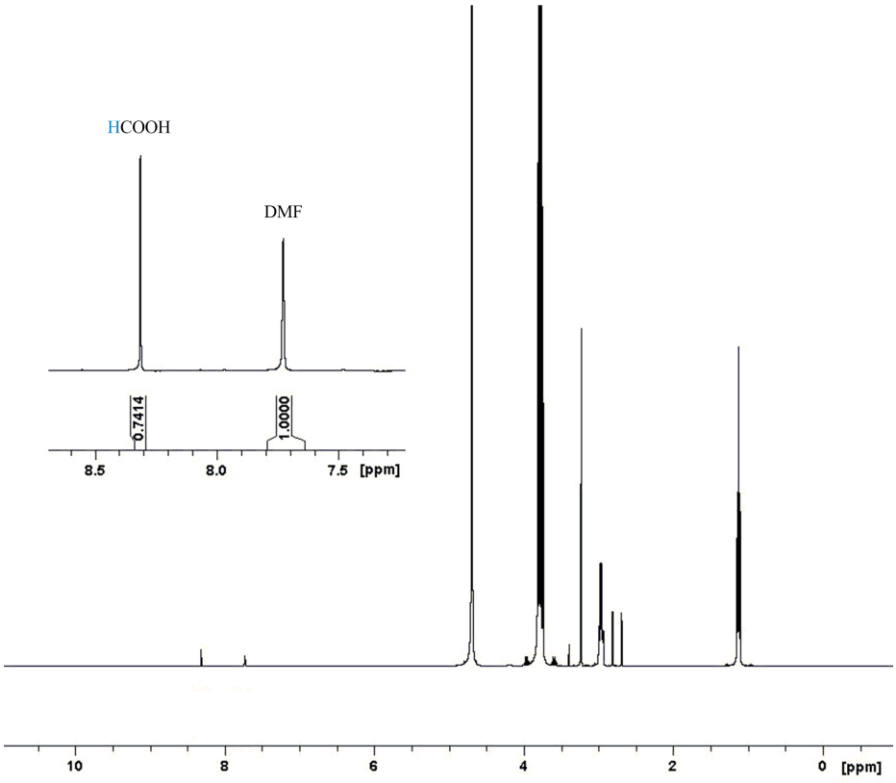

S2. Kinetic measurements:

Figure S8. Left: Formation of formic acid at different precatalyst concentrations with respect to time (complex **1**, 25 bar of CO_2, 25 bar of H_2, 100 °C). Right: Initial rates with respect to precatalyst concentration. (complex **1**, 25 bar of CO_2, 25 bar of H_2, 100 °C)

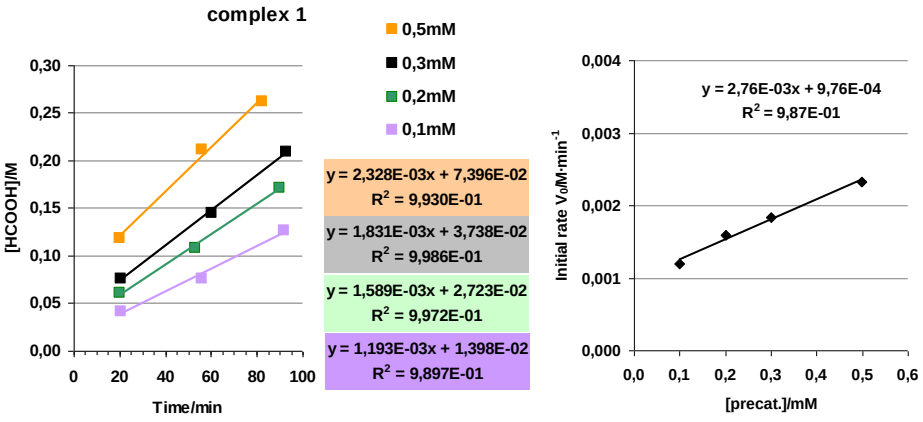

Figure 9. Left: Formation of formic acid at different H_2 pressures with respect to time (0.3 mM of complex **1**, 25 bar of CO_2, 100 °C). ■: 15 bar of H_2, ■: 25 bar of H_2, ■: 35 bar of H_2, ■: 45 bar of H_2 Right: Initial rates with respect to partial pressure of H_2. (0.3 mM of complex **1**, 25 bar of CO_2, 100 °C)

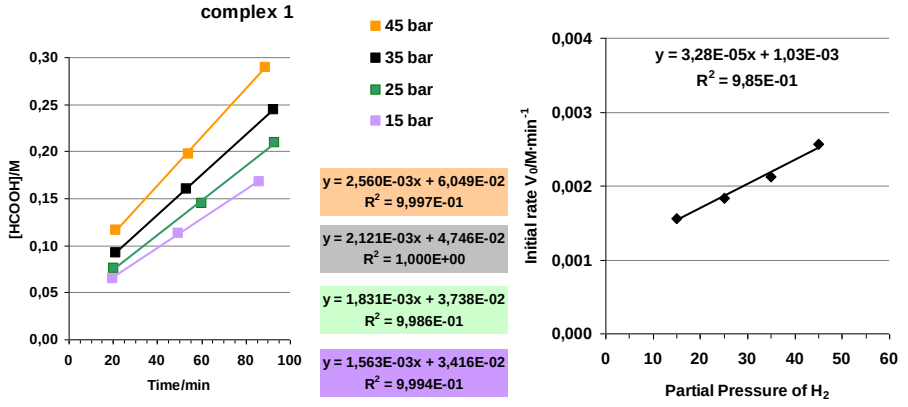

Figure S10. Left: Formation of formic acid at different CO_2 pressures with respect to time (0.3 mM of complex **1**, 25 bar of H_2, 100 °C). ■: 10 bar of CO_2, ■: 25 bar of CO_2, ■: 35 bar of CO_2. Right: Initial rates with respect to partial pressure of CO_2. (0.3 mM of complex **1**, 25 bar of H_2, 100 °C)

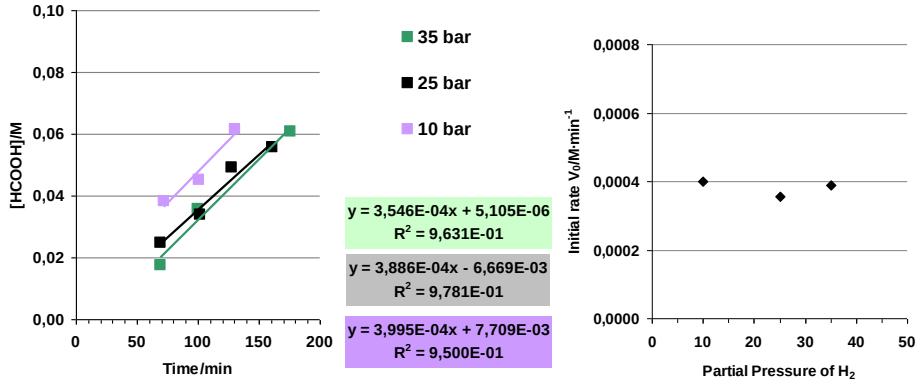

Figure S11. Left: Formation of formic acid at different precatalyst concentrations with respect to time (complex **2**, 25 bar of CO_2, 25 bar of H_2, 100 °C). ■: 0.1 mM, ■: 0.2 mM, ■: 0.3 mM, ■: 0.5 mM. Right: Initial rates with respect to precatalyst concentration. (complex **2**, 25 bar of CO_2, 25 bar of H_2, 100 °C).

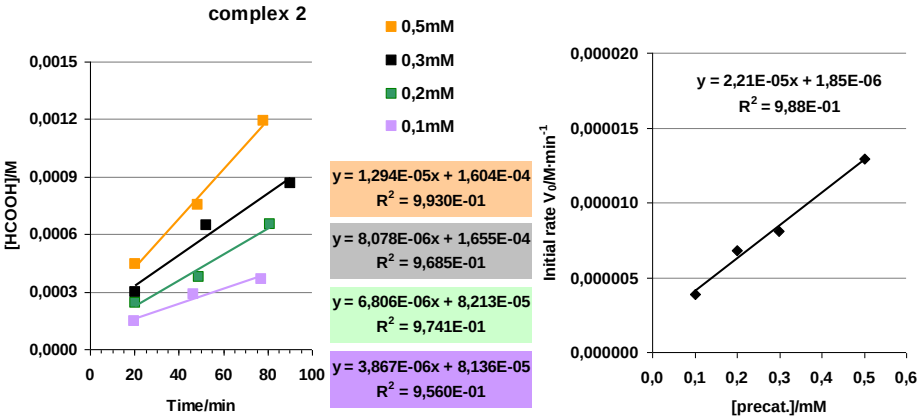

S4. Electrochemistry:

Figure S12. Cyclic voltammograms vs SSCE at a scan rate 100 mV/s in DCM-TBAH (0.1 M), of complex (a) **1**, (b) **1d**, (c) **1w**, (d) **2.**

(a)

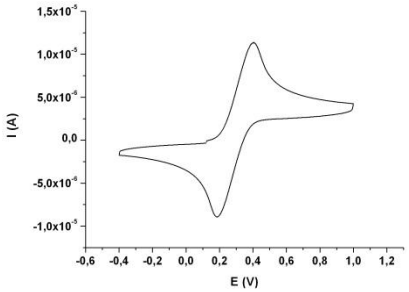

(b)

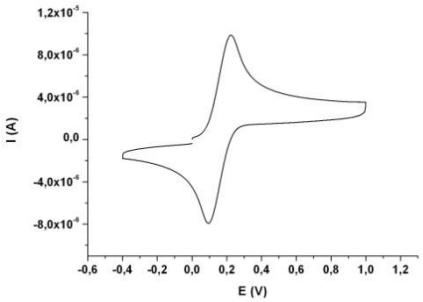

(c)

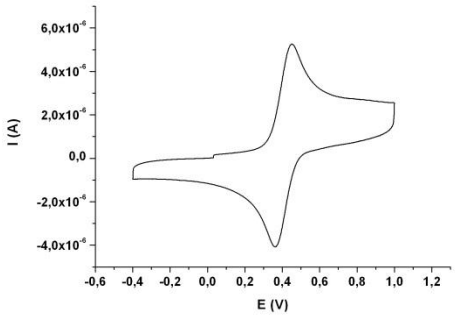

(d)

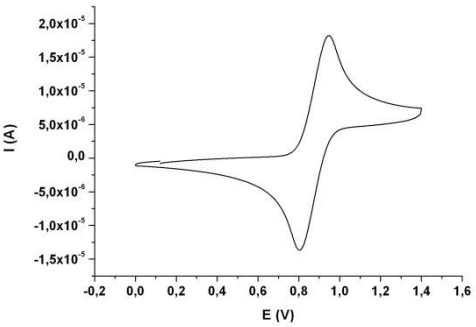

S5. DFT calculations:

Table S1. Gibbs Free energies at the M06-L DFT level of theory of the different steps in the catalytic cycle for compounds **1**, **1d**, **1d'**, **1w**, **1w'** and **2**. Energies in kcal/mol.

	1w	**1w'**	**1**	**1d'**	**1d**	**2**
II	-8.78	-7.70	-9.39	-11.66	-9.60	-9.78
II-a	11.12	10.93	10.19	7.3	9.00	12.23
II-b	-4.32	-4.79	-5.91	-6.33	-4.93	-1.07
II-c	-15.58	-13.83	-13.67	-12.63	-13.68	-20.94
III	12.00	13.23	11.03	10.60	10.45	22.62
III-a	11.47	11.28	11.75	---	---	---
III-b	1.27	0.76	0.28	---	---	---
III-c	-0.74	1.19	-1.00	0.24	-0.72	-1.05
IV-O	3.04	0.72	4.62	7.31	5.41	-4.70
IV-a-O	4.57	5.90	7.97	8.84	9.55	2.53
IV-b-O	-1.53	-5.18	-3.35	-1.52	-4.14	-7.23
IV-N	1.80	-1.14	3.38	3.43	3.48	-5.94
IV-a-N	8.44	6.06	8.78	9.42	9.88	7.42
IV-b-N	6.64	-6.58	-5.40	-3.35	-5.71	-13.36
IV-ON	-1.81	-4.13	-0.23	2.47	0.57	-9.54
$\Delta G^{\neq}_1$	11.12	10.24	10.19	7.30	9.00	12.23
$\Delta G^{\neq}_2$	16.56	19.13	19.00	19.43	22.00	25.16

Figure S13. Computed free energy profiles (kcal/mol) for the catalytic cycles of compounds derived from **1** (red) and $\mathbf{2}^{+}$ (blue).

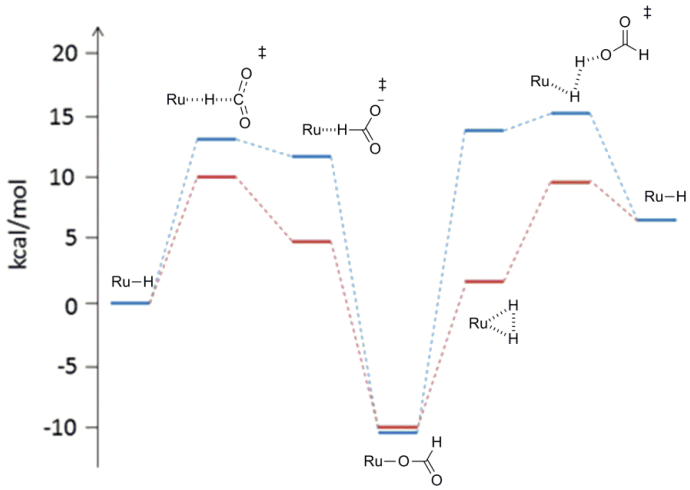

UNIVERSITAT ROVIRA I VIRGILI
SECOND-ROW TRANSITION-METAL COMPLEXES RELEVANT TO CO2 REDUCTION AND WATER OXIDATION
Takashi Ono
DL:T 1108-2014

UNIVERSITAT ROVIRA I VIRGILI
SECOND-ROW TRANSITION-METAL COMPLEXES RELEVANT TO CO2 REDUCTION AND WATER OXIDATION
Takashi Ono
DL:T 1108-2014

Chapter III-2

Carbon Dioxide Reduction Catalyzed by Mononuclear Ruthenium Polypyridyl Complexes: Electronic and Steric Effects

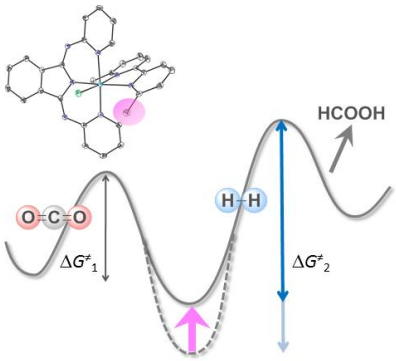

Table of Contents

UNIVERSITAT ROVIRA I VIRGILI
SECOND-ROW TRANSITION-METAL COMPLEXES RELEVANT TO CO2 REDUCTION AND WATER OXIDATION
Takashi Ono
DL:T 1108-2014

III-2.1. Abstract

New mononuclear ruthenium complexes containing tridentate and bidentate polypyridyl ligands have been synthesized and characterized by means of NMR spectroscopy, X-ray crystallography and cyclic voltammetry. Their catalytic performances toward hydrogenative CO_2 reduction were assessed in 2,2,2-trifluoroethanol (TFE) with excess NEt_3. The electronic nature of tridentate and bidentate ligands modulates catalytic activity for hydrogenative CO_2 reduction. A kinetic analysis revealed the relationship between redox potentials for the Ru(III/II) couple and initial turnover frequencies. Furthermore, the influence of steric effect was analysed experimentally and DFT calculations were carried out to clarify the impact of the steric effect in the catalytic process.

III-2.2. Introduction

Carbon dioxide (CO_2) is the primary greenhouse gas and its atmospheric concentration has been rapidly increasing in the last decades because of an increased use of fossil fuels, resulting in global warming[1-2]. Although the contribution of the use of CO_2 toward the decrease of CO_2 emissions is little, the utilization of carbon dioxide (CO_2) as a carbon feedstock is one of the most important areas of the research since CO_2 is abundant, cheap, and non-toxic. In addition, against the depletion of fossil fuels, technologies for carbon neutral energy production are highly desirable. In this regard, the development of the transformation of the thermodynamically stable and kinetically inert CO_2 molecule into liquid or gaseous fuels represents an important challenge.

One promising approach has been the hydrogenative CO_2 reduction catalyzed by transition metal complexes[3-13]. Formic acid is the primary product of the catalytic reaction, and is recognized as a potential hydrogen storage material[14-15]. Recently, the systematic studies based on [Cp*Ir(bpy)Cl]Cl (Cp* = η^5-C_5Me_5, *bpy* = 2,2'-bipyridine) complexes made by Himeda *et al*. showed that the higher the electron donating abilities on 4,4'-R_2-bpy (R = OH as O^- *in situ*, OMe, Me, CO_2H and H) ligand, the higher

UNIVERSITAT ROVIRA I VIRGILI
SECOND-ROW TRANSITION-METAL COMPLEXES RELEVANT TO CO2 REDUCTION AND WATER OXIDATION
Takashi Ono
DL:T 1108-2014

the initial turnover frequencies (TOF_i) obtained.[10] Surprisingly, the catalytic reaction proceeds even in atmospheric pressures of 1:1 mixtures of CO_2:H_2 at 30 °C. Thus, it is of great importance to understand the detailed mechanism.

We previously reported that mononuclear ruthenium-polypyridyl complexes (**1a-c** and **4a**$^+$, see Scheme 1) can catalyze the hydrogenative reduction of CO_2 to formic acid.[12] A kinetic analysis as well as DFT calculations revealed the mechanism for hydrogenative CO_2 reduction and the effect of substituents on the auxiliary ligands.

Here we report an extended study of the hydrogenative CO_2 reduction catalyzed by mononuclear Ru polypyridyl complexes, which consists of the modification of the electronic and steric effects.

III-2.3. Results and Discussion

III-2.3.1. Synthesis, Structure and Redox Properties

Synthesis

Studied complexes for hydrogenative CO_2 reduction are summarized in Scheme 1. Complexes **1a-c**, **4a**$^+$, ***out*-5**$^+$ and ***in*-5**$^+$ were prepared as previously reported from our group[12,16] and others.[17]

New *bid*$^-$ ((1*Z*,3*Z*)-1,3-bis(pyridin-2-ylimino)isoindolin-2-ide) containing complexes **1d-e** and **2** were synthesized in 'one-pot' procedure similarly with those of complexes **1a-c**, that is, by treating Ru(Hbid)Cl_3 with a corresponding ligand in the presence of NEt_3 using EtOH as solvent. However, the purification procedures for **1d-e** were different from **1a-c** and **2**. **1a-c** and **2** are precipitated from the reaction mixture, while higher solubility of **1d-e** in EtOH potentially makes purification difficult (see experimental section).

Complexes **3a-b** containing anionic *dpb*$^-$ (2,6-di(pyridin-2-yl)benzen-1-ide) ligand were synthesized in two steps via the formation of the cyclometalated complex *trans*-[Ru(dpb)(dmso-*s*)$_2$Cl], **6,** as a synthetic intermediate (Scheme 2). The detailed synthetic procedures will be described in Chapter VI. In short, the cyclometalated complex **6** was

Scheme 1. Studied complexes for hydrogenative CO_2 reduction

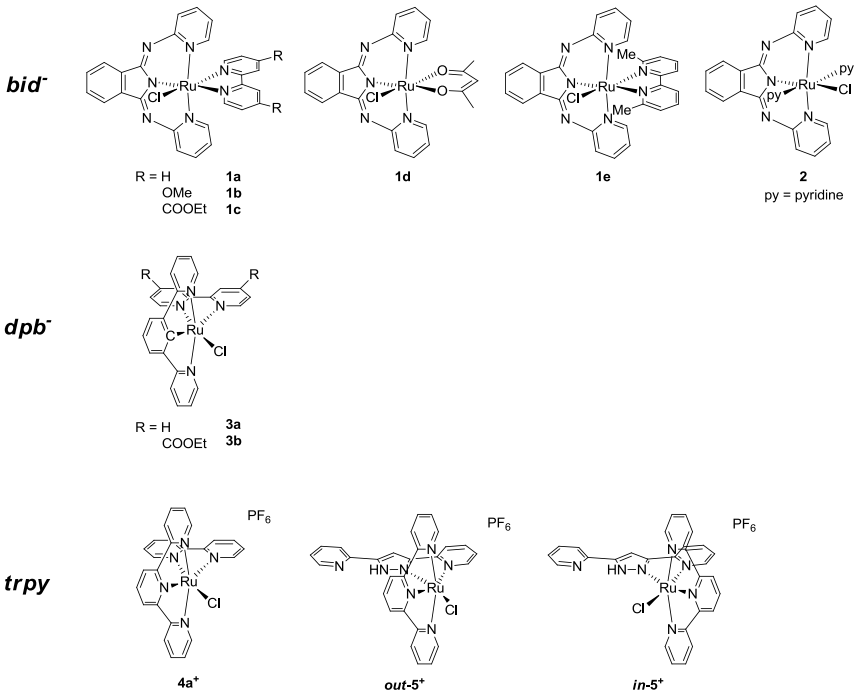

Scheme 2. Synthetic scheme for complexes **3a-b**.

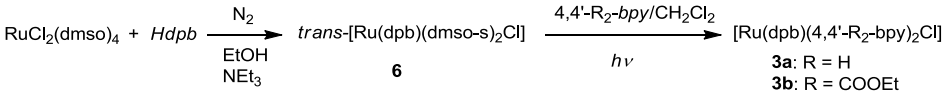

obtained in relatively good yield of 79% by refluxing a mixture of $RuCl_2(dmso)_4$ and *Hdpb* in the presence of NEt_3 Treating **6** with 4,4'-R_2-*bpy* (R = H, COOEt) followed by light irradiation generates neutral Ru-Cl complexes **3a-b**, which were purified by column chromatography using a mixture of dichloromethane and acetone as an eluent to give purple solids.

UNIVERSITAT ROVIRA I VIRGILI
SECOND-ROW TRANSITION-METAL COMPLEXES RELEVANT TO CO2 REDUCTION AND WATER OXIDATION
Takashi Ono
DL:T 1108-2014

Structure

Structural characterization of the new Ru(II) complexes presented in this work was carried out in solution by ^{1}H NMR spectroscopy and in the solid state for **1d** and **1e** based on X-ray diffraction analysis.

Ortep plots for **1d** and **1e** are presented in Figure 1. Selected metric and crystallographic parameters of **1d-e** together with previously reported **1a**[12] are listed in Table 1 and Table S1 in the Supporting Information. In both cases **1d** and **1e** present an octahedral type of geometry with the typical bonding distances expected for a d^5 Ru(III) and d^6 Ru(II) complex respectively.[18] The most interesting feature related to these complexes is the strong distortion suffered by the Ru-Cl bond in **1e**, due to the strong steric effects produced by the Me group at the 6 position of the *bpy* ligand. This is nicely exemplified by the relative angles of the indole type of ligand with regard to that of *bpy*. For ideal octahedral geometry, the angles between those two ligands would be of 90°, and we found a value of 58.4°. The angles between the two pyridyl groups of the *bid*$^-$ ligands also give an indication of the degree of distortion. For ideal octahedral geometry, a 0° value is expected and **1e** presents a value of 34.7° for this angle. This distortion is also manifested in an elongation of Ru-N bond on 6,6'-Me_2-*bpy* by roughly 0.06 Å compared to the more symmetrical **1a**.

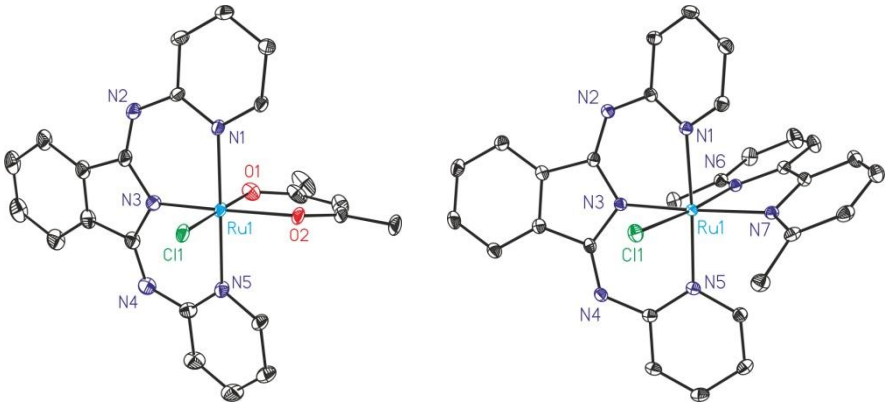

Figure 1. Ortep plots (ellipsoids at 50% probability) of the X-ray crystal structures of **1d** (Left) and **1e** (Right) together with labeling schemes. Color codes: Ru, cyan; N, blue; O, red; Cl, green; C, grey. Hydrogen atoms are not shown for clarity.

UNIVERSITAT ROVIRA I VIRGILI
SECOND-ROW TRANSITION-METAL COMPLEXES RELEVANT TO CO2 REDUCTION AND WATER OXIDATION
Takashi Ono
DL:T 1108-2014

Table 1. Selected Metric Parameters for **1e**, and for Intermediates R-OCHO and TS_2 Related to **1a**, **1e** and **2**. Bond Distances in Å and Angles in deg.

Complex	ph-py[a] (90° ideal)	py-py[b] (0° ideal)	Overall distortion	H-bond/contact[c]	
Ru-Cl, **1e**	58.4	34.7	66.4	2.72/3.18/1.098/109.2 2.91/3.18/1.098/97.2	Cl-HC-Me
Ru-OCHO, **1a**	68.8	27.0	48.2	2.49/3.18/1.089/120.5	O-HC-py
Ru-OCHO, **1e**	51.9	37.7	75.8 (27.6)	2.54/2.95/1.098/100.9 2.53/2.95/1.094/101.6	O-CH-Me
Ru-OCHO, **2**	--	25.3		2.12/2.91/1.086/127.3 2.32/3.05/1.084/123.0 2.58/3.03/1.088/103.4 3.10/3.56/1.088/106.5	O-CH-py
TS_2, **1a**	76.3	16.9	30.6		
TS_2, **1e**	55.1	33.1	68.0 (37.4)		
TS_2, **2**	--	13.2			

a: angle between the best planes formed by the C atoms of the phenyl ring of bid^- and the C,N atoms of the pyridyl ring of bpy cis to the Ru-O bond. b: angle between the best planes formed by the C,N atoms of the pyridyl rings of the bid^- ligand. c: bond length for H-X (Cl or O)/distances between C_α-X/bond lengths for C_α-H/angles for X-H-C_α.

NMR spectroscopic characterization for the newly synthesized complexes is presented in experimental section, in Figure 2 and the Supporting Information (Figures S1-3). As can be seen in Figure 2, the ^{1}H NMR spectrum of **2** shows only one set of coordinated pyridine resonances clearly indicating its *trans* disposition. This is a consequence of the larger thermodynamic stability of the *trans*-**2** isomer with regard to that of *cis*-**2**. This is mainly a consequence of the larger hydrogen bonding interaction in the *trans*-**2** case together with the favourable *trans*-influence for the Ru-N- vs. Ru-Cl bonds. The Ru-Cl interaction with 6-position of protons (H_A in Figure 2) of two pyridyl rings of *bid*$^-$ ligand in **2** are clearly observed from a strongly deshielded doublet (δ_H 10.76 ppm vs 7.5-7.6 ppm for **1a-c**[12]). By contrast, this effect was not

UNIVERSITAT ROVIRA I VIRGILI
SECOND-ROW TRANSITION-METAL COMPLEXES RELEVANT TO CO2 REDUCTION AND WATER OXIDATION
Takashi Ono
DL:T 1108-2014

observed for the protons (δ_H 7.88, H_G) next to the N atom of the monodentate pyridines in NMR time scale due to potential flexibility of the monodentate fashion. Similarly, this kind of deshielding effect can be observed for **1a-c**[12] and **4a**$^+$ as well as **3a-b** (δ_H 10.29 for **3a** and 10.43 for **3b**, respectively) due to the close proximity between the Cl ligand and the proton next to the N atom of one of the pyridyl ring of *bpy* ligand. ^{1}H NMR spectra of **1e** shows that one of the methyl groups appears at lower field (δ_H: 3.32 ppm vs. 1.41 ppm for the other methyl group) as a consequence of the deshielding effect by the adjacent Cl atom (Figure S1).

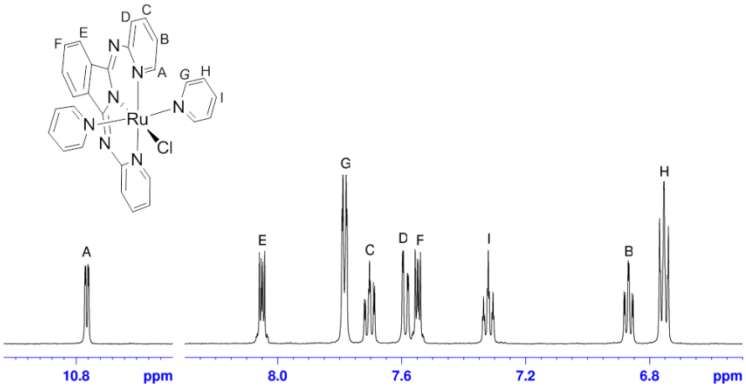

Figure 2. ^{1}H NMR spectrum of complex **2** in CD_2Cl_2 together with the labeling scheme.

Redox properties

The electrochemical properties of all the complexes were examined by means of cyclic voltammetry in dichloromethane and the observed redox couples for Ru(III/II) are collected in Table 2.

The $E_{1/2}$ values (vs SSCE) for Ru(III/II) couple for *bid*$^-$/*bpy* system **1a-c**, **e** are in the range of 0.17 to 0.41 V, varying with electron donating/withdrawing groups on *bpy* ligand, and are shifted 440-700 mV cathodically compared to that of *trpy* analogue **4**$^+$ ($E_{1/2}$ = 0.87 V). These shifts are ascribed to the additional electron density on the metal centre exerted by the anionic character of *bid*$^-$ ligand.

Table 2. Electrochemical data and initial catalytic performances of mononuclear catalysts for hydrogenative CO_2 reduction.

complexes	$E_{1/2}$ for Ru(III/II)[a]	TOF_i[d]	
bid$^-$			
1a	0.30	366.0 (178.4)	Ref 12
1b	0.41	415.7 (259.8)	Ref 12
1c	0.17	212.2 (132.6)	Ref 12
1d	-0.49	0 —	*Tw*
1e	0.30	>1140 (>713)[e]	*Tw*
2	0.29	119.7 (74.8)	*Tw*
dpb$^-$			
3a	0.02	192.6 (120.4)	*Tw*
3b	0.18	211.3 (132.1)	*Tw*
trpy			
4a$^+$	0.87	1.6 (1.0)	Ref 12
***out*-5H**$^+$	0.30[b], (0.63 V)[c]	115.3 (72.1)	*Tw*
***in*-5H**$^+$	0.43[b], (0.82 V)[c]	59.6 (37.3)	*Tw*

a: $E_{1/2}$ (V) obtained from $(E_{p,a} + E_{p,c})/2$ vs SSCE. Scan rate 100 mV/s in glassy carbon working electrode and a Pt disk as auxiliary electrode. b: $E_{1/2}$ values for the deprotonated forms. c: $E_{1/2}$ values for the protonated forms. d: TOF_i in h^{-1}. Initial Turnover Frequencies, considering the first 90 minutes. In parenthesis values normalized with regard to complex **4a**$^+$. Reaction conditions: 0.3 mM solution of complexes dissolved in a 9:1 mixture of TFE and NEt_3 at 25 bar of CO_2 and 25 bar of H_2 at 100°C. *Tw* = This work. e: TOF_i was obtained from first 20 min.

Interestingly, electron donating Me groups on 6,6'-positions of *bpy* does not alter the $E_{1/2}$ value with respect to **1a** (0.30 V for both **1a** and **1e**). This is in contrast to that for the related complex which contains Me groups on 4,4'-positions of *bpy*; the $E_{1/2}$ for $[Ru(trpy)(4,4'\text{-}Me_2\text{-}bpy)Cl]^+$ (0.79 V vs. Ag/AgCl in CH_3CN) is 50 mV lower than that for $Ru(trpy)(bpy)Cl^+$ (0.84 V vs. Ag/AgCl in CH_3CN).[19] In addition, a similar trend has been found for $[Ru(trpy)(2,9\text{-}Me_2\text{-}phen)Cl]^+$ (phen = 1,10-phenanthroline) whose $E_{1/2}$ value (0.83 V vs SSCE in CH_3CN) is even 20 mV higher than that for non-substituted one, $[Ru(trpy)(phen)Cl]^+$ (0.81 V vs SSCE in CH_3CN).[20] This can be explained by that the electron donating abilities of the auxiliary ligands is decreased due to distorted geometry as can be seen in the X-ray structure of **1e** (Figrue 1). The replacement of *bpy* ligand by strong σ-donating anionic *acac*$^-$ ligand decreases its redox potential by nearly 800 mV, resulting in the dominant oxidation state of **1d** as Ru(III).

Figure 3. Cyclic voltammogram vs. SSCE at a scan rate 100 mV/s in DCM-TBAH (0.1 M), of complex **3a** (0.5 mM).

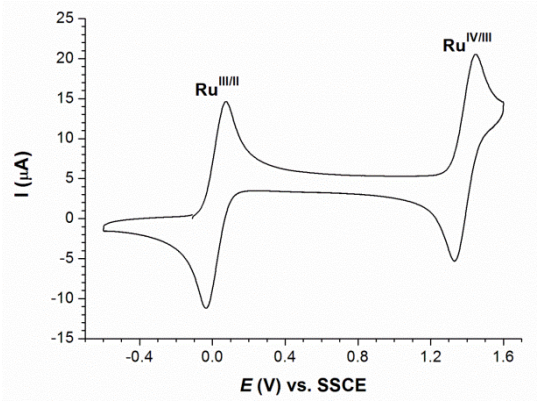

The incorporation of the metal-carbon *σ*-bond in **3a** resulted in a large cathodic shift of Ru(III/II) couple ($E_{1/2}$ = 0.02 V) by more than *800 mV* with regard to *trpy* analogue **1a** and the observation of a chemically and electrochemically reversible wave for the IV/III couple ($E_{1/2}$ = 1.39 V) as can be seen in Figure 3. The latter is only 100 mV anodically shifted with regard to the III/II for $Ru(bpy)_3^{2+}$ or $Ru(tpry)_2$ ($E_{1/2}$ = 1.28 V in CH_3CN for both[21]). This huge cathodic shift is also observed in related complexes: $E_{1/2}$ = 0.51 V for $[Ru(dpb)(trpy)]^+$,[21] in CH_3CN.

Complexes *out*-**5**$^+$ and *in*-**5**$^+$, containing pyrazolylic protons, can be deprotonated in the basic conditions used for the catalytic reaction. Their $E_{1/2}$ values for protonated forms are 0.63 and 0.82 V close to that of **4a**$^+$, while deprotonation resulted in significantly lowering $E_{1/2}$ values (0.30 and 0.43 V, Figure S6) which would potentially alter their catalytic performance compared to **4a**$^+$.

III-2.3.2. Catalytic Experiments

Complexes **1d-e**, **2**, **3a-b**, *out*-**5**$^+$ and *in*-**5**$^+$ were tested as catalyst precursors for the hydrogenative reduction of CO_2 in 2,2,2-trifluoroethanol as solvent with added NEt_3, and in all cases, formic acid was the sole product detected as was found with the other complexes **1a-c**, **4a**$^+$ reported previously[12]. Catalytic activities are reported in

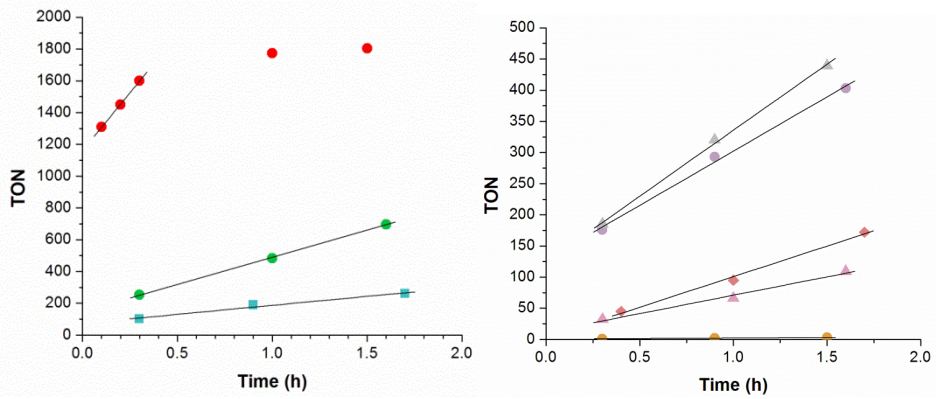

Figure 4. Initial catalytic performance of a 0.3 mM solution of complexes ●: **1a** ●: **1e**, ■: **2**, ●: **3a**, ▲: **3b**, ●: **4a**$^+$, ◆: *out*-**5**$^+$, ▲: *in*-**5**$^+$, dissolved in a 9:1 mixture of TFE and NEt_3 at 25 bar of CO_2 and 25 bar of H_2 at 100 °C.

Table 2 as in terms of initial turnover frequencies (TOF_i) measured over the first 90 minutes except for complex **1e** whose TOF_i was obtained, considering the first 20 minutes due to the much faster reactivity of this complex (TOF_i >1140 h^{-1} for **1e** vs 366 h^{-1} for **1a**, see Figure 4). Figure 4 also reports the time profiles for the generation of HCOOH for the complexes tested in the present work.

By comparing the effect of stronger σ-donating *dpb*$^-$ ligand with *bid*$^-$ ligand, **3a** showed lower catalytic activity (TOF_i: 211 h^{-1}) than that of *bid*$^-$ analogue **1a** (TOF_i: 366 h^{-1}). Complex **3b** containing electron withdrawing group (-COOEt) on *bpy* showed higher activity than **3a** as we found similar trend in *bid*$^-$ system (**1a-b**).[12]

1d which has the lowest $E_{1/2}$ value (-0.49 V) in this study, exerted by the bidentate anionic *acac*$^-$ ligand, resulted in no activity. In contrast to this, a series of *trpy* complexes showed opposite result; that is, the replacement of *bpy* by anionic *bpp*$^-$ formed by *in-situ* deprotonation from complexes *in*-**5**$^+$ and *out*-**5**$^+$ resulted in 37 and 72 times higher catalytic activity than that of *bpy* analogue **4a**$^+$.

Complex **2**, which has reactive site *trans* to the centre ring of the tridentate ligand unlike the others where reactive site locates in *cis* position, showed lower catalytic activity compared with that of **1a**.

UNIVERSITAT ROVIRA I VIRGILI
SECOND-ROW TRANSITION-METAL COMPLEXES RELEVANT TO CO2 REDUCTION AND WATER OXIDATION
Takashi Ono
DL:T 1108-2014

III-2.3.3. Mechanistic Proposal and DFT Calculations

We have earlier proposed a mechanism for mononuclear *bid*$^-$ complexes that is presented in Figure 5 and that also applies here. The mechanism is based on the first order behaviour of catalyst and H_2 pressure and is independent of CO_2 pressure. It consists on a two steps, replacement of formato ligand by H_2 (step III, see Figure 5), and subsequent heterolytic activation of H_2 (step IV-a-O, Figure 5).

Figure 6 shows a relationship between TOF_i and $E_{1/2}$ for the Ru(III/II) couple of the catalysts studied here. Figure 6 clearly shows that for the complexes having anionic tridentate ligand (*bid*$^-$ or *dpb*$^-$) TOF_i increases with an increase of the redox potential. By contrast, a series of complexes having neutral *trpy* ligand shows opposite results; TOF_i increases with a decrease of $E_{1/2}$. In addition it is striking to see the different behaviour of **1a**, **1e** and **2** that have practically the same $E_{1/2}$ but radically different TOF_i.

In order to shed light to all this questions and have a deeper and more complete understanding of the potential mechanisms that occurring here we have carried out DFT calculations for the complete mechanistic cycle for **1a**, **1e** and **2**. The results are shown in Figure 7 and 8 and Table 1 and 3.

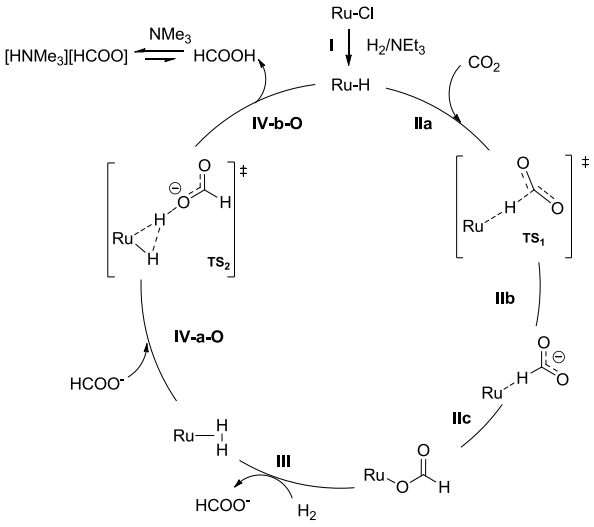

Figure 5. Proposed catalytic cycle for hydrogenative CO_2 reduction.

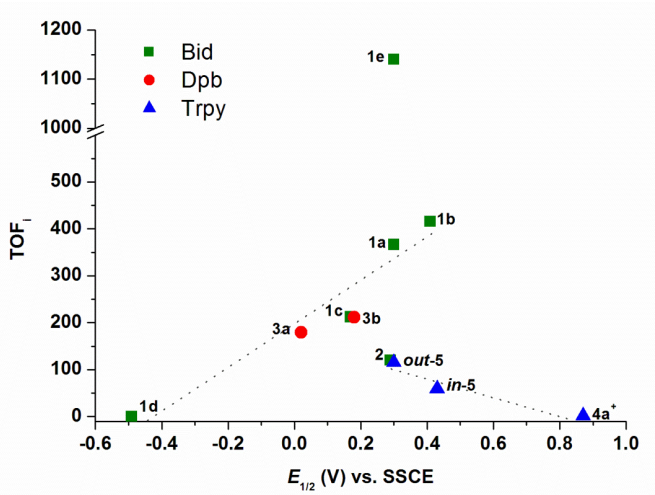

Figure 6. Plot of TOF_i with respect to $E_{1/2}$ for Ru(III/II) couple of complexes containing: *bid*$^-$ (■), *dpb*$^-$ (●), and *trpy* (▲) ligands with a labeling of complexes.

Table 3. Computed and Experimental Rate Constants and Energies for the Species Involved in the CO_2 Hydrogenation Catalytic Cycle with **1a**, **1e**, and **2.**

		Complex		
		1e	**1a**	**2**
Intermediates and TSs	Ru-H+CO_2	0	0	0
	TS_1	9.4	9.2	8.9
	Ru-HCO_2	4.3	3.7	0.0
	Ru-OCHO	-7.3	-10.2	-13.8
	Ru-H_2	3.7	1.4	-3.1
	TS_2	10.8	9.1	6.1
Catalytic steps	IIa	9.4	9.2	8.9
	IIb	-5.1	-5.5	-8.9
	IIc	-11.6	-13.9	-13.8
	III	11.0	11.6	10.7
	IV-a-O	7.1	7.7	9.2
	IV-b-O	-5	-3.4	-0.4
Activation energies	$\Delta G_1^{\neq}$ (IIa)	9.4	9.2	8.9
	$\Delta G_2^{\neq}$ (III+IV-a-O)	18.1	19.3	19.9
TOF_i (h^{-1})	Exp.	>1140 (>9.5)[a]	366.0 (3.0)[a]	119.7 (1.0)[a]
	Calc.	2.0×10^{-20} (11.7)[a]	3.9×10^{-21} (2.3)[a]	1.7×10^{-21} (1.0)[a]

a: Parenceces shows relative rates with respect to complex **2**.

Figure 7. Mercury representation of DFT calculated structures for Ru-OCHO intermediates(left) and TS_2 (right) for **1a**, **1e** and **2**, respectively.

1a

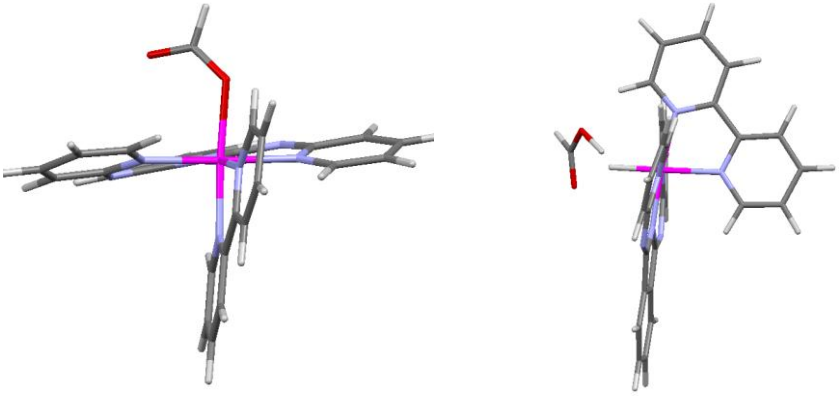

1e

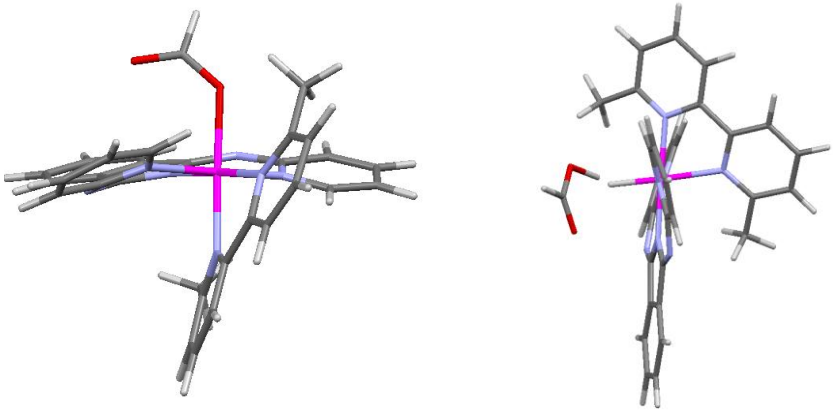

2

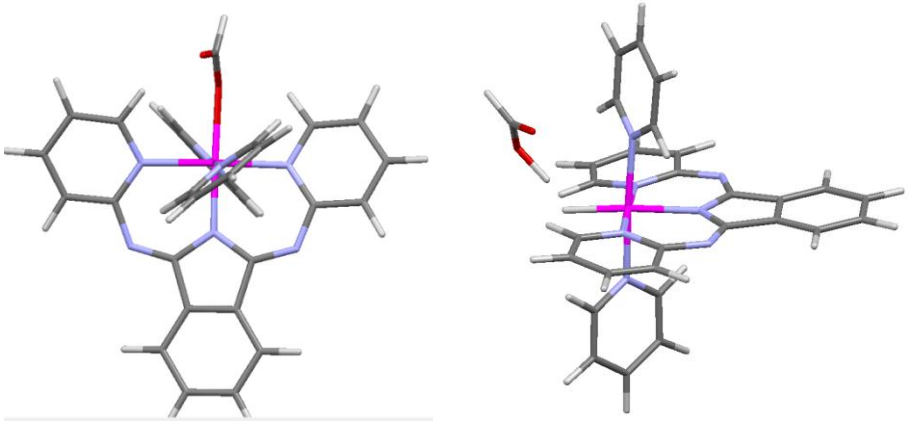

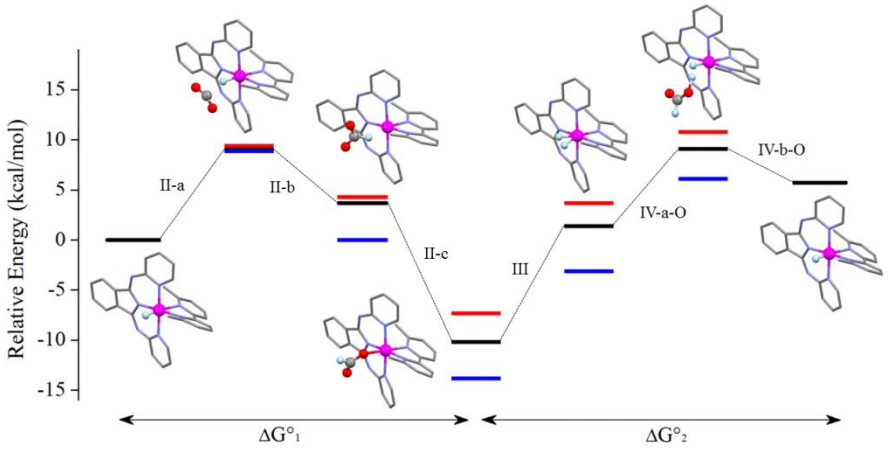

Figure 8. Free energy diagram (kcal/mol) of the catalytic cycle species associated with complex **1a** (black), **1e** (red), and **2** (blue) with electronic energies computed by M06-L.. Free energies are relative to the starting materials [Ru-H] + H_2 + CO_2.

The catalytic cycle is graphically described in Figure 8 and contains all the species and transition states previously shown in the qualitative diagram in Figure 5. Assuming that the $\Delta G_2^{\neq}$ is the rate-determining step for the systems studied, there are two species that are fundamental in order to understand the mechanism and the different perturbation exerted by electron donating and withdrawing substituents as well as by other structural perturbations. This two species are the Ru-OCHO intermediates and the TS_2. Table 1 contains structural parameter for intermediates R-OCHO and TS_2 related to **1a**, **1e** and **2** that are fundamental for the qualitative understanding of the relative energies obtained by DFT, since they are involved in $\Delta G_2^{\neq}$. From this Table 1 there are two very important conclusions that can be drawn: a) in **1e**, there is a strong distortion of the octahedral geometry both in Ru-OCHO intermediate and to a lesser extent to TS_2, with regard to either **1a** or **2**, and b) **2** contains the less distorted geometry and in addition significant H-boding occurs at the Ru-O bond that is the active site of the molecule.

With this in mind together with the energies displayed in Table 3, the following conclusions/considerations can be made.

UNIVERSITAT ROVIRA I VIRGILI
SECOND-ROW TRANSITION-METAL COMPLEXES RELEVANT TO CO2 REDUCTION AND WATER OXIDATION
Takashi Ono
DL:T 1108-2014

1. In our earlier DFT results,[12] the superiority of complexes having anionic *bid*$^-$ ligand with respect to *trpy* complex **4a**$^+$ was explained by the fact that a higher degree of positive effect in step III than that of the negative effect in step IV-a-O resulted in the lower overall $\Delta G_2^{\neq}$. For the *bid*$^-$/*dpb*$^-$ containing complexes, an increase of TOF_i with an increase of $E_{1/2}$ was observed. This can be rationalized based on the DFT catalytic cycle. For the anionic *dpb*$^-$ ligand, the high capacity to transmit σ-donation electronic density to the metal centre with respect to *bid*$^-$ ligand produces complexes that would facilitate the OCHO/H_2 substitution (step III). However, the decreased TOF_i for *dpb*$^-$ complexes with respect to *bid*$^-$ complexes implies that there is significant negative effect in the step of heterolytic H_2 cleavage (step IV-a-O) due to decreased acidity of the coordinated H_2. No catalytic activity of **1d** can be explained by that high electron density on metal centre would significantly increase the latter step. In addition, the latter step will be certainly favoured by increasing the electron withdrawing nature of the auxiliary ligands (*bpy* vs 4,4'-$(COOEt)_2$-bpy) as can be seen in an increase of reactivity upon an increase of $E_{1/2}$.

2. On the other hand, the opposite effect was observed for the *trpy* systems, where an increase of TOF_i with a decrease of $E_{1/2}$ was observed. This can be rationalized that the potentially medium electron donor of the *bpp*$^-$ ligand among *bpy*, *bpp*$^-$ and *bid*$^-$ would increase the ΔG in step III and decrease ΔG in step IV-a-O, but to a lesser degree for both steps, compared with those for *bid*$^-$ systems, and thus it can be considered that TOF_i for *out*-**5**$^+$ and *in*-**5**$^+$ located in between those of **1a** and **4a**$^+$.

3. Finally it is interesting to discuss the TOF_i of complexes **1a**, **1e** and **2** that have practically the same $E_{1/2}$ but that contains ligands that produce strong geometrical distortions due to steric effects and/or hydrogen bonding interactions.

4. For the particular case of **1e**, one of the methyls situated at the 6,6' position of the *bpy* strongly interacts with the Ru-Cl bond, which is the active site, where later on the Ru-H and Ru-O bonds will be formed over the catalytic cycle. This strong

distortion as can be seen in Figure 1 for the Ru-Cl bond is also strongly manifested for the Ru-OCHO intermediates (Fiugur 7) that, as a result, is de-stabilized by 2.9 kcal/mol with regard to complex **1a**. This de-stabilization also influences TS_2 but to a lower extent, by 1.7 kcal/mol, since now the steric influence for a Ru-H is lower than for a Ru-OCHO. As consequence of these two effects, the activation energy for the second step, $\Delta G_2^{\neq}$, is lowered by 1.2 kcal/mol. This is in very good agreement with the experimental observation that the CO_2 reduction by **1e** is more than 3 times faster than for **1a**.

5. For the case of **2**, the change of a *bpy* by two monodentate pyridine ligands produces geometry closer to the ideal octahedral one due to the liberation of the angular constrains imposed by the chelate ligand. On the other hand, the Cl ligand is now *trans* to the central *bid* ligand, although judging from redox pots this does not significantly influence electronic density around the Ru metal centre. However the new geometry produces four H atoms from the C_α to the N coordinating atoms that will be very close to the active site, Ru-H, Ru-O. Detailed analysis is presented in Table 1. This hydrogen bonding produces a strong stabilization of the Ru-OCHO intermediate, 3.6 kcal/mol with regard to the related intermediate from **1a**. On the other hand, the stabilization of the TS_2 takes place with a lower extent, in this case by 3.0 kcal/mol. Overall the two effects combined generate a $\Delta G_2^{\neq}$ barrier that is now 0.6 kcal/mol higher than in the initial *bpy* complex, **1a**. This is again in very good agreement with the experimental observation that now the TOF_i decreases approximately by three times.

III-2.4. Conclusions

We have studied a family of mononuclear Ru complexes as catalysts for the hydrogenative CO_2 reduction from the point of view of their electronic and steric properties. A kinetic analysis of the reaction revealed the relationship between TOF_i and redox potentials for the Ru(III/II) couple of the corresponding Ru-Cl complexes,

UNIVERSITAT ROVIRA I VIRGILI
SECOND-ROW TRANSITION-METAL COMPLEXES RELEVANT TO CO2 REDUCTION AND WATER OXIDATION
Takashi Ono
DL:T 1108-2014

which support the previously obtained computational results, where the rate-determining step consist of two elementary steps (III and IV-a-O in Figure 3) that vary energetically in the opposite way with electronic properties of the ancillary ligands. It is of interest to see that the radically different catalytic behaviour of **1a**, **1e** and **2** regardless of their similar $E_{1/2}$. Theoretical means were able to accurately predict the correct reactivity trend for these catalysts, and rationalize their amplified/impeded catalytic activity by considering the key structural features in the catalytic intermediates.

III-2.5. Experimental Section

Materials

All reagents used in the present work were obtained from Aldrich Chemical Co. or Alfa Aesar and were used without further purification. Synthesis grade organic solvents were obtained from SDS and were routinely degassed with N_2. 2,2,2-Trifluoroethanol (TFE) was obtained from Alfa Aesar and was used without further purification. CO_2 (Premier with a purity code of 4.5; $H_2O \leq 7$ ppm, $O_2 \leq 10$ ppm, $CO \leq 2$ ppm, $N_2 \leq 25$ ppm, THC ≤ 5ppm, THC: total hydrocarbons) and H_2 (BIP with a purity code of 5.7; Premier; $H_2O \leq 0.02$ ppm, $O_2 \leq 0.1$ ppm, $CO + CO_2 \leq 0.5$ ppm, $N_2 \leq 2$ ppm, THC ≤ 0.01 ppm) gases were obtained from Carburos Metálicos S.A.. The compounds $RuCl_3$(Hbid),[22-23] $RuCl_2(dmso)_4$,[24] [Ru(bid)(bpy)(Cl)] (**1a**),[12] [Ru(bid)(4,4'-OMe_2-bpy)(Cl)] (**1b**),[12] [Ru(bid)(4,4'-$COOEt_2$-bpy)(Cl)] (**1c**),[12] [Ru(trpy)(bpy)(Cl)](PF_6) (**[4a](PF$_6$)**),[17] *out*-[Ru(trpy)(Hbpp)(Cl)](PF_6) (**[*out*-5](PF$_6$)**),[16] *in*-[Ru(trpy)(Hbpp)(Cl)](PF_6) (**[*in*-5](PF$_6$)**)[16] and Hdpb (1,3-di(pyridin-2-yl)benzene)[21] were prepared as described in the literature. All synthetic manipulations were routinely performed under N_2 atmosphere using Schlenk and vacuum-line techniques.

Synthesis

Scheme 2. NMR Labeling scheme. Top: *bid*$^-$ complexes, bottom: *dpb*$^-$ complexes.

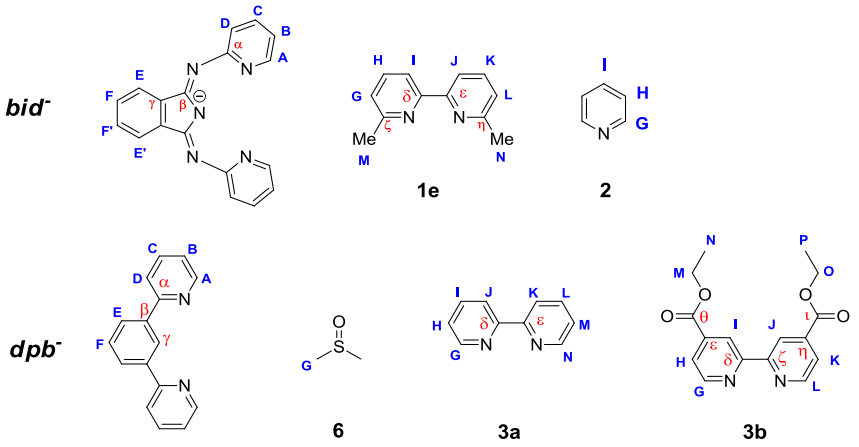

Synthesis of [Ru^{III}(bid)(acac)(Cl)]·0.25CH_2Cl_2 (1d·0.25CH_2Cl_2)

208.7 mg (0.411 mmol) of $RuCl_3$(Hbid), 56 μL (0.55 mmol, 1.3 equiv.) of acetylacetone and 20 mL of degassed EtOH were added into a two-necked 50 mL round bottom flask under N_2 atmosphere, which was heated to reflux for one hour. Then, 50 μL (0.36 mmol) of NEt_3 and 84 mg (2.0 mmol, 5 equiv.) of LiCl were added into the resulting solution, which was refluxed for one hour. After cooling down to room temperature, the resulting solution was stirred under air overnight. All the volatile was removed by rotary evaporator and the residue was purified by recrystallization (Slow evaporation of CH_2Cl_2 from the mixture with EtOH) to give brown needle-type of crystals, which was filtered and washed with Et_2O (3 mL x 5) and dried under vacuum. Yield 123 mg (0.230 mmol) 56%. Anal. Calcd. for $C_{23}H_{19}ClN_5O_2Ru$: C, 51.74; H, 3.59; N, 16.64. Found: C, 50.33; H, 3.79; N, 12.72. Anal. Calcd. for $C_{23}H_{19}ClN_5O_2Ru·0.25CH_2Cl_2$: C, 50.30; H, 3.54; N, 12.61. MALDI(+)-MS (CH_2Cl_2): *m/z* 535.3 ([M+H]$^+$). NMR specta were not taken because **1d** couldn't be reduced to Ru(II) species with reductants such as NEt_3, ascorbic acid, and zinc amalgam.

UNIVERSITAT ROVIRA I VIRGILI
SECOND-ROW TRANSITION-METAL COMPLEXES RELEVANT TO CO2 REDUCTION AND WATER OXIDATION
Takashi Ono
DL:T 1108-2014

Synthesis of [Ru(bid)(6,6'-Me_2-bpy)(Cl)]·CH_2Cl_2 (1e·CH_2Cl_2)

51.3 mg (0.101 mmol) of Ru(Hbid)Cl_3, 20.7 mg (0.237 mmol) of 6,6'-Me_2-bpy were charged into a 20 mL Schlenk tube with Teflon plug valve, which was purged with N_2. Then, 10 mL of degassed EtOH was added and the mixture was heated to reflux for 1 h. 43 μL (0.31 mmol, 3 equiv.) of NEt_3 was added into the resulting solution, which was refluxed for more two hours. After the reaction time, the solvent was removed under reduced pressure to leave a residue, which was dried at 60 °C overnight. The resulting residue was extracted with 10 mL of dry THF and transferred into a Schlenk thorough syringe with filter paper. THF extract was evaporated to give green solid, which was purified by recrystallization from CH_2Cl_2/Et_2O (2/10 mL) to give green microcrystals. Yield 30.7 mg (0.050 mmol) 49%. Anal. calcd. for $C_{30}H_{24}ClN_7Ru$: C, 58.20; H, 3.91; N, 15.84. Found: C, 53.03; H, 4.05; N, 13.99. Anal. calcd. for $C_{30}H_{24}ClN_7Ru·CH_2Cl_2$: C, 52.89; H, 3.72; N, 13.93. ^{1}H NMR (500 MHz, CD_2Cl_2 with NEt_3, 298 K): δ 8.11 (dd, 2H, J_{EF} = 5.4 Hz, $J_{EF'}$ = 3.0 Hz, H_E), 7.91 (d, 1H, J_{JK} = 7.7 Hz, H_J), 7.86 (t, 1H, J_{KJ} = J_{KL} = 7.7 Hz, H_K), 7.62 (d, 1H, J_{IH} = 7.4 Hz, H_I), 7.58 (dd, 2H, J_{FE} = 5.4 Hz, $J_{FE'}$ = 3.0 Hz, H_F), 7.55-7.43 (m, 7H, H_A, H_B, H_D and H_L), 7.29 (t, 1H, J_{HG} = J_{HI} = 7.4 Hz, H_H), 6.67 (d, 1H, J_{GH} = 7.4 Hz, H_G), 6.40 (td, 1H, J_{BA} = J_{BC} = 6.4 Hz, J_{BD} = 1.7 Hz, H_B), 3.32 (s, 3H, H_N), 1.41 (s, 3H, H_M). ^{13}C NMR (125 MHz, CD_2Cl_2 with NEt_3, 298 K): δ 168.0 (C_η), 165.8 (C_ζ), 161.1 (C_δ), 160.6 (C_ε), 158.7 (C_α), 155.5 (C_D), 152.6 (C_β), 141.6 (C_γ), 135.5 (C_K), 134.2 (C_B), 134.0 (C_H), 129.6 (C_F), 126.9 (C_A), 126.6 (C_L), 124.2 (C_G), 121.2 (C_E), 120.5 (C_J), 119.5 (C_I), 115.6 (C_C), 27.9 (C_N), 24.2 (C_M). MALDI(+)-MS (CH_2Cl_2): *m/z* 584.2 ([M-Cl]$^+$).

Synthesis of *trans*-[Ru(bid)($py)_2$(Cl)] (2)

50.8 mg (0.100 mmol) of Ru(Hbid)Cl_3, 16 μL (0.20 mmol, 2 equiv.) of pyridine and 10 mL of degassed EtOH were added into a two-necked 25 mL round bottom flask under N_2 atmosphere, which was heated to reflux for one hour. Then, 50 μL (0.36 mmol) of NEt_3 was added into the resulting solution, which was refluxed for one hour. After cooling down to room temperature, a solid precipitated in the solution was filtered off under air and was washed with EtOH (3 mL x 3) and Et_2O (5 mL x 5) and dried under

vacuum. Yield 43.6 mg (0.074 mmol) 74%. Anal. calcd. for $C_{28}H_{22}ClN_7Ru$: C, 56.71; H, 3.74; N, 16.53. Found: C, 56.38; H, 4.19; N, 16.25. ^{1}H NMR (500 MHz, CD_2Cl_2 with NEt_3, 298 K): δ 10.76 (dd, 2H, J_{AB} = 6.6 Hz, J_{AC} = 1.7 Hz, H_A), 8.05 (dd, 2H, J_{EF} = 5.5 Hz, $J_{EF'}$ = 3.0 Hz, H_E), 7.78 (dd, 4H, J_{GH} = 6.6 Hz, J_{GI} = 1.5 Hz, H_G), 7.70 (ddd, 2H, J_{CD} = 7.8 Hz, J_{CB} = 6.6 Hz, J_{CA} = 1.7 Hz, H_C), 7.59 (dd, 2H, J_{DC} = 7.8 Hz, J_{DB} = 1.5 Hz, H_D), 7.55 (dd, 2H, J_{FE} = 5.5 Hz, $J_{FE'}$ = 3.0 Hz, H_F), 7.32 (dd, 2H, J_{IH} = 7.6 Hz, J_{IG} = 1.5 Hz, H_I), 6.87 (dd, 2H, J_{BA} = J_{BC} = 6.6 Hz, J_{BD} = 1.5 Hz, H_B), 6.75 (dd, 4H, J_{HI} = 7.6 Hz, J_{HG} = 6.6 Hz, H_H). ^{13}C NMR (125 MHz, CD_2Cl_2 with NEt_3, 298 K): δ 157.5 (C_A), 157.3 (C_α), 154.3 (C_G), 151.5 (C_β), 141.7 (C_γ), 135.1 (C_I), 134.6 (C_C), 129.5 (C_F), 127.7 (C_D), 123.8 (C_H), 120.5 (C_E), 116.7 (C_B). MALDI(+)-MS (CH_2Cl_2): *m/z* 435.3 ([M-2pyridine]$^+$).

Synthesis of *trans*-Ru(dpb)(dmso-*s*)$_2$(Cl) (6)

Into three-necked 500 mL round-bottom flask equipped with a condenser, 1.20 g (2.48 mmol) of $RuCl_2(dmso)_4$, 693 mg (2.98 mmol, 1.2 equiv.) of Hdpb and 170 mL of EtOH were added. After N_2 was bubbled into the mixture for 30 min, NEt_3 (1.7 mL, 12 mmol, 5 equiv.) was added and the mixture was refluxed for 24 h. After cooling to room temperature, a solid was precipitated in the solution and the solution was removed with syringe filter under N_2 atmosphere and the solid was washed with EtOH (5 mL x 3) and diethyl ether (15 mL x 3), which was dried under vacuum. Yield. 1.03 g (1.97 mmol), 79%. Anal. calcd. for $C_{20}H_{23}ClN_2O_2RuS_2$: C, 45.84; H, 4.42; N, 5.23; S, 12.24. Found: C, 45.41; H, 4.51; N, 5.23; S, 12.13. ^{1}H NMR (500 MHz, CD_2Cl_2, 298 K): δ 9.05 (d, 2H, J_{AB} = 5.5 Hz, H_A), 7.94 (d, 2H, J_{DC} = 7.1 Hz, H_D), 7.85 (td, 2H, J_{CD} = 7.1 Hz, J_{CA} = 1.6 Hz, H_C), 7.82 (d, 2H, J_{EF} = 7.6 Hz, H_E), 7.27 (ddd, 2H, J_{BC} 7.1 Hz, J_{BA} = 5.5 Hz, J_{BD} = 1.4 Hz, H_B), 7.21 (t, 1H, J_{FE} = $J_{FE'}$ = 7.6 Hz, H_F), 2.39 (s, 12H, Me of dmso). ^{13}C NMR (125 MHz, CD_2Cl_2, 298 K): δ 206.9 (C_γ), 168.3 (C_α), 154.4 (C_A), 144.9 (C_β), 136.8 (C_C), 124.3 (C_E), 122.9 (C_B), 120.3 (C_F), 119.5 (C_D), 42.3 (Me of dmso). ESI-MS (MeOH): *m/z* 411.0 ([M-Cl-dmso]$^+$).

Synthesis of [Ru(dpb)(bpy)(Cl)] (3a)

Into three-necked 250 mL round-bottom flask equipped with a condenser, 506 mg (0.966 mmol) of **6** and 159 mg (1.02 mmol, 1.05 equiv.) of 2,2'-bipyridine were charged

UNIVERSITAT ROVIRA I VIRGILI
SECOND-ROW TRANSITION-METAL COMPLEXES RELEVANT TO CO2 REDUCTION AND WATER OXIDATION
Takashi Ono
DL:T 1108-2014

and the system was purged with N_2. After adding 80 mL of degassed CH_2Cl_2, the solution was stirred for one hour at room temperature. Then, the mixture was further stirred in the presence of tungsten lamp (100 W x 2) overnight. The resulting brown solution was purified over neutral alumina column using CH_2Cl_2/Acetone (90/10, v/v) as eluent. The first purple fraction was collected and the solvent was evaporated to give purple solid, which was washed with Et_2O (10 mL x 3) and dried under vacuum. Yield. 406 mg (0.77 mmol), 81%. Anal. calcd. for $C_{26}H_{19}ClN_4Ru$: C, 59.60; H, 3.65; N, 10.69. Found: C, 59.42; H, 3.65; N, 10.29. ^{1}H NMR (500 MHz, CD_2Cl_2, 298 K): δ 10.29 (d, 1H, J = 5.1 Hz, H_N), 8.33 (d, 1H, J = 8.2 Hz, H_K), 8.05-7.98 (m, 3H, H_E, H_L), 7.95 (d, 1H, J = 7.4 Hz, H_J), 7.93-7.87 (m, 3H, H_D, H_M), 7.63 (d, 2H, J = 6.8 Hz, H_A), 7.49 (td, 2H, J = 6.8 Hz, J = 1.4 Hz, H_C), 7.17 (td, 1H, J = 7.4 Hz, J = 1.2 Hz, H_I), 7.10-7.03 (m, 2H, H_F, H_G), 6.72 (t, 2H, J = 6.8 Hz, J = 1.2 Hz, H_B), 6.51 (td, 1H, J = 7.4 Hz, J = 1.2 Hz, H_H). ^{13}C NMR (125 MHz, CD_2Cl_2, 298 K): δ 223.3 (C_γ), 168.4 (C_α), 161.2 (C_δ), 156.7 (C_G), 154.6 (C_ε), 153.3 (C_A), 150.8 (C_N), 144.9 (C_β), 133.9 (C_C), 133.7 (C_L), 129.9 (C_I), 126.4 (C_M), 124.2 (C_H), 122.2 (C_E), 122.1 (C_J), 121.5 (C_K), 121.2 (C_B), 119.0 (C_F), 118.9 (C_D). ESI-MS (MeOH): *m*/*z* 524.0 (M^+).

Synthesis of [Ru(dpb)(4,4'-$COOEt_2$-bpy)(Cl)] (3b)

Into three-necked 250 mL round-bottom flask equipped with a condenser, 302 mg (0.575 mmol) of **6** and 173 mg (0.577 mmol, 1 equiv.) of 4,4'-$COOEt_2$-2,2'-bipyridine were charged and the system was purged with N_2. After adding 100 mL of degassed CH_2Cl_2, the solution was stirred for one hour at room temperature. Then, the mixture was further stirred in the presence of tungsten lamp (100 W x 2) overnight. The resulting brown solution was purified over neutral alumina column using CH_2Cl_2/Acetone (95/5, v/v) as eluent. The first purple fraction was collected and the solvent was evaporated to give purple residue, which was recrystallized from CH_2Cl_2/pentane to give purple microcrystals, which was washed with pentane (3 mL x 3) and dried under vacuum. Yield. 42.3 mg (0.063 mmol), 11%. Anal. calcd. for $C_{32}H_{27}ClN_4O_4Ru$: C, 57.53; H, 4.07; N, 8.39. Found: C, 57.08; H, 3.91; N, 8.08. Anal. calcd. for $C_{32}H_{27}ClN_4O_4Ru{\cdot}0.5H_2O$: C, 56.76; H, 4.17; N, 8.27. ^{1}H NMR (500 MHz, CD_2Cl_2,

298 K): δ 10.43 (d, 1H, J_{LK} = 5.7 Hz, H_L), 8.99 (s, 1H, H_J), 8.59 (d, 1H, J_{IH} = 1.7 Hz, H_I), 8.45 (dd, 1H, J_{KL} = 5.7 Hz, J_{KJ} = 1.5 Hz, H_K), 8.06 (d, 2H, J_{EF} = 7.6 Hz, H_E), 7.87 (d, 2H, J_{DC} = 8.2 Hz, H_D), 7.51 (ddd, 2H, J_{CD} = 8.2 Hz, J_{CB} = 7.0 Hz, J_{CA} = 1.4 Hz, H_C), 7.44 (d, 1H, J_{GH} = 6.2 Hz, H_G), 7.39, (d, 2H, J_{AB} = 5.5 Hz, H_A), 7.11 (dd, 1H, J_{HG} = 6.2 Hz, J_{HI} = 1.7 Hz, H_H), 6.96 (t, 1H, J_{FE} = 7.6 Hz, H_F), 6.68 (ddd, 2H, J_{BC} = 7.0 Hz, J_{BA} = 5.5 Hz, J_{BD} = 1.1 Hz, H_B), 4.58 (q, 2H, J_{OP} = 7.2 Hz, H_O), 4.29 (q, 2H, J_{MN} = 7.1 Hz, H_M), 1.54 (t, 3H, J_{PO} = 7.2 Hz, H_P), 1.30 (t, 3H, J_{NM} = 7.1 Hz, H_N). ^{13}C NMR (125 MHz, CD_2Cl_2, 298 K): δ 217.9 (C_γ), 167.8 (C_α), 165.4 (C_ι), 164.9 (C_θ), 162.1 (C_δ), 157.5 (C_G), 155.1 (C_ζ), 153.0 (C_A), 151.2 (C_L), 144.4 (C_β), 135.0 (C_C), 134.2 (C_η), 129.9 (C_ε), 125.8 (C_K), 123.2 (C_H), 122.3 (C_E), 121.7 (C_I), 121.6 (C_B), 121.5 (C_J), 121.1 (C_F), 119.4 (C_D), 62.6 (C_O), 62.1 (C_M), 14.6 (C_P), 14.3 (C_N). ESI-MS (MeOH): *m/z* 690.9 ($[M+Na]^+$).

Standard procedure for catalytic hydrogenative CO_2 reduction

Catalytic reactions were run with an SPR16 Slurry Phase Reactor, which is a completely automated reactor system consisting 16 autoclaves (15 mL capacity). Once the program started, a leak test for each autoclave was done and then each reactor was purged with nitrogen gas. Afterward, a complex solution (4.0 mL; solvent/amine = 9/1) was added to each autoclave of the reactor from the top of the vessel under N_2. Once all the solvents and reagents were distributed in all the vessels, stirring at 1000 rpm was started, followed by pressurizing with CO_2 gas and then H_2 gas at the desired pressures. Then the temperature was increased to the desired value, at which point was considered the initial time. At the end of the reaction each reactor was cooled to room temperature and depressurized. The samples were analyzed by ^{1}H NMR spectroscopy, taking the reaction solution (0.3 mL) and mixing it with D_2O (0.2 mL) containing DMF (an internal standard; 120 μL in 10 mL of D_2O). Two replicates were performed for each measurement.

UNIVERSITAT ROVIRA I VIRGILI
SECOND-ROW TRANSITION-METAL COMPLEXES RELEVANT TO CO2 REDUCTION AND WATER OXIDATION
Takashi Ono
DL:T 1108-2014

Instrumentation and measurements

Cyclic voltammetric (CV) experiments were performed in a IJ-Cambria IH-660 potentiostat, using a three electrode cell. Glassy carbon disk electrodes (3 mm diameter) from BAS were used as working electrode, platinum wire as auxiliary and SSCE as the reference electrode. Cyclic voltammograms were recorded at 100 mV/s scan rate under nitrogen atmosphere. The complexes were dissolved in previously degassed dichloromethane containing the necessary amount of (n-Bu_4N)(PF_6), used as supporting electrolyte, to yield a 0.1 M ionic strength solution. All $E_{1/2}$ values reported in this work were estimated from cyclic voltammetry as the average of the oxidative and reductive peak potentials ($E_{p,a}$+$E_{p,c}$)/2. Unless explicitly mentioned the concentration of the complexes were approximately 1 mM. The NMR spectroscopy was performed on Bruker Avance 400 MHz Bruker Avance II and Bruker Avance 500 MHz. Samples were run in DMF-d_7. The ESI mass spectroscopy experiments were performed on a Waters Micromass LCT Premier equipment, respectively. UV-Vis spectroscopy was performed on a Cary bio 50 UV-vis spectrophotometer with 1 cm quartz cells.

X-Ray structure determination

Suitable Crystals of complex **1d·0.5CH_2Cl_2** and **1e·CH_2Cl_2** were grown from slow evaporation of dichloromethane from a mixture with ethanol, and dichloromethane/diethyl ether, respectively. **1d·0.5CH_2Cl_2**: The asymmetric unit contains one molecule of the complex and a half molecule of dichloromethane. The dichloromethane is disordered around a center of inversion. **1e·CH_2Cl_2**: The asymmetric unit contains one molecule of the metal complex and one molecule of dichloromethane. The measured crystals were prepared under inert conditions immersed in perfluoropolyether as protecting oil for manipulation.

***Data collection**:* Crystal structure determinations were carried out using a Bruker-Nonius diffractometer equipped with an APPEX 2 4K CCD area detector, a FR591 rotating anode with MoK_α radiation, Montel mirrors as monochromator, and a Kryoflex low temperature device (T = -173 °C). Full-sphere data collection was used

with ω and φ scans. APEX-2 (for Data collection),[25] Bruker Saint V/.60A (for data reduction),[26] and SADABS (for absorption correction).[27]

***Structure Solution and Refinement**:* Crystal structure solution was achieved using direct methods as implemented in SHELXTL[28] and visualized using the program XP. Missing atoms were subsequently located from difference Fourier synthesis and added to the atom list. Least-squares refinement on F^2 using all measured intensities was carried out using the program SHELXTL. All non-H atoms were refined, including anisotropic displacement parameters.

Computational Details

All geometries were fully optimized at the M06-L level[29] of density functional theory with the Gaussian 09 electronic structure program suite[30] using the Stuttgart [8s7p6d2f | 6s5p3d2f] ECP28MWB contracted pseudopotential basis set on Ru,[31] the MIDI! basis set[32] on nitrogen-based ligands and the 6-31G(d) basis set on all the other atoms.[33] Integral evaluation made use of the grid defined as ultrafine in the Gaussian 09 program. The nature of all stationary points was verified by analytic computation of vibrational frequencies, which were also used for the computation of zero-point vibrational energies and molecular partition functions for use in computing 298 K thermal contributions to free energy.[34] Solvent effects of 2,2,2-trifluoroethanol were included with the SMD continuum solvation model.[35] The energies were subsequently computed with a larger basis set using the same basis set on Ru[31] but the 6-311+G(2df,2p) basis set on all other atoms.[33] Ethyl groups of NEt_3 were modeled as methyl groups for efficiency.

III-2.6. Acknowledgements

Support from MINECO (CTQ-2010-21497). T.O. thanks MINECO for a doctoral grant.

I have carried out experimental parts. DFT calculations were performed by Michlle A. Johnson in the group of Prof. C. J. Cramer at the University of Minnesota.

UNIVERSITAT ROVIRA I VIRGILI
SECOND-ROW TRANSITION-METAL COMPLEXES RELEVANT TO CO2 REDUCTION AND WATER OXIDATION
Takashi Ono
DL:T 1108-2014

III-2.7. References

(1) Karl, T. R.; Trenberth, K. E. *Science* **2003**, *302*, 1719-1723.
(2) Raupach, M. R.; Marland, G.; Ciais, P.; Le Quéré, C.; Canadell, J. G.; Klepper, G.; Field, C. B. *Proc. Natl. Acad. Sci. U.S.A.* **2007**, *104*, 10288-10293.
(3) Jessop, P. G.; Joó, F.; Tai, C.-C. *Coord. Chem. Rev.* **2004**, *248*, 2425-2442.
(4) Jessop, P. G.; Ikariya, T.; Noyori, R. *Chem. Rev.* **1995**, *95*, 259-272.
(5) Federsel, C.; Boddien, A.; Jackstell, R.; Jennerjahn, R.; Dyson, P. J.; Scopelliti, R.; Laurenczy, G.; Beller, M. *Angew. Chem., Int. Ed.* **2010**, *49*, 9777-9780.
(6) Ziebart, C.; Federsel, C.; Anbarasan, P.; Jackstell, R.; Baumann, W.; Spannenberg, A.; Beller, M. *J. Am. Chem. Soc.* **2012**, *134*, 20701-20704.
(7) Federsel, C.; Ziebart, C.; Jackstell, R.; Baumann, W.; Beller, M. *Chem. —Eur. J.* **2012**, *18*, 72-75.
(8) Langer, R.; Diskin-Posner, Y.; Leitus, G.; Shimon, L. J. W.; Ben-David, Y.; Milstein, D. *Angew. Chem., Int. Ed.* **2011**, *50*, 9948-9952.
(9) Tanaka, R.; Yamashita, M.; Nozaki, K. *J. Am. Chem. Soc.* **2009**, *131*, 14168-14169.
(10) Himeda, Y.; Onozawa-Komatsuzaki, N.; Sugihara, H.; Kasuga, K. *Organometallics* **2007**, *26*, 702-712.
(11) Hull, J. F.; Himeda, Y.; Wang, W.-H.; Hashiguchi, B.; Periana, R.; Szalda, D. J.; Muckerman, J. T.; Fujita, E. *Nat. Chem.* **2012**, *4*, 383-388.
(12) Planas, N.; Ono, T.; Vaquer, L.; Miro, P.; Benet-Buchholz, J.; Gagliardi, L.; Cramer, C. J.; Llobet, A. *Phys. Chem. Chem. Phys.* **2011**, *13*, 19480-19484.
(13) Ono, T.; Planas, N.; Miró, P.; Ertem, M. Z.; Escudero-Adán, E. C.; Benet-Buchholz, J.; Gagliardi, L.; Cramer, C. J.; Llobet, A. *ChemCatChem* **2013**, *5*, 3897-3903.
(14) Fukuzumi, S.; Suenobu, T. *Dalton Trans.* **2013**, *42*, 18-28.
(15) Fujita, E.; Muckerman, J. T.; Himeda, Y. *Biochimica et Biophysica Acta (BBA) - Bioenergetics* **2013**, *1827*, 1031-1038.
(16) Sens, C.; Rodríguez, M.; Romero, I.; Llobet, A.; Parella, T.; Benet-Buchholz, J. *Inorg. Chem.* **2003**, *42*, 8385-8394.
(17) Rasmussen, S. C.; Ronco, S. E.; Mlsna, D. A.; Billadeau, M. A.; Pennington, W. T.; Kolis, J. W.; Petersen, J. D. *Inorg. Chem.* **1995**, *34*, 821-829.
(18) Camerano, J. A.; Rodrigues, A.-S.; Rominger, F.; Wadepohl, H.; Gade, L. H. *J. Organomet. Chem.* **2011**, *696*, 1425-1431.
(19) Yoshikawa, N.; Matsumura-Inoue, T.; Kanehisa, N.; Kai, Y.; Takashima, H.; Tsukahara, K. *Anal. Sci.* **2004**, *20*, 1639-1644.
(20) Kaveevivitchai, N.; Zong, R.; Tseng, H.-W.; Chitta, R.; Thummel, R. P. *Inorg. Chem.* **2012**, *51*, 2930-2939.
(21) Bomben, P. G.; Robson, K. C. D.; Sedach, P. A.; Berlinguette, C. P. *Inorg. Chem.* **2009**, *48*, 9631-9643.
(22) Marks, D. N.; Siegl, W. O.; Gagne, R. R. *Inorg. Chem.* **1982**, *21*, 3140-3147.
(23) Gagne, R. R.; Marritt, W. A.; Marks, D. N.; Siegl, W. O. *Inorg. Chem.* **1981**, *20*, 3260-3267.
(24) Evans, I. P.; Spencer, A.; Wilkinson, G. *J. Chem. Soc., Dalton Trans.* **1973**, 204-209.
(25) *Data collection with APEX II* versions v1.0-22, v2009.1-0 and v2009.1-02, Bruker AXS inc., Madison, Wisconsin, USA, **2007**
(26) *Data reduction with Bruker SAINT* versions V.2.10(2003), V/.60A and V7.60A, Bruker AXS inc., Madison, Wisconsin, USA, **2007**
(27) *SADABS:* V.2.10(2003); V2008 and V2008/1, Bruker AXS inc., Madison, Wisconsin, USA, **2001**

(28) Sheldrick, G. M. *Acta Crystallogr. Sect. A* **2008**, *64*, 112-122.
(29) Zhao, Y.; Truhlar, D. G. *J. Chem. Phys.* **2006**, *125*, 194101.
(30) Gaussian 09, Revision A.1, Frisch, M. J.; Trucks, G. W.; Schlegel, H. B.; Scuseria, G. E.; Robb, M. A.; Cheeseman, J. R.; Scalmani, G.; Barone, V.; Mennucci, B.; Petersson, G. A.; Nakatsuji, H.; Caricato, M.; Li, X.; Hratchian, H. P.; Izmaylov, A. F.; Bloino, J.; Zheng, G.; Sonnenberg, J. L.; Hada, M.; Ehara, M.; Toyota, K.; Fukuda, R.; Hasegawa, J.; Ishida, M.; Nakajima, T.; Honda, Y.; Kitao, O.; Nakai, H.; Vreven, T.; Montgomery, J., J. A.; Peralta, J. E.; Ogliaro, F.; Bearpark, M.; Heyd, J. J.; Brothers, E.; Kudin, K. N.; Staroverov, V. N.; Kobayashi, R.; Normand, J.; Raghavachari, K.; Rendell, A.; Burant, J. C.; Iyengar, S. S.; Tomasi, J.; Cossi, M.; Rega, N.; Millam, J. M.; Klene, M.; Knox, J. E.; Cross, J. B.; Bakken, V.; Adamo, C.; Jaramillo, J.; Gomperts, R.; Stratmann, R. E.; Yazyev, O.; Austin, A. J.; Cammi, R.; Pomelli, C.; Ochterski, J. W.; Martin, R. L.; Morokuma, K.; Zakrzewski, V. G.; Voth, G. A.; Salvador, P.; Dannenberg, J. J.; Dapprich, S.; Daniels, A. D.; Farkas, Ö.; Foresman, J. B.; Ortiz, J. V.; Cioslowski, J.; Fox, D. J., Gaussian, Inc., Wallingford CT, 2009.
(31) Andrae, D.; Häußermann, U.; Dolg, M.; Stoll, H.; Preuß, H. *Theoret. Chim. Acta* **1990**, *77*, 123-141.
(32) Easton, R. E.; Giesen, D.; Welch, A.; Cramer, C.; Truhlar, D. *Theoret. Chim. Acta* **1996**, *93*, 281-301.
(33) Sheldon, R. A.; Kochi, J. K. *Metal-Catalyzed Oxidations of Organic Compounds*; Academic Press: New York, 1981.
(34) Cramer, C. J. *Essentials of Computational Chemistry: Theories and Models*; 2nd ed.; Wiley: Chichester, 2004.
(35) Marenich, A. V.; Cramer, C. J.; Truhlar, D. G. *J. Phys. Chem. B* **2009**, *113*, 6378-6396.

UNIVERSITAT ROVIRA I VIRGILI
SECOND-ROW TRANSITION-METAL COMPLEXES RELEVANT TO CO2 REDUCTION AND WATER OXIDATION
Takashi Ono
DL:T 1108-2014

UNIVERSITAT ROVIRA I VIRGILI
SECOND-ROW TRANSITION-METAL COMPLEXES RELEVANT TO CO2 REDUCTION AND WATER OXIDATION
Takashi Ono
DL:T 1108-2014

Supporting Information for:

Carbon Dioxide Reduction Catalyzed by Mononuclear Ruthenium Polypyridyl Complexes: Electronic and Steric Effects

Table of contents

UNIVERSITAT ROVIRA I VIRGILI
SECOND-ROW TRANSITION-METAL COMPLEXES RELEVANT TO CO2 REDUCTION AND WATER OXIDATION
Takashi Ono
DL:T 1108-2014

S1. NMR

Figure S1. 1D and 2D NMR spectra (500 MHz, 298K, CD_2Cl_2 with NEt_3) for complex Ru(bid)(6,6'-Me_2-bpy)(Cl) (**1e**)**:** (a) ^{1}H-NMR, (b) COSY, and (c) NOESY.

(a)

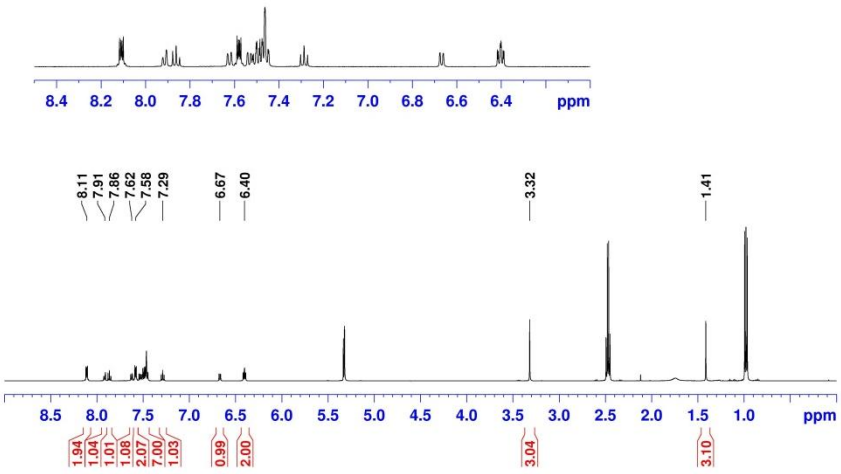

(b)

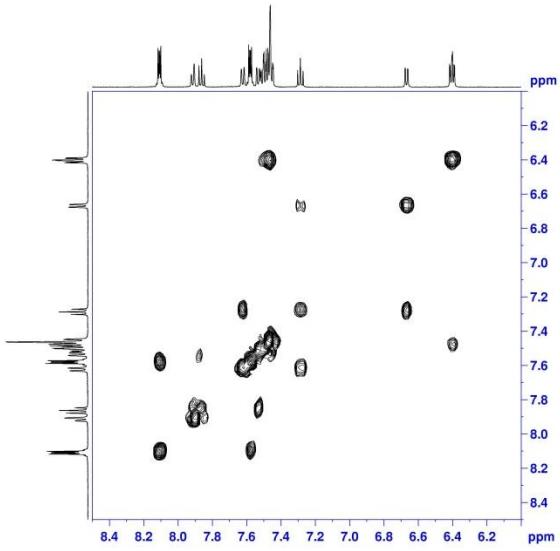

(c)

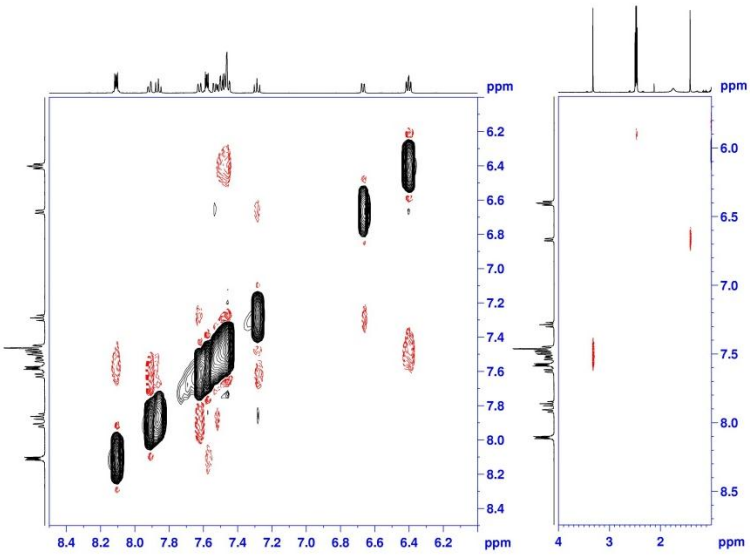

Figure S2. 1D and 2D NMR spectra (500 MHz, 298K, CD_2Cl_2 with NEt_3) for complex *trans*-Ru(bid)$(py)_2$(Cl) (**2**)**:** (a) COSY, and (b) NOESY.

(a)

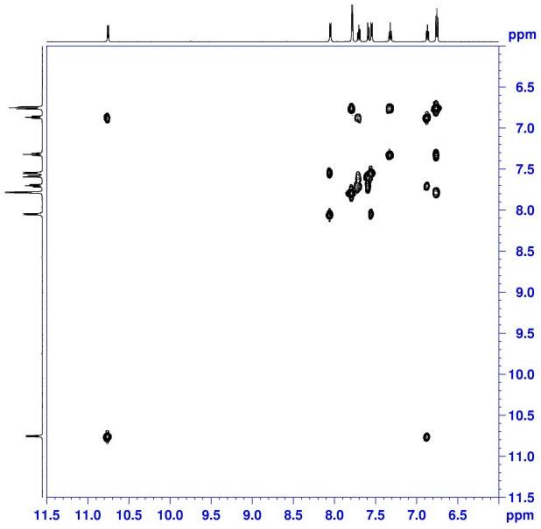

UNIVERSITAT ROVIRA I VIRGILI
SECOND-ROW TRANSITION-METAL COMPLEXES RELEVANT TO CO2 REDUCTION AND WATER OXIDATION
Takashi Ono
DL:T 1108-2014

(b)

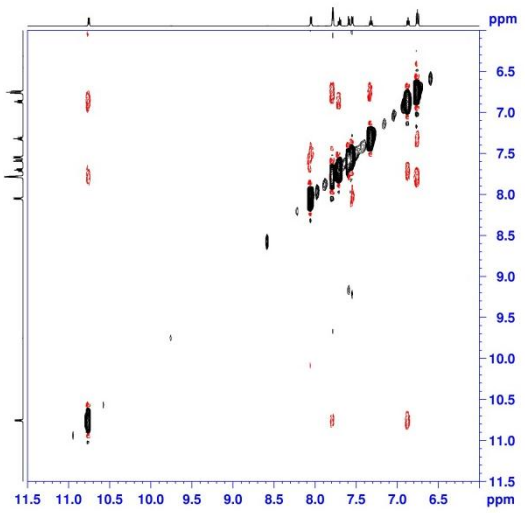

Figure S3. 1D and 2D NMR spectra (500 MHz, 298K, CD_2Cl_2) for complex Ru(dpb)(4,4'-$(COOEt)_2$-bpy)(Cl) (**3b**)**:** (a) ^{1}H-NMR, (b) COSY, and (c) NOESY.

(a)

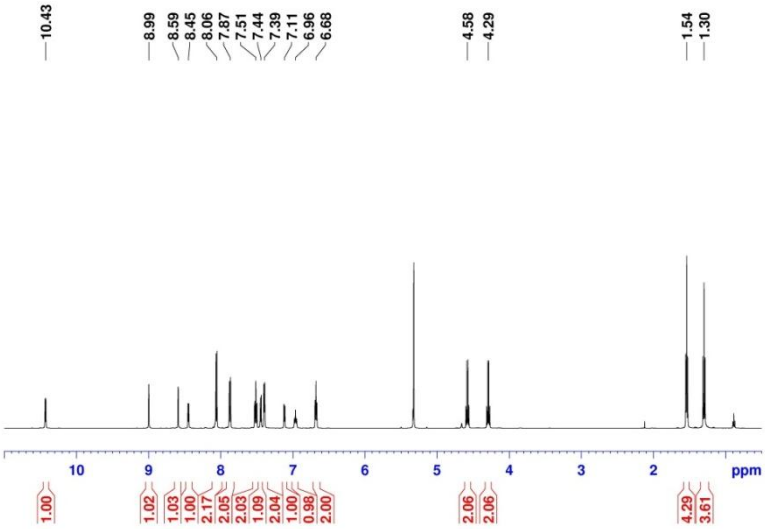

(b)

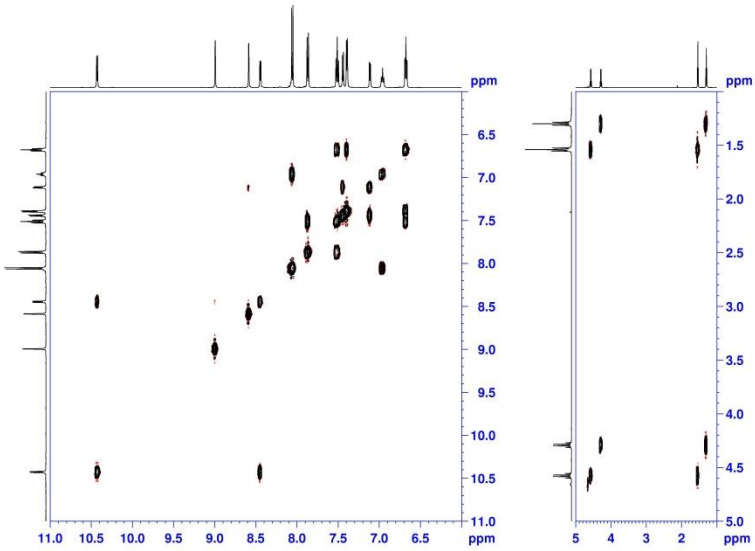
ppm
6.5
7.0
7.5
8.0
8.5
9.0
9.5
10.0
10.5
11.0
11.0 10.5 10.0 9.5 9.0 8.5 8.0 7.5 7.0 6.5 ppm
ppm
1.5
2.0
2.5
3.0
3.5
4.0
4.5
5.0
5 4 3 2 ppm

(c)

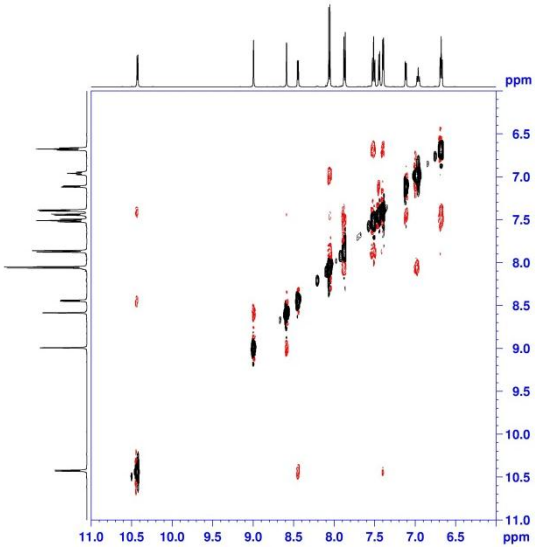
ppm
6.5
7.0
7.5
8.0
8.5
9.0
9.5
10.0
10.5
11.0
11.0 10.5 10.0 9.5 9.0 8.5 8.0 7.5 7.0 6.5 ppm

UNIVERSITAT ROVIRA I VIRGILI
SECOND-ROW TRANSITION-METAL COMPLEXES RELEVANT TO CO2 REDUCTION AND WATER OXIDATION
Takashi Ono
DL:T 1108-2014

Figure S4. Catalytic example: ^{1}H NMR spectrum of aliquot solution in D_2O after the catalytic reaction (using 0.3 mM of complex **1e**, CO_2 25 bar and H_2 25 bar at 100 °C for 20 min).

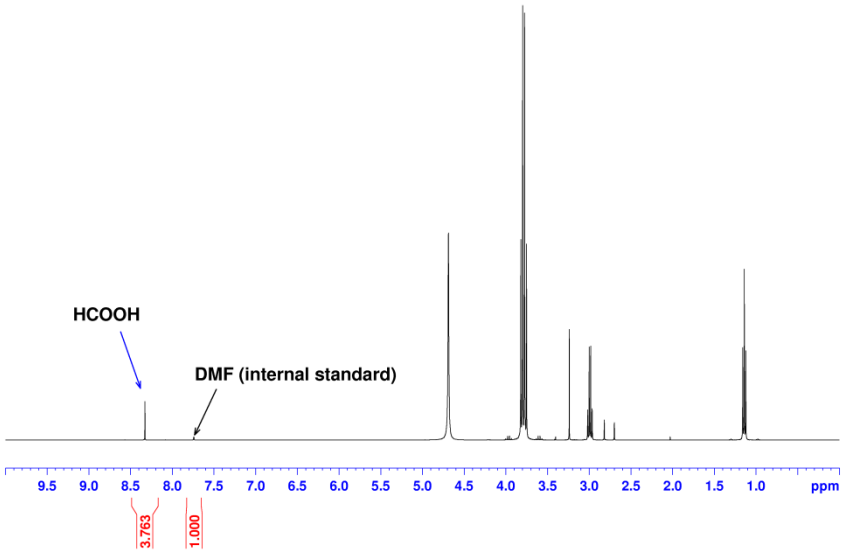

S2. X-ray

Table S1. Crystal data for **1d·0.5CH_2Cl_2** and **1e·CH_2Cl_2**.

	1d·0.5CH_2Cl_2		**1e·CH_2Cl_2**	
Empirical formula	$C_{23.50}H_{20}Cl_2N_5O_2Ru$		$C_{31}H_{26}Cl_3N_7Ru$	
Formula weight	576.41		704.01	
Temperature	100(2) K		100(2) K	
Wavelength	0.71073 Å		0.71073 Å	
Crystal system	Triclinic		Monoclinic	
Space group	P-1		P2(1)/c	
Unit cell dimensions	a = 9.0709(6) Å	α= 98.381(3)°	a = 10.3114(15) Å	α= 90.00°
	b = 10.4947(8) Å	β = 102.016(3)°	b = 14.828(2) Å	β = 92.380(5)°
	c = 12.7717(10) Å	γ = 101.289(3)°	c = 18.855(3) Å	γ = 90.00°
Volume	1143.91(15) $Å^3$		2880.5(7) $Å^3$	
Z	2		4	
Density (calculated)	1.673 Mg/m^3		1.623 Mg/m^3	
Absorption coefficient	0.951 mm^{-1}		0.859 mm^{-1}	
F(000)	580		1424	
Crystal size	0.20 x 0.10 x 0.10 mm^3		0.20 x 0.12 x 0.05 mm^3	
Theta range for data collection	2.02 to 36.47 °.		1.98 to 30.43 °.	
Index ranges	-15 <=h<=15 ,-16 <=k<=17 ,-21 <=l<=20		-14 <=h<=14 ,-19 <=k<=21 ,-26 <=l<=24	
Reflections collected	11122		40554	
Independent reflections	10198 [R(int) = 0.0516]		7889 [R(int) = 0.0374]	
Completeness to	theta =36.47° 0.990 %		theta =25.40° 0.904%	
Absorption correction	Empirical		Empirical	
Max. and min. transmission	0.9109 and 0.8325		0.9583 and 0.8470	
Refinement method	Full-matrix least-squares on F^2		Full-matrix least-squares on F^2	
Data / restraints / parameters	11122 / 0 / 318		7889 / 0 / 381	
Goodness-of-fit on F^2	1.055		1.037	
Final R indices [I>2sigma(I)]	R1 = 0.0668 , wR2 = 0.1866		R1 = 0.0272 , wR2 = 0.0636	
R indices (all data)	R1 = 0.0704 , wR2 = 0.1946		R1 = 0.0315 , wR2 = 0.0661	
Largest diff. peak and hole	4.255 and -7.506 e.$Å^{-3}$		1.421 and -1.207 e.$Å^{-3}$	

UNIVERSITAT ROVIRA I VIRGILI
SECOND-ROW TRANSITION-METAL COMPLEXES RELEVANT TO CO2 REDUCTION AND WATER OXIDATION
Takashi Ono
DL:T 1108-2014

S3. Electrochemistry

Figure S5. Cyclic voltammograms vs. SSCE at a scan rate 100 mV/s in DCM-TBAH (0.1 M), of complex (a) **1d** (0.25 mM), (b) **1e** (0.13 mM), (c) **2** (0.5 mM), and (d) **3b** (0.5 mM).

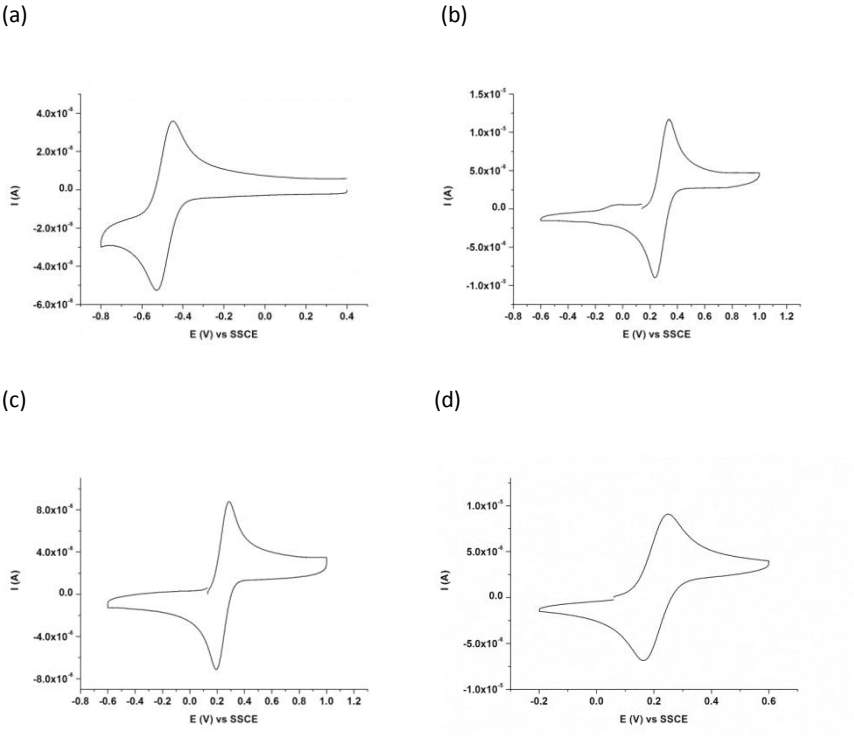

Figure S6. Cyclic voltammograms vs. SSCE of (a) *out*-$\mathbf{5}^{+}$ (0.5 mM) and (b) *in*-$\mathbf{5}^{+}$ (0.5 mM), with added NEt_3 (0, 0.2, 0.5, 1.0, 2.0, 5.0 equiv.) in 0.1 M DCM-$TBAPF_6$. Scan rate 100 mV/s. *: due to oxidation of excess amount of NEt_3.

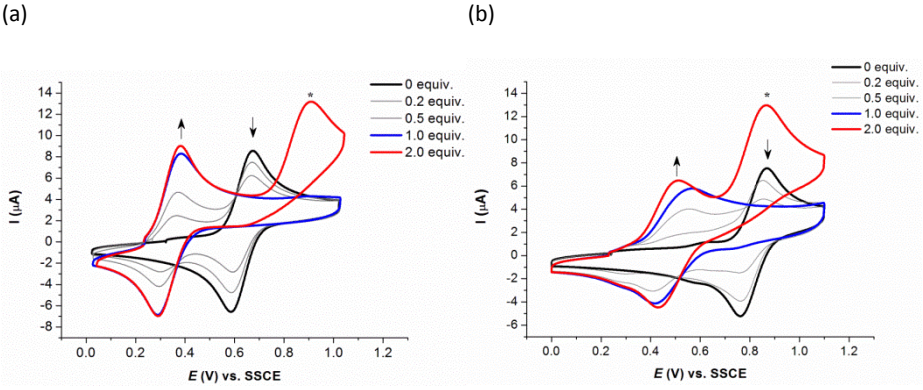

Chapter IV-1

Carbon Dioxide Reduction Catalyzed by Mononuclear Ruthenium Polypyridyl Complexes

ChemCatChem **2013**, 5, 3897–3903. DOI: 10.1002/cctc.201300372

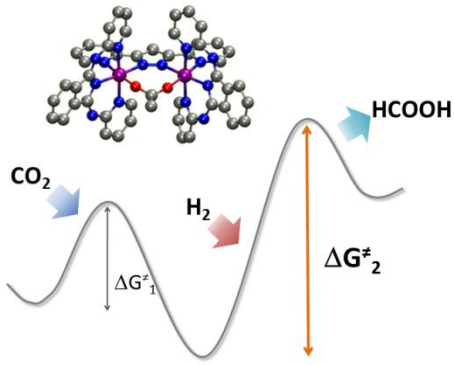

Table of Contents

UNIVERSITAT ROVIRA I VIRGILI
SECOND-ROW TRANSITION-METAL COMPLEXES RELEVANT TO CO2 REDUCTION AND WATER OXIDATION
Takashi Ono
DL:T 1108-2014

IV-1.1. Abstract

Dinuclear ruthenium complexes with formula $[(Ru(bid))_2(\mu\text{-bpp})(\mu\text{-OAc})]$ and $[(Ru(trpy))_2(\mu\text{-bpp})(\mu\text{-X})]^{2+}$ (X= Cl^-, OAc^- and $OCHO^-$) (*bid*$^-$ is (1*Z*,3*Z*)-1,3-bis(pyridin-2-ylimino)isoindolin-2-ide; *trpy* is 2,2':6',2''-terpyridine) were tested as catalysts for the hydrogenative reduction of carbon dioxide in 2,2,2-trifluoroethanol (TFE) as solvent in the presence of excess amine (NEt_3). Significant amounts of formic acid were produced by these catalysts and a kinetic analysis based on initial rate constants was carried out. These catalytic systems were investigated by means of density functional theory calculations (DFT) to elucidate the hydrogenative reduction mechanism. Results are compared to those obtained with previously reported mononuclear catalyst counterparts.

IV-1.2. Introduction

Higher plants, green algae, and cyanobacteria use sunlight to generate molecular oxygen and fix atmospheric carbon dioxide.[1] This process generates an aerobic atmosphere and a readily available carbon energy source, both of which are required to sustain almost all life on our planet. During the last few decades, research pursuing a catalyst that captures CO_2 and transforms it in the form of a "solar fuel" has become a highly relevant challenge.[2-3] Carbon dioxide is the most abundant greenhouse gas present in the atmosphere and nowadays the scientific community agrees that the increase of its concentration during the last century is mainly anthropogenic.[4-6] Consequently, the use of CO_2 as a cheap and highly abundant starting material for chemical synthesis has become a hot topic mainly driven by environmental, legal, and social concerns.

Hydrogenative CO_2 reduction catalyzed by organometallic complexes allows the synthesis of a wide variety of reduced products such as formic acid, formaldehyde, methanol and, ultimately, methane.[7-27] The production of formic acid represents the initial step for all these reduction processes.

UNIVERSITAT ROVIRA I VIRGILI
SECOND-ROW TRANSITION-METAL COMPLEXES RELEVANT TO CO2 REDUCTION AND WATER OXIDATION
Takashi Ono
DL:T 1108-2014

We previously studied a set of mononuclear ruthenium-polypyridyl catalysts for the hydrogenative reduction of CO_2 to formic acid having the general formula $[Ru(T)(bpy)(Cl)]^{n+}$, where T is a *bid*$^-$ or *trpy* meridional ligand. The *bpy* and *bid*$^-$ ligands of these compounds were sequentially functionalized with electron donor/withdrawing groups to alter their electronic properties and consequently their catalytic performance.[28]

In this paper we report a combined experimental and computational study of Ru polypyridyl catalysts for the hydrogenative reduction of CO_2 to formic acid. The catalytic performances of complex $[(Ru(bid))_2(\mu\text{-bpp})(\mu\text{-OAc})]$ (**1**) and the family of complexes $[(Ru(trpy))_2(\mu\text{-bpp})(\mu\text{-X})]^{2+}$ (**2-X^{2+}**) (X= Cl^-, OAc^- and $OCHO^-$), where *bid*$^-$ is (1*Z*,3*Z*)-1,3-bis(pyridin-2-ylmethylene)isoindolin-2-ide and *trpy* is 2,2':6',2''-terpyridine (Figures 1 and 2), have been investigated. The dependence of their activity on pressure, temperature, and concentration has been carefully analyzed.

The previously studied mononuclear compounds [Ru(bid)(bpy)(Cl)] (**3**) and $[Ru(trpy)(bpy)(Cl)]^+$ (**4$^+$**) can be considered the mononuclear homologues of the dinuclear catalysts **1** and **2-Cl^{2+}**, respectively. The direct comparison of the properties of these two sets of catalysts, both from an experimental and theoretical perspective, permits further analysis of the effects of catalyst nuclearity and ligand nature on the catalytic performance of ruthenium polypyridyl complexes.

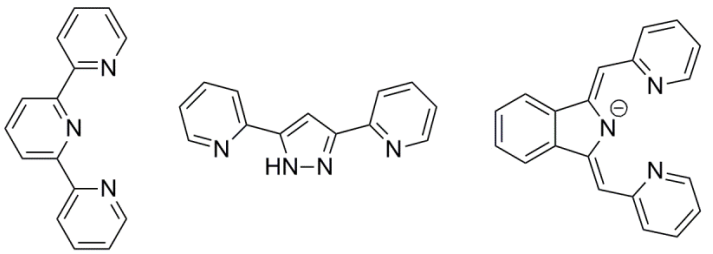

Figure 1. Nitrogenated polydentate ligands employed. From left to right: 2,2':6',2''-terpyridine (*trpy*), bis(2-pyridyl)-3,5-pyrazole (*Hbpp*) and (1*Z*,3*Z*)-1,3-bis(pyridin-2-ylimino)isoindolin-2-ide (*bid*$^-$).

IV-1.3. Results and Discussion

IV-1.3.1. Synthesis and structure

Synthesis

Scheme 1. Synthetic procedures for **2-OCHO^{2+}**

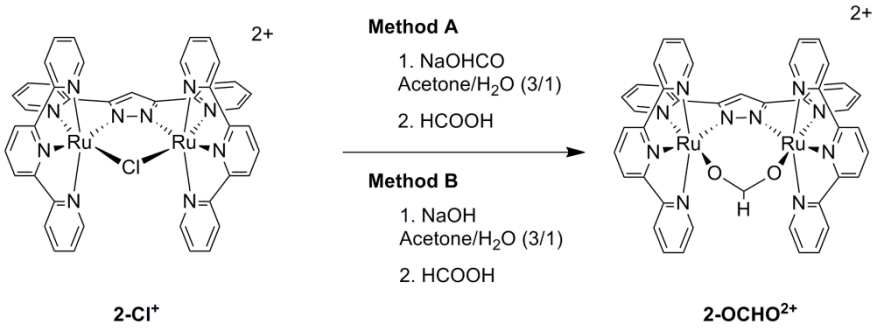

All compounds except [(Ru(trpy))$_2$(μ-bpp)(μ-OCHO)](PF$_6$)$_2$ (**[2-OCHO](PF$_6$)$_2$**) were synthesized as previously reported.[28-31] In order to obtain compound **2-OCHO^{2+}**, the μ-Cl bridge in **2-Cl^{2+}** was replaced by a μ-OCHO bridge when the former was reacted with excess amount of sodium formate under reflux conditions in an acetone/water (3/1) solution, followed by the addition of formic acid (Scheme 1, see experimental section for further details). The addition of KPF$_6$, and consequent volume reduction, yielded a solid precipitate. Recrystallization from acetone/diethyl ether yielded crystals of **[2-OCHO](PF$_6$)$_2$·2Me$_2$CO** suitable for single-crystal X-ray structure determination (Figure 2).

As in other dinuclear Ru-*Hbpp* complexes[30] **2-OCHO^{2+}** has a pseudo-C_2 symmetry axis passing through the centre of the pyrazole ring, both ruthenium metal centres adopt a slightly distorted octahedral geometry where the *bpp*$^-$ ligand is bound to the two metal centres with an almost coplanar disposition of its three rings. The *trpy* ligands are quasi-perpendicular to the Ru-*Hbpp* moiety. The octahedral geometry is slightly distorted by the constrained bite angles of the chelating ligands and crystal packing in the solid state. Bond lengths for **1** and for the **2^{2+}** family from calculated DFT structures are in good agreement with the experimental X-ray structure of **2-OCHO^{2+}**

UNIVERSITAT ROVIRA I VIRGILI
SECOND-ROW TRANSITION-METAL COMPLEXES RELEVANT TO CO2 REDUCTION AND WATER OXIDATION
Takashi Ono
DL:T 1108-2014

and the other previously reported ruthenium-*Hbpp* complexes.[30,32-33] However, calculated and measured angles between the metal center and the ligands are in less good agreement due to crystal packing effects on both *bid*$^-$ and *trpy* ligands (Table 1).

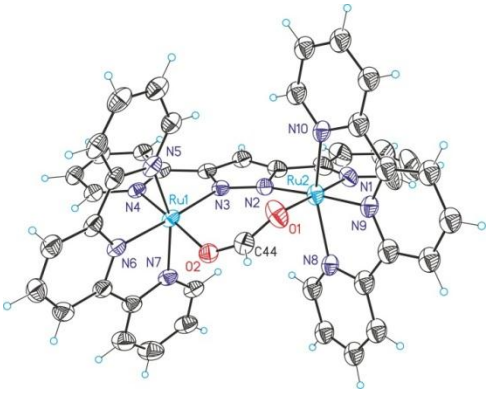

Figure 2. Ortep plot (ellipsoids at 50% probability) of the X-ray crystal structure of the cationic moiety of **2-OCHO**$^{2+}$ together with labeling scheme. Color codes: Ru, violet; N, blue; O, red; C, grey. Hydrogen atoms are not shown for clarity except the hydrogen atom in the formate moiety.

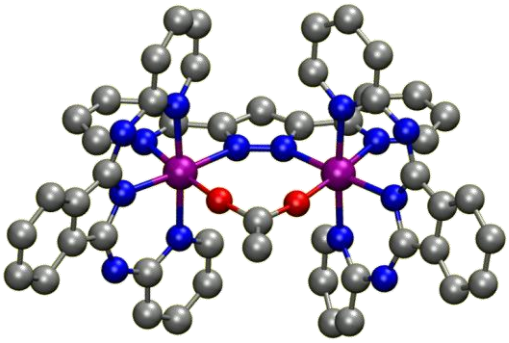

Figure 3. Ball and stick representation of DFT-optimized structure of [(Ru(bid))$_2$(μ-bpp)(μ-OAc)] (**1**). Hydrogen atoms are omitted. Right, Ortep plot (ellipsoids at 50% probability) of the X-ray crystal structure of the cationic moiety of **2-OCHO**$^{2+}$ together with labeling scheme. Color codes: Ru, violet; N, blue; O, red; C, grey.

Table 1. Selected bond lengths (Å) and angles (°) for complexes **1-OCHO**, **2OCHO**$^{2+}$, and **2-Cl**$^{2+}$ (same labeling scheme used for **1-OCHO** and **2-OCHO**$^{2+}$).

	1-OCHO	**2-OCHO**$^{2+}$		**2-Cl**$^{2+}$	
	DFT	**DFT**	**X-ray**	**DFT**	**X-ray**[b]
Ru-L[a]	2.20	2.18	2.16	2.53	2.45
Ru-N3	2.07	2.06	2.06	2.07	2.06
Ru-N4	2.05	2.05	2.04	2.07	2.08
Ru-N5	2.09	2.06	2.07	1.97	1.97
Ru-N6	2.03	1.96	1.96	2.07	2.06
Ru-N7	2.13	2.08	2.07	2.01	2.00
N3-Ru-L[a]	101.8	102.4	102.4	92.1	90.4
N5-Ru-L[a]	87.3	88.4	89.4	91.9	91.3
N3-Ru-N6	175.6	175.6	174.0	91.2	96.1
N3-Ru-N7	90.5	101.3	101.7	99.6	95.4

[a] Distance to the ruthenium coordinated atom of the bridging ligand between the metal centers, L = $HCOO^-$ for **1** and **2-OCHO**$^{2+}$ and L=Cl^- for **2-Cl**$^{2+}$. [b] Ref 30

IV-1.3.2. Catalytic experiments

Compound **1** and the series of **2-X**$^{2+}$ were tested as catalyst precursors for the hydrogenative reduction of CO_2 in TFE, and in all cases formic acid was the sole product detected. In addition, two mononuclear catalysts, $[Ru(trpy)(bpy)(Cl)]^+$ (**3**) and [Ru(bid)(bpy)(Cl)] (**4**), previously reported by our group were tested simultaneously for comparative purposes.[28]

Turnover number (TON) and initial turnover frequencies (TOF_i) were calculated after 3 days and 90 minutes respectively and are reported in Table 2, for catalysts **1**, **2-Cl**$^{2+}$, **3** and **4**$^+$. A typical profile of the catalysts performances versus time is offered in Figure 4. It can be observed that after 3 days the mononuclear catalysts are deactivated, while the dinuclear ones are still active. The enhance stability of the dinuclear complexes with regard to the mononuclear ones is associated with the polychelating nature of the *bpp*$^-$ bridging ligand that when coordinated to the two metal centres generates a very stable structure that avoids potential decomposition pathways.

After 3 days, a TON of 1427 was reached by **1**, (Table 2) which represents a 30% improvement compared to its mononuclear analogue **3**. For the *trpy* complexes, dinuclear complex **2-Cl**$^{2+}$ reached a TON of 409 after 3 days, which is 17 times higher than that of its mononuclear analogue **4**$^{+}$.

Table 2. Catalytic performances of dinuclear (**1**, **2-Cl**$^{2+}$, **2-OCHO**$^{2+}$ and **2-OAc**$^{2+}$) and mononuclear (**3** and **4**$^{+}$) CO_2 reduction catalysts.[a]

Catalyst		$E_{1/2}$[b]	TOF_i[c]	TON[d]
1	$[(Ru(bid))_2(\mu\text{-bpp})(\mu\text{-OAc})]$	0.108, 0.517[e]	288.3 (178.4)	1427
2-Cl^{2+}	$[(Ru(trpy))_2(\mu\text{-bpp})(\mu\text{-Cl})]^{2+}$	0.710, 1.116[f]	7.0 (4.3)	409
2-OCHO^{2+}	$[(Ru(trpy))_2(\mu\text{-bpp})(\mu\text{-OCHO})]^{2+}$	0.754, 1.074	7.4 (4.6)	—
2-OAc^{2+}	$[(Ru(trpy))_2(\mu\text{-bpp})(\mu\text{-OAc})]^{2+}$	0.742, 1.053[f]	—	—
3	[Ru(bid)(bpy)(Cl)]	0.295[g]	366.0 (226.5)[g]	1101
4^{+}	$[Ru(trpy)(bpy)(Cl)]^{+}$	0.865[g]	1.6 (1.0)[g]	24

[a] Reaction conditions: 0.3 mM solution of complexes dissolved in a 9:1 mixture of TFE and NEt_3 at 25 bar of CO_2 and 25 bar of H_2 at 100°C. [b] $E_{1/2}$ (V) obtained from $(E_{p,a} + E_{p,c})/2$ vs SSCE. Scan rate 100 mV/s in glassy carbon working electrode and a Pt disk counter electrode. [c] TOF_i in h^{-1}. Initial Turnover Frequencies, considering the first 90 minutes. In parenthesis values normalized with regard to complex **4**$^{+}$. [d] TON of HCOOH detected after three days. [e] Ref 29. [f] Ref 30. [g] Ref 28.

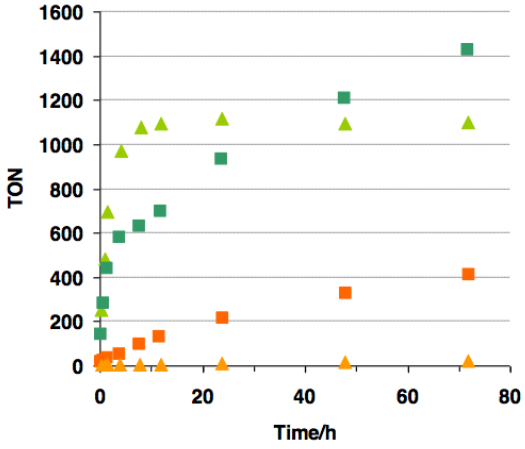

Figure 4. Catalytic performance of a 0.3 mM solution of complexes **1** (■), **2-Cl**$^{2+}$ (■), **3** (▲) and **4**$^{+}$ (▲) dissolved in a 9:1 mixture of TFE and NEt_3 at 25 bar of CO_2 and 25 bar of H_2 at 100 °C.

By comparing the effect of the anionic *bid*$^-$ ligand with that of the *trpy* ligand, we found that complex **1** converts CO_2 into formic acid 41 times faster than **2-Cl**$^{2+}$ under identical conditions.

For *bid*$^-$-containing complexes, we found that the TOF_i of dinuclear complex **1** is 21% lower than that of mononuclear complex **3**, whereas for the *trpy*-containing complexes the TOF_i of the dinuclear complex **2-Cl**$^{2+}$ is 4.3 times higher than that of mononuclear complex **4**$^+$. The reactivity of **2-Cl**$^{2+}$ and **2-OCHO**$^{2+}$ give similar results within the experimental error.

The rate of formic acid formation was studied for complex **1** as a function of catalyst concentration, H_2 pressure, and CO_2 pressure (Figures S4-S6). The initial rates of formate formation are consistent with a first-order behaviour with respect to catalyst concentration and H_2 pressure, whereas the initial rates were found to be independent of CO_2 pressure. Similarly, in the case of **2-Cl**$^{2+}$ first-order behaviour with respect to catalyst concentration is found (Figures S7-8).

IV-1.3.3. DFT Calculations

DFT calculations using the M06-L functional were performed to study the reaction pathways for the overall catalytic process and to rationalize the observed ligand effect on the catalytic activity. We studied a mechanism analogous to that previously proposed for the mononuclear catalysts.[28] The mechanism consists of three general steps: 1) CO_2 insertion into an intermediate Ru-H species, 2) displacement of the newly formed "formato" ligand by H_2, and 3) regeneration of the reactive hydride by the heterolytic cleavage of the H-H bond assisted by a base (Figure 5).

The optimized intermediate and transition state (TS) structures for compound **2-X**$^{2+}$ and the energy profiles for the catalytic cycles of both **1** and **2-X**$^{2+}$ systems are shown in Figure 6. The initial active species features a ruthenium hydride at one centre and a weakly coordinated CO_2 at the second centre. This weak coordination can be observed in the Ru-L bond lengths: 1.639 and 1.633 Å for Ru-H and 2.466 and 2.976 Å for Ru-CO_2 for **1** and **2-X**$^{2+}$, respectively. The initial hydride attack on CO_2 generates, through a TS structure (**I-TS**) with associated free energy of activation $\Delta G^{\neq}_1$, a formato

UNIVERSITAT ROVIRA I VIRGILI
SECOND-ROW TRANSITION-METAL COMPLEXES RELEVANT TO CO2 REDUCTION AND WATER OXIDATION
Takashi Ono
DL:T 1108-2014

ligand bridging between the two ruthenium centres (**II**). Then, a H_2 molecule coordinates with one of the ruthenium centres, displacing one of the formato-coordinated O atoms; this process is predicted to be endergonic in nature (**III**).

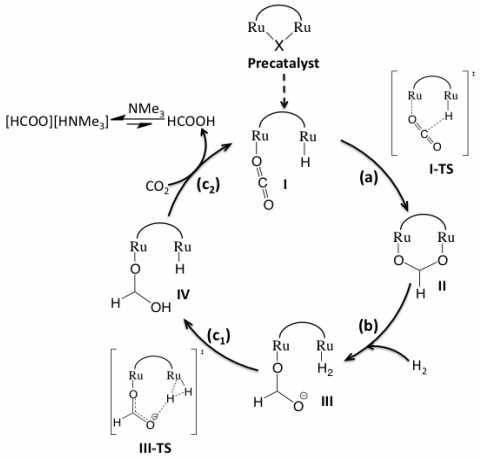

Figure 5. Proposed catalytic cycle for CO_2 reduction.

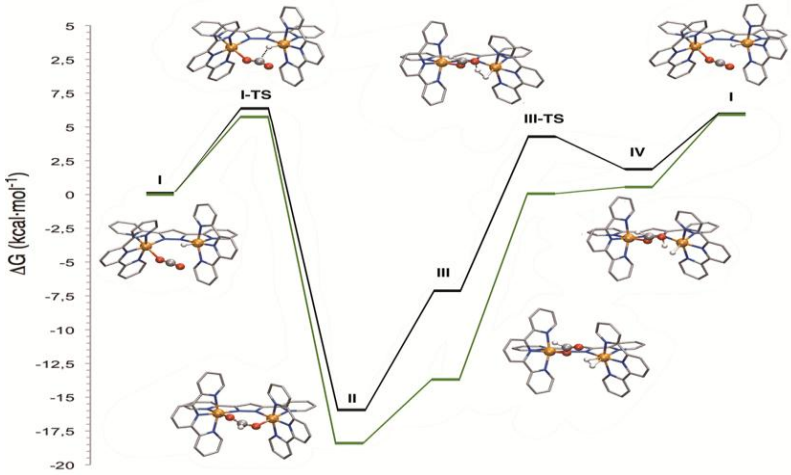

Figure 6. Computed free energy profiles (kcal/mol) for the proposed catalytic cycles of complexes **1** (green) and **2-X^{2+}** (black). The initial [(Ru(T)(CO_2))(Ru(T)(H))(μ-bpp)] species (with T = *trpy* and *bid*$^-$), define the relative zero of energy. Only optimized structures of **2-X^{2+}** are shown and H atoms on the ruthenium ligands are omitted for clarity. *Note: Gas phase electronic energies of **III-TS** for catalyst **1** is 1.4 kcal/mol lower in energy but after including the zero point energy, entropy and solvation contributions it becomes 0.5 kcal/mol higher.*

The heterolytic cleavage of the H-H bond is assisted by the formato ligand (still bound to the second metal center) (**III-TS**), which regenerates the Ru-H center and produces a formic acid molecule. In the final step of the catalytic cycle, a CO_2 molecule displaces the newly formed formic acid; this regenerates **I**. The free energy of activation associated with the H-H heterolytic cleavage by free amine acting as the base was also considered. In all cases, higher free energies of activation were obtained for the amine assisted TS compared with the formato ligand-assisted TS (**III-TS**) depicted in Figure 7.

The presence of the amine is critical, however, as its activity as a base is used to drive the catalytic process through the formation of an ammonium salt of the generated formic acid, which contributes 4.8 kcal/mol of additional driving force; hence, with an overpressure of H_2 and/or CO_2, the catalytic process is net exergonic. For both ligand systems, the free energy of activation associated with the TS structure for the heterolytic cleavage of the dihydrogen intermediate from the formato intermediate ($\Delta G^{\neq}_2$) was found to be the rate-determining step. The free energies of activation ($\Delta G^{\neq}_2$) are computed to be 18.4 and 20.1 kcal/mol for **1** and **2-X^{2+}**, respectively. This trend is consistent with the relative rates summarized in Table 2 and Figure 7.

The key effect of the *bid*$^-$ ligand in **1**, compared to the *trpy* ligand in **2-X^{2+}**, which leads to a significantly improved catalytic activity of the former compound, is the destabilization of the formato intermediate relative to the dihydrogen-substituted intermediate. This effect is associated with the anionic character of the *bid*$^-$ ligand. Although this leads to a free energy of activation for the heterolytic cleavage (Figure 5, step c_1) that is 2.3 kcal/mol higher for **1** than for **2-X^{2+}**, the H_2 coordination to the formato-bridged species (step b) is 4.0 kcal/mol less favourable for **2-X^{2+}** than for **1**, which results in an overall lower free energy of activation for the rate-determining step ($b+c_1$) for **1**.

In line with the experimental findings (Table 2), the calculated free energies of activation for the rate–determining steps ($\Delta G^{\neq}_2$) indicate that the dinuclear catalyst **1** is expected to have a slightly higher activity compared to its mononuclear analogue **3**

UNIVERSITAT ROVIRA I VIRGILI
SECOND-ROW TRANSITION-METAL COMPLEXES RELEVANT TO CO2 REDUCTION AND WATER OXIDATION
Takashi Ono
DL:T 1108-2014

whereas **2-X**$^{2+}$ is predicted to demonstrate significantly higher activity compared to its mononuclear analogue **4**$^{+}$. The free energy of activation for the rate-determining steps b and c_1 varies significantly, both in net magnitude and in individual components, over the various complexes studied (Table 3).

Table 3. Activation energies for the CO_2 insertion into the ruthenium hydride ($\Delta G^{\neq}_1$) and the rate-determining step with its contributions (substitution of the formato ligand by dihydrogen and the Ru-H_2 moiety heterolytic cleavage) for dinuclear (**1** and **2-X**$^{2+}$) and mononuclear (**3** and **4**$^{+}$) catalysts.[a]

	Catalyst	$\Delta G^{\neq}_1$	OCHO/H_2 ligand exchange	Heterolytic cleavage	$\Delta G^{\neq}_2$
1	[(Ru(bid))$_2$(μ-bpp)(μ-OAc)]	5.6	4.7	13.7	18.4
2-X^{2+}	[(Ru(trpy))$_2$(μ-bpp)(μ-X)]$^{2+}$	6.1	8.7	11.4	20.1
3	[Ru(bid)(bpy)(Cl)]	10.2	11.0[b]	8.0[b]	19.0[b]
4^{+}	[Ru(trpy)(bpy)(Cl)]$^{+}$	12.2	22.6[b]	2.5[b]	25.1[b]

[a] Energies in kcal/mol. [b] Reference 28.

The formate/dihydrogen ligand exchange activation energy is strongly affected by the relative σ-donation of the *bid*$^{-}$ and *trpy* ligands. For dinuclear complexes, the free energy of activation increases from 4.7 to 8.7 kcal/mol for the *bid*$^{-}$ and *trpy* complexes, respectively, which implies that the strong electron donation supplies sufficient electron density to the metal center so that it facilitates the breaking of one of the Ru-O bonds of the formato bridge and thus generates a pseudo-pentacoordinated complex[33] ready for H_2 coordination. The opposite trend is observed for the next step, however; heterolytic H_2 splitting is disfavored for the strong σ-donating ligands as they reduce the acidity of the coordinated H_2 fragment. Because the overall energy of activation is a combination of these two factors acting in opposite directions, limited opportunities exist for the exploitation of ligand substitution effects.

IV-1.4. Conclusions

We have studied a family of dinuclear ruthenium complexes containing neutral and monoanionic meridional ligands, such as [(Ru(bid))$_2$(μ-bpp)(μ-OAc)] (**1**) and [(Ru(trpy))$_2$(μ-bpp)(μ-X)]$^{2+}$ (**2-X^{2+}** ; X=Cl$^-$, OAc$^-$, OCHO$^-$; bpp$^-$ = 3,5-bis(2-pyridyl)pyrazolato; bid$^-$ = (1*Z*,3*Z*)-1,3-bis(pyridin-2-ylimino)isoindolin-2-ide; trpy = 2,2':6',2"-terpyridine) and evaluated their activity as hydrogenative CO_2 reduction catalysts to form formic acid. Their activity has been compared with that of the previously reported mononuclear catalysts [Ru(bid)(bpy)(Cl)] (3; bpy=2,2'-bypiridine) and [Ru(trpy)(bpy)(Cl)]$^+$ (**4$^+$**). The use of anionic *bid*$^-$ as a meridional ligand in **1** and **3** increases both turnover number (TON) and initial turnover frequency (TOF_i) compared to their *trpy*-based analogues (**2-X^{2+}** and **4$^+$**). For instance, the dinuclear catalyst **1** has a TOF_i of 228 whereas **2-Cl^{2+}** is only 7.0.The mononuclear complex **3** has a TOF_i higher than that of **1**; however, it deactivates earlier, which leads to a lower TON than that of **1**, appearing stable in the long run. For the dinuclear compounds **1** and **2-Cl^{2+}**, the initial rate was studied as a function of catalyst concentration, H_2 pressure, and CO_2 pressure. The results indicate that the catalytic process is first order with respect to catalyst concentration and H_2 pressure but zero order with respect to CO_2 pressure. These observations are consistent with the rate-determining step, as predicted by theory, which encompasses OCHO/H_2 ligand substitution (step b) followed by H_2 heterolytic cleavage (step c_1). The accelerating effect on the catalytic performance associated with the presence of negatively charged ligands is rationalized owing to DFT calculations. Increasing electron density on the metal center decreases the free energy change associated with step b but increases the free energy of activation for subsequent step c_1. The evidently stronger effect of electronic effects on step b relative to step c_1 is ultimately responsible for the increased reactivity observed with anionic ligands.

UNIVERSITAT ROVIRA I VIRGILI
SECOND-ROW TRANSITION-METAL COMPLEXES RELEVANT TO CO2 REDUCTION AND WATER OXIDATION
Takashi Ono
DL:T 1108-2014

IV-1.5. Experimental Section

Materials

All reagents used in the present work were obtained from Aldrich Chemical Co. or Alfa Aesar and were used without further purification. Synthesis grade organic solvents were obtained from SDS and were routinely degassed with Argon. 2,2,2-Trifluoroethanol (TFE) was obtained from Alfa Aesar and was used without further purification. Carbon dioxide (Premier) and hydrogen (BIP) gases were obtained from Carburos Metálicos S. A.. The complexes $[(Ru(bid))_2(\mu\text{-bpp})(\mu\text{-OAc})]$ (**1**),[29] $[(Ru(trpy))_2(\mu\text{-bpp})(\mu\text{-Cl})](PF_6)_2$ (**[2-Cl](PF$_6$)$_2$**),[30] $[(Ru(trpy))_2(\mu\text{-bpp})(\mu\text{-OAc})](PF_6)_2$ (**[2-OAc](PF$_6$)$_2$**),[30] [Ru(bid)(bpy)(Cl)] (**3**)[28] and $[Ru(trpy)(bpy)(Cl)](PF_6)$ (**[4](PF$_6$)**)[31] were prepared as described in the literature. All synthetic manipulations were routinely performed under an argon atmosphere using Schlenk and vacuum-line techniques.

Synthesis

Synthesis of $[(Ru(trpy))_2(\mu\text{-bpp})(\mu\text{-OCHO})](PF_6)_2$ ([2-OCHO](PF$_6$)$_2$)

***Method A*:** 120 mg (0.0987 mmol) of $[(Ru(trpy))_2(\mu\text{-bpp})(\mu\text{-Cl})](PF_6)_2$, **[2-Cl](PF$_6$)$_2$** and 67.5 mg (0.993 mmol, 10 equiv.) of sodium formate were dissolved in 20 mL of acetone-water (3:1) and heated at reflux for 7 h. The resulting solution was filtered and 1 mL of saturated aqueous solution of KPF_6 was added. Upon reducing the volume, a solid came out of the solution that washed with water and ether. To this solid dissolved in 5 mL of acetone 1 mL (26.5 mmol) of formic acid was added and stirred at room temperature for 30 min. To this solution 1 mL of saturated aqueous solution of KPF_6 and 5 mL of water was added. Upon reducing the volume, a solid came out of the solution that was washed with water and ether and dried under vacuum. Yield: 97.1 mg (80%). ***Method B*:** To a solution of 200 mg (0.164 mmol) of $[(Ru(trpy))_2(\mu\text{-bpp})(\mu\text{-Cl})](PF_6)_2$, **[2-Cl](PF$_6$)$_2$**, in 24 mL of acetone, 8.0 mL of 0.5 M aqueous NaOH (4.0 mmol) was added and heated at reflux for 4 h. After cooling to room temperature 1 mL of saturated aqueous solution of KPF_6 was added to the resulting solution. Upon reducing the volume, a solid came out of the solution that washed with water and ether. To this

solid dissolved in 10 mL of acetone 1.5 mL (39.8 mmol) of formic acid was added and stirred at room temperature for 30 min. To this solution 1 mL of saturated aqueous solution of KPF_6 and 10 mL of water was added. Upon reducing the volume, a solid came out of the solution that washed with water and ether and dried under vacuum. Yield: 160.0 mg (80%). Anal. Calcd. for $C_{44}H_{33}F_{12}N_{10}O_{2.5}P_2Ru_2 \cdot 0.5\ H_2O$: C, 42.49; H, 2.84; N, 11.26; Found: C, 42.67 ; H, 2.84; N, 11.14. The NMR assignment is keyed in Scheme 2. ^{1}H NMR (500 MHz, Acetone-d_6, 298 K): δ 8.71 (d, 4H, J_{JK} = 8.1 Hz, H_J), 8.60 (d, 4H, J_{IH} = 7.6 Hz, H_I), 8.54 (s, 1H, H_A), 8.50 (d, 4H, J_{FG} = 5.6 Hz, H_F), 8.21 (t, 2H, J_{KJ} = $J_{KJ'}$ = 8.1 Hz, H_K), 8.20 (d, 2H, J_{BC} = 7.6 Hz, H_B), 8.03 (td, 4H, J_{HG} = J_{HI} = 7.6 Hz, J_{HF} = 0.9 Hz, H_H), 7.74 (td, 2H, J_{CB} = J_{CD} = 7.6 Hz, J_{CE} = 1.3 Hz, H_C), 7.57 (ddd, 4H, J_{GH} = 7.6 Hz, J_{GF} = 5.6 Hz, J_{GI} = 1.4 Hz, H_G), 7.46 (d, 2H, J_{ED} = 5.7 Hz, H_E), 7.16 (s, 1H, H_L), 6.84 (ddd, 2H, J_{DC} = 7.6 Hz, J_{DE} = 5.7 Hz, J_{DB} = 1.4 Hz, H_D). ^{13}C NMR (125 MHz, Acetone-d_6, 298 K): δ 179.9 (C_L), 161.0 (C_γ), 160.6 (C_δ), 157.5 ($C_{\alpha'}$), 154.8 (C_F), 153.9 (C_E), 152.9 (C_α), 138.4 (C_H), 136.8 (C_C), 135.4 (C_K), 128.4 (C_G), 124.6 (C_I), 123.6 (C_J), 123.2 (C_D), 120.4 (C_B), 105.0 (C_A). ESI-MS (MeOH): *m/z* 1080.8 ($[M\text{-}PF_6]^+$).

Scheme 2. NMR labeling scheme

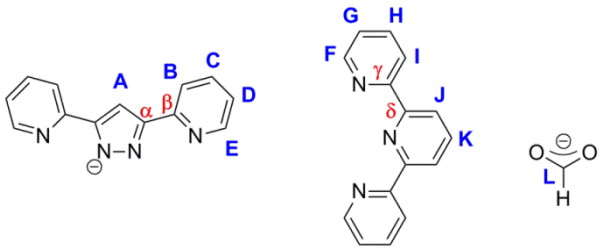

Standard procedure for catalytic hydrogenative CO_2 reduction

Catalytic reactions were run with an SPR16 Slurry Phase Reactor, which is a completely automated reactor system consisting 16 autoclaves (15 mL capacity). Once the program started, a leak test for each autoclave was done and then each reactor was purged with nitrogen gas. Afterward, a complex solution (4.0 mL; solvent/amine = 9/1) was added to each autoclave of the reactor from the top of the vessel under N_2. Once

UNIVERSITAT ROVIRA I VIRGILI
SECOND-ROW TRANSITION-METAL COMPLEXES RELEVANT TO CO2 REDUCTION AND WATER OXIDATION
Takashi Ono
DL:T 1108-2014

all the solvents and reagents were distributed in all the vessels, stirring at 1000 rpm was started, followed by pressurizing with CO_2 gas and then H_2 gas at the desired pressures. Then the temperature was increased to the desired value, at which point was considered the initial time. At the end of the reaction each reactor was cooled to room temperature and depressurized. The samples were analyzed by ^{1}H NMR spectroscopy, taking the reaction solution (0.3 mL) and mixing it with D_2O (0.2 mL) containing DMF (an internal standard;120 μL in 10 mL of D_2O). Two replicates were performed for each measurement.

Instrumentation and measurements

Cyclic voltammetric (CV) experiments were performed in a IJ-Cambria IH-660 potentiostat, using a three electrode cell. Glassy carbon disk electrodes (3 mm diameter) from BASi were used as working electrode, platinum wire as auxiliary and SSCE as the reference electrode. Cyclic voltammograms were recorded at 100 mV/s scan rate under nitrogen atmosphere. The complexes were dissolved in previously degassed dichloromethane containing the necessary amount of (n-Bu_4N)(PF_6), used as supporting electrolyte, to yield a 0.1 M ionic strength solution. All $E_{1/2}$ values reported in this work were estimated from cyclic voltammetry as the average of the oxidative and reductive peak potentials ($E_{p,a}$+$E_{p,c}$)/2 or from differential pulse voltammetry (DPV; pulse amplitudes of 0.05 V, pulse widths of 0.05 s, sampling width of 0.02 s, and a pulse period of 0.1 s). Unless explicitly mentioned the concentration of the complexes were approximately 1 mM. The NMR spectroscopy was performed on bruker avance 400 MHz bruker avance II and bruker avance 500 MHz. The ESI mass spectroscopy experiments were performed on a Waters Micromass LCT Premier equipment, respectively. UV-Vis spectroscopy was performed on a Cary bio 50 UV-vis spectrophotometer with 1 cm quartz cells.

X-Ray structure determination

Suitable Crystals of complex **[2-OCHO](PF_6)$_2$·2Me_2CO** were grown from acetone/diethyl ether. The measured crystals were prepared under inert conditions

immersed in perfluoropolyether as protecting oil for manipulation. **[2-OCHO](PF$_6$)$_2$·2Me$_2$CO**: In the crystal structure the Ruthenium centers showed disorder with one of the bridging ligands that corresponded to formato:chlorido ratio of 90:10. The origin of the chlorido ligand was unclear; however, that ligand could havecome from the trace amounts of chloride counter anion associated with the **2-OCHO^{2+}**, which have ended up substituting the bridging ligand. One of the *trpy* ligands of the complex was disordered in two positions with an occupation ratio of 50:50. One PF_6 was disordered in two positions with occupation ratio 70:30. The asymmetric unit also contains two molecules of acetone disordered in three positions. CCDC 928293 contains the supplementary crystallographic data for complex [**2-OCHO][PF$_6$]$_2$·2Me$_2$CO**. These data can be obtained free of charge from the Cambridge Crystallographic Data Centre via www.ccdc.cam.ac.uk/data_request/cif.

***Data collection**:* Crystal structure determinations were carried out using a Bruker-Nonius diffractometer equipped with an APPEX 2 4K CCD area detector, a FR591 rotating anode with MoK$_\alpha$ radiation, Montel mirrors as monochromator, and a Kryoflex low temperature device (T = -173 °C). Full-sphere data collection was used with ω and φ scans. APEX-2 (for Data collection),[34] Bruker Saint V/.60A (for data reduction),[35] and SADABS (for absorption correction).[36]

***Structure Solution and Refinement**:* Crystal structure solution was achieved using direct methods as implemented in SHELXTL[37] and visualized using the program XP. Missing atoms were subsequently located from difference Fourier synthesis and added to the atom list. Least-squares refinement on F^2 using all measured intensities was carried out using the program SHELXTL. All non-H atoms were refined, including anisotropic displacement parameters.ç

Computational Details

All geometries were fully optimized at the M06-L level[38] of density functional theory with the Gaussian 09 electronic structure program suite[39] using the Stuttgart [8s7p6d2f | 6s5p3d2f] ECP28MWB contracted pseudopotential basis set on ruthenium,[40] the MIDI! basis set[41] on the supporting ligands and the 6-31G(d,p) basis set on all other

UNIVERSITAT ROVIRA I VIRGILI
SECOND-ROW TRANSITION-METAL COMPLEXES RELEVANT TO CO2 REDUCTION AND WATER OXIDATION
Takashi Ono
DL:T 1108-2014

atoms (i.e., those reacting as part of the catalytic cycle).[42] Integral evaluation made use of the grid defined as ultrafine in the Gaussian 09 program. The nature of all stationary points was verified by analytic computation of vibrational frequencies. These were employed for the computation of zero-point vibrational energies and molecular partition functions for use in computing 298 K thermal contributions to free energy.[43] Solvent effects of 2,2,2-trifluoroethanol were included with the SMD continuum solvation model.[44] Single point energy calculations were also performed increasing the basis set, size for the non-metal atoms to 6-311+G(2df,p).[42] Ethyl groups in NEt_3 were modeled as methyl groups for efficiency.

IV-1.6. Acknowledgments

Support from MINECO (CTQ-2010-21497) and the US National Science Foundation (NSF) (CHE-0952054). T.O. thanks MINECO for a doctoral grant. N.P. and L.G. acknowledge the NSF (CHE-1212575).

I have carried out experimental part. DFT calculations were performed by Dr. P. Miro and Dr. M. Z. Ertem in the group of Prof. C. J. Cramer at the University of Minnesota.

IV-1.7. References

(1) Barber, J. *Chem. Soc. Rev.* **2009**, *38*, 185-196.
(2) Takeda, H.; Ishitani, O. *Coord. Chem. Rev.* **2010**, *254*, 346-354.
(3) Morris, A. J.; Meyer, G. J.; Fujita, E. *Acc. Chem. Res.* **2009**, *42*, 1983-1994.
(4) Canadell, J. G.; Le Quéré, C.; Raupach, M. R.; Field, C. B.; Buitenhuis, E. T.; Ciais, P.; Conway, T. J.; Gillett, N. P.; Houghton, R. A.; Marland, G. *Proc. Natl. Acad. Sci. U.S.A.* **2007**, *104*, 18866-18870.
(5) Raupach, M. R.; Marland, G.; Ciais, P.; Le Quéré, C.; Canadell, J. G.; Klepper, G.; Field, C. B. *Proc. Natl. Acad. Sci. U.S.A.* **2007**, *104*, 10288-10293.
(6) Karl, T. R.; Trenberth, K. E. *Science* **2003**, *302*, 1719-1723.
(7) Wang, W.; Wang, S.; Ma, X.; Gong, J. *Chem. Soc. Rev.* **2011**, *40*, 3703-3727.
(8) Jessop, P. G.; Joó, F.; Tai, C.-C. *Coord. Chem. Rev.* **2004**, *248*, 2425-2442.
(9) Jessop, P. G. In *The Handbook of Homogeneous Hydrogenation*; Wiley-VCH Verlag GmbH: 2008, p 489-511.
(10) Hutschka, F.; Dedieu, A.; Eichberger, M.; Fornika, R.; Leitner, W. *J. Am. Chem. Soc.* **1997**, *119*, 4432-4443.
(11) Gassner, F.; Leitner, W. *J. Chem. Soc., Chem. Commun.* **1993**, 1465-1466.
(12) Graf, E.; Leitner, W. *J. Chem. Soc., Chem. Commun.* **1992**, 623-624.

(13) Munshi, P.; Main, A. D.; Linehan, J. C.; Tai, C.-C.; Jessop, P. G. *J. Am. Chem. Soc.* **2002**, *124*, 7963-7971.
(14) Jessop, P. G.; Hsiao, Y.; Ikariya, T.; Noyori, R. *J. Am. Chem. Soc.* **1996**, *118*, 344-355.
(15) Jessop, P. G.; Ikariya, T.; Noyori, R. *Nature* **1994**, *368*, 231-233.
(16) Ng, S. M.; Yin, C.; Yeung, C. H.; Chan, T. C.; Lau, C. P. *Eur. J. Inorg. Chem.* **2004**, *2004*, 1788-1793.
(17) Urakawa, A.; Jutz, F.; Laurenczy, G.; Baiker, A. *Chem. —Eur. J.* **2007**, *13*, 3886-3899.
(18) Maenaka, Y.; Suenobu, T.; Fukuzumi, S. *Energy Environ. Sci.* **2012**, *5*, 7360-7367.
(19) Hull, J. F.; Himeda, Y.; Wang, W.-H.; Hashiguchi, B.; Periana, R.; Szalda, D. J.; Muckerman, J. T.; Fujita, E. *Nat. Chem.* **2012**, *4*, 383-388.
(20) Tanaka, R.; Yamashita, M.; Nozaki, K. *J. Am. Chem. Soc.* **2009**, *131*, 14168-14169.
(21) Himeda, Y.; Onozawa-Komatsuzaki, N.; Sugihara, H.; Kasuga, K. *Organometallics* **2007**, *26*, 702-712.
(22) Ziebart, C.; Federsel, C.; Anbarasan, P.; Jackstell, R.; Baumann, W.; Spannenberg, A.; Beller, M. *J. Am. Chem. Soc.* **2012**, *134*, 20701-20704.
(23) Federsel, C.; Ziebart, C.; Jackstell, R.; Baumann, W.; Beller, M. *Chem. —Eur. J.* **2012**, *18*, 72-75.
(24) Federsel, C.; Boddien, A.; Jackstell, R.; Jennerjahn, R.; Dyson, P. J.; Scopelliti, R.; Laurenczy, G.; Beller, M. *Angew. Chem., Int. Ed.* **2010**, *49*, 9777-9780.
(25) Langer, R.; Diskin-Posner, Y.; Leitus, G.; Shimon, L. J. W.; Ben-David, Y.; Milstein, D. *Angew. Chem., Int. Ed.* **2011**, *50*, 9948-9952.
(26) Wesselbaum, S.; vom Stein, T.; Klankermayer, J.; Leitner, W. *Angew. Chem., Int. Ed.* **2012**, *51*, 7499-7502.
(27) Huff, C. A.; Sanford, M. S. *J. Am. Chem. Soc.* **2011**, *133*, 18122-18125.
(28) Planas, N.; Ono, T.; Vaquer, L.; Miro, P.; Benet-Buchholz, J.; Gagliardi, L.; Cramer, C. J.; Llobet, A. *Phys. Chem. Chem. Phys.* **2011**, *13*, 19480-19484.
(29) Planas, N.; Christian, G. J.; Mas-Marzá, E.; Sala, X.; Fontrodona, X.; Maseras, F.; Llobet, A. *Chem. —Eur. J.* **2010**, *16*, 7965-7968.
(30) Sens, C.; Romero, I.; Rodríguez, M.; Llobet, A.; Parella, T.; Benet-Buchholz, J. *J. Am. Chem. Soc.* **2004**, *126*, 7798-7799.
(31) Rasmussen, S. C.; Ronco, S. E.; Mlsna, D. A.; Billadeau, M. A.; Pennington, W. T.; Kolis, J. W.; Petersen, J. D. *Inorg. Chem.* **1995**, *34*, 821-829.
(32) Bozoglian, F.; Romain, S.; Ertem, M. Z.; Todorova, T. K.; Sens, C.; Mola, J.; Rodríguez, M.; Romero, I.; Benet-Buchholz, J.; Fontrodona, X.; Cramer, C. J.; Gagliardi, L.; Llobet, A. *J. Am. Chem. Soc.* **2009**, *131*, 15176-15187.
(33) Planas, N.; Christian, G.; Roeser, S.; Mas-Marzá, E.; Kollipara, M.-R.; Benet-Buchholz, J.; Maseras, F.; Llobet, A. *Inorg. Chem.* **2012**, *51*, 1889-1901.
(34) *Data collection with APEX II* versions v1.0-22, v2009.1-0 and v2009.1-02, Bruker AXS inc., Madison, Wisconsin, USA, **2007**
(35) *Data reduction with Bruker SAINT* versions V.2.10(2003), V/.60A and V7.60A, Bruker AXS inc., Madison, Wisconsin, USA, **2007**
(36) *SADABS:* V.2.10(2003); V2008 and V2008/1, Bruker AXS inc., Madison, Wisconsin, USA, **2001**
(37) Sheldrick, G. M. *Acta Crystallogr. Sect. A* **2008**, *64*, 112-122.
(38) Zhao, Y.; Truhlar, D. G. *J. Chem. Phys.* **2006**, *125*, 194101.
(39) Gaussian 09, Revision A.1, Frisch, M. J.; Trucks, G. W.; Schlegel, H. B.; Scuseria, G. E.; Robb, M. A.; Cheeseman, J. R.; Scalmani, G.; Barone, V.; Mennucci, B.; Petersson, G. A.; Nakatsuji, H.; Caricato, M.; Li, X.; Hratchian, H. P.; Izmaylov, A. F.; Bloino, J.; Zheng, G.; Sonnenberg, J. L.; Hada, M.; Ehara, M.; Toyota, K.; Fukuda, R.; Hasegawa, J.; Ishida, M.;

Nakajima, T.; Honda, Y.; Kitao, O.; Nakai, H.; Vreven, T.; Montgomery, J., J. A.; Peralta, J. E.; Ogliaro, F.; Bearpark, M.; Heyd, J. J.; Brothers, E.; Kudin, K. N.; Staroverov, V. N.; Kobayashi, R.; Normand, J.; Raghavachari, K.; Rendell, A.; Burant, J. C.; Iyengar, S. S.; Tomasi, J.; Cossi, M.; Rega, N.; Millam, J. M.; Klene, M.; Knox, J. E.; Cross, J. B.; Bakken, V.; Adamo, C.; Jaramillo, J.; Gomperts, R.; Stratmann, R. E.; Yazyev, O.; Austin, A. J.; Cammi, R.; Pomelli, C.; Ochterski, J. W.; Martin, R. L.; Morokuma, K.; Zakrzewski, V. G.; Voth, G. A.; Salvador, P.; Dannenberg, J. J.; Dapprich, S.; Daniels, A. D.; Farkas, Ö.; Foresman, J. B.; Ortiz, J. V.; Cioslowski, J.; Fox, D. J., Gaussian, Inc., Wallingford CT, 2009.

(40) Andrae, D.; Häußermann, U.; Dolg, M.; Stoll, H.; Preuß, H. *Theoret. Chim. Acta* **1990**, *77*, 123-141.

(41) Easton, R. E.; Giesen, D.; Welch, A.; Cramer, C.; Truhlar, D. *Theoret. Chim. Acta* **1996**, *93*, 281-301.

(42) Sheldon, R. A.; Kochi, J. K. *Metal-Catalyzed Oxidations of Organic Compounds*; Academic Press: New York, 1981.

(43) Cramer, C. J. *Essentials of Computational Chemistry: Theories and Models*; 2nd ed.; Wiley: Chichester, 2004.

(44) Marenich, A. V.; Cramer, C. J.; Truhlar, D. G. *J. Phys. Chem. B* **2009**, *113*, 6378-6396.

UNIVERSITAT ROVIRA I VIRGILI
SECOND-ROW TRANSITION-METAL COMPLEXES RELEVANT TO CO2 REDUCTION AND WATER OXIDATION
Takashi Ono
DL:T 1108-2014

Supporting Information for:

Carbon Dioxide Reduction Catalyzed by Dinuclear Ruthenium Polypyridyl Complexes

Table of contents

UNIVERSITAT ROVIRA I VIRGILI
SECOND-ROW TRANSITION-METAL COMPLEXES RELEVANT TO CO2 REDUCTION AND WATER OXIDATION
Takashi Ono
DL:T 1108-2014

S1. NMR:

Figure S1. 1D and 2D NMR spectra (500 MHz, 298K, Acetone-d_6) for complex **2-OCHO^{2+}:** (a) ^{1}H-NMR, (b) COSY, and (c) NOESY.

(a)

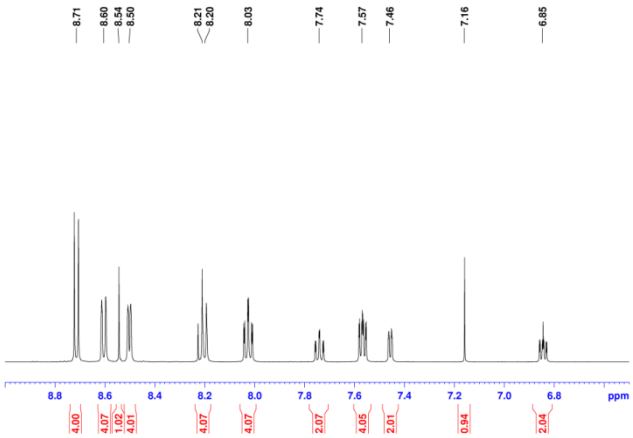

(b)

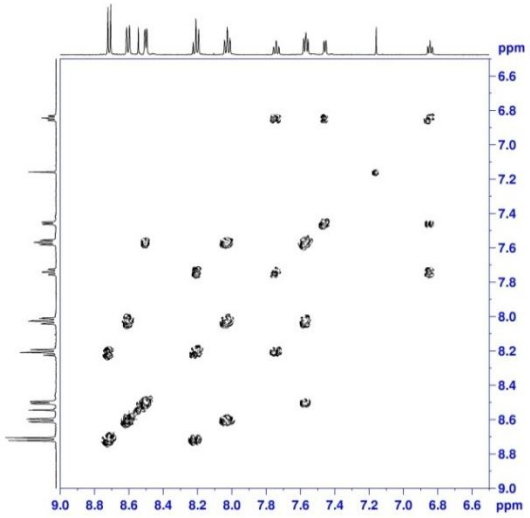

(c)

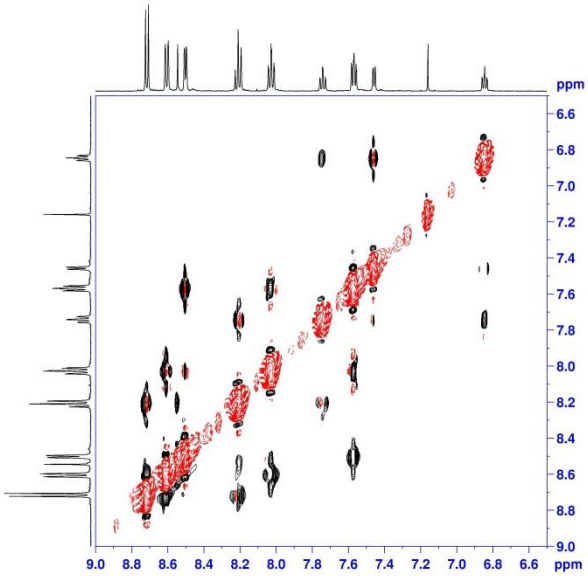

Figure S2. Catalytic example: ^{1}H NMR spectrum of aliquot solution in D_2O after catalytic reaction (using 0.3 mM of complex **1**, CO_2 25 bar and H_2 25 bar at 100 °C for 20 min).

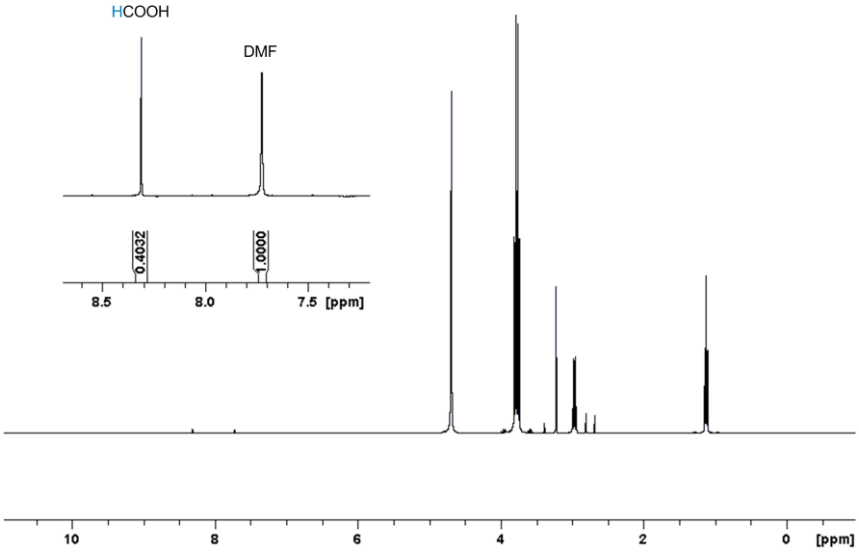

UNIVERSITAT ROVIRA I VIRGILI
SECOND-ROW TRANSITION-METAL COMPLEXES RELEVANT TO CO2 REDUCTION AND WATER OXIDATION
Takashi Ono
DL:T 1108-2014

S2. Kinetic measurements:

Figure S3. Initial catalytic performance of a 0.3 mM solution of complexes **1**, **2-Cl**$^{2+}$, **2-OCHO**$^{2+}$, **3** and **4**$^{+}$ dissolved in a 9:1 mixture of TFE and NEt_3 at 25 bar of CO_2 and 25 bar of H_2 at 100 °C. ■: **1**, ■: **2-Cl**$^{2+}$, ■: **2-OCHO**$^{2+}$, ▲: **3**, ▲: **4**$^{+}$.

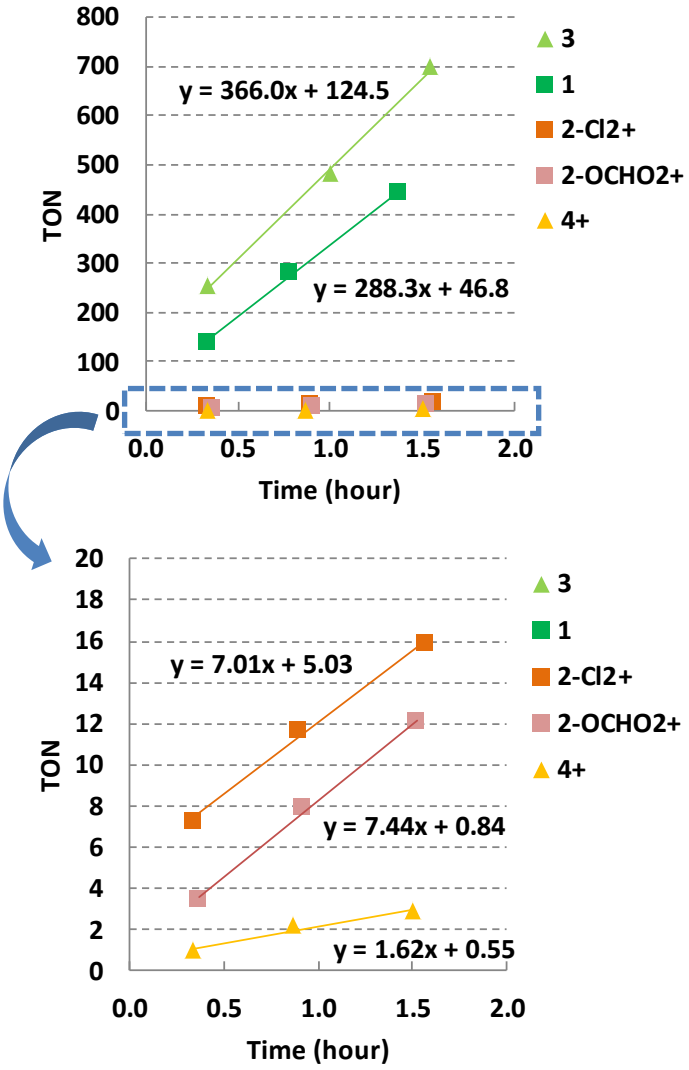

Figure S4. Left: Formation of formic acid at different concentrations of complex **1** with respect to time. Right: Initial rates with respect to precatalyst concentration. (complex **1**, 25 bar of CO_2, 25 bar of H_2, 100 °C)

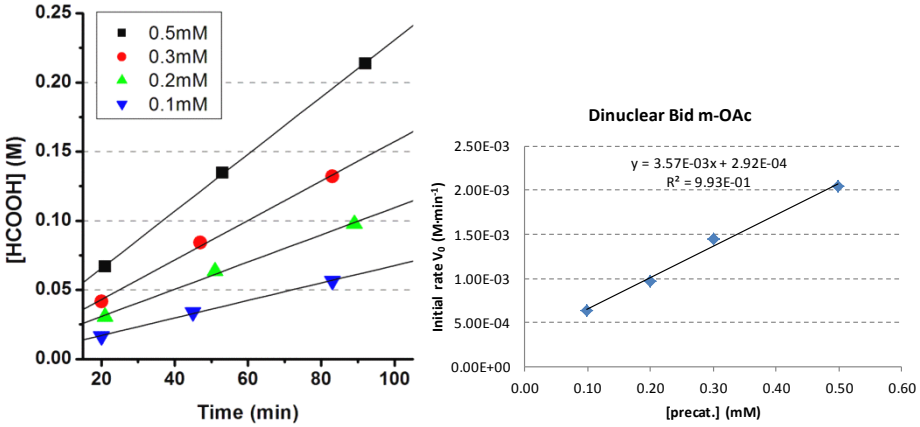

Figure S5. Left: Formation of formic acid at different H_2 pressures with respect to time Right: Initial rates with respect to partial pressure of H_2. (0.3 mM of complex **1**, 25 bar of CO_2, 100 °C)

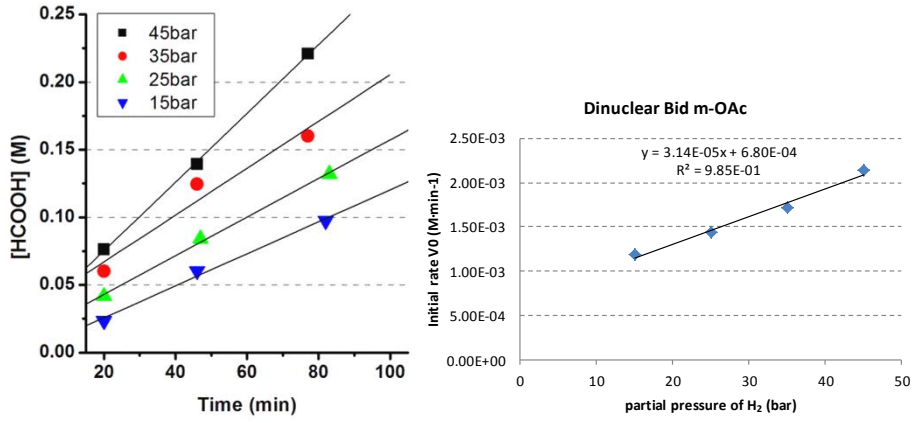

Figure S6. Left: Formation of formic acid at different CO_2 pressures with respect to time Right: Initial rates with respect to partial pressure of CO_2. (0.3 mM of complex **1**, 25 bar of H_2, 100 °C)

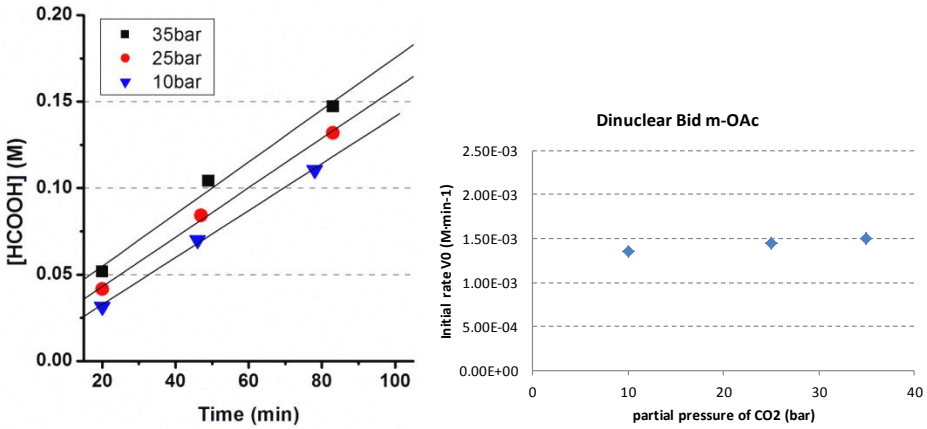

Figure S7. Left: Formation of formic acid at different precatalyst concentrations with respect to time (complex **2-Cl**$^{2+}$, 25 bar of CO_2, 25 bar of H_2, 100 °C). ■: 0.1 mM, ■: 0.2 mM, ■: 0.3 mM, ■: 0.5 mM. Right: Initial rates with respect to precatalyst concentration. (complex **2**, 25 bar of CO_2, 25 bar of H_2, 100 °C)

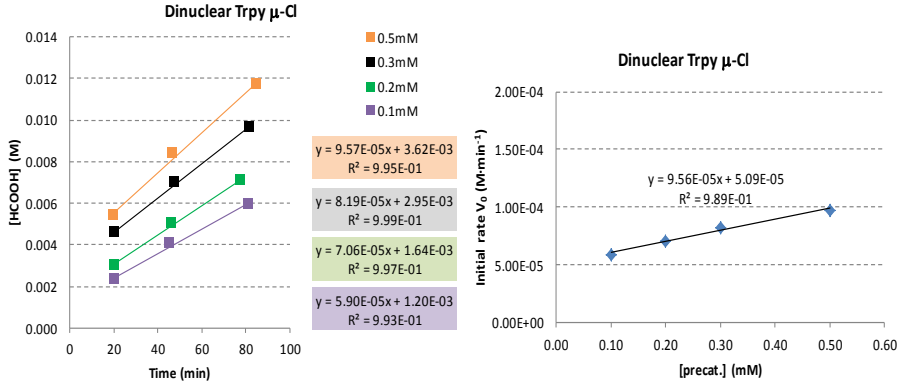

UNIVERSITAT ROVIRA I VIRGILI
SECOND-ROW TRANSITION-METAL COMPLEXES RELEVANT TO CO2 REDUCTION AND WATER OXIDATION
Takashi Ono
DL:T 1108-2014

Chapter IV-2

Dinuclear Ruthenium Hydride Complexes Containing Hbpp and Terpyridine Ligands: Synthesis and Reactivity

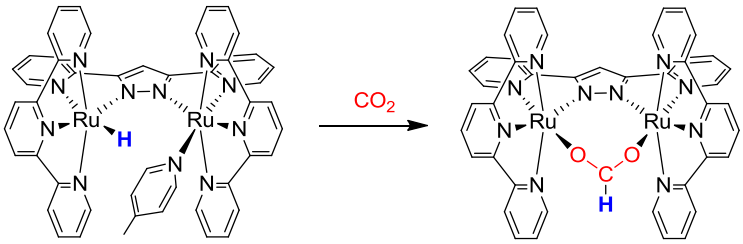

Table of Contents

UNIVERSITAT ROVIRA I VIRGILI
SECOND-ROW TRANSITION-METAL COMPLEXES RELEVANT TO CO2 REDUCTION AND WATER OXIDATION
Takashi Ono
DL:T 1108-2014

IV-2.1. Abstract

Treatment of dinuclear ruthenium complex $\{[Ru(trpy)]_2(\mu\text{-bpp})(\mu\text{-Cl})\}^{2+}$, $\mathbf{1}^{2+}$, (*trpy*: 2,2':6',6''-terpyridine, *bpp*$^-$: 3,5-bis(2-pyridyl)pyrazolate) with excess sodium borohydride, $NaBH_4$ in pyridine-d_5 produces a mixture of hydride species, ending up with three different dinuclear dihydride species, namely *in*,*in*-, *in*,*out*-, and *out*,*out*-$\mathbf{3}^+$ (*in*/*out* reflects the direction of metal hydride bonds with respect to inside or outside of the chelating *bpp*$^-$ ligand), which were tentatively assigned by 1D and 2D NMR spectroscopy. Additionally, non-symmetric dinuclear mono-hydride species *in*,*in*-$\{[Ru(trpy)(H)][Ru(trpy)(L)]\}(\mu\text{-bpp})^{2+}$ (L = 4-picoline) has been cleanly *in-situ* generated by treating *in*,*in*-$\{[Ru(trpy)(L)]_2(\mu\text{-bpp})\}^{3+}$, $\mathbf{4}^{3+}$, with equimolar amount of $NaBH_4$ in dimethylformamide-d_7 and characterized by spectroscopic and electrochemical techniques. Finally its reactivity toward CO_2 has been examined.

IV-2.2. Introduction

Recently, we have found that dinuclear ruthenium polypyridyl complexes, $\{[Ru(trpy)]_2(\mu\text{-bpp})(\mu\text{-Cl})\}^{2+}$, $\mathbf{1}^{2+}$, (*trpy*:2,2':6',6''-terpyridine, *bpp*$^-$: 3,5-bis(2-pyridyl)pyrazolate) and $[(Ru(bid))_2(\mu\text{-bpp})(\mu\text{-OAc})]$, **2**, (*bid*$^-$: (1*Z*,3*Z*)-1,3-bis(pyridin-2-ylimino)isoindolin-2-ide) are the precatalyst for the hydrogenative CO_2 reduction with initial turnover frequencies (TOF_i) of 7.0 h^{-1} and 288.3 h^{-1}, respectively and turnover number (TON) of 409 and 1427, respectively.[1] Interestingly, their stabilities were drastically improved compared to their mononuclear analogues $[Ru(trpy)(bpy)Cl]^+$ and $[Ru(bid)(bpy)Cl]$[2]. The improved stability of dinuclear complexes with respect to mononuclear ones is associated with chelating *bpp*$^-$ ligand.

As well as reactivity of these mononuclear and dinuclear Ru complexes, it is of great importance to carry out the characterization of catalytic intermediate species by means of isolation and/or spectroscopic techniques[3-7] in order to understand the catalytic mechanism.

Although polypyridyl ruthenium-hydrido complexes have been proposed to be intermediates in the reduction reaction of CO_2, CO, and formaldehyde,[8-10] and in

UNIVERSITAT ROVIRA I VIRGILI
SECOND-ROW TRANSITION-METAL COMPLEXES RELEVANT TO CO2 REDUCTION AND WATER OXIDATION
Takashi Ono
DL:T 1108-2014

hydrogen evolution,[11-12] only a few of Ru-H complexes without π-acidic ligand have been isolated including $[Ru(trpy)(bpy)H]^+$,[13] because of their high instability.

Here we report synthesis and characterization of dinuclear ruthenium hydrido complexes which can be considered as a catalytic intermediate equivalent, and its reactivity toward CO_2.

IV-2.3. Results and Discussion

IV-2.3.1. Reaction of dinuclear μ-Cl complex with $NaBH_4$

Scheme 1. The reaction of the μ-Cl complex $\mathbf{1}^{2+}$ with $NaBH_4$.

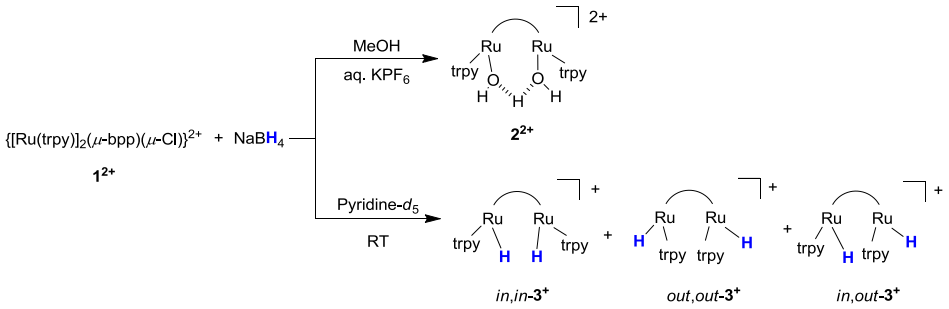

Following the similar procedure for the synthesis of $[Ru(trpy)(bpy)(H)]^+$ [13] (*bpy*: 2,2'-bipyridine), dinuclear complex $\mathbf{1}^{2+}$ was treated with $NaBH_4$ as a hydride source in MeOH, followed by the addition of aqueous KPF_6 solution to precipitate a purple solid (Scheme 1, top). This, however, resulted in the complex mixture containing mainly hydrolyzed compound $\mathbf{2}^{2+}$ [14] and no hydride species was observed. This is marked difference from $[Ru(trpy)(bpy)H]^+$, which had been isolated from the aqueous solution.[13] This can be explained by that formed Ru-H, which would have the increased nucleophilicity assisted by anionic bpp^- ligand with regard to neutral *bpy*, can react with protic solvent such as MeOH and water and that the thermodynamic stability of the bridging HO-H-OH ligand favours the reaction.

Changing the solvent from MeOH to aprotic solvent, pyridine-d_5, resulted in the successful generation of hydride species (Scheme 1, bottom). The reaction was

monitored by ^{1}H NMR spectroscopy over the course of 22 hours at room temperature. The ^{1}H NMR spectra and time profiles of the formation of hydride species are presented in Figure 1 and Figure 2, respectively. As can be seen in Figure 1a, at the beginning of the reaction, main species showed non-symmetric pattern for *bpp*$^-$ ligand, which is unexpected for the C_{2v} symmetric μ-Cl complex **1**$^{2+}$. This is presumably due to the coordination of pyridine-d_5 molecule to one metal centre. This non-symmetric species starts converting to many hydride species and finally ended up to mainly three species. As will be discussed later, these hydride species are three isomers of dinuclear dihydride species, having different orientations of Ru-H bonds, namely, *in*,*in*/*in*,*out*/*out*,*out* with a ratio of 1/1/2 (Figure 1e and 2). The observed chemical shifts at -16.37 (*in*,*in*-**3**$^+$), -16.09 and -16.83 (*in*,*out*-**3**$^+$), and -18.06 (*out*,*out*-**3**$^+$) ppm are in similar range to that for [Ru(trpy)(bpy)H]$^+$ (δ_H: -14.64 in dmso-d_6).

The *out*,*out*-isomer (δ_H: -18.06 ppm) was tentatively assigned by 2D NOESY experiment (Figure S2), showing the correlation between Ru-H and 6- positions of pyridyl protons of *bpp*$^-$ ligand. It is of great interest to observe here that the conformation change of the *trpy* ligand took place during the substitution reaction, because no such a reactivity was observed for the related complex *in*,*in*-{[Ru(trpy)(py)]$_2$(μ-bpp)}$^{3+}$ in the substitution reaction by acetonitrile.[15]

As can be seen in Figure 2, two different hydride signals (δ_H: -16.09 and -16.83) start growing at the same rate after 5 hours of reaction time. Therefore, it can be considered that these two hydride signals are derived from *in,out*-**3**$^+$ which should have magnetically different two hydrides. Although there is no clear evidence for the other main species (δ_{Ru-H} = -16.37 ppm), this one could be assigned as *in,in*-**3**$^+$ species taking into account following two observations; 1) the formation of dihydride species rather than monohydride species is favoured in the presence of large excess amount of $NaBH_4$ (40 equiv.) as both *in*,*out*-**3**$^+$ and *out*,*out*-**3**$^+$ were observed as main species at the end of the reaction, and 2) the subjected dihydride species start growing at the beginning of the reaction.

Aromatic region

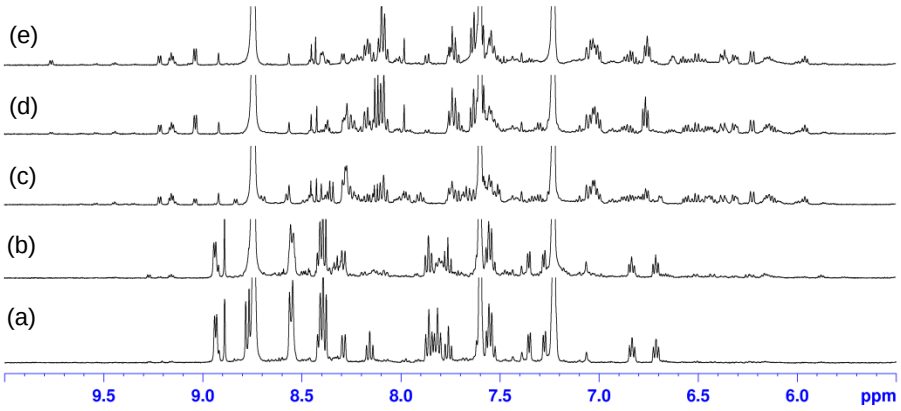

Hydride region

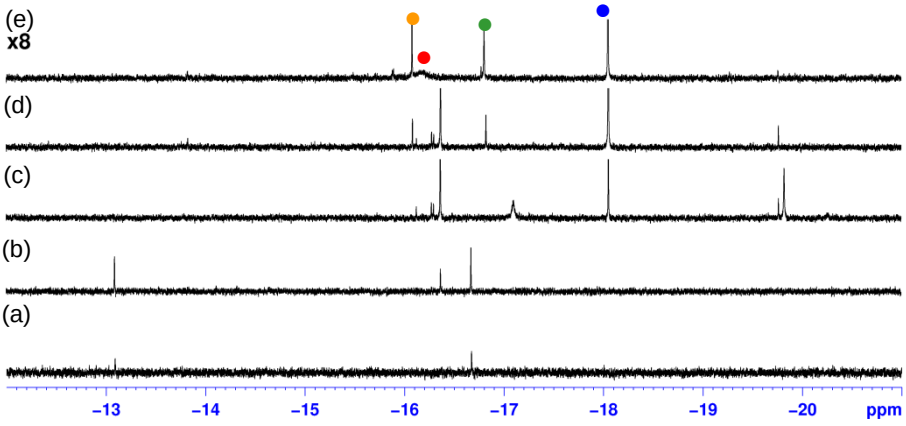

Figure 1. ^{1}H NMR spectra of reaction mixture of {Ru(trpy)}$_2$(μ-bpp)(μ-Cl)}$(PF_6)_3$ (**1**$^{2+}$) with $NaBH_4$ in pyridine-d_5. Top: 12 to -20 ppm, middle: aromatic region and bottom: hydride region. (a) as mixed, (b) 1 hour, (c) 5 hours, (d) 10 hours, (e) 22 hours at room temperature. Aromatic region (top), and hydride region (bottom). ●: *in,in*-dihydride, ● and ●: *in,out*-dihydride.

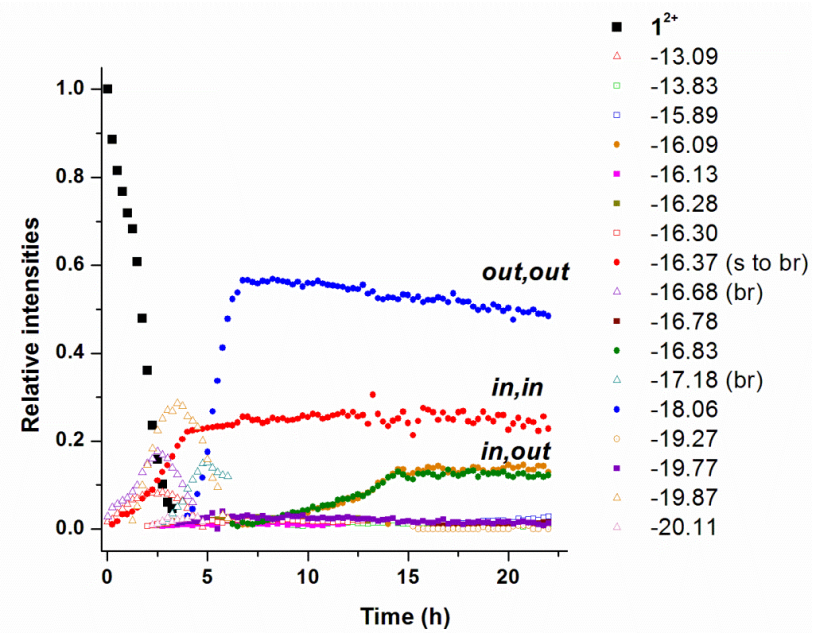

Figure 2. The relative intensities of hydride signals during reaction time. The values in the figure correspond to chemical shifts in ^{1}H NMR. ■: starting complex **1**$^{2+}$, ●: *out,out*-dihydride, ●: *in,in*-dihydride, ● and ●: *in,out*-dihydride. The other species couldn't be assigned. s: sharp, br: broad signals. A ratio of the dihydride species at 22 hours: *out,out*/*in,in*/*in,out* = 2/1/1.

IV-2.3.2. Synthesis and Characterization of dinuclear mono hydride complex

In order to avoid the difficulty caused by the coordination of solvent molecule and second substitution by hydride, two different methods were attempted in the presence of equimolar amount of $NaBH_4$, both of which would provide less complicated reaction pathway: 1) the use of an aprotic weak coordinating solvent, such as dimethylformamide (DMF), and 2) the use of bis-pyridine type of complex as a starting complex. First attempt ended up in a failure because no reactivity at room temperature, and no hydride species but rather a mixture of decomposition products were observed at elevated temperature.

On the other hand, with the second method, using pyridine-d_5 as a solvent, the reaction failed due to no formation of detectable hydride species. However, when using DMF-d_7 as a solvent, dinuclear hydride species was successfully generated (Scheme 2). The starting *in,in*-bis(4-picoline) complex, **4**$^{3+}$, was synthesized following a

UNIVERSITAT ROVIRA I VIRGILI
SECOND-ROW TRANSITION-METAL COMPLEXES RELEVANT TO CO2 REDUCTION AND WATER OXIDATION
Takashi Ono
DL:T 1108-2014

reported literature procedure[16] with the use of 4-picoline instead of pyridine and was characterized by spectroscopic (Figure S1) and analytical techniques. Treating $\mathbf{4}^{3+}$ with 1.0 equiv. of $NaBH_4$ in dry DMF-d_7 at room temperature for 4 hours resulted in the formation of new hydride species $\mathbf{5}^{2+}$ (δ_H: -17.19, Figure 3) along with the appearance of non-symmetric pattern for the *bpp*$^-$ protons, one coordinated 4-picoline, and free 4-picoline. This clearly indicates that each Ru centre in $\mathbf{5}^{2+}$ is bonded to hydrido and 4-picoline, respectively. The conformation of both hydrido and coordinated 4-picoline was assigned to be *in,in* by 2D NOESY experiment (Figure S3). The *in-situ* generated $\mathbf{5}^{2+}$ was stable at least for one week in solution under inert atmosphere.

Scheme 2. The reaction of bis-(4-picoline) complex $\mathbf{4}^{3+}$ with $NaBH_4$

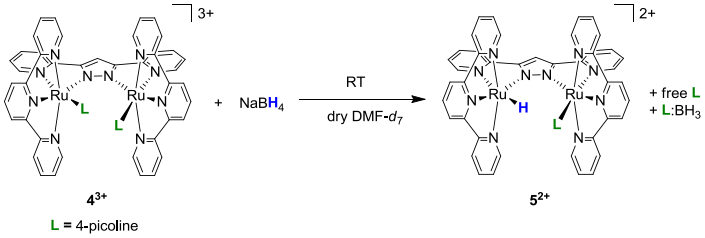

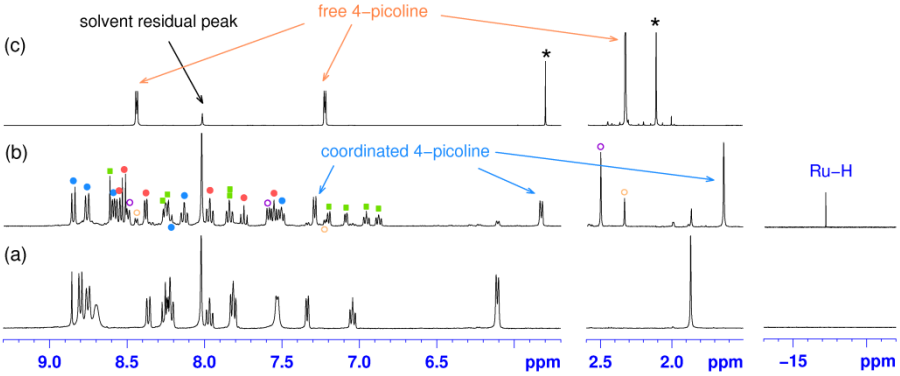

Figure 3. ^{1}H NMR spectra of reaction mixture of $\mathbf{4}^{3+}$ with $NaBH_4$ in DMF-d_7. (a) 10 min at RT, (b) 4 hours at RT, and (c) free 4-picoline. ●: one of the *trpy*, ●: the other *trpy*, ■: *bpp*$^-$, ○: free 4-picoline, ○: BH_3:4-picoline adduct, *: CH_2Cl_2, acetone.

Redox property of dinuclear mono-hydride species $\mathbf{5}^{2+}$

The electrochemical property of $\mathbf{5}^{2+}$ was investigated by means of cyclic voltammetry (CV), and differential pulse voltammetry (DPV) (Figure 4). CVs were carried out in CH_2Cl_2 by mixing a DMF-d_7 solution of the *in-situ* generated $\mathbf{5}^{2+}$.

As can be seen in Figure 4a, first reversible wave at 0.02 V (vs $Ag/AgNO_3$) can be assigned to the Ru(III/II) couple of the Ru-H site by comparing $E_{p,a}$ (-0.12 V vs $Ag/AgNO_3$ in CH_3CN) of the mononuclear analogue $[Ru(trpy)(bpy)H]^+$.[13] It is interesting to see the reduction wave for the Ru-H species because it has been proposed that in the case of $[Ru(trpy)(bpy)H]^+$, disproportionation of $1e^-$ oxidized species takes place, followed by proton loss from $2e^-$ oxidized species with a parent $[Ru(trpy)(bpy)H]^+$ acting as a proton acceptor to form solvent coordinated species $[Ru(trpy)(bpy)S]^{2+}$ (S = CH_3CN) in CH_3CN.[17] The observed stability for the $1e^-$ oxidized species of $\mathbf{5}^{2+}$ could be probably the consequence of the stabilization of Ru(III) centre by electronic coupling between two Ru centres. When the potential was further increased (Figure 4b,c), the two processes ($E_{p,a}$ = 0.70 and 0.99 V), which are quasi-reversible, were found along with the decreased intensity for the reduction of Ru(III)-H species in the reverse scan. By repeating scan, two new waves were gradually increased ($E_{p,a}$ ≈ 0.77 and 1.1 V, marked with an asterisk in Figure 4) together with the decreased intensities of original species. These results indicate that once the oxidation state of the $\mathbf{5}^{2+}$ reached to Ru_2(III,III), decomposition takes place to generate new species that could be bis-4-picoline complex $\mathbf{4}^{3+}$ (Figure 4d). A newly coordinated 4-picoline molecule is derived from the one released when $\mathbf{5}^{2+}$ was *in-situ* generated (Scheme 2).

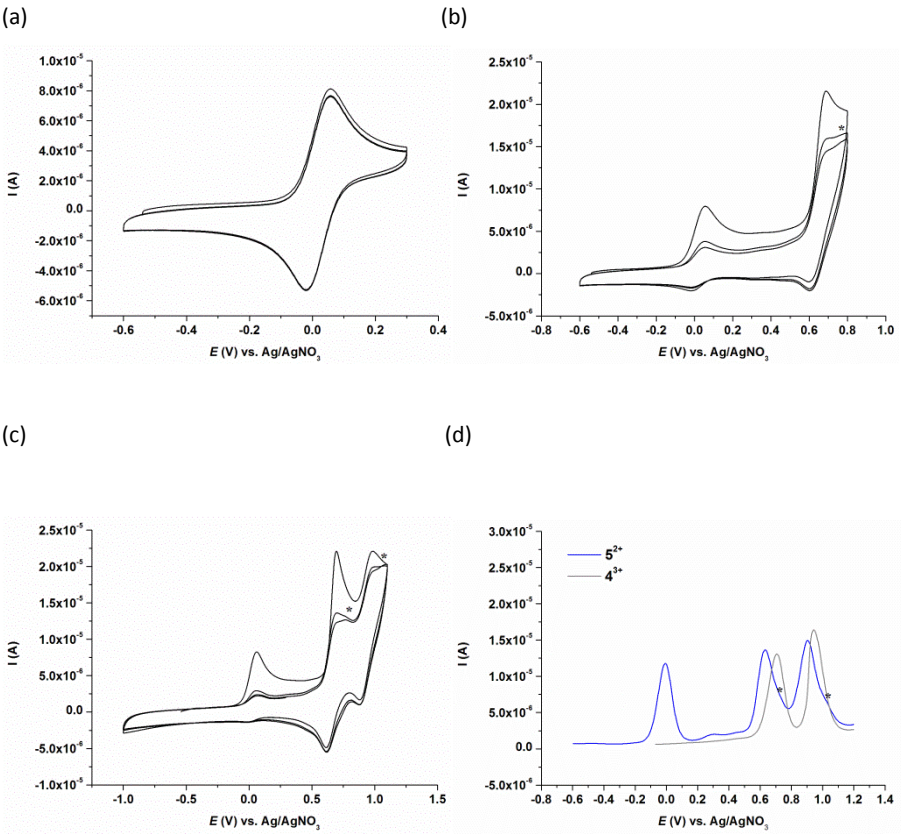

Figure 4. CVs of (a)-(c) $\mathbf{5}^{2+}$ (0.5 mM in DCM/DMF-d_7 = 9/1), and (d) DPVs of $\mathbf{5}^{2+}$ (0.5 mM in DCM/DMF-d_7 = 9/1) and $\mathbf{4}^{3+}$ (0.5 mM in DCM). Glassy carbon working electrode, Pt disk counter electrode and $Ag/AgNO_3$ reference electrode. Scan rate 100 mV s^{-1}

IV-2.3.3. Reactivity of dinuclear mono-hydride toward CO_2

The reactivity of *in-situ* generated $\mathbf{5}^{2+}$ toward CO_2 was examined. The reaction was carried out in the presence of *ca*. 1 bar of CO_2. No change was observed at room temperature for 1 day. At elevated temperature, the reaction proceeded and for complete conversion of $\mathbf{5}^{2+}$ to new species required 4 hours at 80 °C. As can be seen ^{1}H NMR spectra (Figure 5), the newly formed species has been assigned to the bridged formate complex, $\{[Ru(trpy)]_2(\mu\text{-bpp})(\mu\text{-OCHO})\}^{2+}$, reported previously[1] by comparing their chemical shifts. This reactivity is quite different from those of the mononuclear $[Ru(bid)(bpy)H]$[2] and $[Ru(trpy)(bpy)H]^+$[13], which react with CO_2 at room temperature to

form the corresponding formate complexes. The observed low reactivity can be explained by the steric hindrance around Ru-H site surrounded by the coordinated 4-picoline bonded to the other metal centre, which avoids CO_2 molecule from approaching to the reactive site. It can be considered that at elevated temperature, dissociation of 4-picoline and subsequent CO_2 insertion with/without coordination to the vacant coordination site takes place to form thermodynamically stable bridged formate complex.

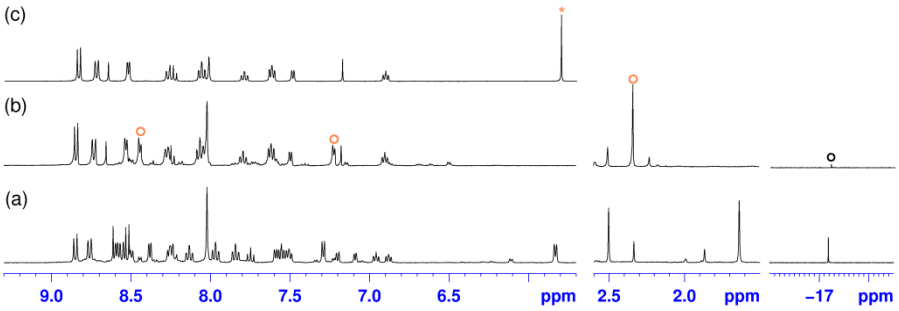

Figure 5. ^{1}H NMR spectra of reaction mixture in DMF-d_7 of (a) *in-situ* generated $\mathbf{5}^{2+}$, (b) 4 hours at 80 °C in the presence of *ca*. 1 bar of CO_2, and (c) $\mathbf{6}^{2+}$. ○: free 4-picoline, *: CH_2Cl_2, acetone. . o: the other hydride species

IV-2.4. Conclusions

New dinuclear ruthenium-hydrido species have been generated *in situ* by using $NaBH_4$ as hydride source in aprotic solvent, such as pyridine and DMF due to their instability toward protic solvent, whose reactivity differs from mononuclear analogue $[Ru(trpy)(bpy)H]^+$ that is stable in water. This is associated with anionic nature of the chelating *bpp*$^-$ ligand, which increase nucleophilicity of Ru-H. The substitution reaction of the Cl ligand in $\mathbf{1}^{2+}$ by $NaBH_4$ shows no selectivity, leading to three dihydride isomers, *in*,*in*-,*in*,*out*-, and *out*,*out*-$\mathbf{3}^+$, which are tentatively assigned by NMR spectroscopy. Unlike the substitution reaction of related complex $\{[Ru(trpy)(py)]_2(\mu\text{-bpp})\}^{3+}$ by acetonitrile, this unexpected reactivity can be associated with high nucleophilicity of

UNIVERSITAT ROVIRA I VIRGILI
SECOND-ROW TRANSITION-METAL COMPLEXES RELEVANT TO CO2 REDUCTION AND WATER OXIDATION
Takashi Ono
DL:T 1108-2014

$NaBH_4$. On the other hand, we could selectively generate and characterize the dinuclear mono-hydride species *in*,*in*-{[Ru(trpy)(H)][Ru(trpy)(4-picoline)](μ-bpp)}$^{2+}$, **5**$^{2+}$, using bis 4-picoline complex **4**$^{3+}$ as the precursor. The complex **5**$^{2+}$ represents a catalytic intermediate equivalent in the mechanism for the hydrogenative CO_2 reduction proposed previously, and we further examined its reactivity toward CO_2. Although hydrido ligand in **5**$^{2+}$ would have similar nucleophilicity with respect to the analogues complex [Ru(trpy)(bpy)H]$^{+}$, the formation of the bridged formate complex from the reaction of **5**$^{2+}$ with CO_2 undergoes only at elevated temperature, suggesting that the dissociation of 4-picoline is necessary for CO_2 approaching to the reactive site.

IV-2.5. Experimental Section

Materials

All reagents used in present work were obtained from Aldrich Chemical Co.or Alfa Aesar and were used without further purification. Synthesis grade organic solvents were obtained from SDS and were routinely degassed with Argon. Methanol was distilled from Mg/I_2. dichloromethane, hexane and diethyl ether were used from the SPS. $NaBH_4$ was purchased from Aldrich Chemical Co. Carbon dioxide was obtained from Carburos Metálicos S. A.. Pyridine-d_5 was used without purification. DMF-d_7 was dried with molecular sieves 3A and stored under N_2. {[Ru(trpy)]$_2$(μ-bpp)(μ-Cl)}$^{2+}$, **1**$^{2+}$,[18] {[Ru(trpy)]$_2$(μ-bpp)(μ-OAc)}$^{2+}$,[18] and {[Ru(trpy)]$_2$(μ-bpp)(μ-OCHO)}$^{2+}$ [1] were prepared as described in the literature. All synthetic manipulations were routinely performed under argon or nitrogen atmosphere using Schlenk and vacuum line techniques.

Synthesis

Monitoring the formation of dinuclear hydride species by the reaction of 1^{2+} with $NaBH_4$

0.30 mL of 7.5 mM pyridine-d_5 solution of complex **1**$^{2+}$ (2.3 μmol), 0.30 mL of 300 mM pyridine-d_5 solution of $NaBH_4$ (90 μmol, 40 equiv.) were added into a J-young NMR tube and shaken. The reaction was monitored every 15 min for 22 hours by ^{1}H NMR spectroscopy.

Scheme 3. NMR Labeling scheme.

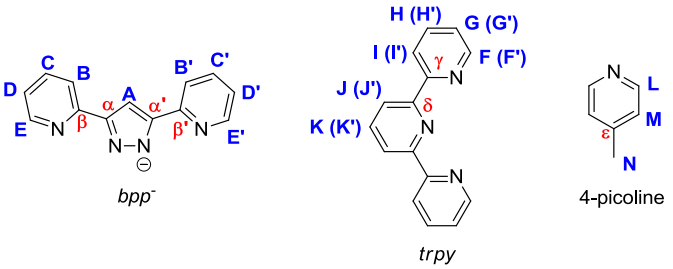

Sinthesis of {[(Ru(trpy)(4-picoline)]$_2$(μ-bpp)}(PF$_6$)$_3$ ([4](PF$_6$)$_3$)

100 mg (0.0807 mmol) of [(Ru(trpy))$_2$(μ-bpp)(μ-OAc)](PF$_6$)$_2$, was dissolved in 40 mL of acetone-water (3:1) and then 2 mL of a pH = 1 water solution (triflic acid) was added. After the addition of 0.15 mL of 4-picoline, the mixture was then heated under reflux for 6 hours. Upon cooling to room temperature, the unreacted starting material was filtered and 1 mL of a saturated aqueous solution of KPF_6 was added to the solution. After evaporation of the acetone in a rotary evaporator, a brown-black solid was obtained which was recrystallized from CH_2Cl_2/Et_2O yielding black microcrystals. Yield: 79.4 mg (65%). Anal. Calcd. for $C_{55}H_{45}F_{18}N_{12}P_3Ru_2$: C, 43.72; H, 3.00; N, 11.12. Found: C, 43.43; H, 3.06; N, 10.99. ^{1}H NMR (500 MHz, Acetone-d_6, 298 K): 8.68 (s, 1H, H_A), 8.66 (brd, 4H, H_F), 8.62 (d, 4H, J_{JK} = 8.1 Hz, H_J), 8.58 (d, 4H, J_{IH} = 7.7 Hz, H_I), 8.30 (d, 2H, J_{BC} = 7.7 Hz, H_B), 8.17 (t, 2H, J_{KJ} = 8.1 Hz, H_K), 8.16 (td, 4H, J_{HI} = J_{HG} = 7.7 Hz, J_{HF} = 1.3 Hz, H_H), 7.89 (td, 2H, J_{CB} = J_{CD} = 7.7 Hz, J_{CE} = 1.4 Hz, H_C), 7.78 (ddd, 4H, J_{GH} = 7.7 Hz, J_{GF} = 5.7 Hz, J_{GI} = 1.2 Hz, H_G), 7.59 (brd, 4H, H_L), 7.33 (d, 2H, J_{ED} = 5.7 Hz, H_E), 6.98 (ddd, 2H, J_{DC} = 7.7 Hz, J_{DE} = 5.7 Hz, J_{DB} = 1.3 Hz, H_D), 6.11 (d, 4H, J_{ML} = 6.2 Hz, H_M), 1.84 (s, 6H, H_N). ^{13}C NMR (125 MHz, Acetone-d_6, 298 K): δ 160.5 ($C_δ$), 159.5 ($C_γ$), 156.6 ($C_α$), 155.8 ($C_β$), 154.8 (C_F), 152.1 (C_L), 150.9 (C_E), 150.2 ($C_ε$), 139.5 (C_H), 138.5 (C_C), 136.5 (C_K), 130.0 (C_G), 126.2 (C_M), 125.7 (C_I), 124.8 (C_J), 124.5 (C_D), 121.6 (C_B), 106.9 (C_A), 20.5 (C_N). ESI-MS (MeOH): *m/z* 360.3 ([M-3PF$_6$]$^{3+}$).

UNIVERSITAT ROVIRA I VIRGILI
SECOND-ROW TRANSITION-METAL COMPLEXES RELEVANT TO CO2 REDUCTION AND WATER OXIDATION
Takashi Ono
DL:T 1108-2014

In-situ generation of dinuclear mono-hydride species $\mathbf{5}^{2+}$ followed by the reaction with CO_2

Generation of $\mathbf{5}^{2+}$: In a drybox, 0.30 mL of 10 mM dry DMF-d_7 solution of complex $\mathbf{5}^{3+}$ (3.0 μmol), 0.20 mL of 15 mM dry DMF-d_7 solution of $NaBH_4$ (3.0 μmol, 1.0 equiv.) and additionally 0.10 mL of dry DMF-d_7 were added into a J-young NMR tube and shaken. Almost conversion of $\mathbf{4}^{3+}$ into $\mathbf{5}^{2+}$ was observed in 4 hours. ^{1}H NMR (500 MHz, DMF-d_7, 298 K) : δ 8.84 (brd, 2H, H_J or $H_{J'}$), 8.76 (d, 2H, $J_{IH \text{ or } I'H'}$ = 8.1 Hz, H_I or $H_{I'}$), 8.61 (s, 1H, H_A), 8.59 (d, 2H, $J_{FG \text{ or } F'G'}$ = 4.9, H_F or $H_{F'}$), 8.56 (d, 2H, $J_{I'H' \text{ or } IH}$ = 7.5 Hz, $H_{I'}$ or H_I), 8.52 (d, 2H, $J_{JK \text{ or } J'K'}$ = 8.0 Hz, $H_{J'}$ or H_J), 8.38 (d, 2H, $J_{F'G' \text{ or } FG}$ = 5.7 Hz, $H_{F'}$ or H_F), 8.28-8.20 (m, 3H, H_B, $H_{B'}$ and H_K or $H_{K'}$), 8.13 (br, 2H, H_H or $H_{H'}$), 7.97 (td, 2H, $J_{H'I' \text{ or } HI}$ = $J_{H'G' \text{ or } HG}$ = 7.5 Hz, $J_{H'F' \text{or } HF}$ = 1.3 Hz, $H_{H'}$ or H_H), 7.87-7.81 (m, 2H, H_C, $H_{C'}$), 7.75 (t, 1H, $J_{K'J' \text{ or } KJ}$ = 8.0 Hz, $H_{K'}$ or H_K), 7.55 (ddd, 2H, $J_{G'H' \text{ or } GH}$ = 7.5 Hz, $J_{G'F' \text{ or } GF}$ = 5.7 Hz, $J_{G'I' \text{ or } GI}$ = 1.2 Hz, $H_{G'}$ or H_G), 7.50 (br, 2H, H_G or $H_{G'}$), 7.29 (d, 2H, J_{LM} = 6.2 Hz, H_L), 7.20 (d, 1H, $J_{ED \text{ or } E'D'}$ = 5.7 Hz, H_E or $H_{E'}$), 7.09 (d, 1H, $J_{E'D' \text{ or } ED}$ = 5.3 Hz, $H_{E'}$ or H_E), 6.96 (ddd, 1H, $J_{DC \text{ or } D'C'}$ = 7.2 Hz, $J_{DE \text{ or } D'E'}$ = 5.7 Hz, $J_{DB \text{ or } D'B'}$ = 1.3 Hz, H_D or $H_{D'}$), 6.88 (ddd, 1H, $J_{D'C' \text{ or } DC}$ = 7.3 Hz, $J_{D'E' \text{ or } DE}$ = 5.3 Hz, $J_{D'B' \text{ or } DB}$ = 1.1 Hz, $H_{D'}$ or H_D), 5.83 (d, 2H, J_{ML} = 6.2 Hz, H_M), 1.64 (s, 3H, H_N), -17.19 (s, 1H, Ru-H).

Reaction with CO_2: After applying freeze-pump-saw cycle (3 times) to the NMR tube which contains *in-situ* generated $\mathbf{5}^{2+}$ in DMF-d_7 as stated above, *ca*. 1 bar of CO_2 was introduced to the tube through the glass adopter equipped to the Teflon cap. The reaction was monitored at room temperature for one day, and then the reaction mixture was heated at 80 °C for 4 hours. The obtained new species was determined to the bridged formate complex by comparing the chemical shifts of the complex prepared in the other procedure reported previously.[1]

Instrumentation and measurements

Cyclic voltammetric (CV) experiments were performed in a IJ-Cambria IH-660 potentiostat, using a three electrode cell. Glassy carbon disk electrodes (3 mm diameter) from BASi were used as working electrode, platinum wire as auxiliary and SSCE as the reference electrode. Cyclic voltammograms were recorded at 100 mV/s scan rate under nitrogen atmosphere. The complexes were dissolved in previously

degassed dichloromethane containing the necessary amount of (n-Bu_4N)(PF_6), used as supporting electrolyte, to yield a 0.1 M ionic strength solution. All $E_{1/2}$ values reported in this work were estimated from cyclic voltammetry as the average of the oxidative and reductive peak potentials ($E_{p,a}$+$E_{p,c}$)/2 or from differential pulse voltammetry (DPV; pulse amplitudes of 0.05 V, pulse widths of 0.05 s, sampling width of 0.02 s, and a pulse period of 0.1 s). Unless explicitly mentioned the concentration of the complexes were approximately 1 mM. The NMR spectroscopy was performed on Bruker Avance 400 MHz Bruker Avance II and Bruker Avance 500 MHz. The ESI mass spectroscopy experiments were performed on a Waters Micromass LCT Premier equipment, respectively.

IV-2.6. Acknowledgements

Support from MINECO (CTQ-2010-21497) is gratefully acknowledged TO thanks MINECO for a doctoral grant.

IV-2.7. References

(1) Ono, T.; Planas, N.; Miró, P.; Ertem, M. Z.; Escudero-Adán, E. C.; Benet-Buchholz, J.; Gagliardi, L.; Cramer, C. J.; Llobet, A. *ChemCatChem* **2013**, *5*, 3897-3903.
(2) Planas, N.; Ono, T.; Vaquer, L.; Miro, P.; Benet-Buchholz, J.; Gagliardi, L.; Cramer, C. J.; Llobet, A. *Phys. Chem. Chem. Phys.* **2011**, *13*, 19480-19484.
(3) Ng, S. M.; Yin, C.; Yeung, C. H.; Chan, T. C.; Lau, C. P. *Eur. J. Inorg. Chem.* **2004**, *2004*, 1788-1793.
(4) Urakawa, A.; Jutz, F.; Laurenczy, G.; Baiker, A. *Chem. —Eur. J.* **2007**, *13*, 3886-3899.
(5) Getty, A. D.; Tai, C.-C.; Linehan, J. C.; Jessop, P. G.; Olmstead, M. M.; Rheingold, A. L. *Organometallics* **2009**, *28*, 5466-5477.
(6) Ziebart, C.; Federsel, C.; Anbarasan, P.; Jackstell, R.; Baumann, W.; Spannenberg, A.; Beller, M. *J. Am. Chem. Soc.* **2012**, *134*, 20701-20704.
(7) Federsel, C.; Ziebart, C.; Jackstell, R.; Baumann, W.; Beller, M. *Chem. —Eur. J.* **2012**, *18*, 72-75.
(8) Ogo, S.; Kabe, R.; Hayashi, H.; Harada, R.; Fukuzumi, S. *Dalton Trans.* **2006**, 4657-4663.
(9) Creutz, C.; Chou, M. H. *J. Am. Chem. Soc.* **2007**, *129*, 10108-10109.
(10) Bruce, M. R. M.; Megehee, E.; Sullivan, B. P.; Thorp, H. H.; O'Toole, T. R.; Downard, A.; Pugh, J. R.; Meyer, T. J. *Inorg. Chem.* **1992**, *31*, 4864-4873.
(11) Chen, Z.; Glasson, C. R. K.; Holland, P. L.; Meyer, T. J. *Phys. Chem. Chem. Phys.* **2013**, *15*, 9503-9507.
(12) Chen, Z.; Kang, P.; Zhang, M.-T.; Meyer, T. J. *Chem. Commun.* **2014**, *50*, 335-337.
(13) Konno, H.; Kobayashi, A.; Sakamoto, K.; Fagalde, F.; Katz, N. E.; Saitoh, H.; Ishitani, O. *Inorg. Chim. Acta* **2000**, *299*, 155-163.

UNIVERSITAT ROVIRA I VIRGILI
SECOND-ROW TRANSITION-METAL COMPLEXES RELEVANT TO CO2 REDUCTION AND WATER OXIDATION
Takashi Ono
DL:T 1108-2014

(14) Bozoglian, F.; Romain, S.; Ertem, M. Z.; Todorova, T. K.; Sens, C.; Mola, J.; Rodríguez, M.; Romero, I.; Benet-Buchholz, J.; Fontrodona, X.; Cramer, C. J.; Gagliardi, L.; Llobet, A. *J. Am. Chem. Soc.* **2009**, *131*, 15176-15187.

(15) Planas, N.; Christian, G.; Roeser, S.; Mas-Marzá, E.; Kollipara, M.-R.; Benet-Buchholz, J.; Maseras, F.; Llobet, A. *Inorg. Chem.* **2012**, *51*, 1889-1901.

(16) Planas, N.; Christian, G. J.; Mas-Marzá, E.; Sala, X.; Fontrodona, X.; Maseras, F.; Llobet, A. *Chem. —Eur. J.* **2010**, *16*, 7965-7968.

(17) Matsubara, Y.; Fujita, E.; Doherty, M. D.; Muckerman, J. T.; Creutz, C. *J. Am. Chem. Soc.* **2012**, *134*, 15743-15757.

(18) Sens, C.; Romero, I.; Rodríguez, M.; Llobet, A.; Parella, T.; Benet-Buchholz, J. *J. Am. Chem. Soc.* **2004**, *126*, 7798-7799.

UNIVERSITAT ROVIRA I VIRGILI
SECOND-ROW TRANSITION-METAL COMPLEXES RELEVANT TO CO2 REDUCTION AND WATER OXIDATION
Takashi Ono
DL:T 1108-2014

Supporting Information for:

Dinuclear Ruthenium Hydride Complexes Containing Hbpp and Terpyridine Ligands: Synthesis and Reactivities

Table of contents

UNIVERSITAT ROVIRA I VIRGILI
SECOND-ROW TRANSITION-METAL COMPLEXES RELEVANT TO CO2 REDUCTION AND WATER OXIDATION
Takashi Ono
DL:T 1108-2014

S1. NMR:

Figure S1. 1D and 2D NMR spectra (500 MHz, 298K, CD_2Cl_2) for complex **4a**$^{3+}$: (a) 1H, (b) COSY, (c) NOESY, (d) DEPTQ135, (e) HSQC, and (f) HMBC

(a)

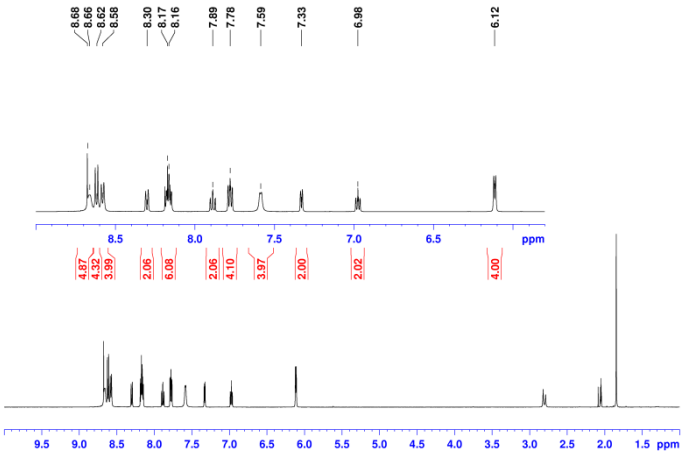

(b)

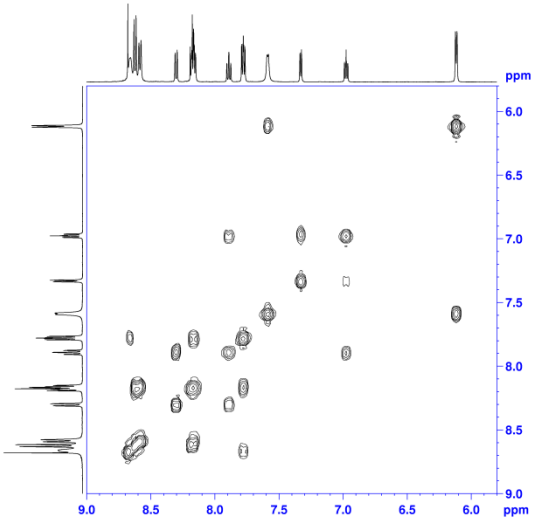

(c)

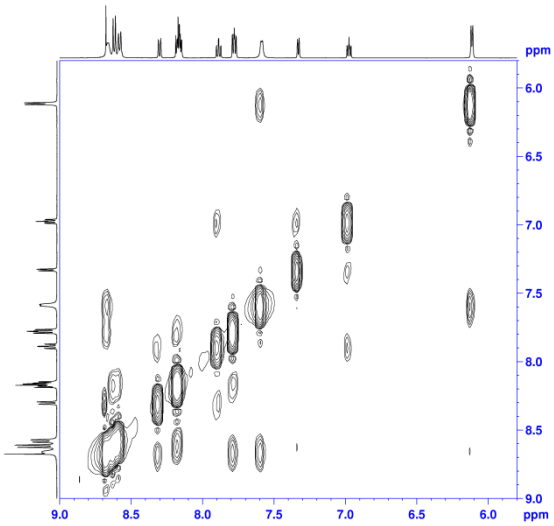
ppm
6.0
6.5
7.0
7.5
8.0
8.5
9.0
9.0
8.5
8.0
7.5
7.0
6.5
6.0
ppm

(d)

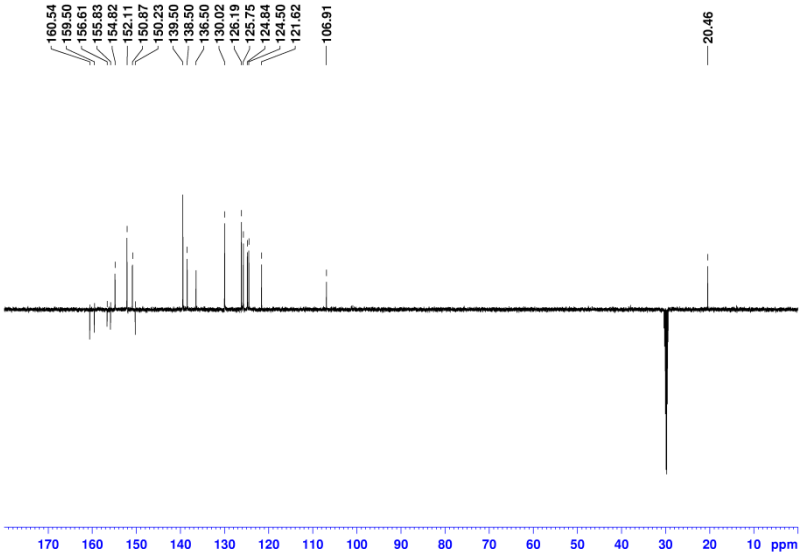
160.54
159.50
156.61
155.83
154.82
152.11
150.87
150.23
139.50
138.50
136.50
130.02
126.19
125.75
124.84
124.50
121.62
106.91
20.46
170
160
150
140
130
120
110
100
90
80
70
60
50
40
30
20
10
ppm

(e)

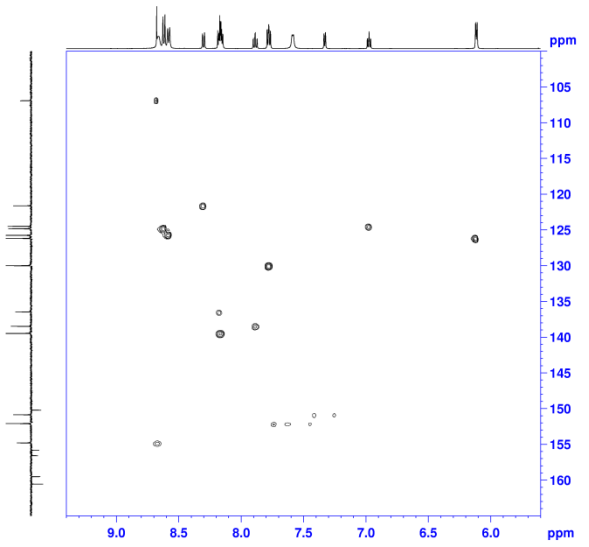
ppm
105
110
115
120
125
130
135
140
145
150
155
160
9.0
8.5
8.0
7.5
7.0
6.5
6.0
ppm

(f)

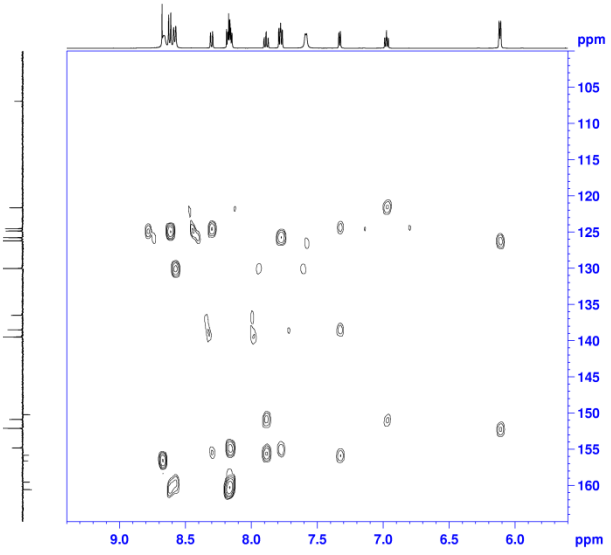
ppm
105
110
115
120
125
130
135
140
145
150
155
160
9.0
8.5
8.0
7.5
7.0
6.5
6.0
ppm

Figure S2. Top: ^{1}H NMR spectra of reaction mixture of $\mathbf{1}^{2+}$ with $NaBH_4$ in pyridine-d_5.in the scan window between 12 to -20 ppm. (a) as mixed, (b) 1 hour, (c) 5 hours, (d) 10 hours, (e) 22 hours at room temperature. Bottom: 2D NOESY spectrum of reaction mixture in pyridine-d_5 after 22 hours and schematic representation of the observed correlation.

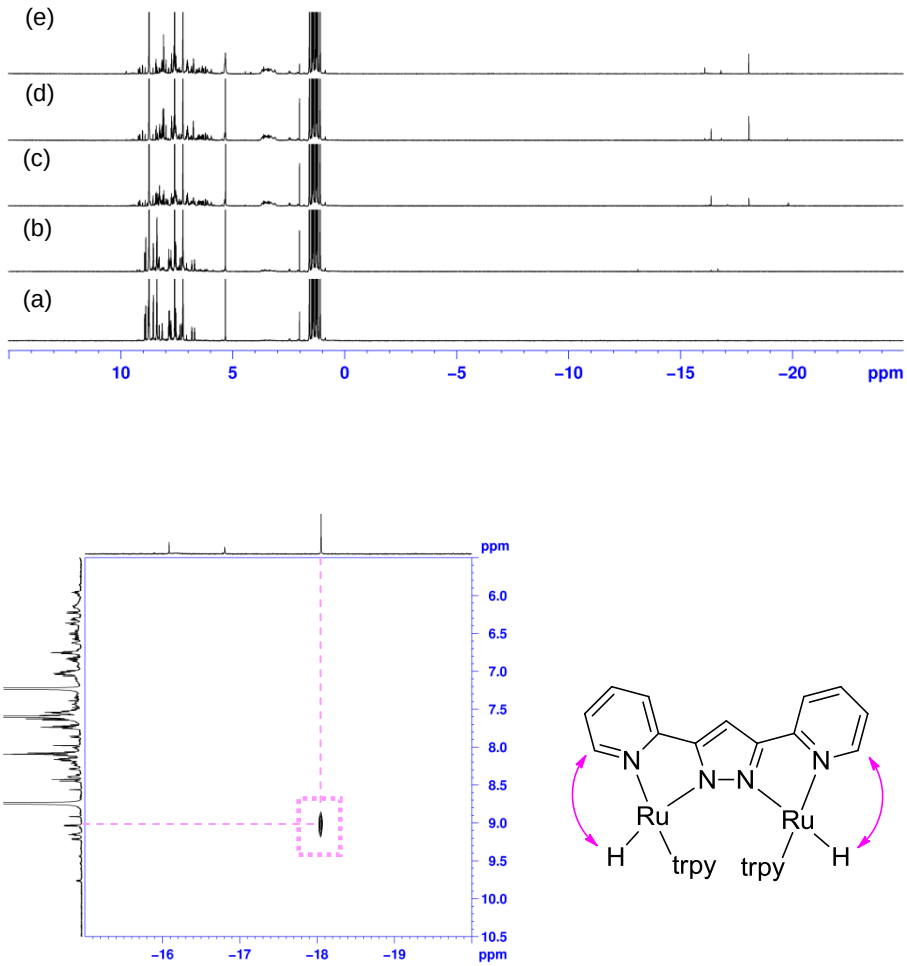

Figure S3. 2D spectra of 4 hours reaction mixture of $\mathbf{4}^{3+}$ with $NaBH_4$ in DMF-d_7. (a) COSY, and (b) NOESY together with schematic representation of the observed correlation

(a)

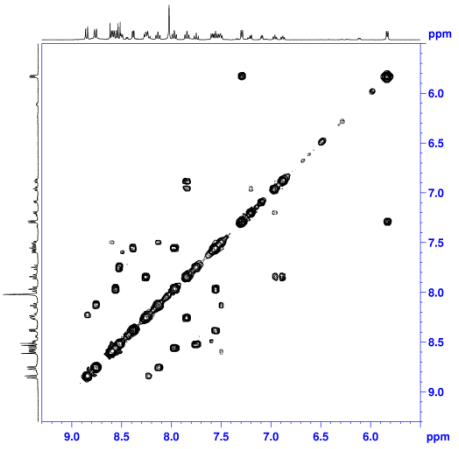

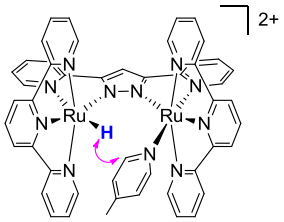

(b)

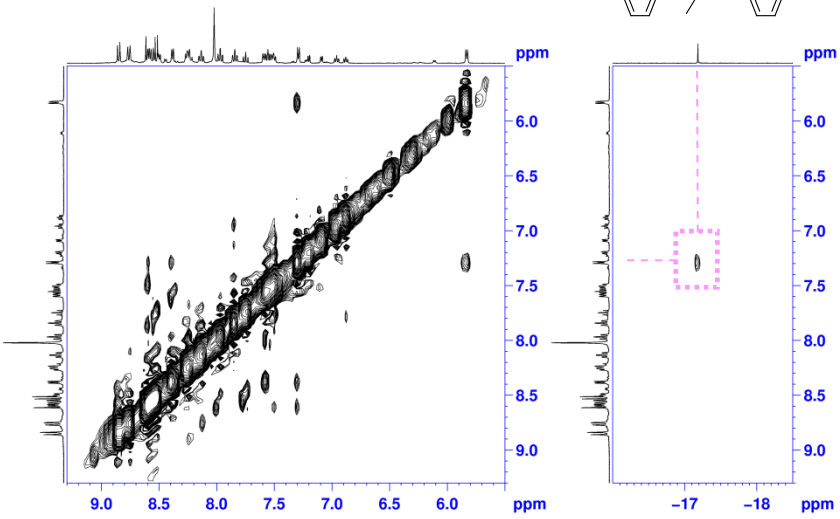

Chapter V

Uptake of one and two molecules of CO_2 by the molybdate dianion: a soluble, molecular oxide model system for carbon dioxide

Chem. Sci. **2014**, *5*, 1772–1776. DOI: 10.1039/c4sc00132j

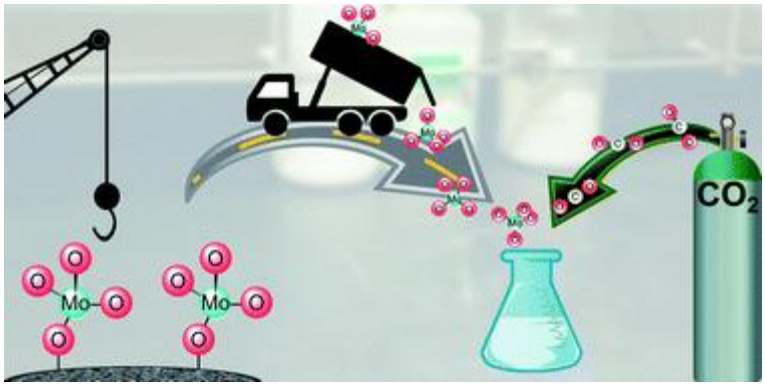

Table of Contents

UNIVERSITAT ROVIRA I VIRGILI
SECOND-ROW TRANSITION-METAL COMPLEXES RELEVANT TO CO2 REDUCTION AND WATER OXIDATION
Takashi Ono
DL:T 1108-2014

V.1. Abstract

Tetrahedral $[MoO_4]^{2-}$ readily binds CO_2 at room temperature to produce a robust monocarbonate complex, $[MoO_3(\kappa^2\text{-}CO_3)]^{2-}$, that does not release CO_2 even at modestly elevated temperatures (up to 56 °C in solution and 70 °C in the solid state). In the presence of excess carbon dioxide, a second molecule of CO_2 binds to afford a pseudo-octahedral dioxo dicarbonate complex, $[MoO_2(\kappa^2\text{-}CO_3)_2]^{2-}$, the first structurally characterized transition-metal dicarbonate complex derived from CO_2. The monocarbonate $[MoO_3(\kappa^2\text{-}CO_3)]^{2-}$ reacts with triethylsilane in acetonitrile under an atmosphere of CO_2 to produce formate (69% isolated yield) together with silylated molybdate (quantitative conversion to $[MoO_3(OSiEt_3)]^-$, 50% isolated yield) after 22 hours at 85 °C. This system thus illustrates both the reversible binding of CO_2 by a simple transition-metal oxoanion and the ability of the latter molecular metal oxide to facilitate chemical CO_2 reduction.

V.2. Introduction

Metal oxide catalysts for CO_2 transformations are advantageous based on considerations of cost, ease of re-use, and stability,[1-3] but these advantages come at the expense of our ability to readily characterize such systems at a molecular level of detail. Intrigued by the paucity of soluble transition-metal oxide systems known to react with CO_2 in a well-defined manner (*e.g.*, eqn (1)),[4-6] we decided to investigate salts of the molybdate dianion in this respect, in order to determine the behaviour and mode of reaction (if any) of a simple oxoanion with carbon dioxide as either the potential basis for a new homogeneous catalytic system or as a soluble model for known heterogeneous oxide catalysts. Accordingly, herein we report the finding that molybdate absorbs not just one but two equivalents of CO_2 (the second, reversibly) together with complete characterization including single-crystal X-ray diffraction studies of the resulting mono- and dicarbonate complexes.

$$L_nM{=}O + CO_2 \rightarrow L_nM(CO_3) \qquad (1)$$

UNIVERSITAT ROVIRA I VIRGILI
SECOND-ROW TRANSITION-METAL COMPLEXES RELEVANT TO CO2 REDUCTION AND WATER OXIDATION
Takashi Ono
DL:T 1108-2014

As our studies were in progress, it was reported that the related tungstate dianion indeed serves as a homogeneous catalyst for CO_2 fixation,[7-8] but so far the reaction intermediates in that system have not been isolated. The structural, spectroscopic, and computational details we disclose herein form an excellent point of reference both for understanding tungstate-catalyzed CO_2 fixation processes and for developing analogous systems based upon molybdate. Toward the latter goal, we show herein the ability of molybdate to mediate the triethylsilane reduction of CO_2 to formate. The present work follows and improves upon our earlier report of titanium trisanilide oxoanion CO_2 binding[4] in that the present system utilizes essentially non-interacting organic cations (in the earlier system oxophilic alkali-metal cations such as lithium were a necessary ingredient for CO_2 uptake) and in that the molybdate dianion is an entirely inorganic species well suited as a discrete, molecular analogue of a solid-state metal oxide. Also serving as a precursor to the present work is our report of a cycle for CO_2 reduction to CO at a niobium nitride binding site; that system represented our initial foray into ligand-based strategies for CO_2 conversion.[9]

V.3. Results and Discussion

We began our studies with the commercially available sodium molybdate, but soon determined that this organic- media insoluble salt does not react with CO_2 under aqueous conditions (as assessed by ^{95}Mo NMR spectroscopy).[10] In order to endow the molybdate dianion with solubility in organic media, we prepared $[PPN]_2[MoO_4]$ (PPN^+ = $(Ph_3P)_2N^+$) in one step from Ag_2MoO_4 and [PPN]Cl using a modified literature procedure.[11] Upon addition of CO_2 to a 0.04 M acetonitrile solution of $[PPN]_2[MoO_4]$ at room temperature, a new species quickly formed. The ^{95}Mo NMR spectrum of the isolated product exhibits a new resonance at +46.7 ppm, no unreacted starting material (+13.2 ppm), but also a small amount of $[Mo_2O_7]^{2-}$ by-product identified by a signal at -3.8 ppm.[12] A new characteristic carbonyl stretch at 1638 cm^{-1} could also be observed by IR spectroscopy.[13]

A preliminary X-ray crystal structure of the CO_2-addition product revealed a κ^2-bound carbonate moiety and enabled us to formulate the major product obtained as $[PPN]_2[MoO_3(\kappa^2\text{-}CO_3)]$. In the interest of obtaining high quality crystallographic data, $[NEt_4]_2[MoO_4]$ (previously reported in the literature and used to prepare examples of well-behaved and crystallographically characterized molybdenum complexes)[14-15] was used to obtain the $[MoO_3(\kappa^2\text{-}CO_3)]^{2-}$dianion as its tetraethylammonium salt. Colourless crystals were grown by vapour diffusion of Et_2O into a CH_3CN solution of $[NEt_4]_2[MoO_3(\kappa^2\text{-}CO_3)]$, and the structure obtained in the ensuing crystallographic investigation is shown in Figure 1. The C-O distances are elongated from 1.162 Å in free CO_2[16] to 1.2258(13) Å, 1.3048(13) Å, and 1.3357(14) Å in the carbonate unit. The average Mo-O distance is 1.739 Å for the three molybdenum oxo bonds, shorter than the average Mo-O distance of 1.776 Å in tetrahedral $[MoO_4]^{2-}$.[17] The carbonate ligand is associated with longer Mo-O interatomic distances at 2.0674(9) and 2.2191(9) Å. The slight asymmetry of the carbonate binding mode is apparently induced by the *trans* influence of one of the molybdenum oxo ligands (O3-Mo1-O6 148.75(3)° and C1-O3-

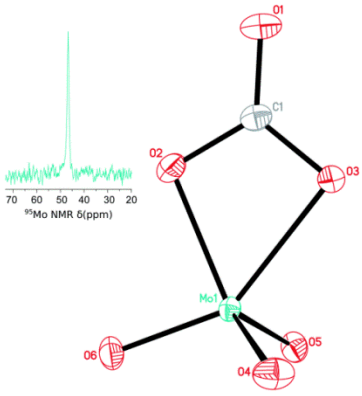

Figure 1. Left: ^{95}Mo NMR resonance of $[MoO_3(\kappa^2\text{-}CO_3)]^{2-}$. Right: solid-state structure of $[NEt_4]_2[MoO_3(\kappa^2\text{-}CO_3)]$ (ellipsoids at the 50% probability level, cations omitted for clarity). Representative interatomic distances [Å] and angles [°]: C1-O1 1.2258(13), C1-O2 1.3357(14), C1-O3 1.3048(13), Mo1-O2 2.0674(9), Mo1-O3 2.2191(9), Mo1-O4 1.7351(8), Mo1-O5 1.7390(8), Mo1-O6 1.7436(8); C1-O2-Mo1 97.75(6), C1-O3-Mo1 91.74(7), O6-Mo1-O3 148.75(3), O4-Mo1-O2 120.28(4), O5-Mo1-O2 121.93(4), O4-Mo1-O5 110.10(4), O4-Mo1-O6 105.15(4), O5-Mo1-O6 105.34(4); C1-O3-Mo1-O6 2.09(11), C1-O2-Mo1-O4 75.02(8), C1-O2-Mo1-O5 71.35(8).

UNIVERSITAT ROVIRA I VIRGILI
SECOND-ROW TRANSITION-METAL COMPLEXES RELEVANT TO CO2 REDUCTION AND WATER OXIDATION
Takashi Ono
DL:T 1108-2014

Mo1-O6 2.09(11)°) as reflected in the Mo-O bond lengths that differ by approximately 0.15 Å, but also in the different Mo-O-C angles of 97.75(6) and 91.74(7)°. This κ^2 binding mode is not surprising given the lack of steric bulk around the molybdenum centre, in contrast to the arrangement in $[(\kappa^1\text{-}CO_3)TiX_3]^-$ (X = N[^{t}Bu](3,5-$Me_2C_6H_3$)) for which a combination of ancillary ligand steric bulk and external carbonate complexation by an alkali-metal counterion promotes κ^1-binding of $[CO_3]^{2-}$ to the titanium centre.[4]

Solid $[PPN]_2[MoO_3(\kappa^2\text{-}CO_3)]$ is moderately stable in air, and does not lose CO_2 even after being heated at 70 °C under vacuum for 1 h. In solution, $[PPN]_2[MoO_3(\kappa^2\text{-}^{13}CO_3)]$ was heated to 56 °C without any observable loss of $^{13}CO_2$ as monitored by ^{13}C NMR spectroscopy. However, this compound is moisture sensitive, undergoing conversion to $[PPN]_2[MoO_4]$ when even a few equivalents of water are added to a solution of $[PPN]_2[MoO_3(\kappa^2\text{-}CO_3)]$. On the other hand, solid $[NEt_4]_2[MoO_3(\kappa^2\text{-}CO_3)]$ is hygroscopic and converts to molybdate and dimolybdate in *ca*. 15 minutes by absorbing moisture from the ambient atmosphere, as monitored by IR spectroscopy. Prepared and isolated using $^{13}CO_2$, $[PPN]_2[MoO_3(\kappa^2\text{-}^{13}CO_3)]$ displays a sharp ^{13}C NMR resonance at 165.7 ppm, this being in a region of the spectrum that is characteristic for carbonates.[4-5,18] In its IR spectrum, an isotope-shifted carbonyl stretch is present at 1599 cm^{-1} , in good agreement with the theoretical 1602 cm^{-1} predicted using the harmonic oscillator approximation. A small peak due to a minor impurity at 158.9 ppm could also be observed by ^{13}C NMR spectroscopy, correlated with the trace dimolybdate by-product detected by ^{95}Mo NMR spectroscopy. Adding $[PPN][HCO_3]$[19] to a mixture of $[PPN]_2[MoO_3(\kappa^2\text{-}^{13}CO_3)]$ and this unknown species yielded an increase in the intensity of the 158.9 ppm signal and no additional resonances, allowing us to conclusively assign the minor impurity as bicarbonate anion. The minor $[HCO_3]$ impurity may originate from the reaction of $[MoO_4]^{2-}$ with $[MoO_3(\kappa^2\text{-}CO_3)]^{2-}$ to yield $[Mo_2O_7]^{2-}$ and free $[CO_3]^{2-}$, the latter converting to bicarbonate upon protonation, presumably from adventitious water.

Under 1 atm of $^{13}CO_2$, the room temperature ^{13}C NMR spectrum of a $[PPN]_2[MoO_4]$ solution features two broad signals: one for the free $^{13}CO_2$ at 125.8 ppm,

and one for the molybdenum carbonate at 165.3 ppm, the broad nature of the resonances suggesting that a chemical exchange is occurring on the NMR time scale. A new major resonance appeared at 162.8 ppm when acquiring the spectrum at -19 °C, but disappeared after degassing the sample. The ratio of the unknown species at 162.8 ppm to $[MoO_3(\kappa^2\text{-}^{13}CO_3)]^{2-}$ increases at higher pressure of $^{13}CO_2$ (3 atm), and at lower temperature (-31 °C). These data are indicative of additional reversible binding of $^{13}CO_2$ to the $[MoO_3(\kappa^2\text{-}CO_3)]^{2-}$ dianion.

The existence of a dicarbonate species was confirmed by X-ray crystallography, as colourless diffraction quality crystals were grown by slowly cooling a CH_3CN solution of $[PPN]_2[MoO_4]$ under an atmosphere of CO_2. In the solid state, both carbonate ligands are bound κ^2 (Figure 2), with Mo-O distances of 2.198(2) and 2.024(2), 2.175(2) and 2.0145(19) Å, respectively. The molybdenum oxo distances are 1.695(2) and 1.705(3) Å, shorter still than in $[MoO_3(\kappa^2\text{-}CO_3)]^{2-}$ as the Mo-O π character is shared over fewer

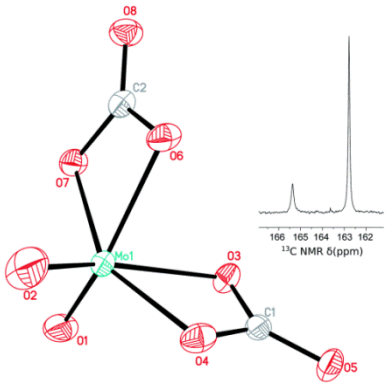

Figure 2. Right: ^{13}C NMR spectrum showing the distribution of $[MoO_3(\kappa^2\text{-}CO_3)]^{2-}$ (165.4 ppm) and $[MoO_2(\kappa^2\text{-}CO_3)_2]^{2-}$ (162.8 ppm) at −19 °C under 1 atm of $^{13}CO_2$. Left: solid-state structure of $[PPN]_2[MoO_2(\kappa^2\text{-}CO_3)_2]$ (ellipsoids at the 50% probability level, cations and solvent molecules omitted for clarity). Representative interatomic distances [Å] and angles [°]: C1–O3 1.302(4), C1–O4 1.352(4), C1–O5 1.228(4), C2–O6 1.303(3), C2–O7 1.358(3), C2–O8 1.223(3), Mo1–O1 1.695(2), Mo1–O2 1.705(3), Mo1–O3 2.198(2), Mo1–O4 2.024(2), Mo1–O6 2.175(2), Mo1–O7 2.0145(19); O3–C1–O4 110.4(2), O6–C2–O7 109.9(2), O4–Mo1–O7 149.44(6), O3–Mo1–O2 152.29(10), O6–Mo1–O1 152.10(8), O1–Mo1–O2 104.86(18); C1–O3–Mo1–O2 18.3(2), C1–O4–Mo1–O6 −79.04(11), C1–O4–Mo1–O1 80.37(14), C2–O6–Mo1–O1 27.3(2), C2–O7–Mo1–O2 86.70(15), C2–O7–Mo1–O3 −76.00(12).

UNIVERSITAT ROVIRA I VIRGILI
SECOND-ROW TRANSITION-METAL COMPLEXES RELEVANT TO CO2 REDUCTION AND WATER OXIDATION
Takashi Ono
DL:T 1108-2014

centres. The carbonate ligand binding mode is characterized by the same type of asymmetry as seen in $[MoO_3(\kappa^2\text{-}CO_3)]^{2-}$ due to the trans influence of the oxo ligands (O3-Mo1-O2 152.29(10)°, O6-Mo1-O1 152.10(8)°, C1-O3-Mo1-O2 18.3(2)°, C2-O6-Mo1-O1 27.3(2)°). While we were able to find several examples of κ^2-bound molybdenum carbonates reported in the Cambridge Structural Database,[20-24] this is the first example of a molybdenum complex with two κ^2-carbonates. To the best of our knowledge, $[PPN]_2[MoO_2(\kappa^2\text{-}CO_3)_2]$ is also the first transition-metal dicarbonate complex obtained directly from CO_2.[25]

In order to gain further insight into the energetics and potential energy landscape of this system, we turned to computational methods (Figure 3). Binding of the first CO_2 molecule is exothermic and exergonic with a $\Delta H°$(298 K) = -14.2 kcal/mol and $\Delta G°$(298 K) = -5.2 kcal/mol. The stability of the $[MoO_3(\kappa^2\text{-}CO_3)]^{2-}$ species is explained by the considerable activation energy of $\Delta G^{‡}$(298 K) = 17.2 kcal/mol for regenerating the molybdate dianion with loss of CO_2. This is consistent with our inability to remove CO_2 under vacuum at room temperature from this material. As expected, binding of the second CO_2 is slightly endergonic ($\Delta G°$(298 K) = 3.2 kcal/mol), being favoured at higher CO_2 pressures and lower temperatures as observed in our ^{13}C-labeling experiments. The possibility of binding a third CO_2 molecule was also investigated. However, producing such a species is endergonic with a $\Delta G°$ (298 K) = 14.6 kcal/mol, as well as $\Delta H° > 0$ and $\Delta S° < 0$. In contrast to the findings of Mizuno *et al*. who reported a calculated κ_1 structure for the related tungstate-CO_2 adduct,[8] we were unable to locate minima corresponding to κ_1 structures for any of the molybdenum carbonate complexes studied herein.

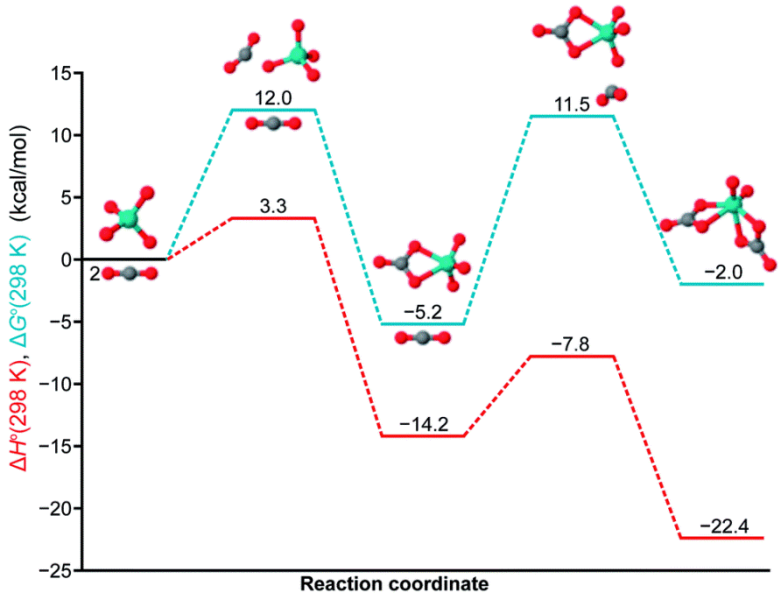

Figure 3. Combined calculated potential energy diagram for the first and second CO_2 binding events. Electronic structure calculations were carried out using the M06[26] density functional with the Def2-QZVPP[27] basis set for molybdenum, incorporating the SDD[28] effective core potential, and 6-311+G(3df) for all other atoms as implemented in the Gaussian 09 suite of programs.[29] The CPCM model[30-31] for CH_3CN was used to describe solvation effects, and the final single-point energies were calculated with QCISD(T)[32-33] at the optimized M06 geometries.

Curious to see whether the new molybdenum carbonate complexes can serve as a source of activated CO_2, we subjected $[PPN]_2[MoO_3(\kappa^2\text{-}CO_3)]$ to the mild hydride donor triethylsilane, which exhibits no background reactivity with CO_2 according to a control experiment.[34] A test reaction revealed a new resonance at δ 8.73 ppm (^{1}NMR spectroscopy), this being located in a region characteristic for formyl protons, as well as a new molybdenum species having a ^{95}Mo NMR signal at -23.7 ppm, a shift essentially identical to that reported for the $[MoO_3(OSiMe_3)]^-$ anion.[12] The production of formate improves from 16% to 71% if the reaction is run under an atmosphere of CO_2, raising the question of whether the active species facilitating CO_2 reduction is the monocarbonate complex $[MoO_3(\kappa^2\text{-}CO_3)]^{2-}$ or the dicarbonate complex $[MoO_2(\kappa^2\text{-}CO_3)_2]^{2-}$. After optimization, clean conversion to [PPN][OCHO] and $[PPN][MoO_3(OSiEt_3)]$ (eqn (2)) as the sole products can be obtained after 22 h at 85 °C, as evidenced by the

UNIVERSITAT ROVIRA I VIRGILI
SECOND-ROW TRANSITION-METAL COMPLEXES RELEVANT TO CO2 REDUCTION AND WATER OXIDATION
Takashi Ono
DL:T 1108-2014

^{1}H NMR spectrum of the crude reaction mixture. We were able to isolate [PPN][OCHO] in 69% yield, along with [PPN][MoO_3(OSiEt_3)] in 50% yield by taking advantage of their differential solubilities in THF.

$$[PPN]_2[MoO_3(\kappa^2\text{-}CO_3)] + Et_3SiH \rightarrow [PPN][MoO_3(OSiEt_3)] + [PPN][OCHO] \quad (2)$$

V.4. Conclusions

In summary, we have synthesized and characterized two molybdenum oxo carbonate species obtained from the uptake of CO_2 by the molybdate dianion and begun exploring their reactivity in the context of CO_2 reduction to formate.[35-39] ^{13}C-labeling experiments and computational analysis suggest that the first binding event to form $[MoO_3(\kappa^2\text{-}CO_3)]^{2-}$ is irreversible, while the second CO_2 molecule binds in a reversible process. We are currently investigating potential uses of $[MoO_4]^{2-}$ as a nucleophilic catalyst for CO_2 fixation[40-45] (encouraged by the methods already developed using the analogous tungstate dianion),[7-8] while also making efforts to develop an improved mechanistic understanding of this rich, yet simple system. This work illustrates the finding that a discrete, soluble molecular metal oxide system unencumbered by organic spectator ligands and unobstructed by hydrogen bonding with water is sufficient for CO_2 activation and conversion to formate in conjunction with a mild hydride source.

V.5. Acknowledgements

SABIC (Saudi Basic Industries Corporation) is acknowledged for partly funding the work of IK. TO would like to thank the Spanish Ministry of Education, Culture and Sport (MECD) for financial support. MT acknowledges the Spanish Ministry of Economy and Competitiveness under CTQ2012-36966 for financial support. DT was funded by the National Science Foundation under CHE-1111357.

I have carried out a part of synthesis, characterization including preparation of X-ray sample during my short stay at the group of Prof. C. C. Cummins at at Massachusetts Institute of Technology (MIT). Ioana Knopf, Ph.D. student in the group of Prof. C. C. Cummins at MIT, has completed the other experimental part. DFT calculations were performed by Prof. M. Temprado at the Universidad de Alcalá. X-ray structure analyses were carried out by Dr. Peter Müller

V.6. Associated contents

Full experimental crystallographic, spectroscopic, and computational data in Supporting Information. CIF data of CCDC 978136, 978137, and 981116.can be obtained free of charge from the Cambridge Crystallographic Data Centre via www.ccdc.cam.ac.uk/data_request/cif.

V.7. References

(1) Wang, S.; Murata, K.; Hayakawa, T.; Hamakawa, S.; Suzuki, K. *Applied Catalysis A: General* **2000**, *196*, 1-8.
(2) Bhanage, B. M.; Fujita, S.-i.; Ikushima, Y.; Arai, M. *Applied Catalysis A: General* **2001**, *219*, 259-266.
(3) Matsuoka, M.; Anpo, M. *Journal of Photochemistry and Photobiology C: Photochemistry Reviews* **2003**, *3*, 225-252.
(4) Silvia, J. S.; Cummins, C. C. *Chemical Science* **2011**, *2*, 1474-1479.
(5) Krogman, J. P.; Bezpalko, M. W.; Foxman, B. M.; Thomas, C. M. *Inorg. Chem.* **2013**, *52*, 3022-3031.
(6) Tsvetkov, N. P.; Andino, J. G.; Fan, H.; Verat, A. Y.; Caulton, K. G. *Dalton Trans.* **2013**, *42*, 6745-6755.
(7) Kimura, T.; Kamata, K.; Mizuno, N. *Angew. Chem., Int. Ed.* **2012**, *51*, 6700-6703.
(8) Kimura, T.; Sunaba, H.; Kamata, K.; Mizuno, N. *Inorg. Chem.* **2012**, *51*, 13001-13008.
(9) Silvia, J. S.; Cummins, C. C. *J. Am. Chem. Soc.* **2010**, *132*, 2169-2171.
(10) *Sodium molybdate dihydrate (50 mg, 0.2 mmol, 1 equiv.) was dissolved in ca. 0.8 mL D_2O. Carbon dioxide (20 mL, 0.8 mmol, 4 equiv.) was bubbled through this solution, after which it was stirred for 10 min. The ^{95}Mo NMR spectrum of the resulting solution showed only the molybdate resonance at δ = 0 ppm and no other species.*
(11) Briggs, J. R.; Harrison, A. M.; Robson, J. H. *Polyhedron* **1986**, *5*, 281-287.
(12) Do, Y.; Simhon, E. D.; Holm, R. H. *Inorg. Chem.* **1985**, *24*, 1831-1838.
(13) Busca, G.; Lorenzelli, V. *Materials Chemistry* **1982**, *7*, 89-126.
(14) Partyka, D. V.; Holm, R. H. *Inorg. Chem.* **2004**, *43*, 8609-8616.
(15) Groysman, S.; Wang, J.-J.; Tagore, R.; Lee, S. C.; Holm, R. H. *J. Am. Chem. Soc.* **2008**, *130*, 12794-12807.

UNIVERSITAT ROVIRA I VIRGILI
SECOND-ROW TRANSITION-METAL COMPLEXES RELEVANT TO CO2 REDUCTION AND WATER OXIDATION
Takashi Ono
DL:T 1108-2014

(16) Herzberg, G. *Electronic Spectra and Electronic Structure of Polyatomic Molecules*; Van Nostrand: New York, N.Y., 1966.
(17) Roman, P.; San Jose, A.; Luque, A.; Gutierrez-Zorrilla, J. M.; Martinez-Ripoll, M. *Acta Crystallographica Section C* **1994**, *50*, 1189-1191.
(18) Darensbourg, D. J.; Sanchez, K. M.; Rheingold, A. L. *J. Am. Chem. Soc.* **1987**, *109*, 290-292.
(19) Meckfessel Jones,. L. M., Texas A&M University, 1994.
(20) Chatt, J.; Kubota, M.; Leigh, G. J.; March, F. C.; Mason, R.; Yarrow, D. J. *J. Chem. Soc., Chem. Commun.* **1974**, 1033-1034.
(21) Carmona, E.; Gonzalez, F.; Poveda, M. L.; Marin, J. M.; Atwood, J. L.; Rogers, R. D. *J. Am. Chem. Soc.* **1983**, *105*, 3365-3366.
(22) Curtis, M. D.; Han, K. R. *Inorg. Chem.* **1985**, *24*, 378-382.
(23) Belmore, K. A.; Vanderpool, R. A.; Tsai, J. C.; Khan, M. A.; Nicholas, K. M. *J. Am. Chem. Soc.* **1988**, *110*, 2004-2005.
(24) Contreras, L.; Paneque, M.; Sellin, M.; Carmona, E.; Perez, P. J.; Gutierrez-Puebla, E.; Monge, A.; Ruiz, C. *New J. Chem.* **2005**, *29*, 109-115.
(25) Krivovichev, S. V.; Burns, P. C. *Radiochemistry* **2004**, *46*, 12-15.
(26) Zhao, Y.; Truhlar, D. *Theor. Chem. Acc.* **2008**, *120*, 215-241.
(27) Weigend, F.; Ahlrichs, R. *Phys. Chem. Chem. Phys.* **2005**, *7*, 3297-3305.
(28) Andrae, D.; Häußermann, U.; Dolg, M.; Stoll, H.; Preuß, H. *Theoret. Chim. Acta* **1990**, *77*, 123-141.
(29) Gaussian 09, Revision C.1, Frisch, M. J.; Trucks, G. W.; Schlegel, H. B.; Scuseria, G. E.; Robb, M. A.; Cheeseman, J. R.; Scalmani, G.; Barone, V.; Mennucci, B.; Petersson, G. A.; Nakatsuji, H.; Caricato, M.; Li, X.; Hratchian, H. P.; Izmaylov, A. F.; Bloino, J.; Zheng, G.; Sonnenberg, J. L.; Hada, M.; Ehara, M.; Toyota, K.; Fukuda, R.; Hasegawa, J.; Ishida, M.; Nakajima, T.; Honda, Y.; Kitao, O.; Nakai, H.; Vreven, T.; Montgomery, J., J. A.; Peralta, J. E.; Ogliaro, F.; Bearpark, M.; Heyd, J. J.; Brothers, E.; Kudin, K. N.; Staroverov, V. N.; Keith, T.; Kobayashi, R.; Normand, J.; Raghavachari, K.; Rendell, A.; Burant, J. C.; Iyengar, S. S.; Tomasi, J.; Cossi, M.; Rega, N.; Millam, J. M.; Klene, M.; Knox, J. E.; Cross, J. B.; Bakken, V.; Adamo, C.; Jaramillo, J.; Gomperts, R.; Stratmann, R. E.; Yazyev, O.; Austin, A. J.; Cammi, R.; Pomelli, C.; Ochterski, J. W.; Martin, R. L.; Morokuma, K.; Zakrzewski, V. G.; Voth, G. A.; Salvador, P.; Dannenberg, J. J.; Dapprich, S.; Daniels, A. D.; Farkas, Ö.; Foresman, J. B.; Ortiz, J. V.; Cioslowski, J.; Fox, D. J., Gaussian, Inc., Wallingford CT, 2010.
(30) Klamt, A.; Schuurmann, G. *Journal of the Chemical Society, Perkin Transactions 2* **1993**, 799-805.
(31) Barone, V.; Cossi, M. *The Journal of Physical Chemistry A* **1998**, *102*, 1995-2001.
(32) Knowles, P. J.; Werner, H.-J. *Chem. Phys. Lett.* **1985**, *115*, 259-267.
(33) Pople, J. A.; Head-Gordon, M.; Raghavachari, K. *J. Chem. Phys.* **1987**, *87*, 5968-5975.
(34) *Triethylsilane (23 mg, 0.2 mmol) was dissolved in ca. 1 mL CD_3CN and transferred to a Schlenk tube which was brought outside the glovebox. The solution was frozen using liquid nitrogen, the headspace was evacuated and the tube refilled with 1 atm of CO_2. The tube was sealed and heated at 85 °C overnight. The solution was analysed by ^1H NMR spectroscopy, showing that no reaction had occurred.*
(35) Itagaki, S.; Yamaguchi, K.; Mizuno, N. *J. Mol. Catal. A: Chem.* **2013**, *366*, 347-352.
(36) Sattler, W.; Parkin, G. *J. Am. Chem. Soc.* **2012**, *134*, 17462-17465.
(37) Motokura, K.; Kashiwame, D.; Miyaji, A.; Baba, T. *Org. Lett.* **2012**, *14*, 2642-2645.
(38) Lalrempuia, R.; Iglesias, M.; Polo, V.; Sanz Miguel, P. J.; Fernández-Alvarez, F. J.; Pérez-Torrente, J. J.; Oro, L. A. *Angew. Chem., Int. Ed.* **2012**, *51*, 12824-12827.

(39) Jansen, A.; Pitter, S. *J. Mol. Catal. A: Chem.* **2004**, *217*, 41-45.
(40) Wang, Y.-B.; Wang, Y.-M.; Zhang, W.-Z.; Lu, X.-B. *J. Am. Chem. Soc.* **2013**, *135*, 11996-12003.
(41) Seayad, J.; Seayad, A. M.; Ng, J. K. P.; Chai, C. L. L. *ChemCatChem* **2012**, *4*, 774-777.
(42) Yang, Z.-Z.; He, L.-N.; Peng, S.-Y.; Liu, A.-H. *Green Chemistry* **2010**, *12*, 1850-1854.
(43) Riduan, S. N.; Zhang, Y.; Ying, J. Y. *Angew. Chem., Int. Ed.* **2009**, *48*, 3322-3325.
(44) Zhou, H.; Zhang, W.-Z.; Liu, C.-H.; Qu, J.-P.; Lu, X.-B. *The Journal of Organic Chemistry* **2008**, *73*, 8039-8044.
(45) Sit, W. N.; Ng, S. M.; Kwong, K. Y.; Lau, C. P. *The Journal of Organic Chemistry* **2005**, *70*, 8583-8586.

UNIVERSITAT ROVIRA I VIRGILI
SECOND-ROW TRANSITION-METAL COMPLEXES RELEVANT TO CO2 REDUCTION AND WATER OXIDATION
Takashi Ono
DL:T 1108-2014

UNIVERSITAT ROVIRA I VIRGILI
SECOND-ROW TRANSITION-METAL COMPLEXES RELEVANT TO CO2 REDUCTION AND WATER OXIDATION
Takashi Ono
DL:T 1108-2014

Supporting Information for:

Uptake of one and two molecules of CO_2 by the molybdate dianion: a soluble, molecular oxide model system for carbon dioxide

Table of contents

UNIVERSITAT ROVIRA I VIRGILI
SECOND-ROW TRANSITION-METAL COMPLEXES RELEVANT TO CO2 REDUCTION AND WATER OXIDATION
Takashi Ono
DL:T 1108-2014

1. General Methods

All manipulations were performed using standard Schlenk techniques or in a nitrogen atmosphere glovebox, unless otherwise stated. All reagents were purchased from Sigma Aldrich or Alfa Aesar. U.S.P. grade carbon dioxide was purchased from Airgas, while $^{13}CO_2$ (99% ^{13}C) was purchased from Cambridge Isotopes. Ag_2MoO_4[1] and [PPN][HCO_3][2] were prepared using reported methods. [NEt_4]$_2$[MoO_4] was synthesized from commercially available [NEt_4]OH and H_2MoO_4 following a literature procedure for a similar compound, [N^nBu_4]$_2$[WO_4].[3] Solvents (EMD Chemicals) were either used as received or purified on a Glass Contour Solvent Purification System built by SG Water USA, LLC. IR spectra were recorded on a Bruker Tensor37 Fourier transform IR (FTIR) spectrometer. Elemental analyses were performed by Robertson Microlit Laboratories, Inc. NMR solvents were obtained from Cambridge Isotope Laboratories, and NMR spectra were obtained on a Bruker 400 MHz spectrometer. ^{95}Mo NMR spectra were acquired on saturated CD_3CN samples using a sweep width of 800 ppm, an acquisition time of 2 s per scan, and, depending on the sample, acquiring 200 to 500 scans. For variable temperature NMR experiments, all reported temperatures were calibrated using a methanol standard ($T \leq 25$ °C) or an ethylene glycol standard ($T \geq 25$ °C). ^{1}H NMR and $^{13}C\{^1H\}$ NMR chemical shifts are referenced to residual protio-solvent signals, ^{95}Mo NMR spectra are referenced to a 2 M Na_2MoO_4 in D_2O external standard (δ = 0 ppm), and ^{31}P NMR spectra are referenced to a 85% H_3PO_4 external standard (δ = 0 ppm). Low-temperature (100 K) X-ray diffraction data were collected on a either a Bruker X8 Kappa DUO four-circle diffractometer coupled to a Bruker Smart APEX2 CCD detector or a Siemens Platform three-circle diffractometer coupled to a Bruker-AXS Smart Apex CCD detector, with graphite-monochromated Mo Kα radiation (λ = 0.71073 Å). The structures were solved by direct methods using SHELXS or intrinsic phasing using SHELXT and refined against F^2 on all data by full-matrix least squares with SHELXL-97 or SHELXL-2012 using established methods. All non-hydrogen atoms were refined anisotropically. All hydrogen atoms were included in the model at geometrically calculated positions and refined using a riding model.

2. $[PPN]_2[MoO_4]$

2.1. Synthesis of $[PPN]_2[MoO_4]$

The following procedure was used in lieu of that reported by Briggs *et al*.[4] Outside the glovebox, Ag_2MoO_4 (9.93 g, 26.4 mmol, 1.1 equiv.) and PPNCl (27.56 g , 48.0 mmol, 2 equiv.) were placed into a 2 L round bottom flask. A solvent mixture (900 mL of 2:1 CH_3CN:H_2O at pH 8) was added to the solids, the flask was sealed with a septum and shielded from light with aluminum foil. The slurry was stirred vigorously at room temperature for 24 h. The mixture was filtered through Celite, then the filtrate was concentrated to 200 mL using a rotary evaporator. Most of the remaining water was removed under vacuum on the Schlenk line. The solid product was collected by filtration and washed with cold water at pH 8 (2×40 mL). The white solid was transferred to a flask and dried under vacuum overnight, after which it was slurried for 30 min in 130 mL of dry Et_2O, collected by filtration, and dried on the frit. The resulting powder was transferred to a 500 mL round bottom flask and dried under vacuum overnight. The solid was split into smaller batches and dried under vacuum at room temperature over P_2O_5 to yield 23.31 g of material (18.8 mmol, 79% yield).

2.2. Characterization of $[PPN]_2[MoO_4]$

^{1}H NMR (CD_3CN, 25 °C, 400.1 MHz) δ: 7.67 (1H, m), 7.57 (2H, m), 7.48 (2H, m) ppm.

$^{13}C\{^{1}H\}$ NMR (CD_3CN, 25 °C, 100.6 MHz) δ: 134.6 (s), 133.2 (m), 130.4 (m), 128.2 (d, $^{1}J_{PC}$ =108 Hz) ppm.

^{95}Mo NMR (CD_3CN, 25 °C, 26.1 MHz) δ: 13.2 ppm.

$^{31}P\{^{1}H\}$ NMR (CD_3CN, 25 °C, 162.0 MHz) δ: 22.0 ppm.

ATR-IR: 3045, 1639, 1586, 1481, 1436, 1282, 1241 (s, PPN), 1184, 1110 (s, PPN), 1026, 996, 811 (s, Mo-O), 788, 753, 721 (vs, PPN), 690 (vs, PPN), 615 cm^{-1}.

Elemental analysis [%] found (calculated for C72H60MoN2O4P4): C 69.72 (69.90), H 4.71 (4.89), N 2.09 (2.26)

^{1}H NMR spectrum of $[PPN]_2[MoO_4]$ in CD_3CN at 25 °C

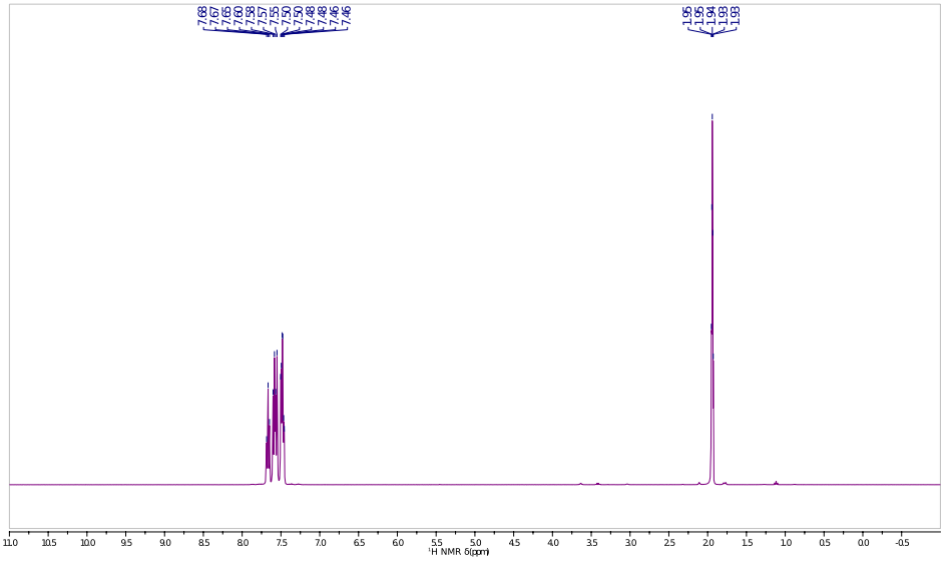

^{13}C NMR spectrum of $[PPN]_2[MoO_4]$ in CD_3CN at 25 °C

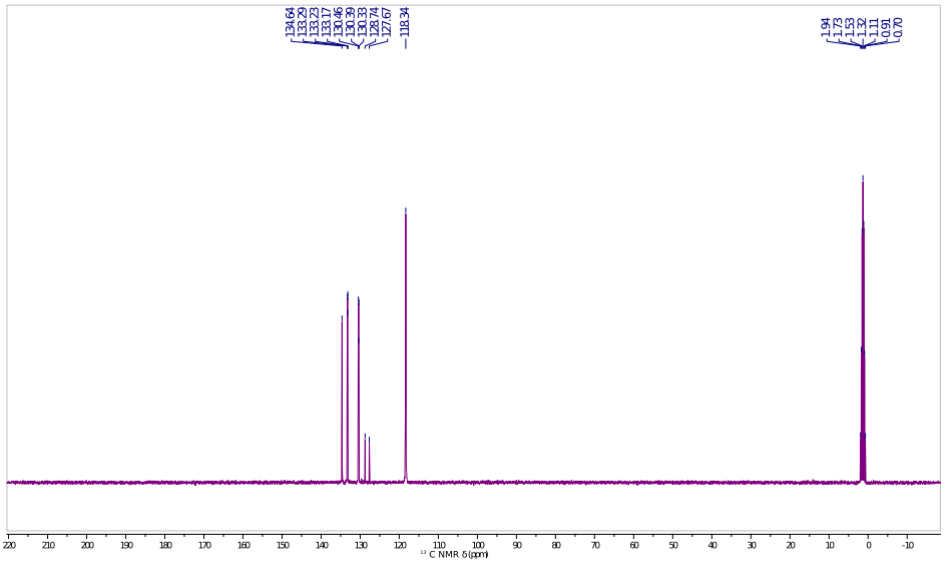

^{95}Mo NMR spectrum of $[PPN]_2[MoO_4]$ in CD_3CN at 25 °C

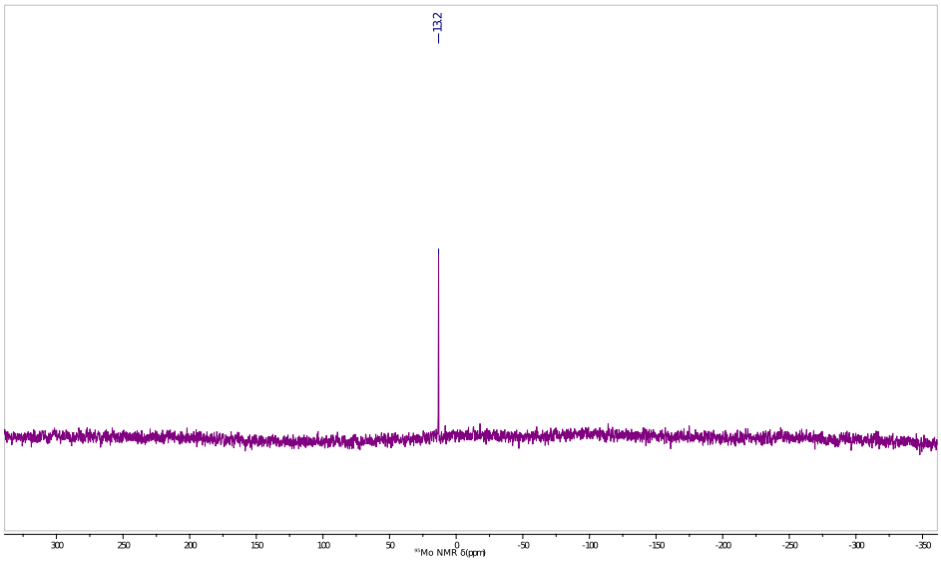

^{31}P NMR spectrum $[PPN]_2[MoO_4]$ in CD_3CN at 25 °C

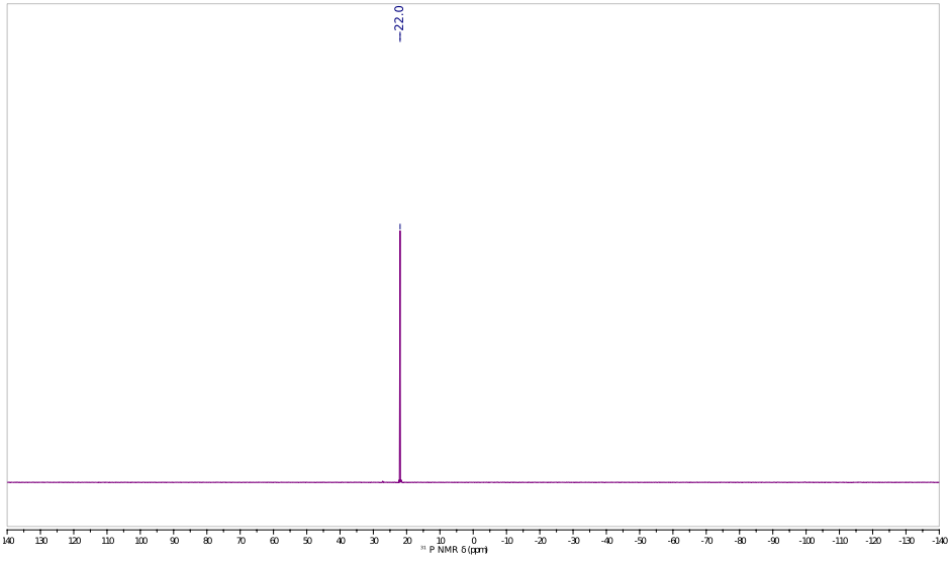

ATR-IR spectrum of $[PPN]_2[MoO_4]$

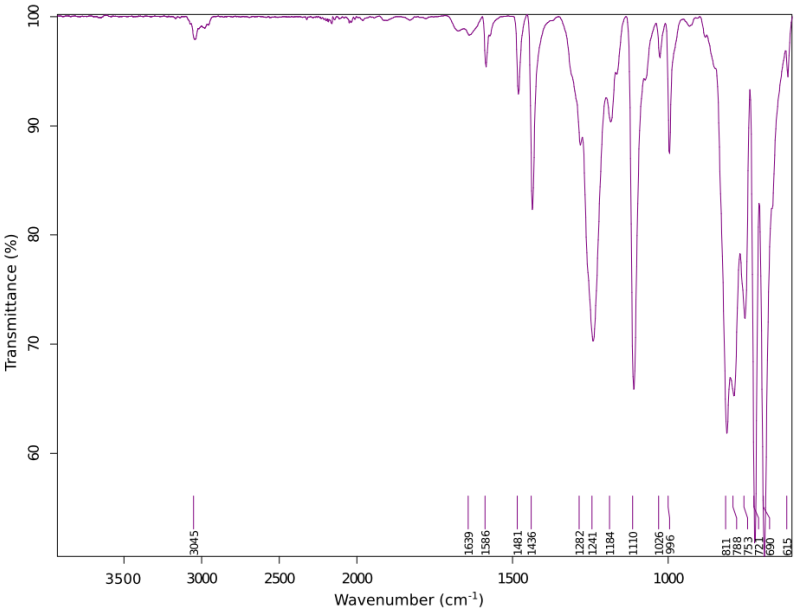

3. $[PPN]_2[MoO_3(\kappa^2\text{-}CO_3)]$

3.1. Synthesis of $[PPN]_2[MoO_3(\kappa^2\text{-}CO_3)]$

$[PPN]_2[MoO_4]$ (1.24 g, 1 mmol, 1 equiv.) was dissolved in CH_3CN (25 mL) and transferred to a round bottom flask that was then capped with a septum. The flask was taken outside the glovebox where CO_2 (60 mL, 2.5 mmol, 2.5 equiv.) was bubbled through the solution. After 5 min, the solvent was removed under vacuum, the flask was brought into the glovebox and the white solid triturated with Et_2O (3×5 mL). The white product obtained through this method (1.15 g, 0.9 mmol, 90% yield) contains $[PPN]_2[MoO_3(\kappa^2\text{-}CO_3)]$ and $[PPN]_2[Mo_2O_7]$ (identified by its characteristic ^{95}Mo NMR chemical shift)[5] in a 18:1 ratio (assessed by ^{95}Mo NMR spectroscopy). We were unable to separate the two compounds due to their very similar solubility properties. Given our ^{13}C-labeling studies (section 7.1), $[PPN][HCO_3]$ is also a by-product in this reaction, therefore the product obtained is a 18:1:2 mixture of $[PPN]_2[MoO_3(\kappa^2\text{-}CO_3)]$:$[PPN]_2[Mo_2O_7]$:$[PPN][HCO_3]$.

3.2. Characterization of $[PPN]_2[MoO_3(\kappa^2\text{-}CO_3)]$

^{1}H NMR (CD_3CN, 25 °C, 400.1 MHz) δ: 7.66 (1H, m), 7.57 (2H, m), 7.48 (2H, m) ppm.

$^{13}C\{^1H\}$ NMR (CD_3CN, 25 °C, 100.6 MHz) δ: 134.6 (s), 133.2 (m), 130.4 (m), 128.2 (d, $^1J_{PC}$ = 108 Hz) ppm.

^{95}Mo NMR (CD_3CN, 25 °C, 26.1 MHz) δ: 46.7 ($[MoO_3(\kappa^2\text{-}CO_3)]^{2-}$), -3.8 ($[Mo^2O^7]^{2-}$) ppm.

$^{31}P\{^1H\}$ NMR (CD_3CN, 25 °C, 162.0 MHz) δ: 21.9 ppm.

ATR-IR: 3050, 1676, 1638 (s, C=O), 1586, 1481, 1436, 1247 (s, PPN), 1180, 1163, 1109 (s, PPN), 1022, 997, 903 (m, Mo-O), 836 (s, Mo-O), 800 (m, Mo-O), 760, 750, 721 (vs, PPN), 689 (vs, PPN), 615 cm^{-1}

Elemental analysis [%] found (calculated for C73H60.1MoN2O6.05P4): C 68.71 (68.39), H 4.70 (4.73), N 1.98 (2.19)

^{1}H NMR spectrum of $[PPN]_2[MoO_3(\kappa^2\text{-}CO_3)]$ in CD_3CN at 25 °C

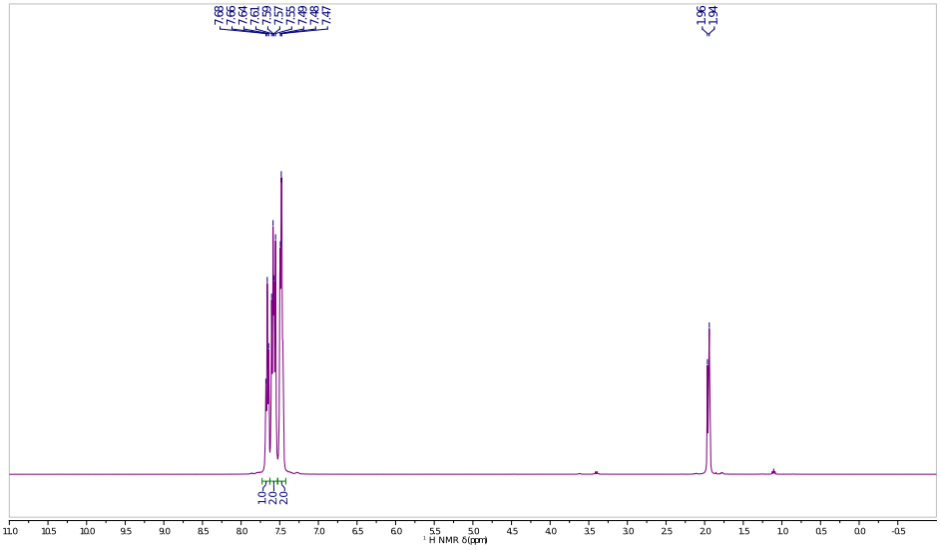

^{13}C NMR spectrum of $[PPN]_2[MoO_3(\kappa^2\text{-}CO_3)]$ in CD_3CN at 25 °C

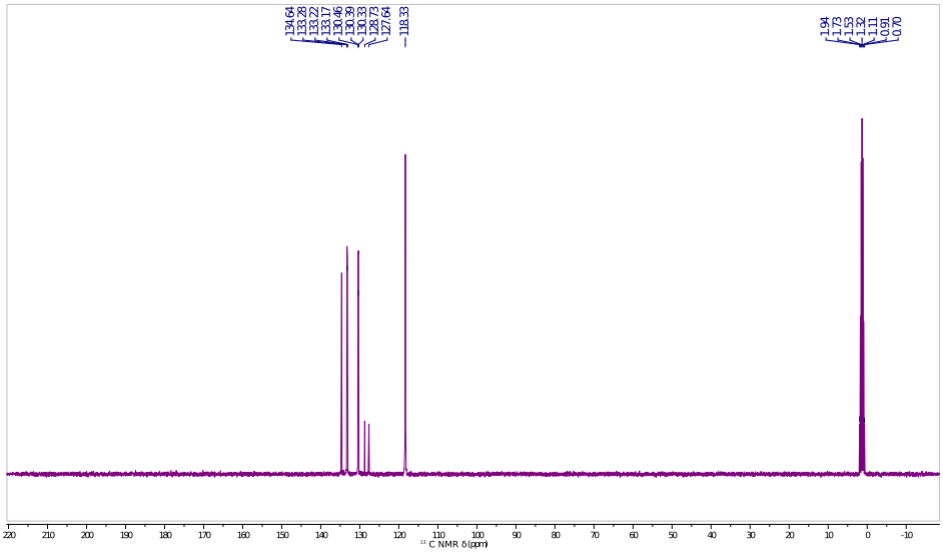

^{95}Mo NMR spectrum of $[PPN]_2[MoO_3(\kappa^2\text{-}CO_3)]$ in CD_3CN at 25 °C

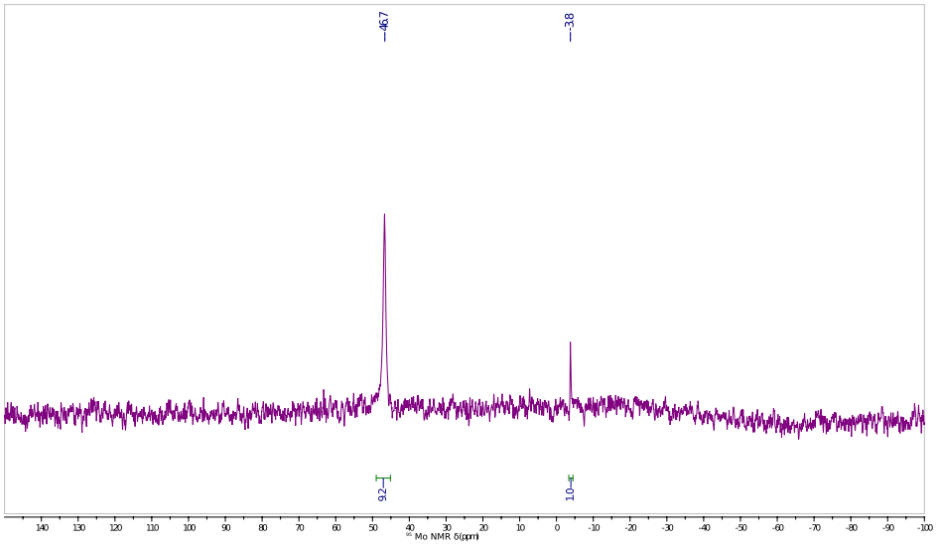

^{31}P NMR spectrum of $[PPN]_2[MoO_3(\kappa^2\text{-}CO_3)]$ in CD_3CN at 25 °C

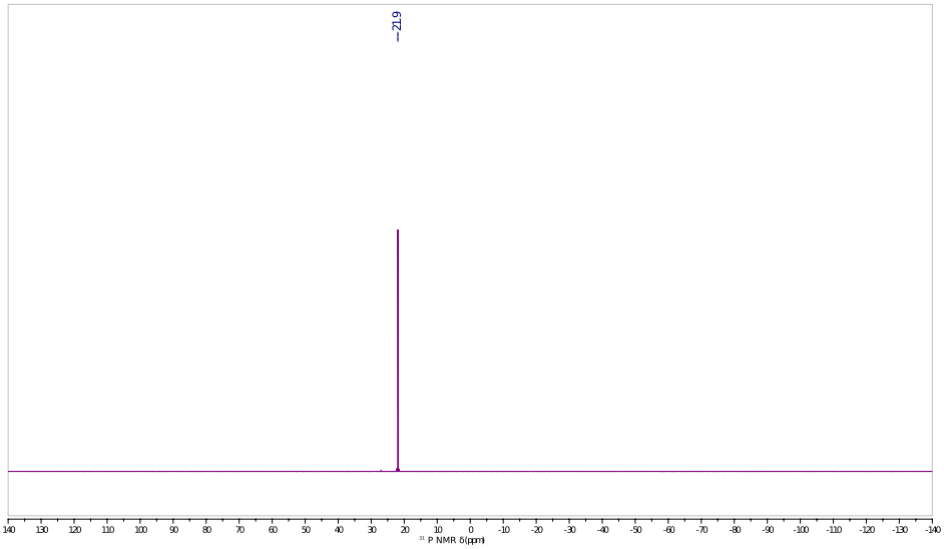

ATR-IR spectrum of $[PPN]_2[MoO_3(\kappa^2\text{-}CO_3)]$

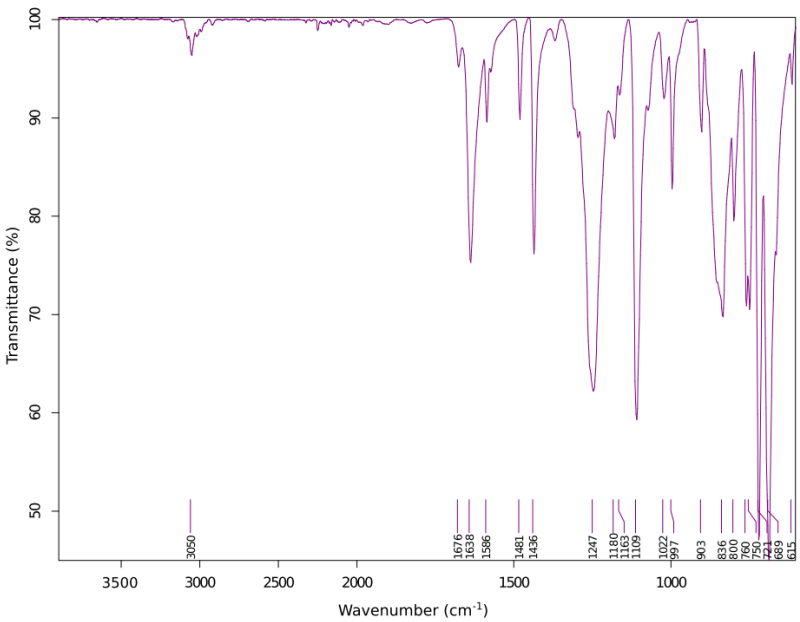

4. $[NEt_4]_2[MoO_3(\kappa^2\text{-}CO_3)]$

4.1. Synthesis of $[NEt_4]_2[MoO_3(\kappa^2\text{-}CO_3)]$

$[NEt_4]_2[MoO_4]$ (840 mg, 2.0 mmol, 1 equiv.) was dissolved in CH_3CN (40 mL) and transferred to a Schlenk flask that was then capped with a septum. The flask was taken outside the glovebox where CO_2 (120 mL, 5.0 mmol, 2.5 equiv.) was bubbled through the solution. After 10 min, the solvent was removed under vacuum, after which the flask was brought into the glovebox. A white solid (800 mg, 1.7 mmol, 85% yield) was thus obtained.

4.2. Characterization of $[NEt_4]_2[MoO_3(\kappa^2\text{-}CO_3)]$

^{1}H NMR (CD_3CN, 25 °C, 400.1 MHz) δ: 3.26 (2H, q, $^3J_{HH}$ = 7.3 Hz), 1.22 (3H, t, $^3J_{HH}$ = 7.3 Hz) ppm.

$^{13}C\{^1H\}$ NMR (CD_3CN, 25 °C, 100.6 MHz) δ: 165.6, 53.1, 7.9 ppm.

^{95}Mo NMR (CD_3CN, 25 °C, 26.1 MHz) δ: 46.4 ppm.

ATR-IR: 2984, 1628 (s, C=O), 1453, 1394, 1265, 1185, 1019, 1005, 901 (m, Mo-O), 839 (s, Mo-O), 807 (vs, Mo-O), 757, 676, 626 cm^{-1}

Elemental analysis [%] found (calculated for C17H40MoN2O6): C 43.71 (43.96), H 8.93 (8.68), N 6.27 (6.03).

^{1}H NMR spectrum of $[NEt_4]_2[MoO_3(\kappa^2\text{-}CO_3)]$ in CD_3CN at 25 °C

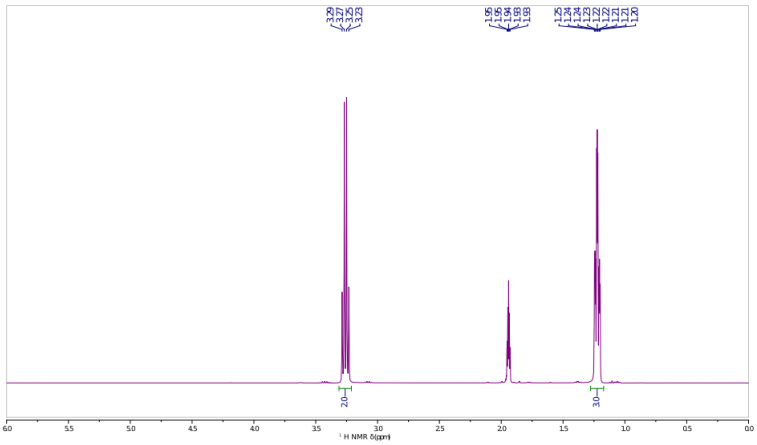

^{95}Mo NMR spectrum of $[NEt_4]_2[MoO_3(\kappa^2\text{-}CO_3)]$ in CD_3CN at 25 °C

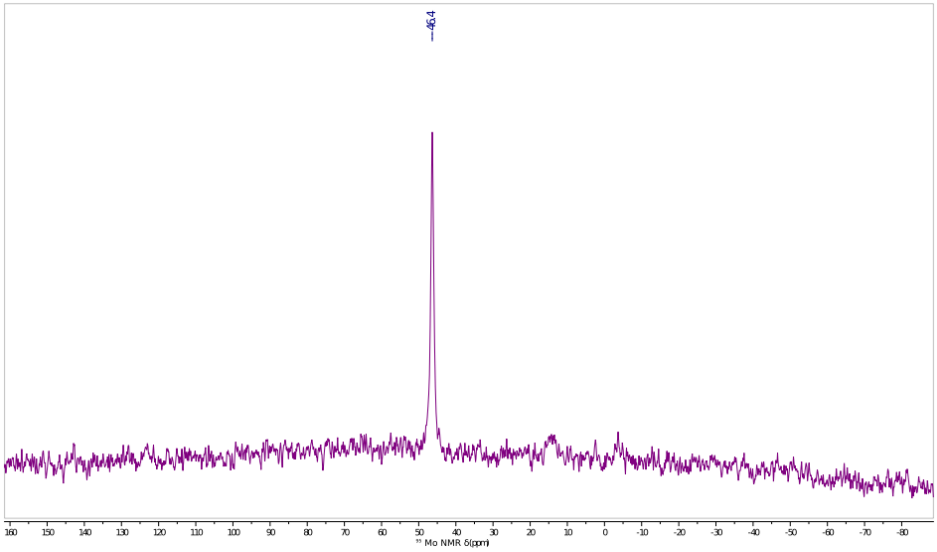

^{13}C NMR spectrum of $[NEt_4]_2[MoO_3(\kappa^2\text{-}CO_3)]$ in CD_3CN at 25 °C

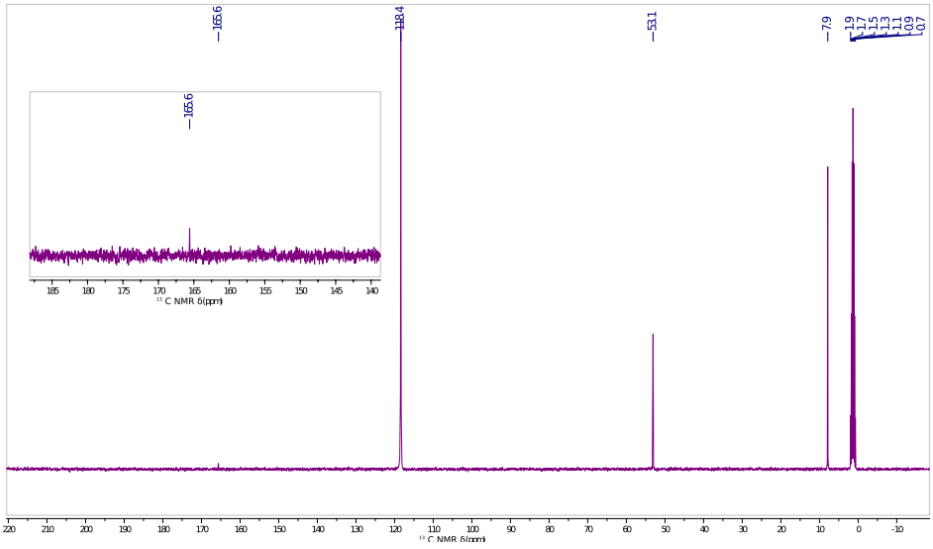

ATR-IR spectrum of $[NEt_4]_2[MoO_3(\kappa^2\text{-}CO_3)]$ in CD_3CN at 25 °C

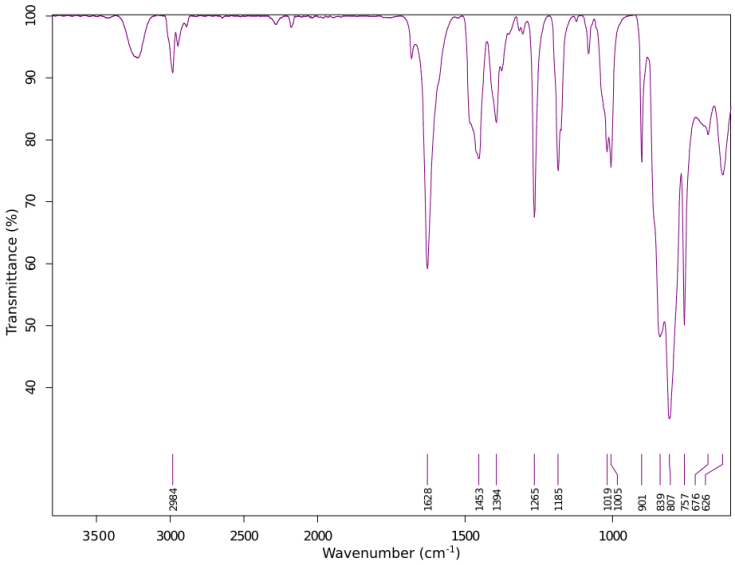

5. Reaction of $[PPN]_2[MoO_3(\kappa^2\text{-}CO_3)]$ with Et_3SiH

5.1. General procedure

$[PPN]_2[MoO_3(\kappa^2\text{-}CO_3)]$ (513 mg, 0.4 mmol, 1 equiv.) was dissolved in CH_3CN (6 mL) and transferred to a Schlenk tube to which a solution of triethylsilane (140 mg, 1.2 mmol, 3 equiv.) in CH_3CN (4 mL) was then added. The Schlenk tube was sealed and taken outside the glovebox, where it was connected to the Schlenk line and degassed using 4 freeze-pump-thaw cycles. The tube was then refilled with CO_2 (1 atm) from the manifold, closed, and heated at 85 ◦C for 22 h. The solvent was removed under vacuum and the flask was brought into the glovebox. The crude residue was triturated with Et_2O (5×8 mL) to remove traces of CH_3CN and obtain an off-white powder. This crude solid was placed on a frit and washed with 3×3 mL THF. The THF insoluble white solid collected was analyzed by NMR and IR spectroscopy and confirmed to be [PPN][OCHO] (162 mg, 0.28 mmol, 69% yield). The THF filtrate was concentrated and triturated with Et_2O (3×3 mL). The solid collected (284 mg) was confirmed to be $[PPN][MoO_3(OSiEt_3)]$ with a small amount of [PPN][OCHO]

contamination. The product was crystallized by slow cooling of a 3:1 THF:Et_2O solution, collected by filtration, and washed with 3×1 mL Et_2O to give pure [PPN][$MoO_3(OSiEt_3)$] (161 mg, 0.2 mmol, 50% yield).

^{1}H NMR spectrum of the crude reaction mixture in CD_3CN at 25 °C

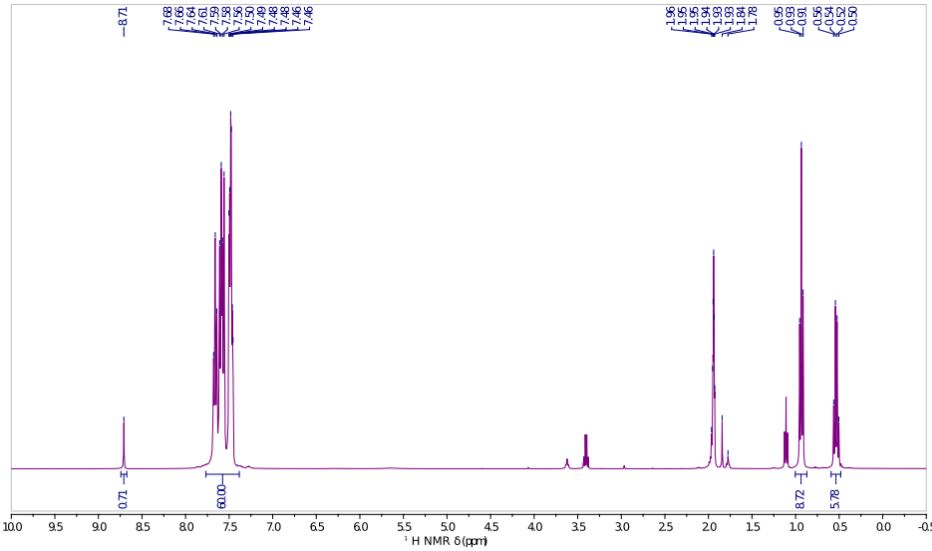

5.2 Characterization of [PPN][OCHO]

^{1}H NMR (CD_3CN, 25 °C, 400.1 MHz) δ: 8.73 (s, 1H, $^1J_{CH}$ = 173 Hz), 7.66 (6H, m), 7.57 (12H, m), 7.48 (12H, m) ppm.

$^{13}C\{^1H\}$ NMR (CD_3CN, 25 °C, 100.6 MHz) δ: 166.4 (s), 134.6 (s), 133.2 (m), 130.4 (m), 128.2 (d, $^1J_{PC}$ = 108 Hz) ppm.

$^{31}P\{^1H\}$ NMR (CD_3CN, 25 °C, 162.0 MHz) δ: 22.1 ppm.

ATR-IR: 3056, 2594 (w, formate C–H), 1600 (vs, C=O), 1584, 1482, 1435, 1365, 1333, 1287, 1264 (s, PPN), 1186, 1162, 1111 (vs, PPN), 1026, 997, 797, 765, 745, 722 (vs, PPN), 692 (vs, PPN), 664, 616 cm^{-1}

Elemental analysis [%] found (calculated for C37H31NO2P2): C 73.43 (76.15), H 4.96 (5.35), N 2.28 (2.40)

UNIVERSITAT ROVIRA I VIRGILI
SECOND-ROW TRANSITION-METAL COMPLEXES RELEVANT TO CO2 REDUCTION AND WATER OXIDATION
Takashi Ono
DL:T 1108-2014

The spectral data shown below pertain to the [PPN][OCHO] obtained in the above-mentioned reaction. In order to unequivocally confirm the identity of this product, [PPN][OCHO] was also synthesized independently from [PPN]Cl and Na[OCHO] following a literature procedure for preparing bis(triphenylphosphine)iminium carboxylates.[6] The material obtained through this route is spectroscopically identical. (^{1}H NMR, ^{13}C NMR, ^{31}P NMR, and ATR-IR) to that obtained via reduction of $[PPN]_2[MoO_3(\kappa^2\text{-}CO_3)]$ with triethylsilane.

^{1}H NMR spectrum of [PPN][OCHO] in CD3CN at 25 °C

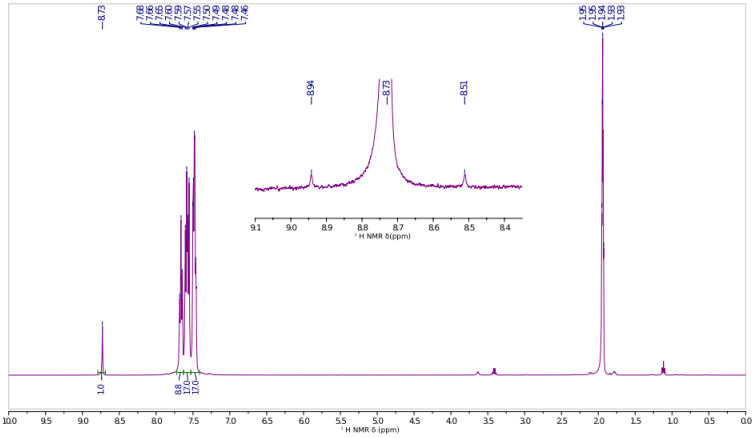

^{13}C NMR spectrum of [PPN][OCHO] in CD_3CN at 25 °C

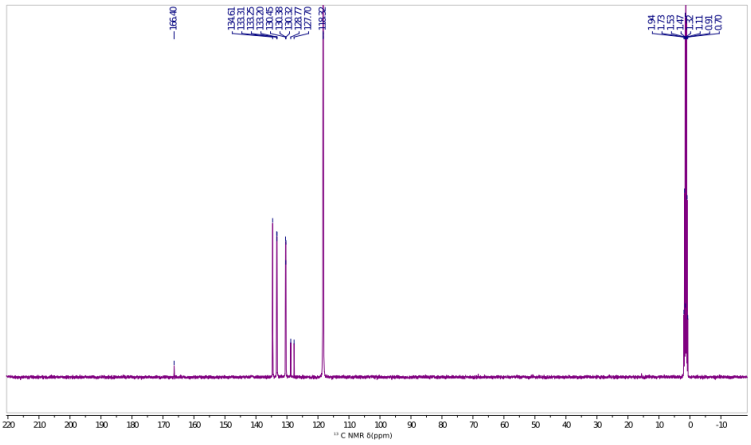

^{31}P NMR spectrum of [PPN][OCHO] in CD_3CN at 25 °C

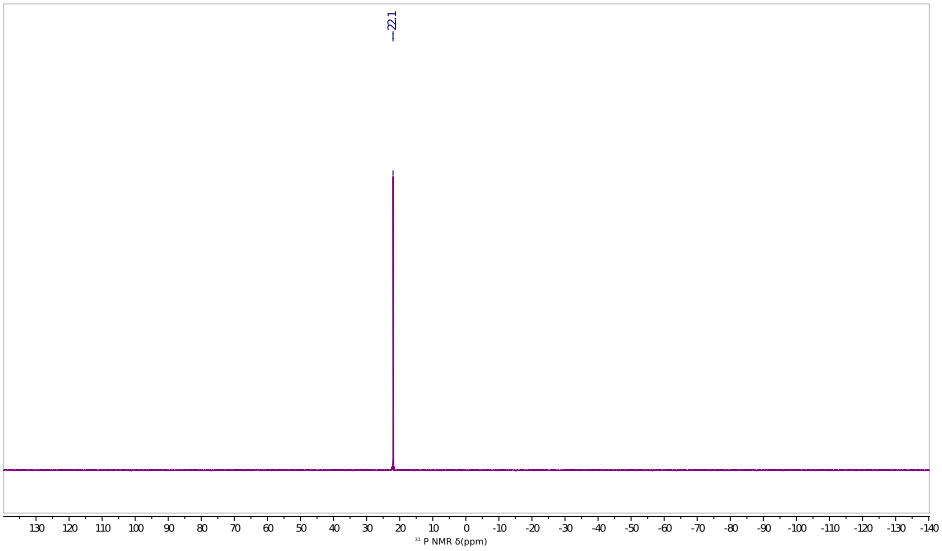

ATR-IR spectrum of [PPN][OCHO]

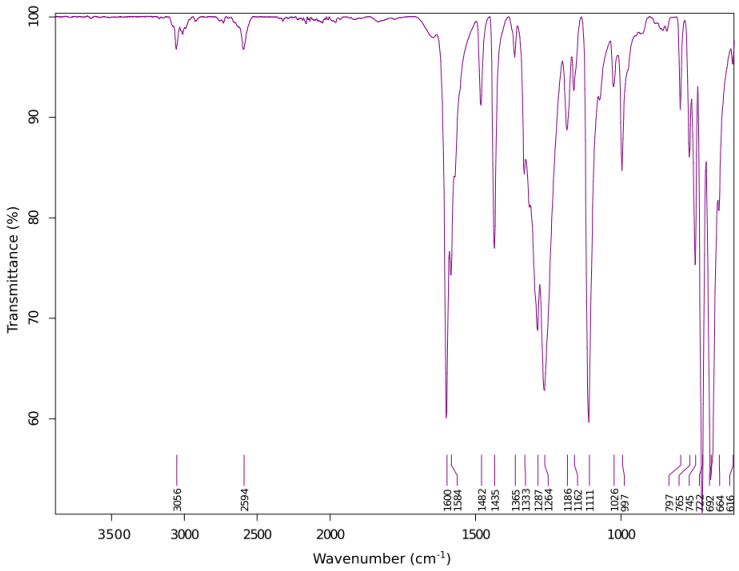

UNIVERSITAT ROVIRA I VIRGILI
SECOND-ROW TRANSITION-METAL COMPLEXES RELEVANT TO CO2 REDUCTION AND WATER OXIDATION
Takashi Ono
DL:T 1108-2014

5.3. Characterization of [PPN][$MoO_3(OSiEt_3)$]

^{1}H NMR (CD_3CN, 25 °C, 400.1 MHz) δ: 7.66 (6H, m), 7.58 (12H, m), 7.48 (12H, m), 0.95 (9H, t, $^{3}J_{HH}$ = 7.9 Hz), 0.55 (6 H, q, $^{3}J_{HH}$ = 7.9 Hz) ppm.

^{13}C{^{1}H} NMR (CD_3CN, 25 °C, 100.6 MHz) δ: 134.6 (s), 133.2 (m), 130.4 (m), 128.2 (d, $^{1}J_{PC}$ = 108 Hz), 7.23 (s), 7.04 (s) ppm.

^{95}Mo NMR (CD_3CN, 25 °C, 26.1 MHz) δ: -23.7 ppm.

For comparison, $[MoO_3(OSiMe_3)]^-$ has a ^{95}Mo NMR resonance at δ = -24 ppm.[5]

^{31}P{^{1}H} NMR (CD_3CN, 25 °C, 162.0 MHz) δ: 22.0 ppm.

ATR-IR: 3056, 2955, 2874, 1588, 1483, 1460, 1436, 1284, 1260 (s, PPN), 1184, 1160, 1113 (s, PPN), 998, 950 (m, Mo-O), 878 (vs, Mo-O), 800, 745, 721 (s, PPN), 691 (s, PPN), 616 cm^{-1}

Elemental analysis [%] found (calculated for C42H45MoNO4P2Si): C 61.94 (61.99), H 5.30 (5.57), N 1.64 (1.72)

^{1}H NMR spectrum of [PPN][$MoO_3(OSiEt_3)$] in CD_3CN at 25 °C

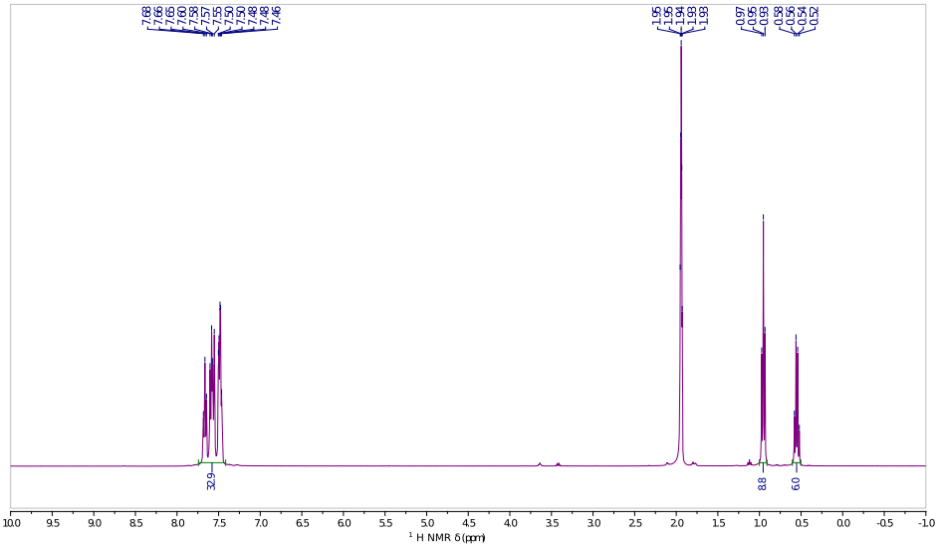

^{13}C NMR spectrum of [PPN][MoO_3($OSiEt_3$)] in CD_3CN at 25 °C

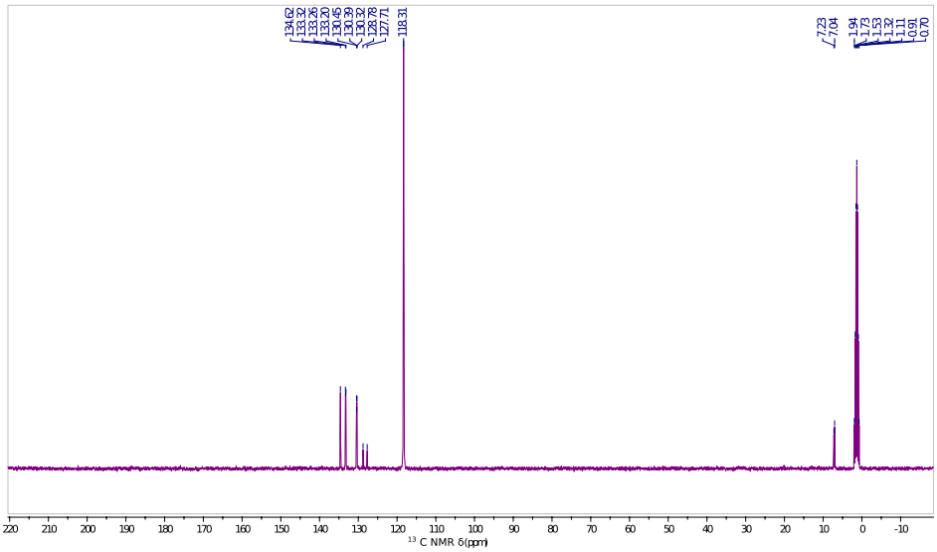

^{95}Mo NMR spectrum of [PPN][MoO_3($OSiEt_3$)] in CD_3CN at 25 °C

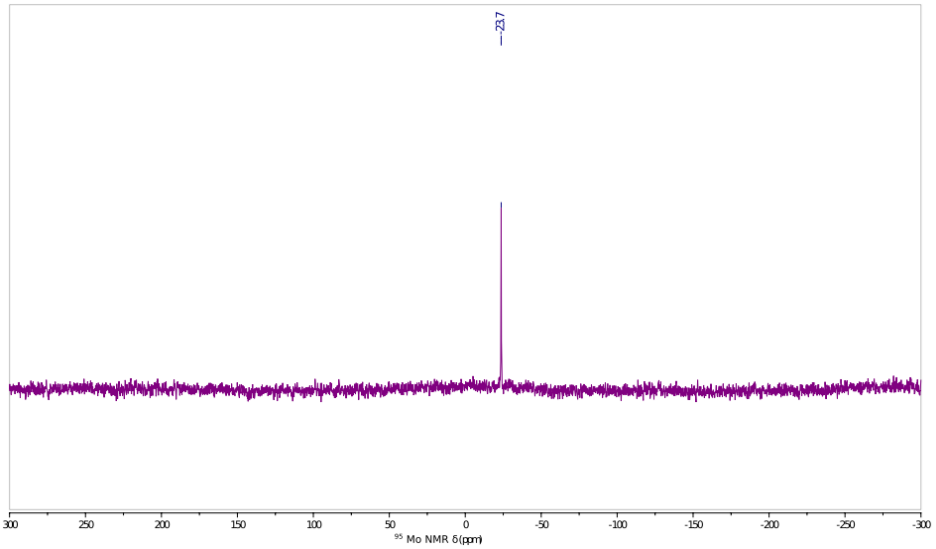

UNIVERSITAT ROVIRA I VIRGILI
SECOND-ROW TRANSITION-METAL COMPLEXES RELEVANT TO CO2 REDUCTION AND WATER OXIDATION
Takashi Ono
DL:T 1108-2014

^{31}P NMR spectrum of [PPN][$MoO_3(OSiEt_3)$] in CD_3CN at 25 °C

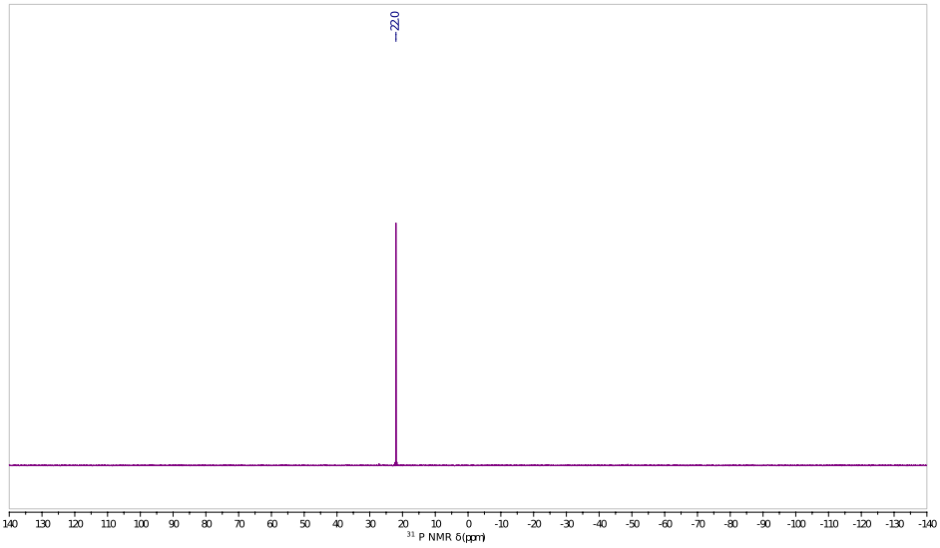

ATR-IR spectrum of [PPN][$MoO_3(OSiEt_3)$]

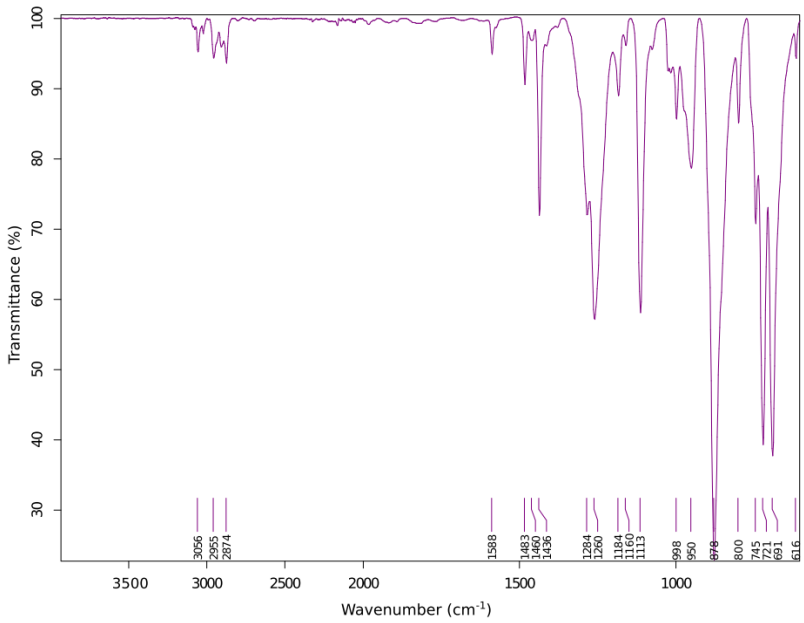

6. Stability studies on $[PPN]_2[MoO_3(\kappa^2\text{-}CO_3)]$ and $[NEt_4]_2[MoO_3(\kappa^2\text{-}CO_3)]$

6.1. Thermal stability of $[PPN]_2[MoO_3(\kappa^2\text{-}CO_3)]$

In the solid state: A small amount (*ca*. 30 mg) of $[PPN]_2[MoO_3(\kappa^2\text{-}CO_3)]$ was placed in a Schlenk flask and brought outside the glovebox. The flask was heated under dynamic vacuum in an oil bath at 70 °C for 1 hour. The resulting solid was analyzed by ATR-IR, showing an identical spectrum to the initial material with no decomposition or decrease in the carbonyl band at 1638 cm^{-1}. In solution: $[PPN]_2[MoO_3(\kappa^2\text{-}^{13}CO_3)]$* (30 mg) was dissolved in *ca*. 0.6 mL of CD_3CN and transferred to an NMR tube glass blown onto a 14/20 female adapter. A vacuum adapter was added, and the sealed system was brought outside the box. The solution was frozen using liquid nitrogen, the system was evacuated, then the tube was flame sealed. ^{13}C NMR spectra were taken at room temperature, 38 °C and 56 °C. No free $^{13}CO_2$ was observed in solution. In contrast to the broad signal observed in the presence of excess $^{13}CO_2$ (see section 7.2), the signal of $[MoO_3(\kappa^2\text{-}^{13}CO_3)]^{2-}$ remained sharp, indicating that no chemical exchange was occurring.

^{13}C NMR spectrum of the $[PPN]_2[MoO_3(\kappa^2\text{-}^{13}CO_3)]$ solution in CD_3CN at 56 °C

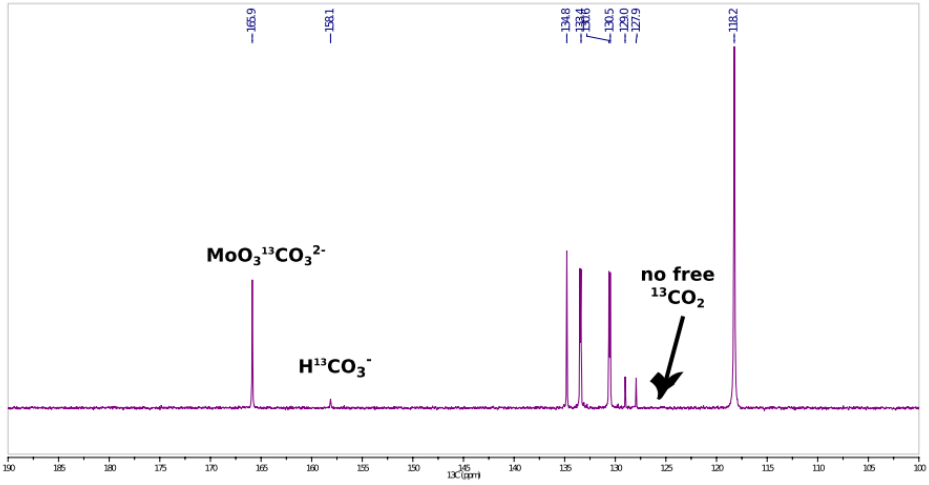

* $[PPN]_2[MoO_3(\kappa^2\text{-}^{13}CO_3)]$ was prepared via the same procedure as $[PPN]_2[MoO_3(\kappa^2\text{-}CO_3)]$, but using $^{13}CO_2$ (99% ^{13}C) instead of naturally abundant CO_2.

6.2. Addition of water to $[PPN]_2[MoO_3(\kappa^2\text{-}^{13}CO_3)]$ monitored by ^{13}C NMR

$[PPN]_2[MoO_3(\kappa^2\text{-}^{13}CO_3)]$ (26 mg, 0.02 mmol, 1 equiv.) was dissolved in *ca*. 0.6 mL of CD_3CN, transferred to an NMR tube, and capped with a septum. A stock solution of H_2O (ACS grade) in CH_3CN was prepared by adding 36 µL H_2O to *ca*. 0.97 mL CH_3CN. ^1H NMR and ^{13}C NMR spectra of the initial sample were taken. Stoichiometric amounts of water were added via microsyringe from the stock solution in 100 µL increments. Each 100 µL of the stock solution contain 0.02 mmol (1 equiv.) H2O. ^1H NMR and ^{13}C NMR spectra were collected after the addition of 1, 2, 4.5 and 9 equiv. of water. The ^1H NMR spectra were used to confirm the stoichiometry. The ^{13}C NMR spectra were diagnostic for the stability of the$[PPN]_2[MoO_3(\kappa^2\text{-}^{13}CO_3)]$. Although water elicits an increase in the amount of HCO_3^-, the $[PPN]_2[MoO_3(\kappa^2\text{-}^{13}CO_3)]$ is still present in solution after the addition of 9 equivalents of water.

^1H NMR spectrum of the $[PPN]_2[MoO_3(\kappa^2\text{-}^{13}CO_3)]$ solution with increasing water content

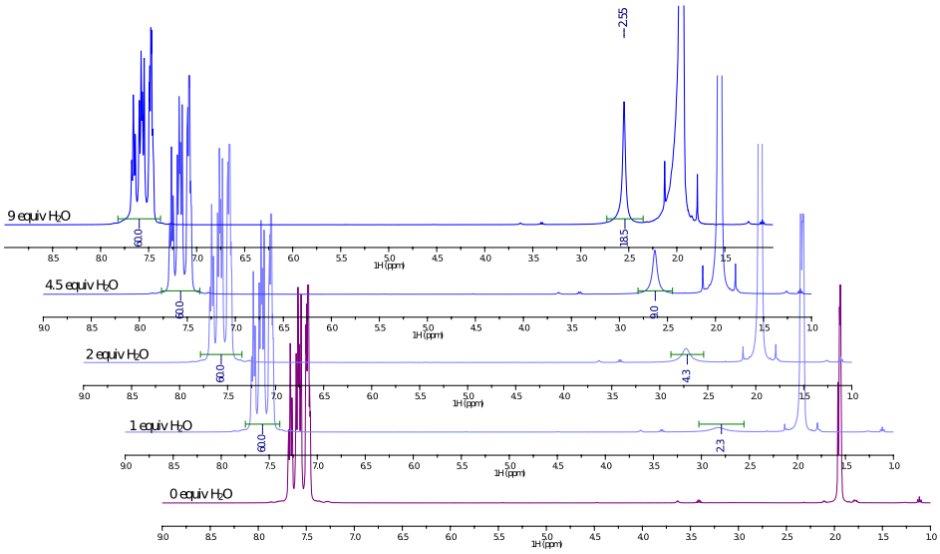

^{13}C NMR spectrum of the $[PPN]_2[MoO_3(\kappa^2\text{-}^{13}CO_3)]$ solution with increasing water content

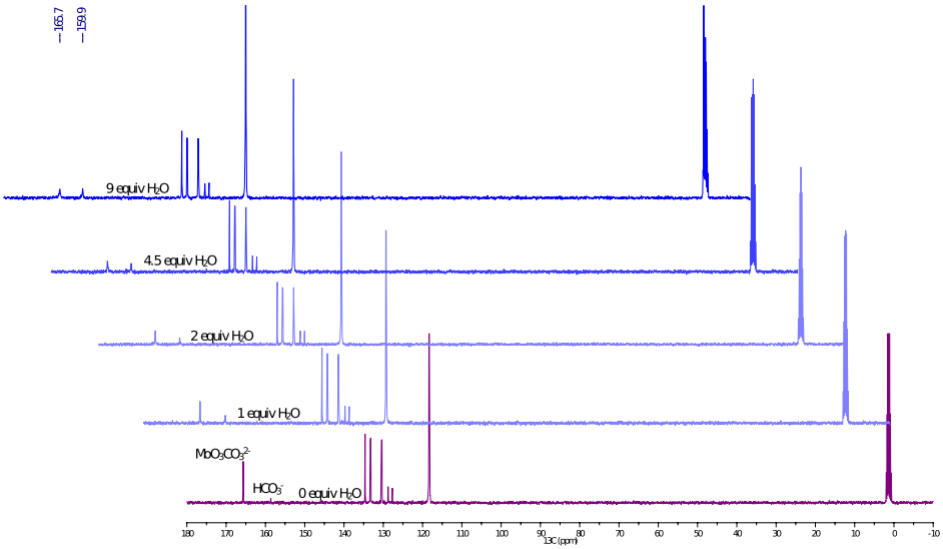

6.3. Addition of water to $[PPN]_2[MoO_3(\kappa^2\text{-}CO_3)]$ monitored by ATR-IR

A small amount of $[PPN]_2[MoO_3(\kappa^2\text{-}CO_3)]$ (20 mg, 0.0156 mmol) was dissolved in 1 mL CH_3CN in a vial that was then capped with a septum. The vial was taken outside the glovebox where water (10 µL, 10 mg, 0.555 mmol, 35 equiv.) was injected using a microsyringe. The solution was stirred for 10 min, all volatile materials were removed, and the residue analyzed by ATR-IR. ATR-IR spectrum of $[PPN]_2[MoO_3(\kappa^2\text{-}CO_3)]$ before (orange) and after (purple) the addition of excess water.

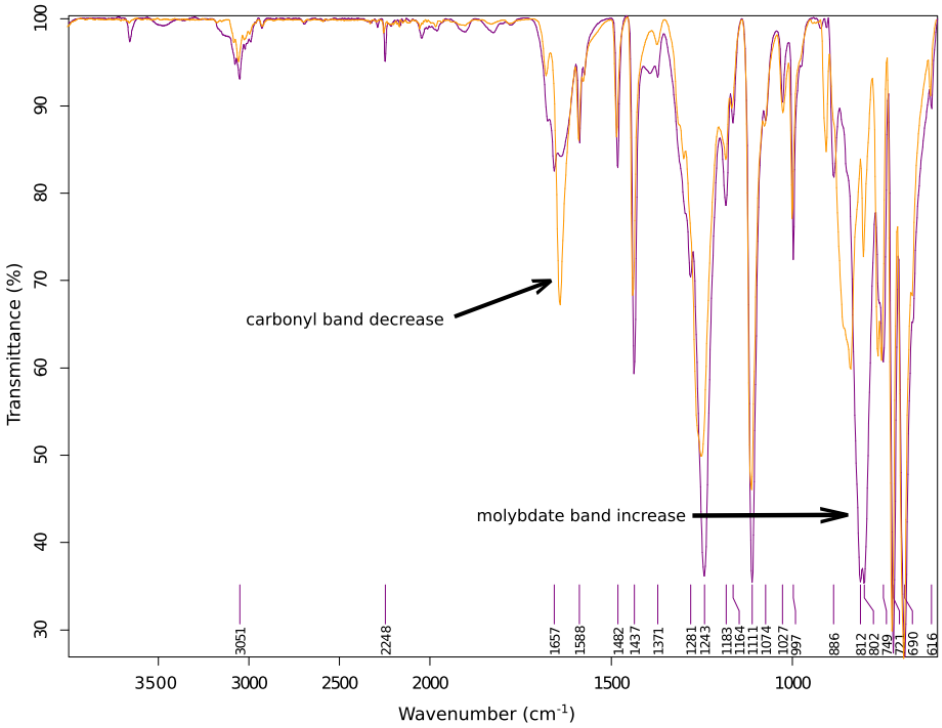

6.4. Hygroscopy of $[NEt_4]_2[MoO_3(\kappa^2\text{-}CO_3)]$ monitored by ATR-IR

A small amount (*ca*. 5 mg) of $[NEt_4]_2[MoO_3(\kappa^2\text{-}CO_3)]$ was placed on the ATR plate and the IR spectrum of this sample was recorded. Additional spectra of the same sample were recorded every 2-3 minutes for a total of 15 minutes, time during which the sample remained in air on the ATR plate and was absorbing atmospheric moisture. The overlay below shows the correlation between the disappearance of the carbonate band and the growth of the broad water OH band. The end product displays bands in the metal oxo region of the spectrum corresponding to molybdate and dimolybdate.

Evolution of the ATR-IR spectrum of $[NEt_4]_2[MoO_3(\kappa^2\text{-}CO_3)]$ over the course of 15 min in air

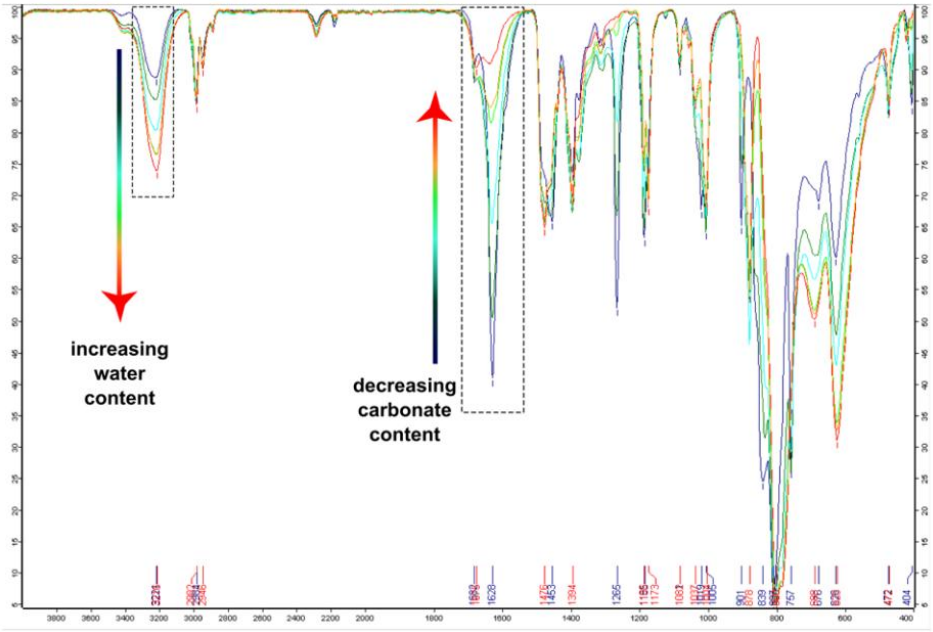

6.5. Formation of $[PPN]_2[MoO_3(\kappa^2\text{-}CO_3)]$ in wet aerobic conditions

$[PPN]_2[MoO_4]$ (100 mg, 0.08 mmol, 1 equiv.) was dissolved in non-degassed ACS grade acetonitrile (2 mL) under air. Carbon dioxide (40 mL, 1.64 mmol, 20 equiv.) was bubbled through the stirring molybdate solution. The reaction was allowed to stir open to air for 10 minutes, after which an aliquot was taken for NMR analysis. The ^{95}Mo NMR spectrum of the crude reaction mixture indicates formation of $[PPN]_2[MoO_3(\kappa^2\text{-}CO_3)]$ and $[PPN]_2[Mo_2O_7]$ in a 1.6:1 ratio.

^{95}Mo NMR of the crude reaction mixture at 25 °C

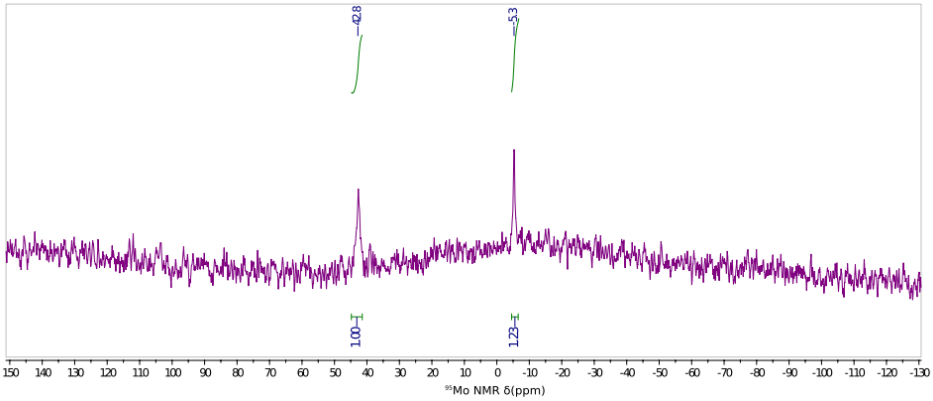

7. ^{13}C-labeling experiments

7.1. Identifying HCO_3^- in the ^{13}C NMR of $[PPN]_2[MoO_3(\kappa^2\text{-}^{13}CO_3)]$

$[PPN]_2[MoO_4]$ (30.4 mg, 0.025 mmol, 1 equiv.) was dissolved in *ca*. 0.6 mL of CD_3CN, transferred to an NMR tube and capped with a septum. The tube was taken outside the glovebox and the solution submitted to 3 freeze-pump-thaw cycles. $^{13}CO_2$ (0.6 mL, 0.025 mmol, 1 equiv.) was added by syringe, after which the tube was shaken vigorously. A ^{13}C NMR spectrum of the reaction mixture was acquired, then the tube was brought into the glovebox where a small amount of $[PPN][HCO_3]$[2] was added to the solution. A ^{13}C NMR spectrum of this mixture was taken, confirming the identity of the upfield carbonate peak.

^{13}C NMR spectrum of the initial reaction mixture

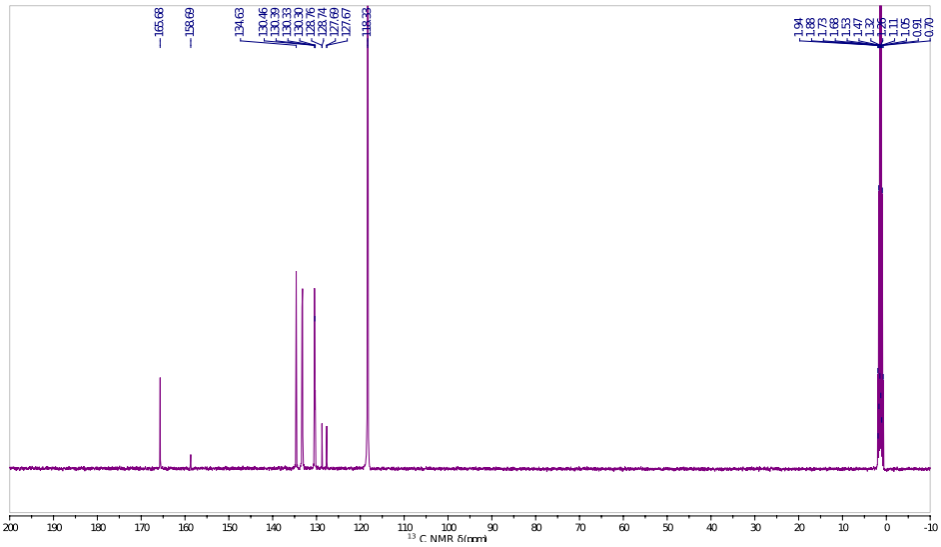

^{13}C NMR spectrum of the reaction mixture after [PPN][HCO_3] was added

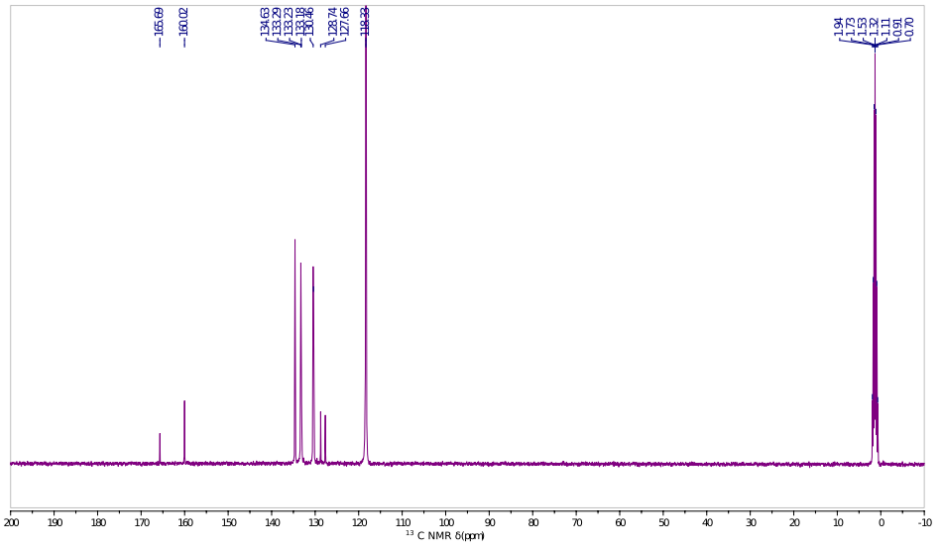

UNIVERSITAT ROVIRA I VIRGILI
SECOND-ROW TRANSITION-METAL COMPLEXES RELEVANT TO CO2 REDUCTION AND WATER OXIDATION
Takashi Ono
DL:T 1108-2014

7.2. Product distribution under 1 atm of $^{13}CO_2$

$[PPN]_2[MoO_4]$ (30.4 mg, 0.025 mmol) was dissolved in *ca*. 0.6 mL of CD_3CN and transferred to a J-Young NMR tube. The tube was brought outside the glovebox, and the solution was submitted to 3 freeze-pump-thaw cycles. After the sample warmed up to room temperature, $^{13}CO_2$ was introduced via syringe, allowing the solution to equilibrate to 1 atm for 1 min while gently shaking the tube, after which the J-Young valve was sealed. The ^{13}C NMR spectrum of this sample under 1 atm of $^{13}CO_2$ is shown below, at room temperature and at -19 °C. The sample was then submitted to 3 freeze-pump-thaw cycles in order to remove the excess $^{13}CO_2$. A ^{13}C NMR spectrum of the resulting solution is also shown in the overlay below.

^{13}C NMR spectrum of $[PPN]_2[MoO_4]$ under 1 atm of $^{13}CO_2$ and after removing the $^{13}CO_2$

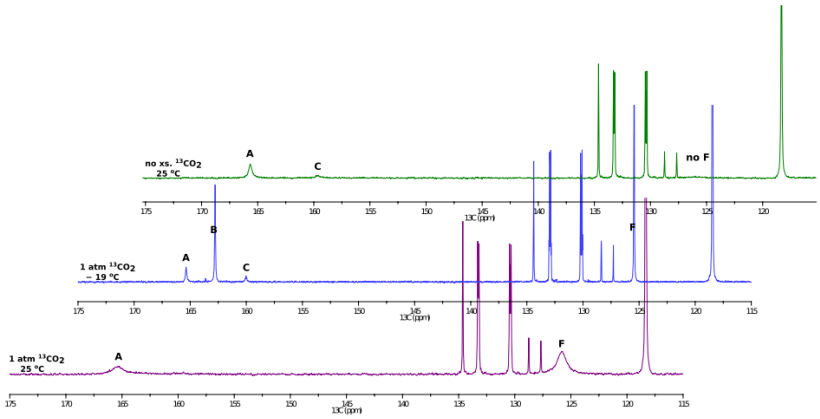

A: $[PPN]_2[MoO_3(\kappa^2\text{-}^{13}CO_3)]$
B: $[PPN]_2[MoO_2(\kappa^2\text{-}^{13}CO_3)_2]$
C: $[PPN][HCO_3]$
F: free $^{13}CO_2$

7.3. Product distribution under 3 atm of $^{13}CO_2$

Inside the glovebox, $[PPN]_2[MoO_4]$ (35 mg, 0.028 mmol) was dissolved in *ca*. 0.6 mL of CD_3CN and transferred to an NMR tube glass blown onto a 14/20 female adapter. A vacuum adapter was added, and the sealed system was brought outside the

glovebox. The solution was degassed using 5 freeze-pump-thaw cycles. The system was refilled with 1 atm of $^{13}CO_2$ via syringe, then closed. The NMR tube was placed in liquid nitrogen and flame sealed. The pressure (3 atm) was calculated based on the relative integration of the free $^{13}CO_2$ (δ = 125.8 ppm) and the solvent (δ = 118.3 ppm) resonances at room temperature, which was 3 times the value of the corresponding ratio from the sample prepared under 1 atm in section 7.2.

^{13}C NMR spectrum of $[PPN]_2[MoO_4]$ under 1 and 3 atm of $^{13}CO_2$ at low temperature

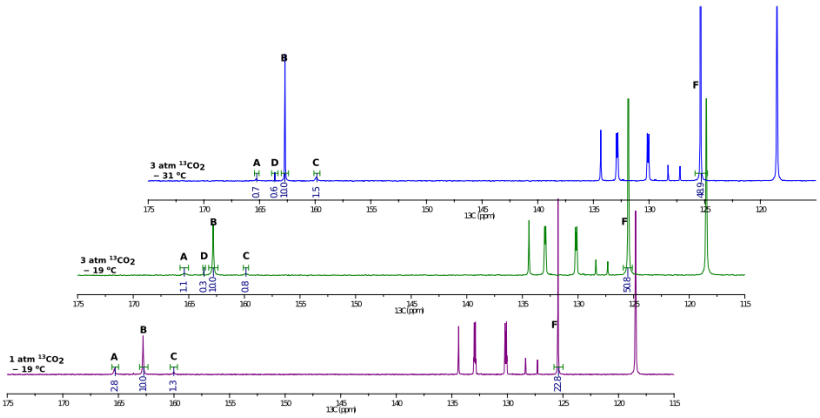

A: $[PPN]_2[MoO_3(\kappa2\text{-}^{13}CO_3)]$
B: $[PPN]_2[MoO_2(\kappa2\text{-}^{13}CO_3)_2]$
C: $[PPN][HCO_3]$
D: species likely due to binding of $^{13}CO_2$ to $[PPN]_2[Mo_2O_7]$ at low temperature under excess $^{13}CO_2$, as evidenced by the spectrum below.
F: free $^{13}CO_2$

^{13}C NMR spectrum of $[PPN]_2[Mo_2O_7]$ under 1 atm of $^{13}CO_2$ at low temperature

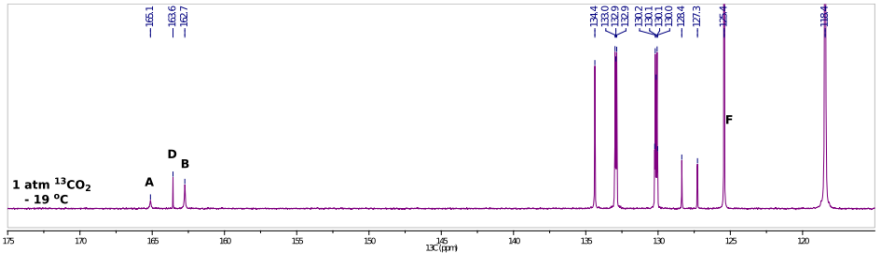

UNIVERSITAT ROVIRA I VIRGILI
SECOND-ROW TRANSITION-METAL COMPLEXES RELEVANT TO CO2 REDUCTION AND WATER OXIDATION
Takashi Ono
DL:T 1108-2014

8. Computational Data

8.1. Computational Details

Electronic structure calculations were carried out using the M06[7] density functional with the Def2-QZVPP[8] basis set for molybdenum, incorporating the SDD[9] effective core potential, and 6-311+G(3df) for all other atoms as implemented in the Gaussian 09 suite of programs.[10] Minimum energy and transition state structures were optimized in CH_3CN solution using the CPCM model[11-12] to describe solvation effects. The obtained stationary points were characterized by performing energy second derivatives, confirming them as minima or transition states by the number of negative eigenvalues of the hessian matrix of the energy (zero and one negative eigenvalues respectively). Finally, single-point energies were calculated with the quadratic configuration interaction method with single and double excitation and perturbative corrections for triple excitations (QCISD(T))[13-14] at the optimized M06 geometries.

8.2. XYZ coordinates for all computed species

CO_2

C	0.00000000	0.00000000	0.00000000
O	0.00000000	0.00000000	1.15384300
O	0.00000000	0.00000000	−1.15384300

$[MoO_4]^{2-}$

Mo	0.00000000	0.00000000	0.00000000
O	1.01811200	1.01811200	1.01811200
O	−1.01811200	−1.01811200	1.01811200
O	1.01811200	−1.01811200	−1.01811200
O	−1.01811200	1.01811200	−1.01811200

TS1 ($[MoO_4]^{2-} + CO_2 \rightarrow [MoO_3(\kappa^2\text{-}CO_3)]^{2-}$)

C	−2.55986400	0.02439000	−0.00006200
O	−3.27956000	−0.90856700	−0.00011200
O	−2.36024300	1.18712000	0.00020900
O	−0.82667800	−0.77271000	−0.00097700

Mo	0.82267800	−0.02825700	−0.00003900
O	1.02641700	0.96430300	1.42417400
O	1.02747200	0.96632500	−1.42274500
O	2.01343000	−1.30641300	−0.00029700

$[MoO_3(\kappa^2\text{-}CO_3)]^{2-}$

C	−1.97701500	0.02314300	−0.00006400
O	−3.19936200	0.12536000	0.00003500
O	−1.30161800	−1.08065000	−0.00025200
O	−1.16215000	1.07167300	0.00028700
Mo	0.63401800	0.00248800	0.00007500
O	1.17608100	−0.83419200	−1.40906100
O	1.17647200	−0.83319500	1.40963700
O	1.46474200	1.52058500	−0.00099300

TS2 ($[MoO_3(\kappa^2\text{-}CO_3)]^{2-} + CO_2 \rightarrow [MoO_2(\kappa^2\text{-}CO_3)_2]^{2-}$)

Mo	0.34057700	−0.71319200	−0.03143300
O	0.96201000	−1.96647100	−1.02020200
O	0.32804900	−1.26071100	1.58205900
O	−2.96600900	1.17472800	−1.00799000
O	−1.36528300	−0.55856200	−0.54763200
O	0.32573100	1.41320100	0.07781900
O	2.16592700	0.31843400	−0.11687200
C	1.63073000	1.51676600	0.01087700
C	−2.62730000	0.61598200	−0.01939800
O	−2.75229700	0.46421700	1.14998900
O	2.26127300	2.55985900	0.05423900

$[MoO_2(\kappa^2\text{-}CO_3)_2]^{2-}$

Mo	0.00001700	0.65798100	−0.00000800
O	0.37506200	1.68532700	−1.29156000
O	−0.37501000	1.68535000	1.29153300
O	1.06193300	−1.04391100	−0.94557000
O	1.71440300	0.02671700	0.81582700
O	−1.06208800	−1.04375800	0.94571600
O	−1.71432300	0.02667400	−0.81589600
C	−1.98476900	−0.97227800	0.05195100

UNIVERSITAT ROVIRA I VIRGILI
SECOND-ROW TRANSITION-METAL COMPLEXES RELEVANT TO CO2 REDUCTION AND WATER OXIDATION
Takashi Ono
DL:T 1108-2014

C	1.98473200	−0.97234400	−0.05192800
O	2.98016000	−1.66620200	0.05612300
O	−2.98019900	−1.66613200	−0.05614600

$[MoO(\kappa^2\text{-}CO_3)_3]^{2-}$

Mo	−0.00040700	−0.22639800	0.34214600
O	2.03921400	0.19925800	0.38382500
O	1.21991600	−1.45227800	−0.68501600
O	−1.22228500	−1.45202500	−0.68367100
O	−2.03909900	0.20299500	0.38151000
O	0.00281900	1.25959700	−1.19639200
O	0.00044300	1.70732000	0.91547700
C	0.00196300	2.22179800	−0.31808200
C	−2.35218200	−0.81773800	−0.37158100
C	2.35082900	−0.82059800	−0.37094700
O	−0.00062400	−0.82858500	1.89209800
O	3.45179500	−1.15264700	−0.73500000
O	0.00315300	3.41629600	−0.53880100
O	−3.45365100	−1.14893700	−0.73483900

9. Crystallographic details for $[PPN]_2[MoO_3(\kappa^2\text{-}CO_3)]$

Colourless, diffraction quality crystals of $[PPN]_2[MoO_3(\kappa^2\text{-}CO_3)]$ were obtained by vapour diffusion of Et_2O into a concentrated solution of CH_2Cl_2. The salt crystallized in the monoclinic space group $P2_1/c$ with one $[MoO_3(\kappa^2\text{-}CO_3)]^{2-}$ dianion, two PPN cations, and 3.5 CH_2Cl_2 solvent molecules per asymmetric unit. The largest residual electron density in the vicinity of the $[MoO_3(\kappa^2\text{-}CO_3)]^{2-}$ dianion could not be assigned and refined satisfactorily to another carbonate position. However, some of this residual electron density could be modelled as a $[MoO_4]^{2-}$ dianion disorder. The occupancy of the independent O atom of the $[MoO_4]^{2-}$ was refined freely, yielding a distribution of 10% oxygen (completing a $[MoO_4]^{2-}$ dianion) to 90% carbonate (completing a $[MoO_3(\kappa^2\text{-}CO_3)]^{2-}$ dianion). Three of the CH_2Cl_2 solvent molecules were refined over two positions. The last half molecule of solvent was located near the inversion centre and could only be refined satisfactorily if the second position was modelled as an Et_2O

molecule instead of CH_2Cl_2. Similarity restraints on 1–2 and 1–3 distances and displacement parameters as well as rigid bond restraints for anisotropic displacement parameters were applied to all the disordered parts, with more stringent restraints applied to the ether molecule. The ratios between the two components of the solvent disorders were refined freely, and the sum of the two occupancies for each pair was constrained to unity yielding ratios of 61:39, 57:43, 97:3, and, for the one close to the inversion centre, 54:46.

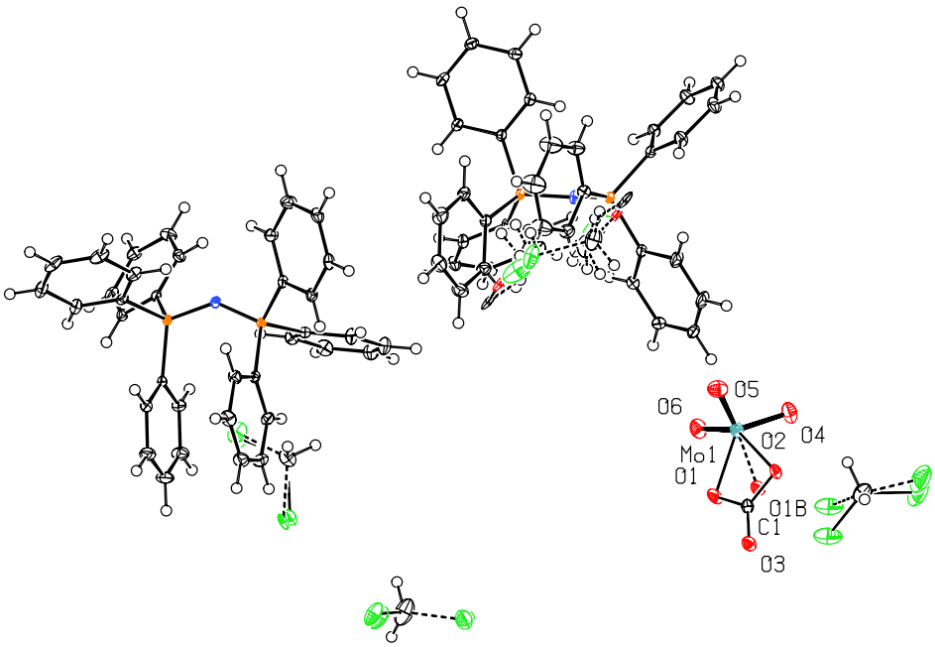

Asymmetric unit of $[PPN]_2[MoO_3(\kappa^2\text{-}CO_3)]$. Select distances [Å]: Mo1-O5 1.728(3), Mo1-O6 1.733(2), Mo1-O4 1.741(3), Mo1-O1B 1.804(15), Mo1-O1 2.062(3), Mo1-O2 2.195(2), Mo1-C1 2.590(3), O1-C1 1.332(4), O2-C1 1.304(4), C1-O3 1.226(4).

UNIVERSITAT ROVIRA I VIRGILI
SECOND-ROW TRANSITION-METAL COMPLEXES RELEVANT TO CO2 REDUCTION AND WATER OXIDATION
Takashi Ono
DL:T 1108-2016

Table 1 Crystallographic data for $[PPN]_2[MoO_3(\kappa^2\text{-}CO_3)]$

	$[PPN]_2[MoO_3(\kappa^2\text{-}CO_3)]$
Reciprocal Net code / CCDC no.	12071 / 981116
Empirical formula, FW (g/mol)	$C_{76.5}H_{67}MoP_2Cl_7N_2O_6$, 1544.47
Crystal size (mm^3)	$0.53 \times 0.16 \times 0.06$
Wavelength (Å)	1.54178
Crystal system, Space group	Monoclinic, $P2_1/c$
Unit cell dimensions (Å, °)	$a = 21.931(8)$, $\alpha = 90$
	$b = 12.235(5)$, $\beta = 92.141(6)$
	$c = 26.654(10)$, $\gamma = 90$
Volume ($Å^3$)	7147(5)
Z	4
Density (calc., g/cm^3)	1.500
Absorption coefficient (mm^{-1})	0.557
$F(000)$	3336
Theta range for data collection (°)	0.93 to 29.13
Index ranges	$-30 \leq h \leq 30$, $-16 \leq k \leq 16$, $-36 \leq l \leq 36$
Reflections collected	180065
Independent reflections, R_{int}	19233 (0.0433)
Completeness to θ_{max} (%)	100.0
Max. and min. transmission	0.9674 and 0.7569
Data / restraints / parameters	19233 / 165 / 966
Goodness-of-fit[a]	1.048
Final R indices[b] $[I > 2\sigma(I)]$	$R_1 = 0.0596$, $wR_2 = 0.1653$
R indices[b] (all data)	$R_1 = 0.0716$, $wR_2 = 0.1785$
Largest diff. peak and hole ($e \cdot Å^{-3}$)	4.118 and −1.686

[a] GooF $= \left[\frac{\Sigma[w(F_o^2 - F_c^2)^2]}{(n-p)}\right]^{\frac{1}{2}}$ [b] $R_1 = \frac{\Sigma||F_o|-|F_c||}{\Sigma|F_o|}$; $wR_2 = \left[\frac{\Sigma[w(F_o^2-F_c^2)^2}{\Sigma[w(F_o^2)^2]}\right]^{\frac{1}{2}}$; $w = \frac{1}{\sigma^2(F_o^2)+(aP)^2+bP}$; $P = \frac{2F_c^2+\max(F_o^2,0)}{3}$

Table 2 Crystallographic details for $[NEt_4]_2[MoO_3(\kappa^2\text{-}CO_3)]$ and $[PPN]_2[MoO_2(\kappa^2\text{-}CO_3)_2]$

	$[NEt_4]_2[MoO_3(\kappa^2\text{-}CO_3)]$	$[PPN]_2[MoO_2(\kappa^2\text{-}CO_3)_2]$
Reciprocal Net code / CCDC no.	X8_13178 / 978136	X8_13097 / 978137
Empirical formula, FW (g/mol)	$C_{17}H_{40}MoN_2O_6$, 464.45	$C_{74}H_{60}MoN_2O_8P_4{\cdot}4\,CH_3CN$, 1489.344
Color / Morphology	Colorless / Needle	Colorless / Block
Crystal size (mm^3)	$0.42 \times 0.10 \times 0.07$	$0.45 \times 0.35 \times 0.20$
Temperature (K)	100(2)	100(2)
Wavelength (Å)	0.71073	0.71073
Crystal system, Space group	Monoclinic, $P2_1/n$	Monoclinic, $P2_1$
Unit cell dimensions (Å, °)	$a = 14.997(3)$, $\alpha = 90$	$a = 10.7577(11)$, $\alpha = 90$
	$b = 8.3386(15)$, $\beta = 99.979(3)$	$b = 13.0244(13)$, $\beta = 90.884(2)$
	$c = 17.151(3)$, $\gamma = 90$	$c = 25.943(3)$, $\gamma = 90$
Volume (Å^3)	2112.4(7)	3634.5(6)
Z	4	2
Density (calc., g/cm^3)	1.460	1.361
Absorption coefficient (mm^{-1})	0.654	0.330
$F(000)$	984	1544
Theta range for data collection (°)	1.667 to 30.508	1.570 to 30.51
Index ranges	$-21 \le h \le 21$, $-11 \le k \le 11$, $-24 \le l \le 24$	$-15 \le h \le 15$, $-19 \le k \le 19$, $-38 \le l \le 38$
Reflections collected	65759	203085
Independent reflections, R_{int}	6441 (0.0290)	24166 (0.0406)
Completeness to θ_{max} (%)	100.0	99.9
Max. and min. transmission	0.7462 and 0.6504	0.937 and 0.866
Data / restraints / parameters	6441 / 0 / 243	24166 / 1 / 913
Goodness-of-fit[a]	1.074	1.087
Final R indices[b] $[I > 2\sigma(I)]$	$R_1 = 0.0181$, $wR_2 = 0.0470$	$R_1 = 0.0355$, $wR_2 = 0.0910$
R indices[b] (all data)	$R_1 = 0.0198$, $wR_2 = 0.0479$	$R_1 = 0.0373$, $wR_2 = 0.0918$
Largest diff. peak and hole ($e \cdot$ Å^{-3})	0.429 and −0.440	1.737 and −0.501

[a] GooF = $\left[\frac{\Sigma[w(F_o^2-F_c^2)^2]}{(n-p)}\right]^{\frac{1}{2}}$ [b] $R_1 = \frac{\Sigma||F_o|-|F_c||}{\Sigma|F_o|}$; $wR_2 = \left[\frac{\Sigma[w(F_o^2-F_c^2)^2]}{\Sigma[w(F_o^2)^2]}\right]^{\frac{1}{2}}$; $w = \frac{1}{\sigma^2(F_o^2)+(aP)^2+bP}$; $P = \frac{2F_c^2+\max(F_o^2,0)}{3}$

UNIVERSITAT ROVIRA I VIRGILI
SECOND-ROW TRANSITION-METAL COMPLEXES RELEVANT TO CO2 REDUCTION AND WATER OXIDATION
Takashi Ono
DL:T 1108-2014

References

(1) Rösner, C.; Lagaly, G. *J. Solid State Chem.* **1984**, *53*, 92-100.
(2) Meckfessel Jones, M. L., Texas A&M University, 1994.
(3) Che, T. M.; Day, V. W.; Francesconi, L. C.; Fredrich, M. F.; Klemperer, W. G.; Shum, W. *Inorg. Chem.* **1985**, *24*, 4055-4062.
(4) Briggs, J. R.; Harrison, A. M.; Robson, J. H. *Polyhedron* **1986**, *5*, 281-287.
(5) Do, Y.; Simhon, E. D.; Holm, R. H. *Inorg. Chem.* **1985**, *24*, 1831-1838.
(6) Derringer, D. R.; Buck, E. A.; Esjornson, S. M. V.; Fanwick, P. E.; Walton, R. A. *Polyhedron* **1990**, *9*, 743-750.
(7) Zhao, Y.; Truhlar, D. *Theor. Chem. Acc.* **2008**, *120*, 215-241.
(8) Weigend, F.; Ahlrichs, R. *Phys. Chem. Chem. Phys.* **2005**, *7*, 3297-3305.
(9) Andrae, D.; Häußermann, U.; Dolg, M.; Stoll, H.; Preuß, H. *Theoret. Chim. Acta* **1990**, *77*, 123-141.
(10) Gaussian 09, Revision C.1, Frisch, M. J.; Trucks, G. W.; Schlegel, H. B.; Scuseria, G. E.; Robb, M. A.; Cheeseman, J. R.; Scalmani, G.; Barone, V.; Mennucci, B.; Petersson, G. A.; Nakatsuji, H.; Caricato, M.; Li, X.; Hratchian, H. P.; Izmaylov, A. F.; Bloino, J.; Zheng, G.; Sonnenberg, J. L.; Hada, M.; Ehara, M.; Toyota, K.; Fukuda, R.; Hasegawa, J.; Ishida, M.; Nakajima, T.; Honda, Y.; Kitao, O.; Nakai, H.; Vreven, T.; Montgomery, J., J. A.; Peralta, J. E.; Ogliaro, F.; Bearpark, M.; Heyd, J. J.; Brothers, E.; Kudin, K. N.; Staroverov, V. N.; Keith, T.; Kobayashi, R.; Normand, J.; Raghavachari, K.; Rendell, A.; Burant, J. C.; Iyengar, S. S.; Tomasi, J.; Cossi, M.; Rega, N.; Millam, J. M.; Klene, M.; Knox, J. E.; Cross, J. B.; Bakken, V.; Adamo, C.; Jaramillo, J.; Gomperts, R.; Stratmann, R. E.; Yazyev, O.; Austin, A. J.; Cammi, R.; Pomelli, C.; Ochterski, J. W.; Martin, R. L.; Morokuma, K.; Zakrzewski, V. G.; Voth, G. A.; Salvador, P.; Dannenberg, J. J.; Dapprich, S.; Daniels, A. D.; Farkas, Ö.; Foresman, J. B.; Ortiz, J. V.; Cioslowski, J.; Fox, D. J., Gaussian, Inc., Wallingford CT, 2010.
(11) Barone, V.; Cossi, M. *The Journal of Physical Chemistry A* **1998**, *102*, 1995-2001.
(12) Klamt, A.; Schuurmann, G. *Journal of the Chemical Society, Perkin Transactions 2* **1993**, 799-805.
(13) Pople, J. A.; Head-Gordon, M.; Raghavachari, K. *J. Chem. Phys.* **1987**, *87*, 5968-5975.
(14) Knowles, P. J.; Werner, H.-J. *Chem. Phys. Lett.* **1985**, *115*, 259-267.

UNIVERSITAT ROVIRA I VIRGILI
SECOND-ROW TRANSITION-METAL COMPLEXES RELEVANT TO CO2 REDUCTION AND WATER OXIDATION
Takashi Ono
DL:T 1108-2014

Chapter VI

New Mononuclear Ruthenium Polypyridyl Complexes Containing Anionic Dpb Ligand: Synthesis, Characterization and Oxidation Reactions

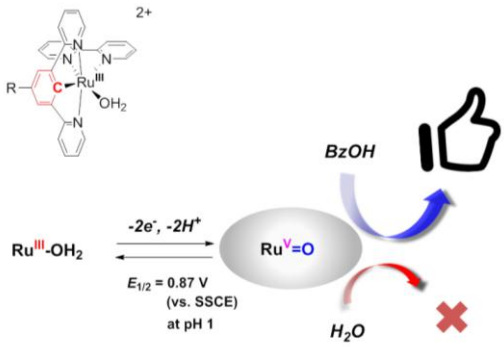

VI

Table of Contents

UNIVERSITAT ROVIRA I VIRGILI
SECOND-ROW TRANSITION-METAL COMPLEXES RELEVANT TO CO2 REDUCTION AND WATER OXIDATION
Takashi Ono
DL:T 1108-2014

VI.1. Abstract

New mononuclear ruthenium complexes containing an anionic tridentate *dpb*$^-$ (2,6-di(pyridin-2-yl)benzen-1-ide) ligand with the general formula [Ru(R-dpb)(bpy)(X)]$^{n+}$ (*bpy* = 2,2'-bipyridine; R = H, X = Cl (**3a**), OH_2 (**4a**$^{2+}$), Py (pyridine) (**5a**$^+$) and CH_3CN (**6a**$^+$); R = F, X = Cl (**3b**) and OH_2 (**4b**$^{2+}$)) are reported. These complexes and their synthetic intermediates *trans*-[Ru(R-dpb)(dmso-*s*)$_2$Cl] (R = H (**1a**) and R = F (**1b**)) have been characterized by the usual analytic techniques and by spectroscopic and electrochemical methods. Complexes **1a**, **1b**, **4b**$^{2+}$, and **5a**$^+$ were additionally characterized by X-ray crystallography. The Ru-aqua complexes **4a**$^{2+}$, **4b**$^{2+}$, which have the dominant oxidation state of Ru(III), showed single 2e$^-$ oxidation wave ($E_{1/2}$ = 0.87 V vs. SSCE for **4a**$^{2+}$ and 0.89 V for **4b**$^{2+}$) corresponding to the formation of Ru(V)=O species at pH 1 in aqueous triflic acid solution. Their $E_{1/2}$ values are drastically reduced with respect to the *trpy* analogue, Ru(trpy)(bpy)$(OH_2)^{2+}$ ($E_{1/2}$ = 1.56 V for Ru(V/IV) couple) due to strong σ-donation of anionic *dpb*$^-$ ligand. **4a**$^{2+}$ and **4b**$^{2+}$ were tested as catalysts for chemical water oxidation using $(NH_4)_2Ce^{IV}(NO_3)_6$ as an oxidant, resulting in the formation of mainly carbon dioxide. The reactivity of the electrogenerated Ru(V)=O species toward benzyl alcohol was studied, showing a second-order rate constant $k_{cat} = 2.7 \pm 0.1 \times 10^3$ $M^{-1} \cdot s^{-1}$.

VI.2. Introduction

High-valent mteal-oxo complexes have been widely investigated because of their applicability in a number of oxidation reactions.[1-3] One of the methods to achieve the formation of metal-oxo species is proton-coupled electron transfer (PCET),[4-5] the key process in Photosystem II where water oxidation takes place to generate molecular oxygen. It has been proposed that manganese-aquo site in the Mn_4CaO_5 cluster in the OEC is oxidized through a successive PCET processes to generate a Mn(V)=O species, which catalyzes 4e$^-$ oxidation of water. [6-9]

Since the discovery of the first mononuclear water oxidation catalyst (WOC) in 2005,[10] a number of mononuclear Ru-WOCs has been developed.[11-24] Most of the

UNIVERSITAT ROVIRA I VIRGILI
SECOND-ROW TRANSITION-METAL COMPLEXES RELEVANT TO CO2 REDUCTION AND WATER OXIDATION
Takashi Ono
DL:T 1108-2014

reported Ru-based WOCs consist of neutral N-donor ligand,[11-18] which generally suffers from their high oxidation potential for the formation of the Ru(V)=O species. This prevents utilizing commonly used photosensitizer, $[Ru(bpy)_3]^{3+}$ type of complexes, being indispensable for the development of photochemical water oxidation system. Related with this, some promising results have recently appeared in which the catalyst contains negatively charged ligand (such as carboxylate, phenolate groups), showing significant effect on lowering the oxidation potentials of high-valent Ru species as well as overpotential toward the water oxidation reaction. [19-24]

These results motivate us to explore the complexes containing negatively charged ligand. From the structural similarity to *trpy*, we decided to use anionic *dpb*$^-$ ligand (2,6-di(pyridin-2-yl)benzen-1-ide, Figure 1) that would stabilize higher oxidation states due to strong σ donation through metal-carbon bond. Herein, we report the synthesis and characterization of new mononuclear ruthenium complex containing anionic *dpb*$^-$ ligand as well as reactivity toward oxidation reactions.

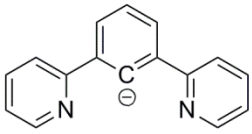

dpb$^-$

Figure 1. Anionic tridentate *dpb*$^-$ (2,6-di(pyridin-2-yl)benzen-1-ide) ligand.

VI.3. Results and Discussion

VI.3.1. Synthesis, Structure and Redox Properties

Synthesis

The 1,3-di(pyridin-2-yl)benzene (*Hdpb*) ligand was prepared as described in the literature.[25] Fluoro substituted Hdpb (F-*Hdpb*) was also prepared with a yield of 34% following the similar procedure as for the synthesis of *Hdpb* ligand and was confirmed by ^{1}H NMR spectroscopy by comparing with the reported chemical shifts.[26] The

Scheme 1. Reaction scheme for the mononuclear *dpb*$^-$ complexes

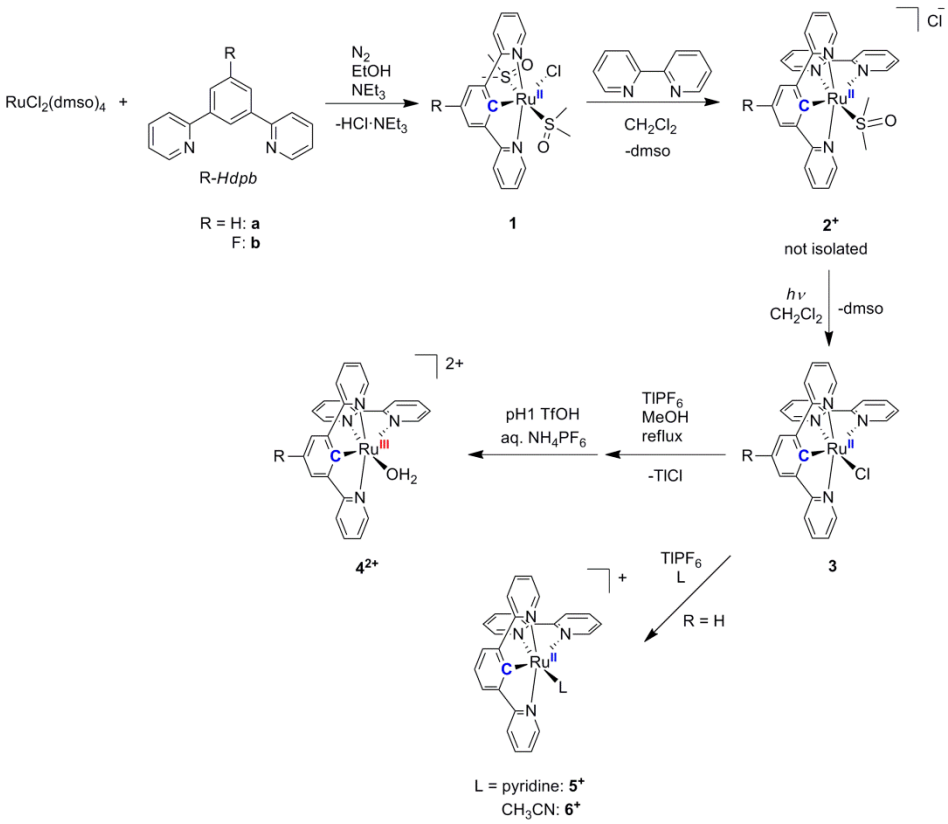

synthetic scheme for mononuclear *dpb*$^-$ complexes is shown in Scheme 1. Mononuclear Ru-*dpb*$^-$ precursors *trans*-Ru(R-dpb)(dmso-*s*)$_2$Cl (**1a**: R = H, **1b**: R = F) were synthesized by the reaction of Ru(dmso)$_4$Cl$_2$ with R-*Hdpb* in the presence of NEt_3 as a base under reflux condition in degassed EtOH. ^{1}H NMR spectrum of **1** in CD_2Cl_2 showed two sets of signals for *dpb*$^-$ ligand, which have a ratio of main (**1**)/minor (**1'**) = 90/10 for R = H, 84/16 for R = F, respectively (Figure 2b and Figure S2). Main species **1** has two chemically equivalent DMSO ligands at 2.39 ppm for both R = H and R =F, while minor one **1'** has only one molecule of coordinated DMSO ligand (at 2.10 ppm for **1a'** and 1.99 ppm for **1b'**, respectively) with respect to one *dpb*$^-$ ligand and in addition to this, was found free DMSO with the same intensity as the coordinated dmso ligand of **1'**.

UNIVERSITAT ROVIRA I VIRGILI
SECOND-ROW TRANSITION-METAL COMPLEXES RELEVANT TO CO2 REDUCTION AND WATER OXIDATION
Takashi Ono
DL:T 1108-2014

Interestingly, in the presence of added DMSO (Figure 2a and Figure S2), the signals corresponding to **1'** disappeared and only **1** was found.

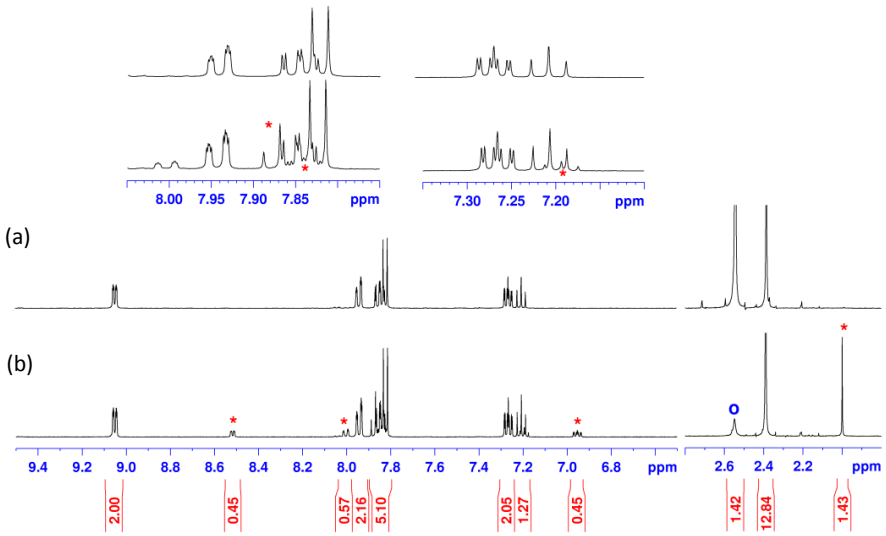

Figure 2. ^{1}H NMR of complex **1a** in CD_2Cl_2. (a) with, (b) without added DMSO. *: minor species **1a'**, o: free DMSO.

Cyclic voltammogram of **1** in CH_2Cl_2 (Figure 3 and Figure S15) shows one main reversible wave ($E_{1/2}$ = 0.47 V vs. SSCE for **1a** and 0.49 V for **1b**) corresponding to the main species and two consecutive oxidation waves at $E_{1/2}$ = 0.25 and 0.64 V for **1a'**, $E_{1/2}$ = 0.30 and 0.68 V for **1b'**. The small difference ($\Delta E_{1/2}$ = 0.39 V for **1a'**, 0.38 for **1b'**) between two redox potentials in organic solvent indicates the formation of dinuclear species which undergoes two consecutive oxidations at each metal centre (eqn. 1) rather than the mononuclear scenario, leading to Ru^{IV} from Ru^{II} through two $1e^-$ oxidations (eqn. 2), that is unlikely to take place. These spectroscopic and

$$Ru^{III}Ru^{III} \xrightarrow{1e^-} Ru^{III}Ru^{II} \xrightarrow{1e^-} Ru^{II}Ru^{II} \quad (1)$$

$$Ru^{IV} \xrightarrow{1e^-} Ru^{III} \xrightarrow{1e^-} Ru^{II} \quad (2)$$

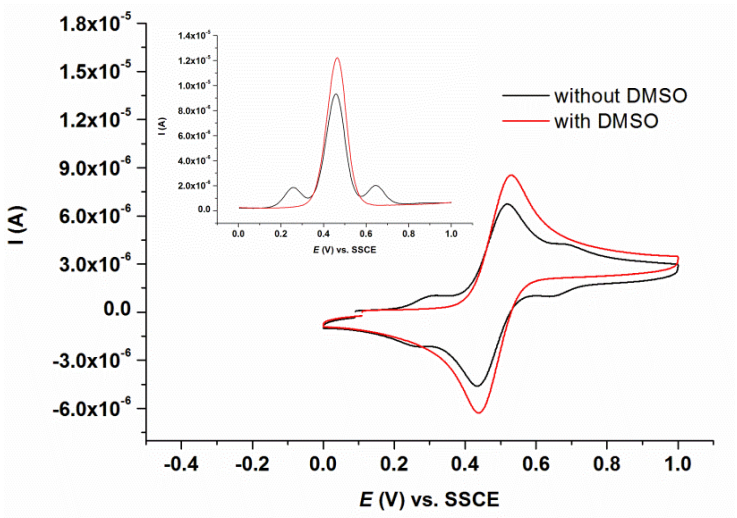

Figure 3. Cyclic voltammograms of **1a** in 0.1 M CH_2Cl_2-$TBAPF_6$ without DMSO (—) and with added DMSO (—). Inset shows differential pulse voltammograms. Glassy carbon working electrode, Pt disk counter electrode and SSCE reference electrode. Scan rate 100 mV s^{-1}.

electrochemical observations suggest that in solution, mononuclear **1** and dinuclear **1'** exist in equilibrium as shown in Scheme 2 together with a plausible dinuclear structure.

Scheme 2. An equilibrium between mononuclear **1** and dinuclear **1'**

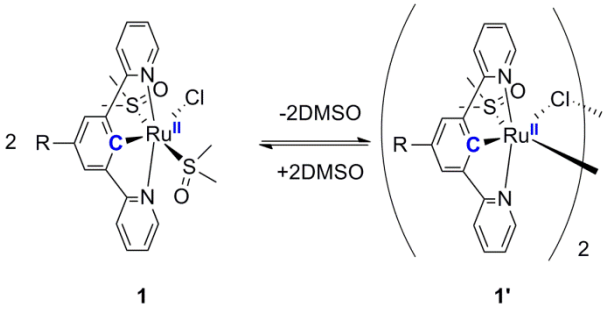

Complexes Ru(R-dpb)(bpy)Cl, **3a-b**, were synthesized in 2 steps: 1) the reaction of complex **1** with *bpy* (2,2'-bipyridine) ligand and 2) subsequent light irradiation, as shown in Scheme 1. In the first step, the substitution of one DMSO and one chlorido ligands by bidentate *bpy* undergoes within 30 minutes at room temperature. The

formed [Ru(R-dpb)(bpy)(dmso)](Cl), **2a-b**$^{+}$ were tentatively assigned by ^{1}H NMR spectroscopy, showing one coordinated DMSO at 2.07 ppm for both **2a**$^{+}$ and **2b**$^{+}$ (Figure S9). In the second step, as was found for Ru(II) polypyridyl complexes,[27-28] photoinduced ligand exchange of DMSO to chlorido, in this case, derived from counter chloride anion produces Ru-Cl complexes **3a-b**.

Finally, Ru-aqua complexes, Ru^{III}(dpb)(bpy)$(OH_2)^{2+}$, **4a-b**$^{2+}$ were obtained by replacing the remaining chlorido ligand with H_2O in the presence of $TlPF_6$, followed by aerial oxidation. Their reduced Ru(II)-OH_2 species were characterized by 1D and 2D NMR spectroscopy in the presence of ascorbic acid as a reductant in a mixture of D_2O and acetone-d_6 (Figures S5-6). The ESI-MS spectra of **4a**$^{2+}$ and **4b**$^{2+}$ in H_2O show peak at m/z = 506.0 and 524.1, respectively, which can be assigned to the cation [Ru^{III}(R-dpb)(bpy)(OH)]$^{+}$ (Figures S11-12). This is because **4a**$^{2+}$ and **4b**$^{2+}$ lose one proton from the coordinated OH_2 group. This is consistent with their pK_a values of the Ru(III) state (p$Ka_{,III}$ = 4.9 for **4a**$^{2+}$:, 4.8 for **4b**$^{2+}$:, respectively), which were determined by spectrophotometric acid-base titration (Figures S13-14). In addition, complexes **5a**$^{+}$ and **6a**$^{+}$ were synthesized in the similar manner as the synthesis of **4a**$^{2+}$ but in the presence of pyridine and acetonitrile, respectively.

Structure

Complexes **1a**, **1b**, **4b**$^{2+}$, and **5a**$^{+}$ were successfully characterized by X-ray diffraction analysis. Their Ortep plots are presented in Figure 4. Selected bond lengths, angles and crystallographic parameters are listed in Table 1, and Tables S1-2 in Supporting Information.

The structure of **1a** shows the Ru atom in a roughly octahedral environment with the *dpb*$^{-}$ ligand coordinated in a meridional fashion. The chlorine atom is located in *trans* position to Ru1-C1 bond, whereas two coordinated DMSO ligands are located in *trans* position one another, bonded through sulfur atoms. Bond distances and angles of Ru-*dpb*$^{-}$ moiety (Ru1-C1: 1.9410(17) Å, Ru1-N1: 2.0977(19), Ru1-N2: 2.103(2) Å, N1-Ru1-N2: 158.46(6)°)) are typical for those of Ru(II)-*dpb*$^{-}$ complexes.[29-32] One of the interesting features was found for the Ru1-Cl1 bond distance to be 2.5558(4) Å, which

is about 0.1 Å longer than of typical Ru^{II}-Cl bond, due to *trans* influence of σ-donating *dpb*$^-$ ligand. Slightly longer Ru-sulfur lengths (Ru1-S1: 2.2996(6) Å, Ru1-S2: 2.3045(6) Å) than that of reported Ru(II)-DMSO complexes[33-35], and shorter S-O bond lengths (O1-S1: 1.4838(19) Å, O2-S2: 1.4844(16) Å) than that of free DMSO (1.492(1) Å)[36] were found, indicating that Ru-S bonds in **1a** is relatively weakened compared to those for typical Ru(II)-DMSO complexes. This phenomenon is typical for *trans*-bis DMSO complexes.[36] These two structural features results in a facile substitution by *bpy* in mild reaction condition. The structure of **1b** is very similar to that of **1a**. The differences found between **1a** and **1b** are the S1-Ru1-Cl1 and S2-Ru1-Cl1 angles (S1-Ru1- Cl1: 91.00(2)° for **1a**, 86.52(2)° for **1b**; S2-Ru1-Cl1: 91.57(2)° for **1a**, 93.78 (2)° for **1b**). These differences can be explained by considering the conformation of methyl groups of DMSO in the crystal structure; in **1a**, each one of the two methyl groups in both DMSO ligand are located roughly in the same plane with Cl atom, whereas in **1b**, two methyl groups of one DMSO ligand are located up and down of the Cl1-Ru1-S1 plane and as a result of less steric repulsion between Cl atom and the Me groups, Ru1-Cl1 bond is slightly bent toward the S1 atom.

The cation of $\mathbf{4b}^{2+}$ was crystallized as the oxidation state of Ru(III) along with two counter anions. One of the anions is a triflate anion (OTf^-), making a hydrogen bonding with one (H1w) of the hydrogen atoms of OH_2 ligand (1.83 Å) and the second anion is a disordered mixture of PF_6^- and OTf^- (a ratio of 60:40). The *bpy* ligand is disordered in two positions with a ratio of 75:25. Longer bond length of Ru1-N2 (2.123(4) Å) compared to that of Ru1-N1 (2.089(4) Å) is presumably caused by the distorted geometry of the *bpy* ligand as a consequence of reducing the steric repulsion with one of the counter anions (a mean plane of *bpy* is inclined at 9.6° from C-Ru1-O1 plane). On the other hand, longer bond length found for Ru1-N3 (2.173(9) Å) compared to that of Ru1-N4 (2.080(8) Å) is largely due to *trans* influence of *dpb*$^-$ ligand. The Ru1-O1 bond distance is 2.063(4) Å which is shortened compared to that of typical Ru(II)-OH_2 [18]

The structure of [**5a**](PF_6) contains one disordered diethyl ether molecule (ratio 50:50). The *dpb*$^-$ and *bpy* ligands are partially disordered in two orientations (ratios: 54:46 and 65:35). The bond lengths and angles for $\mathbf{5a}^+$ are unremarkable except for the

UNIVERSITAT ROVIRA I VIRGILI
SECOND-ROW TRANSITION-METAL COMPLEXES RELEVANT TO CO2 REDUCTION AND WATER OXIDATION
Takashi Ono
DL:T 1108-2014

distorted geometry (Ru1-N1: 1.952(11) Å, Ru1-N2: 2.178(10) Å) presumably caused by steric interaction between the hydrogen atom on the carbon next to the N2 atom and one pyridyl ring of the *bpy* ligand that is slightly inclined due to the steric interaction with monodentate pyridine ligand.

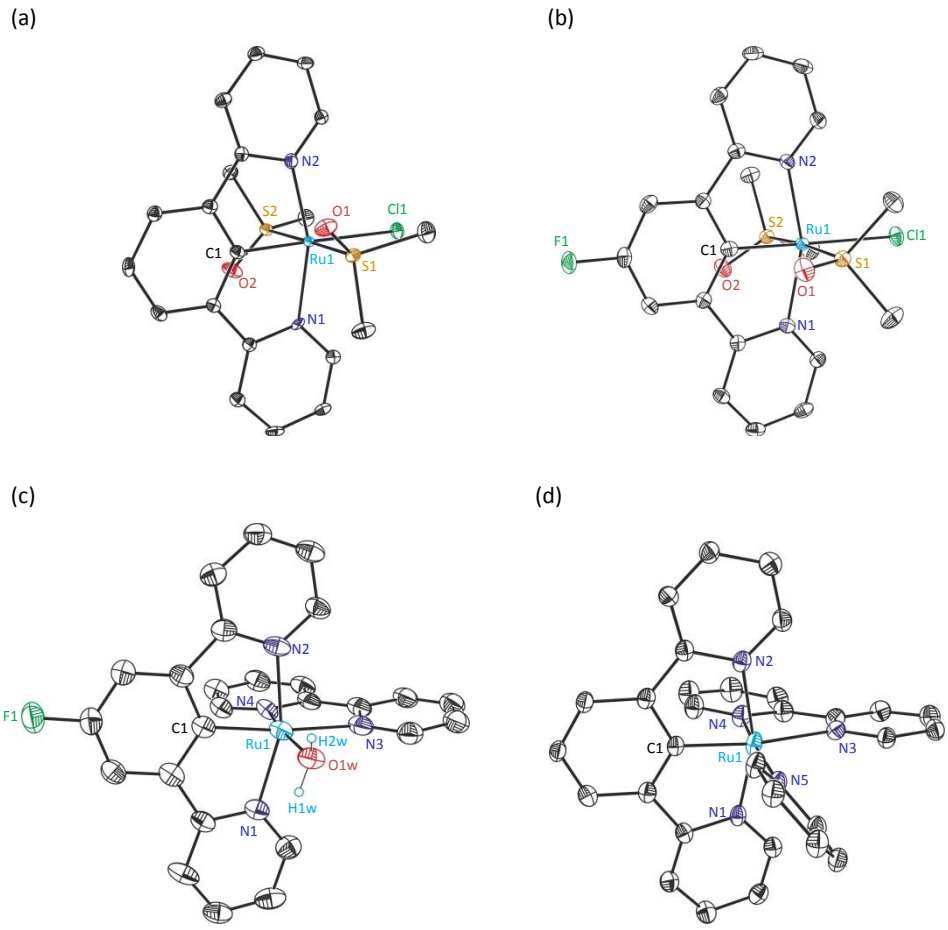

Figure 4. Ortep plots (ellipsoids at 50% probability) of the X-ray crystal structures of (a) **1a**, (b) **1b**, (c) **4b**$^{2+}$, and (d) **5a**$^{+}$. Color codes: Ru, cyan; N, blue; O, red; Cl, green; F, green; S, yellow; C, grey. Hydrogen atoms are not shown for clarity. Labeling schemes were unified for the compared purpose.

Table 1. Selected Bond Distances (Å) and Angles (°) for **1a**, **1b**, **4b**$^{2+}$ and **5a**$^{+}$. Labeling schemes are shown in Figure 4.

	1a	**1b**	**4b**$^{2+}$	**5a**$^{+}$
Ru1-N1	2.0977(19)	2.102(2)	2.089(4)	1.952(11)
Ru1-N2	2.103(2)	2.104(2)	2.123(4)	2.178(10)
Ru1-C1	1.9410(17)	1.943(3)	1.946(5)	1.908(10)
Ru1-S1	2.2996(6)	2.3001(6)	—	—
Ru1-S2	2.3045(6)	2.2900(6)	—	—
Ru1-Cl	2.5558(4)	2.5524(6)	—	—
Ru1-N3	—	—	2.173(9)	2.165(9)
Ru1-N4	—	—	2.080(8)	2.062(8)
Ru1-O1w	—	—	2.063(4)	—
Ru1-N5	—	—	—	2.096(4)
O1-S1	1.4838(19)	1.4844(18)	—	—
O2-S2	1.4844(16)	1.480(2)	—	—
N1-Ru1-N2	158.46(6)	158.39(8)	159.36(18)	160.4(4)
S1-Ru1-S2	177.427(19)	176.17(2)	—	—
S1-Ru1-C1	89.36(11)	89.77(7)	—	—
C1-Ru1-Cl1	178.62(8)	176.04(18)	—	—
S1-Ru1-Cl1	91.00(2)	86.52(2)	—	—
S2-Ru1-Cl1	91.57(2)	93.78(2)	—	—
N1-Ru1-Cl1	99.33(5)	102.21(6)	—	—
N1-Ru1-N3	—	—	104.1(4)	100.8(8)
N2-Ru1-N3	—	—	96.5(4)	98.6(7)
N1-Ru1-N4	—	—	91.1(4)	85.2(10)
N2-Ru1-N4	—	—	92.6(5)	96.6(7)
C-Ru1-O1	—	—	94.37(17)	—
N1-Ru1-O1w	—	—	88.20(16)	—
N3-Ru1-O1w	—	—	93.6(2)	—
C-Ru-N5	—	—	—	91.2(7)
N1-Ru1-N5	—	—	—	90.8(10)
N3-Ru1-N5	—	—	—	97.5(2)

UNIVERSITAT ROVIRA I VIRGILI
SECOND-ROW TRANSITION-METAL COMPLEXES RELEVANT TO CO2 REDUCTION AND WATER OXIDATION
Takashi Ono
DL:T 1108-2014

Redox properties

The electrochemical properties of all the complexes were examined by means of cyclic voltammetry (CV), differential pulse voltammetry (DPV), and square wave voltammetry (SQWV) and the observed redox couples are collected in Tables 2 and 3.

In CH_2Cl_2, Ru-Cl complex **3a** undergoes a reversible $1e^-$ oxidation corresponding to the Ru(III/II) couple at 0.02 V (vs. SSCE). $E_{1/2}$ value for the Ru(III/II) couple is shifted more than 0.8 V cathodically with respect to *trpy* analogue, $[Ru(trpy)(bpy)Cl]^+$ ($E_{1/2}$ = 0.87 V),[25] representing strong σ-donating property of anioninc *dpb*$^-$ ligand through metal-carbon bond. This large potential shift was also observed for the related complexes: $E_{1/2}$ = 0.51 V for $[Ru(trpy)(dpb)]^+$, 1.28 V for $[Ru(trpy)_2]^{2+}$ in CH_3CN.[25] Interestingly, at higher potential, one more $1e^-$ reversible wave was observed at 1.39 V, corresponding to the Ru(IV/III) couple. Introducing fluoro substituent on *dpb*$^-$ ligand increase potentials by 40 mV for the Ru(III/II), and by 30 mV for the Ru(IV/III) couples. $E_{1/2}$ for the Ru(III/II) couple of the synthetic intermediate species **2a**$^+$, **2b**$^+$ which contain a coordinated DMSO ligand, are 0.87 V and 0.92 V, respectively. This is associated with a π-acceptor *S*-bonded DMSO which stabilizes metal dπ orbital and hence increases the redox potential with respect to Ru-Cl complexes **3a-b**.[35] Complexes **5a**$^+$ and **6a**$^+$ show a reversible $1e^-$ oxidation wave at 0.50 V and 0.55 V, respectively, which are about 0.7 V lower than their *trpy* analogues.

In pH 1 aqueous triflic acid solution, Ru-OH_2 complexes showed one quasi-reversible reduction (**4a**$^{2+}$: 0.04 V, **4b**$^{2+}$: 0.07 V) and one quasi-reversible oxidation (**4a**$^{2+}$: 0.87 V, **4b**$^{2+}$: 0.88 V) waves (Figure 5a and S17). The former event corresponds to the Ru(III/II) couple, whereas the latter can be assigned as single $2e^-$ oxidation to Ru(V) species by considering that the difference of peak potentials is 48 mV ($E_{p,a}$ = 899 mV, $E_{p,c}$ = 851 mV) for **4a**$^{2+}$ and 43 mV ($E_{p,a}$ = 903 mV, $E_{p,c}$ = 860 mV) for **4b**$^{2+}$, respectively, which is significantly smaller than 57 mV for ideal $1e^-$ process at 25 °C. At pH 7 in phosphate buffer, the latter oxidation wave splits into two $1e^-$ oxidation waves and 43 mV ($E_{p,a}$ = 903 mV, $E_{p,c}$ = 860 mV) for **4b**$^{2+}$, respectively, which is significantly smaller than 57 mV for ideal $1e^-$ process at 25 °C. At pH 7 in phosphate buffer, the latter

Table 2. Redox potentials (V vs. SSCE) for **1**, **1'**, **2**$^{+}$, **3**, **5**$^{+}$, and **6**$^{+}$ in 0.1 M CH_2Cl_2-$TBAPF_6$ together with related complexes.

Complex		$E_{1/2}$ (V) vs. SSCE	
		III/II	**IV/III**
1a	*trans*-bis DMSO	0.47	—
1b		0.49	—
2a^{+}	DMSO	0.87	—
2b^{+}		0.92	—
3a	Cl	0.02	1.39
3b		0.06	1.42
5a^{+}	pyridine	0.50	—
6a^{+}	CH_3CN	0.55	—
$Ru(trpy)(bpy)Cl^{+}$		0.87	—
$Ru(trpy)(bpy)(py)^{2+}$		1.24[a]	—
$Ru(trpy)(bpy)(CH_3CN)^{2+}$		1.31[a]	—
		III,II/II,II	**III,III/III,II**
1a'		0.25	0.64
1b'		0.30	0.68

a: In CH_3CN. Reference 37.

Table 3. Redox potentials (V vs. SSCE) for **4a**$^{2+}$, **4b**$^{2+}$ and related complex $[Ru^{II}(trpy)(bpy)(OH_2)]^{2+}$ [a,b] at pH 1 and at pH 7 and their pK_a values. $E_{1/2}$ values were taken from square wave voltammetry.

complex	pH	$E_{1/2}$ (V) vs. SSCE				p$K_{a,II}$	p$K_{a,III}$
		III/II	**IV/III**	**V/IV**	**V/III**		
4a^{2+}	1	0.04	—	—	0.87	—	4.9
	7	-0.05	0.37	0.83	—		
4b^{2+}	1	0.07	—	—	0.88	—	4.8
	7	-0.03	0.41	0.85	—		
$Ru(trpy)(bpy)(OH_2)^{2+}$	1	0.80[a]	0.99[a]	1.56[a]	—	9.8[b]	1.7[b]
	7	0.48[b]	0.59[b]	1.62[b]	—		

a: Reference 14, b: Reference 18

UNIVERSITAT ROVIRA I VIRGILI
SECOND-ROW TRANSITION-METAL COMPLEXES RELEVANT TO CO2 REDUCTION AND WATER OXIDATION
Takashi Ono
DL:T 1108-2014

oxidation wave splits into two $1e^-$ oxidation waves (**4a**$^{2+}$: 0.37 V and 0.83 V for the Ru(IV/III) and Ru (V/IV) couples, respectively, **4b**$^{2+}$: 0.41 V and 0.85 V for the Ru(IV/III) and Ru (V/IV) couples, respectively) as shown in Figure 5b and Figure S17.

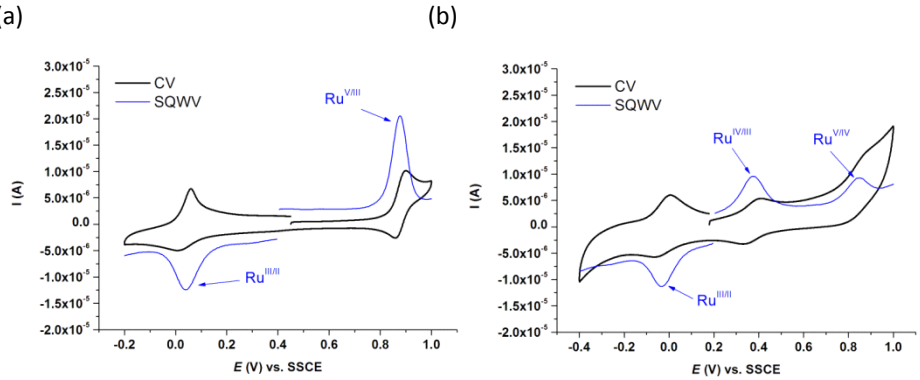

Figure 5. CVs and SQWVs of complex **4a**$^{2+}$ (0.25 mM), (a) at pH 1 in 0.1 M aqueous triflic acid solution, and (b) at pH 7 in 0.1 M phosphate buffer. Glassy carbon working electrode, Pt disk counter electrode and Hg/Hg_2SO_4 reference electrode, and potentials were converted to vs. SSCE. Scan rate 100 mV s^{-1} for CV, frequency 15 s^{-1} for SQWV.

Further to understand better the thermodynamic stability of each species with a different degree of protonation and/or oxidation, the Pourbaix diagram has been constructed for complex **4a**$^{2+}$ within the range of pH 1 to 13 as shown in Figure 6.

Below pH 2, two redox events can be observed, while above pH 2, three redox events can be observed. For the Ru(III/II) couple, its potential is independent on pH between pH 1 and pH 4.9 and decreases by 50 mV/pH unit between pH 4.9 and 12. For the Ru(IV/III) couple, its potential decreases by 111 mV/pH unit between pH 2 and 4.9 and then by 62 mV/pH unit between pH 4.9 and 13. For the Ru(V/IV) couple, its potential is independent on pH between 2 and 13.

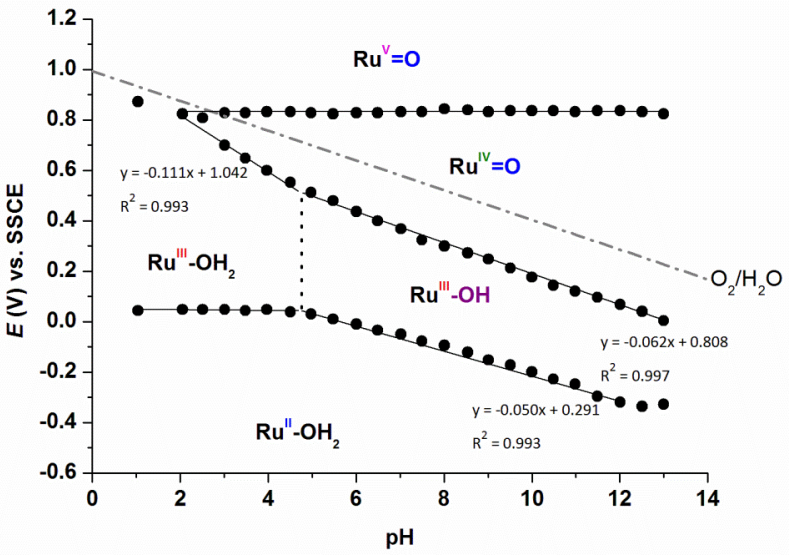

Figure 6. Pourbaix diagram for bis aqua complex **4a**$^{2+}$. The diagram was built by CV or SQWV experiments in aqueous solution at different pH (I = 0.1 M). Glassy carbon working electrode, Pt disk counter electrode and Hg/Hg_2SO_4 reference electrode, and potentials were converted to vs. SSCE. Scan rate 100 mV s^{-1} for CV, frequency 15 s^{-1} for SQWV.

By comparing experimentally derived slopes and the calculated values from the Nernst equation (eq. 3)

$$E_{1/2} = E_{1/2}^{o} - (0.059(\text{mV}) \cdot m/n)\text{pH} \qquad (3)$$

(where *m* is the number of protons, *n* is the number of electrons, and $E_{1/2}^{o}$ is the half-wave potential at pH 0), the reaction in the different pH regions can be expressed by the following equations(eqns.4-11):

$1 < pH < 2$

$$Ru^{III}\text{-}OH_2 + 1e^- \rightarrow Ru^{II}\text{-}OH_2 \qquad (4)$$

$$Ru^{V}{=}O + 2H^+ + 2e^- \rightarrow Ru^{III}\text{-}OH_2 \qquad (5)$$

$2 < pH < 4.9$

$$Ru^{III}\text{-}OH_2 + 1e^- \rightarrow Ru^{II}\text{-}OH_2 \qquad (6)$$

$$Ru^{IV}{=}O + 2H^+ + 1e^- \rightarrow Ru^{III}\text{-}OH_2 \qquad (7)$$

$$Ru^{V}{=}O + 1e^- \rightarrow Ru^{IV}{=}O \qquad (8)$$

UNIVERSITAT ROVIRA I VIRGILI
SECOND-ROW TRANSITION-METAL COMPLEXES RELEVANT TO CO2 REDUCTION AND WATER OXIDATION
Takashi Ono
DL:T 1108-2014

4.9 < pH < 12

Ru^{III}-OH + $1H^+$ + $1e^-$ → Ru^{II}-OH_2 (9)

Ru^{IV}=O + $1H^+$ + $1e^-$ → Ru^{III}-OH (10)

Ru^{V}=O + $1e^-$ → Ru^{IV}=O (11)

It is interesting to see that at pH 1, Ru(V)-oxo species, Ru(V)=O, is generated at 0.87 V, which is nearly 0.7 V lower than that generated from *trpy* analogue $[Ru^{II}(trpy)(bpy)(OH_2)]^{2+}$. Additionaly, p$K_a$ of oxidation state Ru(III) was calculated from the intersection of two lines (Figure 6) to be 4.8, in good agreement with the value obtained from acid-base titration stated above. This value is 3 log unit bigger than that for the *trpy* analogue (4.8 vs. 1.7). At higher potential catalytic current was observed, even though it is small at both pH1 and pH 7 (Figure 7 and S18).

(a) (b)

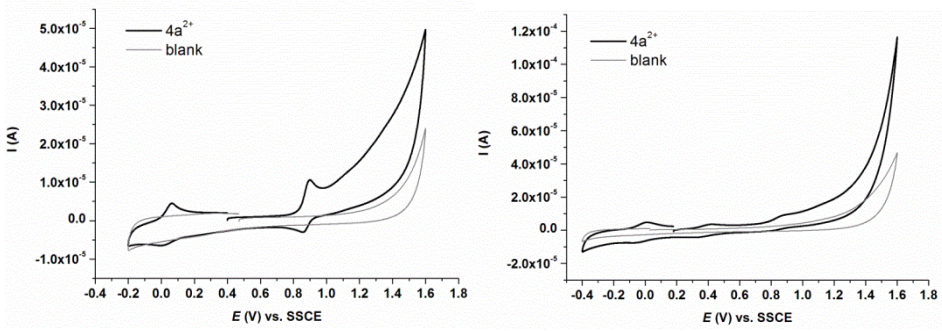

Figure 7. Cyclic voltammograms (CVs) in the presence(—) and absence(—) of complex **4a**$^{2+}$ (0.25 mM), (a) at pH 1 in 0.1 M aqueous triflic acid solution, and (b) at pH 7 in 0.1 M phosphate buffer. Glassy carbon working electrode, Pt disk counter electrode and Hg/Hg_2SO_4 reference electrode and potentials were converted to vs. SSCE. Scan rate 100 mV s^{-1}.

UV-vis

The UV-vis absorption spectra of complexes **3a**, **3b**, **5a**$^+$, and **6a**$^+$ in CH_2Cl_2, and **4a**$^{2+}$ and **4b**$^{2+}$ in phosphate buffer (at pH 2.2) are presented in Figures 8-9 and their UV-Vis features are listed in Table 4.

All the complexes exhibit intense bands in the region between 200 nm and 350 nm due to the intraligand π-π* transitions and unsymmetrical broad metal-to-ligand charge transfer (MLCT) bands in the region of 350-700 nm. As was found for the polypyridyl complexes containing cyclometalated ligand,[25,29-32,38-39] MLCT bands are highly broadened with respect to polypyridyl complexes consisting of neutral ligands, $Ru(trpy)(bpy)L^{n+}$ (L = Cl^-, OH_2, Figures 8-9). This broad nature can be explained by that the higher energy transitions involve excited states associated with *dpb*$^-$, whereas the lower energy transitions involve excited-states localized to *bpy*.[25,32] In addition, the loss of degeneracy of dπ orbitals due to electronic repulsion with electron rich π orbital on phenyl ring of *dpb*$^-$ ligand is involved (Scheme 3).[25,32]

The λ_{max} values for Ru-Cl complexes **3a** and **3b** are red-shifted compared to **4a**$^+$, **4b**$^+$, **5a**$^+$ and **6a**$^+$ which contain neutral ligands (OH_2, pyridine or acetonitrile), as a consequence of a destabilized HOMO because of the repulsion of the filled metal dπ orbitals with the filled p orbitals of the chloride ligand (Scheme3). The UV-vis spectra of Ru(III)-OH_2 complexes **4a**$^{2+}$ and **4b**$^{2+}$ show two features: the higher energy transition around 300-450 nm due to MLCT and the lower-energy transitions in the region of 500-700 nm, which can be assigned to ligand-to-metal charge transfer (LMCT) [38-39]

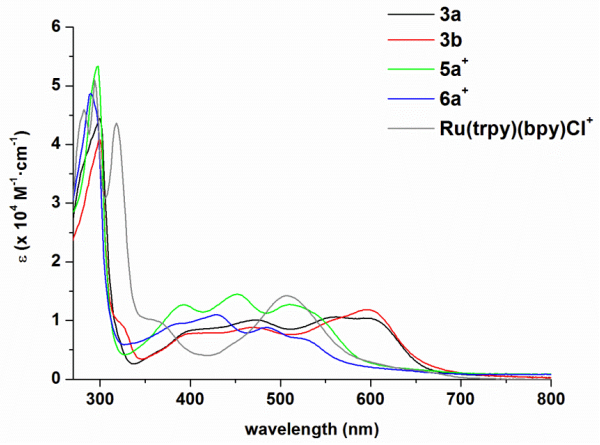

Figure 8. UV-vis spectra for complexes **3a** (black), **3b** (red), **5a**$^+$ (green), **6a**$^+$ (blue), and $Ru(trpy)(bpy)Cl^+$ (gray) in CH_2Cl_2.

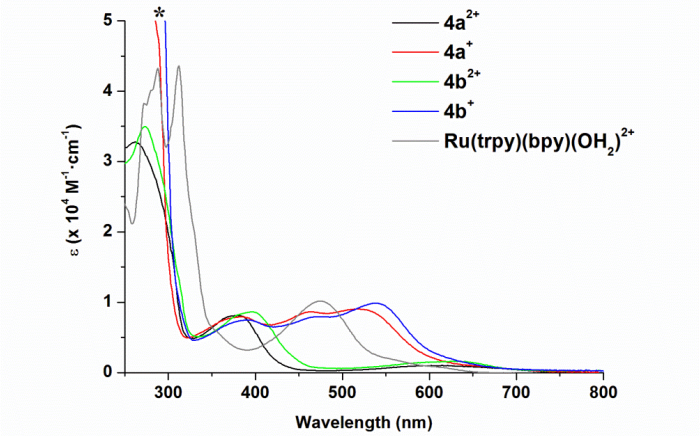

Figure 9. UV-vis spectra in phosphate buffer at pH 2.2, for complexes **4a**$^{2+}$ (black), **4b**$^{2+}$ (green) and their reduced species **4a**$^{+}$ (red), and **4b**$^{+}$ (blue). Slightly excess amount of ascorbic acid was used as reductant. *: due to the absorption of ascorbic acid.

Scheme 3. Relative energies of HOMOs and LUMOs for *dpb*$^{-}$/*bpy* (blue) and *trpy*/*bpy* (black) systems with schematic representation of Ru(NXN)(NN)(L). NXN: tridentate ligand (X =N, *trpy*; X = C^{-}, *dpb*$^{-}$), NN: *bpy* and L: monodentate ligand.

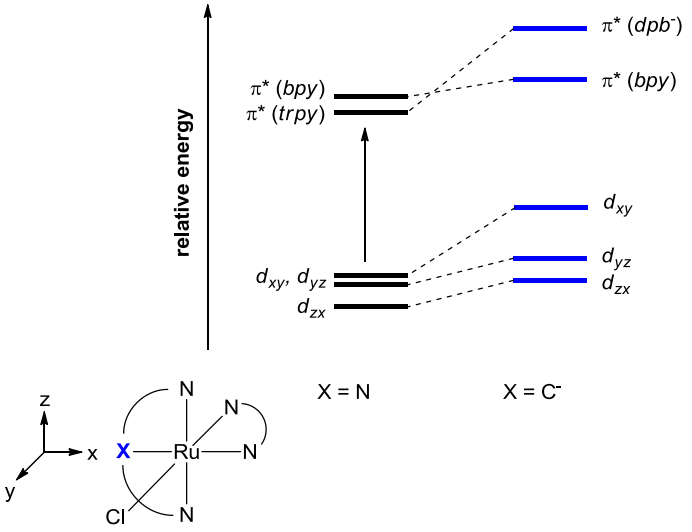

Table 4. UV-vis spectroscopic data for the complexes **3a**, **3b**, **5a**$^{+}$, and **6a**$^{+}$ in CH_2Cl_2 and **4a**$^{2+}$ and **4b**$^{2+}$ in phosphate buffer at pH 2.2.

Complex	assignment	λ_{max}, nm (ε, $M^{-1}\cdot cm^{-1}$)
		In CH_2Cl_2
3a	π-π* dπ-π*	251 (30425), 300 (44419 397(8205), 473(10072), 561 (10624), 597 (10393)
3b	π-π* dπ-π*	245 (29006), 299 (40906) 324 (9320), 397 (7737), 470 (8838), 558 (sh,10079), 595 (11848)
5a^{+}	π-π* dπ-π*	248 (41405), 298 (53347) 392 (12688), 452 (14475), 510 (12725)
6a^{+}	π-π* dπ-π*	246 (40763), 290 (48725) 388 (9495), 430 (11008), 486 (8796), 522 (6990)
		In phosphate buffer (pH 2.2)
Ru(II)		
4a^{+}	π-π* dπ-π*	—* 371 (sh, 7525), 392 (7944), 472 (8648), 524 (9046)
4b^{+}	π-π* dπ-π*	—* 392 (7489), 468 (7946), 538 (9856)
Ru(III)		
4a^{2+}	π-π* dπ-π* π-dπ	240 (33794), 268 (32789) 385 (8090) 608 (br,1080)
4b^{2+}	π-π* dπ-π* π-dπ	237 (31815),273 (34962) 380 (sh), 397 (8660), 583 (sh), 634 (br, 1604)

*: Overlap with the absorption of ascorbic acid. sh: sholder, br:broad.

VI.3.2. Catalytic Experiments

Water oxidation catalysis

$[Ru^{III}(R\text{-}dpb)(bpy)(OH_2)]^{2+}$, **4a**$^{2+}$ (R = H), **4b**$^{2+}$ (R =F), have been tested as a potential water oxidation catalysts by using $(NH_4)_2Ce^{IV}(NO_3)_6$ as chemical oxidant. The

UNIVERSITAT ROVIRA I VIRGILI
SECOND-ROW TRANSITION-METAL COMPLEXES RELEVANT TO CO2 REDUCTION AND WATER OXIDATION
Takashi Ono
DL:T 1108-2014

catalytic properties of complexes $\mathbf{4}^{2+}$ and $\mathbf{4b}^{2+}$ were analyzed by monitoring evolved gases by on-line manometry and MS spectrometry. In both cases, the catalytic reactions were carried out in the following conditions: [Cat] = 1.0 mM, [Ce^{IV}] = 100 mM in 2 mL of 0.1 M aqueous triflic acid solution (pH 1) at 25 °C. The obtained results are shown in Figures 10-11 and listed in Table 5. Both complexes showed poor catalytic activity with mainly the formation of CO_2. These catalytic behaviours are clearly different from that of *trpy* analogue that generates only O_2 with TON of 18.3 in the same reaction condition reported earlier.[18] These difference can be explained by that the redox potential for the Ru(V/III) couple of *dpb*$^-$ complexes is lower than the standard potential for O_2/H_2O, that is, the reaction is thermodynamically unfavourable, and that electron-rich cyclometalated ring of *dpb*$^-$ ligand is oxidatively unstable, leading to degradation of the catalysts during the reaction. It is interesting to point out the different composition of the gases evolved for the two catalysts tested. MS experiment for $\mathbf{4a}^{+}$ shows 4% of O_2, while $\mathbf{4b}^{2+}$ containing fluoro substituent on *dpb*$^-$ ligand generates 8% of O_2 (Figure 11) . These results suggest that decreasing electron density on the cyclometalated ring of *dpb*$^-$ ligand by electron withdrawing group as well as relatively stronger C-F bond with respect to C-H bond would increase the stability of *dpb*$^-$ ligand and hence, of the catalyst.

Table 5. TON and O_2/CO_2 ratios for the evolved gases using $\mathbf{4a}^{2+}$ and $\mathbf{4b}^{2+}$ together with reported $[Ru(trpy)(bpy)(OH_2)]^{2+}$

Complex	TON			O_2/CO_2	
	total	O_2	CO_2		
$\mathbf{4a}^{2+}$	2.6	0.1	2.5	4/96	*Tw*
$\mathbf{4a}^{2+}$	2.8	0.2	2.6	8/92	*Tw*
$Ru(trpy)(bpy)(OH_2)^{2+}$	18.3	18.3	—	—	a

Catalytic conditions: [cat.] = 1 mM, [Ce^{IV}] = 100 mM, in 2mL of 0.1 M aqueous trifli acid solution.
Tw = This work. a: Reference 18.

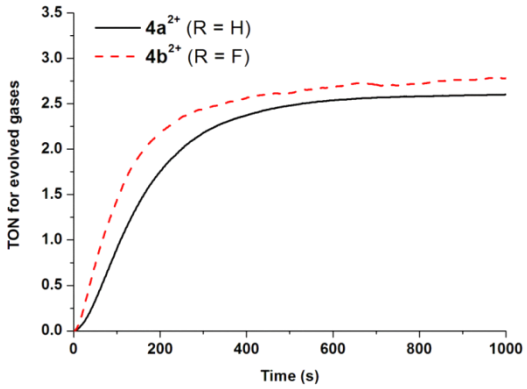

Figure 10. On-line manometric time profiles for the evolved gases, of **4a**$^{2+}$ (—) and **4b**$^{2+}$ (---) (1 mM) at pH 1.0 in 0.1 M triflic acid solution in the presence of $(NH_4)_2Ce(NO_3)_6$ (100 mM) as sacrificial oxidant.

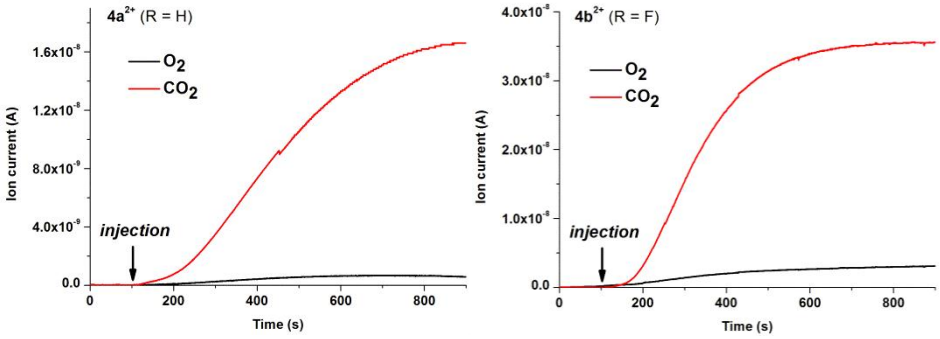

Figure 11. On-line gases evolution profiles monitored by MS upon addition of 100 equiv. of $(NH_4)_2Ce^{IV}(NO_3)_6$ (at 100 seconds) to 1 mM of **4a**$^{2+}$ (left) and **4b**$^{2+}$ (right) in 0.1 M triflic acid solution. Oxygen (—) and carbon dioxide (—).

Electrocatalytic Oxidation of BzOH

In order to evaluate the potential reactivity of Ru(V)=O species toward organic substrates, electrochemistry of **4a**$^{2+}$ was studied in 0.1 M aqueous triflic acid solution at pH 1 by means of cyclic voltammetry in the presence of benzyl alcohol (BzOH) as organic substrate. As can be seen in Figure 12, a catalytic current was observed in the presence of added BzOH, while no current was observed in the CV of only BzOH. The appearance of the catalytic current can be explained by the oxidation of BzOH

catalyzed by the electrogenerated Ru(V)=O species (Scheme 4). We believe that the product formed is benzaldehyde as was found for the other Ru systems for the oxidation of BzOH listed in Table 6.

Scheme 4. Schematic representation of $2e^-$ oxidation of BzOH to benzaldehyde catalyzed by Ru(V) species.

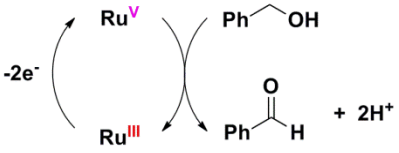

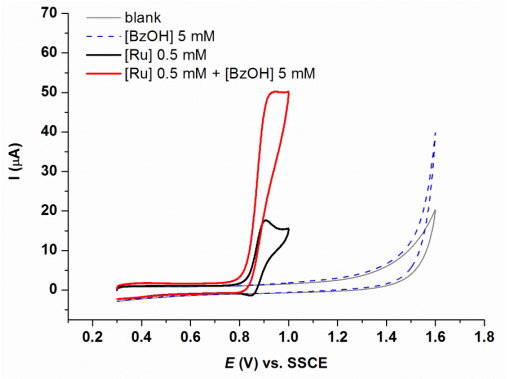

Figure 12. Cyclic voltammograms of $\mathbf{4}^{2+}$ (0.5 mM) in 0.1 M aqueous triflic acid solution at pH 1, in the absence (—) and presence (—) of BzOH (5mM, 10-fold molar excess) together with CVs of 5 mM BzOH(---) and blank solution(—). Glassy carbon working electrode, Pt disk counter electrode and Hg/Hg_2SO_4 reference electrode and potentials were converted to vs. SSCE. Scan rate 100 mV s^{-1}.

In the range of scan rate 10-100 mV/s, catalytic currents at 0.91 V (vs. SSCE) are practically independent of the scan rate (Figure S19), indicating that the catalytic reaction is under steady state. Under these conditions, the catalytic current can be expressed by the following equation[40] (eqn. 12):

$$i_{cat} = nFA[\mathrm{Ru}]D^{1/2}k_{cat}{}^{1/2}[\mathrm{BzOH}]^{1/2} \qquad (12)$$

, where n is the number of electron transferred (n = 2 for the oxidation of BzOH to benzaldehyde), F is Faraday constant, A is the electrode surface area, D and [Ru] are diffusion coefficient and concentration of the catalyst, respectively, [BzOH] is concentration of BzOH, and k_{cat} is the second-order rate constant. As shown in Figure S20, i_{cat} increases linearly with the increase of complex concentration from 0.02 to 0.06 mM in agreement with eq. 12. Furthermore, Figure S21 shows a series of CVs of **4a**$^{2+}$ (0.04 mM) with increasing concentrations of added BzOH (0.2 to 0.6 mM; 5 to 15-fold molar excess) at a scan rate of 20 mV/s. Second-order rate constant k_{cat} can be calculated from the following equation 13 derived from eqn. 12 and the Randles-Sevcik equation (eqn. 14).

$$i_{cat}/i_p = \frac{(RT)^{1/2} k_{cat}^{1/2}}{0.4463(nF\nu)^{1/2}} [\text{BzOH}]^{1/2} \qquad (13)$$

$$i_p = 0.4463 \left(\frac{F^3}{RT}\right)^{1/2} n^{3/2} A D^{1/2} [\text{Ru}] \nu^{1/2} \qquad (14)$$

,where i_p is peak current without BzOH, n' is number of electrons involved in the electrochemical process, (n' = 2 for the Ru(V/III) couple), ν is scan rate, R is the gas constant, and T is temperature. The plot of i_{cat}/i_p with respect to $[\text{BzOH}]^{1/2}$ varies linearly in the range of BzOH concentrations 0.2-0.6 mM in agreement with eq. 13 (Figure S21). From its slope, k_{cat} was determined to be 2730(40) $M^{-1}{\cdot}s^{-1}$. As can be seen in Table 6, the rate constant for **4a**$^{2+}$ is about two orders of magnitude higher than those for the Ru(IV)=O systems and is comparable to the value (3230(50) $M^{-1}{\cdot}s^{-1}$) obtained for the Ru(V)=O system of $[Ru(Mebimpy)(bpy)(OH_2)]^{2+}$ (Mebimpy = 2,6-bis(1-methylbenzimidazol-2-yl)pyridine) reported earlier[41] (Table 6). However, it is noteworthy that our catalyst **4a**$^{2+}$ triggers the reaction at more than 500 mV lower potential.

UNIVERSITAT ROVIRA I VIRGILI
SECOND-ROW TRANSITION-METAL COMPLEXES RELEVANT TO CO2 REDUCTION AND WATER OXIDATION
Takashi Ono
DL:T 1108-2014

Table 6. Second-order rate constants for the oxidation of BzOH catalyzed by **4a**$^{2+}$ and other reported Ru complexes.

Complex		k_{cat} [$M^{-1}\cdot s^{-1}$]	$E_{1/2}$ (V)	
Ru(V)=O species				
			V/III	
4a^{2+}		2730(40)	0.87	pH 1
			V/IV	
Ru(Mebimpy)(bpy)$(OH_2)^{2+}$		3230(50)[a]	1.41	pH 1
Ru(IV)=O species				
			IV/II	
Ru(trpy)(bpy)$(OH_2)^{2+}$		36.1(15)[b]	*ca*. 0.30	pH 13
Ru(trpy)(bpz)$(OH_2)^{2+}$		23.0(7)[b]	*ca*. 0.50	pH 11
Ru(trpy)(R_2Dppi)$(OH_2)^{2+}$	R = H	22(1)[c]	0.39	pH 11
	Me	9(3)[c]	0.37	pH 11
	Cl	6(4)[c]	0.42	pH 11
			IV/III	
Ru(Mebimpy)(bpy)$(OH_2)^{2+}$		16(1)[a]	0.71	pH 7.4

$E_{1/2}$ vs. SSCE. a: Reference 41, b: Reference 42, c: Reference 43.

VI.4. Conclusions

We have shown the synthesis and characterization of new mononuclear ruthenium complexes containing anionic *dpb*$^-$ (2,6-di(pyridin-2-yl)benzen-1-ide) ligand. From electrochemical study, it was shown that strong σ donation of *dpb*$^-$ ligand let the higher oxidation state thermodynamically stable; for instance, Ru(V)-oxo species from $[Ru^{III}$(R-dpb)(bpy)$(OH_2)]^{2+}$ (R = H: **4a**$^{2+}$, R = F: **4b**$^{2+}$) are generated at significantly low redox potential with regard to *trpy* analogue (**4a**$^{2+}$: 0.87 V vs. SSCE, **4b**$^{2+}$: 0.88 V, vs. $[Ru^{II}$(trpy)(bpy)$(OH_2)]^{2+}$: 1.56 V). Complexes **4a**$^{2+}$ and **4b**$^{2+}$ showed poor catalytic activity toward oxidation of water with mainly the formation of CO_2 although the gas compositions of each catalytic reaction are slightly different (O_2/CO_2 = 4/96 for **4a**$^{2+}$ and 8/92 for **4b**$^{2+}$). The reason for their poor catalytic activity can be explained by that the reaction is thermodynamically unfavourable due to low redox potential of Ru(V)=O species with respect to standard potential for O_2/H_2O as well as that the cyclometalated ring of the *dpb*$^-$ ligand is unstable toward oxidation due to its high

electron density. Associated with this, a slight difference of the gas compositions can be rationalized by considering that electron-withdrawing substituent in **4b**$^{2+}$ decreases electron density on the cyclometalated ring of *dpb*$^{-}$ ligand and therefore, increases the stability toward oxidation. Additionally, we have shown the reactivity of the Ru(V)=O species toward organic substrate, BzOH, with a second-order rate constant of (2.7± 0.1) x 10^3 $M^1 \cdot s^{-1}$. From the system found here which is the formation of easily accessible Ru(V)=O species combined with its high reactivity toward BzOH, one would associate with an application for light-driven oxidation reaction of organic substrates.

VI.5. Experimental Section

Materials

All reagents used in the present work were obtained from Aldrich Chemical Co., Alfa Aesar or Strem Chemicals inc. and were used without further purification. Synthesis grade organic solvents were obtained from SDS and were routinely degassed with N_2. The compounds $RuCl_2(dmso)_4$,[44] and Hdpb (1,3-di(pyridin-2-yl)benzene)[25] were prepared as described in the literature. F-Hdpb (2,2'-(5-fluoro-1,3-phenylene)dipyridine) was synthesized with 35% yield following the procedure for the synthesis of Hdpb described in the literature. NMR assignment of F-Hdpb has been reported previously in the literature.[26] All synthetic manipulations were routinely performed under N_2 atmosphere using Schlenk and vacuum-line techniques.

Scheme 5. NMR Labeling scheme for: *dpb*$^{-}$ complexes

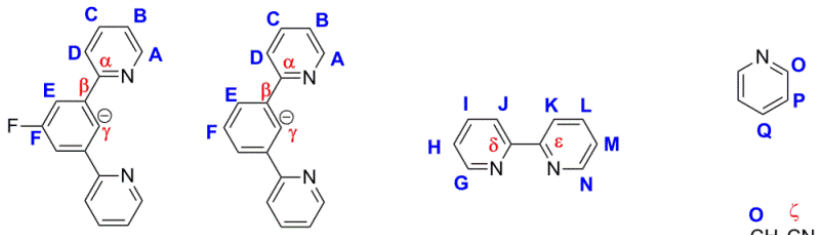

UNIVERSITAT ROVIRA I VIRGILI
SECOND-ROW TRANSITION-METAL COMPLEXES RELEVANT TO CO2 REDUCTION AND WATER OXIDATION
Takashi Ono
DL:T 1108-2014

Synthesis

Synthesis of *trans*-Ru^{II}(dpb)(dmso-*s*)$_2$(Cl), 1a

Into three-necked 500 mL round-bottom flask equipped with a condenser, 1.20 g (2.48 mmol) of $RuCl_2(dmso)_4$, 693 mg (2.98 mmol, 1.2 equiv.) of Hdpb and 170 mL of EtOH were added. After N_2 was bubbled into the mixture for 30 min, NEt_3 (1.7 mL, 12 mmol, 5 equiv.) was added and the mixture was refluxed for 24 h. After cooling to room temperature, a solid was precipitated in the solution and the solution was removed with syringe filter under N_2 atmosphere and the solid was washed with EtOH (5 mL x 3) and diethyl ether (15 mL x 3), which was dried under vacuum. Yield. 1.03 g (1.97 mmol), 79%. Anal. calcd. for $C_{20}H_{23}ClN_2O_2RuS_2$: C, 45.84; H, 4.42; N, 5.23; S, 12.24. Found: C, 45.41; H, 4.51; N, 5.23; S, 12.13. ^{1}H NMR (500 MHz, CD_2Cl_2, 298 K): δ 9.05 (d, 2H, J_{AB} = 5.5 Hz, H_A), 7.94 (d, 2H, J_{DC} = 7.1 Hz, H_D), 7.85 (td, 2H, J_{CD} = 7.1 Hz, J_{CA} = 1.6 Hz, H_C), 7.82 (d, 2H, J_{EF} = 7.6 Hz, H_E), 7.27 (ddd, 2H, J_{BC} 7.1 Hz, J_{BA} = 5.5 Hz, J_{BD} = 1.4 Hz, H_B), 7.21 (t, 1H, J_{FE} = $J_{FE'}$ = 7.6 Hz, H_F), 2.39 (s, 12H, Me of dmso). ^{13}C NMR (125 MHz, CD_2Cl_2, 298 K): δ 206.9 (C_γ), 168.3 (C_α), 154.4 (C_A), 144.9 (C_β), 136.8 (C_C), 124.3 (C_E), 122.9 (C_B), 120.3 (C_F), 119.5 (C_D), 42.3 (Me of dmso). ESI-MS (MeOH): *m/z* 411.0 ([M-Cl-dmso]$^+$).

Synthesis of *trans*-Ru^{II}(F-dpb)(dmso-*s*)$_2$(Cl), 1b

Following the similar procedure for the synthesis of **1a**, **1b** was obtained with 39% yield. Anal. Calc. for $C_{20}H_{22}ClFN_2O_2RuS_2$: C, 44.32; H, 4.09; N, 5.17; S, 11.83. Found: C, 45.44; H, 3.19; N, 5.51; S, 8.62. It was unsuccessful to obtain a satisfactory result for the elemental analysis of complex **1b** due to its instability under air even in solid state. ^{1}H NMR (500 MHz, CD_2Cl_2 + one drop of DMSO, 298 K): δ 9.07 (d, 2H, J_{AB} = 5.6 Hz, H_A), 7.9-7.84 (m, 4H, H_C and H_D), 7.62 (d, 2H, $^3J_{H\text{-}F}$ = 10.4 Hz, H_E), 7.31 (ddd, 2H, J_{BC} = 7.1 Hz, J_{BA} = 5.6 Hz, J_{BD} = 2.0 Hz, H_B), 2.39 (s, 12H, Me of dmso). ^{13}C NMR (125 MHz, CD_2Cl_2+ one drop of DMSO, 298 K): δ 199.4 (C_γ), 167.6 (C_α, $^4J_{CF}$ = 5.0 Hz), 159.7 (C_F, $^1J_{CF}$ = 234 Hz), 154.6 (C_A), 144.8 (C_β, $^1J_{CF}$ = 8.0 Hz), 136.9 (C_C), 123.4 (C_B), 119.9 (C_D), 111.7 (C_E, $^1J_{CF}$ = 23.0 Hz), 42.3 (Me of dmso). ^{19}F NMR (376 MHz, CD_2Cl_2 + one drop of DMSO, 298 K):

δ -124.0 (t, $^{3}J_{H\text{-}F}$ = 10.4 Hz). ESI-MS (MeOH): *m/z* 461.0 ([M-Cl-dmso+MeOH]$^{+}$), 493.0 ([M-Cl-dmso+2MeOH]$^{+}$).

Synthesis of [Ru^{II}(dpb)(bpy)(Cl)], 3a

Into three-necked 250 mL round-bottom flask equipped with a condenser, 506 mg (0.966 mmol) of **6** and 159 mg (1.02 mmol, 1.05 equiv.) of 2,2'-bipyridine were charged and the system was purged with N_2. After adding 80 mL of degassed CH_2Cl_2, the solution was stirred for one hour at room temperature. Then, the mixture was further stirred in the presence of tungsten lamp (100 W x 2) overnight. The resulting brown solution was purified over neutral alumina column using CH_2Cl_2/Acetone (90/10, v/v) as eluent. The first purple fraction was collected and the solvent was evaporated to give purple solid, which was washed with Et_2O (10 mL x 3) and dried under vacuum. Yield. 406 mg (0.77 mmol), 81%. Anal. calcd. for $C_{26}H_{19}ClN_4Ru$: C, 59.60; H, 3.65; N, 10.69. Found: C, 59.42; H, 3.65; N, 10.29. ^{1}H NMR (500 MHz, CD_2Cl_2, 298 K): δ 10.29 (d, 1H, J = 5.1 Hz, H_N), 8.33 (d, 1H, J = 8.2 Hz, H_K), 8.05-7.98 (m, 3H, H_E, H_L), 7.95 (d, 1H, J = 7.4 Hz, H_J), 7.93-7.87 (m, 3H, H_D, H_M), 7.63 (d, 2H, J = 6.8 Hz, H_A), 7.49 (td, 2H, J = 6.8 Hz, J = 1.4 Hz, H_C), 7.17 (td, 1H, J = 7.4 Hz, J = 1.2 Hz, H_I), 7.10-7.03 (m, 2H, H_F, H_G), 6.72 (t, 2H, J = 6.8 Hz, J = 1.2 Hz, H_B), 6.51 (td, 1H, J = 7.4 Hz, J = 1.2 Hz, H_H). ^{13}C NMR (125 MHz, CD_2Cl_2, 298 K): δ 223.3 (C_γ), 168.4 (C_α), 161.2 (C_δ), 156.7 (C_G), 154.6 (C_ε), 153.3 (C_A), 150.8 (C_N), 144.9 (C_β), 133.9 (C_C), 133.7 (C_L), 129.9 (C_I), 126.4 (C_M), 124.2 (C_H), 122.2 (C_E), 122.1 (C_J), 121.5 (C_K), 121.2 (C_B), 119.0 (C_F), 118.9 (C_D). ESI-MS (MeOH): *m/z* 524.0 (M^{+}).

Synthesis of [Ru^{II}(F-dpb)(bpy)(Cl)]·0.5H$_2$O, 3b·0.5H$_2$O

Following the similar procedure for the synthesis of **3a**, **3b** was obtained with 78% yield. Anal. Calc. for $C_{26}H_{18}ClFN_4Ru$: C, 57.62; H, 3.35; N, 10.34. Found: C, 56.63; H, 3.15; N, 9.89. Anal. Calcd for $C_{26}H_{18}ClFN_4Ru{\cdot}0.5H_2O$: C, 56.68; H, 3.48; N, 10.17. ^{1}H NMR (500 MHz, DMSO-d_6, 7298 K): d 10.10 (d, 1H, J_{NM} = 4.7 Hz, H_N), 8.75 (d, 1H, J_{KL} = 8.2 Hz, H_K), 8.37 (d, 1H, J_{JI} = 8.1 Hz, H_J), 8.21-8.14 (m, 3H, H_D and H_L), 8.08-8.01 (m, 3H, H_E and H_M), 7.63 (t, 2H, J_{CB} = J_{CD} = 6.8 Hz, H_C), 7.55 (d, 2H, J_{AB} = 6.8 Hz, H_A), 7.35 (t, 1H, J_{IH} = J_{IJ} =

UNIVERSITAT ROVIRA I VIRGILI
SECOND-ROW TRANSITION-METAL COMPLEXES RELEVANT TO CO2 REDUCTION AND WATER OXIDATION
Takashi Ono
DL:T 1108-2014

7.7 Hz, H_I), 6.89 (t, 2H, $J_{BA} = J_{BC}$ = 6.8 Hz, H_B), 6.80-6.70 (m, 2H, H_G and H_H). ^{13}C NMR (125 MHz, DMSO-d_6, 298 K): δ 206.5 (C_γ), 167.2 (C_α, br), 160.3 (C_δ), 158.5 (C_F, brd, $^1J_{CF}$ = 244 Hz), 155.1 (C_G), 154.0 (C_ε), 152.1 (C_A, br), 149.3 (C_N), 143.8 (C_β, br), 134.2 (C_L), 133.8 (C_C), 130.6 (C_I), 126.1 (C_M), 124.5 (C_H), 122.7 (C_J), 122.1 (C_K), 121.5 (C_B), 119.4 (C_D), 109.3 (C_E, brd, $^2J_{CF}$ = 24 Hz). ^{19}F NMR (376 MHz, DMSO-d_6, 298 K): δ -126.4 (br). ESI-MS (MeOH): *m/z* 565.0 ($[M+Na]^+$).

Synthesis of $[Ru^{III}(dpb)(bpy)(OH_2)](PF_6)(OTf)$, [4a](PF$_6$)(OTf)

105 mg (0.200 mmol) of Ru(dpb)(bpy)(Cl) **3a**, 106 mg (0.304 mmol, 1.5 equiv.) of $TlPF_6$ were charged into a 20 mL Schlenk tube with Teflon plug valve, which was purged with N_2. Then, 10 mL of degassed MeOH was added and the mixture was heated to reflux for 1 hour. After cooling down to room temperature, white precipitate, TlCl was filtered off through a pad of Celite. Into the wine red filtrate, 10 mL of pH1 triflic acid was added and the volume was reduced by rotary evaporator to give a green solution. After adding 1 mL of saturated aqueous NH_4PF_6, the flask was kept into fridge overnight to give green crystalline precipitate, which was filtered and washed with small amount of cold water and Et_2O and dried under vacuum. Yield 132 mg (0.165 mmol) 82%. Anal. Calcd. for $C_{27}H_{21}F_9N_4O_4PRuS$: C, 40.51; H, 2.64; N, 7.00; S, 4.01. Found: C, 40.45; H, 3.01; N, 6.88; S, 3.71. ^{1}H NMR (500 MHz, D_2O/Acetone-d_6 = 3/2 with ascorbic acid and NEt_3, 298 K): δ 9.58 (d, 1H, J_{NM} = 5.3 Hz, H_N), 8.57 (d, 1H, J_{KL} = 8.1 Hz, H_K), 8.16 (t, 1H, J_{LK} = 8.1 Hz, H_L), 8.12 (d, 1H, J_{JI} = 8.0 Hz, H_J), 8.01-7.94 (m, 5H, H_D, H_M and H_E), 7.62 (d, 2H, J_{AB} = 5.8 Hz, H_A), 7.58 (t, 2H, J_{CD} = 7.8 Hz, H_C), 7.21 (t, 1H, J_{IJ} = 8.0 Hz, H_I), 7.15 (t, 1H, J_{FE} = 7.6 Hz, H_F), 6.87 (d, 1H, J_{GH} = 6.3 Hz, H_G), 6.79 (t, 2H, J_{BA} = 5.8 Hz, H_B), 6.47 (t, 1H, J_{HG} = 6.3 Hz, H_H). ^{13}C NMR (125 MHz, D_2O/Acetone-d_6 = 3/2 with ascorbic acid and NEt_3, 298 K): δ 224.6 (C_γ), 169.3 (C_α), 161.3 (C_δ), 156.6 (C_G), 154.3 (C_ε), 152.8 (C_A), 148.7 (C_N), 145.2 (C_β), 136.0 (C_C), 135.6 (C_L), 131.8 (C_I), 127.4 (C_M), 124.5 (C_H), 123.5 (C_E), 123.0 (C_J and C_K), 122.2 (C_B), 119.4 (C_D), 119.3 (C_F). ESI-MS (H_2O): *m/z* 506.0 ($[M-2PF_6-H]^+$).

Synthesis of $[Ru^{III}(F\text{-}dpb)(bpy)(OH_2)](PF_6)_2$, $[\mathbf{4b}](PF_6)_2$

Following the similar procedure for the synthesis of **4a**$^{2+}$, **4b**$^{2+}$ was obtained with 77% yield. Anal. Calcd. for $C_{26}H_{20}F_{13}N_4OP_2Ru$: C, 38.34; H, 2.48; N, 6.88. Found: C, 38.58; H, 2.76; N, 6.83. ^{1}H NMR (500 MHz, D_2O/Acetone-d_6 = 2/1 with ascorbic acid and NEt_3, 298 K): δ 9.54 (d, 1H, J_{NM} = 5.3 Hz, H_N), 8.55 (d, 1H, J_{KL} = 8.1 Hz, H_K), 8.19-8.10 (m, 2H, H_J and H_L), 8.03-7.93 (m, 3H, H_D, and H_M), 7.99 (d, 2H, $^3J_{H\text{-}F}$ = 11.0 Hz, H_E), 7.66 (d, 2H, J_{AB} = 6.5 Hz, H_A), 7.61 (t, 2H, J_{CD} = 6.5 Hz, H_C), 7.23 (t, 1H, J_{IJ} = 7.0 Hz, H_I), 6.86-6.81 (m, 3H, H_B and H_G), 6.50 (t, 1H, J_{HG} = 7.0 Hz, H_H). ^{13}C NMR (125 MHz, D_2O/Acetone-d_6 = 2/1 with ascorbic acid and NEt_3, 298 K): δ 216.7 (C_γ), 168.5 (C_α, $^4J_{C\text{-}F}$ = 5 Hz), 161.3 (C_δ), 159.4 (C_F, $^1J_{C\text{-}F}$ = 229 Hz), 156.5 (C_G), 154.4 (C_ε), 153.1 (C_A), 148.8 (C_N), 145.4 (C_β, $^3J_{C\text{-}F}$ = 8 Hz), 136.0 (C_C), 135.7 (C_L), 132.1 (C_I), 127.4 (C_M), 124.7 (C_H), 123.1 (C_K), 123.0 (C_J), 122.7 (C_B), 120.0 (C_D), 110.7 (C_E, $^2J_{C\text{-}F}$ = 24 Hz). ^{19}F NMR (376 MHz, D_2O/Acetone-d_6 = 2/1 with ascorbic acid and NEt_3,, 298 K): δ -69.5 (d, 12F, PF_6), -123.0 (t, 1F, $^3J_{H\text{-}F}$ = 11.0 Hz, F-dpb). ESI-MS (H_2O): *m/z* 524.1 ($[M\text{-}2PF_6\text{-}H]^+$).

Synthesis of $[Ru^{II}(dpb)(bpy)(py)](PF_6)$, $[\mathbf{5}](PF_6)$

50.1 mg (0.0954 mmol) of Ru(dpb)(bpy)(Cl) **3a**, 50.8 mg (0.145 mmol, 1.5 equiv.) of $TlPF_6$ were charged into a 20 mL Schlenk tube with Teflon plug valve, which was purged with N_2. Then, 6 mL of degassed MeOH and 38 μL (0.47 mmol, 5equiv.) of pyridine were added and the mixture was heated to reflux for 1 hour. After cooling down to room temperature, white precipitate, TlCl was filtered off through a pad of Celite. Into the filtrate, 1 mL of saturated aqueous KPF_6 was added. Upon reducing the volume, brown precipitate appeared which was filtered and washed with Et_2O (5 mL x 3) and dried under vacuum. Slow evaporation of Et_2O into the acetone solution of the compound gave microcrystals, which was washed with Et_2O (5 mL x 3) and dried under vacuum. Yield 34.0 mg (0.0477 mmol) 50%. Anal. Calcd. for $C_{31}H_{24}F_6N_5PRu$: C, 52.25; H, 3.39; N, 9.83. Found: C, 52.13; H, 3.77; N, 9.72. ^{1}H NMR (500 MHz, Acetone-d_6, 298 K): δ 9.02 (d, 1H, J_{NM} = 5.4 Hz, H_N), 8.86 (d, 1H, J_{KL} = 7.7 Hz, H_K), 8.51 (d, 1H, J_{JI} = 7.7 Hz, H_J),

UNIVERSITAT ROVIRA I VIRGILI
SECOND-ROW TRANSITION-METAL COMPLEXES RELEVANT TO CO2 REDUCTION AND WATER OXIDATION
Takashi Ono
DL:T 1108-2014

8.32 (td, 1H, $J_{LK} = J_{LM} = 7.7$ Hz, $J_{LN} = 1.4$ Hz, H_L), 8.23 (d, 2H, $J_{DC} = 7.6$ Hz, H_D), 8.13 (d, 2H, $J_{EF} = 7.6$ Hz, H_E), 7.99 (ddd, 1H, $J_{ML} = 7.7$ Hz, $J_{MN} = 5.4$ Hz, $J_{MK} = 1.1$ Hz H_M), 7.88 (d, 2H, $J_{AB} = 5.6$ Hz, H_A), 7.84-7.78 (m, 4H, H_C and H_O), 7.68-7.58 (m, 2H, H_I and H_Q), 7.26 (t, 1H, $J_{FE} = 7.6$ Hz, H_F), 7.19 (d, 1H, $J_{GH} = 5.8$ Hz, H_G), 7.12 (t, 2H, $J_{PO} = J_{PQ} = 7.1$ Hz, H_P), 7.04 (ddd, 2H, $J_{BC} = 7.6$ Hz, $J_{BA} = 5.6$ Hz, $J_{BD} = 1.3$ Hz, H_B), 6.92 (ddd, 1H, $J_{HI} = 7.7$ Hz, $J_{HG} = 5.8$ Hz, $J_{HJ} = 1.2$ Hz, H_H). ^{13}C NMR (500 MHz, Acetone-d_6, 298 K): δ 223.3 (C_γ), 169.3 (C_α), 159.4 (C_δ), 155.7 (C_ε), 155.2 (C_G), 153.3 (C_O), 153.2 (C_A) 149.9 (C_N), 144.6 (C_β), 136.7 (C_C), 136.6 (C_L), 136.6 (C_Q), 134.8 (C_I), 128.1 (C_M), 126.1 (C_H), 125.9 (C_P), 124.9 (C_E), 124.3 (C_K), 123.8 (C_J), 123.5 (C_B), 120.6 (C_D), 120.5 (C_F). ESI-MS (H_2O): *m/z* 568.1 ([M-PF_6]$^+$).

Synthesis of [Ru^{II}(dpb)(bpy)(ACN)](PF_6)·0.5H_2O, [6](PF_6)·0.5H_2O

50.8 mg (0.0970 mmol) of Ru(dpb)(bpy)(Cl) **3a**, 50.4 mg (0.144 mmol, 1.5 equiv.) of $TlPF_6$ were charged into a 20 mL Schlenk tube with Teflon plug valve, which was purged with N_2. Then, 10 mL of degassed acetonitrile was added and the mixture was heated to reflux for 1 hour. After cooling down to room temperature, white precipitate, TlCl was filtered off through a pad of Celite. Into the filtrate, 1 mL of saturated aqueous KPF_6 was added. Upon reducing the volume, brown precipitate appeared which was filtered and washed with Et_2O (5 mL x 3) and dried under vacuum. Slow evaporation of Et_2O into the CH_2Cl_2 solution of the compound gave microcrystals, which was washed with Et_2O (5 mL x 3) and dried under vacuum. Yield 47.8 mg (0.0709 mmol) 73%. Anal. Calcd. for $C_{31}H_{24}F_6N_5PRu$: C, 49.86; H, 3.29; N, 10.38. Found: C, 49.29; H, 3.65; N, 10.10. Anal. Calcd. for $C_{31}H_{24}F_6N_5PRu·0.5H_2O$: C, 49.20; H, 3.39; N, 10.25. ^{1}H NMR (500 MHz, Acetone-d_6, 298 K): δ 9.87 (d, 1H, $J_{NM} = 5.2$ Hz, H_N), 8.81 (d, 1H, $J_{KL} = 7.9$ Hz, H_K), 8.46 (d, 1H, $J_{JI} = 7.8$ Hz, H_J), 8.33 (td, 1H, $J_{LK} = J_{LM} = 7.9$ Hz, $J_{LN} = 1.5$ Hz, H_L), 8.19 (d, 2H, $J_{DC} = 7.8$ Hz, H_D), 8.12 (d, 2H, $J_{EF} = 7.6$ Hz, H_E), 8.07 (ddd, 1H, $J_{ML} = 7.9$ Hz, $J_{MN} = 5.2$ Hz, $J_{MK} = 1.2$ Hz, H_M), 7.81-7.74 (m, 4H, H_A and H_C), 7.62 (td, 1H, $J_{IH} = J_{IJ} = 7.8$ Hz, $J_{IG} = 1.5$ Hz, H_I), 7.31 (t, 1H, $J_{FE} = 7.6$ Hz, H_F), 7.17 (d, 1H, $J_{GH} = 5.8$ Hz, H_G), 6.98 (ddd, 2H, $J_{BC} = 7.6$ Hz, $J_{BA} = 5.7$ Hz, $J_{BD} = 1.4$ Hz, H_B), 6.94 (ddd, 1H, $J_{HI} = 7.8$ Hz, $J_{HG} = 5.8$ Hz, $J_{HJ} = 1.3$ Hz, H_H), 2.23 (s, 3H, H_O). ^{13}C NMR (125 MHz, Acetone-d_6, 298 K): δ 219.0 (C_γ),

169.5 (C_α), 159.7 (C_δ), 155.3 (C_ε), 154.8 (C_G), 153.3 (C_A), 150.6 (C_N), 144.9 (C_β), 136.8 (C_C), 136.6 (C_L), 134.9 (C_I), 128.1 (C_M), 126.1 (C_H), 126.0 (C_ζ), 124.6 (C_E), 124.0 (C_K), 123.7 (C_J), 122.9 (C_B), 120.7 (C_F), 120.2 (C_D), 3.7 (C_O). ESI-MS (H_2O): *m/z* 529.9 ([M-PF_6]$^+$).

Instrumentation and measurements

Cyclic voltammetric (CV) experiments were performed in a IJ-Cambria IH-660 potentiostat, using a three electrode cell. Glassy carbon disk electrodes (3 mm diameter) from BASi were used as working electrode, platinum wire as auxiliary and SSCE as the reference electrode. Cyclic voltammograms were recorded at 100 mV/s scan rate under nitrogen atmosphere. The complexes were dissolved in previously degassed dichloromethane containing the necessary amount of (*n*-Bu_4N)(PF_6), used as supporting electrolyte, to yield a 0.1 M ionic strength solution. All $E_{1/2}$ values reported in this work were estimated from cyclic voltammetry as the average of the oxidative and reductive peak potentials ($E_{p,a}$+$E_{p,c}$)/2 or from differential pulse voltammetry (DPV; pulse amplitudes of 0.05 V, pulse widths of 0.05 s, sampling width of 0.02 s, and a pulse period of 0.1 s). Unless explicitly mentioned the concentration of the complexes were approximately 1 mM. The NMR spectroscopy was performed on Bruker Avance 400 MHz Bruker Avance II and Bruker Avance 500 MHz. The ESI mass spectroscopy experiments were performed on a Waters Micromass LCT Premier equipment, respectively. UV-Vis spectroscopy was performed on a Cary bio 50 UV-vis spectrophotometer with 1 cm quartz cells. Manometric measurements were performed with homemade water-jacket glass reactor coupled to a Testo 521 manometer. Composition of the gaseous phase was determined by online mass-spectrometry with an OmniStar GSD 301 C (Pfeiffer) quadrupole mass-spectrometer. In a typical experiment, 2 μmol of complex was charged in a glass vial closed with septum and connected to capillary adaptor. Then, vacuum/N_2-refilling were applied three times. Afterwards, 1.85 mL of degassed aqueous triflic acid solution at pH 1 was added into the vial, followed by additional degasification with N_2. And this reactor was connected to MS spectrometer. A 0.15 mL of previously degassed $(NH_4)_2Ce^{IV}(NO_3)_6$

UNIVERSITAT ROVIRA I VIRGILI
SECOND-ROW TRANSITION-METAL COMPLEXES RELEVANT TO CO2 REDUCTION AND WATER OXIDATION
Takashi Ono
DL:T 1108-2014

solution (200 μmol) was then added directly into the reaction solution with a Hamilton syringe.

X-Ray structure determination

Suitable crystals of **1a** and **1b** were grown by cooling the hot methanol-d_4 solutions of **1a** and **1b**, respectively. **1a** was crystallized as a merohedral twin (TWIN law: 0 1 0 1 0 0 0 0 -1; BASF: 0.51288). Suitable Crystal of complex **[4b](PF$_6$)$_2$** was grown as **[4b](PF$_6$)$_{0.6}$(OTf)$_{1.4}$** by slow evaporation of a mixture of acetone and aqueous triflic acid (HOTf) solution. The asymmetric unit contains one molecule of the metal complex and two anions. One of the anions is a triflate anion (OTf^-). The second anion is a disordered mixture of OTf^- and PF_6^- (ratio 40:60). The bpy ligand of the main molecule is disordered in two positions with a ratio of 75:25. Suitable Crystal of complex **[5a](PF$_6$)** was grown as **[5a](PF$_6$)·Et$_2$O** from dichloromethane/diethyl ether. The asymmetric unit contains one molecule of the metal complex, one PF_6 anion and one diethyl ether molecule. The main molecule is partially disordered in two orientations (ratios: 54:46 and 65:35). The diethyl ether molecule is also disordered in two positions (ratio 50:50). The measured crystals were prepared under inert conditions immersed in perfluoropolyether as protecting oil for manipulation.

***Data collection**:* Crystal structure determinations were carried out using a Bruker-Nonius diffractometer equipped with an APPEX 2 4K CCD area detector, a FR591 rotating anode with MoK_α radiation, Montel mirrors as monochromator, and a Kryoflex low temperature device (T = -173 °C). Full-sphere data collection was used with ω and φ scans. APEX-2 (for Data collection),[45] Bruker Saint V/.60A (for data reduction),[46] and SADABS (for absorption correction).[47]

***Structure Solution and Refinement**:* Crystal structure solution was achieved using direct methods as implemented in SHELXTL[48] and visualized using the program XP. Missing atoms were subsequently located from difference Fourier synthesis and added to the atom list. Least-squares refinement on F^2 using all measured intensities was carried out using the program SHELXTL. All non-H atoms were refined, including anisotropic displacement parameters.

VI.6. Acknowledgements

Support from MINECO (CTQ-2010-21497) is gratefully acknowledged TO thanks MINECO for a doctoral grant.

X-ray structure analyses were carried out by Dr. Jordi Benet-Buchholz at the Institute of Chemical Research of Catalonia (ICIQ)

VI.7. References

(1) Sheldon, R. A.; Kochi, J. K. *Metal-Catalyzed Oxidations of Organic Compounds*; Academic Press: New York, 1981.
(2) Punniyamurthy, T.; Velusamy, S.; Iqbal, J. *Chem. Rev.* **2005**, *105*, 2329-2364.
(3) Gunay, A.; Theopold, K. H. *Chem. Rev.* **2010**, *110*, 1060-1081.
(4) Huynh, M. H. V.; Meyer, T. J. *Chem. Rev.* **2007**, *107*, 5004-5064.
(5) Weinberg, D. R.; Gagliardi, C. J.; Hull, J. F.; Murphy, C. F.; Kent, C. A.; Westlake, B. C.; Paul, A.; Ess, D. H.; McCafferty, D. G.; Meyer, T. J. *Chem. Rev.* **2012**, *112*, 4016-4093.
(6) Cox, N.; Pantazis, D. A.; Neese, F.; Lubitz, W. *Acc. Chem. Res.* **2013**, *46*, 1588-1596.
(7) Siegbahn, P. E. M. *Acc. Chem. Res.* **2009**, *42*, 1871-1880.
(8) Umena, Y.; Kawakami, K.; Shen, J.-R.; Kamiya, N. *Nature* **2011**, *473*, 55-60.
(9) McEvoy, J. P.; Brudvig, G. W. *Chem. Rev.* **2006**, *106*, 4455-4483.
(10) Zong, R.; Thummel, R. P. *J. Am. Chem. Soc.* **2005**, *127*, 12802-12803.
(11) Concepcion, J. J.; Jurss, J. W.; Templeton, J. L.; Meyer, T. J. *J. Am. Chem. Soc.* **2008**, *130*, 16462-16463.
(12) Concepcion, J. J.; Tsai, M.-K.; Muckerman, J. T.; Meyer, T. J. *J. Am. Chem. Soc.* **2010**, *132*, 1545-1557.
(13) Yoshida, M.; Masaoka, S.; Abe, J.; Sakai, K. *Chemistry – An Asian Journal* **2010**, *5*, 2369-2378.
(14) Wasylenko, D. J.; Ganesamoorthy, C.; Henderson, M. A.; Koivisto, B. D.; Osthoff, H. D.; Berlinguette, C. P. *J. Am. Chem. Soc.* **2010**, *132*, 16094-16106.
(15) Roeser, S.; Farràs, P.; Bozoglian, F.; Martínez-Belmonte, M.; Benet-Buchholz, J.; Llobet, A. *ChemSusChem* **2011**, *4*, 197-207.
(16) Polyansky, D. E.; Muckerman, J. T.; Rochford, J.; Zong, R.; Thummel, R. P.; Fujita, E. *J. Am. Chem. Soc.* **2011**, *133*, 14649-14665.
(17) Badiei, Y. M.; Polyansky, D. E.; Muckerman, J. T.; Szalda, D. J.; Haberdar, R.; Zong, R.; Thummel, R. P.; Fujita, E. *Inorg. Chem.* **2013**, *52*, 8845-8850.
(18) Maji, S.; López, I.; Bozoglian, F.; Benet-Buchholz, J.; Llobet, A. *Inorg. Chem.* **2013**, *52*, 3591-3593.
(19) Duan, L.; Fischer, A.; Xu, Y.; Sun, L. *J. Am. Chem. Soc.* **2009**, *131*, 10397-10399.
(20) Duan, L.; Xu, Y.; Gorlov, M.; Tong, L.; Andersson, S.; Sun, L. *Chem. —Eur. J.* **2010**, *16*, 4659-4668.
(21) Xu, Y.; Fischer, A.; Duan, L.; Tong, L.; Gabrielsson, E.; Åkermark, B.; Sun, L. *Angew. Chem., Int. Ed.* **2010**, *49*, 8934-8937.
(22) Duan, L.; Bozoglian, F.; Mandal, S.; Stewart, B.; Privalov, T.; Llobet, A.; Sun, L. *Nat Chem* **2012**, *4*, 418-423.

UNIVERSITAT ROVIRA I VIRGILI
SECOND-ROW TRANSITION-METAL COMPLEXES RELEVANT TO CO2 REDUCTION AND WATER OXIDATION
Takashi Ono
DL:T 1108-2014

(23) Tong, L.; Inge, A. K.; Duan, L.; Wang, L.; Zou, X.; Sun, L. *Inorg. Chem.* **2013**, *52*, 2505-2518.
(24) Kärkäs, M. D.; Åkermark, T.; Johnston, E. V.; Karim, S. R.; Laine, T. M.; Lee, B.-L.; Åkermark, T.; Privalov, T.; Åkermark, B. *Angew. Chem., Int. Ed.* **2012**, *51*, 11589-11593.
(25) Bomben, P. G.; Robson, K. C. D.; Sedach, P. A.; Berlinguette, C. P. *Inorg. Chem.* **2009**, *48*, 9631-9643.
(26) Wang, Z.; Turner, E.; Mahoney, V.; Madakuni, S.; Groy, T.; Li, J. *Inorg. Chem.* **2010**, *49*, 11276-11286.
(27) Hesek, D.; Hembury, G. A.; Drew, M. G. B.; Taniguchi, S.; Inoue, Y. *Inorg. Chem.* **2001**, *40*, 2478-2479.
(28) Vos, J. G.; Pryce, M. T. *Coord. Chem. Rev.* **2010**, *254*, 2519-2532.
(29) Beley, M.; Collin, J. P.; Louis, R.; Metz, B.; Sauvage, J. P. *J. Am. Chem. Soc.* **1991**, *113*, 8521-8522.
(30) Jäger, M.; Smeigh, A.; Lombeck, F.; Görls, H.; Collin, J.-P.; Sauvage, J.-P.; Hammarström, L.; Johansson, O. *Inorg. Chem.* **2010**, *49*, 374-376.
(31) Wadman, S. H.; Havenith, R. W. A.; Hartl, F. e.; Lutz, M.; Spek, A. L.; van Klink, G. P. M.; van Koten, G. *Inorg. Chem.* **2009**, *48*, 5685-5696.
(32) Wadman, S. H.; Lutz, M.; Tooke, D. M.; Spek, A. L.; Hartl, F. e.; Havenith, R. W. A.; van Klink, G. P. M.; van Koten, G. *Inorg. Chem.* **2009**, *48*, 1887-1900.
(33) Sens, C.; Rodríguez, M.; Romero, I.; Llobet, A.; Parella, T.; Sullivan, B. P.; Benet-Buchholz, J. *Inorg. Chem.* **2003**, *42*, 2040-2048.
(34) Benet-Buchholz, J.; Comba, P.; Llobet, A.; Roeser, S.; Vadivelu, P.; Wiesner, S. *Dalton Trans.* **2010**, *39*, 3315-3320.
(35) Roeser, S.; Maji, S.; Benet-Buchholz, J.; Pons, J.; Llobet, A. *Eur. J. Inorg. Chem.* **2013**, *2013*, 232-240.
(36) Calligaris, M.; Carugo, O. *Coord. Chem. Rev.* **1996**, *153*, 83-154.
(37) Konno, H.; Kobayashi, A.; Sakamoto, K.; Fagalde, F.; Katz, N. E.; Saitoh, H.; Ishitani, O. *Inorg. Chim. Acta* **2000**, *299*, 155-163.
(38) Beley, M.; Collin, J. P.; Sauvage, J. P. *Inorg. Chem.* **1993**, *32*, 4539-4543.
(39) Koivisto, B. D.; Robson, K. C. D.; Berlinguette, C. P. *Inorg. Chem.* **2009**, *48*, 9644-9652.
(40) Bard, A. J.; Faulkner, L. R. *Electrochemical Methods: Fundamentals and Applications*; 2nd ed.; Wiley: New York, 2001.
(41) Paul, A.; Hull, J. F.; Norris, M. R.; Chen, Z.; Ess, D. H.; Concepcion, J. J.; Meyer, T. J. *Inorg. Chem.* **2011**, *50*, 1167-1169.
(42) Gerli, A.; Reedijk, J.; Lakin, M. T.; Spek, A. L. *Inorg. Chem.* **1995**, *34*, 1836-1843.
(43) Catalano, V. J.; Heck, R. A.; Immoos, C. E.; Öhman, A.; Hill, M. G. *Inorg. Chem.* **1998**, *37*, 2150-2157.
(44) Evans, I. P.; Spencer, A.; Wilkinson, G. *J. Chem. Soc., Dalton Trans.* **1973**, 204-209.
(45) *Data collection with APEX II* versions v1.0-22, v2009.1-0 and v2009.1-02, Bruker AXS inc., Madison, Wisconsin, USA, **2007**
(46) *Data reduction with Bruker SAINT* versions V.2.10(2003), V/.60A and V7.60A, Bruker AXS inc., Madison, Wisconsin, USA, **2007**
(47) *SADABS:* V.2.10(2003); V2008 and V2008/1, Bruker AXS inc., Madison, Wisconsin, USA, **2001**
(48) Sheldrick, G. M. *Acta Crystallogr. Sect. A* **2008**, *64*, 112-122.

UNIVERSITAT ROVIRA I VIRGILI
SECOND-ROW TRANSITION-METAL COMPLEXES RELEVANT TO CO2 REDUCTION AND WATER OXIDATION
Takashi Ono
DL:T 1108-2014

Supporting Information for:

New Mononuclear Ruthenium Polypyridyl Complexes Containing Anionic Dpb Ligand: Synthesis, Characterization and Oxidation Reactions

Table of contents

UNIVERSITAT ROVIRA I VIRGILI
SECOND-ROW TRANSITION-METAL COMPLEXES RELEVANT TO CO2 REDUCTION AND WATER OXIDATION
Takashi Ono
DL:T 1108-2014

S1. NMR:

Figure S1. 1D and 2D NMR spectra (500 MHz, 298K, CD_2Cl_2) for complex **1a:** (a) ^{1}H-NMR, (b) COSY, and (c) NOESY.

(a)

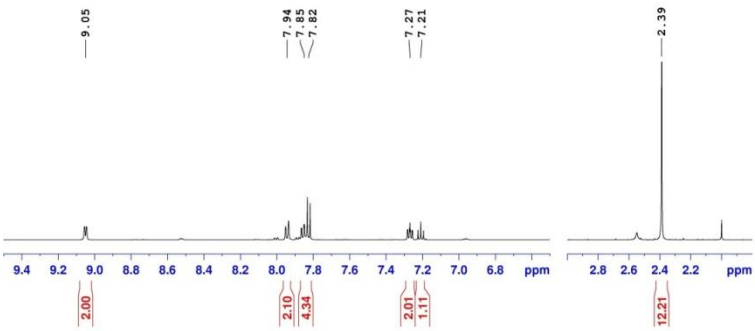

(b)

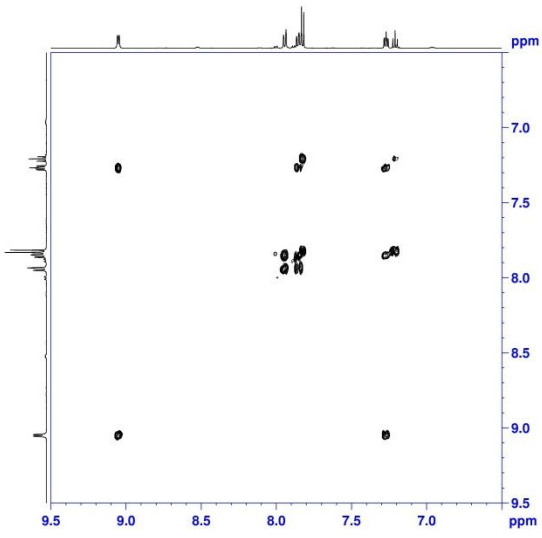

(c)

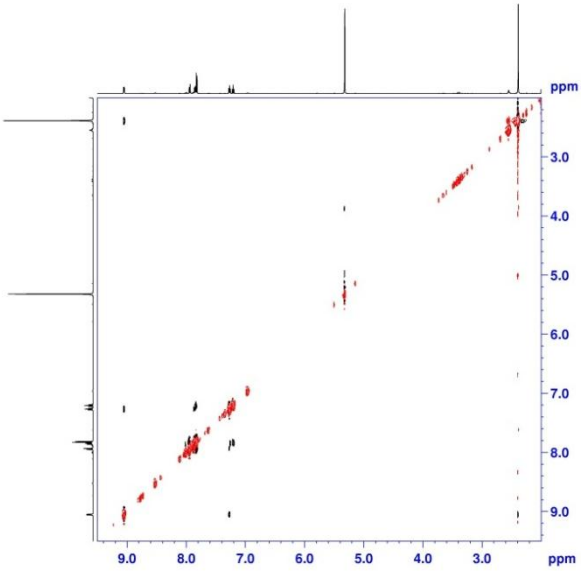

Figure S2. 1D and 2D NMR spectra (500 MHz, 298K, CD_2Cl_2) for complex **1b:** (a) ^{1}H-NMR,top: without, bottom: with added DMSO, (b) ^{1}H{^{19}F} NMR, (c) ^{19}F NMR, (d) COSY, (e) NOESY. (b)-(e): with added DMSO.

(a)

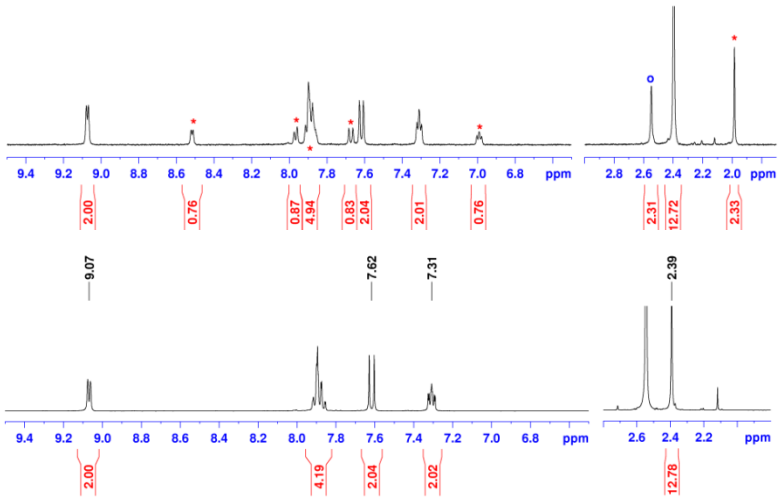

*: equilibrium product. o: free DMSO

(b)

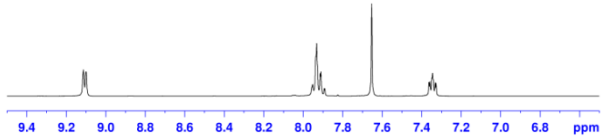

(c)

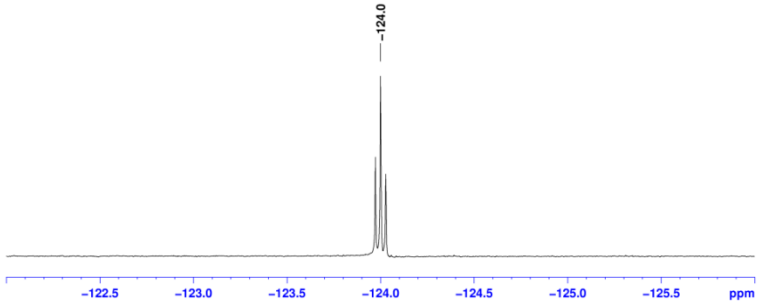

(d)

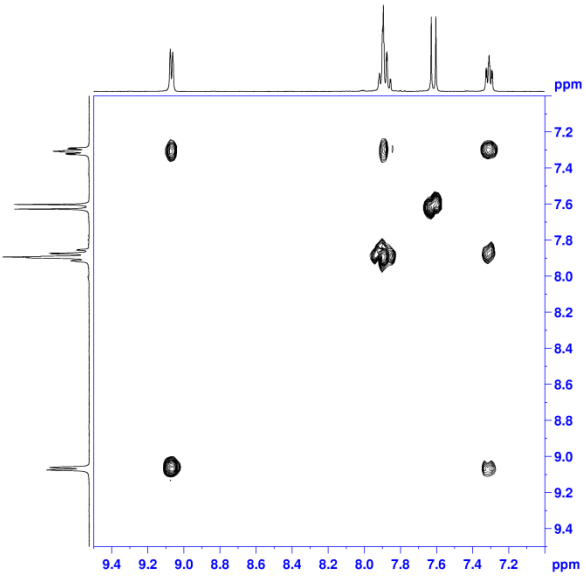
ppm
7.2
7.4
7.6
7.8
8.0
8.2
8.4
8.6
8.8
9.0
9.2
9.4
9.4 9.2 9.0 8.8 8.6 8.4 8.2 8.0 7.8 7.6 7.4 7.2
ppm

(e)

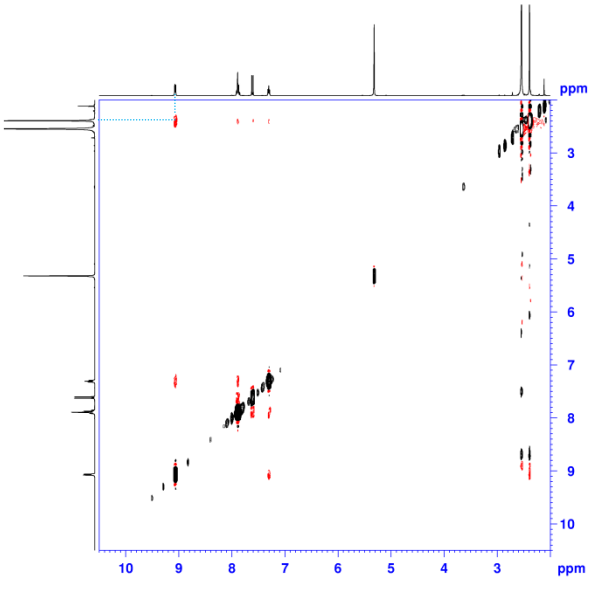
ppm
3
4
5
6
7
8
9
10
10 9 8 7 6 5 4 3
ppm

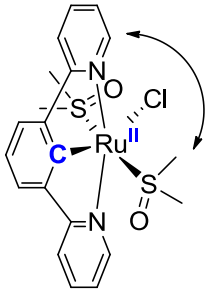
N
O
S
Cl
Ru
II
C
S
O
N

Figure S3. 1D and 2D NMR spectra (500 MHz, 298K, CD_2Cl_2) for complex **3a:** (a) ^{1}H-NMR, (b) COSY, and (c) NOESY.

(a)

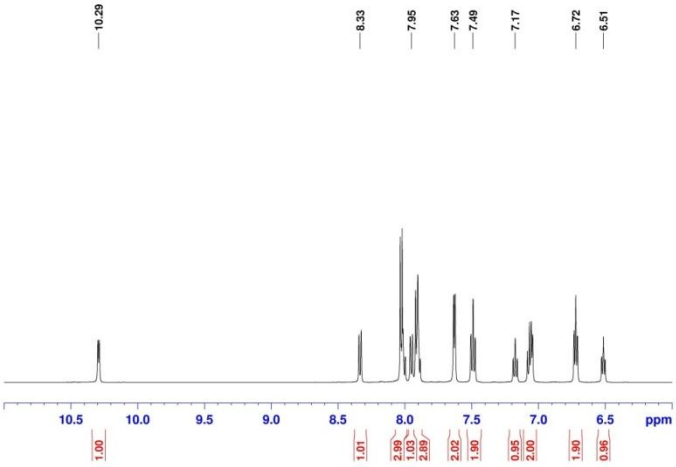

(b)

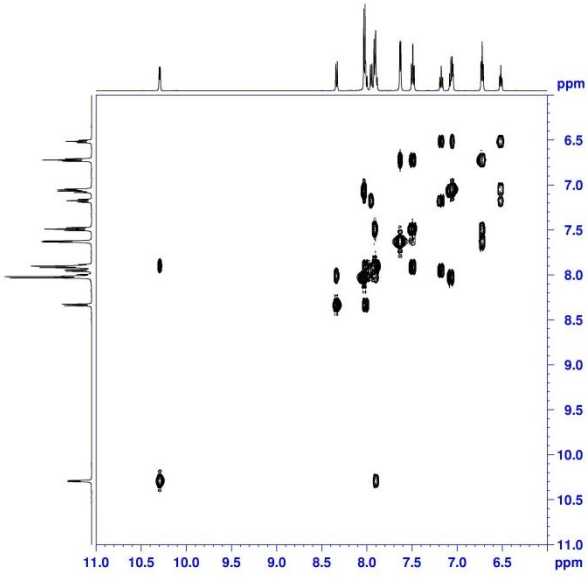

(c)

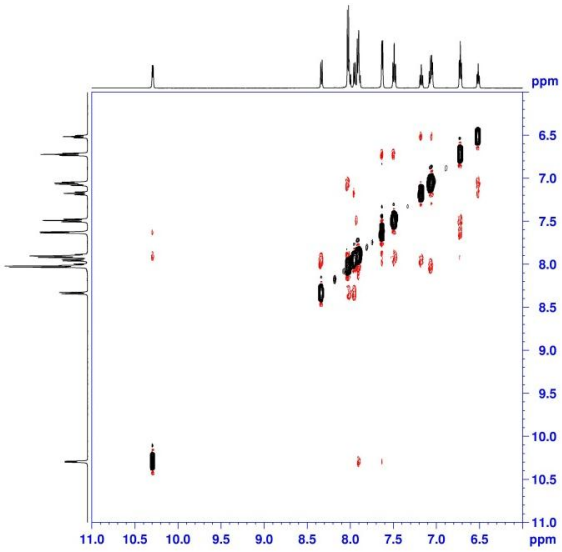

Figure S4. 1D and 2D NMR spectra (500 MHz, 298K, DMSO-d_6) for complex **3b:** (a) top: ^{1}H NMR, bottom: ^{1}H{^{19}F}, (b) ^{19}F, (c) COSY, (d) NOESY.

(a)

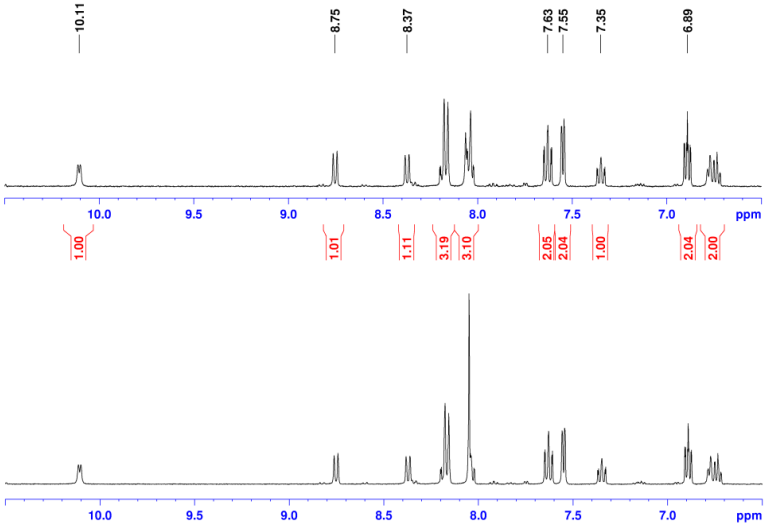

UNIVERSITAT ROVIRA I VIRGILI
SECOND-ROW TRANSITION-METAL COMPLEXES RELEVANT TO CO2 REDUCTION AND WATER OXIDATION
Takashi Ono
DL:T 1108-2014

(b)

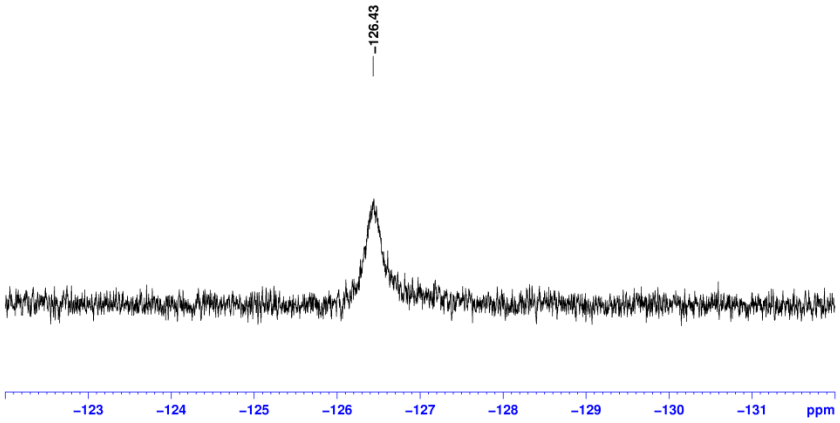

(c)

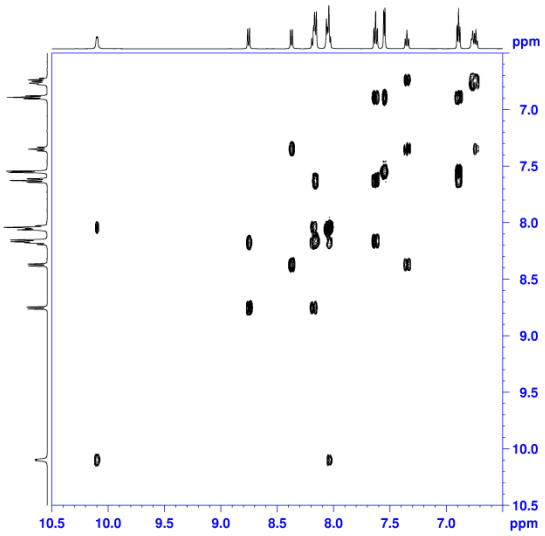

(d)

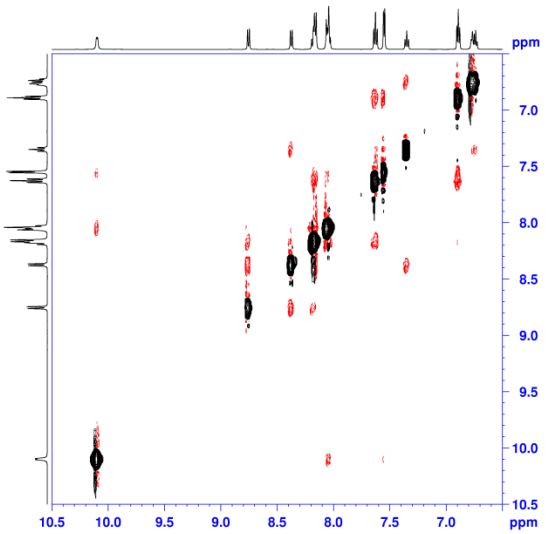

Figure S5. 1D and 2D NMR spectra (500 MHz, 298K, D_2O/Acetone-d_6 = 3/2, with ascorbic acid and NEt_3) for the reduced species of complex **4a^{2+}:** (a) ^{1}H-NMR, (b) COSY, and (c) NOESY.

(a)

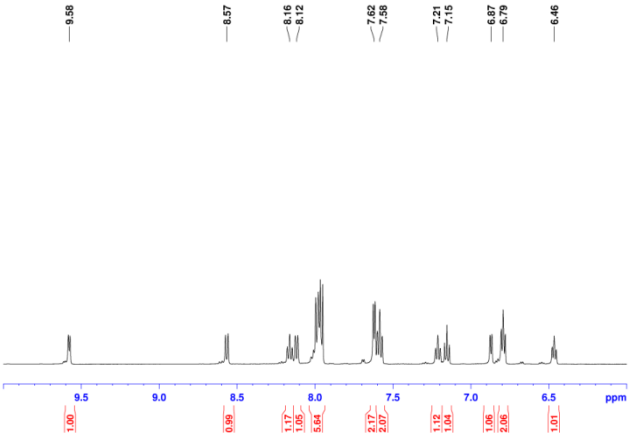

(b)

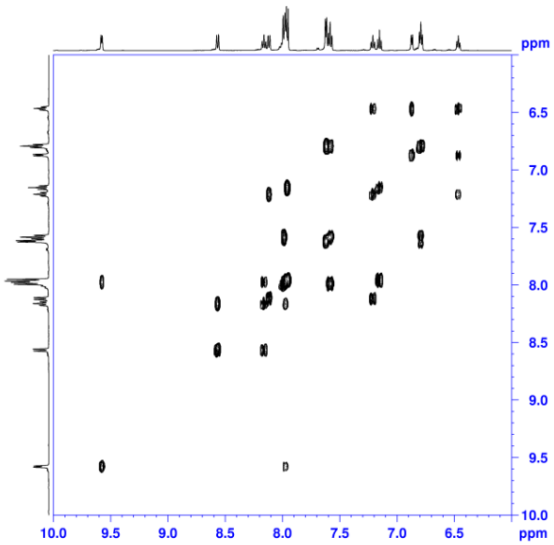
ppm
6.5
7.0
7.5
8.0
8.5
9.0
9.5
10.0
10.0 9.5 9.0 8.5 8.0 7.5 7.0 6.5
ppm

(c)

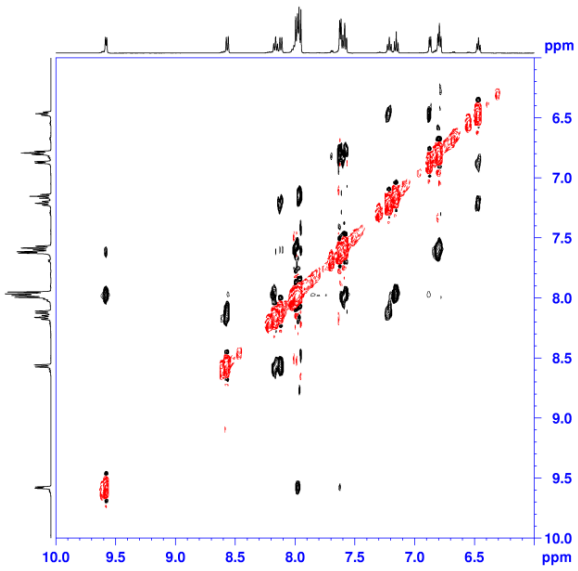
ppm
6.5
7.0
7.5
8.0
8.5
9.0
9.5
10.0
10.0 9.5 9.0 8.5 8.0 7.5 7.0 6.5
ppm

Figure S6. 1D and 2D NMR spectra (500 MHz, 298K, D_2O/Acetone-d_6 = 2/1, with ascorbic acid and NEt_3) for the reduced species of complex **4b^{2+}:** (a) top: ^{1}H NMR, bottom: $^{1}H\{^{19}F\}$, (b) top: ^{19}F, bottom: $^{19}F\{^{1}H\}$, (c) COSY, and (d) NOESY.

(a)

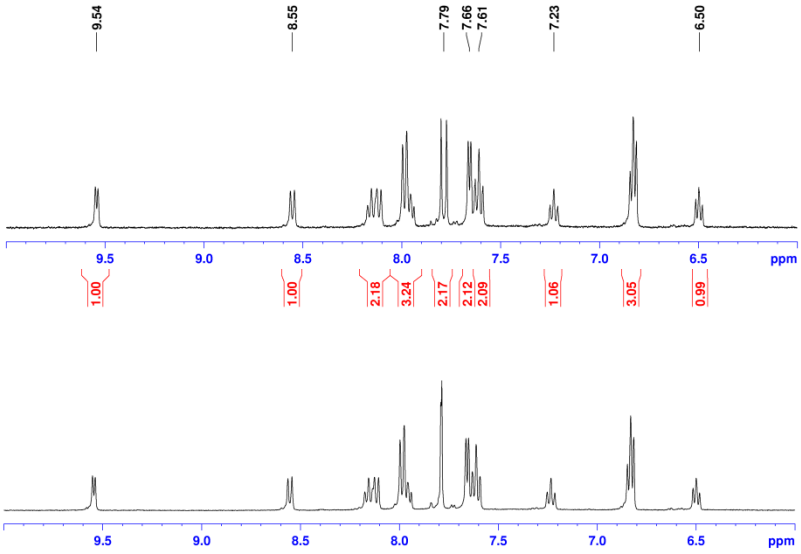

(b)

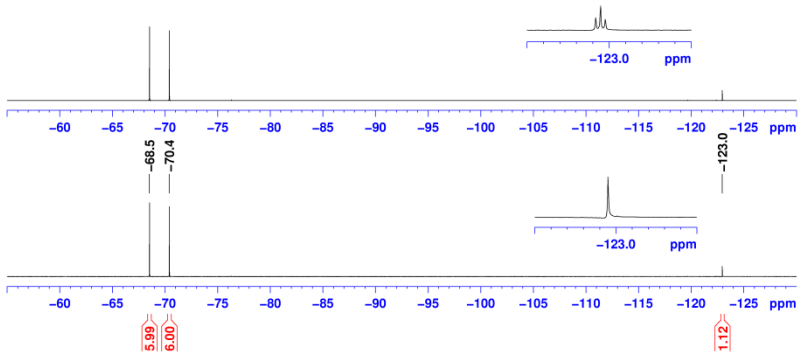

UNIVERSITAT ROVIRA I VIRGILI
SECOND-ROW TRANSITION-METAL COMPLEXES RELEVANT TO CO2 REDUCTION AND WATER OXIDATION
Takashi Ono
DL:T 1108-2014

(c)

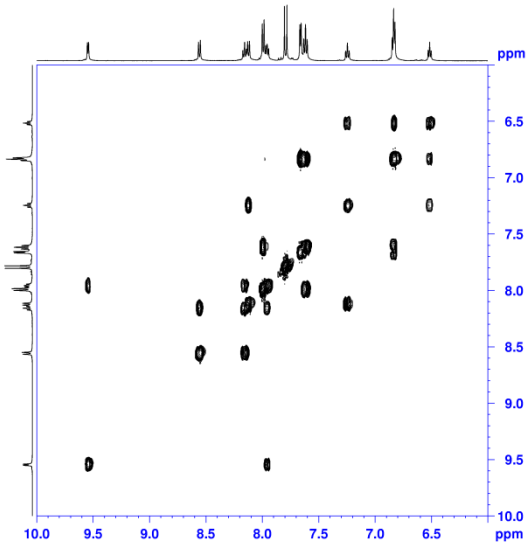

(d)

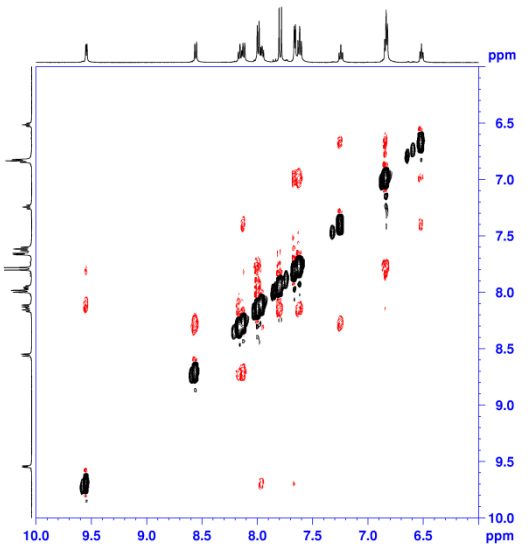

Figure S7 . 1D and 2D NMR spectra (500 MHz, 298K, Acetone-d_6) for complex **5a**$^+$**:** (a) ^{1}H-NMR, (b) COSY, and (c) NOESY.

(a)

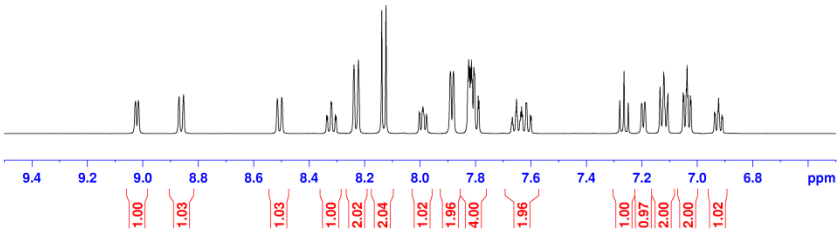

(b)

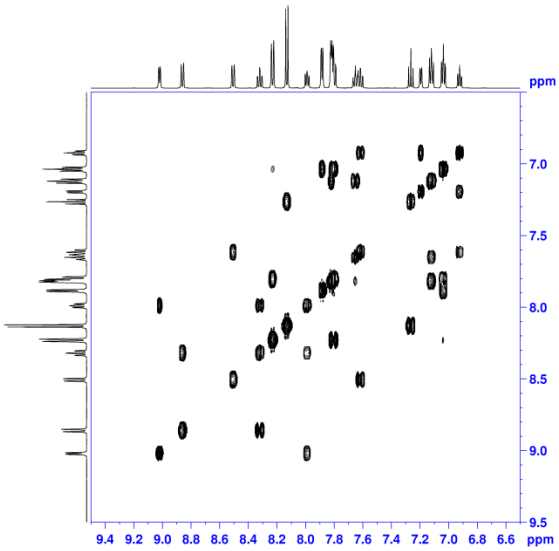

UNIVERSITAT ROVIRA I VIRGILI
SECOND-ROW TRANSITION-METAL COMPLEXES RELEVANT TO CO2 REDUCTION AND WATER OXIDATION
Takashi Ono
DL:T 1108-2014

(c)

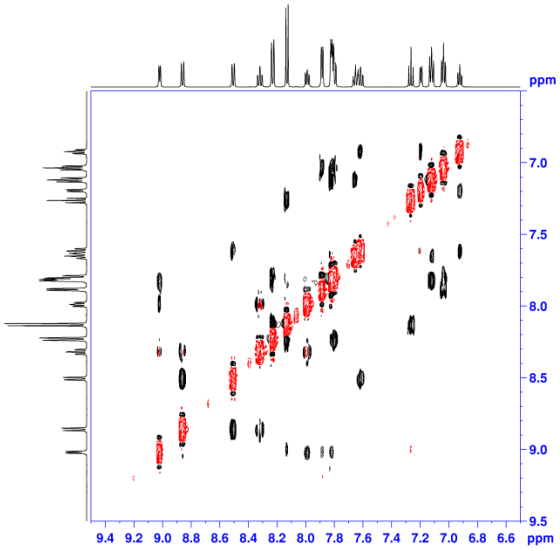

Figure S8. 1D and 2D NMR spectra (500 MHz, 298K, Acetone-d_6) for complex **6a**$^+$ **:** (a) ^{1}H-NMR, (b) COSY, and (c) NOESY.

(a)

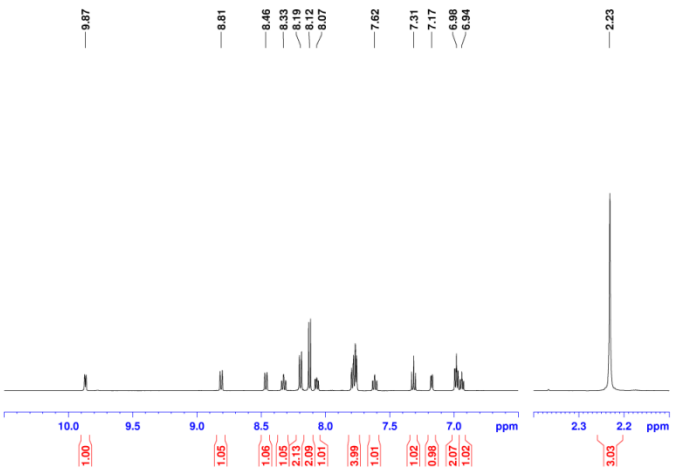

(b)

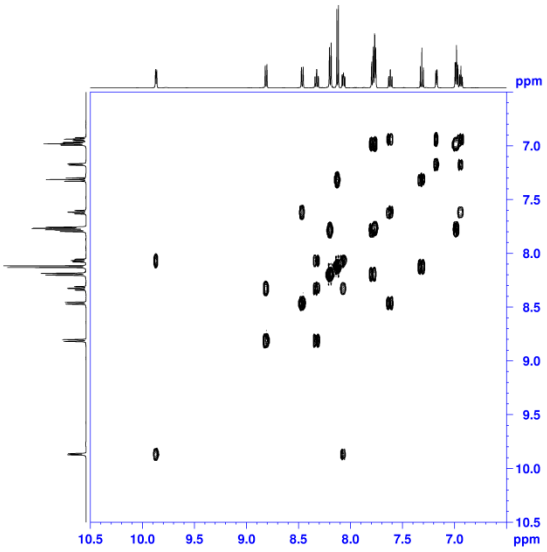
ppm
7.0
7.5
8.0
8.5
9.0
9.5
10.0
10.5
10.5 10.0 9.5 9.0 8.5 8.0 7.5 7.0
ppm

(c)

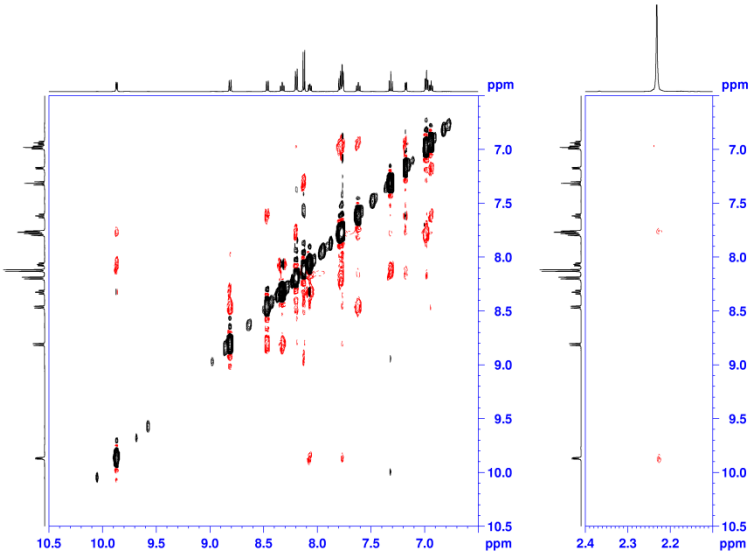
ppm
7.0
7.5
8.0
8.5
9.0
9.5
10.0
10.5
10.5 10.0 9.5 9.0 8.5 8.0 7.5 7.0
ppm
2.4 2.3 2.2
ppm

Figure S9. ^{1}H NMR spectra (500 MHz, 298K, MeOD-d_4) for intermediate species **2a**$^{+}$

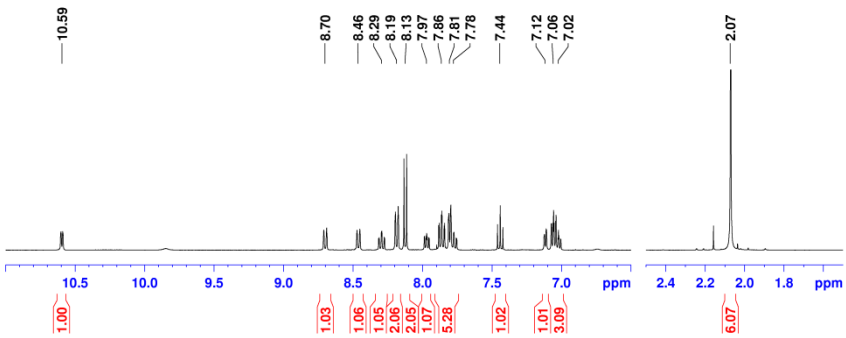

Figure S10 . ^{1}H NMR spectra (500 MHz, 298K, MeOD-d_4) for intermediate species **2b**$^{+}$

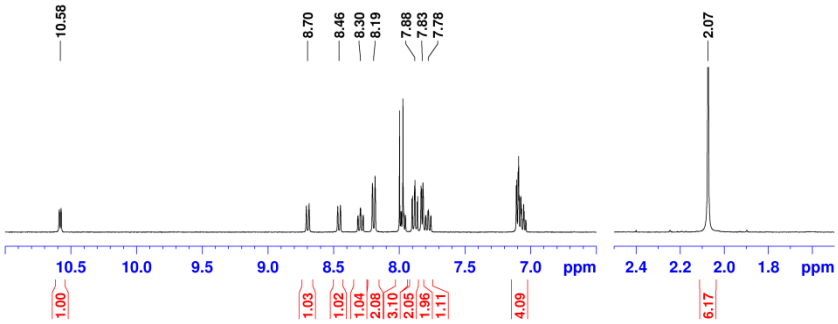

S2. MS:

Figure S11 . ESI-MS spectra of **4a**$^{2+}$

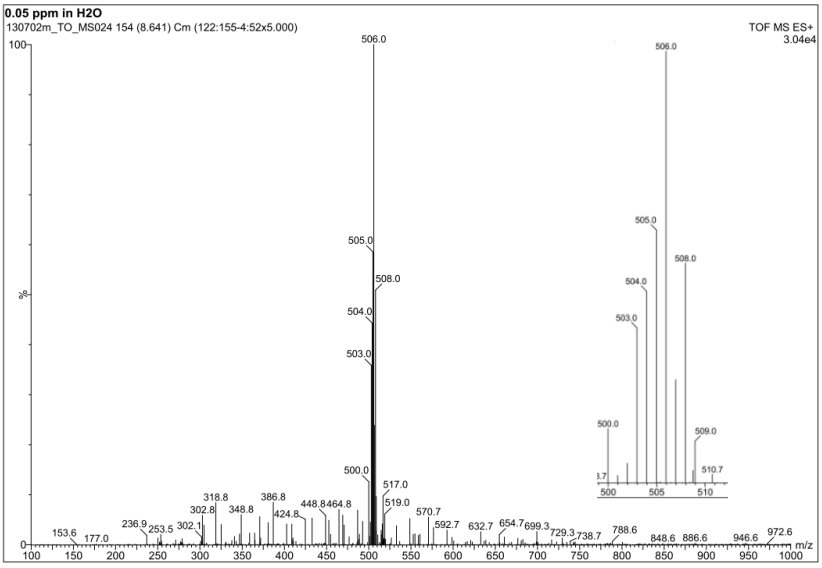

Figure S12 . ESI-MS spectra of **4b**$^{2+}$

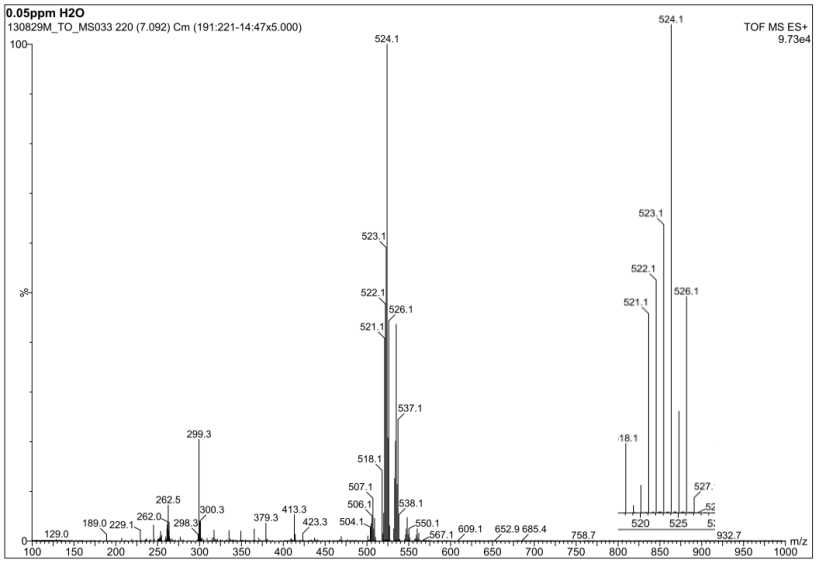

UNIVERSITAT ROVIRA I VIRGILI
SECOND-ROW TRANSITION-METAL COMPLEXES RELEVANT TO CO2 REDUCTION AND WATER OXIDATION
Takashi Ono
DL:T 1108-2014

S3. X-ray:

Table S1. Crystal data for **1a** and **1b**.

	1a		**1b**	
Empirical formula	$C_{20}H_{23}ClN_2O_2RuS_2$		$C_{20}H_{22}ClFN_2O_2RuS_2$	
Formula weight	524.04		542.04	
Temperature	100(2) K		100(2) K	
Wavelength	0.71073 Å		1.54178 Å	
Crystal system	Hexagonal		Monoclinic	
Space group	P6(5)		P2(1)/c	
Unit cell dimensions	a = 9.5162(2) Å	α= 90.00°	a = 15.7897(4) Å	α= 90.00°
	b = 9.5162(2) Å	β = 90.00°	b = 14.3763(4) Å	β = 103.8870(10)°
	c = 38.7539(10) Å	γ = 120.00°	c = 9.4774(3) Å	γ = 90.00°
Volume	3039.30(12) $Å^3$		2088.46(10) $Å^3$	
Z	6		4	
Density (calculated)	1.718 Mg/m^3		1.724 Mg/m^3	
Absorption coefficient	1.131 mm^{-1}		9.374 mm^{-1}	
F(000)	1596		1096	
Crystal size	0.20 x 0.20 x 0.20 mm^3		0.13 x 0.06 x 0.02 mm^3	
Theta range for data collection	1.05 to 1.05°		2.88 to 67.36°	
Index ranges	-12 <=h<=13 ,-13 <=k<=12 ,-52 <=l<=54		-18 <=h<=15 ,-15 <=k<=16 ,-10 <=l<=10	
Reflections collected	5438		11110	
Independent reflections	5437 [R(int) = 0.0222]		3354 [R(int) = 0.0270]	
Completeness to	theta = 30.05°, 0.946 %		theta = 67.36°, 89.4%	
Absorption correction	Empirical		Empirical	
Max. and min. transmission	0.8054 and 0.8054		0.8347 and 0.3754	
Refinement method	Full-matrix least-squares on F^2		Full-matrix least-squares on F^2	
Data / restraints / parameters	5438 / 197 / 258		3354 / 0 / 266	
Goodness-of-fit on F^2	1.321		1.096	
Final R indices [I>2sigma(I)]	R1 = 0.0206, wR2 = 0.0590		R1 = 0.0286, wR2 = 0.0776	
R indices (all data)	R1 = 0.0206, wR2 = 0.0590		R1 = 0.0287, wR2 = 0.0777	
Largest diff. peak and hole	0.783 and -0.511 $e.Å^{-3}$		0.865 and -0.758 $e.Å^{-3}$	

Table S2. Crystal data for **[4b](OTf)1.4(PF6)0.6** and **[5b](PF6)·Et2O**.

	[4b](OTf)$_{1.4}$(PF$_6$)$_{0.6}$		**[5b](PF$_6$)·Et$_2$O**	
Empirical formula	$C_{27.40}H_{20}F_{8.80}N_4O_{5.20}P_{0.60}RuS_{1.40}$		$C_{35}H_{34}F_6N_5OPRu$	
Formula weight	820.21		786.71	
Temperature	100(2) K		100(2) K	
Wavelength	0.71073 Å		0.71073 Å	
Crystal system	Orthorhombic		Monoclinic	
Space group	Pbca		P2(1)/c	
Unit cell dimensions	a = 15.701(2) Å	α = 90.00°	a = 14.5655(8) Å	α = 90.00°
	b = 11.5742(18) Å	β = 90.00°	b = 16.2571(10) Å	β = 115.194(2)°
	c = 32.908(5) Å	γ = 90.00°	c = 15.2796(9) Å	γ = 90.00°
Volume	5980.4(16) Å^3		3273.9(3) Å^3	
Z	8		4	
Density (calculated)	1.822 Mg/m^3		1.596 Mg/m^3	
Absorption coefficient	0.757 mm^{-1}		0.600 mm^{-1}	
F(000)	3269		1600	
Crystal size	0.25 x 0.10 x 0.10 mm^3		0.15 x 0.15 x 0.04 mm^3	
Theta range for data collection	1.24 to 29.58°		1.55 to 27.66°	
Index ranges	-12 <=h<=21 ,-16 <=k<=14 ,-42 <=l<=45		-18 <=h<=19 ,-21 <=k<=21 ,-19 <=l<=19	
Reflections collected	59697		30521	
Independent reflections	8365 [R(int) = 0.0806]		7462 [R(int) = 0.0368]	
Completeness to	theta =29.58°, 99.8%		theta =27.66°, 97.899994%	
Absorption correction	Empirical		Empirical	
Max. and min. transmission	0.9281 and 0.8333		0.9764 and 0.9153	
Refinement method	Full-matrix least-squares on F^2		Full-matrix least-squares on F^2	
Data / restraints / parameters	8365 / 395 / 613		7462 / 1605 / 733	
Goodness-of-fit on F^2	1.788		1.042	
Final R indices [I>2sigma(I)]	R1 = 0.0723, wR2 = 0.2526		R1 = 0.0637, wR2 = 0.1830	
R indices (all data)	R1 = 0.0896, wR2 = 0.2608		R1 = 0.0865, wR2 = 0.2080	
Largest diff. peak and hole	1.992 and -2.046 e.Å^{-3}		3.295 and -3.569 e.Å^{-3}	

UNIVERSITAT ROVIRA I VIRGILI
SECOND-ROW TRANSITION-METAL COMPLEXES RELEVANT TO CO2 REDUCTION AND WATER OXIDATION
Takashi Ono
DL:T 1108-2014

S4. UV-vis:

Figure S13. Top: Acid-base spectrophotometric titration of **4a**$^{2+}$ in 0.1 M H_3PO_4/NaH_2PO_4 buffer. The pH of the solution has been varied by adding drops of 4 M NaOH. pH changes: 3.86, 4.15, 4.24, 4.40, 4.66, 4.96, 5.24, 5.53, 5.81, 6.07 Bottom: Plots for the calculation of the pK_a value. pK_a =4.9

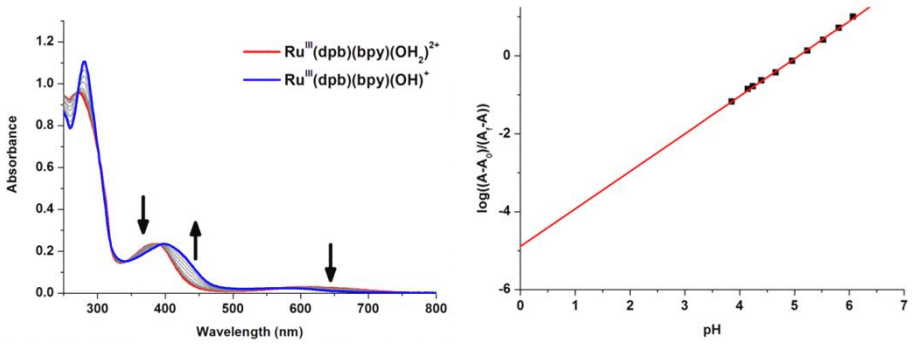

Figure S14. Top: Acid-base spectrophotometric titration of **4b**$^{2+}$ in 0.1 M H_3PO_4/NaH_2PO_4 buffer. The pH of the solution has been varied by adding drops of 4 M NaOH. pH changes: 3.69, 4.21, 4.60, 5.03, 5.40, 5.77, 6.08. Bottom: Plots for the calculation of the pK_a value. pK_a =4.8

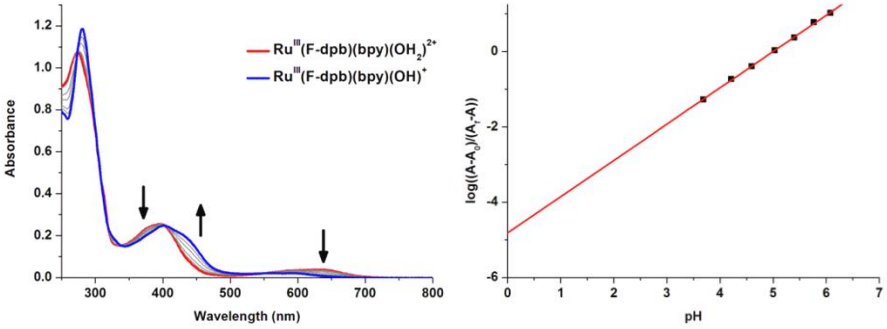

S5. Electrochemistry:

Figure S15. Cyclic voltammograms of **1b** in 0.1 M CH_2Cl_2-$TBAPF_6$ without DMSO (—) and with added DMSO (—). Inset shows differential pulse voltammograms. Glassy carbon working electrode, Pt disk counter electrode and SSCE reference electrode. Scan rate 100 mV s^{-1}

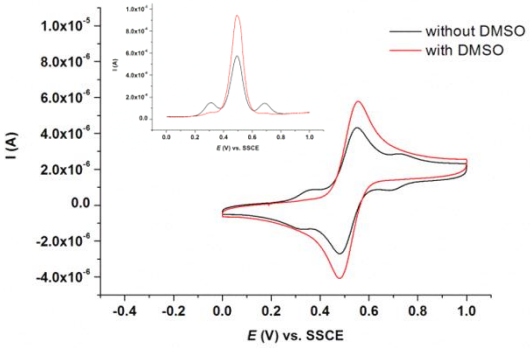

Figure S16. CVs and DPVs of (a) **3a** (0.25 mM), (b) **3b** (0.50 mM), (c) **5a**$^+$ (0.25 mM), and (d) **6a**$^+$ (0.25 mM) in 0.1 M CH_2Cl_2-$TBAPF_6$. Glassy carbon working electrode, Pt disk counter electrode and SSCE reference electrode. Scan rate 100 mV s^{-1}

(a)

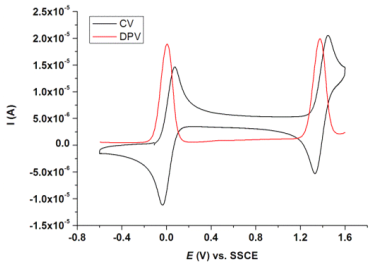

(b)

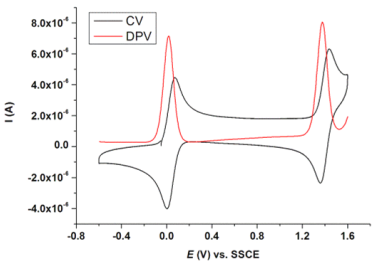

(c)

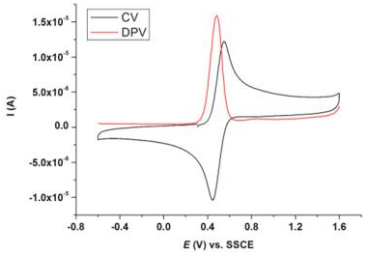

(d)

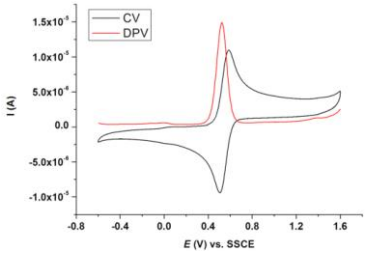

UNIVERSITAT ROVIRA I VIRGILI
SECOND-ROW TRANSITION-METAL COMPLEXES RELEVANT TO CO2 REDUCTION AND WATER OXIDATION
Takashi Ono
DL:T 1108-2014

Figure S17. CVs (left) and SWVs (right) of complex **4b2+** (0.25 mM), (a) at pH 1 in 0.1 M aqueous triflic acid solution, and (b) at pH 7 in 0.1 M phosphate buffer. Glassy carbon working electrode, Pt disk counter electrode and Hg/Hg2SO4 reference electrode, and potentials were converted to vs. SSCE. Scan rate 100 mV s-1 for CV, frequency 15 s-1 for SWV.

(a)

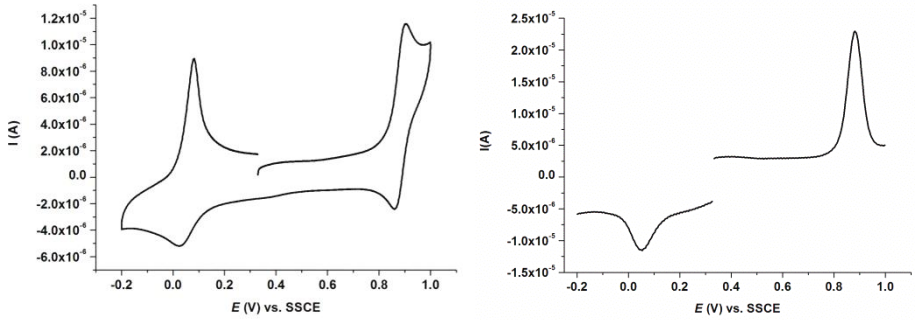

(b)

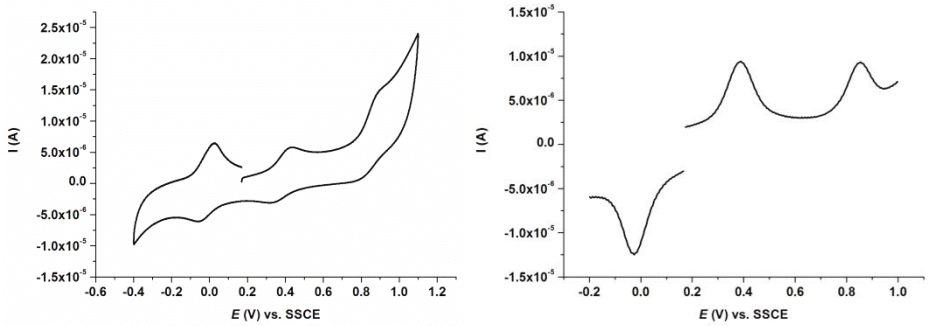

Figure S18. Cyclic voltammograms (CV) in the presence(—) and absence(—) of complex **4b**$^{2+}$ (0.25 mM), (a) at pH 1 in 0.1 M aqueous triflic acid solution, and (b) at pH 7 in 0.1 M phosphate buffer. Glassy carbon working electrode, Pt disk counter electrode and Hg/Hg_2SO_4 reference electrode and potentials were converted to vs. SSCE. Scan rate 100 mV s^{-1}.

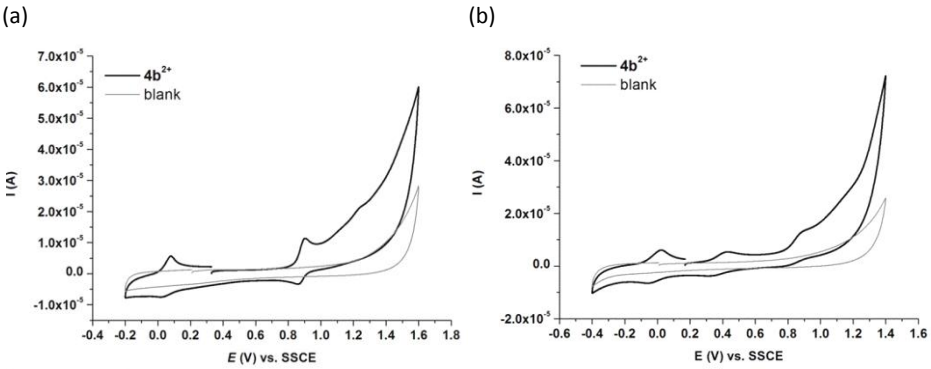

Figure S19. Plot of i_{cat} at 0.91 V (vs. SSCE) with respect to scan rate at [**4a**$^{2+}$]= 0.04 mM and [BzOH] = 4 mM. Catalytic current are practically independent of the scan rate.

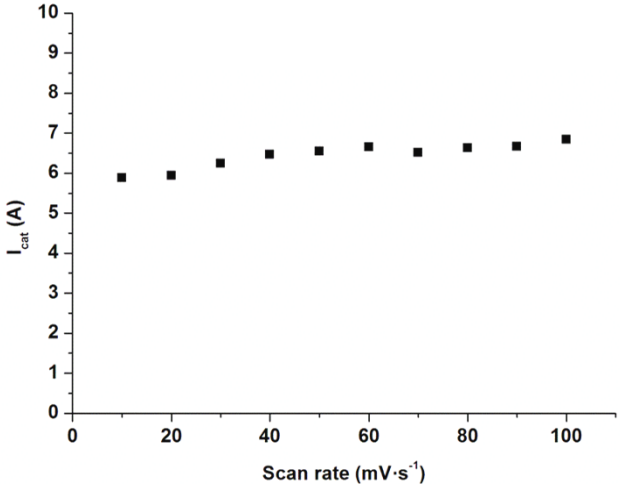

UNIVERSITAT ROVIRA I VIRGILI
SECOND-ROW TRANSITION-METAL COMPLEXES RELEVANT TO CO2 REDUCTION AND WATER OXIDATION
Takashi Ono
DL:T 1108-2014

Figure S20. Top: Cyclic voltammograms (CV) of complex **4a**$^{2+}$ at different concentrations (0.02-0.06 mM) in the presence of BzOH (0.2 mM) in 0.1 M aqueous triflic acid solution at pH 1 Glassy carbon working electrode, Pt disk counter electrode and Hg/Hg_2SO_4 reference electrode and potentials were converted to vs. SSCE. Scan rate 20 mV s^{-1}. Bottom: Plots of i_{cat} at 0.91 V (vs. SSCE) with respect to [Ru] (mM) at different concentrations of BzOH (0.2-0.6 mM).

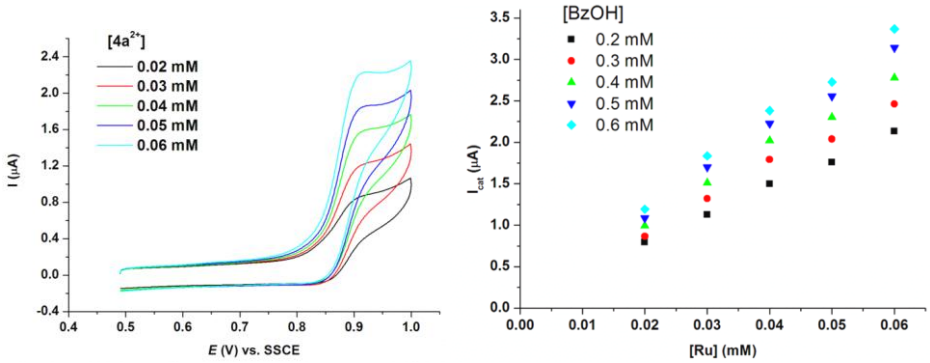

Figure S21. Top: Cyclic voltammograms (CV) of complex **4a**$^{2+}$ (0.04 mM) in 0.1 M aqueous triflic acid solution at pH 1, showing the increase of the catalytic current upon additions of BzOH (0.2-0.6 mM). Glassy carbon working electrode, Pt disk counter electrode and Hg/Hg_2SO_4 reference electrode and potentials were converted to vs. SSCE. Scan rate 20 mV s^{-1}. Bottom: Plots of i_{cat}/i_{p0} at 0.91 V (vs. SSCE) with respect to $[BzOH]^{1/2}$ at different concentrations of **4a**$^{2+}$ (0.02-0.06 mM).

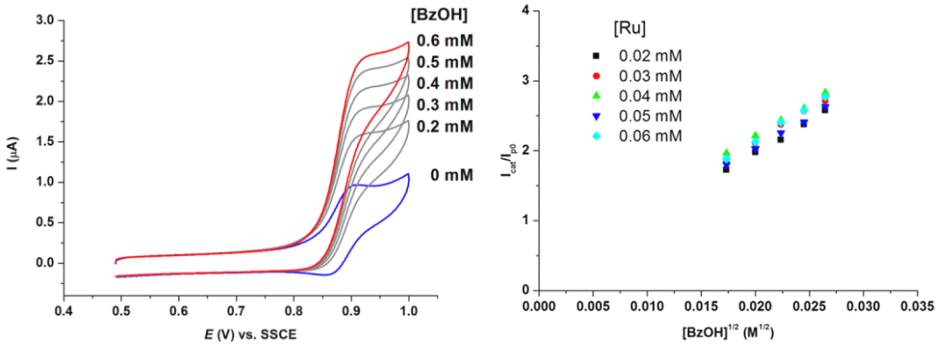

UNIVERSITAT ROVIRA I VIRGILI
SECOND-ROW TRANSITION-METAL COMPLEXES RELEVANT TO CO2 REDUCTION AND WATER OXIDATION
Takashi Ono
DL:T 1108-2014

Chapter VII

New Dinuclear Ruthenium Polypyridyl Complexes Containing Anionic Dpb Ligand: Synthesis, Characterization and Water Oxidation Reaction

'Ru-Hbpp' WOC analogue

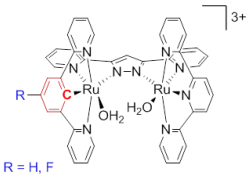

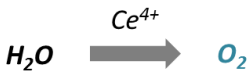

Table of Contents

UNIVERSITAT ROVIRA I VIRGILI
SECOND-ROW TRANSITION-METAL COMPLEXES RELEVANT TO CO2 REDUCTION AND WATER OXIDATION
Takashi Ono
DL:T 1108-2014

VII.1. Abstract

New non-symmetric dinuclear ruthenium complexes containing an anionic tridentate *dpb*$^-$ (2,6-di(pyridin-2-yl)benzen-1-ide), *trpy* (2,2';6',2''-terpyridine) and the dincleating *bpp*$^-$ (3,5-bis(2-pyridyl)pyrazolate) ligands with the general formula {[Ru(R-dpb)][Ru(trpy)](μ-bpp)(μ-X)}$^{n+}$ (R = H: **a**, F: **b**; X = DMSO (**3**$^{2+}$), X = Cl (**5**$^{2+}$) OMe-OH$_2$/OH-OH$_2$ (**6**$^{2+}$)) are reported. These complexes and their synthetic intermediates *in*,*out*-{[Ru(R-dpb)Cl][Ru(trpy)Cl](μ-bpp)}$^+$ (R = H (**4a**$^+$) and R = F (**4b**$^+$)) have been characterized by means of structural (for **3a**$^{2+}$, **3b**$^{2+}$, **4a**$^+$, **5a**$^{2+}$, **6b-X**$^{2+}$ (X = OMe-OH$_2$), and **6b-X**$^{2+}$ (X = OH-OH$_2$)) and electrochemical techniques. The bridged DMSO complexes **3**$^{2+}$ which have a formal oxidation state of Ru$_2$(II,II) were additionally characterized by 1D and 2D NMR spectroscopies. The bis-aqua species **7a**$^{3+}$ and **7b**$^{3+}$ can be smoothly *in-situ* formed by the dissolution of **6a-X**$^{2+}$ and **6b-X**$^{2+}$ in acidic solution at pH 1 and their redox properties are investigated by electrochemical techniques. The bis-aqua species shows four reversible 1e$^-$ redox processes within the potential ranges of -0.2 to 1.2 V (vs SSCE) at pH 1. Each redox species is tentatively assigned by the Pourbaix diagram. The observed electrocataytic wave at an onset potential of *ca*. 1.4 V is associated with the formation of further single 2e$^-$ oxidized Ru$_2^{V,V}$ species ($E_{1/2}$ ≈ 1.55 V) determined by square wave voltammetry technique. Using (NH$_4$)$_2$Ce^{IV}(NO$_3$)$_6$ (100 equiv.) as an oxidant, **7a**$^{3+}$ have been shown to catalytically oxidize water to molecular oxygen with a concomitant formation of carbon dioxide (O$_2$/CO$_2$ = 54/46) with TONs of 5.7 for O$_2$ and 4.8 for CO$_2$. The fluoro-substituted species **7b**$^{3+}$ showed better catalytic performance with TONs of 7.7 for O$_2$ and 3.4 for CO$_2$ (O$_2$/CO$_2$ = 69/31).

VII.2. Introduction

World energy consumption and subsequently caused global warming are becoming serious issues due to increasing human activity.[1-2] These problems could be solved by artificial photosynthesis which produces the renewable and clean energy source, being the alternative of fossil fuels. Water oxidation reaction that generates

UNIVERSITAT ROVIRA I VIRGILI
SECOND-ROW TRANSITION-METAL COMPLEXES RELEVANT TO CO2 REDUCTION AND WATER OXIDATION
Takashi Ono
DL:T 1108-2014

molecular oxygen is a half-reaction of artificial photosynthesis, which accumulates protons for hydrogen production in the other half-reaction.[3] In the last decade, many studies have been done for developing molecular catalysts capable of oxidizing water[4-5] by mimicking the oxygen-evolving complex (OEC) in photosystem (PSII), though it is still underway of finding efficient catalysts because of high thermodynamic demand and kinetic complexity of the reaction.

In 2004, our group have shown that the dinuclear 'Ru-*Hbpp*' catalyst is capable of catalytically oxidizing water to molecular oxygen with turnover number (TON) of 18.6.[6-8] Later on, Thummel *et al*. also found that dinuclear Ru complexes containing bis-tridentate pyridazine-based ligand worked as water oxidation catalysts (WOCs) (Figure 1).[9-10] However, these WOCs based on nitrogen donor ligand requires strong oxidant such as $(NH_4)_2Ce^{IV}(NO_3)_6$ in order to reach high oxidation state whose species can oxidize water. On the other hand, Sun *et al*. have recently focused on the use of ligands containing anionic group such as carboxylate for both mono-[11-15] and dinuclear[16-18] Ru complexes. It has been demonstrated that the carboxylate groups play a very significant role in the electronic properties of the corresponding complexes through σ-donating effect. This approach resulted in considerably lowered redox potentials and showed high catalytic performance. For instance, carboxylate modified dinuclear complex resulted in considerably high TON of 10000[17] (Figuer 1) with respect to the Thummel's one[10] (TON of *ca.* 600) at pH 1 and furthermore it has been shown that the reaction can be driven by $[Ru(bpy)_3]^{2+}$ type of photosensitizer due to the lowered redox potential.[17-18]

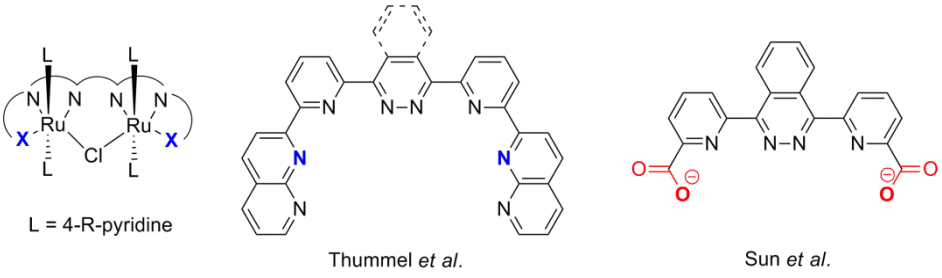

Figure 1. Dinuclear complexes reported by Thummel *et al*. and Sun *et al*..

In Chapter VI, we have shown that anionic *dpb*$^-$ (2,6-di(pyridin-2-yl)benzen-1-ide) ligand (Figure 2) enables the corresponding mononuclear complexes to generate Ru(V)=O species at significantly low redox potential and it is efficient electrocatalyst for oxidation of organic substrate such as benzyl alcohol. This result prompted us to develop dinuclear 'Ru-*Hbpp*' analogues containing anionic *dpb*$^-$ ligand. Herein, we report the synthesis and characterization of new dinuclear complexes containing *dpb*$^-$ ligand. Further, we examined their catalytic performance towards chemical water oxidation.

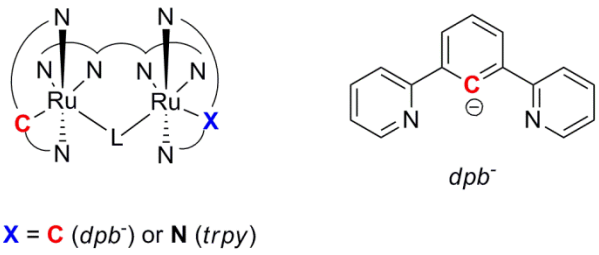

Figure 2. Anionic tridentate *dpb*$^-$ (2,6-di(pyridin-2-yl)benzen-1-ide) ligand.

VII.3. Results and Discussion

VII.3.1. Synthesis, Structure and Redox Properties

Synthesis

All synthetic procedures for the dinuclear complexes are shown in Scheme 1. In order to construct a dinuclear structure of mononuclear *dpb*$^-$ complex, we have used *Hbpp* (=2,2'-(1H-pyrazole-3,5-diyl)dipyridine) ligand as the dinucleating ligand. Refluxing a 2/1 mixture of **1a**/*Hbpp* in the presence of NEt_3 in MeOH, followed by the precipitation by KPF_6 yielded the dinuclear complex **2**$^+$. The complex **2**$^+$ is highly air-sensitive in solution and even in the solid state toward the metal-centred oxidation so that it could be never obtained as the oxidation state of Ru_2(II,II), but rather a mixture with a higher oxidation states. Because of the high thermodynamic stability of the DMSO bridge motif, it was unsuccessful to replace it either by the bridged chlorido or

UNIVERSITAT ROVIRA I VIRGILI
SECOND-ROW TRANSITION-METAL COMPLEXES RELEVANT TO CO2 REDUCTION AND WATER OXIDATION
Takashi Ono
DL:T 1108-2014

Scheme 1. Reaction scheme for the synthesis of dinuclear complexes containing anionic *dpb*$^-$ ligand

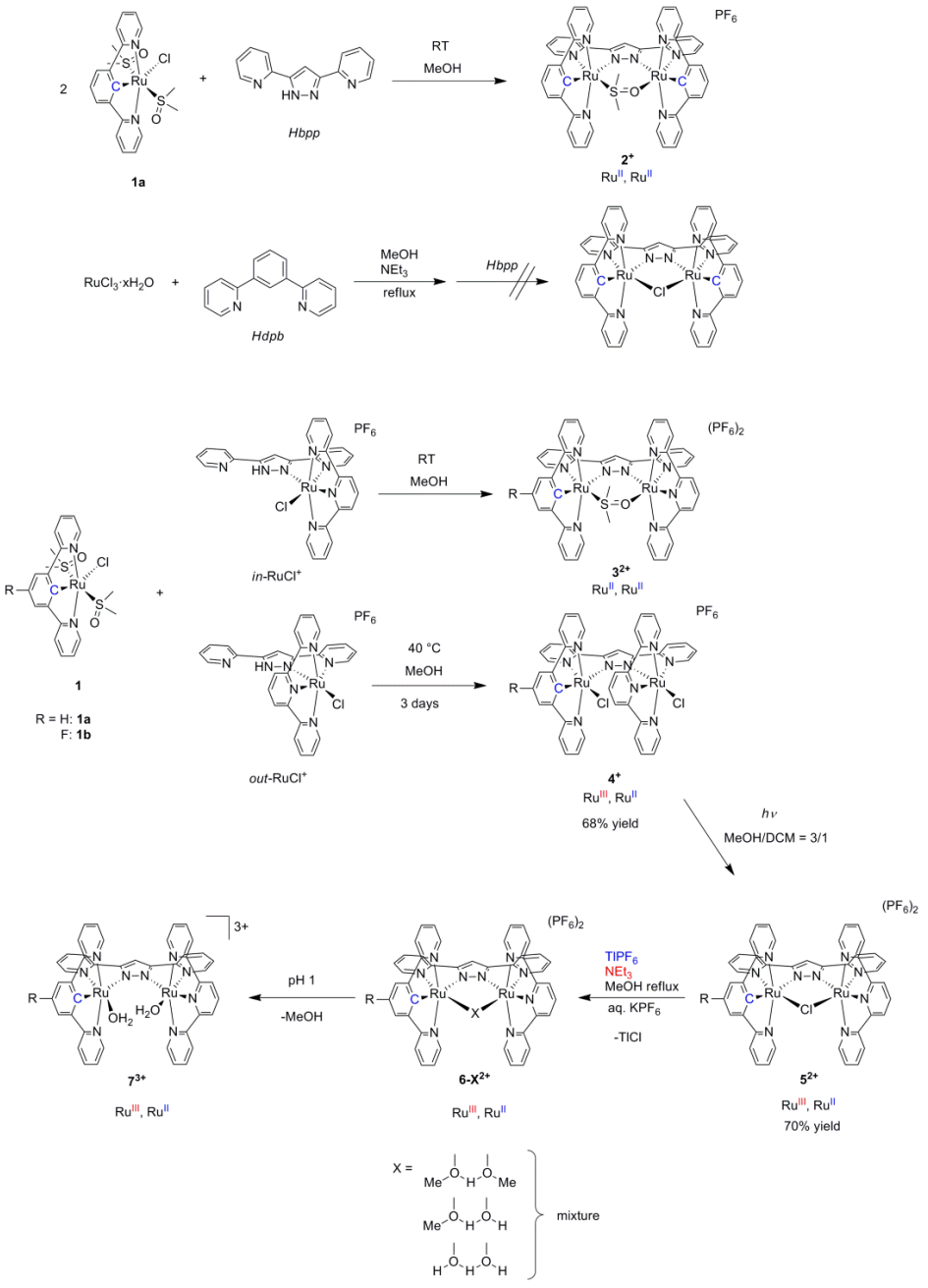

acetato ligands which are the synthetic precursors of the dinuclear Ru-*Hbpp* aqua complex.[6] In order to avoid the undesirable role of DMSO, other procedure was applied, where $RuCl_3$ and *Hdpb* ligand was refluxed in the presence of excess NEt_3 prior to the addition of 0.5 equivalent of *Hbpp*. However, this resulted in the complex mixture and none of new species were isolated and identified.

The terms *in* and *out* used in this chapter indicate whether the monodentate ligand is oriented inside or outside, respectively, of the centre of the *Hbpp* or bpp^- ligand.

Dinuclear complexes containing dpb^- ligand on one metal centre and *trpy* ligand on the other were successfully synthesized by treating dpb^- complex **1a** and *Hbpp-trpy* complexes, *in*-, and *out*-$[Ru(trpy)(Hbpp)Cl]^+$, reported earlier from our group.[19] When **1a** was treated with *in*-$[Ru(trpy)(Hbpp)Cl]^+$, the bridged DMSO complex $\mathbf{3a}^{2+}$ was smoothly formed at room temperature. On the other hand, the reaction of **1a** with *out*-$[Ru(trpy)(Hbpp)Cl]^+$ requires elevated temperature and the products obtained depend on the reaction temperature. When the reaction was carried out under reflux condition in MeOH, the bridged DMSO complexes $\mathbf{3a}^{2+}$ was selectively obtained, whereas under milder reaction conditions (at 40 °C for 3 days), the other species $\mathbf{4a}^+$ was isolated as main product. Its ESI-MS spectrum (Figure S5d) showed a parent peak at m/z = 959.0 corresponding to the bis-chlorido species, $\{[Ru^{III}(dpb)(Cl)][Ru^{II}(trpy)(Cl)](\mu\text{-bpp})\}^+$. From Its X-ray structure discussed later, the conformation of the two Cl ligands was unambiguously determined as that the Cl ligand bonded to Ru(dpb) moiety directs to the inside of the centre point of bpp^- lignad and the other Cl ligand bonded to Ru(trpy) moiety is *out* positioned.

The varieties of the reactivity can be explained by the followings; a) different degrees of the nucleophilicity of the N atoms (pyridyl and pyrazolyl) of the *Hbpp-trpy* monomer towards the incoming dpb^- monomer **1a**, b) a stability of the coordinated *in*-positioned DMSO ligand, and c) a lability of the Cl ligand bonded to a Ru(II) metal centre. A proposed mechanism is shown in Scheme 2. The higher nucleophilicity of pyridyl nitrogen on *Hbpp* ligand and a labile DMSO ligand in **1a** would generate *in*-positioned DMSO species **A** and **B,** both of which are not observed. The intermediate

UNIVERSITAT ROVIRA I VIRGILI
SECOND-ROW TRANSITION-METAL COMPLEXES RELEVANT TO CO2 REDUCTION AND WATER OXIDATION
Takashi Ono
DL:T 1108-2014

species **A** further would undergo a dissociation of the Cl ligand to form **3a**$^{2+}$ due to both the lability of the Cl ligand bonded to Ru(II) metal centre and the thermodynamic stability of the bridged DMSO motif. By contrast, it can be considered that the DMSO ligand in **B** would suffer from a steric repulsion from *in*-positioned *trpy* ligand and thus, be replaced by less hindered Cl ligand to form **4a**, followed by oxidation to a stable **4a**$^{+}$ due to its low redox potential. At higher temperature, a dissociation of the Cl ligand in **B** and/or **4a** would take place to form the DMSO bridged complex **3a**$^{2+}$.

Scheme 2. Plausible reaction mechanism of **1a** with *in*- and *out*-[Ru(trpy)(Hbpp)Cl]$^{+}$

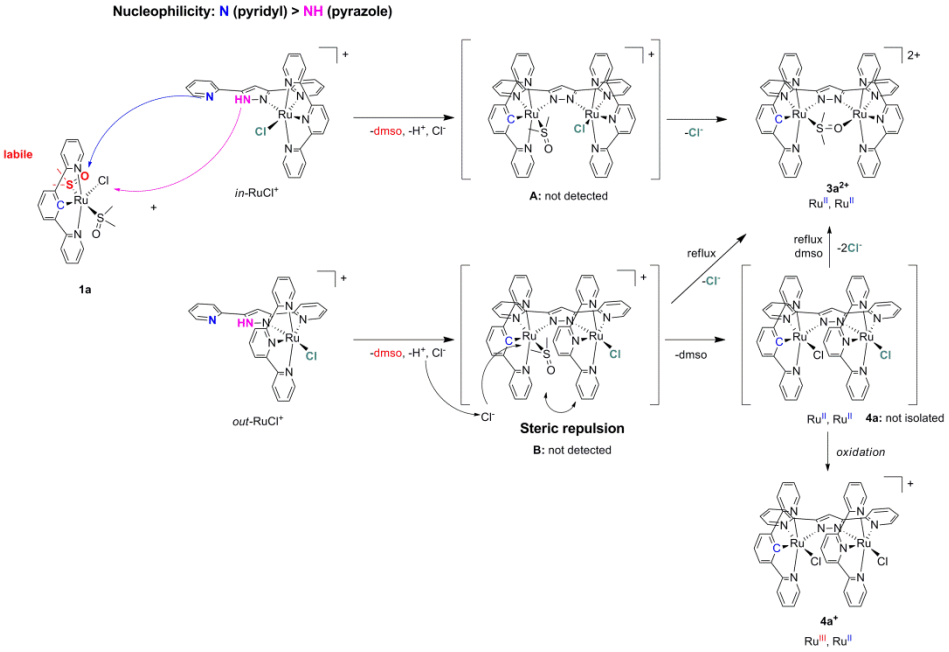

The formation of the μ-chlorido complex **5a**$^{2+}$ was achieved by light irradiation of **4a**$^{+}$. Such reactivity was observed previously for the synthesis of the *trpy*-*trpy* analogue {[Ru(trpy)]$_2$(μ-bpp)(μ-Cl)}$^{2+}$.[6] The Cl ligand in **5a**$^{2+}$ was removed by Tl^{+} as TlCl in the presence of slightly excess amount of NEt$_3$ in MeOH to form **6a-X**$^{2+}$. The bridged ligand X in **6a-X**$^{2+}$ was supposed to be a mixture of the ligands shown in Scheme 1 determined by ^{1}H NMR studies, mass spectrometry, elemental analysis, and X-ray diffraction

analyses, which will be discussed later. Similarly, the complexes **3b**$^{2+}$, **4b**$^{+}$, **5b**$^{+}$, and **6b**$^{2+}$ containing fluoro-substituted *dpb*$^{-}$ (*F-dpb*$^{-}$) ligand were synthesized using **1b** as the precursor.

Finally, the dissolution of **6a**$^{2+}$ and **6b**$^{2+}$ in aqueous solution at pH 1 (0.1 M triflic acid) resulted in the *in-situ* formation of the bis-aqua species **7a**$^{3+}$ and **7b**$^{3+}$, respectively.

Characterization of the dinuclear complexes

The new *dpb*$^{-}$-*dpb*$^{-}$ and *dpb*$^{-}$-*trpy* dinuclear complexes have been characterized by the usual spectroscopic, structural and electrochemical techniques.

NMR spectroscopy

All the dinuclear complexes except the bridged DMSO complexes **3a**$^{2+}$ and **3b**$^{2+}$ showed paramagnetic species. It was unsuccessful to obtain any diamagnetic species by the commonly used reducing agents such as NEt_3 and ascorbic acid. Although some of complexes displayed diamagnetic species using zinc as a reductant, none of them were identified due to the complex mixture with undesired reduced species with the exception of **2**$^{+}$. The diamagnetic complexes **2**$^{+}$, **3a**$^{2+}$ and **3b**$^{2+}$ were characterized by 1D and 2D NMR spectroscopies (Figure 3-4, Figure S1-S3 in Supporting Information)

The ^{1}H NMR spectrum of the bridged DMSO complex **2**$^{+}$ in the presence of zinc in acetone-d_6 (Figure 3a) shows non-symmetric pattern for the chelating *bpp*$^{-}$ ligand backbone, indicative of different coordination environment of each metal centre. This is associated with the existence of one coordinated DMSO molecule (δ_H 1.33 ppm) which binds through both oxygen and sulfur atoms between two metal centres. The observed chemical shift of the methyl protons of the DMSO ligand is shifted significantly upfield with respect to free DMSO molecule. This is presumably due to the ring-current effect of the electron-rich phenyl ring of the two *dpb*$^{-}$ ligands. As we will see in the next, a similar but lesser degree of the effect was observed for **3a**$^{2+}$ with 0.2

UNIVERSITAT ROVIRA I VIRGILI
SECOND-ROW TRANSITION-METAL COMPLEXES RELEVANT TO CO2 REDUCTION AND WATER OXIDATION
Takashi Ono
DL:T 1108-2014

ppm downfield (δ_H 1.53 ppm) due to lesser degree of the π-electroic current from the *trpy* ligand with respect to *dpb*$^-$ ligand.

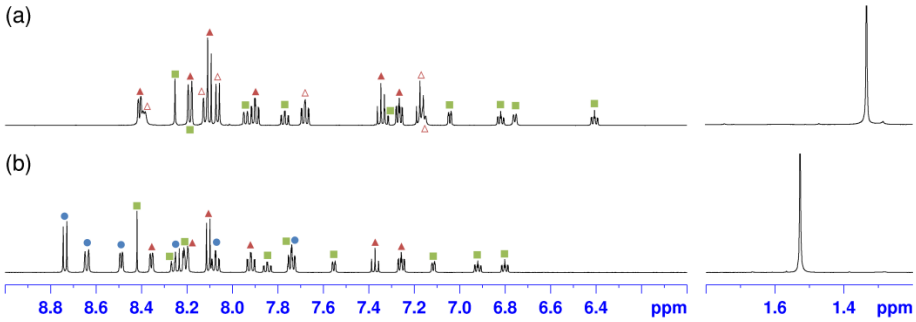

Figure 3. ^{1}H NMR spectrum in acetone-d_6 of (a) **2a**$^+$ (in.the presence of zinc) and (b) **3a**$^{2+}$. ▲: one of the *dpb*$^-$, △: the other *dpb*$^-$, ■: *bpp*$^-$ and ●: *trpy*.

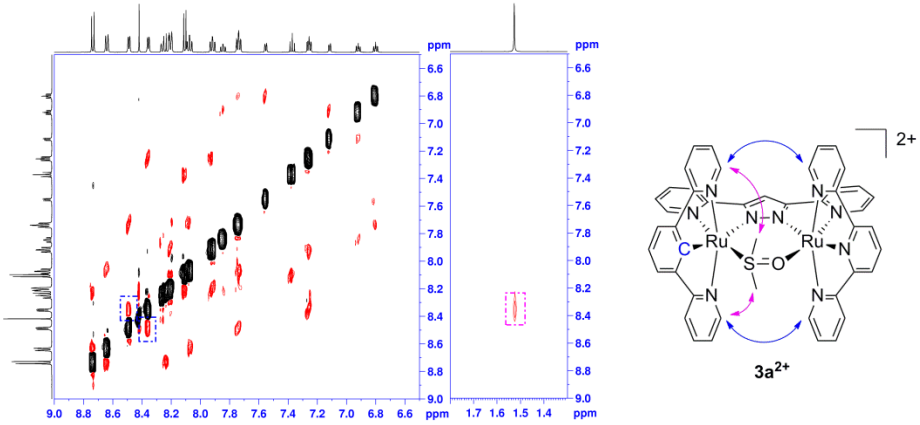

Figure 4. Left: NOESY spectrum of **3a**$^{2+}$ in acetone-d_6. Right: A schematic representation of NOESY correlations of the given protons in **3a**$^{2+}$.

Figure 3b shows a ^{1}H NMR spectrum of **3a**$^{2+}$ in acetone-d_6. It is clear that **3a**$^{2+}$ contains one *dpb*$^{-}$, one *trpy*, one non-symmetric *bpp*$^{-}$ and one coordinated dmso ligands (δ_H 1.53 ppm). As shown in Figure 4, the 2D NOESY spectrum reveals two features; a) a correlation between 6-positions of protons on terminal pyridine rings of *trpy* and 6-positions of protons on pyridine rings of *dpb*$^{-}$, and b) a correlation between methyl protons of the coordinated DMSO and 6-positions of protons on pyridine rings of *dpb*$^{-}$. These points clearly indicate that DMSO ligand is located between two metal centres and is coordinated through S-atom to the metal centre bonded to *dpb*$^{-}$ ligand. As it will be discussed later, the X-ray structure of **3a**$^{2+}$ revealed that the DMSO ligand coordinates to the other metal centre through *O*-coordination, acting as a bridging ligand. Although the other isomer where S atom coordinates to the Ru centre bonded to *trpy* would be possible, only the former was obtained. This can be explained on the basis of HSAB (Hard and Soft Acids and Bases) theory. Strong σ-donating property of *dpb*$^{-}$ ligand weakens the Lewis acidity of the Ru(II) centre with respect to the Ru(II) bonded to *trpy* and thus the DMSO prefers coordination through 'softer base' sulfur atom to Ru(II)-*dpb*$^{-}$ and 'harder base' oxygen atom to Ru(II)-*trpy* .

UNIVERSITAT ROVIRA I VIRGILI
SECOND-ROW TRANSITION-METAL COMPLEXES RELEVANT TO CO2 REDUCTION AND WATER OXIDATION
Takashi Ono
DL:T 1108-2014

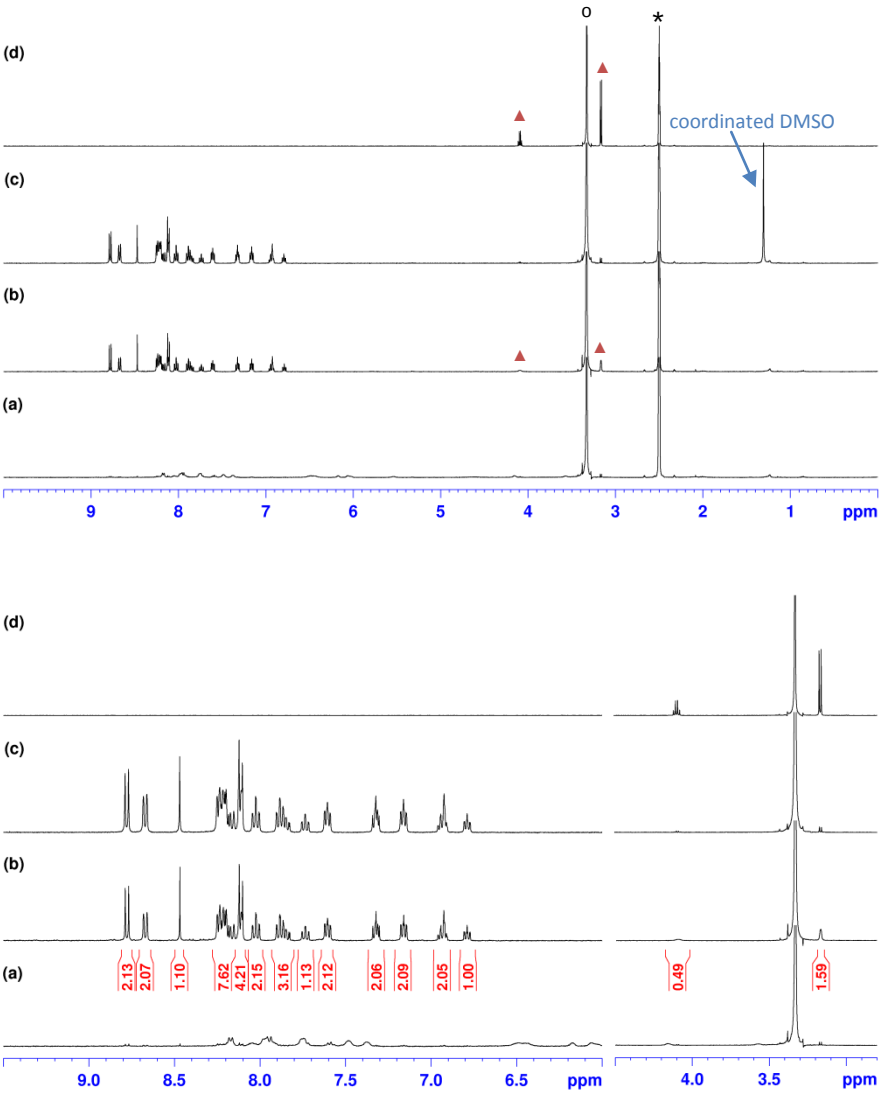

Figure 5. ^{1}H NMR spectra in dmso-d_6 of (a) 10 min (already growing DMSO-d_6 complex), (b) 1 day after dissolving **6a-X**$^{2+}$, (c) isolated bridged dmso complex and (d) free MeOH. Clean transformation of **6a-X**$^{2+}$ into bridged DMSO-d_6 complex along with liberation of free MeOH (bridged dmso complex/free MeOH = 1/0.5). Top: the spectra regions between 10 to 0 ppm, bottom: enlarged views. *: solvent residual peak, o: H_2O, and ▲: free MeOH.

*Characterization of **6a-X**$^{2+}$ and **6b-X**$^{2+}$*

The bridged ligand in **6a-X**$^{2+}$ and **6b-X**$^{2+}$ could be cleanly replaced by DMSO-d_6 ligand in dmso-d_6 solvent at room temperature to form a diamagnetic bridged-DMSO-d_6 complexes along with only one set of new signals corresponding to free MeOH (Figure. 5 and Figure S4). However, it is unclear how the oxidation state is reduced from $Ru^{III}Ru^{II}$ to $Ru^{II}Ru^{II}$. A ratio of formed DMSO-d_6 complexes and free MeOH is about 1/0.5 for both cases, suggesting that half of the bridging ligand in **6-X**$^{2+}$ contains MeOH. As shown in Table 1, the obtained elemental analyses data are in agreement with the values of a 1/1 mixture of the two complexes containing MeO-H-OH/HO-H-OH as the bridged ligands. Additionally, ESI-MS experiments for both complexes were taken in acetonitrile, where the replacement of the bridged ligand X by CH_3CN does not take place within the sample preparation due to the relatively stable bridging motif. As can be seen in Figure 6 and Figure S6, for both complexes the peaks corresponding to $[\overline{Ru\text{-}OMe\ \ Ru}]^{2+}$ species are the parent peaks with small intensities of bridged ligand species. Note, however, that there are additionally MeO-HOMe species although the origins of this species are not known either from the synthesis or during MS measurement.

Table 1. Experimental and calculated values of elemental analysis for the complexes **6a-X**$^{2+}$ and **6b-X**$^{2+}$. The differences between theoretical and experimental values are shown in the parentheses.

		Expt. and theor. values		
		C (%)	H (%)	N (%)
X	**6a-X**$^{2+}$	43.5180	2.6135	10.0858
	MeO-H-OMe	44.52 (-1.00)	3.09 (-0.48)	10.16 (-0.07)
	MeO-H-OH	44.05 (-0.53)	2.96 (-0.35)	10.27 (-0.18)
	HO-H-OH	43.57 (-0.05)	2.83 (-0.22)	10.39 (-0.30)
	1/1 mixture of MeO-H-OH/HO-H-OH	43.81 (-0.29)	2.89 (-0.28)	10.33 (-0.24)
X	**6b-X**$^{2+}$	42.8961	2.7156	9.9015
	MeO-H-OMe	43.89 (-0.99)	2.96 (-0.24)	10.01 (-0.11)
	MeO-H-OH	43.42 (-0.52)	2.83 (-0.11)	10.13 (-0.23)
	HO-H-OH	42.94 (-0.04)	2.70 (+0.02)	10.24 (-0.34)
	1/1 mixture of MeO-H-OH/HO-H-OH	43.18 (-0.28)	2.83 (-0.11)	10.13 (-0.23)

UNIVERSITAT ROVIRA I VIRGILI
SECOND-ROW TRANSITION-METAL COMPLEXES RELEVANT TO CO2 REDUCTION AND WATER OXIDATION
Takashi Ono
DL:T 1108-2014

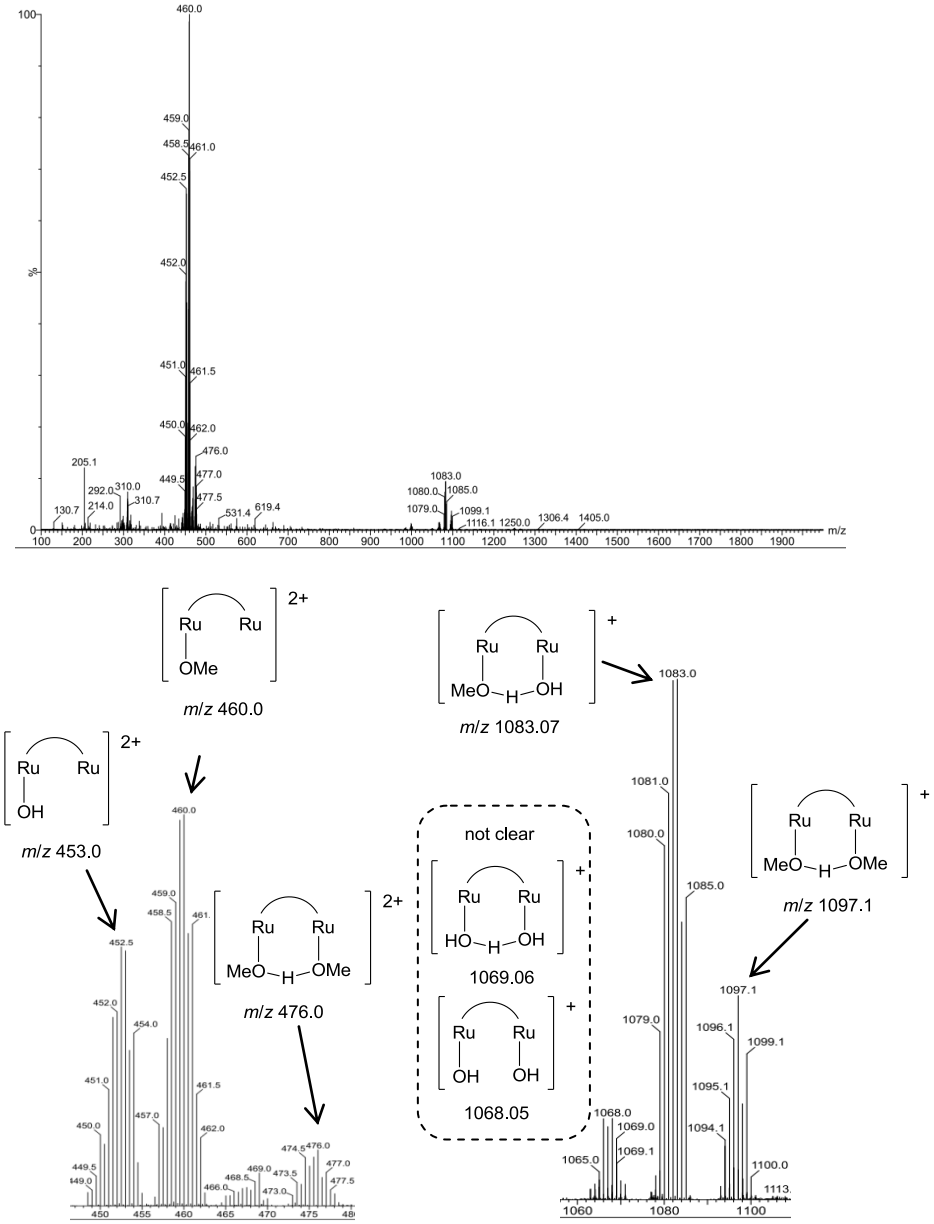

Figure 6. Top: ESI-MS(CH_3CN) spectrum of **6a-X**$^{2+}$. Bottom: Enlarged views of the peaks together with possible structures and their theoretical *m/z* values. *Trpy*, *dpb*$^-$ and *bpp*$^-$ ligands are not shown in their structrues for the sake of simplicity.

Structure

Complexes **3a**$^{2+}$, **3b**$^{2+}$, **4a**$^{+}$, **5a**$^{2+}$, **6b-X**$^{2+}$ (X = MeO-H-OH) and **6b-X**$^{2+}$ (X =HO-H-OH) were successfully characterized by X-ray diffraction analysis. Their Ortep plots are presented in Figure 7. Selected bond lengths, angles and crystallographic parameters are listed in Table 2, and Table S1 in Supporting Information.

Each of the X-ray structures displays the expected geometry where each ruthenium centre coordinates in a distorted octahedral geometry to the tridentate *dpb*$^{-}$ and *trpy* ligands, respectively, in a meridional fashion and is linked by the bridging *bpp*$^{-}$ ligand. The other coordination sites of two Ru centres are occupied either by monodentate chlorido ligands or bridging ligands.

Bond distances and angles of both Ru-*dpb*$^{-}$ and Ru-*trpy* moieties in all the structures obtained here are in typical ranges, whereas bond lengths between Ru atoms and N atoms of *bpp*$^{-}$ ligand are varied with their monodentate or bridged ligands. As a general trend, both Ru1-N3 and Ru1-N4 bonds (2.012(5)-2.231(12) Å) are slightly longer than those for both Ru2-N5 and Ru2-N6 bond distances (2.013(5)-2.13(2) Å), resulting in a narrower bite angle for N3-Ru1-N4 (75.40(7)-78.0(3)°) compared with those for N6-Ru2-N5 (77.69(7)-79.6(8)°). This is in relation mainly to the strong σ-donating property of *dpb*$^{-}$ ligand. In addition, Ru1···Ru2 distances vary from 3.923 to 4.781 Å by accommodating steric environments.

The structure of **3a**$^{2+}$ contains one DMSO ligand acting as a bridging ligand, bonded to Ru-*dpb*$^{-}$ and Ru-*trpy* moieties through sulfur (Ru1-S1: 2.1956(7) Å) and oxygen atoms (Ru2-O1: 2.154(2) Å), respectively. The Ru1-N3 distance at 2.143(2) Å is significantly longer than those for **4a**$^{+}$, **5**$^{2+}$, and **6b**$^{2+}$ due to the *trans* influence of the sulfur atom of the DMSO ligand, as was found for the *S*- bonded Ru(II)-DMSO complexes.[20] The short Ru1-S1 bond length with respect to typical values for the polypyridyl Ru(II)-DMSO complexes[21-22] associated with the clearly elongated S1-O1 bond length (1.515 Å) compared to that in the free dmso molecule (1.472 Å)[20,23] is due to increased degree of back donation from *dpb*$^{-}$-derived electron rich dπ orbital to pπ orbital of the sulfur atom. In addition to this, the elongated S1-O1 bond distance can be also rationalized

UNIVERSITAT ROVIRA I VIRGILI
SECOND-ROW TRANSITION-METAL COMPLEXES RELEVANT TO CO2 REDUCTION AND WATER OXIDATION
Takashi Ono
DL:T 1108-2014

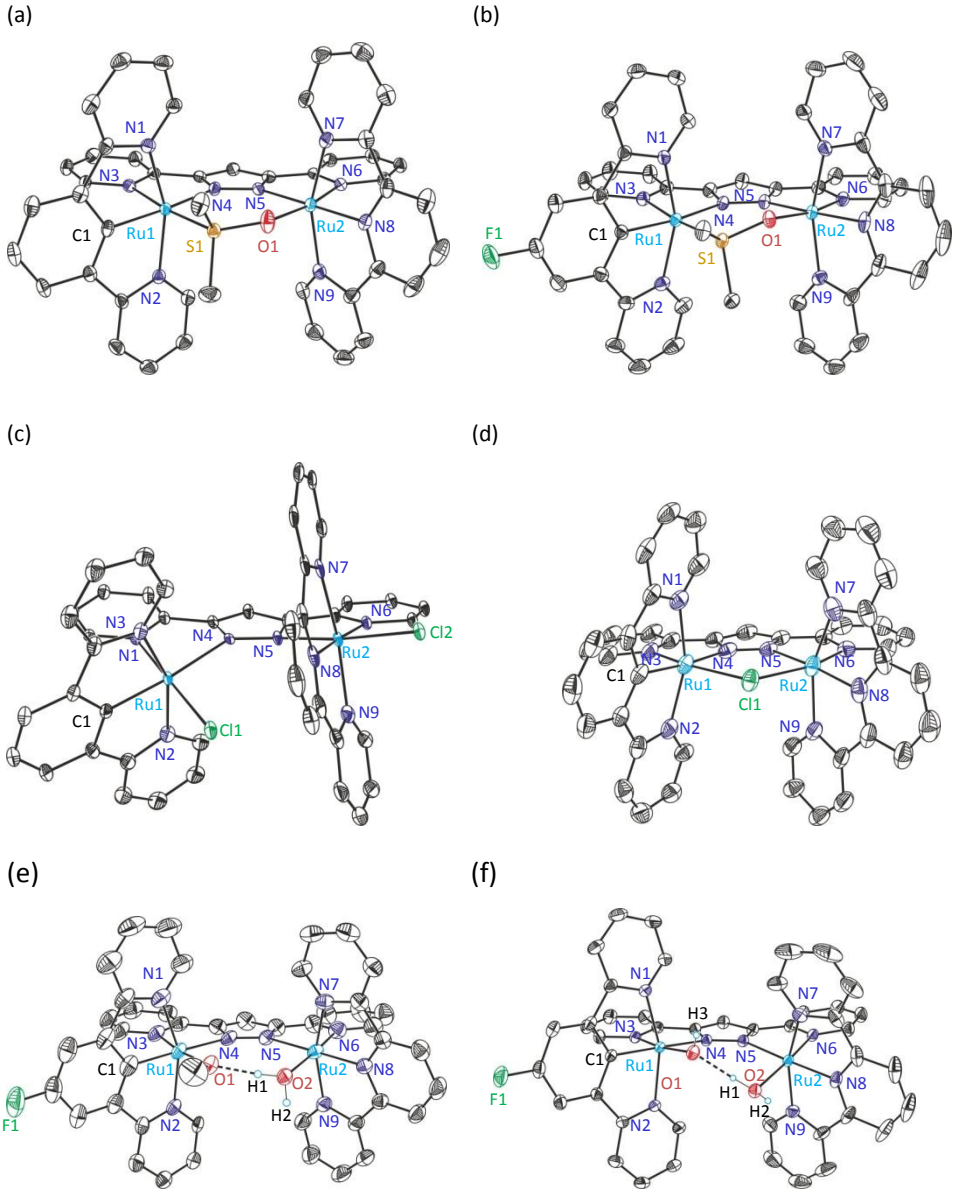

Figure 7. Ortep plots (ellipsoids at 50% probability) of the X-ray crystal structures of (a) **3a**$^{2+}$, (b) **3b**$^{2+}$, (c) **4a**$^{+}$, (d) **5a**$^{2+}$, (e) **6b-X**$^{2+}$ (X = MeO-H-OH), and (f) **6b-X**$^{2+}$ (X = HO-H-OH). Color codes: Ru, cyan; N, blue; O, red; Cl, green; F, green; S, yellow; C, grey. Hydrogen atoms are not shown for clarity. Labeling schemes were unified for the compared purpose.

Table 2. Selected bond distances (Å) and angles (°) for **3a**$^{2+}$, **3b**$^{2+}$, **4a**$^{+}$, **5a**$^{2+}$, **6b-X**$^{2+}$ (X = MeO-H-OH), and **6b-X**$^{2+}$ (X = HO-H-OH). Labeling schemes are shown in Figure 7.

	3a^{2+}	**3b**$^{2+}$	**4a**$^{+}$	**5a**$^{2+}$	**6b-X**$^{2+}$ X = MeO-H-OH	**6b-X**$^{2+}$ X = HO-H-OH
Ru1-N1	2.092(2)	2.096(2)	2.092(9)	2.082(5)	2.078(5)	2.0841(11)
Ru1-C1	1.960(2)	1.960(2)	1.936(8)	1.995(5)	1.934(5)	1.9431(13)
Ru1-N2	2.097(2)	2.112(2)	2.105(7)	2.073(5)	2.104(9)	2.0854(11)
Ru1-N3	2.143(2)	2.138(2)	2.080(7)	2.066(5)	2.087(11)	2.0972(12)
Ru1-N4	2.115(2)	2.124(2)	2.239(6)	2.012(5)	2.231(12)	2.1816(11)
Ru2-N7	2.068(2)	2.068(2)	2.055(8)	2.235(15)	2.054(4)	2.0619(12)
Ru2-N8	1.963(2)	1.967(2)	1.948(7)	2.050(5)	1.944(4)	1.9507(12)
Ru2-N9	2.065(2)	2.058(2)	2.057(8)	1.930(14)	2.060(4)	2.0707(12)
Ru2-N6	2.038(2)	2.043(2)	2.098(7)	2.066(5)	2.02(3)	2.0497(12)
Ru2-N5	2.033(2)	2.031(2)	2.083(8)	2.013(5)	2.13(2)	2.0797(11)
Ru1-S1	2.1956(7)	2.2101(5)	—	—	—	—
Ru2-O1	2.154(2)	2.143((1)	—	—	—	—
S1-O1	1.515(2)	1.526(1)	—	—	—	—
Ru1-Cl1	—	—	2.321(2)	2.4691(14)	—	—
Ru2-Cl2	—	—	2.383(2)	—	—	—
Ru2-Cl1	—	—	—	2.4759(15)	—	—
Ru1-O1	—	—	—	—	1.962(10)	2.0066(10)
Ru2-O2	—	—	—	—	2.103(4)	2.1023(10)
Ru1···Ru2	4.2282(3)	4.2085(2)	4.765(1)	3.9233(8)	4.781(2)	4.5640(5)
N1-Ru1-N2	157.64(8)	156.66(7)	157.7(3)	155.8(2)	157.2(4)	158.47(5)
N3-Ru1-N4	75.73(8)	75.40(7)	78.0(3)	76.3(2)	77.4(5)	76.89(4)
N3-Ru1-C1	93.10(9)	94.59(8)	92.5(3)	103.2(2)	95.3(4)	95.55(5)
N4-Ru1-S1	97.66(6)	96.47(5)	—	—	—	—
C1-Ru1-S1	93.58(7)	93.51(6)	—	—	—	—
N4-Ru1-Cl1	—	—	100.0(2)	87.09(14)	—	—
C1-Ru1-Cl1	—	—	89.2(3)	93.54(19)	—	—
N4-Ru1-O1	—	—	—	—	94.0(5)	94.82(4)
C1-Ru1-O1	—	—	—	—	93.4(3)	92.92(5)
N7-Ru2-N9	157.99(9)	158.84(7)	160.1(3)	153.7(6)	159.05(5)	159.43(6)
N6-Ru2-N5	77.80(8)	77.69(7)	78.1(3)	77.0(2)	79.6(8)	78.48(5)
N5-Ru2-N8	—	—	106.0(3)	—	—	—
N6-Ru2-N8	101.75(9)	99.19(8)	—	98.7(6)	98.1(7)	95.92(5)
N5-Ru2-O1	95.74(8)	95.43(6)	—	—	—	—
N8-Ru2-O1	84.77(8)	87.63(7)	—	—	—	—
N6-Ru2-Cl2	—	—	92.4(2)	—	—	—
N8-Ru2-Cl2	—	—	83.5(2)	—	—	—
N5-Ru2-Cl1	—	—	—	87.09(15)	—	—
N8-Ru2-Cl1	—	—	—	97.0(10)	—	—
N5-Ru2-O2	—	—	—	—	94.7(5)	95.47(4)
N8-Ru2-O2	—	—	—	—	87.46(13)	90.00(5)
Dihedral angle of two pyridyl rings of *bpp*$^{-}$	8.9	4.3	19.3	6.1	7.6	7.5

UNIVERSITAT ROVIRA I VIRGILI
SECOND-ROW TRANSITION-METAL COMPLEXES RELEVANT TO CO2 REDUCTION AND WATER OXIDATION
Takashi Ono
DL:T 1108-2014

by the existence of the *O*-coordination to the other metal centre.

The structure of **3b**$^{2+}$ is similar to that for **3a**$^{2+}$ in large part. The slightly longer Ru1-S1 bond length in **3b**$^{2+}$ (2.2101(5) Å vs. 2.1956(7) in **3a**$^{2+}$) can be probably explained by the weakened back donation exerted by electron-withdrawing fluoro group. Nevertheless, the longer S1-O1 bond distance (1.515(2) Å in **3b**$^{2+}$ vs 1.526(1) Å in **3a**$^{2+}$) was observed. This is probably associated with the strengthen Ru2-O1 bond (2.143(1) Å in **3b**$^{2+}$ vs 2.154 (2) Å in **3a**$^{2+}$)

The structure of **4a**$^{+}$ reveals that each metal centre has monodentate chlorido ligand, and those are located *in*- and *out*- positions for Ru-*dpb*$^{-}$ and Ru-*trpy* moieties, respectively. The steric repulsion between the *in*-Cl atom and *trpy* ligand produces the distortion of the planarity of the *bpp*$^{-}$ ligand, yielding an angle of 19.3° between two pyridyl rings of the *bpp*$^{-}$ ligand, which is more than 10° larger than that for the others (see Table 2). The Ru2-Cl2 bond distance (2.383(2) Å) is within the range for the typical Ru(II)-polypyridyl complexes, whereas the short Ru1-Cl1 bond length (2.321(2)) is due to the formal oxidation state of Ru(III) on Ru-*dpb*$^{-}$ moiety.

In contrast to **4a**$^{+}$, the bond lengths between each Ru and Cl atoms in the structure of **5a**$^{2+}$ dropped into a similar range (Ru1-Cl1: 2.4691(14) and Ru2-Cl2: 2.4759(15) Å) and those are similar to those for the *trpy-trpy* analogue, {[Ru(trpy)]$_2$(μ-Cl)(μ-bpp)]}$^{2+}$ (2.447(6) Å) reported earlier.[6] One interesting feature is that the Ru1-N4 bond length (2.012(5) Å) is significantly shortened compare with that for the other *dpb*$^{-}$*-trpy* complexes (**3a**$^{2+}$: 2.115(2), **3b**$^{2+}$: 2.124(2), **4a**$^{+}$: 2.239(6), **6b-X**$^{2+}$ (X = MeO-H-OH): 2.231(12), and **6b-X**$^{2+}$ (X = HO-H-OH): 2.1816(11) Å). This is because of the reduced flexibility of the two Ru substructures caused by the Cl bridge. This further causes the relatively lengthened Ru1-C1 bond distance (1.995(5) Å) which is *trans* to the N4 atom on pyrazolate moiety and the narrower N1-Ru1-N2 angle (155.8(2)°) due to the *trans* influence by the increased interaction between Ru1 and N4 atoms.

The crystals of **6b-X**$^{2+}$ (X = MeO-H-OH) and **6b-X**$^{2+}$ (X = HO-H-OH) were grown from acetone/Et_2O and from CH_2Cl_2/Et_2O, respectively. No distinctive differences were found between both structures. The significant short Ru1-O1 bond lengths (**6b-X**$^{2+}$,X = MeO-H-OH: 1.962(10), **6b-X**$^{2+}$,X = HO-H-OH: 2.0066(10) Å) with respect to the Ru2-O2

distances (**6b-X**$^{2+}$,X = MeO-H-OH: 2.103(4), **6b-X**$^{2+}$,X = HO-H-OH: 2.1023(10) Å) clearly demonstrate that the anionic OMe and OH ligands are coordinated to Ru centres bonded to F-*dpb*$^{-}$ ligand, respectively, in order to stabilize the oxidation state of Ru(III), and OH_2 ligand is coordinated to Ru(trpy) site. These two ligands build intramolecular hydrogen- bonding, as can be seen in the O1···H1 bond lengths of 1.64 and 1.62 Å for **6b-X**$^{2+}$ (X = MeO-H-OH) and **6b-X**$^{2+}$ (X = HO-H-OH), respectively.

Redox properties

The electrochemical properties of all the dinuclear complexes were investigated by means of cyclic voltammetry (CV), differential pulse voltammetry (DPV), and square wave voltammetry (SQWV) (Figure S7 in Supporting Information) and Detailed data are reported Tables 3 for in CH_2Cl_2 and Table 4 for in aqueous solution together with other related complexes for comparison purposes.

In CH_2Cl_2, all the dinuclear complexes showed at least two redox couples due to two non-symmetric redox active metal centres.

The bridged DMSO complex **2**$^{+}$ containing *dpb*$^{-}$ ligand on each metal centre showed two reversible 1e^{-} oxidations at 0.06 V (vs. SSCE) and 0.88 V corresponding to the Ru_2(III,II/II,II) and Ru_2(III,III/III,II) couples, respectively. This distinct difference of the redox potentials can be explained by the different nature of S- and O-coordination modes of dmso molecule. A π-acceptor *S*-bonded DMSO stabilizes metal dπ orbitals, whereas *O*-bonded DMSO ligand yields a significant change in energy to dπ orbitals due to the destabilization by π-donating property of the O atom and hence stabilizes higher oxidation state at lower potential. In contrast, two reversible redox couples for the *dpb*$^{-}$-*trpy* complex **3a**$^{2+}$ appear at 0.72 V and 1.10 V with a small$\Delta E_{1/2}$ value of 0.38 V with respect to **2**$^{+}$ ($\Delta E_{1/2}$ = 0.82 V). By comparing the $E_{1/2}$ values for the Ru(III/II) couple of the mononuclear analogues [Ru(trpy)(bpy)(dmso)]$^{2+}$ [21] and [Ru(dpb)(bpy)(dmso)]$^{+}$ [24] (see Table 3 for their $E_{1/2}$ values), it is reasonable to assign as that the first oxidation takes place at *S*-bonded Ru(dpb) centre and the second one does at *O*-bonded Ru(trpy) centre.

UNIVERSITAT ROVIRA I VIRGILI
SECOND-ROW TRANSITION-METAL COMPLEXES RELEVANT TO CO2 REDUCTION AND WATER OXIDATION
Takashi Ono
DL:T 1108-2014

Table 3. Redox potentials (V vs. SSCE) for the dinuclear complexes **2**$^{+}$, **3a**$^{2+}$, **3b**$^{2+}$, **4a**$^{+}$, **4b**$^{+}$, **5a**$^{2+}$, **5b**$^{2+}$, **6a-X**$^{2+}$, and **6b-X**$^{2+}$ in 0.1 M CH_2Cl_2-$TBAPF_6$ together with some of the reference complexes for the compared purpose.

Complex		$E_{1/2}$ (V) vs SSCE			$\Delta E_{1/2}$ (V)
dinuclear		**III,II/II,II**	**III,III/III,II**	**IV,III/III,III**	
dpb^{-}-*dpb*$^{-}$					
2^{+}	μ-DMSO	0.06	0.88	—	0.82
dpb^{-}-*trpy*					
3a^{2+}	μ-DMSO	0.72	1.10	—	0.38
3b^{2+}	μ-DMSO	0.74	1.10	—	0.36
4a^{+}	*in,out*-Cl_2	-0.30	0.53	1.36	0.83, 0.83
4b^{+}	*in,out*-Cl_2	-0.26	0.54	1.37	0.80, 0.83
5a^{2+}	μ-Cl	0.01	0.93	—	0.92
5b^{2+}	μ-Cl	0.03	0.92	—	0.89
6a-X^{2+}	μ-X	-0.20	0.71	—	0.91
6b-X^{2+}	μ-X	-0.18	0.72	—	0.92
trpy-trpy					
$\{[Ru(trpy)]_2(\mu\text{-bpp})(\mu\text{-Cl})\}^{2+}$		0.71[a]	1.12[a]	—	0.41
mononuclear		**III/II**	**IV/III**		
$Ru(trpy)(bpy)Cl^{+}$		0.87	—		—
Ru(dpb)(bpy)Cl		0.02[b]	1.39[b]		1.37
$Ru(trpy)(bpy)(dmso)^{2+}$		1.59 (*S*)[c,d]	—		—
		1.06 (*O*)[c,d]	—		—
$Ru(dpb)(bpy)(dmso)^{+}$		0.87 (*S*)[b,d]	—		—

a: Reference 6. b: Reference 24. c: in CH_3CN, reference 21. d: *S* and *O* reflects *S*-bonded and *O*-bonded to metal centre, respectively

The *in,out*-Cl_2 complex **4a**$^{+}$, which has dominant oxidation state of $Ru^{III}Ru^{II}$, undergoes one reversible 1e^{-} reduction at -0.30 V and two reversible 1e^{-} oxidations at 0.53 and 1.36 V, respectively. The comparison with the mononuclear Ru-Cl analogues (see Table 3) allows us to assign all three redox processes to Ru(III/II)-*dpb*$^{-}$, Ru(III/II)-*trpy*, and Ru(IV/III)-*dpb*$^{-}$ couples in the dinuclear structure from the cathodic to anodic processes.

For the bridged Cl complex **5a**$^{2+}$, the observed two 1e$^-$ redox processes at 0.01 and 0.93 V are anodically shifted by 0.31 and 0.40 V, respectively, with regard to **4a**$^+$ containing one more Cl ligand. These shifts can be explained by that the dissociation of σ- and π-donor Cl ligand and subsequent formation of the bridged Cl ligand produces the relative stabilization of dπ orbitals of both metal centres and thus causes the increase of the redox potentials. On the other hand, the cathodic shifts (0.21-0.22 V) for the couples of Ru_2(III,II/II,II) and Ru_2(III,III/III,II) of **6a-X**$^{2+}$ with regard to **5a**$^{2+}$ are the consequence of the substitution of the one Cl ligand by the σ- and π-donor of two O donor ligands.

As can be seen in Table 3, the large $\Delta E_{1/2}$ ($E_{1/2}$(III,III/III,II)- $E_{1/2}$(III,II/II,II)) values of the μ-Cl complexes with regard to *in*,*out*-Cl_2 may indicate that electronic coupling between both metals increases through additional bridging ligand other than the *bpp*$^-$. As can be observed in Figure 8 and Figure S8, dissolving the μ-X-complexes **6a-X**$^{2+}$ and **6b-X**$^{2+}$ in acidic media at pH 1 four reversible redox processes were observed within the potential ranges of -0.2-1.2 V (vs. SSCE), indicative of the PCET processes due to the *in-situ* formation of bis-aqua species **7a**$^{3+}$ and **7b**$^{3+}$. Each redox event can be assigned to 1e$^-$ redox couples of Ru_2(III,II/II,II), Ru_2(III,III/III,II), Ru_2(IV,III/III,III), and Ru_2(IV,IV/IV,III) from the relative current intensities of each wave and those assignments are further supported by the Pourbaix diagram (Figure 9). The Pourbaix diagram of **7a**$^{3+}$ was constructed within the pH range between 1 and 7. Above pH 7, the difficulty faced with both solubility and increased complexity of CV responses probably due to the existence of the non-hydrolysed species consisting of the methoxido/aquo bridge.

UNIVERSITAT ROVIRA I VIRGILI
SECOND-ROW TRANSITION-METAL COMPLEXES RELEVANT TO CO2 REDUCTION AND WATER OXIDATION
Takashi Ono
DL:T 1108-2014

Table 4. Redox potentials (V vs. SSCE) for bis-aqua species **7a**$^{3+}$, **7b**$^{3+}$, and *in*,*in*-{[Ru^{II}(trpy)(H$_2$O)]$_2$(μ-bpp)}$^{3+}$ together with those for the mononuclear analogues at pH 1.

Complex	$E_{1/2}$ (V) vs SSCE				
Dinuclear	**III,II/II,II**	**III,III/III,II**	**IV,III/III,III**	**IV,IV/IV,III**	**V,V/IV,IV**
7a^{3+}	-0.04	0.61	≈ 0.90	0.96	1.55 (2e$^-$)
7b^{3+}	-0.01	0.62	≈ 0.90	0.95	≈ 1.5 (2e$^-$)
in,*in*-{[Ru^{II}(trpy)(H$_2$O)]$_2$(μ-bpp)}$^{3+}$	0.59[a]	0.65[a]	0.88[a]	1.10[a]	—
mononuclear	**III/II**	**IV/III**	**V/IV**	**V/III**	
[Ru(dpb)(bpy)(OH$_2$)]$^{2+}$	0.04[b]	—	—	0.87 (2e$^-$)[b]	
[Ru(trpy)(bpy)(OH$_2$)]$^{2+}$	0.80[c]	0.99[c]	1.56[c]	—	

a: Reference 6. b: Reference 24. c: Reference 25.

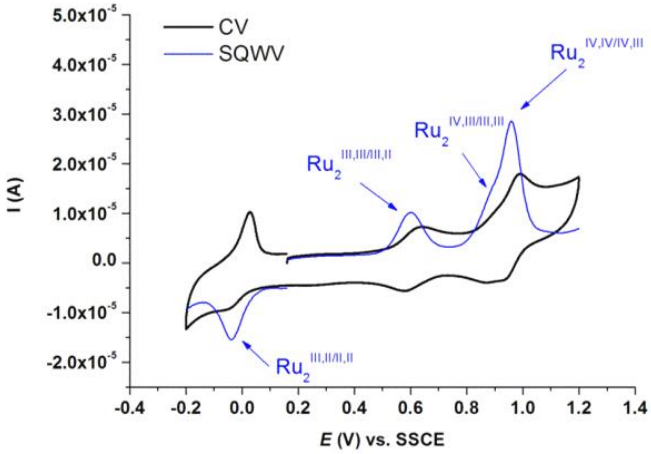

Figure 8. CV and SQWV of bis-aqua species **7a**$^{3+}$ (0.25 mM) in 0.1 M aqueous triflic acid solution at pH 1. Glassy carbon working electrode, Pt disk counter electrode and Hg/Hg$_2$SO$_4$ reference electrode, and potentials were converted to vs. SSCE. Scan rate 100 mV s^{-1} for CV, frequency 15 s^{-1} for SQWV.

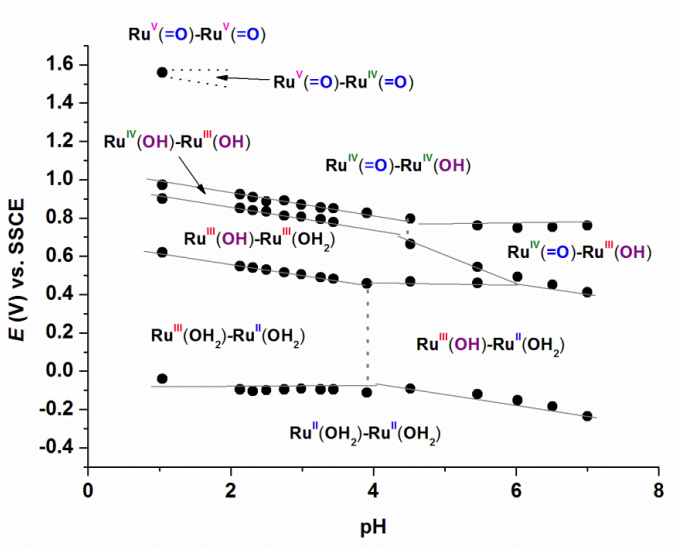

Figure 9. Pourbaix diagram for bis aqua complex **7a**$^{3+}$. The diagram was built by CV or SQWV experiments in aqueous solution at different pH (I = 0.1 M, glassy carbon working electrode, standard potentials vs. SSCE). The potentials for the couples of Ru_2(III,III/III,II), Ru_2(IV,III/III,III), and Ru_2(IV,IV/IV,III) decrease by -56, -50 and -56 mV/pH between pH 1 and 4, indicative of ($1e^-$ + $1H^+$) processes.

Below pH *ca.* 4, the potential for the Ru_2(III,II/II,II) couple is independent on pH values. All the following three redox potentials decrease by *ca*. 55 mV/pH unit between pH 1 and 4. By considering the Nernst equation (eqn. 1)

$$E_{1/2} = E_{1/2}^{o} - (0.059(\text{mV}) \cdot m/n)\text{pH} \qquad (1)$$

(where *m* is the number of protons, *n* is the number of electrons, and $E_{1/2}^{o}$ is the half-wave potential at pH 0), and that each redox processes have relatively similar intensities (Figure 8), the four reversible redox processes at pH 1 can be described by the following equations (eqns.2-5):

$$Ru^{III}\text{-}OH_2\ H_2O\text{-}Ru^{II} + 1e^- \rightarrow Ru^{II}\text{-}OH_2\ H_2O\text{-}Ru^{II} \qquad E_{1/2} = -0.04 \qquad (2)$$

$$Ru^{III}\text{-}OH_2\ \ HO\text{-}Ru^{III} + 1e^- + 1H^+ \rightarrow Ru^{III}\text{-}OH_2\ H_2O\text{-}Ru^{II} \qquad E_{1/2} = 0.61 \qquad (3)$$

$$Ru^{IV}\text{-}OH \quad HO\text{-}Ru^{III} + 1e^- + 1H^+ \rightarrow Ru^{III}\text{-}OH_2 \quad HO\text{-}Ru^{III} \qquad E_{1/2} = 0.90 \qquad (4)$$

$$Ru^{IV}\text{-}OH \quad O{=}Ru^{IV} + 1e^- + 1H^+ \rightarrow Ru^{IV}\text{-}OH \quad HO\text{-}Ru^{III} \qquad E_{1/2} = 0.96 \qquad (5)$$

In contrast to the *trpy-trpy* complex, no reactivity toward water oxidation by the Ru_2(IV,IV) species of *dpb*$^-$*-trpy* complex at least in the CV time scale can be explained by low thermodynamic driving force toward water oxidation ($E(O_2/H_2O)$ = 0.935 V at pH 1 vs. SSCE)

When the potential is increased to 1.7 V, electrocatalytic wave with an onset potential of *ca*. 1.4 V was observed (Figure 10a), indicating that the newly formed species having a oxidation state higher than Ru_2(IV,IV) triggers electrocatalytic water oxidation. Its $E_{1/2}$ value was determined through SQWV to be *ca.* 1.55 V vs. SSCE. By carefully analysing the additional redox process within the pH 1-2 (Figure 10b), SQWV responses of the redox process clearly separates into two processes with increasing pH. Thus, we can conclude that

(a) (b)

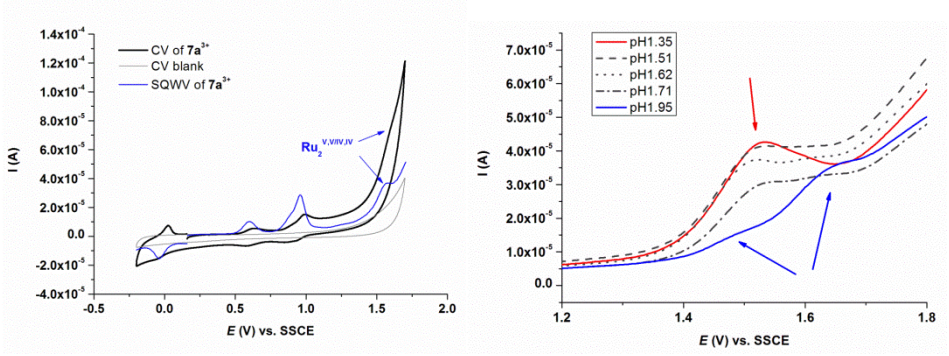

Figure 10. (a) CV and SQWV of **7a**$^{3+}$ (0.25 mM) in 0.1 M aqueous triflic acid solution at pH 1, and (b) SQWVs of **7a**$^{3+}$ (0.25 mM) at different pHs changing by the addition of 0.1 M triflic acid solution into 0.1 M H_3PO_4 / NaH_2PO_4 buffer (pH = 1.95). Glassy carbon working electrode, Pt disk counter electrode and Hg/Hg_2SO_4 reference electrode, and potentials were converted to vs. SSCE. Scan rate 100 mV s^{-1}, SQWV frequency (a) 15 s^{-1} (b) 30 s^{-1}.

the additional redox process consists of single $2e^-$ process at pH 1 and two $1e^-$ processes above pH 1.35. At higher pH, the corresponding redox processes could not be resolved due to low current intensity and non-peak shaped responses overlapped with a catalytic current. The additional redox processes can be described by the following equations (eqns.6-8) depending on the pH values.

pH < 1.35

$$Ru^{V}=O \quad O=Ru^{V} + 2e^- + 1H^+ \rightarrow Ru^{IV}\text{-}OH \quad O=Ru^{IV} \qquad (6)$$

1.35 < pH < 1.95

$$Ru^{V}=O \quad O=Ru^{IV} + 1e^- + 1H^+ \rightarrow Ru^{IV}\text{-}OH \quad O=Ru^{IV} \qquad (7)$$

$$Ru^{V}=O \quad O=Ru^{V} + 1e^- \rightarrow Ru^{V}=O \quad O=Ru^{IV} \qquad (8)$$

And, the observed electrocatalytic current is associated with the following reaction at pH 1 (eqn.9).

$$Ru^{V}=O \quad O=Ru^{V} + 2H_2O \rightarrow Ru^{III}\text{-}OH_2 \quad H_2O\text{-}Ru^{III} + O_2 \qquad (9)$$

Interestingly, except the Ru(III,II/II,II) couple, there is no distinctive difference on $E_{1/2}$ between *dpb*$^-$*-trpy* and *trpy-trpy* systems. Although It is unclear that both oxidation and deprotonation take place either on Ru(dpb) or Ru(trpy) sites, since the first three reactions (eqs.2-4) at pH 1 undergo in the similar manner as those for the *trpy-trpy* complex,[6] one can roughly compare their redox potentials: 1) $E_{1/2}$ of first redox process clearly indicates that the oxidation occurs at Ru(dpb) site. 2) By considering high stability of Ru(III)-dpb exerted by strong σ-donor of the *dpb*$^-$ ligand, it is reasonable to assign that the second oxidation and a loss of one proton is at Ru(trpy)-centered in order to stabilize Ru(III)(trpy) by OH ligand. 3) The next two processes are not clear, but it is possible to assign to $[(dpb)Ru^{IV}\text{-}OH \quad O=Ru^{IV}(trpy)]^{3+}$, at oxidation state of IV,IV. Moreover, the Ru(V,V) species is highly destabilized (at $E_{1/2} \approx 1.55$V) compared to its mononuclear counterpart $Ru(dpb)(bpy)(OH_2)^{2+}$ ($E_{1/2} = 0.87$ V for the Ru(V/III) couple).

UNIVERSITAT ROVIRA I VIRGILI
SECOND-ROW TRANSITION-METAL COMPLEXES RELEVANT TO CO2 REDUCTION AND WATER OXIDATION
Takashi Ono
DL:T 1108-2014

VII.3.2. Catalytic Experiments

Water oxidation catalysis

The bis-aqua complexes **7a**$^{3+}$ (R = H), **7b**$^{3+}$ (R =F), have been tested as water oxidation catalysts by using $(NH_4)_2Ce^{IV}(NO_3)_6$ as chemical oxidant. In both cases, the catalytic reactions were carried out in the following conditions: [Cat] = 1.0 mM, [Ce^{IV}] = 100 mM in 2 mL of 0.1 M aqueous triflic acid solution (pH 1) at 25 °C. The catalytic properties of **7a**$^{3+}$ and **7b**$^{3+}$ were analysed by monitoring evolved gases by on-line manometry and MS spectrometry and the obtained results are shown in Figures 11-12 and listed in Table 5. As can be seen in Figure 12, both catalysts generate a mixture of O_2 and CO_2 during the reaction time, indicating that two competitive reactions, water oxidation and ligand oxidation, are taking place. This is in sharp contrast with *in*,*in*-{[Ru(trpy)(OH_2)]$_2$(μ-bpp)}$^{3+}$, which generates only O_2 with TON 18.6.[6] Consequently, the catalytic efficiencies of **7a**$^{3+}$ and **7b**$^{3+}$ are lower than that for *in*,*in*-{[Ru(trpy)(OH_2)]$_2$(μ-bpp)}$^{3+}$.

It is interesting to see that the rate of O_2 formation using fluoro-substituted catalyst **7b**$^{3+}$ is faster than that of non-substituted one **7a**$^{3+}$. From on-line manometry and MS experiments, TONs for evolved gases can be determined as TONs 5.7 for O_2 and 4.8 for CO_2 using **7a**$^{3+}$, and TONs 7.7 for O_2 and 3.4 for CO_2 using **7b**$^{3+}$. These differences can be associated with the increased stability of the catalyst by the introduction of oxidatively rugged C-F bond on the *dpb*$^-$ ligand as was shown for the mononuclear analogues in chapter VI.

Table 5. TON and O_2/CO_2 ratios for the evolved gases using **7a**$^{3+}$ and **7b**$^{3+}$ together with *in*,*in*-{[Ru(trpy)(OH_2)]$_2$(μ-bpp)}$^{3+}$.

Complex	TON			O_2/CO_2	eff.[a]	
	total	O_2	CO_2			
7a^{3+}	10.5	5.7	4.8	54/46	22.8	*Tw*
7b^{3+}	11.1	7.7	3.4	69/31	30.8	*Tw*
in,*in*-{[Ru(trpy)(OH_2)]$_2$(μ-bpp)}$^{3+}$	18.6	18.6	—	—	74.4	b

Catalytic conditions: [cat.] = 1 mM, [Ce^{IV}] = 100 mM, in 2mL of 0.1 M aqueous triflic acid solution. *Tw* = This work. a: eff. = efficiency. b: Reference 6.

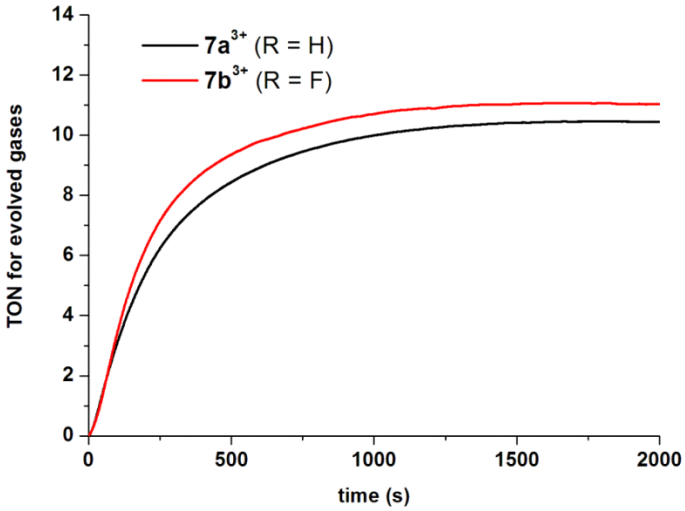

Figure 11. On-line manomtric time profiles for the evolved gases, of **7a**$^{3+}$ (—) and **7b**$^{3+}$ (—) (1 mM) at pH 1.0 in 0.1 M triflic acid solution in the presence of $(NH_4)_2Ce(NO_3)_6$ (100 mM) as sacrificial oxidant.

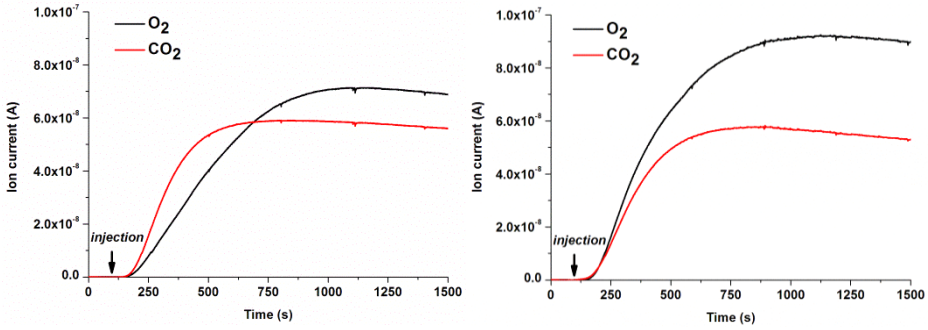

Figure 12. On-line gases evolution profiles monitored by MS upon addition of 100 equiv. of $(NH_4)_2Ce^{IV}(NO_3)_6$ (at 100 seconds) to 1 mM of **7a**$^{3+}$ (Top) and **7b**$^{3+}$ (bottom) in 0.1 M triflic acid solution. Oxygen (—) and carbon dioxide (—).

VII.4. Conclusions

A series of new non-symmetric dinuclear ruthenium complexes containing the anionic *dpb*$^{-}$ (2,6-di(pyridin-2-yl)benzen-1-ide) and *trpy* ligands on each metal centre have been synthesized. The bridged DMSO complexes **3a**$^{2+}$ and **3b**$^{2+}$ were characterized by 1D and 2D NMR spectroscopies. The thermodynamic stability of these complexes can

UNIVERSITAT ROVIRA I VIRGILI
SECOND-ROW TRANSITION-METAL COMPLEXES RELEVANT TO CO2 REDUCTION AND WATER OXIDATION
Takashi Ono
DL:T 1108-2014

be attributable to both the bridged coordination mode through S and O atoms and the strong Ru-S bond due to the back donation from electron-rich metal centre derived from strong σ-donating property of *dpb*$^-$ ligand. The properties of the bridged Cl complex **5a**$^{2+}$ and bis-aqua species **7a**$^{3+}$ in solid state and/or in solution are compared with the previously reported dinuclear *trpy-trpy* analogues. The X-ray structure of **5a**$^{2+}$ showed the structural similarity with *trpy-trpy* analogue, which allowed us to compare their electronic properties. Cyclic voltammograms in CH_2Cl_2 indicate that *dpb*$^-$*-trpy* complexes have lower electronic coupling between both metal centres compared with that for the *trpy-trpy* complex. By contrast, it could be considered that in aqueous solution, electronic coupling relatively increases assisted by the PCET. However, the expected influence of the strong σ-donor of *dpb*$^-$ ligand on lowering both the redox potentials and catalytic onset potential (at *ca.*1.4 V vs SSCE) was not found for the *dpb*$^-$*-trpy* system. This result may imply that highly different electronic properties of both metal centres exerted by mononucleating ligand limit the electronic coupling between both metal centres to a lesser degree compared with symmetric system. The chemical water oxidation reaction by *in-situ* generated bis-aqua complex resulted in low efficiencies and selectivities with regard to the dinuclear 'Ru-Hbpp' WOC, which is attributable to the oxidatively fragile *dpb*$^-$ ligand. The observed better catalytic performance for fluoro-substituted catalyst **7b**$^{3+}$ supports this potential catalyst degradation pathway. Based on these results, a catalyst which consists of three C-F bonds on the phenyl ring of *dpb*$^-$ ligand could be a promising candidate.

VII.5. Experimental Section

Materials

All reagents used in the present work were obtained from Aldrich Chemical Co., Alfa Aesar or Strem Chemicals inc. and were used without further purification. Synthesis grade organic solvents were obtained from SDS and were routinely degassed with N_2. The compounds Hbpp (3,5-bis(2-pyridyl)pyrazole),[26-29] Hdpb (1,3-di(pyridin-2-yl)benzene),[30] *out*-[Ru(trpy)(Hbpp)Cl](PF$_6$)[31] and *in*-[Ru(trpy)(Hbpp)Cl](PF$_6$)[31] were

prepared as described in the literature. The complexes *trans*-Ru(R-dpb)(dmso-*s*)$_2$Cl, **1a** (R =H), **1b** (R =F) were prepared as described in Chapter VI. All synthetic manipulations were routinely performed under N_2 atmosphere using Schlenk and vacuum-line techniques.

Synthesis

Scheme 3. NMR Labeling scheme for: *dpb*$^-$ complexes

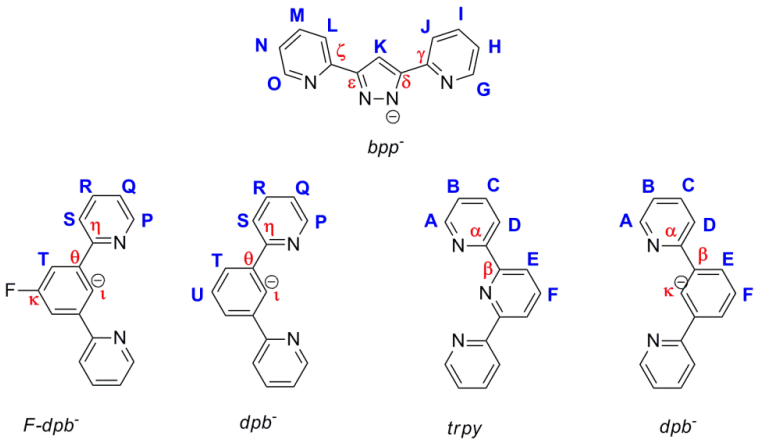

Synthesis of {[Ru^{II}(dpb)][Ru^{II}(dpb)](μ-bpp)(μ-dmso)}(PF$_6$)$_2$, [2](PF$_6$)

A mixture of 30.8 mg (0.058 mmol) of complex **1a**, 6.5 mg (0.29 mmol) of *Hbpp* and 5 μL (0.036 mmol, 1.2 equiv.) of NEt_3 in 5 mL of degassed MeOH was heated at reflux for 1 hour under N_2 atmosphere. After cooling to room temperature, 1 mL of degassed saturated aqueous KPF_6 solution was added into the reaction mixture under N_2, resulting in a formation of brown precipitates. Without an removable of the MeOH solvent, the precipitates were collected by a glass frit, which was quickly washed with water (3 mL x 3) and Et_2O (3 mL x 3), dried under vacuum and stored under N_2. Yield 20.2 mg (0.018 mmol), 62%. NMR measurements were carried out in the presence of zinc as reductant due to the partially oxidized complex. ^{1}H NMR (400 MHz, Acetone-d_6, 298 K, with Zn): δ 8.43-8.36 (m, 4H, H_A and H_P), 8.25 (s, 1H, H_K), 8.21-8.17 (m, 3H, H_S, and H_J or H_L), 8.14-8.08 (m, 4H, H_D and H_T), 8.06 (d, 2H, J_{EF} =7.6 Hz, H_E), 7.94 (d, 1H, J_{LM}

$_{or\ JI}$ = 7.7 Hz, H_L or H_J), 7.90 (td, 2H, $J_{RS} = J_{RQ}$ = 7.6 Hz, J_{RP} = 1.6 Hz, H_R), 7.77 (td, 1H, $J_{IJ\ or\ ML}$ = $J_{IH\ or\ MN}$= 7.6 Hz, $J_{IG\ or\ MO}$ = 1.6 Hz, H_I or H_M), 7.68 (td, 2H, $J_{CD} = J_{CB}$ = 7.8 Hz, J_{CA} = 1.6 Hz, H_C), 7.37-7.32 (m, 2H, H_U, and H_M or H_I), 7.27 (ddd, 2H, J_{QR} = 7.6 Hz, J_{QP} = 5.5 Hz, J_{QS} = 1.5 Hz, H_Q), 7.20-7.14 (m, 3H, H_F and H_B), 7.04 (d, 1H, $J_{GH\ or\ ON}$ = 5.8 Hz, H_G or H_O), 6.82 (ddd, 1H, $J_{HI\ or\ NM}$ = 7.6 Hz, $J_{HG\ or\ NO}$ = 5.8 Hz, $J_{HJ\ or\ NL}$ = 1.5 Hz, H_H or H_N), 6.76 (d, 1H, $J_{ON\ or\ GH}$ = 5.9 Hz, H_O or H_G), 6.41 (ddd, 1H, $J_{NM\ or\ HI}$ = 7.7 Hz, $J_{NO\ or\ HG}$ =5.9 Hz, $J_{NL\ or\ HJ}$ = 1.5 Hz, H_N or H_H), 1.33 (s, 6H, *Me* of DMSO). ESI-MS (MeOH): *m/z* 965.1([M-PF_6]$^+$).

Synthesis of {[Ru^{II}(dpb)][Ru^{II}(trpy)](μ-bpp)(μ-DMSO}$(PF_6)_2$·H_2O, [3a]$(PF_6)_2$·H_2O

Method A: A mixture of 100 mg (0.191 mmol) of complex **1a** and 141 mg (0.191 mmol) of *out*-[Ru(Cl)(Hbpp)(trpy)](PF_6) in 50 mL of MeOH was heated at reflux overnight. After cooling to room temperature, the solvent was evaporated by a rotary evaporator to give brown residue, which was purified by column chromatography using neutral alumina as the solid support. A first brown fraction corresponding to small amount of **4a**$^+$ was eluted with CH_2Cl_2/acetone (50/50) and a desired complex was eluted with MeOH. To this solution, 1 mL of saturated aqueous KPF_6 solution and 5 mL of water was added. Upon reducing the volume, a solid came out of the solution that was washed with water (5 mL x 3) and Et_2O (10 mL x 3) and then dried under vacuum. Yield 110 mg (0.088 mmol), 46%. ***Method B***: A mixture of 51.0 mg (0.0973 mmol) of complex **1a** and 71.9 mg (0.0976 mmol) of *in*-[Ru(Cl)(Hbpp)(trpy)](PF_6) in 25 mL of MeOH was stirred at room temperature for 1 hours. The solvent was evaporated to give brown residue, which was purified by column chromatography using neutral alumina as the solid support. A desired complex was eluted with Acetone/MeOH (80/20). To this solution, 1 mL of saturated aqueous KPF_6 solution and 5 mL of water was added. Upon reducing the volume, a solid came out of the solution that was washed with water (5 mL x 3) and Et_2O (10 mL x 3) and then dried under vacuum. Yield 75.2 mg (0.060 mmol), 61%. Anal. Calcd. for $C_{46}H_{37}F_{12}N_9OP_2Ru_2S$: C, 43.99 ; H, 2.90; N, 10.04; S, 2.55. Found: C, 43.47; H, 3.28; N, 9.85; S, 2.54. Anal. Calcd. for $C_{46}H_{37}F_{12}N_9OP_2Ru_2S·H_2O$: C, 43.49 ; H, 2.96; N, 9.87; S, 2.51. ^{1}H NMR (500 MHz, Acetone-d_6, 298 K): δ 8.73 (d, 2H, J_{EF} = 8.1 Hz, H_E), 8.64 (d, 2H, J_{DC} = 7.9 Hz, H_D), 8.49 (d, 2H, J_{AB} = 5.5 Hz, H_A), 8.42 (s, 1H, H_K),

8.36 (d, 2H, J_{PQ} = 5.5 Hz, H_P), 8.28-8.18 (m, 5H, H_F, H_J, H_L and H_S), 8.11 (d, 2H, J_{TU} = 7.7 Hz, H_T), 8.07 (td, 2H, J_{CD} = J_{CB} = 7.9 Hz, J_{CA} = 1.5 Hz, H_C), 7.92 (td, 2H, J_{RQ} = J_{RS} = 7.6 Hz, J_{RP} = 1.6 Hz, H_R), 7.85 (td, 1H, $J_{ML\ or\ IJ}$ = $J_{MN\ or\ IH}$ = 7.6 Hz, $J_{MO\ or\ IG}$ = 1.5 Hz, H_M or H_I), 7.77-7.71 (m, 3H, H_B and H_I or H_M), 7.55 (d, 1H, $J_{GH\ or\ ON}$ = 5.8 Hz, H_G or H_O), 7.37 (t, 1H, J_{UT} = 7.7 Hz, H_U), 7.26 (ddd, 2H, J_{QR} = 7.6 Hz, J_{QP} = 5.5 Hz, J_{QS} = 1.4 Hz, H_Q), 7.12 (d, 1H, $J_{ON\ or\ GH}$ = 5.7 Hz, H_O or H_G), 6.92 (ddd, 1H, $J_{NM\ or\ HI}$ = 7.6 Hz, $J_{NO\ or\ HG}$ = 5.7 Hz, $J_{NL\ or\ HJ}$ = 1.4 Hz, H_N or H_H), 6.80 (ddd, 1H, $J_{HI\ or\ NM}$ = 7.4 Hz, $J_{HG\ or\ NO}$ = 5.8 Hz, $J_{HJ\ or\ NL}$ = 1.5 Hz, H_H or H_N), 1.53 (s, 6H, *Me* of dmso). ^{13}C NMR (125 MHz, Acetone-d_6, 298 K): δ 207.3 ($C_{\text{⎚}}$), 168.8 (C_η), 160.9 (C_α), 160.5 (C_β), 157.3 ($C_{\gamma\ or\ \zeta}$), 154.8 ($C_{G\ or\ O}$), 154.7 (C_P), 154.4 (C_A), 154.1 ($C_{\zeta\ or\ \gamma}$), 152.7 ($C_{\varepsilon\ or\ \delta}$), 151.4 ($C_{O\ or\ G}$), 151.3 ($C_{\delta\ or\ \varepsilon}$), 145.0 ($C_\theta$), 138.9 ($C_R$), 138.8 ($C_{M\ or\ I}$), 138.7 ($C_C$), 137.1 ($C_{I\ or\ M}$), 135.7 ($C_F$), 128.7 ($C_B$), 125.9 ($C_T$), 124.8 ($C_D$), 124.0 ($C_Q$), 123.6 ($C_E$), 123.3 ($C_{N\ or\ H}$), 123.0 ($C_U$), 122.9 ($C_{H\ or\ N}$), 121.3 ($C_S$), 120.8 ($C_{L\ or\ J}$), 120.5 ($C_{J\ or\ L}$), 104.0 ($C_K$), 42.3 (*Me* of dmso). ESI-MS (MeOH): *m/z* 1111.9 ($[M\text{-}PF_6]^+$), 483.5 ($[M\text{-}2PF_6]^{2+}$).

Synthesis of *in,out*-{[Ru^{III}(dpb)(Cl)][Ru^{II}(trpy)(Cl)](μ-bpp)}(PF_6)·0.75CH_3CN, [4a](PF_6)·0.75CH_3CN

A mixture of 225 mg (0.429 mmol) of complex **1a** and 320 mg (0.434 mmol) of *out*-[Ru(Cl)(Hbpp)(trpy)](PF_6) in 80 mL of MeOH was heated at 45 °C for 3 days. After reaction time, a precipitate appeared was filtered off, which was washed with MeOH (5 mL x 3) and Et_2O (10 mL x 3) and then dried under vacuum. The greenish yellow solid was purified by column chromatography using neutral alumina as the solid support. A first brown fraction was eluted with CH_2Cl_2/CH_3CN (70/30). To this solution 1 mL of saturated aqueous KPF_6 solution and 5 mL of water was added. Upon reducing the volume, a solid came out of the solution that was washed with water (5 mL x 3) and Et_2O (10 mL x 3) and dried under vacuum. Yield 315 mg (0.285 mmol), 67%. The sample for elemental analysis was obtained from recrystallization by slow vapour diffusion of Et_2O into a solution of CH_3CN to give brown crystalline solid. Anal. Calcd. for $C_{44}H_{31}Cl_2F_6N_9PRu_2$: C, 47.88; H, 2.83; N, 11.42. Found: C, 48.26; H, 3.34; N, 12.09. Anal. Calcd. for $C_{44}H_{31}Cl_2F_6N_9PRu_2$·0.75$CH_3CN$: C, 48.17; H, 2.95; N, 12.04. ESI-MS (MeOH): *m/z* 959.0 ($[M\text{-}PF_6]^+$).

UNIVERSITAT ROVIRA I VIRGILI
SECOND-ROW TRANSITION-METAL COMPLEXES RELEVANT TO CO2 REDUCTION AND WATER OXIDATION
Takashi Ono
DL:T 1108-2014

{[Ru^{III}(dpb)][Ru^{II}(trpy)](μ-bpp)(μ-Cl}$(PF_6)_2$, [5a]$(PF_6)_2$

The solution of 234 mg (0.212 mmol) of complex **4a**$^+$ in 60 mL of MeOH/CH_2Cl_2 (3/1) was stirred in the presence of 2 x 100 W tungsten lamp for 2 days. To the resulting solution, 1 mL of saturated aqueous KPF_6 was added. The volume was then reduced on a rotary evaporator until precipitate appeared which was collected on a glass frit and washed with water (5 mL x 3) and Et_2O (10 mL x 3) and dried under vacuum. The solid was once dissolved in a minimal amount of acetone and then evaporated to give brown oily residue, to which 50 mL of CH_2Cl_2 was added and the slurry was stirred for 30 min. The precipitate was then collected on a glass frit and washed with cold CH_2Cl_2 (3 mL x 3) and Et_2O (10 mL x 3) and dried under vacuum. Yield. 191 mg (0.157 mmol), 75%. Anal. Calcd. for $C_{44}H_{31}ClF_{12}N_9P_2Ru_2$: C, 43.56; H, 2.58; N, 10.39. Found: C, 43.21; H, 2.40; N, 10.13. ESI-MS (MeOH): *m/z* 462.0 ([M-2PF_6]$^{2+}$).

{[Ru^{III}(dpb)][Ru^{II}(trpy)](μ-bpp)(μ-X)}$(PF_6)_2$, [6a-X]$(PF_6)_2$

51.2 mg (0.042 mmol) of complex **5a**$^+$, 22.6 mg (0.065 mmol, 1.5 equiv.) of $TlPF_6$ were charged into a 20 mL Schlenk tube with Teflon plug valve, which was purged with N_2. Then, 8 mL of degassed MeOH and 9.0 μL (0.065 mmol, 1.5 equiv.) of NEt_3 were added and the mixture was heated to reflux for 1 hour. After cooling down to room temperature, white precipitate, TlCl was filtered off through a pad of Celite. After adding 1 mL of saturated aqueous KPF_6, the volume was reduced by rotary evaporator to give brown solid, which was filtered and washed with cold water (3 mL x 3) and Et_2O (5 mL x 3) and dried under vacuum. Yield 44.2 mg (0.036 mmol) 86%. Data for elemental analysis and MS spectrum are shown in Table 1 and Figure 6, respectively.

***In-situ* preparation of *in*,*in*-{[Ru^{III}(dpb)(OH_2)][Ru^{II}(trpy)(OH_2)](μ-bpp)}$(PF_6)_3$, [7a]$(PF_6)_3$**

Bis aqua complex can be prepared by hydrolysis of μ-X complex in acidic aqueous media. However, the isolation of bis aqua complex is unsuccessful due to its higher solubility compared to that of m-X complex which is first precipitated upon reducing the volume.

Synthesis of {[Ru^{II}(F-dpb)][Ru^{II}(trpy)](μ-bpp)(μ-dmso)}$(PF_6)_2$·H_2O, [3b]$(PF_6)_2$·H_2O

Method A: Following the similar procedure for the synthesis of **3a**$^{2+}$, **3b**$^{2+}$ was obtained with 37% yield. ***Method B***: Following the similar procedure for the synthesis of **3a**$^{2+}$, **3b**$^{2+}$ was obtained with 46% yield. Anal. Calcd. for $C_{46}H_{36}F_{13}N_9OP_2Ru_2S$: C, 43.37; H, 2.85; N, 9.90; S, 2.52. Found: C, 42.70; H, 2.83; N, 9.80; S, 2.39. Anal. Calcd. for $C_{46}H_{36}F_{13}N_9OP_2Ru_2S·H_2O$: C, 42.76; H, 2.96; N, 9.76; S, 2.48. ^{1}H NMR (500 MHz, Acetone-d_6, 298 K): δ 8.74 (d, 2H, J_{EF} = 8.2 Hz, H_E), 8.65 (d, 2H, J_{DC} = 7.9 Hz, H_D), 8.50 (d, 2H, J_{AB} = 5.4 Hz, H_A), 8.42 (s, 1H, H_K), 8.39 (d, 2H, J_{PQ} = 5.6 Hz, H_P), 8.28-8.18 (m, 5H, H_F, H_J, H_L and H_S), 8.08 (td, 2H, J_{CB} = J_{CD} =7.9 Hz, J_{CA} = 1.4 Hz H_C), 8.00-7.93 (m, 4H, H_R and H_T), 7.86 (td, 1H, $J_{ML\ or\ IJ}$ = $J_{MN\ or\ IH}$ = 7.6 Hz, $J_{MO\ or\ IG}$ = 1.5 Hz, H_M or H_I), 7.77-7.71 (m, 3H, H_B and H_I or H_M), 7.56 (d, 1H, $J_{GH\ or\ ON}$ = 5.7 Hz, H_G or H_O), 7.30 (ddd, 2H, J_{QR} = 7.1 Hz, J_{QP} = 5.6 Hz, J_{QS} = 1.2 Hz, H_Q), 7.14 (d, 1H, $J_{ON\ or\ GH}$ = 5.5 Hz, H_O or H_G), 6.95 (ddd, 1H, $J_{NM\ or\ HI}$ = 7.6 Hz, $J_{NO\ or\ HG}$ = 5.5 Hz, $J_{NL\ or\ HJ}$ = 1.3 Hz, H_N or H_H), 6.81 (ddd, 1H, $J_{HI\ or\ NM}$ = 7.4 Hz, $J_{HG\ or\ NO}$ = 5.7 Hz, $J_{HJ\ or\ NL}$ = 1.4 Hz, H_H or H_N), 1.55 (s, 6H, *Me* of dmso). ^{13}C NMR (125 MHz, Acetone-d_6, 298 K): δ 200.1 (C_ι), 168.2 (d, $^4J_{CF}$ = 4.8 Hz, C_η), 161.6 (d, $^1J_{CF}$ = 234.0 Hz, C_κ) 161.1 (C_α), 160.6 (C_β), 157.5 ($C_{\gamma\ or\ \zeta}$), 155.0 (C_P), 155.0 ($C_{G\ or\ O}$), 154.5 (C_A), 154.2 ($C_{\zeta\ or\ \gamma}$), 152.9 ($C_{\varepsilon\ or\ \delta}$), 151.6 ($C_{O\ or\ G}$), 151.5 ($C_{\delta\ or\ \varepsilon}$), 145.7 (d, $^3J_{CF}$ = Hz, C_θ), 139.1 (C_R), 139.0 ($C_{M\ or\ I}$), 138.9 (C_C), 137.2 ($C_{I\ or\ M}$), 135.8 (C_F), 128.8 (C_B), 125.0 (C_D), 124.7 (C_Q), 123.8 (C_E), 123.6 ($C_{N\ or\ H}$), 123.1 ($C_{H\ or\ N}$), 122.1 (C_S), 121.0 ($C_{L\ or\ J}$), 120.7 ($C_{J\ or\ L}$), 113.4 (d, $^2J_{CF}$ = 23.8 Hz, C_T), 104.2 (C_K), 42.5 (*Me* of dmso). ^{19}F NMR (376.5 MHz, Acetone-d_6, 298 K): δ -72.6 (d, 12F, J_{FP} = 7.7 Hz, *P*F_6), -122.1 (t, 1F, J_{FH} = 10.5 Hz, *F*-dpb). ESI-MS (MeOH): *m/z* 1130.1 ([M-PF_6]$^+$), 492.5 ([M-2PF_6]$^{2+}$).

Synthesis of *in,out*-{[Ru^{III}(F-dpb)(Cl)][Ru^{II}(trpy)(Cl)](μ-bpp)}(PF_6)·1.5H_2O, [4b](PF_6)·1.5H_2O

Following the similar procedure for the synthesis of **4a**$^+$, **4b**$^+$ was obtained with 52% yield. Anal. Calcd. for $C_{44}H_{30}Cl_2F_7N_9PRu_2$: C, 47.11; H, 2.70; N, 11.24. Found: C, 45.94; H, 2.87; N, 10.73. Anal. Calcd. for $C_{44}H_{30}Cl_2F_7N_9PRu_2·1.5H_2O$: C, 46.06; H, 2.90; N, 10.97. ESI-MS (MeOH): *m/z* 977.0 ([M-PF_6]$^+$)

UNIVERSITAT ROVIRA I VIRGILI
SECOND-ROW TRANSITION-METAL COMPLEXES RELEVANT TO CO2 REDUCTION AND WATER OXIDATION
Takashi Ono
DL:T 1108-2014

Synthesis of {[Ru^{III}(F-dpb)][Ru^{II}(trpy)](μ-bpp)(μ-Cl}$(PF_6)_2$, [5b]$(PF_6)_2$

Following the similar procedure for the synthesis of **5a**$^{2+}$, **5b**$^{2+}$ was obtained with 71% yield. Anal. Calcd. for $C_{44}H_{30}ClF_{13}N_9P_2Ru_2$: C, 42.92; H, 2.46; N, 10.24. Found: C, 42.83; H, 2.35; N, 10.23. ESI-MS (MeOH): *m/z* 973.1 ([M-2PF_6+MeOH-H]$^+$).

Synthesis of {[Ru^{III}(F-dpb)][Ru^{II}(trpy)](μ-bpp)(μ-X}$(PF_6)_2$, [6b-X]$(PF_6)_2$

Following the similar procedure for the synthesis of **6a-X**$^{2+}$, **6b-X**$^{2+}$ was obtained with 95%. Data for elemental analysis and MS spectrum are shown in Table 1 and Figure S6 in Supporting Information, respectively.

In-situ **preparation of *in*,*in*-{[Ru^{III}(F-dpb)(OH_2)][Ru^{II}(trpy)(OH_2)](μ-bpp)}$(PF_6)_3$, [7b]$(PF_6)_3$**

Bis aqua complex can be prepared by hydrolysis of the corresponding μ-X complex **6b-X**$^{2+}$ in acidic aqueous media. However, because its solubility is low with regard to non-substituted complex **6a-X**$^{2+}$ electrochemical studies were carried out as slurry.

Instrumentation and measurements

Cyclic voltammetric (CV) experiments were performed in a IJ-Cambria IH-660 potentiostat, using a three electrode cell. Glassy carbon disk electrodes (3 mm diameter) from BASi were used as working electrode, platinum wire as auxiliary and SSCE as the reference electrode. Cyclic voltammograms were recorded at 100 mV/s scan rate under nitrogen atmosphere. The complexes were dissolved in previously degassed dichloromethane containing the necessary amount of (*n*-Bu_4N)(PF_6), used as supporting electrolyte, to yield a 0.1 M ionic strength solution. All $E_{1/2}$ values reported in this work were estimated from cyclic voltammetry as the average of the oxidative and reductive peak potentials ($E_{p,a}$+$E_{p,c}$)/2 or from differential pulse voltammetry (DPV; pulse amplitudes of 0.05 V, pulse widths of 0.05 s, sampling width of 0.02 s, and a pulse period of 0.1 s). Unless explicitly mentioned the concentration of the complexes were approximately 1 mM. The NMR spectroscopy was performed on Bruker Avance 400 MHz Bruker Avance II and Bruker Avance 500 MHz. The ESI mass spectroscopy

experiments were performed on a Waters Micromass LCT Premier equipment, respectively. UV-Vis spectroscopy was performed on a Cary bio 50 UV-vis spectrophotometer with 1 cm quartz cells. Manometric measurements were performed with homemade water-jacket glass reactor coupled to a Testo 521 manometer. Composition of the gaseous phase was determined by online mass-spectrometry with an OmniStar GSD 301 C (Pfeiffer) quadrupole mass-spectrometer. In a typical experiment, 2 μmol of complex was charged in a glass vial closed with septum and connected to capillary adaptor. Then, vacuum/N_2-refilling were applied three times. Afterwards, 1.85 mL of degassed aqueous triflic acid solution at pH 1 was added into the vial, followed by additional degasification with N_2. And this reactor was connected to MS spectrometer. A 0.15 mL of previously degassed $(NH_4)_2Ce^{IV}(NO_3)_6$ solution (200 μmol) was then added directly into the reaction solution with a Hamilton syringe.

X-Ray structure determination

Suitable crystals of the complex **[3a](PF$_6$)$_2$** was grown as **[3a](PF$_6$)$_2$·MeOH** from methanol/diethylether. The asymmetric unit contains one molecule of the metal complex, two PF_6 anions and one methanol molecule. Suitable crystals of the complex **[3b](PF$_6$)$_2$** was grown as **[3b](PF$_6$)$_2$·Et$_2$O·1.5Me$_2$CO** from acetone/diethylether. The asymmetric unit contains one molecule of the metal complex, two PF_6 anions and one molecule of diethylether, and one and half molecules of acetone. These solvent molecules are disordered in two positions for diethylether with a ratio of 0.5/0.5 and three positions for acetone with a ratio of 0.5/0.5 /0.5. Suitable crystals of the complex **[4a](PF$_6$)** was grown as **{[4a](PF$_6$)}$_2$·1.5CH$_2$Cl$_2$** by vapour diffusion of Et_2O into a solution of **[4a](PF$_6$)** in a mixture of dichloromethane and N,N-dimethylformamide. The asymmetric unit contains two independent molecules of the metal complex cation, two PF_6 anions and 1.5 disordered dichloromethane molecules. The dichloromethane molecules are disordered located in seven positions with a ratio of 0.30:0.15:0.35:0.20:020:0.20:0.10. Suitable crystals of the complex **[5a](PF$_6$)$_2$** was grown as **[5a](PF$_6$)$_2$·3Me$_2$CO** from acetone/diethylether. The asymmetric unit contains

UNIVERSITAT ROVIRA I VIRGILI
SECOND-ROW TRANSITION-METAL COMPLEXES RELEVANT TO CO2 REDUCTION AND WATER OXIDATION
Takashi Ono
DL:T 1108-2014

one molecule of the metal complex, two PF_6 anions and three acetone molecules. In the metal complex, *trpy* and *dpb*$^-$ ligands are disordered interchanging its position with a ratio of 60:40. Additionally, one of the ligands is disordered in two orientations with a ratio of 80:20. The two PF_6 anions are disordered in three positions with a ratio 1:0.5:0.5. One of the PF_6 anions is located on a centre of inversion (C_i symmetry) and another is disordered around a twofold axis (ratio 0.5:0.5). One of the acetone molecules is disordered in two positions with a ratio of 70:30. Suitable crystals of the complex **[6b-OMe-H-OH](PF$_6$)$_2$** was grown as **[6b-OMe-H-OH](PF$_6$)$_2$·3.04Me$_2$CO·0.46Et$_2$O** from acetone/diethylether. The asymmetric unit contains one molecule of the metal complex, two PF_6 anions, 3.04 molecules of acetone and 0.46 molecules of diethylether. The metal complex molecule is partially disordered in two orientations with a ratio of 0.56:0.48. The two PF_6 anions are disordered in five positions with a ratio of 1:0.35:0.15:0.27:0.23. The 3.04 acetone molecules are disordered in six positions with a ratio of 1:0.25:0.25:0.66:0.34:0.54. The diethyl ether molecule is sharing its position with one of the acetone molecules with occupancy of 0.46. Suitable crystals of the complex **[6b-OH-H-OH](PF$_6$)$_2$** was grown as **[6b-OH-H-OH](PF$_6$)$_2$·1.25Et$_2$O·2H$_2$O** from dichloromethane/diethylether. The asymmetric unit contains one molecule of the metal complex, two PF_6 anions, 1.25 molecules of diethylether and two molecules of non-coordinated water. One of the PF6 anions is disordered in two orientations (ratio: 0.52:0.48). The diethylether molecules are disordered in three positions with a ratio of 0.75:025:025 and the water molecules are disordered in five positions with a ratio of 0.5:0.5:0.5:0.25:0.25.

***Data collection**:* Crystal structure determinations were carried out using a Bruker-Nonius diffractometer equipped with an APPEX 2 4K CCD area detector, a FR591 rotating anode with MoK_α radiation, Montel mirrors as monochromator, and a Kryoflex low temperature device (T = -173 °C). Full-sphere data collection was used with ω and φ scans. APEX-2 (for Data collection),[32] Bruker Saint V/.60A (for data reduction),[33] and SADABS (for absorption correction).[34]

***Structure Solution and Refinement**:* Crystal structure solution was achieved using direct methods as implemented in SHELXTL[35] and visualized using the program XP.

Missing atoms were subsequently located from difference Fourier synthesis and added to the atom list. Least-squares refinement on F^2 using all measured intensities was carried out using the program SHELXTL. All non-H atoms were refined, including anisotropic displacement parameters.

VII.6. Acknowledgements

Support from MINECO (CTQ-2010-21497) is gratefully acknowledged TO thanks MINECO for a doctoral grant.

X-ray structure analyses were carried out by Dr. Jordi Benet-Buchholz at the Institute of Chemical Research of Catalonia (ICIQ)

VII.7. References

(1) Karl, T. R.; Trenberth, K. E. *Science* **2003**, *302*, 1719-1723.
(2) Canadell, J. G.; Le Quéré, C.; Raupach, M. R.; Field, C. B.; Buitenhuis, E. T.; Ciais, P.; Conway, T. J.; Gillett, N. P.; Houghton, R. A.; Marland, G. *Proc. Natl. Acad. Sci. U.S.A.* **2007**, *104*, 18866-18870.
(3) Berardi, S.; Drouet, S.; Francàs, L.; Gimbert-Surinach, C.; Guttentag, M.; Richmond, C.; Stoll, T.; Llobet, A. *Chem. Soc. Rev.* **2014**. no page later.
(4) Limburg, B.; Bouwman, E.; Bonnet, S. *Coord. Chem. Rev.* **2012**, *256*, 1451-1467.
(5) Hetterscheid, D. G. H.; Reek, J. N. H. *Angew. Chem., Int. Ed.* **2012**, *51*, 9740-9747.
(6) Sens, C.; Romero, I.; Rodríguez, M.; Llobet, A.; Parella, T.; Benet-Buchholz, J. *J. Am. Chem. Soc.* **2004**, *126*, 7798-7799.
(7) Bozoglian, F.; Romain, S.; Ertem, M. Z.; Todorova, T. K.; Sens, C.; Mola, J.; Rodríguez, M.; Romero, I.; Benet-Buchholz, J.; Fontrodona, X.; Cramer, C. J.; Gagliardi, L.; Llobet, A. *J. Am. Chem. Soc.* **2009**, *131*, 15176-15187.
(8) Romain, S.; Bozoglian, F.; Sala, X.; Llobet, A. *J. Am. Chem. Soc.* **2009**, *131*, 2768-2769.
(9) Zong, R.; Thummel, R. P. *J. Am. Chem. Soc.* **2005**, *127*, 12802-12803.
(10) Deng, Z.; Tseng, H.-W.; Zong, R.; Wang, D.; Thummel, R. *Inorg. Chem.* **2008**, *47*, 1835-1848.
(11) Duan, L.; Fischer, A.; Xu, Y.; Sun, L. *J. Am. Chem. Soc.* **2009**, *131*, 10397-10399.
(12) Duan, L.; Xu, Y.; Gorlov, M.; Tong, L.; Andersson, S.; Sun, L. *Chem. —Eur. J.* **2010**, *16*, 4659-4668.
(13) Duan, L.; Bozoglian, F.; Mandal, S.; Stewart, B.; Privalov, T.; Llobet, A.; Sun, L. *Nat Chem* **2012**, *4*, 418-423.
(14) Tong, L.; Wang, Y.; Duan, L.; Xu, Y.; Cheng, X.; Fischer, A.; Ahlquist, M. S. G.; Sun, L. *Inorg. Chem.* **2012**, *51*, 3388-3398.
(15) Tong, L.; Inge, A. K.; Duan, L.; Wang, L.; Zou, X.; Sun, L. *Inorg. Chem.* **2013**, *52*, 2505-2518.
(16) Xu, Y.; Åkermark, T.; Gyollai, V.; Zou, D.; Eriksson, L.; Duan, L.; Zhang, R.; Åkermark, B.; Sun, L. *Inorg. Chem.* **2009**, *48*, 2717-2719.

UNIVERSITAT ROVIRA I VIRGILI
SECOND-ROW TRANSITION-METAL COMPLEXES RELEVANT TO CO2 REDUCTION AND WATER OXIDATION
Takashi Ono
DL:T 1108-2014

(17) Xu, Y.; Fischer, A.; Duan, L.; Tong, L.; Gabrielsson, E.; Åkermark, B.; Sun, L. *Angew. Chem., Int. Ed.* **2010**, *49*, 8934-8937.
(18) Xu, Y.; Duan, L.; Tong, L.; Akermark, B.; Sun, L. *Chem. Commun.* **2010**, *46*, 6506-6508.
(19) Sens, C.; Rodríguez, M.; Romero, I.; Llobet, A.; Parella, T.; Sullivan, B. P.; Benet-Buchholz, J. *Inorg. Chem.* **2003**, *42*, 2040-2048.
(20) Calligaris, M.; Carugo, O. *Coord. Chem. Rev.* **1996**, *153*, 83-154.
(21) Rachford, A. A.; Petersen, J. L.; Rack, J. J. *Inorg. Chem.* **2005**, *44*, 8065-8075.
(22) Benet-Buchholz, J.; Comba, P.; Llobet, A.; Roeser, S.; Vadivelu, P.; Wiesner, S. *Dalton Trans.* **2010**, *39*, 3315-3320.
(23) Calligaris, M. *Coord. Chem. Rev.* **2004**, *248*, 351-375.
(24) *Chapter VI in this thesis*.
(25) Wasylenko, D. J.; Ganesamoorthy, C.; Henderson, M. A.; Koivisto, B. D.; Osthoff, H. D.; Berlinguette, C. P. *J. Am. Chem. Soc.* **2010**, *132*, 16094-16106.
(26) Teixidor, F.; Garcia, R.; Pons, J.; Casabó, J. *Polyhedron* **1988**, *7*, 43-47.
(27) Casabo, J.; Pons, J.; Siddiqi, K. S.; Teixidor, F.; Molins, E.; Miravitlles, C. *J. Chem. Soc., Dalton Trans.* **1989**, 1401-1403.
(28) Pons, J.; López, X.; Benet, E.; Casabó, J.; Teixidor, F.; Sánchez, F. J. *Polyhedron* **1990**, *9*, 2839-2845.
(29) Levine, R.; Sneed, J. K. *J. Am. Chem. Soc.* **1951**, *73*, 5614-5616.
(30) Bomben, P. G.; Robson, K. C. D.; Sedach, P. A.; Berlinguette, C. P. *Inorg. Chem.* **2009**, *48*, 9631-9643.
(31) Sens, C.; Rodríguez, M.; Romero, I.; Llobet, A.; Parella, T.; Benet-Buchholz, J. *Inorg. Chem.* **2003**, *42*, 8385-8394.
(32) *Data collection with APEX II* versions v1.0-22, v2009.1-0 and v2009.1-02, Bruker AXS inc., Madison, Wisconsin, USA, **2007**
(33) *Data reduction with Bruker SAINT* versions V.2.10(2003), V/.60A and V7.60A, Bruker AXS inc., Madison, Wisconsin, USA, **2007**
(34) *SADABS:* V.2.10(2003); V2008 and V2008/1, Bruker AXS inc., Madison, Wisconsin, USA, **2001**
(35) Sheldrick, G. M. *Acta Crystallogr. Sect. A* **2008**, *64*, 112-122.

UNIVERSITAT ROVIRA I VIRGILI
SECOND-ROW TRANSITION-METAL COMPLEXES RELEVANT TO CO2 REDUCTION AND WATER OXIDATION
Takashi Ono
DL:T 1108-2014

Supporting Information for:

New Dinuclear Ruthenium Polypyridyl Complexes Containing Anionic Dpb Ligand: Synthesis, Characterization and Water Oxidation Reaction

Table of contents

UNIVERSITAT ROVIRA I VIRGILI
SECOND-ROW TRANSITION-METAL COMPLEXES RELEVANT TO CO2 REDUCTION AND WATER OXIDATION
Takashi Ono
DL:T 1108-2014

S1. NMR:

Figure S1. 1D and 2D NMR spectra (500 MHz, 298K, CD_2Cl_2) for complex **2a**$^+$: (a) ^{1}H-^{1}H COSY, and (b) NOESY.

(a)

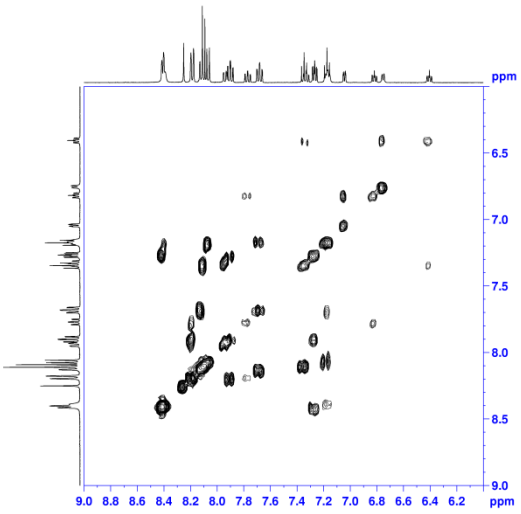

(b)

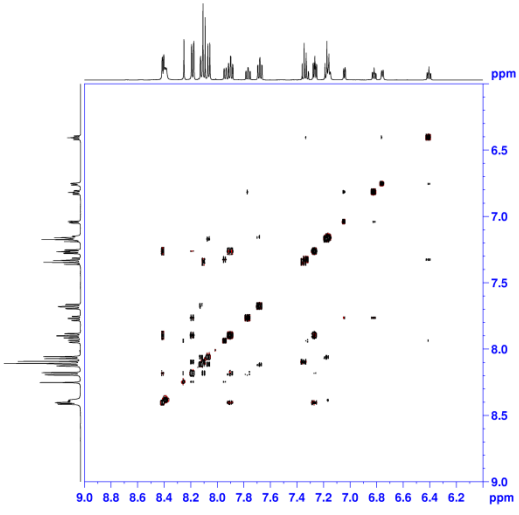

Figure S2. 1D and 2D NMR spectra (500 MHz, 298K, CD_2Cl_2) for complex **3a**$^{2+}$: (a) COSY, (b) DEPTQ135,(c) HSQC, and (d) HMBC.

(a)

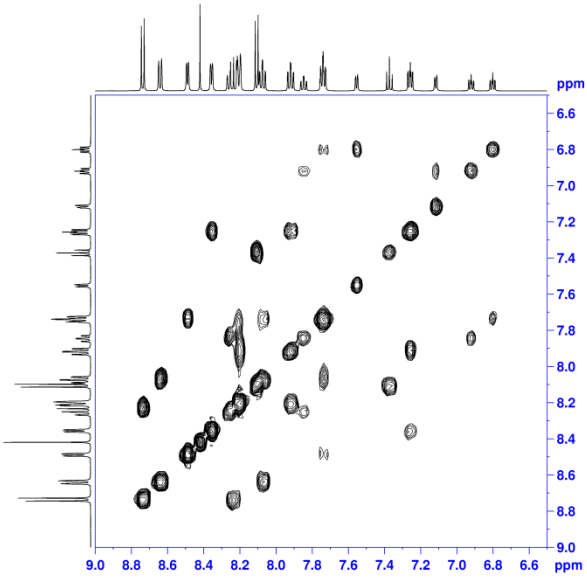

(b)

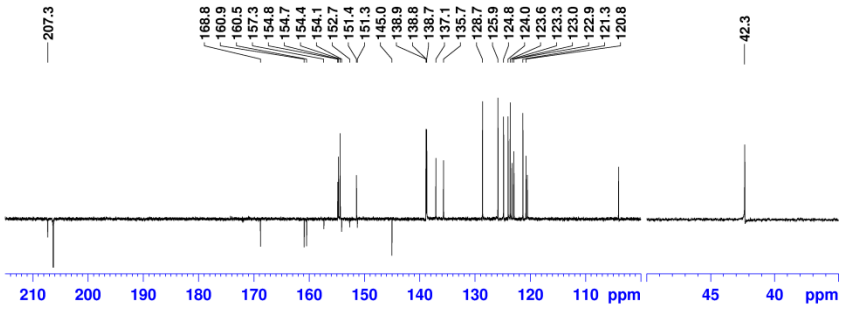

UNIVERSITAT ROVIRA I VIRGILI
SECOND-ROW TRANSITION-METAL COMPLEXES RELEVANT TO CO2 REDUCTION AND WATER OXIDATION
Takashi Ono
DL:T 1108-2014

(c)

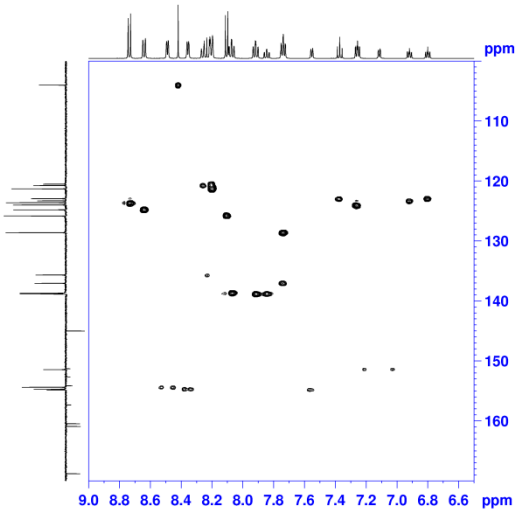

(d)

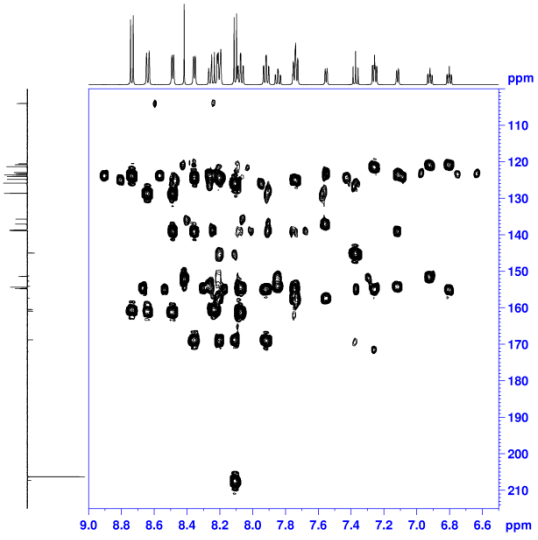

Figure S3. 1D and 2D NMR spectra (500 MHz, 298K, CD_2Cl_2) for complex **3b**$^{2+}$: (a) top: $^{1}H\{^{19}F\}$, bottom: ^{1}H NMR, (b) top: ^{19}F, bottom: $^{19}F\{^{1}H\}$, (c) COSY, (d) NOESY, (e) DEPTQ135,(f) HSQC, and (g) HMBC.

(a)

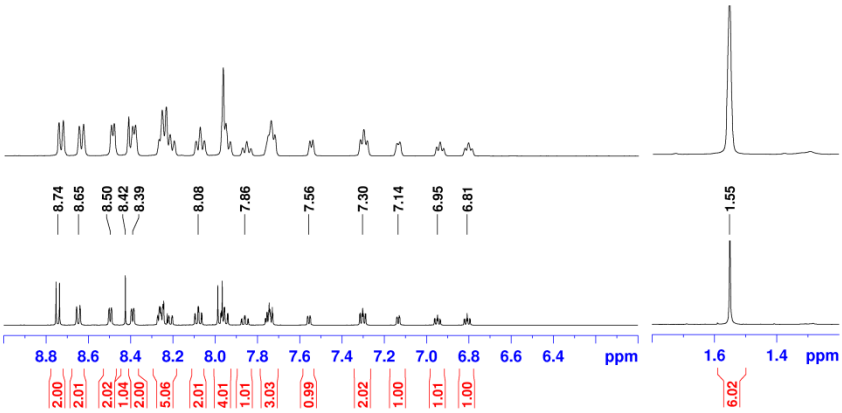

(b)

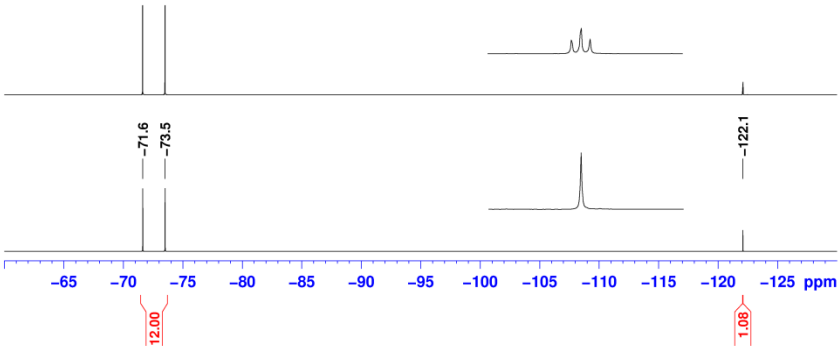

UNIVERSITAT ROVIRA I VIRGILI
SECOND-ROW TRANSITION-METAL COMPLEXES RELEVANT TO CO2 REDUCTION AND WATER OXIDATION
Takashi Ono
DL:T 1108-2014

(c)

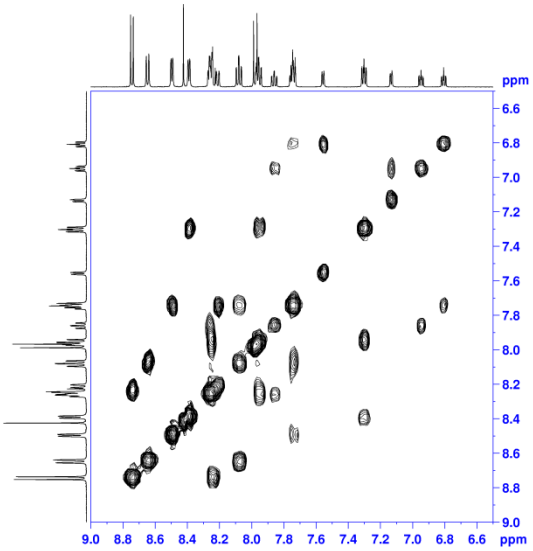

(d)

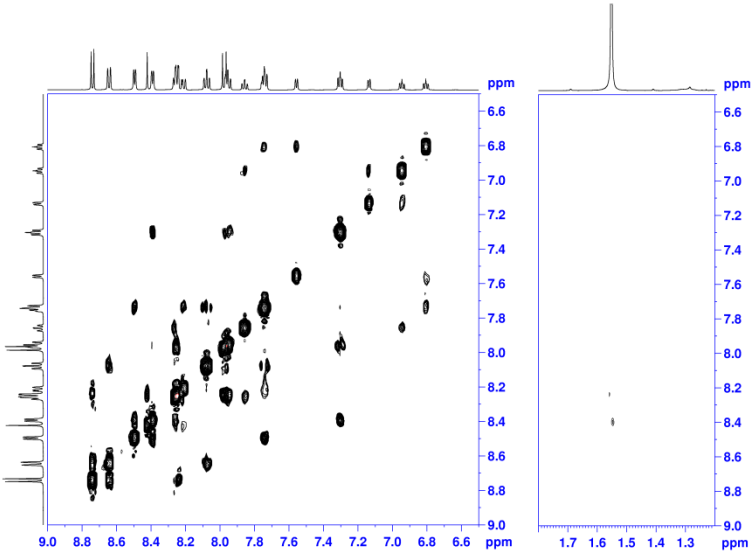

(d)

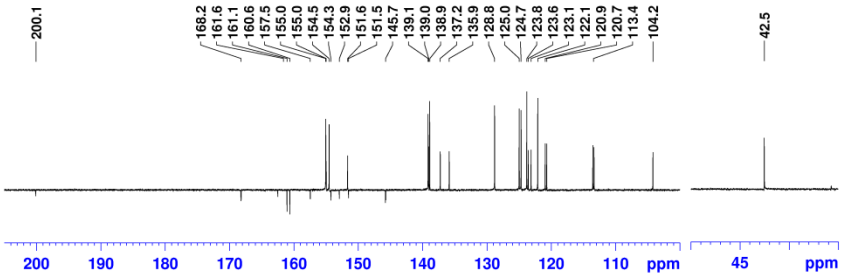
200.1
168.2
161.6
161.1
160.6
157.5
155.0
155.0
154.5
154.3
152.9
151.6
151.5
145.7
139.1
139.0
138.9
137.2
135.9
128.8
125.0
124.7
123.8
123.6
123.1
122.1
120.9
120.7
113.4
104.2
42.5
200
190
180
170
160
150
140
130
120
110
ppm
45
ppm

(e)

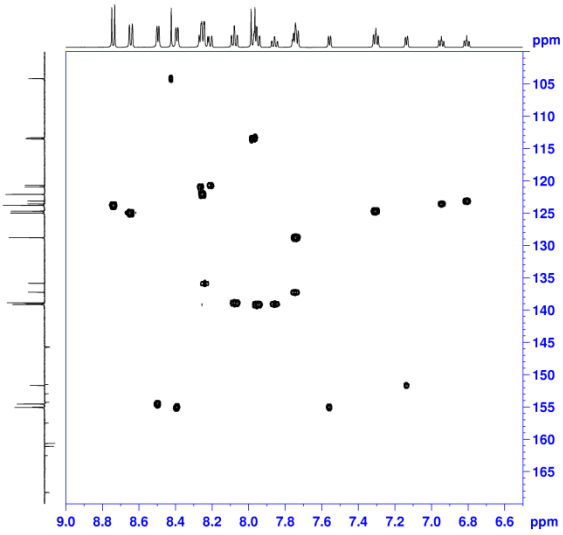
ppm
105
110
115
120
125
130
135
140
145
150
155
160
165
9.0
8.8
8.6
8.4
8.2
8.0
7.8
7.6
7.4
7.2
7.0
6.8
6.6
ppm

UNIVERSITAT ROVIRA I VIRGILI
SECOND-ROW TRANSITION-METAL COMPLEXES RELEVANT TO CO2 REDUCTION AND WATER OXIDATION
Takashi Ono
DL:T 1108-2014

(f)

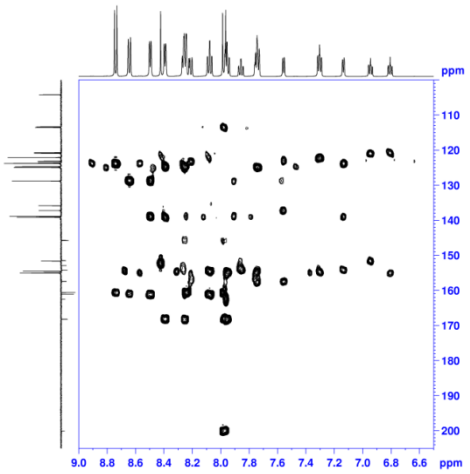

Figure S4. ^{1}H NMR spectra of (a) 10 min, and (b) 1 day, after dissolving **6b-X**$^{2+}$ in dmso-d_6 Clean transformation of **6b-X**$^{2+}$ into bridged DMSO-d_6 complex along with liberation of free MeOH (bridged dmso complex/free MeOH = 1/0.5). *: solvent residual peak, o: H_2O, and ▲: free MeOH.

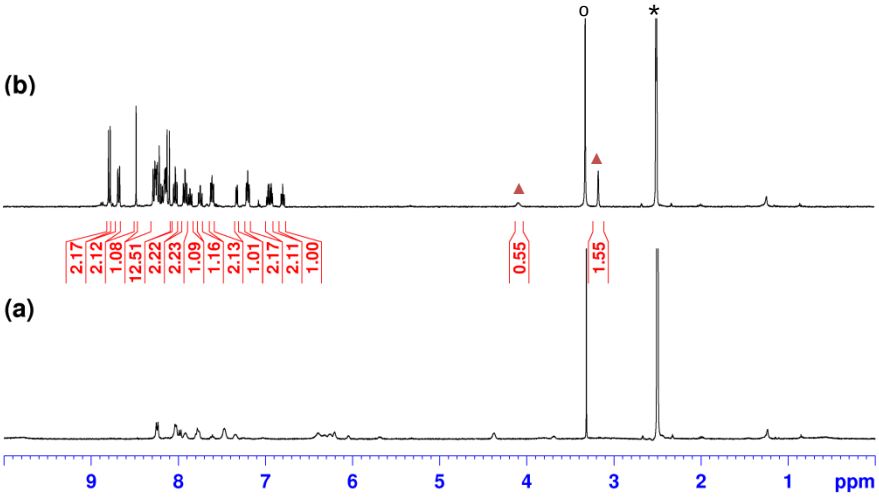

S2. MS:

Figure S5. ESI-MS spectra of (a) **2a**$^{+}$, (b) **3a**$^{2+}$, (c) **3b**$^{2+}$, (d) **4a**$^{+}$, (e) **4b**$^{+}$, (f) **5a**$^{2+}$, and (g) **5b**$^{2+}$.

(a)

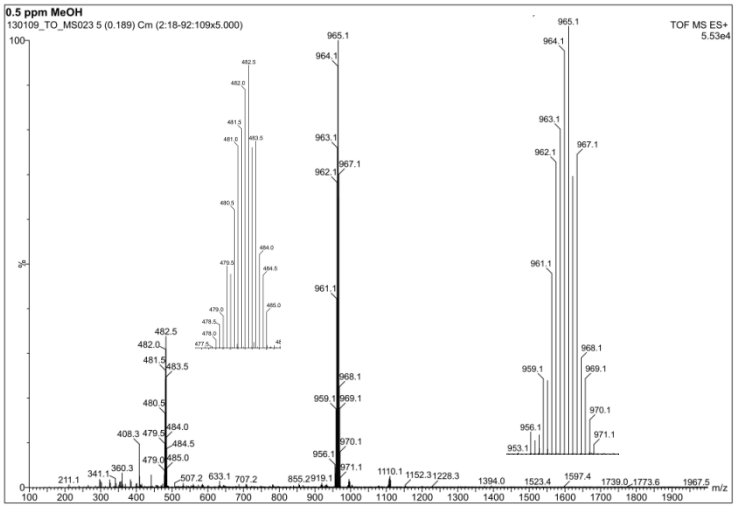

(b)

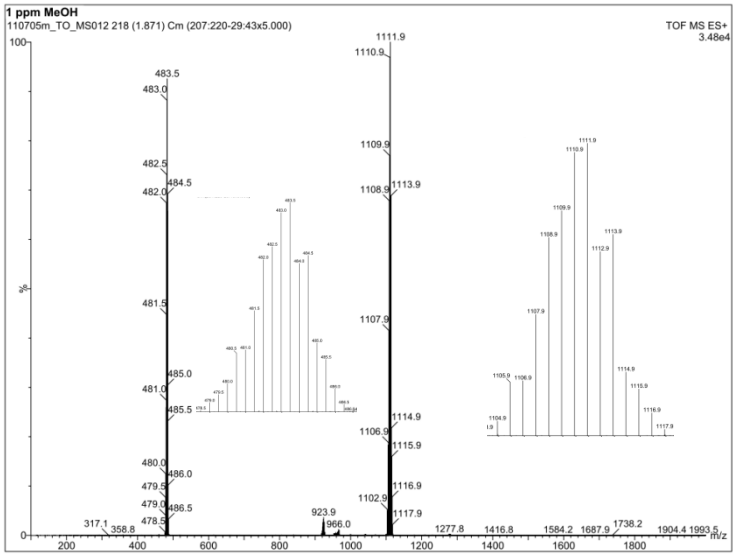

(c)

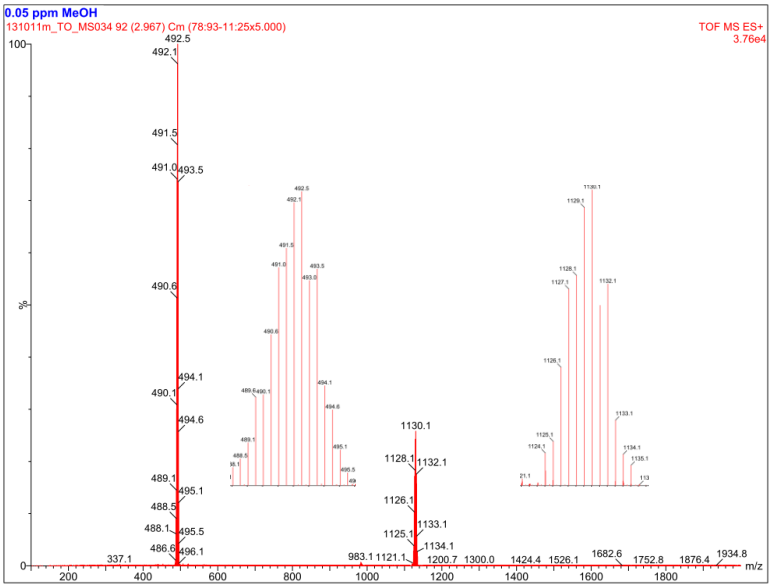
0.05 ppm MeOH
131011m_TO_MS034 92 (2.967) Cm (78:93-11:25x5.000)
TOF MS ES+
3.76e4
100
%
0
492.5
492.1
491.5
491.0
493.5
490.6
494.1
490.1
494.6
489.1
495.1
488.5
488.1
495.5
486.6
496.1
337.1
1130.1
1128.1
1132.1
1126.1
1133.1
1125.1
1134.1
983.1
1121.1
1200.7
1300.0
1424.4
1526.1
1682.6
1752.8
1876.4
1934.8
200
400
600
800
1000
1200
1400
1600
1800
m/z

(d)

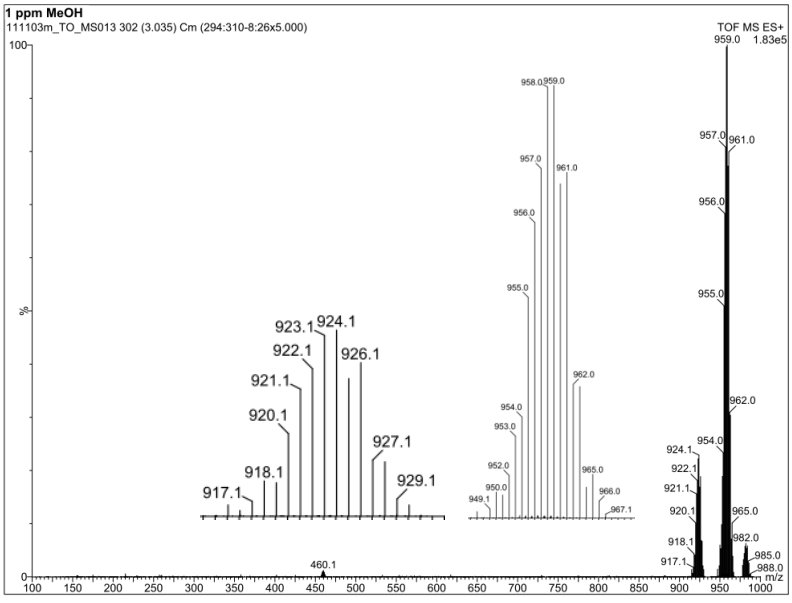
1 ppm MeOH
111103m_TO_MS013 302 (3.035) Cm (294:310-8:26x5.000)
TOF MS ES+
959.0
1.83e5
100
%
0
923.1
924.1
922.1
926.1
921.1
920.1
927.1
918.1
929.1
917.1
460.1
958.0
959.0
957.0
961.0
956.0
955.0
962.0
954.0
953.0
952.0
965.0
950.0
966.0
949.1
967.1
957.0
961.0
956.0
955.0
962.0
954.0
924.1
922.1
921.1
920.1
965.0
918.1
982.0
917.1
985.0
988.0
100
150
200
250
300
350
400
450
500
550
600
650
700
750
800
850
900
950
1000
m/z

(e)

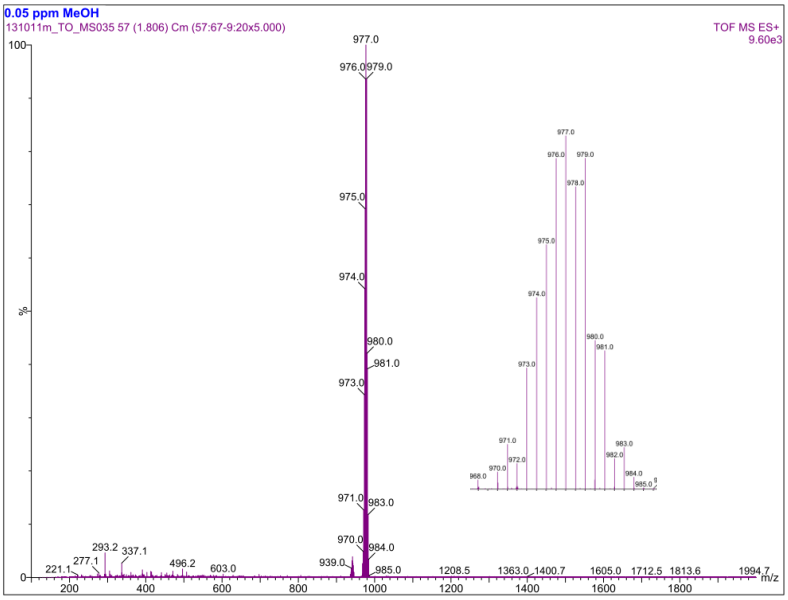
0.05 ppm MeOH
131011m_TO_MS035 57 (1.806) Cm (57:67-9:20x5.000)
TOF MS ES+
9.60e3
977.0
976.0
979.0
975.0
974.0
980.0
981.0
973.0
971.0
983.0
970.0
984.0
293.2
337.1
277.1
496.2
603.0
939.0
985.0
1208.5
1363.0
1400.7
1605.0
1712.5
1813.6
1994.7
m/z

(f)

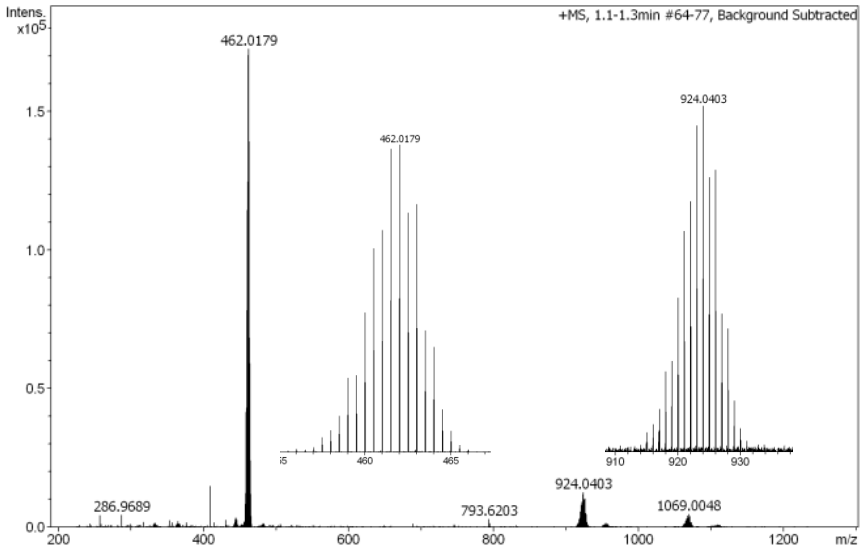
Intens.
x10^5
+MS, 1.1-1.3min #64-77, Background Subtracted
462.0179
924.0403
286.9689
793.6203
1069.0048
m/z

UNIVERSITAT ROVIRA I VIRGILI
SECOND-ROW TRANSITION-METAL COMPLEXES RELEVANT TO CO2 REDUCTION AND WATER OXIDATION
Takashi Ono
DL:T 1108-2014

(g)

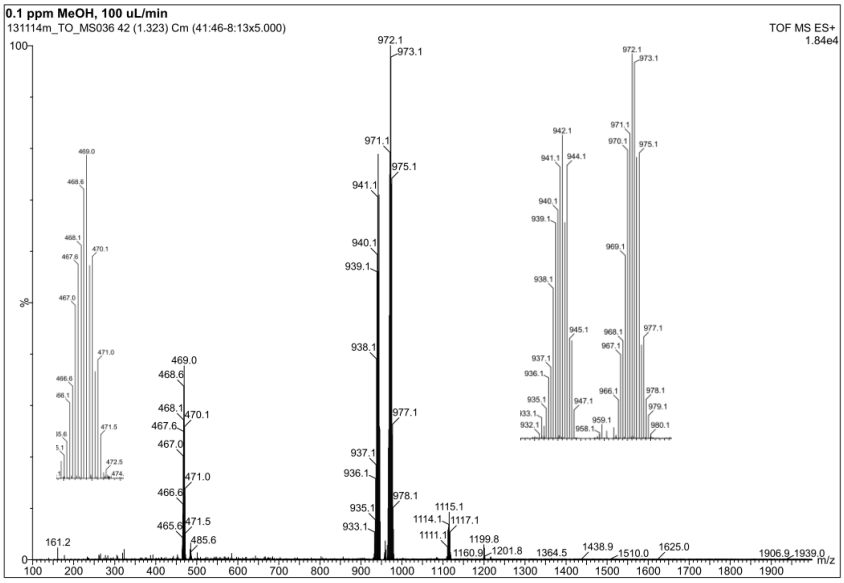

Figure S6. Top: ESI-MS(CH_3CN) spectrum of **6b-X**$^{2+}$. Bottom: Enlarged views of the peaks together with possible structures and their theoretical *m*/*z* values. *Trpy*, *dpb*$^-$ and *bpp*$^-$ ligands are not shown in their structrues for the sake of simplicity.

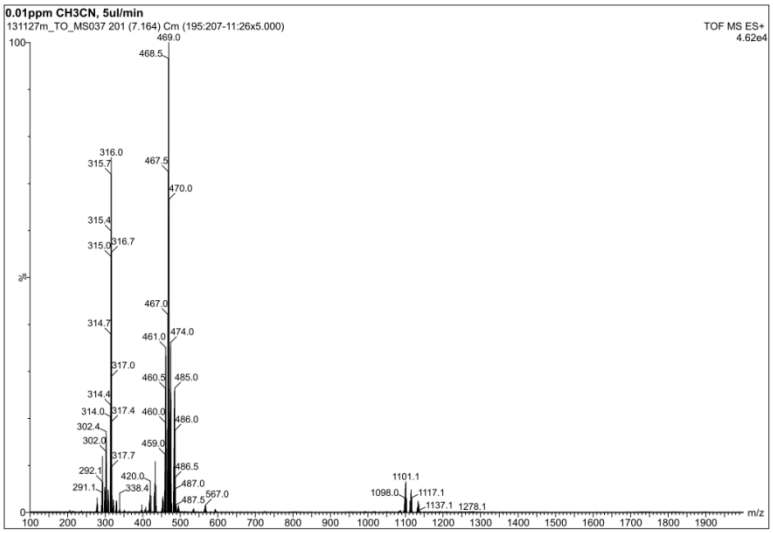

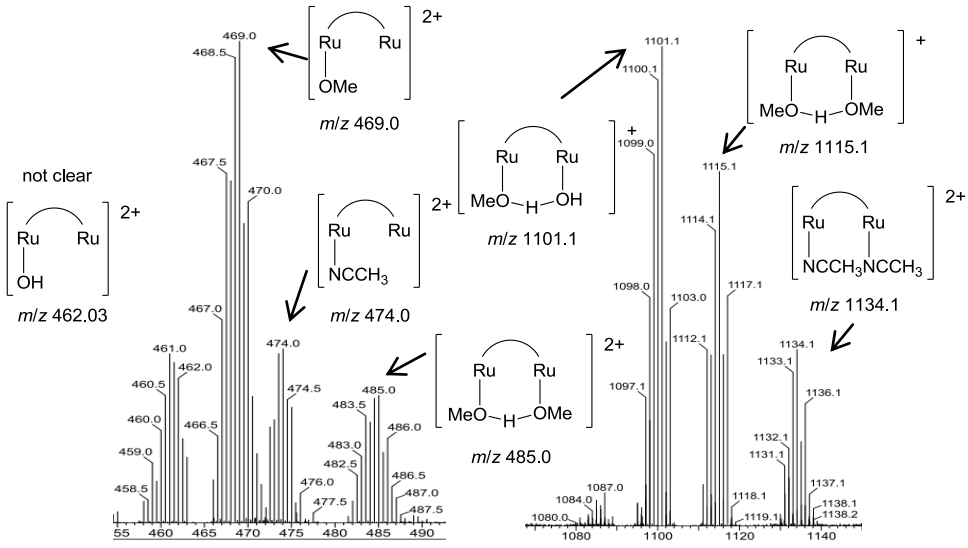

UNIVERSITAT ROVIRA I VIRGILI
SECOND-ROW TRANSITION-METAL COMPLEXES RELEVANT TO CO2 REDUCTION AND WATER OXIDATION
Takashi Ono
DL:T 1108-2014

S3. X-ray:

Table S1. Crystal data for **3a**$^{2+}$, **3b**$^{2+}$, **4a**$^{+}$, **5a**$^{2+}$, **6b-X**$^{2+}$ (X = OMe-H-OH), and **6b-X**$^{2+}$ (X = OH-H-OH)

	[3a](PF$_6$)$_2$·MeOH	**[3b](PF$_6$)$_2$·Et$_2$O·1.5Me$_2$CO**
Empirical formula	$C_{47}H_{41}F_{12}N_9O_2P_2Ru_2S$	$C_{54.50}H_{55}F_{13}N_9O_{3.50}P_2Ru_2S$
Formula weight	1288.03	1435.21
Temperature	100(2) K	100(2) K
Wavelength	0.71073 Å	0.71073 Å
Crystal system	Orthorhombic	Monoclinic
Space group	Pna2(1)	P2(1)/n
Unit cell dimensions	a = 17.8228(8) Å α = 90.00 °.	a = 16.0503(7) Å α = 90.00°
	b = 14.7029(7) Å β = 90.00 °.	b = 16.0262(7) Å β = 94.2940(10)°
	c = 18.3058(9) Å γ = 90.00 °.	c = 22.1920(10) Å γ = 90.00°
Volume	4797.0(4) Å^3	5692.3(4) Å^3
Z	4	4
Density (calculated)	1.783 Mg/m^3	1.675 Mg/m^3
Absorption coefficient	0.839 mm^{-1}	0.720 mm^{-1}
F(000)	2576	2896
Crystal size	0.30 x 0.15 x 0.10 mm^3	0.20 x 0.20 x 0.10 mm^3
Theta range for data collection	1.78 to 30.07°	2.50 to 36.46°.
Index ranges	-24 <=h<=24, -20 <=k<=20, -25 <=l<=25	-26 <=h<=24, -17 <=k<=26, -27 <=l<=36
Reflections collected	12932	81900
Independent reflections	12440 [R(int) = 0.0716]	26692 [R(int) = 0.0398]
Completeness to	theta = 30.07°, 0.952%	theta =36.46°, 95.8%
Absorption correction	Empirical	Empirical
Max. and min. transmission	0.9208 and 0.7870	0.9314 and 0.8693
Refinement method	Full-matrix least-squares on F^2	Full-matrix least-squares on F^2
Data / restraints / parameters	12932 / 58 / 680	26692 / 152 / 877
Goodness-of-fit on F^2	1.038	1.057
Final R indices [I>2sigma(I)]	R_1 = 0.0273, wR_2 = 0.0647	R_1 = 0.0459, wR_2 = 0.1044
R indices (all data)	R_1 = 0.0293, wR_2 = 0.0660	R_1 = 0.0709, wR_2 = 0.1181
Largest diff. peak and hole	0.804 and -0.919 e.Å^{-3}	1.822 and -0.721 e.Å^{-3}

Table S1. (continued)

	{[4a](PF$_6$)}$_2$·1.5CH$_2$Cl$_2$		**[5a](PF$_6$)$_2$·3Me$_2$CO**	
Empirical formula	$C_{89.50}H_{66}Cl_7F_{12}N_{18}P_2Ru_4$		$C_{53}H_{49}ClF_{12}N_9O_3P_2Ru_2$	
Formula weight	2335.97		1387.54	
Temperature	100(2) K		100(2) K	
Wavelength	0.71073 Å		0.71073 Å	
Crystal system	Triclinic		Monoclinic	
Space group	P-1		C2/c	
Unit cell dimensions	a = 13.7814(16) Å	α = 86.933(4)°	a = 13.6534(5) Å	α = 90.00°
	b = 15.2122(16) Å	β = 82.492(4)°	b = 31.5014(12) Å	β = 94.911(2)°
	c = 24.502(3) Å	γ = 65.564(4)°	c = 26.3415(8) Å	γ = 90.00°
Volume	4636.5(9) Å^3		11287.9(7) Å^3	
Z	2		8	
Density (calculated)	1.673 Mg/m^3		1.633 Mg/m^3	
Absorption coefficient	0.956 mm^{-1}		0.731 mm^{-1}	
F(000)	2324		5576	
Crystal size	0.25 x 0.15 x 0.05 mm^3		0.15 x 0.10 x 0.10 mm^3	
Theta range for data collection	0.84 to 25.15°		1.51 to 26.43°	
Index ranges	-15 <=h<=16, -13 <=k<=18, -29 <=l<=29		-16 <=h<=17, -39 <=k<=39, -32 <=l<=32	
Reflections collected	36991		45003	
Independent reflections	16072 [R(int) = 0.0550]		11556 [R(int) = 0.0420]	
Completeness to	theta = 25.15°, 96.6%		theta = 26.43°, 99.4%	
Absorption correction	Empirical		Empirical	
Max. and min. transmission	0.9537 and 0.7960		0.9305 and 0.8983	
Refinement method	Full-matrix least-squares on F^2		Full-matrix least-squares on F^2	
Data / restraints / parameters	16072 / 1129 / 1300		11556 / 1043 / 977	
Goodness-of-fit on F^2	1.133		1.096	
Final R indices [I>2sigma(I)]	R_1 = 0.0785, wR_2 = 0.1777		R_1 = 0.0661, wR_2 = 0.1660	
R indices (all data)	R_1 = 0.1168, wR_2 = 0.1970		R_1 = 0.0993, w$R_2$2 = 0.1954	
Largest diff. peak and hole	1.977 and -1.204 e.Å^{-3}		2.172 and -1.222 e.Å^{-3}	

UNIVERSITAT ROVIRA I VIRGILI
SECOND-ROW TRANSITION-METAL COMPLEXES RELEVANT TO CO2 REDUCTION AND WATER OXIDATION
Takashi Ono
DL:T 1108-2014

Table S1. (continued)

	[6b-OMe-H-OH]$(PF_6)_2$·3.04Me_2CO·0.46Et_2O		**[6b-OH-H-OH]$(PF_6)_2$·1.25Et_2O·2H_2O**	
Empirical formula	$C_{55.95}H_{57.85}F_{13}N_9O_{5.50}P_2Ru_2$		$C_{49}H_{49.50}F_{13}N_9O_{5.25}P_2Ru_2$	
Formula weight	1455.44		1359.55	
Temperature	100(2) K		100(2) K	
Wavelength	0.71073 Å		0.71073 Å	
Crystal system	Triclinic		Triclinic	
Space group	P-1		P-1	
Unit cell dimensions	a = 13.0322(10) Å	α = 96.590(2)°	a = 13.1299(7) Å	α = 67.2250(10)°
	b = 14.4871(11) Å	β = 98.843(2)°	b = 13.8941(7) Å	β = 82.912(2)°
	c = 19.5881(13) Å	γ = 114.633(2)°	c = 15.6968(9) Å	γ = 88.0890(10)°
Volume	3255.2(4) $Å^3$		2619.8(2) $Å^3$	
Z	2		2	
Density (calculated)	1.485 Mg/m^3		1.724 Mg/m^3	
Absorption coefficient	0.602 mm^{-1}		0.741 mm^{-1}	
F(000)	1471		1367	
Crystal size	0.04 x 0.02 x 0.01 mm^3		0.30 x 0.10 x 0.05 mm^3	
Theta range for data collection	1.72 to 27.33°		1.417 to 35.332°	
Index ranges	-15 <=h<=16 ,-18 <=k<=18 ,-17 <=l<=25		-15<=h<=21,-13<=k<=22,-25<=l<=24	
Reflections collected	30202		50281	
Independent reflections	14439 [R(int) = 0.0293]		21033[R(int) = 0.0198]	
Completeness to	theta =27.33°, 98.2%		theta =35.332°, 88.8%	
Absorption correction	Empirical		Empirical	
Max. and min. transmission	0.9940 and 0.9763		0.964 and 0.838	
Refinement method	Full-matrix least-squares on F^2		Full-matrix least-squares on F^2	
Data / restraints / parameters	14439 / 2113 / 1418		21033/ 650/ 932	
Goodness-of-fit on F^2	1.031		1.037	
Final R indices [I>2sigma(I)]	R_1 = 0.0601, wR_2 = 0.1679		R_1 = 0.0351, wR_2 = 0.0868	
R indices (all data)	R_1 = 0.0899, wR_2 = 0.2005		R_1 = 0.0438, wR_2 = 0.0929	
Largest diff. peak and hole	1.708 and -0.884 e.$Å^{-3}$		1.645 and -1.029 e.$Å^{-3}$	

S4. Electrochemistry:

Figure 7. CVs and DPVs of (a) **2a**$^{+}$ (0.5 mM), (b) **3a**$^{2+}$ (0.5 mM), (c) **3b**$^{2+}$ (0.2 mM), (d) **4a**$^{+}$ (0.5 mM), (e) **4b**$^{+}$ (0.5 mM), (f) **5a**$^{2+}$ (0.5 mM), (g) **5b**$^{2+}$ (0.5 mM), (h) **6a-X**$^{2+}$ (0.5 mM), and (i) **6b-X**$^{2+}$ (0.5 mM) in 0.1 M CH_2Cl_2-$TBAPF_6$. Glassy carbon working electrode, Pt disk counter electrode and SSCE reference electrode. Scan rate 100 mV s^{-1}.

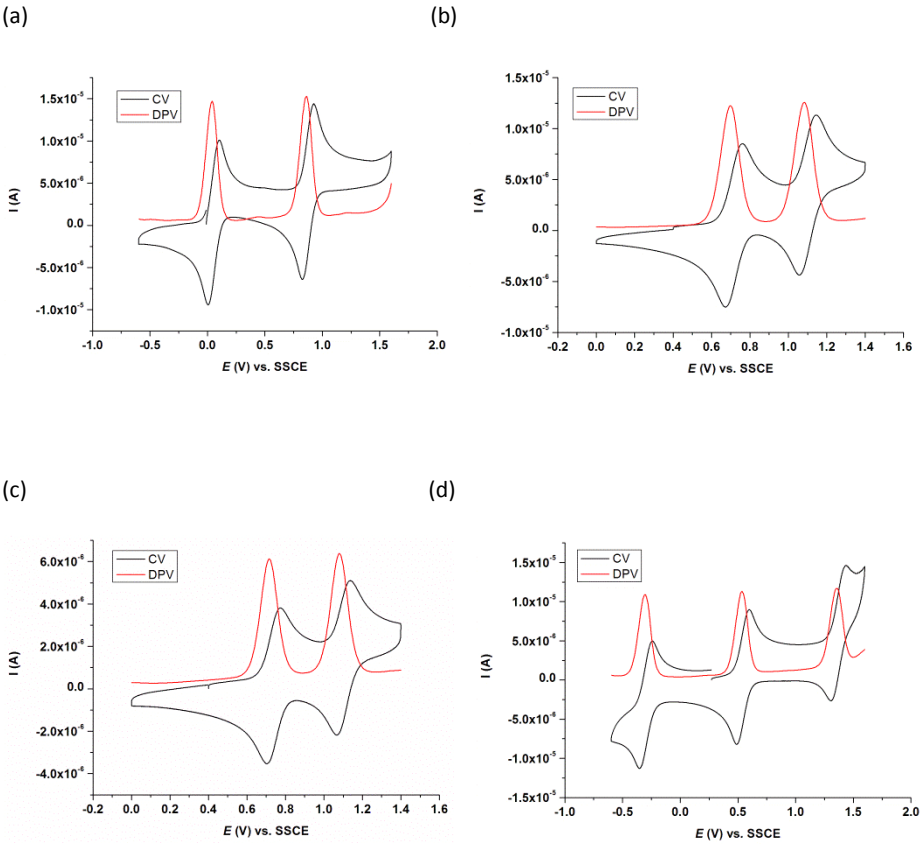

(e)

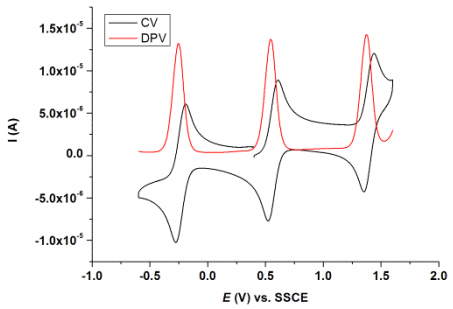
CV
DPV
I (A)
E (V) vs. SSCE

(f)

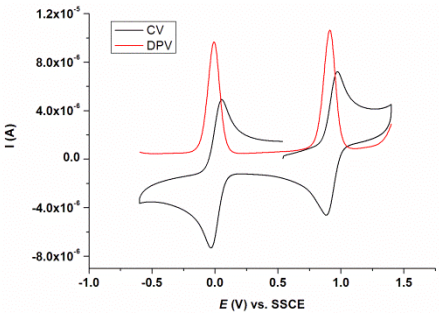
CV
DPV
I (A)
E (V) vs. SSCE

(g)

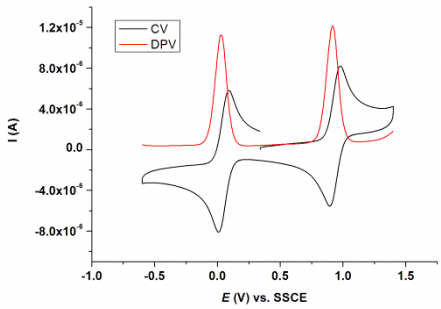
CV
DPV
I (A)
E (V) vs. SSCE

(h)

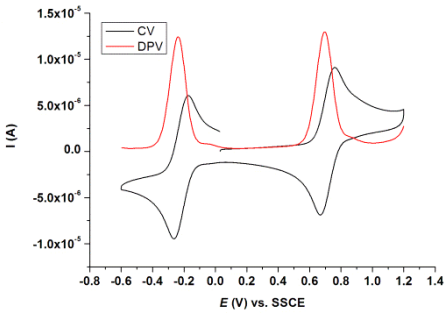
CV
DPV
I (A)
E (V) vs. SSCE

(i)

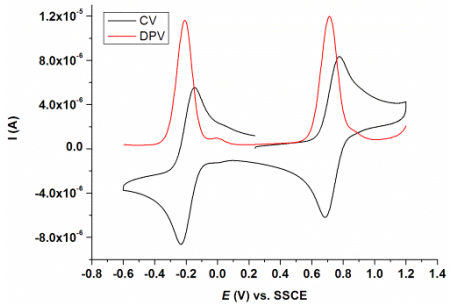
CV
DPV
I (A)
E (V) vs. SSCE

Figure S8. CV and SQWV of bis-aqua species **7b**$^{3+}$ (0.25 mM slurry) in 0.1 M aqueous triflic acid solution at pH 1. Glassy carbon working electrode, Pt disk counter electrode and Hg/Hg_2SO_4 reference electrode, and potentials were converted to vs. SSCE. Scan rate 100 mV s^{-1} for CV, frequency 15 s^{-1} for SQWV.

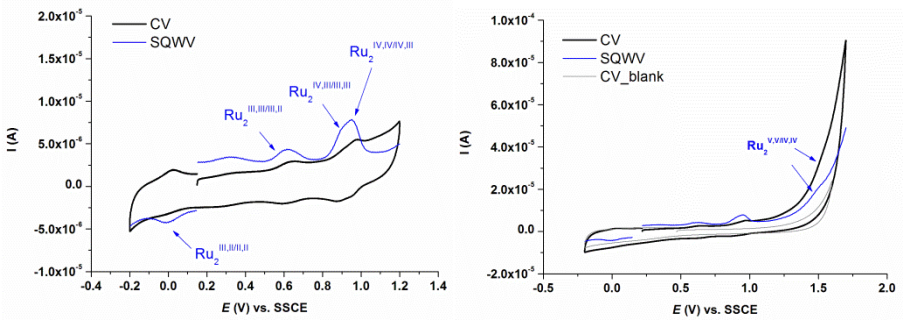

UNIVERSITAT ROVIRA I VIRGILI
SECOND-ROW TRANSITION-METAL COMPLEXES RELEVANT TO CO2 REDUCTION AND WATER OXIDATION
Takashi Ono
DL:T 1108-2014

UNIVERSITAT ROVIRA I VIRGILI
SECOND-ROW TRANSITION-METAL COMPLEXES RELEVANT TO CO2 REDUCTION AND WATER OXIDATION
Takashi Ono
DL:T 1108-2014

Chapter VIII

Summary and Conclusions

UNIVERSITAT ROVIRA I VIRGILI
SECOND-ROW TRANSITION-METAL COMPLEXES RELEVANT TO CO2 REDUCTION AND WATER OXIDATION
Takashi Ono
DL:T 1108-2014

Chapter III

A series of new mononuclear ruthenium polypyridyl complexes of general formula $[Ru(T)(B)Cl]^{n+}$ (T = meridional tridentate ligand, B = bidentate ligand) have been introduced to the catalytic reaction of the hydrogenative reduction of CO_2 to formic acid. The catalytic mechanism has been studied using M06L DFT level of theory.

Chapter III-1

- New mononuclear Ru complexes containing anionic N donor *bid*$^-$ ((1*Z*,3*Z*)-1,3-bis(pyridin-2-ylimino)isoindolin-2-ide) ligand, Ru(bid)(4,4'-R_2-bpy)Cl, (bpy = 2,2'-bipyridine, R = H: **1**, OMe: **1d**, COOEt: **1w**) have been synthesized and characterized.
- Their catalytic performances toward the hydrogenative CO_2 reduction have been compared to that of $[Ru(trpy)(bpy)Cl]^+$, **2**$^+$ (*trpy* = 2,2':6';2''-terpyridine). Substitution of *trpy* by the anionic *bid*$^-$ ligand produces a remarkable enhancement of both TON and TOF_i, showing the importance of electronic perturbation on catalytic performance.
- Further electronic donation exerted by *bpy* resulted in the decrease of the TOF_i with respect to **1**, whereas the introduction of the electron withdrawing substituent increases TOF_i.
- DFT calculations reveals that the rate-determining step consists of two elementally steps; A) substitution of the formato ligand by H_2, and B) heterolytic cleavage of the H-H bond. It has been demonstrated that the former process is favoured with electron-donating ligands, whereas the latter is favoured with electron withdrawing ligands, which agrees with the experimental results.

Chapter III-2

- A series of mononuclear Ru complexes have been assessed for the catalytic reaction from the viewpoint of their electronic and steric properties.
- Electronic properties of the complexes studied were varied by systematically changing the ancillary tridentate or bidentate ligands.
- A kinetic analysis of the reaction revealed the relationship between TOF_i and redox potentials for the Ru(III/II) couple of the corresponding Ru-Cl complexes, These results support the computational results obtained in Chapter III-1, where the rate-determining step consist of two elementary steps that vary energetically in the opposite way with electronic properties of the ancillary ligands.
- For the purpose of studying the steric effect, the *bid*$^-$ complex [Ru(bid)(6,6'-Me_2-bpy)] **1e** having methyl substituents around the reactive site has been newly synthesized and characterized.
- This steric effect resulted in an increase of the catalytic activity with respect to non-substituted complex (TOF_i 1140 h^{-1} for **1e**, 366.0 h^{-1} for **1a**).
- DFT calculation reveals that the increased reaction rate is associated with the high destabilization of the formato intermediate and lesser degree of the destabilization in TS_2.

Chapter IV

This chapter described the hydrogenative CO_2 reduction with dinuclear ruthenium polypyridyl complexes and the related metal-hydrido chemistry.

Chapter IV-1

- A family of dinuclear ruthenium complexes containing anionic and neutral tridentate ligands, $[(Ru(bid))_2(\mu\text{-bpp})(\mu\text{-OAc})]$, **1**, and $[(Ru(trpy))_2(\mu\text{-bpp})(\mu$-

X)]$^{2+}$,**2-X^{2+}**, (X=Cl$^-$, OCHO$^-$; *bpp*$^-$ = 3,5-bis(2-pyridyl)pyrazolato) has been tested as the precatalysts for the hydrogenative CO_2 reduction.

- The use of anionic *bid*$^-$ as a meridional ligand in **1** increases both TON and TOF_i compared to their *trpy* analogues, **2-X^{2+}**.
- The dinuclear complex **1** has a TOF_i lower than that of mononuclear analogue [Ru(bid)(bpy)Cl], **3**; however, the stability in the catalytic cycle drastically increase, leading to a higher TON than that of **3**.
- A kinetic analysis showed that the initial rate follows first order in catalyst concentration and H_2 pressure but zero order in CO_2 pressure.
- These observations are consistent with the rate-determining step, as predicted by DFT calculations, which consists of OCHO/H_2 ligand substitution followed by H_2 heterolytic cleavage.
- The evidently stronger effect of electronic effects on the step of OCHO/H_2 ligand substitution relative to the step of H_2 heterolytic cleavage is ultimately responsible for the increased reactivity observed with anionic ligands.

Chapter IV-2

- New dinuclear ruthenium hydrido species have been generated *in situ* by using $NaBH_4$ as hydride source in aprotic solvent, such as pyridine and DMF due to their instability toward protic solvent such as MeOH and water, whose reactivity differs from mononuclear analogue [Ru(trpy)(bpy)H]$^+$ that is stable in water. This can be due to the increased nucleophilicity of the Ru-H and the high thermodynamic stability of the undesired bridged OH-OH_2 complex **2^{2+}**.
- The reaction of {[Ru(trpy)]$_2$(μ-bpp)(μ-Cl)}$^{2+}$, **1^{2+}**, with excess amount of $NaBH_4$ in pyridine-d_5 ended up with the formation of three isomers of the dinuclear ruthenium bis-hydrido species, which were tentatively assigned

to *in*,*in*-,*in*,*out*-, and *out*,*out*-$\mathbf{3}^{+}$ by NMR spectroscopy. No selectivity of the reaction is associated with the high nucleophilicity of $NaBH_4$.

- The dinuclear mono-hydride species *in*,*in*-{[Ru(trpy)(H)][Ru(trpy)(4-picoline)](μ-bpp)}$^{2+}$, $\mathbf{5}^{2+}$, using bis 4-picoline complex $\mathbf{4}^{3+}$ as the starting complex in DMF-d_7 have been *in-situ* generated and characterized by spectroscopic and electrochemical techniques
- The complex $\mathbf{5}^{2+}$ represents a catalytic intermediate equivalent in the mechanism for the hydrogenative CO_2 reduction proposed in Chapter IV-1.
- The reaction of $\mathbf{5}^{2+}$ toward CO_2 produced the bridged formate complex only at elevated temperature. The observed low reactivity of $\mathbf{5}^{2+}$ with respect to mononuclear analogue $[Ru(trpy)(bpy)H]^{+}$ suggests that the dissociation of 4-picoline is necessary for CO_2 approaching to the reactive site because one would expect that the hydrido ligand in $\mathbf{5}^{2+}$ have similar nucleophilicity to $[Ru(trpy)(bpy)H]^{+}$ from the electrochemical data.

Chapter V

- Two molybdenum oxo carbonate species obtained from the reaction of molybdate dianion with CO_2 have been synthesized and characterized analytically, spectroscopically, and structurally.
- ^{13}C-labeling experiments and computational analysis suggest that the first binding event to form $[MoO_3(\kappa^2\text{-}CO_3)]^{2-}$ is irreversible, while the second CO_2 molecule binds in a reversible process.
- It has been shown that new molybdenum carbonate complexes could serve as a source of activated CO_2, and produces formate by the reaction with mild hydride donor triethylsilane. The production of formate improves from 16% to 71% if the reaction is run under an atmosphere of CO_2, raising the question of whether the active species facilitating CO_2 reduction is the

monocarbonate complex $[MoO_3(\kappa^2\text{-}CO_3)]^{2-}$ or the dicarbonate complex $[MoO_2(\kappa^2\text{-}CO_3)_2]^{2-}$.

Chapter VI

- The synthesis of a new family of mononuclear Ru-complexes containing anionic *dpb*$^-$ (2,6-di(pyridin-2-yl)benzen-1-ide) ligand is presented. All the complexes have been characterized in solution and solid state.
- The electrochemical data of the new complexes have been compared with those of *trpy* analogues. The strong σ donating property of *dpb*$^-$ ligand results in a stabilization of higher oxidation state; for instance, Ru(V)-oxo species from $[Ru^{III}(R\text{-}dpb)(bpy)(OH_2)]^{2+}$ (R = H: **4a**$^{2+}$, R = F: **4b**$^{2+}$) are generated at significantly low redox potential with regard to *trpy* analogue (**4a**$^{2+}$: 0.87 V vs. SSCE, **4b**$^{2+}$: 0.88 V, vs. $[Ru^{II}(trpy)(bpy)(OH_2)]^{2+}$: 1.56 V).
- The catalytic performance of the Ru-aqua complexes **4a**$^{2+}$ and **4b**$^{2+}$ as WOC has been evaluated. The obtained poor catalytic activity can be explained by that the reaction is thermodynamically unfavourable due to low redox potential of Ru(V)=O species with respect to standard potential for O_2/H_2O as well as the instability of *dpb*$^-$ ligand toward oxidation.
- The electrocatalytic activity of the Ru(V)=O species toward BzOH has been examined. The obtained rate constant ((2.7± 0.1) x 10^3 $M^1 \cdot s^{-1}$) is comparable to the highest rate obtained with $[Ru(Mebimpy)(bpy)(OH_2)]^{2+}$ among the related systems. We have shown the superiority of our catalyst in terms of the required lower potential for triggering the reaction.

Chapter VII

- New non-symmetric dinuclear ruthenium complexes containing the anionic *dpb*$^-$ (2,6-di(pyridin-2-yl)benzen-1-ide) and *trpy* ligands on each metal

centre, which represents an analogue of dinuclear 'Ru-*Hbpp*' WOC, have been synthesized and characterized.

- By comparing the electrochemical data of the bridged Cl complex **5a**$^{2+}$ with that of the *trpy-trpy* analogue, it has been found that *dpb*$^{-}$-*trpy* complexes have lower electronic coupling between both metal centres.
- By contrast, it could be considered that in aqueous solution, electronic coupling relatively increases assisted by the PCET.
- The expected influence of the strong electron donor of *dpb*$^{-}$ ligand on lowering both the redox potentials and catalytic onset potential (at *ca.*1.4 V vs SSCE) was not found for the *dpb*$^{-}$-*trpy* system. This result may imply that highly different electronic properties of both metal centres exerted by mononucleating ligand limit the electronic coupling between both metal centres to a lesser degree compared with symmetric system.
- The catalytic performance of the bis-aqua species **7a**$^{3+}$ and **7b**$^{3+}$ as WOC has been evaluated. The obtained low TON and low selectivities (O_2/CO_2) with regard to the dinuclear 'Ru-*Hbpp*' WOC, could be attributable to the oxidatively fragile *dpb*$^{-}$ ligand.-
- The observed better catalytic performance for fluoro-substituted catalyst **7b**$^{3+}$ supports this potential catalyst degradation pathway. Based on these results, a catalyst which consists of three C-F bonds on the phenyl ring of *dpb*$^{-}$ ligand could be a promising candidate.

Resumen

En esta memoria se presentan los resultados obtenidos sobre la reducción del dióxido de carbono CO_2 y de la oxidación del agua a oxígeno, utilizando complejos de metales de transición como catalizadores. En los **Capítulo III** y **IV** se describe la reducción hidrogenativa del CO_2 al ácido fórmico catalizada mediante complejos polypyridyl rutenio. En el capítulo III, se utilizaron en la reducción catalítica hidrogenativa del CO_2 al ácido fórmico una serie de nuevos complejos mononucleares polypyridyl rutenio que tienen como fórmula $[Ru(T)(B)Cl]^{n+}$ (T = ligando tridentado meridional, B = ligando bidentado). En el **Capítulo III-1**, se muestran los resultados sobre la influencia de los efectos electrónicos sobre la actividad catalítica mediante el uso de complejos de Ru mononucleares que contienen un ligando aniónico N donante *bid*$^-$ ((1*Z*,3*Z*)-1,3-bis(piridin-2-ilimino)isoindolin-2-ide), y el ligando *bpy* que está sustituido por grupos electro donadores/aceptores. Las propiedades catalíticas hacia la reducción hidrogenativa del CO_2 muestran la importancia de la perturbación electrónica en el rendimiento catalítico. Los cálculos DFT revelan que el paso clave en el ciclo catalítico consta elementalmente de; A) la sustitución del ligando Formato mediante H_2, y B) el rompimiento heterolítico del enlace H-H. La diferencia sobre las actividades catalíticas permite racionalizar que el primer proceso se ve favorecido con ligandos donantes de electrones, mientras que la segunda fase del proceso catalítico se ve favorecida con ligandos aceptores de electrones. En el **Capítulo III-2** se describen los efectos electrónicos y estéricos extendidos sobre la reducción hidrogenativa del CO_2. Las propiedades electrónicas de los complejos estudiados fueron variadas cambiando sistemáticamente los ligandos tridentado o bidentados. Un análisis cinético reveló la relación entre velocidad inicial (TOF_i) y las propiedades electrónicas del centro metálico. Estos resultados apoyan los cálculos DFT los

cuales se muestran en el **Capítulo III-1**, donde la etapa determinante de la velocidad de reacción consiste en dos pasos elementales que varían energéticamente de manera opuesta con las propiedades electrónicas de los ligandos auxiliares. La actividad catalítica se ve incrementada por la introducción del sustituyente estérico cerca del sitio reactivo. La mejora de la velocidad fue racionalizada mediante cálculos DFT, se encontró que la desestabilización de las especies de Ru-formato hacia la coordinación de H_2 es un paso clave. En el **Capítulo IV-1,** se examinó el rendimiento catalítico de una familia de complejos polypyridyl rutenio dinucleares $\{[Ru(T)]_2(\mu\text{-bpp})(\mu\text{-X})\}^{n+}$ (T = *bid*$^-$ o *trpy*, *bpp*$^-$ = 3,5-bis(2-pyridyl)pyrazolate, X = OAc^-, Cl^-, o $OCHO^-$) en comparación con sus análogos mononucleares. El complejo dinuclear *bid*$^-$ mostró unos valores de TOF_i inferiores a los de su análogo mononuclear [Ru(bid)(bpy)Cl]; Sin embargo, su estabilidad en el ciclo catalítico aumentó drásticamente, lo que llevó a unos valores de TON más altos que los mostrados para su análogo mononuclear. Estudios mecanísticos, incluyendo un análisis de la cinética y cálculos DFT indican que el paso determinante de la velocidad consiste en la sustitución del ligando $OCHO/H_2$ seguido del rompimiento heterolítico del H_2. El efecto acelerador sobre las propiedades catalíticas asociado con el ligando aniónico se debe a que el paso de sustitución del ligando $OCHO/H_2$ está fuertemente afectado por el efecto electrónico en relación con el paso del rompimiento heterolítico del H_2. En el **Capítulo IV-2**, se muestra la síntesis de nuevas especies hidruro de rutenio dinucleares basadas en ligandos *bpp*$^-$/*trpy* consideradas especies clave para la reducción del CO_2. Un par de complejos dinucleares de hidruro fueron sintetizados usando $NaBH_4$ como fuente de hidruro. La baja estabilidad de las especies de hidruro hacia disolvente prótico tal como agua y MeOH con respecto a la análoga mononuclear $[Ru(trpy)(bpy)H]^+$ se explica debido al aumento de la

nucleofilicidad ejercida por Ru-H mediante el ligando aniónico *bpp*$^-$. La generación exitosa de las especies hidruro se consigue mediante el uso de un disolvente aprótico tal como piridina y DMF. La especie dinuclear mono-hidruro *in*,*in*-{[Ru(trpy)(H)][Ru(trpy)(4-picoline)](μ-bpp)}$^{2+}$, que representan un equivalente intermedio catalítico en el mecanismo propuesto para la reducción hidrogenativa del CO_2 descrito en el **Capítulo IV-1**, ha sido generada *in-situ*. El complejo formato puente de la reacción con el CO_2 se obtuvo sólo a temperatura elevada. La baja reactividad observada hacia el CO_2 con respecto a su análogo mononuclear, el cual reacciona con el CO_2 a temperatura ambiente, sugiere que la disociación de 4-picolina es necesaria para que el CO_2 se aproxime al sitio reactivo, ya que segun los datos electroquímicos el ligando hidruro tiene similar nucleofilicidad a [Ru(trpy)(bpy)H]$^+$. En el **Capítulo V** se describe la reactividad del dianión molibdato, $[MoO_4]^{2-}$, el cual puede ser considerado como un modelo soluble de óxidos metálicos heterogéneos, hacia el CO_2. Se han sintetizado y caracterizado analíticamente, espectroscópicamente, y estructuralmente dos especies de molibdeno carbonato oxo lo cuales fueron obtenidos a partir de la reacción del dianión molibdato con CO_2. Experimentos de ^{13}C-etiquetado y análisis computacionales sugieren que el primer evento de enlace para formar $[MoO_3(\kappa^2\text{-}CO_3)]^{2-}$ es irreversible, mientras que la segunda molécula de CO_2 se une en un proceso reversible. Se ha demostrado que los nuevos complejos de carbonato de molibdeno podrían servir como una fuente de CO_2 activado, produciendo formato mediante reacción con un donador de hidruro suave como el trietilsilano. En los **Capítulo VI** y **VII** se describe la síntesis de nuevos complejos de rutenio-aqua mono y dinucleares basados en el ligando tridentado aniónico *dpb*$^-$ (2,6-di(pyridin-2-yl)benzen-1-ide) para ser usados en la reacción de oxidación del agua . En el **Capítulo VI**, una nueva familia de complejos

mononucleares de Ru que contienen el ligando aniónico *dpb*$^-$ (2,6-di(pyridin-2-yl)benzen-1-ide) se ha preparado y caracterizado tanto en solución como en estado sólido. Sus datos electroquímicos se compararon con los de análogos de *trpy*. La propiedad electrodonadora del ligando *dpb*$^-$ resulta en la estabilización del estado de oxidación más alto; por ejemplo, las especies Ru(V)-oxo a partir de $[Ru^{III}(R\text{-}dpb)(bpy)(OH_2)]^{2+}$ (R = H, o F) se generan en un significativamente bajo potencial redox en relación con el análogo *trpy* (R = H: 0.87 V, R = F: 0.88 V,. $[Ru^{II}(trpy)(bpy)(OH_2)]^{2+}$: 1.56 V vs. SSCE). Además, se examinó el comportamiento catalítico de los nuevos complejos Ru-aqua como catalizadores para la oxidación del agua (WOC). La pobre actividad catalítica obtenida se racionalizó ya que la reacción es desfavorable desde un punto de vista termodinámico, así como la inestabilidad del ligando *dpb*$^-$ hacia la oxidación. Además, se demuestra la ventaja del uso de las especies de fácil acceso Ru(V)=O en la oxidación electrocatalítica de sustrato orgánico tal como alcohol de bencilo en términos de alta velocidad de reacción y el menor potencial requerido entre los sistemas relacionados. En el **Capítulo VII**, se establece el método de síntesis de nuevos complejos dinucleares de rutenio no simétricos que contienen ligandos *dpb*$^-$ and *trpy* en cada centro metálico, lo que representa un análogo del catalizador dinuclear 'Ru-*Hbpp*' WOC. La comparación de los datos electroquímicos con los mostrados para el análogo *trpy-trpy* sugiere que los complejos no simétricos *dpb-trpy* tienen menor acoplamiento electrónico entre los dos centros metálicos. Se ha evaluado el comportamiento catalítico de nuevas especies bis-aqua como WOC. Los valores bajos de TON y bajas selectividades (O_2/CO_2) respecto al complejo dinuclear 'Ru-*Hbp*' WOC, se atrbuye a la oxidación del ligando *dpb*$^-$. La leve modificación del catalizador resultó en un mejor rendimiento catalítico, dando una sugerencia para las nuevas mejoras del sistema catalítico.

UNIVERSITAT ROVIRA I VIRGILI
SECOND-ROW TRANSITION-METAL COMPLEXES RELEVANT TO CO2 REDUCTION AND WATER OXIDATION
Takashi Ono
DL:T 1108-2014

UNIVERSITAT ROVIRA I VIRGILI
SECOND-ROW TRANSITION-METAL COMPLEXES RELEVANT TO CO2 REDUCTION AND WATER OXIDATION
Takashi Ono
DL:T 1108-2014